FOREST MANAGEMENT ALTERS FOREST WATER USE AND DROUGHT VULNERABILITY

EDITED BY: Christina (Naomi) Tague, Julia Annick Schwarz, Matthew D. Hurteau and Anthony Parolari

PUBLISHED IN: Frontiers in Forests and Global Change

frontiers Research Topics

ISSN 1664-8714
ISBN 978-2-88966-861-8
DOI 10.3389/978-2-88966-861-8

About Frontiers

Frontiers is more than just an open-access publisher of scholarly articles: it is a pioneering approach to the world of academia, radically improving the way scholarly research is managed. The grand vision of Frontiers is a world where all people have an equal opportunity to seek, share and generate knowledge. Frontiers provides immediate and permanent online open access to all its publications, but this alone is not enough to realize our grand goals.

Frontiers Journal Series

The Frontiers Journal Series is a multi-tier and interdisciplinary set of open-access, online journals, promising a paradigm shift from the current review, selection and dissemination processes in academic publishing. All Frontiers journals are driven by researchers for researchers; therefore, they constitute a service to the scholarly community. At the same time, the Frontiers Journal Series operates on a revolutionary invention, the tiered publishing system, initially addressing specific communities of scholars, and gradually climbing up to broader public understanding, thus serving the interests of the lay society, too.

Dedication to Quality

Each Frontiers article is a landmark of the highest quality, thanks to genuinely collaborative interactions between authors and review editors, who include some of the world's best academicians. Research must be certified by peers before entering a stream of knowledge that may eventually reach the public - and shape society; therefore, Frontiers only applies the most rigorous and unbiased reviews.
Frontiers revolutionizes research publishing by freely delivering the most outstanding research, evaluated with no bias from both the academic and social point of view. By applying the most advanced information technologies, Frontiers is catapulting scholarly publishing into a new generation.

What are Frontiers Research Topics?

Frontiers Research Topics are very popular trademarks of the Frontiers Journals Series: they are collections of at least ten articles, all centered on a particular subject. With their unique mix of varied contributions from Original Research to Review Articles, Frontiers Research Topics unify the most influential researchers, the latest key findings and historical advances in a hot research area! Find out more on how to host your own Frontiers Research Topic or contribute to one as an author by contacting the Frontiers Editorial Office: frontiersin.org/about/contact

FOREST MANAGEMENT ALTERS FOREST WATER USE AND DROUGHT VULNERABILITY

Topic Editors:
Christina (Naomi) Tague, University of California, Santa Barbara, United States
Julia Annick Schwarz, University of Freiburg, Germany
Matthew D. Hurteau, University of New Mexico, United States
Anthony Parolari, Marquette University, United States

Citation: Tague, C., Schwarz, J. A., Hurteau, M. D., Parolari, A., eds. (2021). Forest Management Alters Forest Water Use and Drought Vulnerability. Lausanne: Frontiers Media SA. doi: 10.3389/978-2-88966-861-8

Table of Contents

frontiers in Forests and Global Change

EDITORIAL
published: 13 April 2021
doi: 10.3389/ffgc.2021.671437

Editorial: Forest Management Alters Forest Water Use and Drought Vulnerability

Christina Tague[1]*, *Matthew D. Hurteau*[2] *and Anthony Parolari*[3]

[1] Bren School of Environmental Science and Management, University of California, Santa Barbara, Santa Barbara, CA, United States, [2] Department of Biology, University of New Mexico, Albuquerque, NM, United States, [3] Civil, Construction and Environmental Engineering, Marquette University, Milwaukee, WI, United States

Keywords: species change, thinning, forest density, forest health, drought

Editorial on the Research Topic

Forest Management Alters Forest Water Use and Drought Vulnerability

Widespread, multi-year droughts are an increasing threat to forests throughout the world. Droughts are causing declines in forest productivity, increases in tree mortality, and contributing to increasing frequency and severity of disturbances including wildfire and insect outbreaks. Droughts also alter forest water use and the partitioning of limited precipitation between transpiration, evaporation, groundwater recharge, and streamflow. Ongoing climate change is likely to worsen droughts, with climate model projections indicating increasing duration and frequency in many forested regions of the globe. In the face of these threats, understanding how forests use water, particularly during droughts, and how forests respond to drought is critical for managing the services that these forests provide. Of particular relevance to forest managers is how management interventions might alter forest water use, mitigate drought vulnerability, and minimize losses of key ecosystem services. Management strategies, including changing forest structure through density reduction (thinning) and planting, which are commonly implemented to meet other objectives, have the potential to influence water demand and availability. Given the increasing drought-induced water scarcity, a key question for researchers and managers is how does management impact forest drought response?

This collection of papers provides new insights into how forest management, forest water use and droughts are interrelated. The collection considers both ecohydrologic impacts of changes in *forest density* (through thinning or fire) and impacts that could occur via *species management*.

DENSITY REDUCTION AND FOREST DROUGHT RESPONSES

Papers that examine forest density (Burke et al.; Hwang et al.; Klockhow et al., 2020; Krogh et al.; Roche et al.; Sinacore et al.; van Mantgem et al.) address a wide range of ecohydrologic processes that can change with forest density including snow accumulation and melt, evapotranspiration, streamflow, productivity/growth, fire, and mortality risk. Techniques used in these papers range from observation-based studies with sap flow (Sinacore et al.), tree rings (van Mantgem et al.), remotely sensed vegetation indices (normalized difference vegetation index, NDVI) (Hwang et al.), and eddy-covariance data (Roche) to ecosystem modeling approaches (Krogh et al.; Burke et al.; Saksa et al.).

Many of these papers suggest that density reduction alters forest drought responses, or at least increases water availability and/or productivity of the remaining trees. All of these studies however also emphasize the large range of variation in the impact of density reduction. For example, van Mantgem et al., using tree rings, and Burke et al. using a mechanistic model, both show substantial

Edited and reviewed by:
Kevin J. McGuire, Virginia Tech, United States

***Correspondence:**
Christina Tague
ctague@bren.ucsb.edu

Specialty section:
This article was submitted to Forest Hydrology, a section of the journal Frontiers in Forests and Global Change

Received: *23 February 2021*
Accepted: *18 March 2021*
Published: *13 April 2021*

Citation:
Tague C, Hurteau MD and Parolari A (2021) Editorial: Forest Management Alters Forest Water Use and Drought Vulnerability. Front. For. Glob. Change 4:671437. doi: 10.3389/ffgc.2021.671437

variation in responses to thinning intensity and climate. Burke et al. also highlights the importance of subsurface characteristics that affect plant available water storage capacity and type of thinning as controls on thinning response. Saksa et al. show substantial spatial variation with greater water yield following density reduction for the wetter central California Sierra relative to the drier Southern Sierra. Krogh et al. similarly emphasize spatial heterogeneity by showing how increases in snowmelt recharge with thinning vary spatially, even within relatively small watersheds.

Density reduction impacts are also dynamic and several of the studies note that the change in vegetation water use after density reduction recovers quickly (even within the first 5 years following density reduction) (Burke et al.; Roche et al.). While most papers explore the impacts of density reduction, Hwang et al. complements these by looking at hydrologic impacts of density increases that can occur with fire suppression. More generally, Mrad et al. provide a theoretical perspective on how forest density evolves over time, linking allometric, growth, structural and biomechanical, and metabolic mechanisms to the self-thinning process.

THE ROLE OF SPECIES

A subset of the papers explore interactions among species composition and forest water use and mortality risk (Klockow et al.; Schwarz et al.; van Mantgem et al.). Klockow et al. show that mortality rates and the relationship with stand structure differ across pine species during a recent drought in Texas. Hwang et al. show differences in response between downslope mesophytic trees and upslope xerophytic trees to increasing temperature for a Southern Appalachia site–although they suggest differences may be due to hillslope-scale water subsidy rather than species differences.

How management influences future forests is a function of near-term decision-making that can shape species composition and growth. van Mantgem et al. for example found species differences in drought and thinning responses in their review of tree ring analysis of growth in southwestern US forests.

Changes in precipitation and evaporative demand with climate change and their effects on soil water balances are likely to mediate managed forest drought responses. In a throughfall reduction experiment, Qi et al. showed that deep soil water storage buffered decreases in throughfall inputs. In addition, Hwang et al. showed that downslope water subsidies may decrease with increasing upslope evaporative demand and the vulnerability of downslope mesophytic species to drought. Further, coincident changes in temperature and water availability interact to produce contrasting climate change responses across forests. For example, as shown by Ruiz-Pérez and Vico, increased temperatures increased productivity in water-rich northern Boreal regions, whereas it decreased productivity in already water-limited southern regions.

SUMMARY

Most of the studies in our collection focus on semi-arid environments, where increases in drought-related forest mortality have been widespread in recent years. As climate changes, however, the concepts and findings presented in this collection will be relevant to geographic regions where drought related forest impacts were once relatively rare. Ruiz-Pérez and Vico offer a boreal forest perspective, and map drought vulnerability in Northern Europe to identify where forest management actions, such as those described by other papers in this collection, are likely to be needed in the future.

Taken together the studies in this Research Topic confirm that forest water use and drought responses are intimately tied to forest structure and composition, but that these relationships are sensitive to local-to-regional-scale variability in climate, species, and geologic/topographic setting. Efforts to mitigate drought vulnerability by active forest management must therefore take this variability into account; i.e., a one-size-fits-all approach is unlikely to be successful. New research that integrates both modeling and monitoring tools that can target specific sites and scales where management actually occurs is needed if we are to successfully use forest management to address increasing forest drought vulnerability in our changing climate.

AUTHOR CONTRIBUTIONS

All authors contributed to writing of the editorial.

ACKNOWLEDGMENTS

We thank all of the contributors to this collection and to Julia Schwarz for her help in developing and organizing the theme.

Conflict of Interest: The authors declare that the research was conducted in the absence of any commercial or financial relationships that could be construed as a potential conflict of interest.

frontiers in Forests and Global Change

ORIGINAL RESEARCH
published: 26 November 2019
doi: 10.3389/ffgc.2019.00079

Benefits of Mixtures on Growth Performance of Silver Fir (*Abies alba*) and European Beech (*Fagus sylvatica*) Increase With Tree Size Without Reducing Drought Tolerance

Julia A. Schwarz and Jürgen Bauhus*

Chair of Silviculture, University of Freiburg, Freiburg, Germany

OPEN ACCESS

Edited by:
David Findlay Scott,
University of British Columbia Okanagan, Canada

Reviewed by:
John L. Campbell,
Forest Service (USDA), United States
Mark David Tomer,
Agricultural Research Service (USDA), United States

****Correspondence:***
Julia A. Schwarz
julia.schwarz@waldbau.uni-freiburg.de

Specialty section:
This article was submitted to Forest Hydrology, a section of the journal Frontiers in Forests and Global Change

Received: *16 September 2019*
Accepted: *11 November 2019*
Published: *26 November 2019*

Citation:
Schwarz JA and Bauhus J (2019) Benefits of Mixtures on Growth Performance of Silver Fir (Abies alba) and European Beech (Fagus sylvatica) Increase With Tree Size Without Reducing Drought Tolerance. Front. For. Glob. Change 2:79. doi: 10.3389/ffgc.2019.00079

To mitigate negative impacts of drought stress in the face of climate change, mixtures of tree species such as those between European beech (*Fagus sylvatica*) and silver fir (*Abies alba*) are assumed to lower risks in forest management. This study investigates the influence of mixing beech and fir on tree growth in general and in particular on tree species responses to the extreme drought event of 2003. For this purpose, we analyzed basal area increment series and carbon isotope composition ($\delta^{13}C$) in wood of ∼160 trees from three mixed-species sites in Germany and one site in Croatia. Overall growth performance for both fir and beech increased with proportions of the admixed species when accounting for the interactions with tree size and competition intensity. Mixing improved growth of large trees for both species irrespective of neighborhood density, whereas smaller trees benefitted only in denser neighborhoods. Positive mixing effects on radial growth were more pronounced in fir compared to beech, yet the latter benefitted by admixture of fir with regard to growth recovery following drought. Both the resistance of radial growth against reduction during drought as well as the variation of isotopic composition throughout the drought period were not affected by mixing, indicating that water-use in these two species was not complementary under drought stress. Although trees from both species exhibited growth reductions during the drought, fir maintained higher absolute growth levels than beech during the drought. Both species benefited from growing in mixed neighborhoods but complementary effects depended on tree size and neighborhood density. Mixing fir and beech leads to positive or neutral effects on growth performance of trees, also in response to an extreme drought event. Since increasing tree species richness also spreads the risks associated with extreme events, mixtures of beech and fir can be recommended as a possible alternative for more drought-sensitive stands such as spruce monocultures.

Keywords: climate change, water-use efficiency, neighborhood analysis, radial growth, dendro-ecology, resistance, recovery, resilience

INTRODUCTION

Climate models predict rising average temperatures and also more frequent occurrences of extreme climatic events like storms, floods, heat waves, and droughts for the twenty-first century (Pachauri et al., 2014). In forestry, tree species mixtures are viewed as one of the most important approaches to adapt forests to the uncertainties of global change (Bauhus et al., 2017b). A growing number of studies have reported positive relationships between species diversity and forest productivity (Paquette and Messier, 2011; Vila et al., 2013; Jucker et al., 2014; Forrester and Bauhus, 2016) and tree diversity has also been shown to enhance resistance to pest outbreaks (Bauhus et al., 2017a; Jactel et al., 2017). However, whether diverse forests are also better adapted to more frequent and severe drought stress is less clear. A recent review on this topic concluded that there is no systematic relationship between tree diversity and drought tolerance across different forest ecosystems (Grossiord, 2019). However, Grossiord (2019) found that studies which reported that mixed-species forests are more resistant and resilient to drought stress (e.g., Pretzsch et al., 2013; Gazol et al., 2016) were more common than studies reporting negative effects (e.g., Grossiord et al., 2014a; Paquette et al., 2018). In addition, several studies found mixed effects, positive for one and negative for the admixed species (e.g., Condés and Del Río, 2015). Negative effects on drought tolerance may be expected in mixtures that grow faster than the monocultures of participating species since higher growth rates are typically associated with higher transpiration rates (Law et al., 2002; Forrester, 2015). Hence, the relationship between diversity and drought tolerance of trees is less straightforward as for example the more commonly reported positive effect of tree species diversity on resistance to pest outbreaks of specialist herbivore insects (Bauhus et al., 2017a). The inconsistent evidence regarding drought response of mixtures may be related to the fact that it is highly dependent on both tree species identity and site conditions because both jointly determine the absence or presence of mechanisms that lead to complementary water use such as differing species-specific rooting depths or different phenology (Forrester and Bauhus, 2016).

In Central Europe, tree species mixtures are being promoted to replace vulnerable forest stands that have been identified as areas for priority action in the endeavor to adapt forest landscapes to climate change (Bolte et al., 2009). For example, Norway spruce (*Picea abies*) still dominates large parts of the Central European forest landscape despite its documented susceptibility to droughts and wind throw. Recent observations across Central Europe confirm that the area suitable for Norway spruce cultivation will continue to decline with ongoing changing climate (Hanewinkel et al., 2013) even at higher elevations (Zang et al., 2014). Compared to Norway spruce, European beech (*F. sylvatica*) and silver fir (*A. alba*) have been shown to be less susceptible to summer droughts (Zang et al., 2011; Pretzsch et al., 2013; Vitali et al., 2017). Therefore, mixtures of European beech and silver fir, a natural species combination in many European mountain ranges, is currently promoted as an option for montane and upper montane forests in Central Europe (Zang et al., 2011, 2014). The natural distribution range of beech covers most of continental Europe and this species grows in (pure) broadleaved forests or in mixtures with conifer species including silver fir (Ellenberg, 1996). Studies from central and southern Europe have reported both decreasing (e.g., Jump et al., 2006; Gessler et al., 2007; Piovesan et al., 2008) and increasing growth trends for beech over the recent decades (Dittmar et al., 2003; Pretzsch et al., 2014; Tegel et al., 2014). Beech is considered only moderately drought tolerant and toward its southern distribution limit it may be replaced through actively managing for more drought-tolerant *Quercus*-species (Vitale et al., 2012). Silver fir is native to Europe and has a geographical distribution similar to that of beech but limited to mountainous regions. As fir grew well under the warmer conditions during the mid-Holocene (Tinner et al., 2013; Ruosch et al., 2016), it has been assumed that it would be a good replacement for the more drought-sensitive spruce at higher elevations. For example, in the Black forest, radial growth of spruce was found to more affected by drought than growth of fir and this effect was particularly pronounced at higher altitudes (van der Maaten-Theunissen et al., 2013; Vitali et al., 2017). Likewise, results of a study that included a large number of sites across Southern Germany indicate that fir can maintain growth rates also during severe drought events through its contact to ground water via deep tap roots if sufficient rainfall or snowmelt occurred early in the year (Zang et al., 2011). However, at lower elevations or in regions where high summer temperatures and soil water deficit represent major growth limiting factors, fir has been reported to be also vulnerable to drought (e.g., Battipaglia et al., 2009; Lebourgeois et al., 2010).

Stem growth of beech in mixed stands was reported to be higher than in mono-specific stands for Beech (Bosela et al., 2015; Mina et al., 2018b), and to some extent also for fir (Toigo et al., 2015; Mina et al., 2018b). Yet, with regard to the drought response of these two species, most knowledge stems from mono-specific stands or mixtures with other species. To our knowledge, only two studies have actually assessed the effect of mixing on the drought response of fir-beech mixtures (Lebourgeois et al., 2013; Gazol et al., 2016). In one of these studies, a lower sensitivity of growth to summer drought was found for fir when growing in mixture with beech and the largest benefits occurred at the driest sites (Lebourgeois et al., 2013). Neither of these studies analyzed the growth response of beech to drought when it was mixed with fir, and it remains unclear if benefits for fir came at the expense of beech or if both species benefitted from mixing with regard to their drought response

To study the response of trees to extreme drought events, one can either apply the drought experimentally (Magh et al., 2018), coincidentally measure physiological and growth processes during a drought phase (Isaac-Renton et al., 2018), or use a retrospective approach (Sohn et al., 2013), which was applied in this study. The latter is more suited to study drought influences at multiple sites and thus enable extrapolation of results to a larger population of inference (Gazol et al., 2018). Retrospective approaches analyze the variation of variables contained in the annual growth ring archive of a tree. Radial growth data can be used to understand how tree growth was influenced by forest management and environmental changes, including climate and

weather, at multiple spatial and temporal scales. Yet in temperate regions like Central Europe, where tree growth shows less inter-annual variation (Fritts, 1976), stable carbon isotope ratios ($\delta^{13}C$) in wood have been found to be better or useful additional indicators of environmental variations compared to wood growth alone (Farquhar et al., 1989; Saurer et al., 1997; Schleser, 1999). Since drought conditions reduce stomatal aperture and thus leaf-internal CO_2 partial pressure, photosynthetic discrimination against heavier $^{13}CO_2$ of the atmosphere decreases, which leads to higher values of $\delta^{13}C$ in wood (Farquhar et al., 1989). Therefore, the difference in $\delta^{13}C$ of tree rings formed in wet and dry years is a direct indicator of the level of tree water stress, and this has been used in a number of recent studies to assess the modulating influence of tree species diversity on drought stress in individual species (Grossiord et al., 2014a,b; Forrester et al., 2016). For example, drought stress in trees of a boreal forests, as indicated by stronger increases of $\delta^{13}C$ in the dry compared to the wet year, increased with tree species diversity (Grossiord et al., 2014b).

When analyzing the effect of mixtures of species on tree responses to drought events, one has to take into account additional factors that can have confounding effects on growth (Forrester and Bauhus, 2016). In stands with a large variation in tree size, large trees have been reported to be more severely affected by drought in terms of radial growth reductions than smaller trees (McDowell et al., 2011; Bennett et al., 2015; McDowell and Allen, 2015). In addition, transpiration, and therefore susceptibility to drought stress can be higher in overyielding mixtures that have a higher stand density than the monoculture counterparts (Barrufol et al., 2013; Pretzsch and Biber, 2016; Pretzsch and Schutze, 2016). Therefore, it is important to disentangle density from diversity effects when analyzing drought responses of mixed stands (Forrester, 2014).

So far, no study has investigated the effect of mixing on drought sensitivity in terms of both radial growth and isotopic composition for fir and beech. Therefore, the main aim of this study was to examine, if mixing these two species improves the drought tolerance of both species. For this purpose, we analyzed basal area increment (BAI) of 160 trees from three sites in south-western Germany and from one site in Croatia with a particular focus on periods of extreme drought stress. For beech and fir trees growing in neighborhoods of different admixture proportions, we tested whether mixing influenced the resistance, recovery, and resilience of growth to severe soil drought conditions. In addition, we compared the carbon isotope composition ($\delta^{13}C$) among years with different climatic conditions for trees in mixed vs. monospecific neighborhoods. We hypothesized that for both silver fir and European beech:

(1) Benefits of mixing on overall growth are similar for the two species and show similar patterns over time
(2) Mixing leads to a positive effect on the overall growth performance of both species but benefits vary with tree size and neighborhood competition
(3) Drought tolerance of trees is higher in mixed compared to monospecific neighborhoods

MATERIALS AND METHODS

Study Sites and Stand Selection

Data were collected at four sites, three in the Black Forest in South-western Germany and one that was close to the city of Gospic in Croatia in the Velebit mountains (**Table 1**). Climate among sites in the Black Forest varies with altitude (ranging from 400 to 860 m.a.s.l.) corresponding to a decrease in mean temperature from 9.8 to 8.6°C and an increase of annual

TABLE 1 | Site and stand description for the three study sites in Germany and the fourth site in Croatia.

Parameter/Site	Conventwald	Croatia	Freiamt	Hexental
Coordinates	48°1.3171'N, 7°57.7946'E	44° 33.8617'N, 15° 12.8145'E	48°08.8630'N, 7°54.3310'E	47°54.9986'N, 7°48.7720'E
Elevation range (m asl)	700–860	900–1,000	400	400–500
Mean annual temperature (°C)	8.6	10.1*	9.8	9.8
Annual precipitation sum (mm)	1,370	1,360*	1,130	1,130
Bedrock	Paragneiss	Limestone	Sandstone	Sandstone
Soil type	Hyperdystric Skeletic Folic Cambisol	Chromic cambisol	Dystric Cambisol	Dystric Cambisol
Stand age (years)	140–180	100–120	50–70	70–120
Mean annual basal area increment and standard deviation (SD in brackets) in years 2000–2016 in Beech (B) & Fir (F) in mm²	Beech 2051 (899) Fir 2883 (1838)	B 2011 (1096) F 3427 (1966)	B 2185 (1111) F 2432 (1650)	B 3327 (1638) F 3715 (1893)
Mean diameter at breast height and standard deviation (SD) DBH in 2016 of Beech (B) & Fir (F) in c	B 55.4 (7.4) F 71.5 (7.4)	B 40.2 (7.4) F 56.7 (11.1)	B 29.9 (6.5) F 33.7 (7.0)	B 48.8 (9.5) F 53.1 (8.2)

Climate data were obtained from the closest meteorological station and refer to years 2000–2014 for Croatia and 2000–2015 for the other three sites.
**Only nearby climate station was situated at 600 m asl and hence actual mean temperature at the sites should be lower and precipitation higher.*

precipitation from 1,130 to 1,370 mm (**Table 1**). The Croatian site has similar annual precipitation as the highest-elevation site in the Black Forest. Soils at all sites are Cambisols which developed on limestone in Croatia and on paragneiss or sandstone at the German sites. Forest stands were selected for sampling based on the following criteria:

(1) Mixed stands dominated by fir and beech with each species having at least 30% of total stand basal area; percentage of other species below 15% basal area,
(2) Heterogeneous mixing within the stand; including sections with monospecific patches of each species as well as parts with fine-grained tree-wise mixtures,
(3) More or less even-aged and early mature stands, and
(4) Maximum of one thinning intervention in the last 5 years and stumps had to be datable to permit identification of the timing of interventions during the last decade.

Data Collection, Tree-Ring Analyses, and Identification of the Drought Event

At each site, approximately twenty trees per species were selected evenly across three groups of neighborhood composition reflecting differing mixture proportions of fir and beech comprising trees with mostly conspecific neighbors, trees being surrounded by an even mix of the two species, and trees surrounded by heterospecific neighbors. Additional selection criteria for sample trees were that they had to (1) be of at least co-dominant status; (2) show no visible signs of injuries, damage, or loss in vitality; (3) have not more than one tree of a third species in their neighborhood; (4) have neighborhoods of comparable density (+/– closed conditions), and (5) not be part of the neighborhood of the next sample tree to avoid spatial correlation. The minimum distance between the selected trees within each stand varied among stands depending on their age and size. For each sample (=focal) tree, we recorded tree-ID, species, diameter at breast height (DBH) and extracted at that height two cores with an increment borer from perpendicular directions starting upslope and going in clockwise direction. Assuming that spatial extent of above ground competition also reflects below ground competition, trees were considered to be actual neighbors, and hence competitors of the central tree, if their crown interfered with the crown of the central trees. For each neighbor, we determined species identity and DBH and measured the distance to the central tree to determine neighborhood density and composition.

All increment cores were air-dried and then sanded with increasingly finer sandpaper. The polished cores were scanned and visually cross-dated with the *WinDENDRO* software (Regent Instruments Inc.). Next, the cross-validation software *COFECHA* (Grissino-Mayer, 2001) was used to check for possible cross-dating mistakes. We averaged the two cores per tree, assuming cross-sectional incremental areas of concentric shape. Mean annual basal area increments (BAI, mm^2 $year^{-1}$) of trees were calculated from annual radial increments (mm). Values before 2000 were excluded from further analyses to avoid the confounding impact of natural and thinning-related changes in the neighborhood, which could not be reconstructed prior to 2000 for the majority of stands. Since basal area increment is closely related to crown dimensions, which are rather stable in mature trees, detrending these data was not considered necessary for the short time period of investigation (2000–2016) (Sohn et al., 2016).

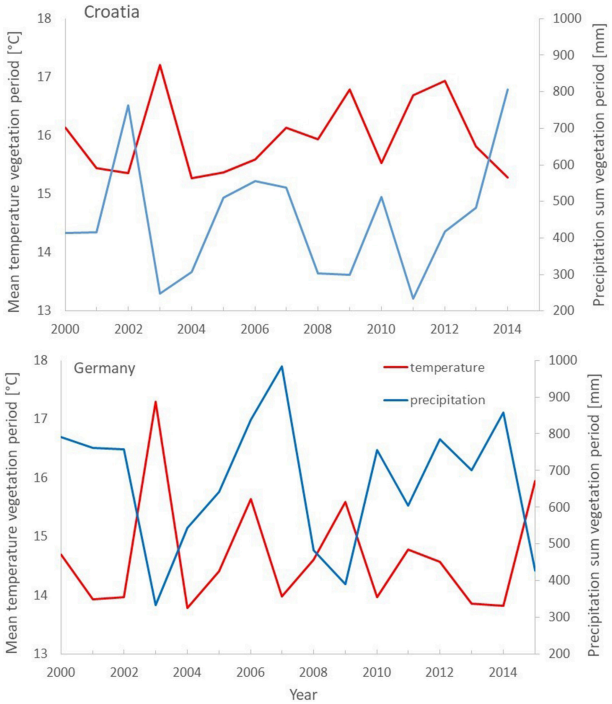

FIGURE 1 | Climate diagrams for two weather stations in Gospic in Croatia (top) and Conventwald in Germany (bottom) depicting mean temperature (red) and sum of precipitation (blue) of the vegetation period (May to September) from 2000 to 2014 (15).

The well-documented Pan-European drought event of 2003, also obvious in precipitation and temperature data at the study sites (**Figure 1**), was selected for analyzing the effect of mixing on the drought response of growth.

Analyses of Stable Carbon Isotopes

The carbon isotopic composition of dried wood samples was analyzed for all sample trees for a period of three consecutive years: 2002, 2003 and 2004, which included the drought event of 2003 as well as 1 year before and after the drought event. Measurements of $\delta^{13}C$ were done using a DeltaPlus isotope ratio mass spectrometer (Thermo Fisher, Bremen, Germany) coupled via a ConFlowIII open-split to an elemental analyzer (Carlo Erba 1100 CE analyzer; Thermo Fisher Scientific, Rodano, Italy). For more details regarding the measurement procedure, see Werner et al. (1999), Werner and Brand (2001) and Brooks et al. (2003). $\delta^{13}C$ values were calculated using the following equation,

$$\delta^{13}C = 13R_{sample} - \left(\frac{13R_{standard}}{(13R_{standard} - 1_{standard}) * 1000}\right) \quad (1)$$

where $13R_{sample}$ is the $^{13}C/^{12}C$ ratio of the sample, and $13R_{standard}$ denotes the $^{13}C/^{12}C$ ratio of the standard. Values are expressed in per mil (‰) by multiplying the δ value with the factor 1000 (Coplen, 2011; Brand et al., 2012). The $\delta^{13}C$ values are given on the δ^{13}CIAEA-603–LSVEC scale by analyzing the samples against a calibrated in-house-standard (Acetanilide: -30.06 ± 0.05‰). A quality control standard (Caffeine: −40.46 ‰) was interspersed between samples. The daily precision of the sequences was equal to or better than 0.1‰.

Data Analyses

To test our hypotheses (H1–H3), three types of analyses were conducted:

(1) Temporal analyses to test for the overall effect of mixing on growth complementarity of the two species over time (H1).
(2) Neighborhood analyses to determine the effect of mixing and other growth-relevant parameters on tree growth for a period for which exact data on neighborhood competition and composition were available (H2).
(3) Drought response analyses to test the influence of mixing on drought tolerance of trees (H3).

General Modeling Framework

To account for the replicated structure (species, trees and sites and years) and hence inherently correlated errors in our dataset, we used linear mixed-effects models (LMMs) to determine the effect of mixing on our response variables for all three analyses. The random structure of the mixed models (random effects, temporal autocorrelation, variance structure) was optimized in the presence of all fixed effects by comparing the AIC of models with different random structures using restricted maximum likelihood (REML) estimation following the procedure described by Zuur et al. (2009).

Fixed effects were selected only for the neighborhood analyses while a fixed set of predictors was used in both temporal and drought analyses (**Table 2**). All continuous, fixed effects were centered and scaled. The validity of model assumptions was evaluated using graphical tools (i.e., residual, autocorrelation and quantile-quantile plots). Models were fit with R (R Core Team, 2014), using the package *nlme* (Pinheiro et al., 2019) to allow for the specification of variance functions, to address heteroscedasticity and to model temporal autocorrelation. *P*-values were calculated with the package *lmerTest* based on Satterthwaite approximations of the degrees of freedom to test for the significance of the fixed effects (Kuznetsova et al., 2017). The modeling framework for each of the three analyses is summarized in the following sections and more detailed descriptions are presented in **Supplementary Materials 1, 2**.

Temporal Analysis: Testing H1

To examine if growth of the two tree species was positively affected by mixing and if mixing effects persisted over time, we calculated the response variable complementarity of annual growth (BAI) of the period 2000–2016 as a modification of the mixing response suggested by Vitali et al. (2018) and Forrester et al. (2013) as:

$$\textit{Complementarity}\ (\%) = \frac{BAI_{Mix} - BAI_{Mono}}{BAI_{Mono}} * 100 \qquad (2)$$

where BAI_{Mix} is the annual BAI of trees growing in mixed neighborhoods, and BAI_{Mono} is the average value of annual BAI of all trees in monospecific neighborhoods from the same species and site (as the mixed tree). Hence, the average growth over time of trees experiencing interspecific interactions is compared to that of trees which are subjected to intraspecific interactions. Complementarity values were transformed using the BoxCox-distribution to approach more normal distributions (see **Supplementary Material 2**). The mixed model included only Species and Year plus their interaction as fixed effects (**Table 2**). The optimal random structure was found to be trees nested in sites and an autocorrelation structure of order 1 (AC function) was included to take account of temporal autocorrelation of repeated measures (**Table 2**, **Supplementary Material 2**). In addition, temporal trends of BAI series were tested separately for each site and species using linear regression.

Neighborhood Analyses: Testing H2

To identify the most important growth-controlling variables for the two species at the tree neighborhood level, we analyzed the effect of admixing on tree growth while accounting for additional confounding factors. As response variable, we calculated mean annual growth by averaging annual values of BAI of the years 2014–2016 (meanBAI_3) for all focal trees as this is more indicative of growth performance than BAI of a single year (2016). (In addition, mean BAI of the last 3 years was highly correlated to BAI in 2016 and to mean BAI of the last 5 years, r >0.9, see **Supplementary Material 3**). The log transformation was applied on the response variable meanBAI_3 to obtain normal residuals. After determining the optimal random structure, we formulated the full hypothesis as:

$$\begin{aligned} &\textit{Log}\,(\textit{meanBAI3}) \sim \textit{Admixed\_prop} + \textit{Hegyi} + \textit{BAL} + \textit{DBH} \\ &+ \textit{Martonne} + \textit{Species} + \textit{Admixed\_prop} * \textit{Species} \\ &+ \textit{Admixed\_prop} * \textit{DBH} + \textit{Admixed\_prop} * \\ &\textit{Hegyi} + \textit{Admixed\_prop} * \textit{BAL} + \textit{Admixed\_prop} * \textit{Martonne}, \\ &\textit{random} = \sim 1|\textit{Site} \end{aligned} \qquad (3)$$

In Equation (3), "*" denotes that main effect and interactions of the respective variables are considered in the model, and the "1|x" notation denotes a random intercept with grouping variable x. The variables in Equation (3) refer to:

(a) *Admixed_prop*: Admixture proportions (%) based on Hegyi-index
(b) *Hegyi:* a modified version of the competition index according to Hegyi (Lee and Gadow, 1997)
(c) *BAL:* Basal area of trees larger than the focal tree in m^2
(d) *Martonne*: an aridity-index (Martonne, 1926)
(e) *DBH*: tree size at breast height in cm
(f) *Species*: binary, fir, and beech
(g) *Site*: location of the measurement

TABLE 2 | Summary statistics (means and standard deviation SD in brackets) for response variables and (continuous) predictors used in the three models related neighborhood analysis (testing H2), temporal analysis (testing H1), and drought response analysis (testing H3).

	Neighborhood analyses	Temporal analysis	Drought analysis
Sample size	$N = 153$	$N = 1{,}564$	$N = 152$
Response variable(s)	$meanBAI_3$ (mm^2): 8519 (5030)	Complementarity (%): 10 (64)	RES_{BAI}: 0.80 (0.21)/REC_{BAI}: 1.07 (0.31)/ $RESIL_{BAI}$: 0.84 (0.28) / RES_{13C}: 1.20 (1.21)/ REC_{13C}: 0.71 (1.10) $RESIL_{13C}$: 0.48 (0.94)
FIXED EFFECTS RELATED TO			
Species identity	Beech ($N = 73$) vs. Fir ($N = 80$)	Beech ($N = 731$) vs. fir ($N = 833$)	Beech ($N = 72$) vs. fir ($N = 80$)
Neighborhood composition	Admixture–%: 47.16 (32.93)	Included in response	Monospecific ($N = 61$) vs. Mixed ($N = 91$)
Neighborhood competition	Hegyi–index: 1.09 (0.48), BAL*: 5.88 (5.46)	Not addressed here	Not available
Age/Tree Size	DBH_{2016} : 49.48 (14.84)	Not addressed here	DBH_{2003}: 43.99 (15.66), BAI_{predr}: 3135 (1895)
Site/climatic conditions	Aridity index "Martonne": 6.00 (1.28)	Years (2000–2016)	Not needed (only 1 year)
RANDOM STRUCTURE			
Random effects	Sites	Trees nested in sites	Sites
Variance structure	Not needed	Not needed	Not needed
Temporal autocorrelation	Not needed	Yes (order 1)	Not needed

In addition, an overview of the random effects structure is provided separately for each analysis. For categorical predictors only sample size (N) is shown.
*$meanBAI_3$, average annual basal area increment in mm^2 from 2014 to 2016; Complementarity, Average annual basal area increments from 2000–2016 from trees in mixed neighborhoods relative to mean of all trees from same species and site growing in monospecific neighborhoods, RES1 = resistance of growth during drought, REC1 recovery of growth from drought, RESIL1 resilience of growth from drought, RES/REC/RESIL_δ13C resistance/recovery/resilience of wood carbon isotope composition. DBH diameter at breast height, Hegyi is competition index modified from Hegyi, BAL summed basal area of trees larger than the sample tree (*was not selected into final model), BAI_{predr} = mean of BAI in 3 years before drought (2000–2002).*

The variables (b–e) are confounding predictors, which were included in the full model because the annual variation of radial growth is known to depend on fluctuations of environmental and stand-related factors (Monserud and Sterba, 1996; Danescu et al., 2016). These confounding predictors and the model selection procedure leading to the final model shown in **Table 2** are described in detail in **Supplementary Materials 1, 3**.

Analyses of the Tree-Level Drought Response: Testing H3

The effect of mixing on drought tolerance of beech and fir trees was analyzed using the following response variables regarding the growth and isotopic variation throughout the drought period. For tree growth, we calculated three drought response variables by dividing the observed growth into resistance of radial growth to drought (RES), its recovery from drought (REC), and the resilience to drought (RESIL) as suggested by Lloret et al. (2011) as

$$RES = \frac{value\ \ DY}{value\ preDY} \tag{4a}$$

$$REC = \frac{value\ postDY}{value\ \ DY} \tag{4b}$$

$$RESIL = \frac{value\ postDY}{value\ \ preDY} \tag{4c}$$

where *value DY is* the annual basal area increment (BAI) of each tree during the drought year (DY) 2003, *value preDY* is the BAI during the year(s) before the drought, and *value postDY* is the BAI during the year(s) following the drought of individual trees. In order increase the robustness of our results, we calculated the Lloret-indices based on both one and 2 year-long pre- and post-drought periods. We restricted this period to 2 years before and after the drought for calculating $RES1/2_{BAI}$, $REC1/2_{BAI}$, and $RESIL1/2_{BAI}$ to avoid any influence of the heavy and partial masting that took place in fir and beech in 2006. The six response variables were relatively independent from each other ($r < 0.67$ see **Supplementary Material 4**) and hence should contain unique information. To obtain normal residuals, a log transformation was applied on all indices (except for $RESIL_{BAI}$ calculated with 2 year periods, which could be directly used without any transformation).

For analyses of carbon isotopic composition ($\delta^{13}C$) in tree-rings, we selected the same years (2002–2004) that were used to calculate growth responses to drought. Analogous to calculations of growth resistance and following the analysis done by Schaefer et al. (2017), the drought resistance of $\delta^{13}C$ (RES_{13C}) was quantified as the ratio between the value of the dry year and the wet pre-DY (Equation 4a) so that, a higher value of RES_{13C} reflects a smaller increase in $\delta^{13}C$ in the dry year indicating a lower stomatal response and thus a lower level of drought stress. In addition, the recovery and resilience of $\delta^{13}C$ following drought was calculated as the ratio between the post-DY 2004 and the DY 2003 (REC_{13C}, Equation 4b) and between the post-DY 2004 and the pre-DY 2002 ($RESIL_{13C}$, Equation 4c). The ratios RES_{13C} and $RESIL_{13C}$ could be directly used, without transformation, as response variables in our models while REC_{13C} had to be log-transformed to obtain a normal distribution.

As we did not extract increment cores from the neighbors of our central trees, and therefore could not calculate DBH of these trees in the past, actual data on neighborhood composition and competition was available only for the time of sampling in 2016.

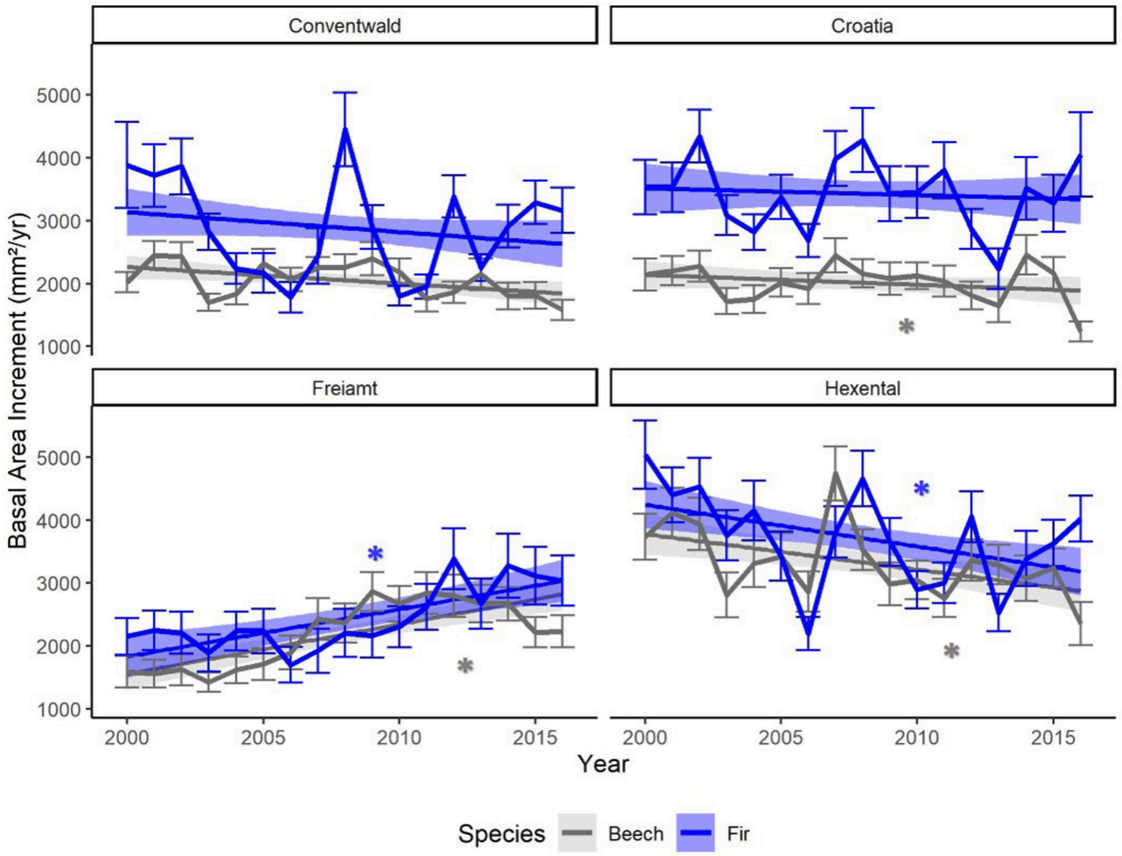

FIGURE 2 | Means of annual basal area increments (BAI) of trees from two species (fir: blue and beech: gray) at four sites (Conventwald, Croatia, Freiamt, Hexental), from 2000 to 2016. Thin bars represent standard deviation. Trend-lines and bands represent smoothed conditional means using linear model (geom_smooth function, ggplot2 in R). Stars indicate a significant trend ($p < 0.05$) over time, which was detected based on linear regression of BAI vs. Year, separately for each site and species.

Therefore, we could not calculate neighborhood characteristics for the drought year 2003 and had to use a different set of predictors as used in the neighborhood analyses (**Table 2** and more details on predictors in **Supplementary Material 1**).

To visualize the overall mixing effect on growth and isotopic response to drought, the complementarity of drought responses was calculated using the same framework as used for BAI (Equation 1) according to Vitali et al. (2018) as:

$$\textit{Complementarity}\ (\%) = \frac{\textit{RespMix} - \textit{RespMono}}{\textit{RespMono}} * 100 \qquad (5)$$

where $Resp_{Mix}$ is the average value of each of the drought response indices (resistance, recovery, and resilience of BAI and 13C) of each tree in mixed neighborhoods, and $Resp_{Mono}$ is the average value of either response of all trees in mono-specific neighborhoods from the same species and site.

RESULTS

General Results

Annual mean BAI was higher in fir than beech in most years at the two higher altitude sites (Conventwald and Croatia, **Figure 2**) while the two species showed similar absolute growth rates at the two lower altitude sites (Hexental and Freiamt) throughout the period 2000–2016. A growth decline during the 2003 drought was visible for both species at all sites (**Figure 2**). Fir displayed a second growth depression in 2006, most likely due to a strong masting event and this decline was even more pronounced than the one in 2003 at the two lower sites (Freiamt and Hexental) (**Figure 2**). At the time of sampling, mean DBH of fir was significantly larger than that of beech at the two higher altitude sites (Conventwald, Croatia) while at the 2 lower sites trees of the two species had comparable average DBH (**Supplementary Material 5**). Yet, the competition index was similar for both species at all sites (**Supplementary Material 5**).

For beech, decreasing BAI trends over time are visible at two sites (Hexental and Croatia), while fir shows decreasing growth only at the Hexental site (**Figure 2**). Both species exhibited

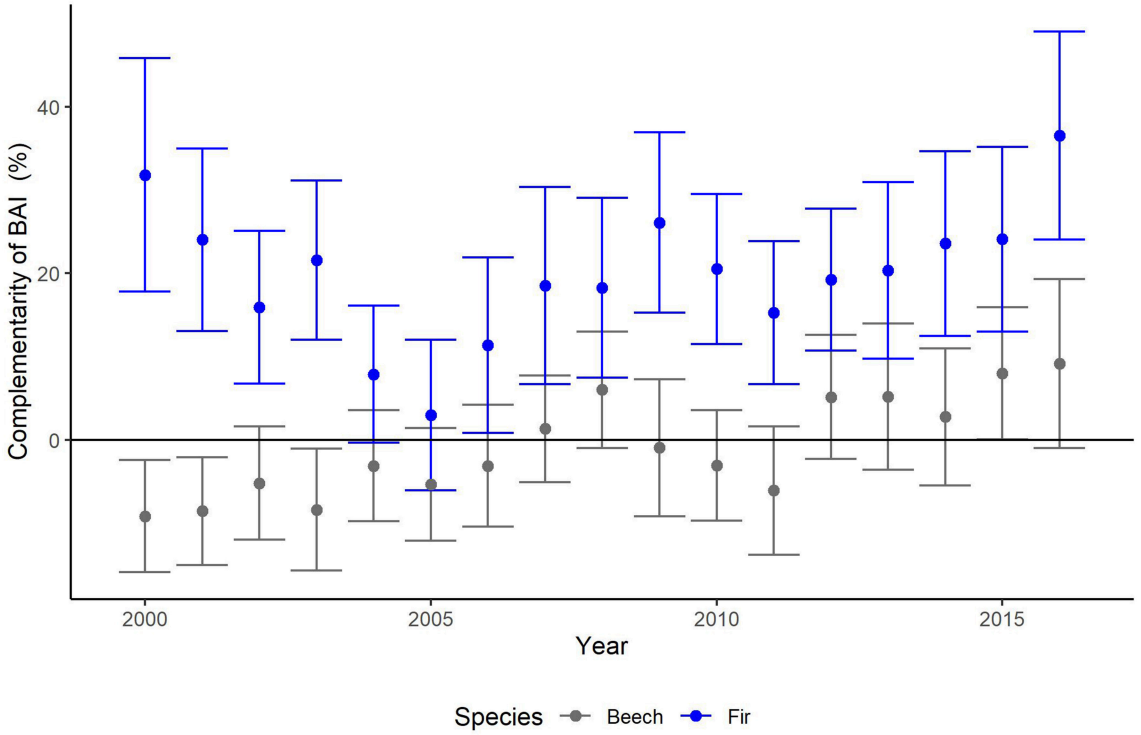

FIGURE 3 | Annual means and SE (thin bars) of complementarity (%) of basal area increments (BAI) of beech (gray) and fir (blue) for years 2000–2016. Complementarity of BAI reflects the average growth (BAI) of trees experiencing interspecific interactions compared to that of trees, which are subjected to intraspecific interactions (see Equation 2 for calculation).

positive BAI trends at the Freiamt site but this is most likely an age-related effect as trees at this site were considerably younger than at the other sites (**Table 1**).

Mixing Effect on Growth and Over Time (H1)

Across all sites, fir had positive values for complementarity of BAI (mean annual growth of all trees in mixed vs. monospecific neighborhoods) with 20% higher growth in mixed as in monospecific neighborhoods when averaging values of years 2000–2016 (range 3–37%) (**Figure 3**). In contrast, for the same period overall lower values of BAI complementarity—including negative ones—were observed in beech leading to a net zero mean (from −9 to +9%) when averaging complementarity values of all years (**Figure 3** and **Supplementary Material 5**).

After applying the BoxCox-transformation (to obtain normal residuals), complementarity of BAI shows an increasing trend regardless of species ($p < 0.01$) (**Table 3**). The selection of random effect structure (using REML) led to trees nested in sites as the most important random effect with a moderate signal among sites and trees (**Supplementary Material 2**): Since complementarity values have, after transformation, approximately a range of 21, the SD of 2 for trees nested in sites represents 10% of the range of the response and the SD of 1.4 for residual error represent 7% of the response range. As the variance explained by the fixed effects in the mixed model was very low (**Table 3**, R^2_{marg}. only 0.03) and in view of the considerable proportion of the variability of the response absorbed by random effects, we looked at the site-specific patterns of growth complementarity over time. At three sites, fir showed positive values of growth complementarity in the majority of years (**Figure 4**) except for three negative values at the Conventwald site from 2005 to 2007 (**Figure 4**). However, at the fourth site (Hexental) negative values of growth complementarity in fir were observed (**Figure 4**). Interestingly this is the only site, where values of growth complementarity were consistently positive and even increased over time for beech (**Figure 4**). At the remaining three sites, growth complementarity of beech was either consistently negative (Croatia) or fluctuated around zero (Conventwald and Freiamt) (**Figure 4**).

Drivers of Tree Growth at the Neighborhood Level (H2)

Average tree growth from 2014 to 2016 ($meanBAI_3$) increased significantly with admixture proportions for fir at two sites while no relationship between $meanBAI_3$ and admixture proportions was found for beech at any site (**Figure 5**). However, results of the most parsimonious mixed model indicate that in the presence of several confounding factors, $meanBAI_3$ was positively related to admixture proportions in both species ($p < 0.05$) (**Table 4**). This highlights the need to take into account additional growth-relevant factors. Results of the mixed model indicated a direct

TABLE 3 | Parameter estimates with standard errors (S.E.) of linear mixed model fit for temporal analyses by REML *t*-tests using Satterthwaite approximations to degrees of freedom for complementarity of BAI.

Response variable: Complementarity of BAI (%)			R^2 marginal	0.03
Transformation: BoxCox			R^2 conditional	0.69
Fixed effects (β_i)	**Estimate**	**S.E.**	**Variance components**	**S.D.**
β_0	8.90***	0.32	$d_i^{2\ Site}$	0.00
Year	0.15**	0.05	$d_{ij}^{2\ trees\ in\ sites}$	2.02
Species_Fir	0.75	0.43	d_ε^2	1.37
Year* Species	−0.04	0.07	ϕ	Phi 0.37

Model results refer to data from years 2000–2016. Marginal R^2 considers only the contribution of fixed effects; conditional R^2 considers the contribution of both fixed and random effects.

*The continuous fixed effect of year was centered and scaled. Significance codes: ***for $p < 0.001$; **for $p < 0.01$; see **Table 2** for explanation of abbreviations of variable the response was coxbox transformed. ϕ is the temporal autocorrelation parameter between successive years (AR1), d_i^2 and d_{ij}^2 are the variance estimates of the random effects site and trees in sites and d_ε^2 is the residual variance. Number of observations, 1564; groups: Site = 4 and trees in site = 92.*

positive effect of DBH on meanBAI$_3$ ($p < 0.001$), and a direct negative effect of the competition index on meanBAI$_3$ ($p < 0.01$). In addition, model outcomes showed two significant positive interactions of the relationship between admixture proportion and meanBAI$_3$ with DBH and the *Hegyi*-index (both $p < 0.001$). The selection of the random effect structure (using REML) led to site as the most important random effect. The random effect variances showed a moderate variability of the signal among sites. Since meanBAI$_3$ values assumed after transformation approximately a range of 3.6, the standard deviation of 0.40 represents 11% of the range of the response (likewise the standard deviation of 0.40 for the residual error represents 11% of the response range).

To obtain a visual comparison of the interactive effects of tree size and competition with mixing, we plotted model predictions of the relationship between the response meanBAI$_3$ with admixture proportions for (a) trees of different dimension in terms of DBH (at average levels of competition) and (b) trees of different levels of neighborhood competition (at average levels of DBH). For the *Martonne* index, we used the median value. As model predictions were similar for fir and beech (as indicated by the lack of interaction between admixing and species, **Table 4**), both species were combined for these predictions.

The relationship between admixture proportions and basal area growth became more positive with increasing tree size; switching from negative to positive for a DBH-value of ∼50 cm (**Figure 6A**). Likewise, the relationship between admixture proportions and basal area growth became more positive with increasing competition levels; switching from negative to positive for a Hegyi-value around 1 (**Figure 6B**). In heterospecific neighborhoods (>70% admixed), tree growth became even higher in denser compared to more open conditions (**Figure 6B**). Note that due to the negative relationship between the competition index and DBH (**Supplementary Material 5**) high levels of competition (*Hegyi*-values of >1.5) were observed only in neighborhoods of trees with a DBH below 45 cm so that our finding of a positive effect of admixing at high competition levels is limited to smaller trees. Based on model predictions, we can summarize that basal area growth increases with admixture proportions in larger trees irrespective of competition levels (due to smaller absolute ranges of the *Hegyi*-index) and for smaller trees in denser neighborhoods (**Figures 6A,B**).

Drought Response of Tree Growth (H3)

Beech showed significantly lower annual growth (BAI) in dry compared to normal years ($P < 0.05$) while BAI of fir was similar in dry and normal years (**Supplementary Material 5**). Fir exhibited significantly higher basal area growth than beech irrespective of climatic conditions (**Supplementary Material 5**). Growth (BAI) decreased on average by 18–20% for both beech and fir during the drought year compared to the previous year(s) across all sites but resistance varied considerably across sites with growth reductions ranging from only ∼5% for beech at the Freiamt site up to ∼30% for beech at the Hexental site (**Supplementary Material 5**). Results of the mixed models indicate that growth resistance during the 2003 drought was similar for the two species and did not differ between mixed and monospecific neighborhoods (**Table 5**, **Figures 7A,B**). Similarly, recovery of growth following drought and growth resilience to drought was similar in mixed and monospecific neighborhoods and neither recovery nor resilience of growth was different between the two species (**Table 5**). However, there was a significant interaction between species and mixing category for growth recovery 1 indicating faster recovery in beech than in fir in mixed neighborhoods (**Table 5** and effect plots in **Supplementary Material 2**). This is also in line with the higher complementarity of recovery in beech compared to fir when comparing all trees across all sites (**Figure 7**). In addition, results of the mixed models indicate no direct effect of tree size on either RES $_{BAI}$, REC $_{BAI}$, or RESIL $_{BAI}$ but a significant interaction indicating that the relationship of REC$_{BAI}$ and RESIL$_{BAI}$ with tree size is more negative in mixed compared to monospecific neighborhoods (**Table 5** and effect plots in **Supplementary Material 2**). However, the proportion of variation explained by our selected predictors (all fixed effects) to test the third hypothesis was overall low and ranged from 2 to 29% (see R^2 marginal values in **Table 5**). The selection of random effect structure (using REML), pointed to site as the most important random effect and the random effect variances showed a low variability of the signal among sites (The standard deviation for site represents merely <7% of the range of the responses, and the standard deviation for residual error represents <18% of the response range).

Drought Response of Isotopic Composition (H3)

The inter-annual variation of $\delta^{13}C$ follows a similar pattern in both species with a significant increase from 2002 to the drought year (2003) and a subsequent significant decrease from the drought to the post-drought year (2004) (**Supplementary Material 5**). This pattern was consistent across

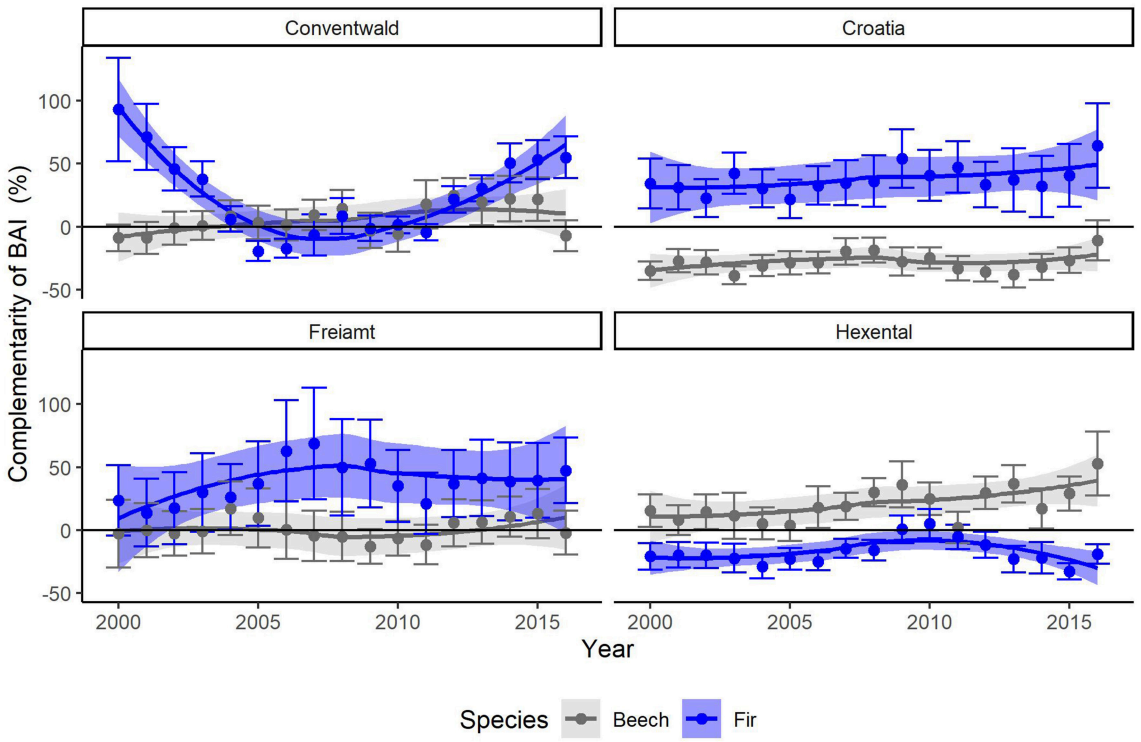

FIGURE 4 | Annual means and SE (thin bars) of complementarity (%) of basal area increments (BAI) of beech (gray) and fir (blue) for years 2000–2016 for the 4 sites (Conventwald, Croatia, Freiamt, and Hexental). Bands represent loess-smoothed conditional means (geom_smooth function with 'loess' and formula "y ~ x" with span =1, ggplot2 in R). Complementarity of BAI reflects the average growth (BAI) of trees experiencing interspecific interactions compared to that of trees which are subjected to intraspecific interactions (see Equation 2 for calculation).

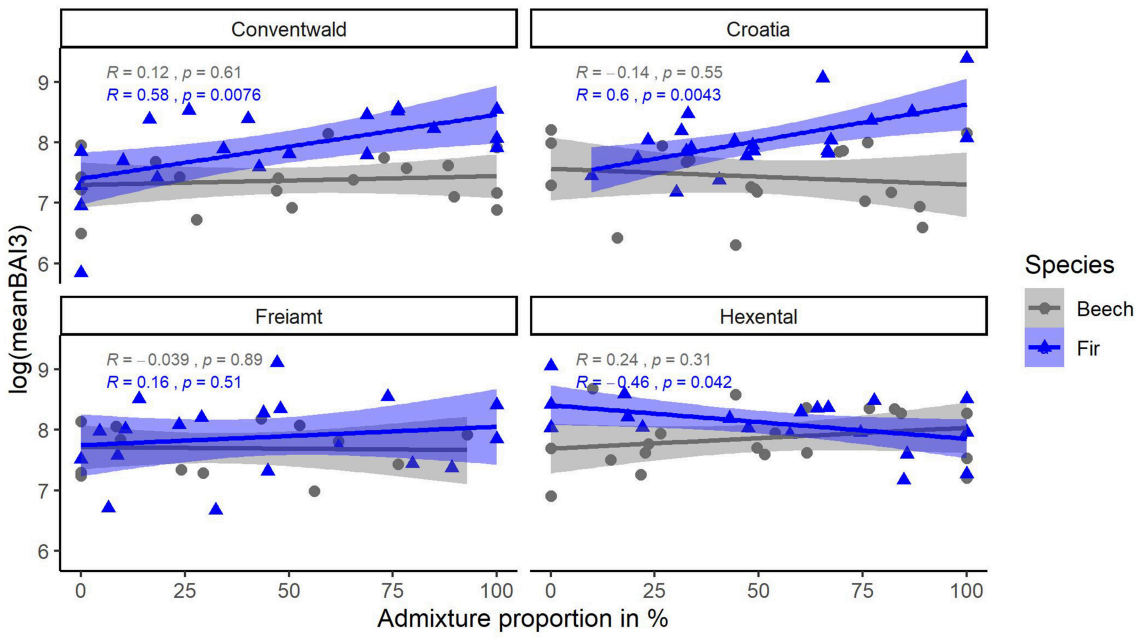

FIGURE 5 | Relationship of (transformed) response variable meanBAI3 (average BAI of last 3 years) with admixture proportions for beech (gray) and fir (blue) trees at 4 sites (Conventwald, Croatia, Freiamt, and Hexental). Pearson-r and *p*-values refer to results of linear regression for each species and site separately, $N = 14–20$.

TABLE 4 | Parameter estimates with standard errors (S.E.) of the best linear mixed model fit for neighborhood analyses by REML *t*-tests using Satterthwaite approximations to degrees of freedom.

Response variable: meanBAI$_3$			**Transformation: log**	
Fixed effects (β_i)	**Estimate**	**S.E.**	**Variance components**	**S.D.**
β_0	7.73***	0.21	$d_i^{2\ Site}$	0.40
Admixture %	0.07*	0.03	d_ε^2	0.40
Hegyi-index	−0.18**	0.06	R^2 marginal = 0.45	
Species fir	0.16	0.08	R^2 conditional = 0.72	
DBH	0.35***	0.07		
Martonne-index	−0.33	0.21		
Admixture % * DBH	0.19***	0.05		
Admixture % * Hegyi-Index	0.24***	0.06		

Marginal R^2 considers only the contribution of fixed effects; conditional R^2 considers the contribution of both fixed and random effects.
*The continuous fixed effects (admixture %, Hegyi-index, DBH, and Martonne index) were centered and scaled to facilitate comparisons. Significance codes: ***for $p < 0.001$; **for $p < 0.01$; *for $p < 0.05$, see **Table 2** for explanation of abbreviations of variables The response was transformed with exponent 0.2., d_i^2 is the variance estimate of the random effect site and d_ε^2 is the residual variance. Number of observations = 153; groups: Site =4.*

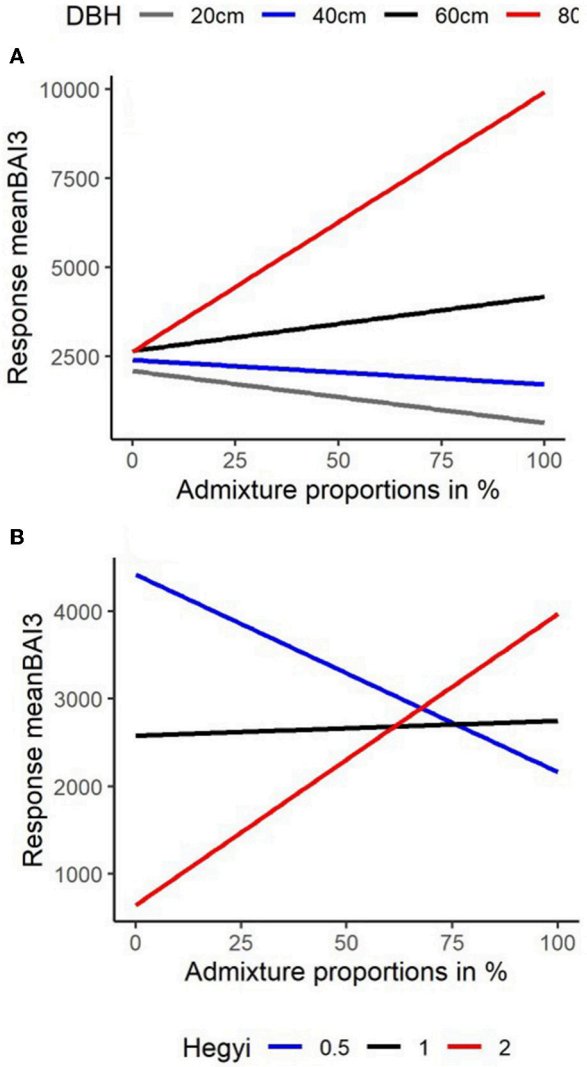

FIGURE 6 | Comparison of model predictions (see **Table 4**) for the relationship between the (back-transformed) response meanBAI$_3$ (y-axis) (average BAI from 2014 to 2016) with increasing admixture proportions (x-axis) in % for **(A)** trees of different dimensions in terms of DBH and **(B)** for 3 levels of neighborhood competition Hegyi = 0.5 (blue), Hegyi = 1.0 (Black), and Hegyi = 2.0 (Red).

sites (**Supplementary Material 5**). Mean annual values of $\delta^{13}C$ were significantly higher for fir as for beech in all years ($p < 0.001$, **Supplementary Material 5**) and at all sites (except for the site Hexental in 2003). Values of $\delta^{13}C$ in each year were similar for trees in monospecific and mixed neighborhoods for both species (**Figure 8**). This is line with results of the mixed models, which indicated that resistance, recovery and resilience of $\delta^{13}C$ was similar for the two species and for trees growing in mixed or monospecific neighborhoods (**Table 5**, **Supplementary Material 5**). Across all sites and trees, complementarity of isotopic response to drought (resistance, recovery and resilience of $\delta^{13}C$) was similar in beech and fir (**Figure 9**).

Results of the mixed models indicate that there is neither a direct effect of DBH on the isotopic drought indices nor an interactive one of DBH with mixing category (**Table 5**). The selection of random effect structure (using REML), again pointed to site as the most important random effect and the random effect variances showed a low to moderate variability of the signal among sites. The standard deviation for site represents merely 0–9% of the range of the responses. The standard deviation for residual error was higher representing 15–17% of the response range. The variance explained by the selected fixed effects in the isotope models was very low with 1–5% (R^2-marginal values in **Table 5**).

DISCUSSION

Results of this study highlight the importance of incorporating data on actual neighborhood composition and competition when examining the effects of mixing on growth performance of individual species. Positive effects of mixing on overall growth performance were more pronounced in fir than in beech, yet the latter benefitted more from admixture of fir with regard to the growth recovery following drought. In contrast to our assumptions, both the growth resistance during drought as well as the variation in isotopic composition throughout the drought period were not affected by mixing. In the following we will first discuss our results in the same order as our hypotheses; regarding (1) effects of mixing on the overall and temporal growth performance of trees, (2) the interactive effect of mixing with other growth-relevant factors on overall growth performance and (3) how mixing affected the drought response of trees.

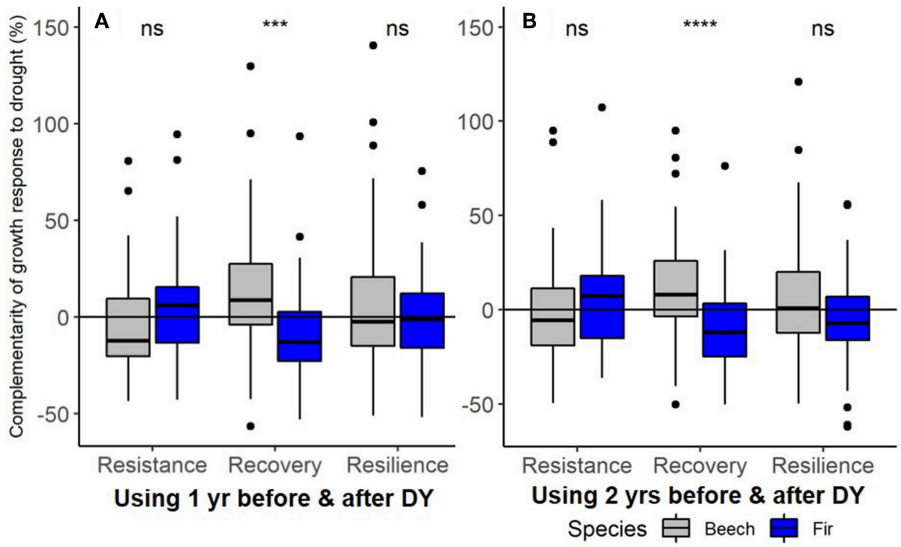

FIGURE 7 | Complementarity effects of mixing on growth responses to the 2003-drought of European beech (gray) and silver fir (blue) in terms of resistance during drought (RES), recovery following drought (REC), and resilience to drought (RESIL) using **(A)** one and **(B)** two year(s) in the pre- and post-drought period. Stars (***$P <$ 0.001 and ****$P <$ 0.0001) indicate significant differences between the 2 species for each index and "ns" indicates no significant difference between the 2 species ($P >$ 0.05) based on t-tests. Note that *T*-test was done for with transformed (^0.25) data while figure depicts raw data.

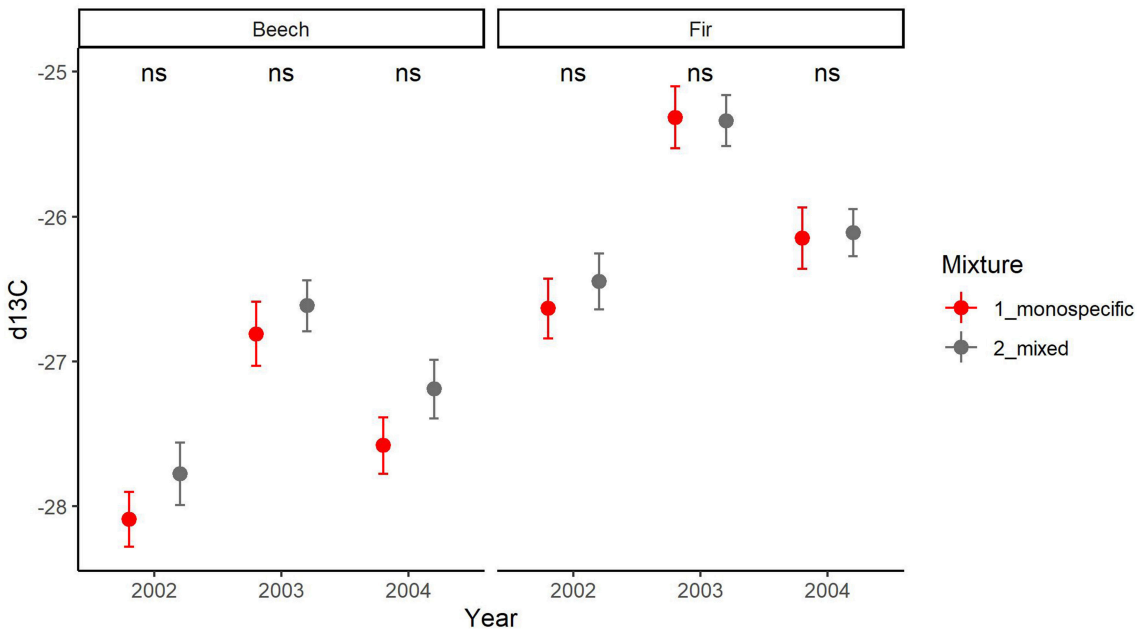

FIGURE 8 | Comparison of means (SE depicted as thin bars) of carbon isotopic composition $\delta^{13}C$ in wood of the years 2002, 2003, and 2004 between trees growing in monospecific (gray) and mixed (red) neighborhoods for beech **(left)** and fir **(right)**. ns indicates that there is no significant difference between mixed and monospecific neighborhoods within species based on *t*-test.

Mixing Effects on Overall Growth Performance and Over Time

Results of the neighborhood analyses indicate increasing growth with admixture proportions for both species, which is in accordance with our first hypothesis and other recent studies. Radial increment of beech and fir in mixtures responded positively to mixing but this was not directly compared with trees experiencing strictly monospecific conditions (Bosela et al., 2015). Several studies reported that growth of European beech increases, compared to mono-specific situations, in

neighborhoods with other species (Pretzsch et al., 2010, 2013; Bosela et al., 2015; Toigo et al., 2015; Metz et al., 2016). Likewise, higher growth rates were observed for firs in functionally diverse neighborhoods when admixed with several species including beech (Gazol et al., 2016) and spruce (Vallet and Pérot, 2011). However, results of two other studies based on periodic stand-level inventories in mixtures of beech and fir indicated either no effects of mixing on growth (BAI) of either species (Del Rio et al., 2014) or positive mixing effects for beech at all sites, whereas positive effects for fir were restricted to sites of lower productivity (Toigo et al., 2015).

Our finding of positive mixing effects on growth of fir and beech indicates that for both species intra-specific competition was greater than inter-specific competition. We can only speculate about potential mechanisms behind the observed growth complementarity. Owing to their strongly different traits such as in crown and root architecture, leaf morphology, phenology, etc. they may use the resources in a complementary way or even facilitate each other (Forrester and Bauhus, 2016; Magh et al., 2018). In case of beech, mixing benefits have been commonly linked to a reduction in strong intra-specific competition and the development of larger crowns (Pretzsch and Biber, 2005; Dieler and Pretzsch, 2013; Mina et al., 2018a). Positive mixing effects on growth performance of fir may be the result of increased crown light capture in spring and autumn when beech is leafless (Ishii and Asano, 2010; Lebourgeois et al., 2010). Whether or not mixing may improve water or nutrient availability of the two species cannot be ascertained on the basis of this study.

In accordance with the second part of our hypothesis, beech displayed more negative growth (BAI) trends compared to fir across our sites but the temporal trajectories of BAI complementarity were positive and did not differ between the two species. Similarly, another European-wide study has reported declining growth trends in European beech but not in silver fir growing in mixed stands for a similar period, concluding that fir is less susceptible to warmer and drier conditions than beech (Bosela et al., 2018). Our findings with regard temporal trends of complementarity and growth should be interpreted with caution, however, as we analyzed only the most recent 16 years. In addition, our study shows that such broad trends may not occur at every site and that variability among sites in magnitude and direction is very high.

Mixing Benefits for Both Species Increase With Tree Size and Neighborhood Density

Results of our neighborhood analyses clearly demonstrate that overall growth performance for both fir and beech increases with admixture proportions when considering the interactions of admixing with tree size and with competition intensity; this is in full agreement with our second hypothesis. Hence, both trees size and the level of neighborhood competition are key factors in shaping species interactions. According to the estimates of our mixed model, the strongest effect, which explained most of the growth variation, was actually derived from the variation in DBH among trees and sites (note that size differences in our study are mainly due to age differences and not due to differences in canopy status). Our finding that mixing benefits increased with tree size in beech is in agreement with results of two recent studies, which reported increasing mixing benefits for beech with tree size/stand age in combination with spruce (Houpert et al., 2018) and pine (Forrester et al., 2017).

Mixing benefits for growth performance increased not only with tree size in both species but this relationship was additionally modulated by competition intensity in tree neighborhoods. This is an indication that for beech-fir mixtures, positive effects of competitive reduction outweigh any negative effects caused by interspecific competition. Two other studies reported also increasing complementarity with stand density in fir and spruce mixtures for both species (Forrester et al., 2013; Mina et al., 2018a). Likewise, the complementarity effect was greater at higher stand densities for beech in mixtures with pine (Condés et al., 2013; Bello et al., 2019).

Increasing complementarity with stand density is more likely to occur in mixtures where interactions lead to improved light capture (Forrester et al., 2013). Under these conditions, positive as well as negative species interactions have been found to be weaker at lower densities and hence complementarity may initially increase with stand density to a certain point (Forrester et al., 2013), which is in agreement with our results. Only at very high densities competition may outweigh any complementarity effects (Forrester et al., 2013). As our stands were at least 60 years old and because we did not sample trees of lower canopy status but only (co-)dominant individuals, it is likely that we never crossed the threshold after which negative density effects on complementarity appear. Since neighborhood density was comparable for trees growing in mixed and monospecific neighborhoods, we can rule out that the mixing effect was mediated by differences in stand density, which is often the case (Forrester, 2014).

Growth and Isotopic Response to Drought

According to our expectations, both species responded with substantial growth reductions of 20% on average to the drought in 2003. Although trees from both species exhibited similar growth resistance, fir maintained higher absolute growth levels as beech during the drought. The similar increase of 1.5‰ $\delta^{13}C$ on average in both species indicates that during the drought year stomatal aperture and hence conductance was strongly and similarly controlled (Farquhar et al., 1989). In accordance with findings of Schaefer et al. (2017), we found a lower $\delta^{13}C$ in the broadleaved compared to the evergreen species indicating a higher c_i due to higher stomatal conductance and/or a lower rate of photosynthesis and accordingly different intrinsic water use efficiencies in the two species. Still, the comparable growth and isotopic response during the 2003 drought points toward a similar physiology and/or a similar length/timing of the wood formation period i.e., similar cambial activity, in these two shade-tolerant species (Zang et al., 2014). In contrast to our findings, Zang et al. (2014) found higher values of resistance, recovery and resilience in fir compared to beech. However, they analyzed several drought events and sites across a larger climatic gradient.

TABLE 5 | Parameter estimates with standard errors (S.E.) of linear mixed model fit for drought analyses by REML *t*-tests using Satterthwaite approximations to degrees of freedom for the response variables reflecting growth and isotopic response to 2003 drought: resistance (RES), recovery (REC), and resilience (RESIL) of BAI and $\delta^{13}C$.

Response variables (Transformed)	**$RES1_{BAI}$(log)**		**$REC1_{BAI}$ (log)**		**$RESIL1_{BAI}$ (log)**		**$RES2_{BAI}$(log)**		**$REC2_{BAI}$ (log)**		**$RESIL2_{BAI}$**		**RES_{13C} (log)**		**REC_{13C}**		**Log($RESIL_{13C}$)**	
R^2 marginal/R^2conditional	**0.02/0.10**		**0.23/0.26**		**0.16/0.28**		**0.05/0.06**		**0.29/0.29**		**0.24/0.25**		**0.05/0.05**		**0.03/0.27**		**0.01/0.01**	
Fixed effects (β_i)	**Estimate**	**(S.E.)**	**Estimate**	**(S.E.)**	**Estimate**	**(S.E.)**	**Estimate**	**(S.E.)**	**Estimate**	**(S.E.)**	**Estimate**	**(S.E.)**	**Estimate**	**S.E.**	**Estimate**	**S.E.**	**Estimate**	**S.E.**
Intercept (β_0)	−0.23***	(0.06)	−0.00	(0.05)	−0.23**	(0.08)	−0.26***	(0.05)	0.07	(0.05)	0.87***	(0.04)	−0.16***	0.04	1.13***	0.07	−0.07*	0.03
Mixing category	−0.07	(0.06)	0.10(*)	(0.06)	0.04	(0.07)	−0.05	(0.06)	0.08	(0.06)	0.04	(0.06)	0.01	0.05	−0.01	0.05	−0.003	0.04
Species	−0.04	(0.07)	0.06	(0.07)	0.01	(0.08)	0.02	(0.06)	−0.02	(0.06)	−0.01	(0.06)	−0.07	0.05	0.04	0.05	−0.01	0.04
DBH_{2003}	−0.01	(0.04)	−0.03	(0.04)	−0.03	(0.05)	−0.04	(0.03)	−0.03	(0.03)	−0.05	(0.03)	0.04	0.03	0.02	0.04	−0.01	0.02
Mixing category * Species	0.12	(0.08)	−0.17*	(0.08)	−0.05	(0.10)	0.10	(0.08)	−0.16*	(0.08)	−0.04	(0.08)	0.01	0.07	−0.01	0.07	0.02	0.05
Mixing category * DBH_{2003}	−0.01	(0.04)	−0.12**	(0.04)	−0.13**	(0.05)	−0.00	(0.04)	−0.12**	(0.04)	−0.10*	(0.04)	0.001	0.03	0.01	0.03	0.03	0.03
SD of variance components $d_I^{2\ Site}$	0.07		0.05		0.12		0.02		0.00		0.03		0.02		0.11		0.00	
d_ε^2	0.24		0.24		0.28		0.23		0.24		0.22		0.20		0.19		0.15	

*Marginal R^2 considers only the contribution of fixed effects; conditional R^2 considers the contribution of both fixed and random effects. The continuous fixed effects (h DBH_{2003} and BAI_{predr}) were centered and scaled to facilitate comparisons. Significance codes: ***for $p < 0.001$, **for $p < 0.01$; *for $p < 0.05$; (*) for $p < 0.1$, see* ***Table 2*** *for explanation of abbreviations of variables. di2 Site is the variance estimate of the random effect site and de2 is the residual variance. Number of observations = 152; groups: Site = 4.*

*For RES/REC/$RESIL_{BAI}$, 1 and 2 refer(s) to 1 and 2 year(s) before and after the drought. The continuous fixed effects (DBH_{2003} and BAI_{predr}) were centered and scaled to facilitate comparisons. Significance codes: ***for $p < 0.001$, **for $p < 0.01$; *for $p < 0.05$; (*) for $p < 0.1$, see* ***Table 2*** *for explanation of abbreviations of variables. di2 Site is the variance estimate of the random effect site and de2 is the residual variance. Number of observations = 152; groups: Site = 4.*

FIGURE 9 | Complementarity effects of mixing on isotopic response to the 2003-drought of European beech (gray) and silver fir (blue) in terms of resistance during drought (RES), recovery following drought (REC) and resilience to drought (RESIL). "ns" Indicates no significant difference ($P > 0.05$) between the 2 species for each index based on *t*-tests.

Mixing Did Not Affect the Resistance of Growth and $\delta^{13}C$ During Drought

In disagreement with our third hypothesis, there was no indication for complementary water-use between these two species during a period of severe water limitations. However, absolute growth (BAI) during the drought year was significantly higher in fir than in beech. The lack of mixing benefits on growth resistance and isotopic response to drought for either of the two species is in accordance with several other studies for beech and fir (Grossiord et al., 2014b); fir (Lebourgeois et al., 2013; Gazol et al., 2016); and beech (Metz et al., 2016; Schaefer et al., 2017). In contrast, results of two other studies indicate mixing benefits for growth resistance in fir in mixture with spruce (Dănescu et al., 2018; Vitali et al., 2018).

Similar response to drought in mixed and monospecific neighborhoods indicate that the entire rooted soil profile dried out during the extreme drought year 2003 and that there was no advantage of deeper-rooted species. Under these conditions, any potential presence of mechanisms related to complementary water-use, such as spatial or temporal stratification, would have been insufficient to buffer soil moisture reductions (Forrester and Bauhus, 2016; Schaefer et al., 2017).

Viewed from another perspective, the finding of comparable growth and resistance of isotopic composition indicates that the overall faster growth of trees in mixed compared

to monospecific neighborhoods was not a disadvantage for either of the species during drought (Forrester, 2014) as has been reported for other species combinations (Metz et al., 2016).

Mixing Improves Growth Recovery Following Drought in Beech

The complementarity of growth recovery was significantly higher in beech than in fir. This finding of greater mixing benefits for beech than for companion species is in agreement with other studies (Mölder and Leuschner, 2014; Metz et al., 2016). In contrast to our finding, fir trees growing in more functionally diverse stands recovered more quickly (Gazol et al., 2016).

The positive effects of fir trees on growth recovery of beech imply lower competitive stress once water became less limiting in the post-drought year. We can only speculate about the actual mechanisms behind the competitive reduction in beech in the year following the drought event. One possible explanation could be that beech fine-root systems with lower construction costs can recover more quickly from the drought (Meier and Leuschner, 2008)

The faster growth recovery of beech in mixed compared to monospecific neighborhoods was not accompanied by a higher recovery of carbon isotopic composition. This inconsistency suggests that growth processes are to some extent decoupled from physiological processes, perhaps through mixing-related changes in allocation patterns to above- or below-ground tissues at the tree level (Forrester and Bauhus, 2016). However, we cannot ascertain if and to what extent mixing beech and fir did indeed lead to structural adaptations at the tree level. The absence of a mixing effect on the recovery of $\delta^{13}C$ may be the result of simultaneous changes in assimilation and stomatal conductance, which both affect $\delta^{13}C$ but in opposing directions (Barbour et al., 2002).

Neither the resilience of growth and of $\delta^{13}C$ was affected by species or mixing which is most likely due to persisting water shortages in 2004. This year was relatively dry at all sites, which is also indicated by $\delta^{13}C$ values and growth not returning to pre-drought levels at the majority of sites.

Tree Size Affects the Growth Response Following Drought

Mixing benefits for growth recovery and resilience varied with tree size whereas no such interaction was found for growth resistance and the isotopic drought response. The relationship of recovery and resilience of growth with tree size was more negative in mixed compared to monospecific neighborhoods. This is in contrast with our findings on general growth performance where mixing benefits increased with tree size. However, results of a recent meta-analysis also indicate increasing drought impacts on stem growth with tree size (Bennett et al., 2015). We are not aware of a study that actually tested the combined effects of mixing and tree size on the drought response of trees and we will refrain from any further interpretations due to the low amount of variance explained by fixed plus random effects in all our drought response models (low R^2s). The incorporation of climactic and/or neighborhood data referring to the pre-drought, drought and post-drought period may have improved the variance explained by our drought models considerably [see for example (Dănescu et al., 2018) but finding the best (most parsimonious model)] was not the aim of our study as we were interested in the overall mixing effect on growth and isotopic response of our tree to the extreme Pan-European drought in 2003.

CONCLUSION

Both species benefited from growing in mixed neighborhoods but complementarity effects were dependent on tree size and neighborhood density. Results of this study demonstrate that mixing silver fir and European beech leads to positive or neutral effects on growth performance of trees also in relation to an extreme drought event. Our results demonstrate that mixing fir and beech offers no advantages for mitigating growth responses during periods of extreme water shortage. However, mixing fir and beech can help to improve the growth recovery following drought in beech but not in fir. In addition, faster growth rates of trees of both species in mixed compared to monospecific neighborhoods have no disadvantages for their response to drought. Therefore, mixtures of beech and fir may be considered at appropriate sites as an alternative for more drought-sensitive Norway spruce forests.

DATA AVAILABILITY STATEMENT

The datasets generated for this study are available at: https://freidok.uni-freiburg.de.

AUTHOR CONTRIBUTIONS

JB conceived the study and acquired funding for the project. JB and JS designed the study and discussed and interpreted the results and contributed to the writing of the final manuscript. JS carried out data collection, performed the analysis, and drafted the manuscript.

FUNDING

Financial support by the Federal Minister of Agriculture (BML) and the Federal Minister of Environment (BMU) via the Federal Institute of Agriculture and Nutrition (BLE) in the frame of the project Buchen-Tannen-Mischwälder zur Anpassung von Wirtschaftswäldern an Extremereignisse des Klimawandels (BuTaKli) within the program Waldklimafondsis gratefully acknowledged (Grant No. FKZ/28W-C-1-069-01).

ACKNOWLEDGMENTS

We gratefully acknowledge the help of district forester Johannes Wiesler from the community Hexental in Breisgau-Hochschwarzwald for his personal support and the provision

of an additional sampling site. The authors thank the forestry districts Breisgau-Hochschwarzwald and Emmendingen in Germany and Mladen Ivankovic from the Croatian Forest Research Institute Gopsic for supporting this study by providing data on tree composition of the forest stands. We also thank Nanja Unger, Nanja Unger, Fekxi Lindicke, Carlos Kuhlmann, Florentin Jäger, and Bárbara Magdalena San Martín for their assistance in fieldwork. We express our gratitude to Sven Hofmann and Nanja Unger for the many hours spend in the lab during sample preparation and processing of growth data.

SUPPLEMENTARY MATERIAL

The Supplementary Material for this article can be found online at: https://www.frontiersin.org/articles/10.3389/ffgc.2019.00079/full#supplementary-material

REFERENCES

Barbour, M. M., Walcroft, A. S., and Farquhar, G. D. (2002). Seasonal variation in delta13C and delta18O of cellulose from growth rings of *Pinus radiata*. *Plant Cell Environ.* 25, 1483–1499. doi: 10.1046/j.0016-8025.2002.00931.x

Barrufol, M., Schmid, B., Bruelheide, H., Chi, X., Hector, A., Ma, K., et al. (2013). Biodiversity promotes tree growth during succession in subtropical forest. *PLoS ONE* 8:e81246. doi: 10.1371/journal.pone.0081246

Battipaglia, G., Saurer, M., Cherubini, P., Siegwolf, R. T. W., and Cotrufo, M. F. (2009). Tree rings indicate different drought resistance of a native (*Abies alba* Mill.) and a nonnative (Picea abies (L.) Karst.) species co-occurring at a dry site in Southern Italy. *For. Ecol. Manage.* 257, 820–828. doi: 10.1016/j.foreco.2008.10.015

Bauhus, J., Forrester, D. I., Gardiner, B., Jactel, H., Vallejo, R., and Pretzsch. H. (2017a). "Ecological stability of mixed-species forests," in *Mixed-Species Forests. Ecology and Management*, eds H. Pretzsch, D. I. Forrester, and J. Bauhus (Berlin, Heidelberg: Springer), 337–382. doi: 10.1007/978-3-662-54553-9_7

Bauhus, J., Forrester, D. I., and Pretzsch, H. (eds.). (2017b). "Mixed-Species Forests: the development of a forest management paradigm," in *Mixed-Species Forests. Ecology and Management*, (Berlin; Heidelberg: Springer), 1–25. doi: 10.1007/978-3-662-54553-9_1

Bello, J., Vallet, P., Perot, T., Balandier, P., Seigner, V., Perret, S., et al. (2019). How do mixing tree species and stand density affect seasonal radial growth during drought events? *For. Ecol. Manage.* 432, 436–445. doi: 10.1016/j.foreco.2018.09.044

Bennett, A. C., McDowell, N. G., and Allen, C. D., and Anderson-Teixeira, K. J. (2015). Larger trees suffer most during drought in forests worldwide. *Nat. Plants* 1:15139. doi: 10.1038/nplants.2015.139

Bolte, A., Ammer, C., Löf, M., Madsen, P. Nabuurs, G. -J., Schall, P., et al. (2009). Adaptive forest management in central Europe: climate change impacts, strategies and integrative concept. *Scand. J. For. Res.* 24, 473–482. doi: 10.1080/02827580903418224

Bosela, M., Lukac, M., Castagneri, D., Sedmák, R., Biber, P., Carrer, M., et al. (2018). Contrasting effects of environmental change on the radial growth of co-occurring beech and fir trees across Europe. *Sci. Total Environ.* 615, 1460–1469. doi: 10.1016/j.scitotenv.2017.09.092

Bosela, M., Tobin, B., Šeben, V., Petráš, R., and Larocque, G., R. (2015). Different mixtures of Norway spruce, silver fir, and European beech modify competitive interactions in central European mature mixed forests. *Can. J. For. Res.* 45, 1577–1586. doi: 10.1139/cjfr-2015-0219

Brand, W. A., and Coplen, T., B. (2012). Stable isotope deltas: tiny, yet robust signatures in nature. *Isotopes Environ. Health Stud.* 48, 393–409. doi: 10.1080/10256016.2012.666977

Brooks, P. D., Geilmann, H., Werner, R. A., and Brand, W. A. (2003). Improved precision of coupled delta13C and delta15N measurements from single samples using an elemental analyzer/isotope ratio mass spectrometer combination with a post-column six-port valve and selective CO2 trapping; improved halide robustness of the combustion reactor using CeO2. *Rapid Commun. Mass Spectrom.* 17, 1924–1926. doi: 10.1002/rcm.1134

Condés, S., and Del Río, M. (2015). Climate modifies tree interactions in terms of basal area growth and mortality in monospecific and mixed *Fagus sylvatica* and *Pinus sylvestris* forests. *Eur. J. For. Res.* 134, 1095–1108. doi: 10.1007/s10342-015-0912-0

Condés, S., Del Rio, M., and Sterba, H. (2013). Mixing effect on volume growth of *Fagus sylvatica* and *Pinus sylvestris* is modulated by stand density. *For. Ecol. Manage.* 292, 86–95. doi: 10.1016/j.foreco.2012.12.013

Coplen, T. B. (2011). Guidelines and recommended terms for expression of stable-isotope-ratio and gas-ratio measurement results. *Rapid Commun. Mass Spectrom.* 25, 2538–2560. doi: 10.1002/rcm.5129

Danescu, A., Albrecht, A. T., and Bauhus, J. (2016). Structural diversity promotes productivity of mixed, uneven-aged forests in southwestern Germany. *Oecologia* 182, 319–333. doi: 10.1007/s00442-016-3623-4

Dănescu, A., Kohnle, U., Bauhus, J., Sohn, J., and Albrecht, A. T. (2018). Stability of tree increment in relation to episodic drought in uneven-structured, mixed stands in southwestern Germany. *For. Ecol. Manage.* 415-416, 148–159. doi: 10.1016/j.foreco.2018.02.030

Del Rio, M., Schutze, G., and Pretzsch, H. (2014). Temporal variation of competition and facilitation in mixed species forests in Central Europe. *Plant Biol.* 16, 166–176. doi: 10.1111/plb.12029

Dieler, J., and Pretzsch, H. (2013). Morphological plasticity of European beech (*Fagus sylvatica* L.) in pure and mixed-species stands. *For. Ecol. Manage.* 295, 97–108. doi: 10.1016/j.foreco.2012.12.049

Dittmar, C., Zech, W., and Elling, W. (2003). Growth variations of Common beech (*Fagus sylvatica* L.) under different climatic and environmental conditions in Europe—a dendroecological study. *For. Ecol. Manage.* 173, 63–78. doi: 10.1016/S0378-1127(01)00816-7

Ellenberg, H. (1996). *Vegetation Mitteleuropas mit den Alpen*. Stuttgart: kologischer, dynamischer und historischer Sicht.

Farquhar, G. D., Ehleringer, J. R., and Hubick, K. T. (1989). Carbon isotope discrimination and photosynthesis. *Annu. Rev. Plant Physiol. Plant Mol. Biol.* 40, 503–537. doi: 10.1146/annurev.pp.40.060189.002443

Forrester, D. I. (2014). The spatial and temporal dynamics of species interactions in mixed-species forests. From pattern to process. *For. Ecol. Manage.* 312, 282–292. doi: 10.1016/j.foreco.2013.10.003

Forrester, D. I. (2015). Transpiration and water-use efficiency in mixed-species forests versus monocultures: effects of tree size, stand density and season. *Tree Physiol.* 35, 289–304. doi: 10.1093/treephys/tpv011

Forrester, D. I., Ammer, C., Annighöfer, P. J., Avdagic, A., Barbeito, I., Bielak, K., et al. (2017). Predicting the spatial and temporal dynamics of species interactions in *Fagus sylvatica* and *Pinus sylvestris* forests across Europe. *For. Ecol. Manage.* 405, 112–133. doi: 10.1016/j.foreco.2017.09.029

Forrester, D. I., and Bauhus, J. (2016). A review of processes behind diversity—productivity relationships in forests. *Curr. For. Rep.* 2, 45–61. doi: 10.1007/s40725-016-0031-2

Forrester, D. I., Bonal, D., Dawud, S., Gessler, A., Granier, A., Pollastrini, M., et al. (2016). Drought responses by individual tree species are not often correlated with tree species diversity in European forests. *J. Appl. Ecol.* 53, 1725–1734. doi: 10.1111/1365-2664.12745

Forrester, D. I., Kohnle, U., Albrecht, A. T., and Bauhus, J. (2013). Complementarity in mixed-species stands *of Abies alba* and *Picea abies* varies with climate, site quality and stand density. *For. Ecol. Manage.* 304, 233–242. doi: 10.1016/j.foreco.2013.04.038

Fritts, H. (1976). *Tree Rings and Climate*. Oxford: Elsevier Science.

Gazol, A., Camarero, J., and Gomez-Aparicio, J. L. (2016). Functional diversity enhances silver fir growth resilience to an extreme drought. *J. Ecol.* 104, 1063–1075. doi: 10.1111/1365-2745.12575

Gazol, A., Camarero, J. J., Sangüesa-Barreda, G., and Vicente-Serrano, S. M. (2018). Post-drought resilience after forest die-off: shifts in regeneration, composition, growth and productivity. *Front. Plant Sci.* 9:1546. doi: 10.3389/fpls.2018.01546

Gessler, A., Keitel, C., Kreuzwieser, J., Matyssek, R., Seiler, W., and Rennenberg, H. (2007). Potential risks for European beech (*Fagus sylvatica* L.) in a changing climate. *Trees* 21, 1–11. doi: 10.1007/s00468-006-0107-x

Grissino-Mayer, H. D. (2001). Evaluating crossdating accuracy: a manual and tutorial for the computer program COFECHA. *Tree-Ring Res.* 57, 2162–4585.

Grossiord, C. (2019). Having the right neighbors: how tree species diversity modulates drought impacts on forests. *N. Phytol.* doi: 10.1111/nph.15667. [Epub ahead of print].

Grossiord, C., Granier, A., Gessler, A., Jucker, T., and Bonal, D. (2014a). Does drought influence the relationship between biodiversity and ecosystem functioning in boreal forests? *Ecosystems* 17, 394–404. doi: 10.1007/s10021-013-9729-1

Grossiord, C., Granier, A., Ratcliffe, S., Bouriaud, O., Bruelheide, H., Checko, E., et al. (2014b). Tree diversity does not always improve resistance of forest ecosystems to drought. *Proc. Natl. Acad. Sci. USA.* 111, 14812–14815. doi: 10.1073/pnas.1411970111

Hanewinkel, M., Cullmann, D. A., Schelhaas, M. -J., Nabuurs, G. -J., and Zimmermann, N. E. (2013). Climate change may cause severe loss in the economic value of European forest land. *Nat. Clim. Chang.* 3, 203–207. doi: 10.1038/nclimate1687

Houpert, L., Brigitte, R., David Forrester, I., Marco, M., and Markus H. O. (2018). Mixing effects in Norway Spruce—European beech stands are modulated by site quality, stand age and moisture availability. *Forests* 9:83. doi: 10.3390/f9020083

Isaac-Renton, M., Montwé, D., Hamann, A., Spiecker, H., Cherubini, P., and Treydte, K. (2018). Northern forest tree populations are physiologically maladapted to drought. *Nat. Commun.* 9:5254. doi: 10.1038/s41467-018-07701-0

Ishii, H., and Asano, S. (2010). The role of crown architecture, leaf phenology and photosynthetic activity in promoting complementary use of light among coexisting species in temperate forests. *Ecol. Res.* 25, 715–722. doi: 10.1007/s11284-009-0668-4

Jactel, H., Bauhus, J., Boberg, J., Bonal, D., Castagneyrol, B., Gardiner, B., et al. (2017). Tree diversity drives forest stand resistance to natural disturbances. *Curr. For. Rep.* 3, 223–243. doi: 10.1007/s40725-017-0064-1

Jucker, T., Bouriaud, O., Avacaritei, D., Dănilă, I., Duduman, G., Valladares, F., et al. (2014). Competition for light and water play contrasting roles in driving diversity-productivity relationships in Iberian forests. *J. Ecol.* 102, 1202–1213. doi: 10.1111/1365-2745.12276

Jump, A. S., Hunt, J. M., and Peñuelas, J. (2006). Rapid climate change-related growth decline at the southern range edge of *Fagus sylvatica*. *Glob. Chang. Biol.* 12, 2163–2174. doi: 10.1111/j.1365-2486.2006.01250.x

Kuznetsova, A., Brockhoff, P. B., and Christensen, R. H. B. (2017). lmerTest package: tests in linear mixed effects models. *J. Stat. Softw.* 82, 1–26. doi: 10.18637/jss.v082.i13

Law, B. E., Falge, E., Gu, L., Baldocchi, D. D., Bakwin, P., Berbigier, P., et al. (2002). Environmental controls over carbon dioxide and water vapor exchange of terrestrial vegetation. *Agri. For. Meteor.* 113, 97–120. doi: 10.1016/S0168-1923(02)00104-1

Lebourgeois, F., Gomez, N., Pinto, P., and Mérian, P. (2013). Mixed stands reduce *Abies alba* tree-ring sensitivity to summer drought in the Vosges mountains, western Europe. *For. Ecol. Manage.* 303, 61–71. doi: 10.1016/j.foreco.2013.04.003

Lebourgeois, F., Rathgeber, C. B. K., and Ulrich, E. (2010). Sensitivity of French temperate coniferous forests to climate variability and extreme events (*Abies alba*, *Picea abies* and *Pinus sylvestris*). *J. Veg. Sci.* 21, 364–376. doi: 10.1111/j.1654-1103.2009.01148.x

Lee, W. K., and Gadow, K. V. (1997). Iterative bestimmung der konkurrenzbäume in *Pinus densiflora* beständen. *Allg. Forst Jagdztg.* 168, 41–45.

Lloret, F., Keeling, E. G., and Sala, A. (2011). Components of tree resilience: effects of successive low-growth episodes in old ponderosa pine forests. *Oikos* 120, 1909–1920. doi: 10.1111/j.1600-0706.2011.19372.x

Magh, R. -K., Grün, M., Knothe, V. E., Stubenazy, T., Tejedor, J., Dannenmann, M., et al. (2018). Silver-fir (*Abies alba* MILL.) neighbors improve water relations of European beech (*Fagus sylvatica* L.), but do not affect N nutrition. *Trees* 32, 337–348. doi: 10.1007/s00468-017-1557-z

Martonne, E. D. (1926). L'indice d'aridité. *Bull. Assoc. Geogr. Fr.* 3, 3–5. doi: 10.3406/bagf.1926.6321

McDowell, N. G., and Allen, C. D. (2015). Darcy's law predicts widespread forest mortality under climate warming. *Nat. Clim. Chang.* 5, 669–672. doi: 10.1038/nclimate2641

McDowell, N. G., Bond, B. J., Dickman, L. T., Ryan, M. G., and Whitehead, D. (2011). "Relationships between tree height and carbon isotope discrimination," *in. Size- and Age-Related Changes in Tree Structure and Function*, eds F. C. Meinzer, B. Lachenbruch, and T. E. Dawson (Dordrech: Springer), 255–286. doi: 10.1007/978-94-007-1242-3_10

Meier, I. C., and Leuschner, C. (2008). Belowground drought response of European beech: fine root biomass and carbon partitioning in 14 mature stands across a precipitation gradient. *Glob. Change. Biol.* 14, 2081–2095. doi: 10.1111/j.1365-2486.2008.01634.x

Metz, J., Annighofer, P., Schall, P., Zimmermann, J., Kahl, T., Schulze, E. -D., et al. (2016). Site-adapted admixed tree species reduce drought susceptibility of mature European beech. *Glob. Change. Biol.* 22, 903–920. doi: 10.1111/gcb.13113

Mina, M., del Río, M., Huber, M. O., Thürig, E., and Rohner, B. (2018a). The symmetry of competitive interactions in mixed Norway spruce, silver fir and European beech forests. *J. Veg. Sci.* 29, 775–787. doi: 10.1111/jvs.12664

Mina, M., Huber, M. O., Forrester, D. I., Thürig, E., and Rohner, B. (2018b). Multiple factors modulate tree growth complementarity in Central European mixed forests. *J. Ecol.* 106, 1106–1119. doi: 10.1111/1365-2745.12846

Mölder, I., and Leuschner, C. (2014). European beech grows better and is less drought sensitive in mixed than in pure stands. Tree neighbourhood effects on radial increment. *Trees* 28, 777–792. doi: 10.1007/s00468-014-0991-4

Monserud, R. A., and Sterba, H. (1996). A basal area increment model for individual trees growing in even- and uneven-aged forest stands in Austria. *For. Ecol. Manage.* 80, 57–80. doi: 10.1016/0378-1127(95)03638-5

Pachauri, R. K., Allen, M. R., Barros, V. R., Broome, J., Cramer, W., Christ, R., et al. (2014). *Climate change 2014*: *Synthesis Report*. Geneva: Contribution of Working Groups I, II and III to the fifth assessment report of the Intergovernmental Panel on Climate Change IPCC.

Paquette, A., Hector, A., Castagneyrol, B., Vanhellemont, M., Koricheva, J., Scherer-Lorenzen, M., et al. (2018). A million and more trees for science. *Nat. Ecol. Evol.* 2, 763–766. doi: 10.1038/s41559-018-0544-0

Paquette, A., and Messier, C. (2011). The effect of biodiversity on tree productivity: from temperate to boreal forests. *Glob. Ecol. Biogeogr.* 20, 170–180. doi: 10.1111/j.1466-8238.2010.00592.x

Pinheiro, J., Bates, D., DebRoy, S., Sarkar D, and, R Core Team. (2019). *nlme: Linear and Nonlinear Mixed Effects Models*. Available online at: https://CRAN.R-project.org/package=nlme (accessed September 27, 2019).

Piovesan, G., Biondi, F., Di Filippo, A., Alessandrini, A., and Maugeri, M. (2008). Drought-driven growth reduction in old beech (*Fagus sylvatica* L.) forests of the central Apennines, Italy. *Glob. Change. Biol.* 14, 1265–1281. doi: 10.1111/j.1365-2486.2008.01570.x

Pretzsch, H., and Biber, P. (2005). A re-evaluation of Reineke's rule and stand density index. *For. Sci.* 51, 304–320. doi: 10.1093/forestscience/51.4.304

Pretzsch, H., and Biber, P. (2016). Tree species mixing can increase maximum stand density. *Can. J. For. Res.* 46, 1179–1193. doi: 10.1139/cjfr-2015-0413

Pretzsch, H., Biber, P., Schütze, G., Uhl, E., and Rötzer, T. (2014). Forest stand growth dynamics in Central Europe have accelerated since 1870. *Nat. Commun.* 5:4967. doi: 10.1038/ncomms5967

Pretzsch, H., Block, J., Dieler, J., Dong, P. H., Kohnle, U., Nagel, J., et al. (2010). Comparison between the productivity of pure and mixed stands of Norway spruce and European beech along an ecological gradient. *Ann. For. Sci.* 67:712. doi: 10.1051/forest/2010037

Pretzsch, H., and Schutze, G. (2016). Effect of tree species mixing on the size structure, density, and yield of forest stands. *Eur. J. For. Res.* 135, 1–22. doi: 10.1007/s10342-015-0913-z

Pretzsch, H., Schutze, G., and Uhl, E. (2013). Resistance of European tree species to drought stress in mixed versus pure forests: evidence of stress release by inter-specific facilitation. *Plant Biol.* 15, 483–495. doi: 10.1111/j.1438-8677.2012.00670.x,

R Core Team (2014). *R: A Language and Environment for Statistical Computing*. Vienna, Austria. Available online at: http://www.R-project.org/ (accessed September 27, 2019).

Ruosch, M., Spahni, R., Joos, F., Henne, P. D., ven der Knaap, W. O., and Tinner, W. (2016). Past and future evolution of *Abies alba* forests in Europe - comparison of a dynamic vegetation model with palaeo data and observations. *Glob. Chang. Biol.* 22, 727–740. doi: 10.1111/gcb.13075

Saurer, M., Borella, S., Schweingruber, F., and Siegwolf, R. (1997). Stable carbon isotopes in tree rings of beech: climatic versus site-related influences. *Trees* 11, 291–297. doi: 10.1007/s004680050087

Schaefer, C., Grams, T., Roetzer, T., Feldermann, A., and Pretzsch, H. (2017). Drought stress reaction of growth and Δ13C in tree rings of European beech and Norway spruce in monospecific versus mixed stands along a precipitation gradient. *Forests* 8:177. doi: 10.3390/f8060177

Schleser, G.-H. (1999). Isotope signals as climate proxies: the role of transfer functions in the study of terrestrial archives. *Quat. Sci. Rev.* 18, 927–943. doi: 10.1016/S0277-3791(99)00006-2

Sohn, J. A., Gebhardt, T., Ammer, C., Bauhus, J., Häberle, K.-H., Matyssek, R., et al. (2013). Mitigation of drought by thinning: short-term and long-term effects on growth and physiological performance of Norway spruce (Picea abies). *For. Ecol. Manage.* 308, 188–197. doi: 10.1016/j.foreco.2013.07.048

Sohn, J. A., Hartig, F., Kohler, M., Huss, J., and Bauhus, J. (2016). Heavy and frequent thinning promotes drought adaptation in *Pinus sylvestris* forests. *Ecol. Appl.* 26, 2190–2205. doi: 10.1002/eap.1373

Tegel, W., Seim, A., Hakelberg, D., Hoffmann, S., Panev, M., Westphal, T., et al. (2014). A recent growth increase of European beech (*Fagus sylvatica* L.) at its Mediterranean distribution limit contradicts drought stress. *Eur. J. For. Res.* 133, 61–71. doi: 10.1007/s10342-013-0737-7

Tinner, W., Colombaroli, D., Heiri, O., Henne, P. D., Steinacher, M., Untenecker, J., et al. (2013). The past ecology of *Abies alba* provides new perspectives on future responses of silver fir forests to global warming. *Ecol. Monogr.* 83, 419–439. doi: 10.1890/12-2231.1

Toigo, M., Vallet, P., Perot, T., Bontemps, J., D., Piedallu, C., and Courbaud, B. (2015). Overyielding in mixed forests decreases with site productivity. *J. Ecol.* 103, 502–512. doi: 10.1111/1365-2745.12353

Vallet, P., and Pérot, T. (2011). Silver fir stand productivity is enhanced when mixed with Norway spruce: evidence based on large-scale inventory data and a generic modelling approach. *J. Veg. Sci.* 22, 932–942. doi: 10.1111/j.1654-1103.2011.01288.x

van der Maaten-Theunissen, M., Kahle, H. -P., and van der Maaten, E. (2013). Drought sensitivity of Norway spruce is higher than that of silver fir along an altitudinal gradient in southwestern Germany. *Ann. For. Sci.* 70, 185–193. doi: 10.1007/s13595-012-0241-0

Vila, M., Carrillo-Gavilan, A., Vayreda, J., Bugmann, H., Fridman, J., Grodzki, W., et al. (2013). Disentangling biodiversity and climatic determinants of wood production. *PLoS ONE* 8:e53530. doi: 10.1371/journal.pone.0053530

Vitale, M., Mancini, M., Matteucci, G., Francesconi, F., Valenti, R., and Attorre, F. (2012). Model-based assessment of ecological adaptations of three forest tree species growing in Italy and impact on carbon and water balance at national scale under current and future climate scenarios. *iFor. Biogeosci. For.* 5, 235–246. doi: 10.3832/ifor0634-005

Vitali, V., Büntgen, U., and Bauhus, J. (2017). Silver fir and Douglas fir are more tolerant to extreme droughts than Norway spruce in south-western Germany. *Glob. Chang. Biol.* 23, 5108–5119. doi: 10.1111/gcb.13774

Vitali, V., Forrester, D. I., and Bauhus, J. (2018). Know your neighbours: drought response of norway spruce, silver fir and douglas fir in mixed forests depends on species identity and diversity of tree neighbourhoods. *Ecosystems* 5:145. doi: 10.1007/s10021-017-0214-0

Werner, R. A., and Brand, W. A. (2001). Referencing strategies and techniques in stable isotope ratio analysis. *Rapid Commun. Mass Spectrom.* 15, 501–519. doi: 10.1002/rcm.258

Werner, R. A., Bruch, B. A., and Brand, W. A. (1999). ConFlo III - an interface for high precision δ13C and δ15N analysis with an extended dynamic range. *Rapid Commun. Mass Spectrom.* 13, 1237–1241. doi: 10.1002/(SICI)1097-0231(19990715)13:13<1237::AID-RCM633>3.0.CO;2-C

Zang, C., Hartl-Meier, C., Dittmar, C., Rothe, A., and Menzel, A. (2014). Patterns of drought tolerance in major European temperate forest trees: climatic drivers and levels of variability. *Glob. Chang. Biol.* 20, 3767–3779. doi: 10.1111/gcb.12637

Zang, C., Rothe, A., Weis, W., and Pretzsch, H. (2011). Zur Baumarteneignung bei Klimawandel: ableitung der Trockenstress-Anfälligkeit wichtiger Waldbaumarten aus Jahrringbreiten. *Allg. Forst. Jagdzt.* 182, 98–112.

Zuur, A. F., Ieno, E. N., Walker, N., Saveliev, A. A., and Smith, G. M. (2009). *Mixed Effects Models and Extensions in Ecology With R*. New York, NY: Springer New York. doi: 10.1007/978-0-387-87458-6

Conflict of Interest: The authors declare that the research was conducted in the absence of any commercial or financial relationships that could be construed as a potential conflict of interest.

frontiers in Forests and Global Change

ORIGINAL RESEARCH
published: 13 December 2019
doi: 10.3389/ffgc.2019.00082

Drought Effects on *Tectona grandis* Water Regulation Are Mediated by Thinning, but the Effects of Thinning Are Temporary

Katherine Sinacore[1], Connor Breton[2], Heidi Asbjornsen[2], Virginia Hernandez-Santana[3] and Jefferson S. Hall[1]*

[1] ForestGEO, Smithsonian Tropical Research Institute, Panama City, Panama, [2] Ecohydrology Lab, Department of Natural Resources and the Environment, University of New Hampshire, Durham, NH, United States, [3] Instituto de Recursos Naturales y Agrobiología de Sevilla, Consejo Superior de Investigaciones Científicas, Seville, Spain

Results from tropical planted forests have demonstrated that tree plantations can have variable growth and water use patterns in response to drought. Yet research on how specific species will perform during a drought and whether this response can be mediated through forest management is still poorly understood. We took advantage of the 2015–2016 El Niño drought in central Panama to test the effects of thinning on sap flux density, transpiration, and growth of planted *Tectona grandis* (teak), a non-native species introduced to Panama for timber production. Despite a reduction in growth of teak during drought for control and thinned sites, tree sap flux density of thinned sights significantly increased after thinning, but the effect was temporary. Sap flux density (J_S) for teak is strongly driven by changes in vapor pressure deficit (VPD), temperature, and radiation; however, J_S declines as temperature rises above 28°C and VPD is above 0.5, suggesting a temperature threshold that could be problematic as droughts and temperatures increase in unison in the future. At the stand-level, all sites reduced transpiration during the drought. Although diameter growth and transpiration declined during drought, the leaf area index after the drought ended returned to pre-drought levels.

Keywords: Agua Salud Project, drought, forest management, sap flow, teak, thinning, transpiration

OPEN ACCESS

Edited by:
Julia Annick Schwarz, University of Freiburg, Germany

Reviewed by:
Norbert Kunert, Smithsonian Institution, United States
Dirk Hölscher, University of Göttingen, Germany

****Correspondence:***
Katherine Sinacore
ksinacore@gmail.com

Specialty section:
This article was submitted to Forest Hydrology, a section of the journal Frontiers in Forests and Global Change

Received: *07 October 2019*
Accepted: *29 November 2019*
Published: *13 December 2019*

Citation:
Sinacore K, Breton C, Asbjornsen H, Hernandez-Santana V and Hall JS (2019) Drought Effects on Tectona grandis Water Regulation Are Mediated by Thinning, but the Effects of Thinning Are Temporary. Front. For. Glob. Change 2:82. doi: 10.3389/ffgc.2019.00082

INTRODUCTION

Tectona grandis (teak) plantations have increased rapidly over the last few decades, especially in Panama, where an estimated 55,000 hectares is covered by planted teak (Kollert and Chrubini, 2012). Although teak can grow well on high nutrient soils in Panama, teak has been associated with dry and degraded soils that are often accompanied with low infiltration rates and high overland flow rates during rain events (Ribolzi et al., 2017, see exceptions: Fernández-Moya et al., 2013, 2014), raising concerns of how teak may affect important ecosystem services in Panama (i.e., water quality, water supply, and carbon sequestration). Although teak is a dry season deciduous and occurs in dry areas across its natural range, with respect to ecosystem services, planting teak in areas of water scarcity, in particular, is of concern given their relatively high transpiration rates and low water use efficiency (Cernusak and Aranda, 2007).

Model predictions are increasingly more confident that climate change induced droughts will become the norm (Allen et al., 2010), but there is large uncertainty of how growth and water use

of trees will respond to these future novel climates. Growing evidence suggests that tree responses to extreme future droughts will likely vary greatly by species traits (Pineda-García et al., 2015), successional status (Bretfeld et al., 2018), tree canopy position (Grote et al., 2016), and may often lead to unexpected and non-linear physiological and stand-level dynamics (Engelbrecht et al., 2007; Allen et al., 2010).

Plantation trees experience similar meteorological effects as upper canopy trees experience in secondary forests. Changes in vapor pressure deficit (VPD), temperature, precipitation, and radiation have all been shown to affect plant water use at hourly, daily, and monthly timescales (Bretfeld et al., 2018; Brum et al., 2018). There are often species-specific thresholds where plant water use begins to decline in response to high VPD, radiation, or temperature (Sinacore et al., in review), which often leads to reduced tree water use and stand transpiration during droughts (Brum et al., 2018; Zhang et al., 2018). With predicted increases in temperature, in particular, understanding at what threshold tree water use begins to decline at high temperatures and VPDs is crucial for modeling future stand and landscape level responses to a changing climate. While precipitation and soil moisture are sometimes decoupled from transpiration on seasonal timescales (del Campo et al., 2019), deficits in soil moisture can still affect long term transpiration trends and growth of trees (Detto et al., 2018).

An adaptive management tool to reduce competition, whereby individual trees are removed to open space so that crowns of individual trees can expand, also known as thinning, can increase photosynthetic capacity and, in turn, productivity. While the effects of thinning are generally considered in terms of growth, recent growing concern over water resources has sparked increasing attention on the effects of thinning as a tool to manage plantations for desirable productivity and water yield outcomes (Lagergren et al., 2008; Gavinet et al., 2019). At the individual tree level, thinning may increase tree water use due to a reduction in competition for resources and an increase in radiation hitting previously shaded leaves (Lagergren et al., 2008; del Campo et al., 2019). However, stand-level transpiration following thinning depends on many factors.

Assuming an increase in tree-level water use due to thinning, it is still possible that no change or even a decline in transpiration may be observed at the stand-level. For example, if trees double their water use, but density after thinning is reduced by more than 50%, stand transpiration in thinned stands may be less than adjacent unthinned stands. As such, thinning offers an opportunity to not only control tree growth, but tree and stand transpiration, both of which have implications for water regulation and landscape scale water availability. Under these conditions, thinning could also serve as a key management tool mitigating the effects of drought. For example, if soil moisture becomes limiting, trees growing in low density thinned stands may have greater access to limited soil moisture, and be able to maintain growth and transpiration rates better than unthinned stands with more intraspecific competition.

Our work focuses on plantations located in the Panama Canal Watershed, where there are many competing uses land, trees, and water. Freshwater from the watershed is used for both drinking water in Panama City and for boats transiting through the Panama Canal. Any changes in climate or land use can affect how much water comes off the watershed (Ogden and Stallard, 2013). In fact, Panama has recently created a National Water Authority (ConAgua), in recognition that, even in a country where water is abundant, access to water is an ever-increasing concern. Since teak is an important land use in Panama, a better understanding of teak management for growth and water use is important, with a strong emphasis on how teak will response to drought.

We asked three questions to better understand the effect that thinning has in mediating water use and growth responses during drought in teak plantations:

1. How does thinning affect teak tree-level water use patterns and growth during drought?
2. What are the implications of thinning on stand-level transpiration during drought?
3. What are the key meteorological variables that predict daily water use of teak?

METHODS

Site Description

The study was conducted in the Agua Salud Project site within the Panama Canal Watershed (9○13′ N, 79○47′W, 330 m amsl). We worked in the 30-ha *T. grandis* plantations that were established in 2008. Trees were planted at a spacing of 3 m between trees and 2.6 m between rows (total of 1,111 trees per hectare), such that trees were planted in a triangular configuration to reduce potential erosion on steeper slopes. Prior to plantation establishment, the land was cleared of forest in the 1970s with the predominant land use being cattle grazing (Weber and Hall, 2009). Since tree establishment in 2008, four yearly understory cleanings occurred from May through August to prevent additional competition with the planted trees. The cleanings reduced to three and then two times a year as the tree canopies began to close. Teak trees were also pruned to maintain 4.9 m (16 ft) of a branch free bole. Teak is characterized as dry season deciduous, but we found it does not lose all of its leaves at once at our site (Fernández-Moya et al., 2014). The topography of the area is characterized by both flat areas and areas with short and steep slopes (Hassler et al., 2011; Mayoral et al., 2018) and the soils are silt clay to clay with pH values ranging from 4.4 to 5.8 (Batterman et al., 2018).

Sampling Design

The sampling design was meant to estimate water use in *T. grandis* stands. During June of 2014, we established five teak plots, measuring 25 m by 25 m in area with $<$10 degrees of inclination to avoid logistical problems with the sapflow cables. At all sites, trees were interacting aboveground, but were not overtopping one another. Between June and August of 2014 and 2015, all trees within each plot were measured for height and diameter at breast height (DBH, 1.3 m above ground). A total of 351 trees were inventoried. Between July and August of each year, the understory of the 30 ha teak plantation was cleaned, which included the teak plots where inventories were established.

In June 2014, we established four subplots within a subset of the monocultures to measure sap flow in selected trees (hereafter referred to as sap flow trees). We selected eight trees per plot for sap flow measurements based on the following criteria: (1) The tree crowns had to be interacting (i.e., the stand has reached canopy closure); and (2) The trees had to be within a 10 m radius of each other to be within reach of the sap flow cables. A total of 32 trees were measured, 17 of which were used for analysis. Trees were excluded from analysis if they were missing >20% of data points. Large data gaps were caused by ant attacks, termite infestations, or lightning. We refer to the two plots that were not thinned as Control 1 and Control 2.

Thinning Experiment

Two of the teak plantation plots received a thinning treatment in June 2015, and the other two were left unthinned as controls (**Table 1**). The thinned plots are referred to as Treatment 1 and Treatment 2. The thinning treatment consisted of removing 50% of the individual trees, which is around the percentage of trees thinned in Panama teak plantations (Griess and Knoke, 2011). Trees were felled with a chainsaw or machete in a direction to avoid damage to study trees. Sap flow trees in the thinned sites had three competing trees removed so that each sap flow tree had three neighbors after the thinning. In the unthinned stands, each sap flow tree had 6 neighbors during the study period.

Drought Index, Micrometeorological, and Soil Moisture Data

Central Panama experiences annual dry seasons that start in mid-December and end in mid-May, with the remainder of the year (May through early December) being considered the wet season. During the period of the study, the El Niño drought occurred such that the normal wet season was dry, essentially connecting the dry season of 2015 with the dry season of 2016, creating what we refer to as a prolonged drought. We selected the Standard Precipitation-Evapotranspiration Index to assess drought conditions based on the recommendation of Slette et al. (2019) for methods to define drought. We calculated the index using the *SPEI* package in R (Begueria and Vicente-Serrano, 2013). The SPEI calculates potential evapotranspiration (PET) using the Penman-Monteith equation. From the package, PET is calculated using the monthly minimum temperature, maximum temperature, average wind speed, sun hours, the site latitude, and site altitude in meters above sea-level. Negative values on the SPEI index (<-1) indicated drought conditions. We calculated the index based on 1 month periods and 6 month periods. We calculated the SPEI using data between 2002 and 2019. Data from 2002 to 2015 were collected from a nearby meteorological (MET) station on Barro Colorado Island. Data from 2015 onward were collected from the Agua Salud MET station (more details below). We also calculated monthly precipitation totals and subtracted precipitation from the PET for a 10 year period from 2009 to 2019 in order to determine the water deficit or surplus.

Two MET stations located within the Agua Salud Project study area collected local climate data for the 2014–2015 study period. From June 2014 through January 2015, MET data were collected from the Property 2 site while data after February 2015 were collected from the Celestino Tower site. Climate data from the Celestino Tower included air temperature (°C) and relative humidity (RH, %) using an HMP60 (Vaisala, Vantaa, Finland), and precipitation (mm) using a 260–250-A tipping bucket (NovaLynx, CA, USA), Vapor pressure deficit (VPD, kPA) was calculated from the air temperature and RH data following (Allen et al., 1998). Small gaps in the dataset exist due to either sensor malfunction or due to the transition period between taking down the Property 2 tower and constructing the Celestino Tower.

The 2014 dry season began December 21, 2013 and ended May 6, 2014 and the 2015 dry season began December 14, 2014 and ended May 16, 2015 (Paton, 2016). Mean annual rainfall for 2014 was 2,203 mm and for 2015 it was 1,810 mm (Paton, 2016). Generally, about 80% of the average annual precipitation falls between May and mid-December. Mean daily maximum and minimum temperatures are 32 and 23°C, respectively (http://striweb.si.edu/esp/physical_monitoring/descrip_bci.htm).

Soil volumetric water content (VWC) was measured using DeltaT PR2 sensors (DeltaT, Cambridge, United Kingdom) at six soil depths (100, 200, 300, 400, 600, and 1,000 mm) starting in December 2014. At each site, three trees with sap flow sensors were randomly selected. An access tube was placed 0.5 m in a random cardinal direction from the bole of the tree. Soil moisture measurements were collected for each tube every 1–4 days. A mean VWC was calculated for the first three depths (100, 200, and 300), where changes in VWC throughout the year were apparent. An ANOVA with a *post-hoc* Tukey test was performed to analyze mean VWC difference between plots.

TABLE 1 | Site characteristics of each plot.

			Transpiration (mm day^{-1})	
Plot	**DBH**	**Height**	**Pre-treatment**	**Thinning + Drought**
Control 1	9.29 (0.44)	7.10 (1.69)	4.10	3.50
Control 2	8.84 (0.98)	6.85 (1.42)	2.16	0.90
Treatment 1	8.84 (0.96)	5.74 (1.24)	4.34	2.94
Treatment 2	10.10 (1.34)	9.56 (1.78)	7.60	1.77

Mean diameter at breast height (DBH) in centimeters and mean height in meters with standard deviations in parentheses are shown for each plot. Stand transpiration estimates for each site (mm day^{-1}). Controls represent unthinned stands and Treatments represent thinned stands. Daily transpiration totals per site shown under Pre-treatment and Thinning + Drought.

Tree Sap Flux Density and Stand Transpiration

We analyzed data from June 15, 2014 through December 15, 2015. Tree-level water use estimates are based on data obtained from individual sap flow trees. Stand-level measurements are scaled using plot inventories and the relationship between DBH and water use (Hernandez-Santana et al., 2015). Sap flow was measured using the heat ratio method (HRM; Burgess et al., 2001). On each tree, one sensor was installed 1.30 m above the base of the tree facing north. Each sensor contained three

probes (a heater probe and two temperature probes, installed equidistantly upstream and downstream from the heater probe, 0.6 cm). Each temperature probe contained three thermocouples located at 0.5, 1.7, and 3.0 cm from the bark of the tree. A heat pulse was automatically sent to the sensors every 15 min. The speed of the heat (*Vh*) was calculated according to Burgess et al. (2001) every 15 min. Heat pulse velocities were corrected (*Vc*) for errors (probe misalignment and wounding) following Burgess et al. (2001). Estimates of each tree's daily sap flux density (J_s) were obtained from *Vc* (Green et al., 2003):

$$J_s = \frac{\rho_d}{\rho_s}\left(\mathrm{MC} + \frac{C_{dw}}{C_s}\right) V_c \quad (1)$$

where ρ_d is the density of sapwood, ρ_s is the density of water, MC is the volumetric water content of the sapwood, C_{dw} is the thermal conductivity of dry wood, and C_s is the thermal conductivity of water.

Cores were taken from trees where sensors were not actively measuring sap flow to determine conducting sapwood area. No cores across the range of sampled tree diameters (7.1 to 13.3 cm at breast height) revealed heartwood, so the entire diameter cross section of each study tree was treated as conducting sapwood for the transpiration calculations. We found a significant but weak relationship ($p < 0.001$, $R^2 = 0.04$) between DBH and whole tree water use. We calculated the daily water use of each sap flow tree (Equation 2):

$$Q = (0.093402 \times \log(DBH) + 2.351654)^2 \quad (2)$$

Where *Q* is the daily water use of an individual tree and DBH is the diameter at breast height of the tree. Each *Q* was summed for the site and then divided by the ground area of the site to measure transpiration in mm day^{-1}.

Radial Profile Characterization

The middle sap flux density (thermocouple 1.7 cm from the bark) was divided by the outer sap flux density (thermocouple 0.5 cm from the bark) to determine where sap flux density was greatest throughout the study period. If the sap flux ratio (J_s ratio) is >1, the sap flux density is greater in the outer portion of the tree than the middle. Conversely, if the ratio is <1, the sap flux density is greater in the middle portion of the tree than the outer. We calculated the ratio for every 15 min reading and then averaged the ratio by week for thinned and unthinned sites across the study length (1.5 years).

Growth and Leaf Area Index Characterization

Relative growth rate (RGR) was calculated for all sap flow trees ($n = 32$) using aboveground tree biomass (AGB) and (Equation 3):

$$RGR = \frac{\ln AGB_2 - AGB_1}{t_2 - t_1} \quad (3)$$

For the year before thinning, RGR was calculated using the 2015 (AGB_2) and 2014 (t_1, AGB_1), while 2016 (AGB_3) and 2015 (AGB_2). Diameter at breast height measurements for each year were used to calculate AGB based on equations from Kraenzel et al. (2003).

Leaf area index (LAI) of the teak canopies were estimated using hemispherical photography photos. Photos were taken at two different time points—May 2015 (pre-treatment) and October 2015 (post-treatment). The teak canopies were fully foliated in May 2015 and October 2015, but during October 2015, the photos represent the end of the drought period. Photos were taken with a Canon Eos Xs 1000D (Canon, Ota, Tokio, Japan) with an attached Sigma 4.5 mm fisheye lens with an equisolid projection (Sigma, Ronkonkoma, New York, USA). A total of six photos were taken per plot at three different time points. Tubes were placed at each point so the same location could be used over the study period. At each tube, three photos were taken with a self-timer and automatic exposure compensation and bracketing at −2.0, −1.0, and 0. The camera was placed on a tripod so that the lens was one meter above the ground and level. If there were leaves at a distance <0.6 meters from the lens, they were pulled from the view of the lens. Photos were taken only if there was no direct sunlight or rain (typically occurring during the late morning. We took photos during the wet season prior to the drought/thinning and after the drought/thinning. Hemispherical photo analyses were performed with the *Hemiphot* package (ter Steeg, 2018).

Statistical Analyses

All statistical analyses were performed in R (R Core Team, 2017) and figures were produced with *ggplot2* (Wickham, 2016). The *lme4* package (Bates et al., 2015) was used to perform mixed effects models to determine differences in (1) pooled J_s by temperature and VPD and (2) stand transpiration by treatment. All mixed effects models included an additional interaction of pre-treatment or thinning. The *dabestr* package (Ho et al., 2019) was used to create estimation graphics for both RGR and LAI analyses. We selected the Ho et al. (2019) method of estimating effect sizes and their uncertainty to take advantage of plotting full sampling curves and effect sizes to show the variability in the data.

RESULTS

Drought Conditions at Site Based on SPEI

Based on the SPEI calculation, the time period of the study that experienced a drought in 2015/2016 coincided with an El Niño Southern Oscillation Event (ENSO). The SPEI was <−1 (moderately dry) at the beginning of the ENSO event, approaching −2 (extremely dry) toward the end of the ENSO event (**Figure S1**). Prior to and after the ENSO event, the annual precipitation was greater than the annual PET. There was always a PRCP-PET deficit during the dry seasons, but the deficit was longer (8 months) during the ENSO event than the other years (4–5 months). Additionally, the higher PRCP-PET during the ENSO event was lower than the previous years (**Figure S2**).

After thinning, 50% of the trees were removed in two of the plots. In the other two control plots, no trees were thinned. Around the same time of the thinning (June 2015), Panama experienced an El Niño Southern Oscillation Event (ENSO). At

the sites, there was a 54% decrease in precipitation in comparison to the previous year (**Figure 1E**) and nearly a 32% reduction from the average (since 1927) in cumulative rainfall, based on a nearby site of Barro Colorado Island (Paton, 2016). The ENSO event also corresponded with increases in net radiation (40%) and VPD (20%). Volumetric water content (VWC) was not significantly different between treatments at the beginning of the study (dry season 2015) but started to become significantly different after the thinning. Notably, the thinned sites had 10% higher VWC than the unthinned sites from July until October 2015 ($p < 0.001$). After October, the VWC of the unthinned and thinned sites were no longer significantly different.

Responses of Sap Flux Density

J_s of teak generally increased with increasing VPD and temperatures, independent of treatment (**Figure 2**). At 28°C, J_s began to decline as VPD increased, with the exception of 34°C. The slopes of the lines ranged from 1.20 for 20°C to −0.01 for 28°C, and did not follow a consistent pattern (i.e., decreasing slopes with increasing temperatures). All models relating J_s with VPD and temperature were significant, but the R^2 ranged from 0.24 to <0.01. Unlike the relationship of VPD and temperature, radiation had a pattern of decreasing slopes with increasing VPD. J_s increased with increasing VPD and net radiation, until radiation reached 450 W m^{-2} (**Figure 3**), and notably, the rate of change decreased at each increase in net radiation of 50 W m^{-2}.

Prior to thinning, both treatments had trees with similar J_s (**Figure 1A**), except for a period immediately preceding the thinning, possibly due to a small rainfall event and differences in leaf cover among sites. The thinned sites began to have greater J_s that corresponded with increases in VWC and the thinning, with the exception of a brief period in August when J_s did not significantly differ. An increase in the ratio of outer to middle J_s occurred in the thinned sites after the thinning (with no change in the control sites; **Figures S3**).

Stand Growth, Transpiration, and LAI Before and After Thinning

Relative growth rates (RGR) for all trees declined during the drought (**Figure 4**). The effect size was calculated to compare the thinning and drought treatment to the control (unthinned sites). The RGR effect size was negative for thinning + drought. The

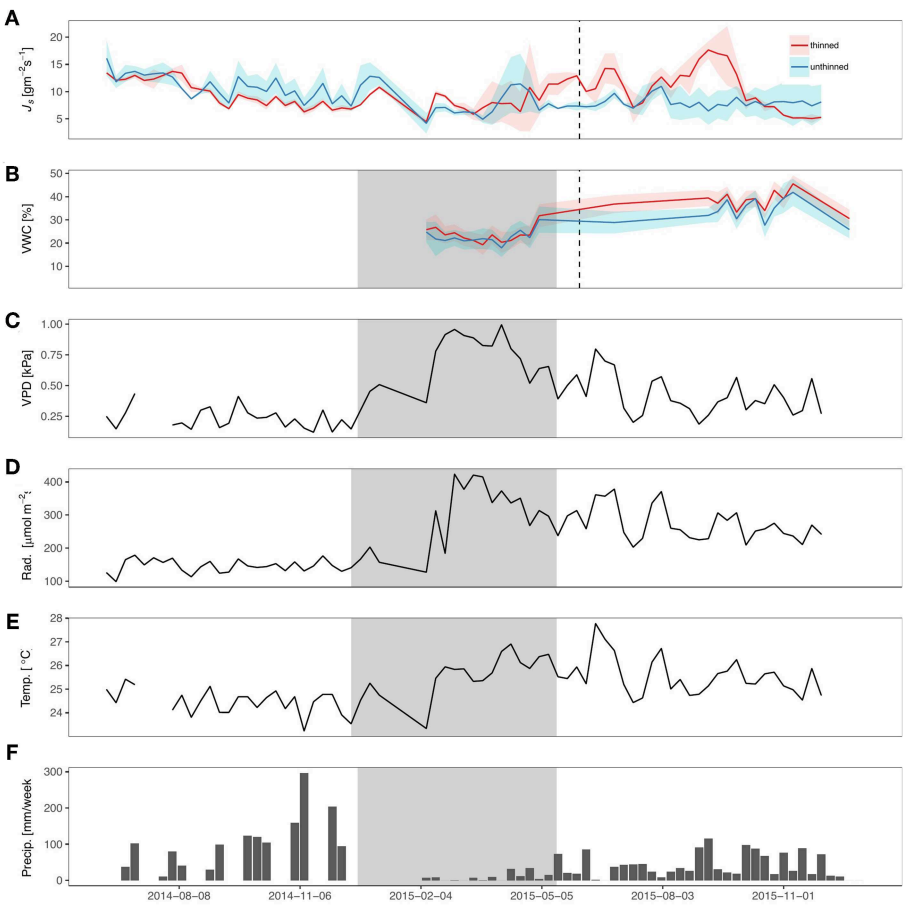

FIGURE 1 | Sap flux density and meteorological variables during sampling period. **(A)** Mean sap flux density (J_s; gm^{-2} s^{-1}), **(B)** mean volumetric water content (VWC; %) for top 30 cm, **(C)** Vapor pressure deficit (VPD; kPa), **(D)** net radiation (Rad; W m^{-2}), **(E)** temperature (Temp.; °C), and **(F)** precipitation (precip.; mm week^{-1}) from June 2014 through June 2016. Gray shading represents dry season and dashed line represents the timing of the thinning.

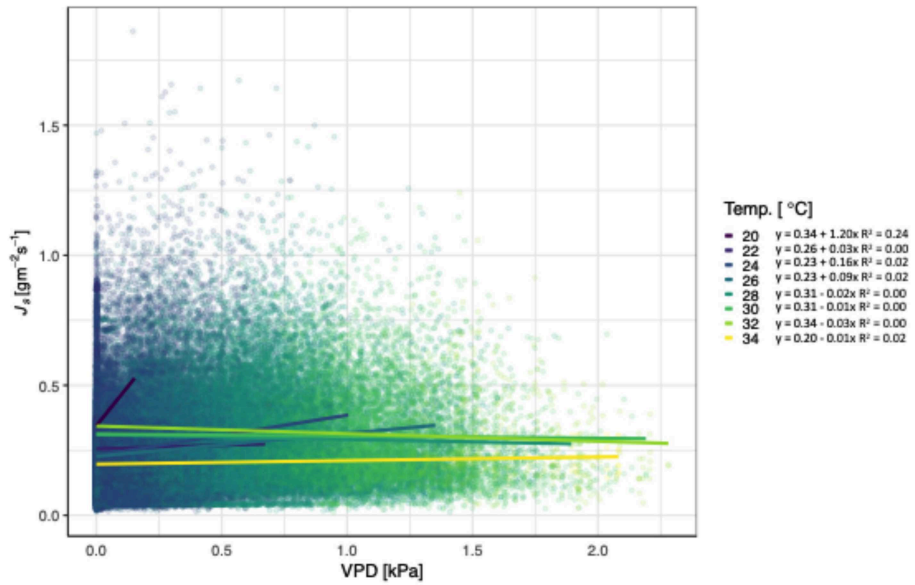

FIGURE 2 | Relationship between vapor pressure deficit (VPD; kPa), sap flux density (J_s; gm^{-2} s^{-1}), and air temperature (Temp. °C) for *Tectona grandis*. Treatments (thinned and unthinned) are pooled. Colors represent binned hourly mean air temperatures (by 2°C) during daylight hours (07:00 to 18:00). Model equations for each temperature bin shown. R^2 values included for all models where $p < 0.0001$).

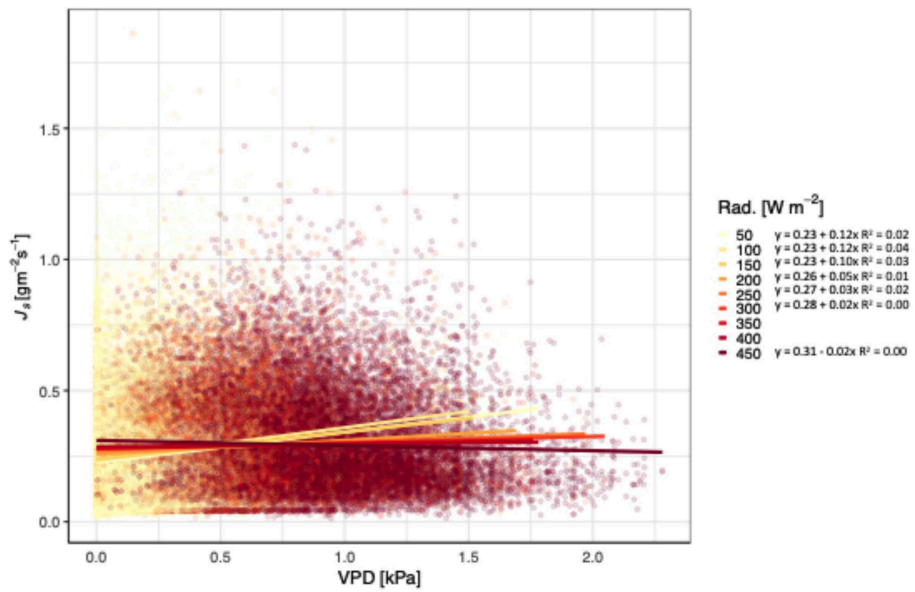

FIGURE 3 | Relationship between vapor pressure deficit (VPD; kPa), sap flux density (J_s; gm^{-2} s^{-1}), and net radiation (Rad. Wm^{-2}) for *Tectona grandis*. Treatments (thinned and unthinned) are pooled. Colors represent binned hourly mean net radiation (by 50 Wm^{-2}) during daylight hours (07:00 to 18:00). Model equations for each temperature bin shown. R^2 values included for all models where $p < 0.0001$).

distribution of changes for RGR was greater for sites that were thinned than for the controls (**Figure 4**). Leaf area index (LAI) before the drought/thinning and after the drought/thinning did not vary (**Figure 5**). The effect size of the drought year was not significantly different from the control, regardless of whether the sites were thinned. Stand transpiration (E) was significantly different among sites pre-treatment, with one site having the greatest E with 7.60 mm day^{-1}. All sites had lower E during the drought/post-thinning period. The two thinned sites had lower E (2.94 and 1.77 mm day^{-1}) than one of the control sites which had the highest E during the second half of the study (3.50 mm day^{-1}) (**Table 1**).

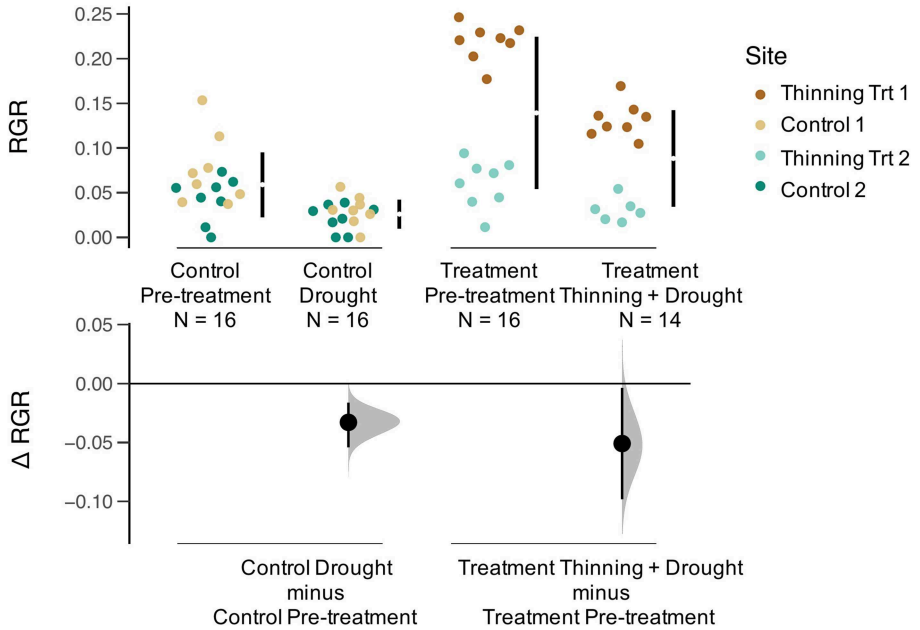

FIGURE 4 | Gardner-Altman plot of relative growth rate (RGR, kg yr^{-1}) for Pre-treatment Control, Drought Control, Pre-treatment, and Thinning + Drought Treatment. Colors represent the four sites. The change in RGR (Δ RGR, or effect size) is compared between the control and treatment, as well as pre-treatment and drought/drought+thinning conditions.

DISCUSSION

Water Use and Transpiration Mediated by Thinning

Stand transpiration was on average lower in the thinned sites than the unthinned sites because of the reduction of trees. Additionally, thinning increased tree sap flux density for a short period and not enough to compensate for the lower stand density experienced in the thinned sites (**Figure 1**, **Table 1**). This result suggests that stands can be thinned to regulate stand transpiration. During the dry season or a drought event, when there is significantly less rainfall than the wet season and a normal year, respectively, reducing the evaporative demand of plantations by reducing the density can potentially benefit both individual tree growth and downstream water resources in the short-term, although long-term changes (i.e., 1 year +) in stand transpiration are still not fully understood. Stand transpiration was notably variable (**Table 1**), which may be partially attributable to the differences in stand LAI (**Figure 4**), but also could be caused by differences in soil nutrients or even slope, which have an effect on the growth of some native species in the adjacent area (Mayoral et al., 2018). All of these factors, when scaled to the stand-level, can result in significant differences in transpiration.

Although we expected teak to reduce LAI during the drought (like it does during the dry season), the teak trees did not fully lose leaves. In fact, LAI trended toward an increase during the drought regardless of whether the stands were thinned or not (**Figure 5**). Higher growth rates and altered leaf flushing to take advantage of the higher than normal radiation experienced during an El Niño event is common among some species in secondary forests (Detto et al., 2018; Schnabel et al., 2019). Our work shows, however, that even within the same species, drought can differentially affect tree-level and stand-level growth rates, J_s, and transpiration.

One limitation of our conclusions at the stand-level is that the number of plots is a constraint and limits the generalizability of our results. However, this is a common limitation inherent to sapflow studies, given the high costs, labor, and resources involved in fully instrumenting and maintaining the plots. Although plot sample size was small, we were able to collect sapflow data on 32 trees, which we argue provides sufficient statistical power to draw robust conclusions for our specific study sites about sap flux density and stand transpiration.

Although thinning may decrease competition for soil moisture, the remaining trees after the thinning may experience higher levels of radiation on the sides of their crowns. Simultaneously, greater exposure of soil to radiation may increase evaporation from the upper soil layer faster than in unthinned plots due to reduced shading by trees. Based on thinning principles, we expected that relative growth rate of released trees to be greater than the year before the release, but we did not find this to be true. Both the controls and thinned stands had lower RGR during the ENSO event (**Figure 4**) suggesting that the drought had a negative impact on aboveground growth that overrode any positive growth impacts associated with thinning. However, despite decreases in RGR, LAI a year after thinning and the drought returned to pre-thinning levels (**Figure 5**). Since RGR is based on increases in DBH, this metric does not represent any below

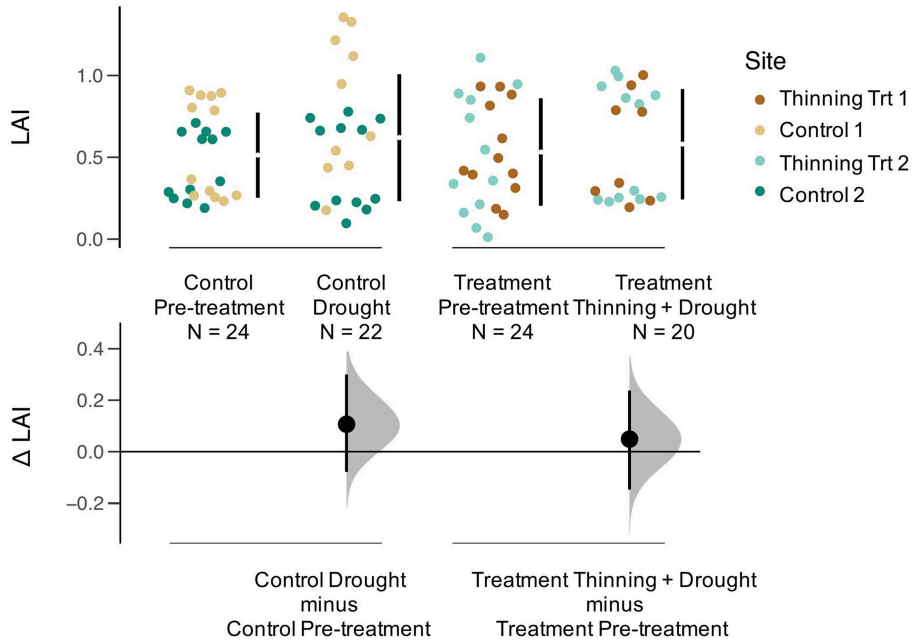

FIGURE 5 | Gardner-Altman plot of leaf area index (LAI) for Pre-treatment Control, Drought Control, Pre-treatment, and Thinning + Drought Treatment. Colors represent the four sites. The change in LAI (Δ LAI, or effect size) is compared between the control and treatment, as well as pre-treatment and drought/thinning+drought conditions.

ground growth that could have been occurring in response to drought (Markesteijn and Poorter, 2009).

Thinning had an initial effect on tree J_s, but this effect subsided when precipitation increased. Initially, there was an increase in tree J_s after the thinning compared to the trees in the control sites, despite the presence of a drought. During a brief rainy period during the drought in September where precipitation was >PET (see **Figure S1**), J_s of the trees in thinned and control sites were not significantly different. However, when PET shifted and was higher than precipitation, the differences between J_s were more pronounced, with tree J_s in thinned sites being higher than J_s of trees in control sites. Soon after, when precipitation returned to more normal conditions and precipitation was higher than PET, J_s of both treatments were no longer significantly different. The results from PET and precipitation also follow closely with VWC, in which VWC was initially higher in thinned sites than controls, but closely tracked differences in PET and precipitation. Based on these results, the increase in tree J_s due to thinning was significant, but the effect was temporary (<6 months) and did not necessarily override the effect of the drought. This suggests that thinning might be a useful tool to use when trees are experiencing water shortages (e.g., low VWC), to increase access to VWC while a drought persists. However, since the effect appears short for teak, thinning may be more useful for longer droughts or for species that are slower to recover LAI. Although not directly tested here, thinning can affect the boundary layer and canopy roughness, which can result in trees losing more water. For example, trees growing next to forest edges in the Amazon and spruce trees in Denmark have higher water use due to changes in the boundary layer (Hernandez-Santana et al., 2011; Ringgaard et al., 2012; Kunert et al., 2015). A change in the boundary layer, combined with a reduction in competition for soil water for remaining trees after thinning, can in the short-term increase water use. However, for open stands (like the ones in this study), droughts can dry out the top soil layer faster, limiting the accessibility of water for the remaining trees, which will fade the effect of thinning over the long-term.

Also notable is that there was a transition to higher J_s in the outer portion of the sapwood area after the thinning (**Figure S3**). Generally, J_s is higher toward the bark of the tree, where newer wood is being added (Alvarado-Barrientos et al., 2013). The change to higher J_s in the outer thermocouple post thinning, despite the drought, can be explained by the LAI of the thinned stands. The fact that the thinned stands were able to return to pre-thinned LAI within a year, suggests an increase in leaf production, which would necessitate greater water use by the tree, primarily in the outer portion of the tree which is preferentially connected to the newest leaves. Similarly, the control plots did not have an increase or decrease in LAI between the pre-treatment and treatment + drought years, which is expected.

High Radiation, Temperature, and Vapor Pressure Deficit Decrease Sap Flux Densities

In addition to tree species or site-specific characteristics (Hassler et al., 2018), atmospheric conditions and soil water availability are the primary controls of hourly, daily and yearly changes in sap flux density (J_s) (Bovard et al., 2005). While some meteorological

variables that affect J_s are highly correlated with one another, others can interact and have opposite effects on J_s. For example, while VPD, temperature, and radiation are tightly linked, they can have opposite effects on J_s. For example, J_s increases in the morning with increasing VPD and then often declines in the afternoon because radiation forces stomatal closure despite similar VPD levels (Zeppel et al., 2004).

Although J_s generally increases with VPD and temperature, we found that teak hits a temperature and radiation threshold at high VPD (**Figures 2**, **3**). Irrespective of treatment, J_s increased with increasing VPD until 28°C, at which point, J_s began to decline. In contrast, locally adapted species in adjacent sites had temperature thresholds up to 30°C (Sinacore et al., in revision). Given that climate change induced temperature increases are expected at our sites and may influence the ability of teak to regulate water, these results are particularly notable, especially when compared to native species alternatives. Radiation also had a negative effect on J_s at higher VPD, with the threshold 450 W m^{-2}, which was near the maximum radiation during the course of our study. Despite trees in tropical forests generally having positive responses to increasing VPD and radiation (i.e., through higher growth rates), predicted increases in temperatures may cause an opposite effect in the future, a concept that requires further investigation.

CONCLUSIONS

Thinning had short-term effects on plant water use and growth that mediated the effects of drought. At the tree-level, thinning increased J_s and VWC during a period when drought conditions persisted. Once the drought ended, however, J_s and VWC returned back to the levels in the unthinned treatment, providing evidence that thinning can be used as a short-term management strategy to reduce the water stress trees may face during a drought. At the stand-level, reducing tree density by 50% can have a significant impact on reducing transpiration, which has potential positive consequences for downstream water availability. While tree growth declined during drought and was not benefitted through thinning, leaf production was sufficient that LAI returned to pre-thinned levels following the drought, setting up the stands to be highly productive once the drought ended. Finally, we emphasize that more work on temperature and radiation thresholds is crucial to better predict how teak will respond to future droughts.

DATA AVAILABILITY STATEMENT

The raw data supporting the conclusions of this article will be made available by the authors upon reasonable request.

AUTHOR CONTRIBUTIONS

KS, JH, and CB: data curation. KS and VH-S: formal analysis. JH: funding acquisition. JH and HA: supervision. KS, JH, VH-S, CB, and HA: writing original draft, reviewing, and editing.

FUNDING

KS was supported by grants and fellowships from the Smart Reforestation® program of the Smithsonian Tropical Research Institute, Mr. Stanley Motta, the Silicon Valley Foundation, the Heising-Simons Foundation, and the University of New Hampshire. CB was supported by grants and fellowships from the Smithsonian Tropical Research Institute and the University of New Hampshire International Research Opportunities Program.

ACKNOWLEDGMENTS

We are grateful for the work of DanielaWeber, Estrella Yanguas, and Federico Davis for managing the plantation and providing field and lab support. We would also like to thank Señor Rosendo for protecting the plantation from fires and sharing many cups of coffee with us in the field. We are also grateful to Guillermo Fernandez, Mario Bailon, Miguel Nuñez, Andrea Miller, Adrián Brox, Victor Garcia, Lea Bernath, Andrés Rodriguez, Rand Snyder, and Martyna Glodowska who all spent many hours and days collecting sap flow, LAI, soil moisture, and physical growth measurements. We could not have done the thinning without the help of Carlos Días and Victorino Montenegro who carefully cut trees without damaging adjacent ones. The Agua Salud Project is part of ForestGEO and is a collaboration between the Smithsonian Tropical research Institute, the Panama Canal Authority (ACP), and the Panamanian Ministry of the Environment (MiAMbiente).

SUPPLEMENTARY MATERIAL

The Supplementary Material for this article can be found online at: https://www.frontiersin.org/articles/10.3389/ffgc.2019.00082/full#supplementary-material

REFERENCES

Allen, C., Macalady, A., Chenchouni, H., Bachelet, D., Mcdowell, N., Vennetier, M., et al. (2010). A global overview of drought and heat induced tree mortality reveals emerging climate change risk for forests. *For. Ecol. Manage.* 259, 660–684. doi: 10.1016/j.foreco.2009.09.001

Allen, R. G., Pereira, L. S., Raes, D., and Smith, M. (1998). *Crop Evapotranspiration: Guidelines for Computing Crop Water Requirements*. Rome: FAO.

Alvarado-Barrientos, M. S., Hernandez-Santana, V., and Asbjornsen, H. (2013). Variability of the radial profile of sap velocity in Pinus patula from contrasting stands within the seasonal cloud forest zone of Veracruz, Mexico. *Agric. For. Meteorol.* 168, 108–119. doi: 10.1016/j.agrformet.2012.08.004

Bates, D., Maechler, M., Bolker, B., and Walker, S. (2015). Fitting linear mixed-effects models using lme4. *J. Stat. Softw.* 67, 1–48. doi: 10.18637/jss.v067.i01

Batterman, S. A., Hall, J. S., Turner, B. L., Hedin, L. O., LaHaela Walter, J. K., Sheldon, P., et al. (2018). Phosphatase activity and nitrogen fixation reflect species differences, not nutrient trading or nutrient balance, across tropical rainforest trees. *Ecol. Lett.* 21, 1486–1495. doi: 10.1111/ele.13129

Begueria, S., and Vicente-Serrano, S. M. (2013). *SPEI: Calculation of the Standardised Precipitation-Evapotranspiration Index*. R package version, 1, 6.

Bovard, B. D., Curtis, P. S., Vogel, C. S., Su, H. B., and Schmid, H. P. (2005). Environmental controls on sap flow in a northern hardwood forest. *Tree Physiol.* 25, 31–38. doi: 10.1093/treephys/25.1.31

Bretfeld, M., Ewers, B. E., and Hall, J. S. (2018). Plant water use responses along secondary forest succession during the 2015-2016 El Niño drought in Panama. *New Phytol.* 219, 885–899. doi: 10.1111/nph.15071

Brum, M., Gutierrez-Lopez, J., Asbjornsen, H., Licata, J., Pypker, T., Sanchez, G., et al. (2018). ENSO effects on the transpiration of eastern Amazon trees. *Philos. Trans. R. Soc. B Biol. Sci.* 373:20180085. doi: 10.1098/rstb.2018.0085

Burgess, S. S. O., Adams, M. A., Turner, N. C., Beverly, C. R., Ong, C. K., Khan, A. A. H., et al. (2001). An improved heat pulse method to measure low and reverse rates of sap flow in woody plants. *Tree Physiol.* 21, 589–598. doi: 10.1093/treephys/21.9.589

Cernusak, L., and Aranda, J. (2007). Large variation in whole-plant water-use efficiency among tropical tree species. *New Phytol.* 173, 294–305. doi: 10.1111/j.1469-8137.2006.01913.x

del Campo, A. D., González-Sanchis, M., García-Prats, A., Ceacero, C. J., and Lull, C. (2019). The impact of adaptive forest management on water fluxes and growth dynamics in a water-limited low-biomass oak coppice. *Agric. For. Meteorol.* 264, 266–282. doi: 10.1016/j.agrformet.2018.10.016

Detto, M., Wright, S. J., Calderón, O., and Muller-Landau, H. C. (2018). Resource acquisition and reproductive strategies of tropical forest in response to the El Niño-Southern Oscillation. *Nat. Commun.* 9, 1–8. doi: 10.1038/s41467-018-03306-9

Engelbrecht, B. M., Comita, L. S., Condit, R., Kursar, T. A., Tyree, M. T., Turner, B. L., et al. (2007). Drought sensitivity shapes species distribution patterns in tropical forests. *Nature* 447, 80–82. doi: 10.1038/nature05747

Fernández-Moya, J., Alvarado, A., Forsythe, W., and Marchamalo-Sacristán, M. (2013). Effect of teak (*Tectona grandis*) plantations on hydraulic conductivity and porosity of Alfisols in Costa Rica. *J. Trop. For. Sci.* 25, 259—267. Available online at: www.jstor.org/stable/23617041

Fernández-Moya, J., Alvarado, A., Forsythe, W., Ramírez, L., Algeet-Abarquero, N., and Marchamalo-Sacristán, M. (2014). Soil erosion under teak (*Tectona grandis* L.f.) plantations: general patterns, assumptions and controversies. *Catena* 123, 236–242. doi: 10.1016/j.catena.2014.08.010

Gavinet, J., Ourcival, J., and Limousin, J. (2019). Rainfall exclusion and thinning can alter the relationships between forest functioning and drought. *New Phytol.* 223, 1267–1279. doi: 10.1111/nph.15860

Green, S., Clothier, B., and Jardine, B. (2003). Theory and practical application of heat pulse to measure sap flow. *Agron. J.* 95, 1371–1379. doi: 10.2134/agronj2003.1371

Griess, V. C., and Knoke, T. (2011). Can native tree species plantations in Panama compete with Teak plantations? An economic estimation. *New For.* 41, 13–39. doi: 10.1007/s11056-010-9207-y

Grote, R., Gessler, A., Hommel, R., Poschenrieder, W., and Priesack, E. (2016). Importance of tree height and social position for drought-related stress on tree growth and mortality. *Trees Struct. Funct.* 30, 1467–1482. doi: 10.1007/s00468-016-1446-x

Hassler, S. K., Weiler, M., and Blume, T. (2018). Tree-, stand- and site-specific controls of landscape-scale patterns of transpiration. *Hydrol. Earthy Syst. Sci.* 22, 13–30. doi: 10.5194/hess-22-13-2018

Hassler, S. K., Zimmermann, B., van Breugel, M., Hall, J. S., and Elsenbeer, H. (2011). Recovery of saturated hydraulic conductivity under secondary succession on former pasture in the humid tropics. *For. Ecol. Manage.* 261, 1634–1642. doi: 10.1016/j.foreco.2010.06.031

Hernandez-Santana, V., Asbjornsen, H., Sauer, T., Isenhart, T., Schilling, K., and Schultz, R. (2011). Enhanced transpiration by riparian buffer trees in response to advection in a humid temperate agricultural landscape. *For. Ecol. Manage.* 261, 1415–1427. doi: 10.1016/j.foreco.2011.01.027

Hernandez-Santana, V., Hernandez-Hernandez, A., Vadeboncoeur, M. A., and Asbjornsen, H. (2015). Scaling from single-point sap velocity measurements to stand transpiration in a multispecies deciduous forest: uncertainty sources, stand structure effect, and future scenarios. *Can. J. For. Res.* 45, 1489–1497. doi: 10.1139/cjfr-2015-0009

Ho, J., Tumkaya, T., Aryal, S., Choi, H., and Claridge-Chang, A. (2019). Moving beyond *P*-values: data analysis with estimation graphics. *Nat. Methods* 16, 565–566. doi: 10.1038/s41592-019-0470-3

Kollert, W., and Chrubini, L. (2012). "Teak resources and market assessment 2010," in *FAO Plant. For. Trees Work. Pap. F.P. 47E*. Rome: FAO.

Kraenzel, M., Castillo, A., Moore, T., and Potvin, C. (2003). Carbon storage of harvest-age teak (*Tectona grandis*) plantations, Panama. *For. Ecol. Manage.* 173, 213–225. doi: 10.1016/S0378-1127(02)00002-6

Kunert, N., Aparecido, L. M. T., Higuchi, N., dos Santos, J., and Trumbore, S. (2015). Higher tree transpiration due to road-associated edge effects in a tropical moist lowland forest. *Agric. For. Meteorol.* 213, 183–192. doi: 10.1016/j.agrformet.2015.06.009

Lagergren, F., Lankreijer, H., Kučera, J., Cienciala, E., Mölder, M., and Lindroth, A. (2008). Thinning effects on pine-spruce forest transpiration in central Sweden. *For. Ecol. Manage.* 255, 2312–2323. doi: 10.1016/j.foreco.2007.12.047

Markesteijn, L., and Poorter, L. (2009). Seedling root morphology and biomass allocation of 62 tropical tree species in relation to drought- and shade-tolerance. *J. Ecol.* 97, 311–325. doi: 10.1111/j.1365-2745.2008.01466.x

Mayoral, C., van Breugel, M., Turner, B., Asner, G., Vaughn, N. R., and Hall, J. S. (2018). Predicting the effect of microsite quality and species composition on tree growth: a new modeling approach. *For. Ecol. Manage.* 432, 534–545. doi: 10.1016/j.foreco.2018.09.047

Ogden, F. L., and Stallard, R. F. (2013). Land use effects on ecosystem service provisioning in tropical watersheds, still an important unsolved problem. *Proc. Natl. Acad. Sci. U.S.A.* 110:E5037. doi: 10.1073/pnas.1314747111

Paton, S. (2016). *Meteorological and Hydrological Summary for Barro Colorado Island*. Panama City, FL: Smithsonian Tropical Research Institute.

Pineda-García, F., Paz, H., Meinzer, F. C., and Angeles, G. (2015). Exploiting water versus tolerating drought: water-use strategies of trees in a secondary successional tropical dry forest. *Tree Physiol.* 36, 208–217. doi: 10.1093/treephys/tpv124

R Core Team (2017). *A Language and Environment for Statistical Computing*. Available online at: https://www.R-project.org/ (accessed January 6, 2014).

Ribolzi, O., Evrard, O., Huon, S., De Rouw, A., Silvera, N., Latsachack, K. O., et al. (2017). From shifting cultivation to teak plantation: effect on overland flow and sediment yield in a montane tropical catchment. *Sci. Rep.* 7, 1–12. doi: 10.1038/s41598-017-04385-2

Ringgaard, R., Herbst, M., and Friborg, T. (2012). Partitioning of forest evapotranspiration: the impact of edge effects and canopy structure. *Agric. For. Meteorol.* 166, 86–97. doi: 10.1016/j.agrformet.2012.07.001

Schnabel, F., Schwarz, J. A., Dănescu, A., Fichtner, A., Nock, C. A., Bauhus, J., et al. (2019). Drivers of productivity and its temporal stability in a tropical tree diversity experiment. *Glob. Chang. Biol.* 25, 4257–4272. doi: 10.1111/gcb.14792

Slette, I. J., Post, A. K., Awad, M., Even, T., Punzalan, A., Williams, S., et al. (2019). How ecologists define drought, and why we should do better. *Glob. Change Biol.* 25, 3193–3200. doi: 10.1111/gcb.14747

ter Steeg, H. (2018). *Hemiphot.R: Free R Scripts to Analyse Hemispherical Photographs for Canopy Openness, Leaf Area Index and Photosynthetic Active Radiation Under Forest Canopies*. Panama City, FL. Available online at: https://github.com/Hans-ter-Steege/Hemiphot

Weber, D., and Hall, J. S. (2009). *Resumen del Proyecto Agua Salud*. Panama City, FL.

Wickham, H. (2016). *ggplot2: Elegant Graphics for Data Analysis*. New York, NY: Springer. doi: 10.1007/978-3-319-24277-4

Zeppel, M. J. B., Murray, B. R., Barton, C., and Eamus, D. (2004). Seasonal responses of xylem sap velocity to VPD and solar radiation during drought in a stand of native trees in temperate Australia. *Funct. Plant Biol.* 31, 461–470. doi: 10.1071/FP03220

Zhang, Q., Jia, X., Shao, M., Zhang, C., Li, X., and Ma, C. (2018). Sap flow of black locust in response to short-Term drought in southern Loess Plateau of China. *Sci. Rep.* 8, 1–10. doi: 10.1038/s41598-018-24669-5

Conflict of Interest: The authors declare that the research was conducted in the absence of any commercial or financial relationships that could be construed as a potential conflict of interest.

frontiers in Forests and Global Change

ORIGINAL RESEARCH
published: 31 January 2020
doi: 10.3389/ffgc.2019.00093

Throughfall Reduction × Fertilization: Deep Soil Water Usage in a Clay Rich Ultisol Under Loblolly Pine in the Southeast USA

Ji Qi[1,2]*, *Daniel Markewitz*[1], *Mary Anne McGuire*[1], *Lisa Samuelson*[3] and *Eric Ward*[4,5]

[1] Warnell School of Forestry and Natural Resources, University of Georgia, Athens, GA, United States, [2] The Jones Center at Ichauway, Newton, GA, United States, [3] School of Forestry and Wildlife Sciences, Auburn University, Auburn, AL, United States, [4] U. S. Geological Survey, Wetland and Aquatic Research Center, Lafayette, LA, United States, [5] Department of Forestry and Environmental Resources, North Carolina State University, Raleigh, NC, United States

Forests in the Southeast USA are predicted to experience a moderate decrease in precipitation inputs over this century that may result in soil water deficiency during the growing season. The potential impact of a drier climate on the productivity of managed loblolly pine (*Pinus taeda* L.) plantations in the Southeast USA is uncertain. Access to water reserves in deep soil during drought periods may help buffer these forests from the effects of water deficits. To better understand the potential impact of drought on deep soil water, we studied the combined effects of throughfall reduction and fertilization on soil water usage in a clay rich Piedmont Ultisol to a depth of 3 m. In a 6-year-old loblolly pine plantation, we applied a throughfall reduction treatment (ambient vs. ∼30% throughfall reduction) and a fertilization treatment (no fertilization vs. fertilization). Over 28 months, throughfall reduction lowered soil moisture for all depths and differences were significant in the surface soils (0–0.3 m) (1.2–3.6%) and deep soils (below 2 m) (2.6–3.6%). Fertilization also lowered soil moisture for all depths and differences were significant at 0.3–0.6 m (2.9%) and 1.94–3.06 m (4.5%). Fertilization when combined with the throughfall reduction treatment significantly decreased soil water at 0.1–0.9 m depth. Soils of all depths were rarely depleted of plant available water with the exception of 0–0.1 m, mainly during the growing season. Under throughfall reduction treatment, soil below 0.9 m consistently accounted for more than half of the change in plant available water during months when transpiration exceeded precipitation. When considering the whole soil profile in this clay rich Ultisol, soil water storage buffered transpirational demand in the face of decreasing throughfall input.

Keywords: deep soil, soil moisture, drought, fertilization, loblolly pine

OPEN ACCESS

Edited by:
Christina Tague, University of California, Santa Barbara, United States

Reviewed by:
John T. Van Stan, Georgia Southern University, United States
Cate Macinnis-Ng, The University of Auckland, New Zealand

***Correspondence:**
Ji Qi
jill.qi@swfwmd.state.fl.us

Specialty section:
This article was submitted to Forest Hydrology, a section of the journal Frontiers in Forests and Global Change

Received: *30 July 2019*
Accepted: *23 December 2019*
Published: *31 January 2020*

Citation:
Qi J, Markewitz D, McGuire MA, Samuelson L and Ward E (2020) Throughfall Reduction × Fertilization: Deep Soil Water Usage in a Clay Rich Ultisol Under Loblolly Pine in the Southeast USA. Front. For. Glob. Change 2:93. doi: 10.3389/ffgc.2019.00093

INTRODUCTION

Deep root (>1 m) water uptake can be important for forest ecosystems during drought (Nepstad et al., 1994; Fensham and Fairfax, 2007; Padilla and Pugnaire, 2007; Maeght et al., 2013). Drought stresses plants and lowers productivity (Borken and Matzner, 2009) and access to deep water reserves can buffer plants from these stresses (Belk et al., 2007). Predicting plant responses to a changing climate requires an understanding of deep soil water access under drought conditions.

Forests in the Southeast USA are predicted to experience more variable precipitation over this century with up to three times more extreme daily precipitation events (a daily amount that occurs once in 20 years) (Meehl et al., 2007; Kunkel et al., 2013), and a 2.5% or more per decade decrease in water yield (Sun, 2013). Uncertainty in future precipitation patterns still remains because the Southeast is straddled in the transition zone between the Northeast with projected wetter conditions and the Southwest with projected drier conditions (Kunkel et al., 2013). Variable precipitation could result in soil drying during the growing season, a critical period for plant growth (Teskey and Sheriff, 1996). Positive relationships between rooting depth and resistance to drought have been demonstrated (Fensham and Fairfax, 2007; Padilla and Pugnaire, 2007). For example, in Brazilian Amazonian forests, about half of the closed forests rely on water extracted by deep roots to maintain evergreen canopies during the dry season (Nepstad et al., 1994). In a similar Amazonian forest, it was estimated that soil water at the 2.5–5.5 m depth contributed ∼20% of water demand and the 5.5–11.5 m depth contributed ∼10% (Markewitz et al., 2010). A global review of 565 root profiles, across 15 terrestrial biomes, indicated that soil depths of 0.4, 0.7, and 1.1 m correspond to cumulative root biomass proportions of 80, 90, and 95%, respectively (Schenk and Jackson, 2002). As such, studying water uptake by deep roots is critical to increase our understanding of plant water uptake and soil water availability under changing climate (Harper and Tibbett, 2013; Maeght et al., 2013).

Understanding the impact of a potentially drier climate is particularly important in managed loblolly pine (*Pinus taeda* L.) forests in the Southeast USA, which are the most intensively managed and fastest growing commercial pine species in the region covering ∼20 million hectares (Fox et al., 2007). However, loblolly pine is not highly drought tolerant so is uncommon on the driest soil types (e.g., Quartzipsamments). Low soil water availability has been shown to reduce net photosynthesis (Wertin et al., 2010), decrease both above and below ground growth, and shift root distribution of loblolly pine (Torreano and Morris, 1998). Depending on stand structure and climate, mid-rotation loblolly pine stands in Georgia use ∼300–650 mm of water per year (Bartkowiak et al., 2015). Six hundred and fifty mm represents about 55% of the rain this region receives (1,109 mm, 30-year average) (http://www.ncdc.noaa.gov). During the growing season, loblolly pine relies on soil water storage as transpiration often exceeds precipitation (McNulty et al., 1996).

Fertilization is often combined with other management practices in loblolly pine plantations and significantly improves productivity (Jokela et al., 1991; Kyle et al., 2005; Fox et al., 2007). Although fertilization can increase productivity (Fox et al., 2007), when combined with low soil water availability stands may exhibit little response to fertilization (Tang et al., 2004; Goldstein et al., 2013). This research is part of a recent region wide (Florida, Georgia, Oklahoma, Virginia) loblolly pine fertilization x throughfall reduction experiment that specifically addressed the interaction effects of fertilization and decreased water availability on loblolly pine (Will et al., 2015). A few published papers from this region wide research have examined the combined effects of fertilization and decreased water availability (Samuelson et al., 2014, 2018; Bartkowiak et al., 2015; Ward et al., 2015; Maggard et al., 2016, 2017). Previous results have demonstrated that fertilization may intensify the impact of drought (Bartkowiak et al., 2015; Ward et al., 2015). Responses, however, have been site and soil specific and only the Georgia site has reported on soil moisture content below 60 cm (Qi et al., 2018b).

In this research we report on how drought and fertilization affect soil hydrological processes to a depth of 3 m. Here we report on our empirical measurements during 28 months of this experiment while our previous work focused on model simulations (Qi et al., 2018b). Predicting how these loblolly pine forests might respond to drought is critical for understanding how forests might be altered under a changing climate. This research was designed to test these hypotheses: (1) throughfall reduction treatment will reduce soil moisture for the whole soil profile, and when combined with fertilization the soil moisture reduction will be greater than throughfall reduction or fertilization alone; (2) under throughfall reduction treatment, soil moisture storage change will be greater in deep soil when compared with ambient throughfall, and when combined with fertilization the soil moisture change will be greater than throughfall reduction or fertilization alone.

METHODS

Site Descriptions

The experiment was established in a loblolly pine plantation in Taliaferro County, Georgia owned by Plum Creek Timber Company. The study site is at an elevation of 152 m with latitude 33°37′32.61″ N and longitude 82°47′56.54″ W. This site was clear-cut in 2004 and both chemical and mechanical site preparation were applied in 2005. This included an aerial application of Velpar ULW herbicide (5.97 kg/ha), debris management, and combination plowing. In 2006, bare root seedlings (seed orchard mix) were hand planted at 1,544 trees/ha. Herbaceous weed control was applied banded at ∼220 ml/ha of Oust Extra in 2006. Refer to Will et al. (2015) for more details.

The soils of this research site are a Cecil-Lloyd complex. The Lloyd series is a fine, kaolinitic, thermic Rhodic Kanhapludult, while the Cecil series is a fine, kaolinitic, thermic Typic Kanhapludult. The Rhodic designation indicates an influence of mafic parent material on soil color. These soils are typical in the region. These soil series descriptions are based on USDA-NRCS Soil Survey Division (https://soilseries.sc.egov.usda.gov).

The 30-year (1983–2012) average annual precipitation is 1,119 mm and the 30-year (1983–2012) average daily maximum and minimum temperature is 22.7 and 10.1°C (http://www.ncdc.noaa.gov). During the study period, monthly Palmer Drought Severity Index indicated mild drought from June 2014 to June 2015 ranging from -1.00 to -1.99 and moderate drought for July 2015 with values ranging from -2.00 to -2.99 (http://www.ncdc.noaa.gov/temp-and-precip/drought/historical-palmers/psi/201303-201507).

FIGURE 1 | Throughfall reduction structure covering 30% of the plot area with troughs to capture and funnel throughfall away from the plots. Taliaferro County, Georgia in 2012 when loblolly pines were 6 years old. Data collection period was May 2013 to August 2015.

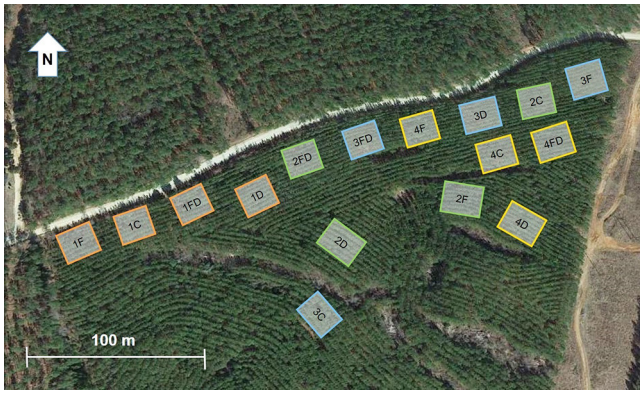

FIGURE 2 | Map of experimental treatments and blocks located in Taliaferro County, Georgia. Four treatments were randomly assigned in each of the four blocks: control (C), fertilization (F), throughfall reduction (D) and combined treatment of FD. Fertilizer additions included N, P, K and micronutrients and throughfall reduction diverted 30% of throughfall off of the plot. Blocks were established by grouping plots with similar tree height (6.34 ± 0.58 m average at time of treatment initiation in 2012) and basal area (8.79 ± 1.58 m^2/ha average at time of treatment initiation).

Experimental Design

The treatment area for each plot was 34 × 28 m with a 21 × 14 m measurement area in the center and a 6 m untreated buffer area between each treatment area. Throughfall exclusion structures (**Figure 1**) were installed to reduce throughfall by 30%, which is at the extreme end of predictions for precipitation reduction associated with climate change for the region (Collins et al., 2013; Walsh et al., 2014). Furthermore, because most planted pine forests are nutrient limited and nutrient management is widespread, it is important to examine the interaction of throughfall exclusion treatment with an imposed nutritional gradient. This study was designed as a 2x2 factorial experiment with four blocks and the following treatments were assigned randomly: Control (C)–no treatment; Fertilization (F)–fertilizer additions to achieve "optimum" nutrition; Throughfall reduction (D)–troughs installed in understory to divert 30% of throughfall off of the plot (**Figure 1**); Fertilization and throughfall reduction (FD)–combined fertilization and throughfall reduction treatments (**Figure 2**) (PINEMAP 2013). Blocks were established by grouping plots with similar tree height (6.34 ± 0.58 m average at time of treatment initiation) and basal area (8.79 ± 1.58 m^2/ha average at time of treatment initiation) (Will et al., 2015). The fertilizer rates were 224 kg/ha N, 28 kg/ha P, 56 kg/ha K and a micro-nutrient mix at the rate of 22.4 kg/ha containing 6% S, 5% B, 2% Cu, 6% Mn, and 5% Zn (Southeast Mix, Cameron Chemicals, Inc., Virginia Beach, VA, USA) evenly broadcast by hand to ensure even distribution.

The throughfall reduction structures were made of plastic troughs and were installed between tree rows in the forest understory starting May 2012 (**Figure 1**). These troughs covered 30% of the plot area to capture ∼30% of incoming throughfall and channeled the water to outside of the experimental treatment areas. The 30% covered area does not necessarily exactly equal a 30% reduction in throughfall, although similar designs have been effectively applied for exclusion experiments (Hanson et al., 1998; Nepstad et al., 2002). In addition, large lengths of trough have been demonstrated to be most effective in reducing error in estimates of throughfall volume <5% or ∼4 cm in this location (Zimmermann et al., 2010). Stemflow is another potential source of error but as a proportion of precipitation in pine plantations is generally <10% (Swank, 1972) and often ranged from 5 to <1% or ∼2 cm (Abrahamson et al., 1998; Zarnoch et al., 2002; Bryant et al., 2005). Currently there is little evidence supporting the influence of stemflow on deep soil water (Levia and Germer, 2015). For example, in a desert shrubland, stemflow generated preferential flow along roots, however, this preferential flow did not reach beyond 40 cm in the soil (Jian et al., 2014). Vertical infiltration of preferential flow along roots was hampered due to low hydraulic conductivity of clay rich soil in a European beech stand (Schwärzel et al., 2012). Considering the small amount of stemflow and the clay rich Ultisol, stemflow impact on deep soil was deemed minimal at this study site. Studies at this location and other companion sites using the same trough structure to reduce throughfall have already demonstrated impacts on soil moisture and plant water usage responses such as transpiration (Samuelson et al., 2014, 2018; Ward et al., 2015; Maggard et al., 2016, 2017; Wightman et al., 2016). Finally, using the same experiment site, a study modeling the effect of changing precipitation inputs on deep soil water utilization was able to calibrate and validate water balances using the same field measurements (Qi et al., 2018a).

Soil Texture and Chemical Analysis

One soil profile was sampled to 3 m in the middle of each plot. Soils were collected in eight depths: 0–0.1, 0.1–0.2, 0.2–0.5, 0.5–1.0, 1.0–1.5, 1.5–2.0, 2.0–2.5 and 2.5–3.0 m. All samples were air-dried and homogenized by sieving through a 2 mm screen.

A subsample was analyzed in replicate for soil texture, pH, total carbon and nitrogen. Textural analysis followed Gee and Or (2002) and soil water pH tests followed the method of Thomas (1996) with a 1:1 soil:water ratio. For carbon and nitrogen analysis samples were further oven-dried at 65°C and ball mill ground. Total carbon and nitrogen were analyzed on a CE Elantech NC 2100 Soil Analyzer (CE Elantech Inc., Lakewood, NJ) using the Dumas method as described in Bremner (1996).

Soil Moisture Measurements

At the approximate center of the plot, sets of 6.5 mm diameter welding rods were installed within tree rows (in all plots), between tree rows (in all plots), and under throughfall reduction structures (only in D and FD plots) to cover these 4 depth increments: 0–0.1, 0–0.3, 0–0.6, and 0–0.9 m. These rods were used for soil moisture measurements and were left exposed at the surface for later reading (Greco and Guida, 2008). In addition, using these same welding rods, 0.12-m rods were constructed with coaxial cable and epoxy (Evett and Ruthardt, 2005) and installed at 1.94–2.06 m (centered at 2 m) and 2.94–3.06 m (centered at 3 m) depths with the cable exposed at the surface. Soil volumetric water content (VWC) was measured by attaching a Riser Bond Model 1205CXA Coaxial Metallic Time Domain Reflectometer (TDR) (Radiodetection, Raymond, Maine) to the rods or coaxial cable with alligator clips. The wave forms were measured to estimate VWC. Soil moisture probes were measured approximately monthly from May 2013 to August 2015. The surface soil moisture measurements were later partitioned into separate depths: 0–0.1, 0.1–0.3, 0.3–0.6, and 0.6–0.9 m, using:

$$D_e = \sum_{i=1}^{n} \theta_i D_i$$

where D_e [L] is depth of water equivalent, θ_i and D_i are the VWCs and layer thicknesses, respectively, of each layer (Radcliffe and Šimunek, 2010).

To better capture the soil moisture changes during the growing season, in March 2014 logging TDR probes (CS655 0.12 m Soil Water Content Reflectometer, Campbell Scientific, Inc., Logan, Utah) were installed vertically at 0.54–0.66 m at the approximate center of each plot in blocks 2 and 4 (total of eight probes). They were programmed to collect data every 30 min from March 2014 to October 2015. These data were logged automatically (CR23X, Campbell Scientific, Inc., Logan, Utah), then downloaded and averaged by day from March 2014 to August 2015.

Plant Available Water

To calculate plant available water (PAW), soil water retention curves were determined using Tempe cells (SoilMoisture Equipment Corp., Santa Barbara, CA) and a WP4C Dewpoint PotentialMeter (Decagon Devices. Inc., Pullman, WA). Core samples were collected in each plot at 0–75 mm and 100–175 mm. Core samples were also collected at 0.5, 1.0, 1.5, 2.0, 2.5, and 3.0 m from the walls of two soil pits dug on site.

Tempe cells were used for <1 MPa and WP4C Dewpoint PotentialMeter was used for >1 MPa. Results from both measurements were then combined to form soil water retention curve equations following Van Genuchten (1980):

$$S_e(h) = \frac{1}{\left[1 + (\alpha h)^n\right]^m}$$

where α [L^{-1}], n [–], and m [–] are fitting parameters, h is pressure [L] and $S_e(h)$ [–] is the effective soil water saturation calculated following Van Genuchten (1980):

$$S_e = \frac{\theta - \theta_r}{\theta_s - \theta_r}$$

where θ is the VWC, θ_s is the saturated VWC and θ_r is the residual VWC, defined as the VWC where hydraulic conductivity approaches zero (Van Genuchten, 1980). PAW (θ_{PAW}) was calculated as the amount of soil water held at tensions between -0.01 and -1.5 MPa (θ_{wp}), determined from soil moisture retention curves. The PAW of each soil layer was calculated using:

$$\theta_{PAW} = \theta - \theta_{wp}$$

where θ of 0–0.1, 0.1–0.3, 0.3–0.6, and 0.6–0.9 m soils were measured as noted above; θ of 0.9–2 m were averaged between VWC measurements at 0.6–0.9 and 2 m; and θ of 2–3 m were averaged between VWC measurements at 2 and 3 m. The PAWs of 0–0.1, 0.1–0.3, 0.3–0.6, 0.6–0.9, 0.9–2.0, and 2.0–3.0 m were calculated approximately monthly from May 2013 to August 2015.

Precipitation and Transpiration

Precipitation records were obtained from six weather stations located within 90 km of the research site (www.georgiaweather.net). Due to the lack of any one weather station being in extremely close proximity, the mean precipitation between six locations from March 2013 to August 2015 were used to estimate the water balance during the experiment (**Figure 3**). Transpiration on a ground area basis was calculated by averaging sap flow (kg/min) across sample tress in a treatment plot, dividing by measurement plot area, and multiplying by the ratio of sapwood area to the average sapwood area of sap flow trees measured at diameter at breast height in November 2012. The sap flow measurements and scaling approaches were detailed in Bartkowiak et al. (2015). Data collected in 2013 were previously reported in Bartkowiak et al. (2015). In 2014, sap flux was collected and scaled similarly with the addition of gap filling of missing data using methods described by Bell et al. (2015) (**Figure 3**).

Statistical Analysis

Soil VWC data of different depths (0–0.1, 0.1–0.3, 0.3–0.6, 0.6–0.9, 1.94–2.06, and 2.94–3.06 m) were tested for main and interactive treatment effects of fertilization and throughfall reduction ($\alpha = 0.05$). Among 5,185 data points, there were 62 VWC measurements below zero, ∼1% of the total data collected. These data points were not included in data analysis. The experimental unit of replication was the plot. Block was treated as a random factor. Between rows, within row, and under trough positions (within unit repeated measurements) were averaged

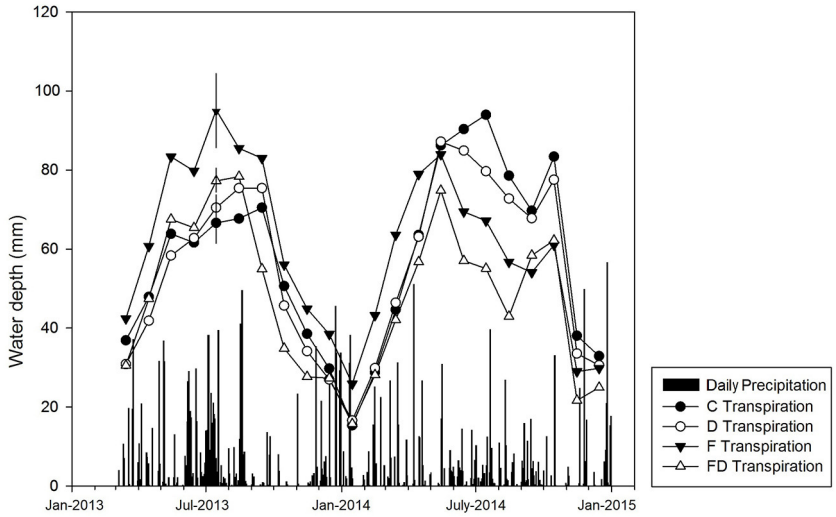

FIGURE 3 | Daily precipitation (black bars) and monthly transpiration in treatments of control (C), fertilization (F), throughfall reduction (D), and combined treatment of FD in a loblolly pine plantation in Taliaferro County, Georgia for the period of March 2013 to December 2014. Error bars (±1 SE, $n = 4$) shown only for July 2013 transpiration to maintain clarity. The transpiration was determined from sap flux measurements and scaling approaches detailed in Bartkowiak et al. (2015).

to represent plot level VWC. These data were analyzed using a mixed effect, repeated measures model with date as the repeated factor. Tukey's significance test at the level of $\alpha = 0.05$ was used to separate treatment effect on VWCs at the same depth. The SAS statistical package (SAS Institute Inc., Cary, North Carolina) was used for all data analyses.

RESULTS

Soil Physical and Chemical Properties

Soils of all depths were acidic, with pH ranging from 5.2 to 5.8. Mean carbon concentrations ranged from 1.92% in 0-0.1 m and decreased with depth to ∼0.5% below 1 m. Mean nitrogen concentrations were 0.1% at the surface and decreased to 0–0.01% below 1 m.

The clay content ranged from 24–47%, with lowest clay contents in the 0–0.1 and 2.5–3.0 m layers, while 0.2–2.5 m soils had >40% clay throughout (**Figure 4**). Wilting point VWCs (θ_{wp}) ranged from 10–19% (**Figure 4**). In correspondence with clay contents, θ_{wp} were highest in the middle of the soil profile but decreased toward the surface and the bottom of the profile (**Figure 4**).

Volumetric Water Content

Soil Volumetric Water Contents (VWC, data could be found in **Supplementary Material**) were generally higher during winters and lower during summers (**Figure 5**), and the effect of time was significant ($p < 0.0001$ for all depths). This was more obvious in surface soils, while deep soil VWC varied proportionally less over the observed time. There were no significant time by treatment interactions for any depth (p value ranged from 0.4–0.9).

The main effect of fertilization was reduced VWC for all depths (**Table 1**). The effect was more prominent below 0.3 m with 1.3–4.5% lower VWC in fertilized plots. The differences were significant within the 0.3–0.6 m depth increment (2.9%, $p < 0.0001$) and 2.94–3.06 m increment (4.5%, $p < 0.0001$). Surface soil moisture was only 0.4–0.5% lower in the fertilized plots, and these differences were not significant.

The main effect of throughfall reduction treatment was also lowered soil moisture for all depths, ranging from 0.8 to 3.6% VWC (**Table 1**). The differences were significant for surface soils, 0–0.1 ($p < 0.0001$) and 0.1–0.3 m ($p = 0.0253$), with 3.6 and 1.2% lower VWC, respectively. Differences from 0.3–0.6 to 0.6–0.9 m were not significantly different. Deep soils did differ, 1.94–2.06 m ($p = 0.0006$) and 2.94–3.06 m ($p = 0.0252$) had significantly lower VWC, with 3.6 and 2.6% lower VWC, respectively.

The interaction effect of fertilization and throughfall reduction was significant at 0.1–0.3 m ($p < 0.0001$), 1.94–2.06 m ($p = 0.0002$), and 2.94–3.06 m ($p < 0.0001$) soils (**Table 1**). In these cases, throughfall reduction without fertilization (i.e., C vs. D) significantly lowered soil moisture while the effect of throughfall reduction with fertilization (i.e., F vs. FD) was not significant. For example, for soils at 1.96–2.04 m depth, without throughfall reduction, fertilization significantly reduced soil moisture (i.e., C vs. F); while with throughfall reduction fertilization didn't have a significant effect on soil moisture (i.e., D vs. FD) (**Figure 6**).

Water Balance

Plant available water (PAW) varied with season. In general, plots with FD treatment had the lowest PAW, while C had the highest (**Figure 7**). Soils of all depths were never depleted of PAW, except for the 0–0.1 m soils under D, F, and FD treatments. Among these soils, there was no PAW in 0–0.1 m soil under D treatments for 6 months, 4 months for FD plots, and 2 months for F plots (mainly being depleted during the growing season) (**Figure 7**).

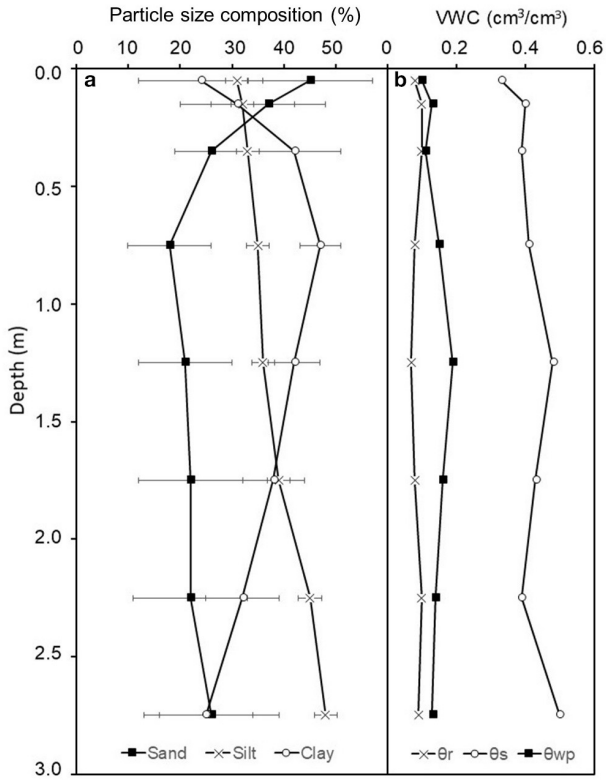

FIGURE 4 | (a) Soil sand, silt, and clay percentage for all treatment plots at Taliaferro County, Georgia. Values are mean ±1 SE ($n = 16$). **(b)** Soil water retention curve parameters for 0–0.1 and 0.1–0.2 m, eight samples were collected and data points from all eight samples were used to create one soil water retention curve, and for soils below 0.2 m, two samples were collected. Samples were collected in August 2013. Where θ_r is the residual volumetric water content, θ_s is the saturated volumetric water content, and θ_{wp} is the volumetric water content at −1.5 MPa, determined from soil moisture retention curves.

Transpiration exceeded precipitation for 4–8 months in the growing seasons during the experimental period, with D plots having the longest duration of precipitation deficit (May– October 2014). Soil water storage change over time showed similar trends as precipitation-transpiration, often being negative during the growing season and positive during winter. Plots under FD treatment experienced the longest time period (11 months) with the total $\Delta PAW < 0$, while C plots had the shortest time (8 months) (**Figure 8**).

During the months that transpiration exceeded precipitation, the contribution of soil below 0.9 m to ΔPAW varied widely: 1.0–7.2 cm in C plots, 1.0–7.5 cm in D, 0.1–10.3 cm in F, and 0.4–19.0 cm in FD (**Figure 8**). The FD soils below 90 cm contributed the highest amount of water (19.0 cm), which occurred in May 2014. During this month, VWC at 2 m changed from 54.6 to 39.7%, accounting for 78% of the total ΔPAW. The highest proportion of soil water from below 0.9 m that contributed to total ΔPAW for any month was 98%, which occurred in plots under FD treatment during November 2013 (**Figure 8**). Overall, D plots had a consistently large proportion (62–81%) of total ΔPAW coming from soils below 0.9 m, while the proportions varied widely under other treatments (C: 40–86%, F: 18–81%, and FD: 11–98%) (**Figure 8**).

Growing Season Analysis

The VWC data collected by dataloggers every 30 min followed the same trend as VWC measured monthly (**Figure 9**). Soil VWCs were generally higher during winters and lower during summers. These higher temporal resolution data better captured daily variability in VWC. Soils under all four treatments experienced a similar increase and decrease in VWC, with smaller daily variances for D and FD soils.

DISCUSSION

We hypothesized that throughfall reduction would reduce soil moisture for the whole soil profile, and when combined with fertilization the reduction in soil moisture would be greater than with throughfall reduction or fertilization alone. Under the treatment of throughfall reduction, there was lower soil moisture throughout the whole soil profile relative to the ambient throughfall plots, with both surface (0–0.3 m) and deep (2–3 m) soils having significantly lower soil moisture (**Table 1** and **Figure 5**). In the surface, lower soil moisture might be explained by lower throughfall inputs and high fine root biomass that would increase root water uptake. In 0.3–2.0 m soils, the absence of significant effects might be attributed to the high clay content, which requires a large water content difference to induce a relatively small change in water potential that may not have been statistically detectable (**Figure 4**). In deep soil horizons, lower soil moisture could be caused by higher root water uptake or continued soil drainage. The absence of VWC values above θ_s (**Figure 4**), however, suggests limited potential for drainage and therefore, lower VWC in 2–3 m soils are likely caused by higher root water uptake (the presence of roots in deep soil was reported in Qi et al., 2018a).

Fertilized plots also had consistently lower soil moisture than unfertilized plots. In a study conducted on the same research site in 2013, fertilization significantly increased leaf area index (Bartkowiak et al., 2015). Higher leaf area index could result in more canopy interception and thus reduced throughfall input. Another possible explanation is that lower VWC under fertilization was caused by higher root water uptake to meet canopy transpirational demand. In 2013, transpirational demand in fertilizer treatments (64.9 ± 5.5 cm year^{-1}) was not significantly greater than non-fertilized (58.0 ± 4.0 cm year^{-1}) (Bartkowiak et al., 2015). The soil moisture differences between fertilized and unfertilized plots were especially prominent below 0.3 m, with significant differences at 0.3–0.6 m and 2.94–3.06 m (**Table 1** and **Figure 5**). Finally, under FD treatment VWC was significantly lower in the 0.1–0.9 m depths (**Figure 5**). These results do indicate some increased drying (lower VWC) of the surface under FD (0.1–0.9 m) compared to D (0–0.3 m). On a water content basis, in the upper 0.9 m this translated into a greater depletion of 2.38 cm of PAW in FD compared to D. The

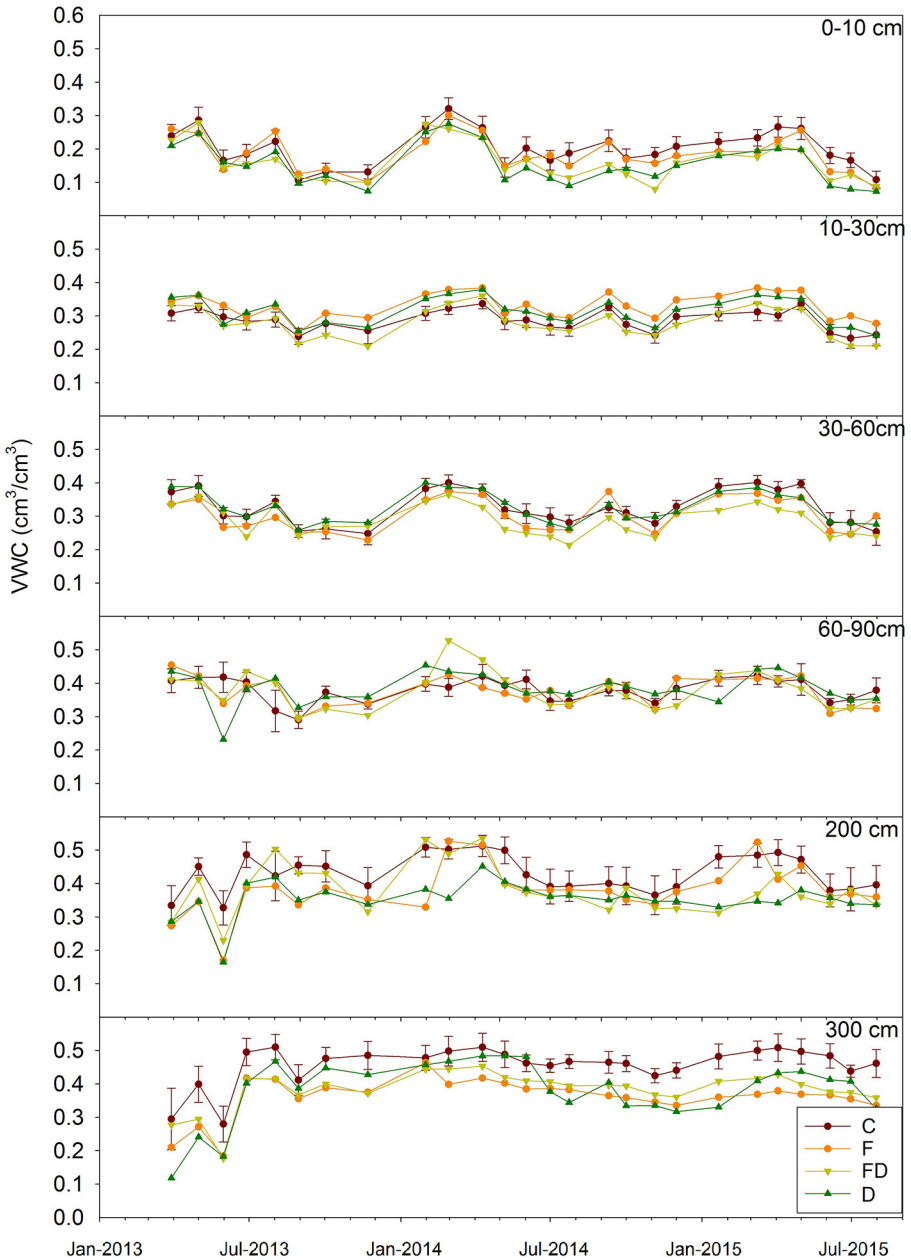

FIGURE 5 | Mean soil volumetric water content (VWC) of six depths for March 2013 to July 2015. Treatments are control (C), fertilization (F), throughfall reduction (D), and combined treatment of FD. Bars representing ±1 SE are given only for C to maintain clarity ($n = 4$).

depletion in the upper 0.9 m compromised ∼80% of the depletion over the entire 3 m in FD.

Our second hypothesis addressed deep soil moisture, proposing that under throughfall reduction treatment, ΔPAW would be greater in deep soil when compared with ambient throughfall, and when combined with fertilization the change in deep soil moisture would be greater than throughfall reduction or fertilization alone. We found consistently greater ΔPAW below 0.9 m under throughfall reduction treatment compared to ambient throughfall. During months when transpiration > precipitation, 0–0.9 m soil rarely (5 of the 37 months) contributed more than half of total ΔPAW. In D plots, soils below 0.9 m consistently contributed more than half of ΔPAW, while the proportion varied widely in ambient throughfall soils (18–86%) (**Figure 7**). Under FD treatment, soils below 0.9 m contributed 98% of ΔPAW during November 2013, which is the maximum percent contribution throughout all months of the experiment under all treatments.

Within the soils of the current study site, even though we excluded ∼30% of throughfall, which is at the extreme end of

TABLE 1 | Treatment effects of fertilization, throughfall reduction, and their interaction ($n = 4$) on soil volumetric water content (VWC), and %VWC change.

Depth (m)	Fertilization		Throughfall reduction		Interaction
	Δ VWC (%)	*P*-value	Δ VWC (%)	*P*-value	*P*-value
0–0.1	−0.49	0.5162	−3.58	<0.0001	0.1334
0.1–0.3	−0.41	0.4221	−1.19	0.0253	<0.0001
0.3–0.6	−2.94	<0.0001	−0.80	0.2551	0.2676
0.6–0.9	−1.24	0.1202	−0.81	0.3131	0.2948
1.94–2.06	−1.27	0.223	−3.58	0.0006	0.0002
2.94–3.06	−4.51	<0.0001	−2.64	0.0252	<0.0001

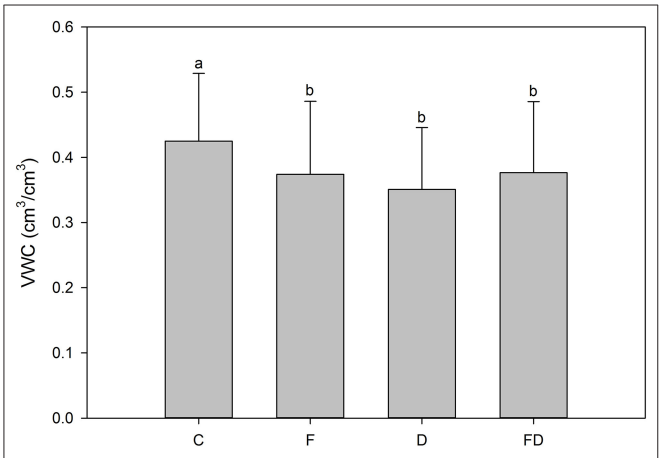

FIGURE 6 | Treatment [control (C), fertilization (F), throughfall reduction (D), and FD] effects on volumetric water content (VWC) of 1.94–2.06 m soils. Bars represent the means of VWC (over the period of March 2013 to July 2015) and error bars represent ±1 SE ($n = 108$). Letters indicating differences for Tukey's significance test at the level of $\alpha = 0.05$ were used to separate treatment effect on VWC.

predictions for precipitation reduction associated with climate change for the region (Collins et al., 2013; Walsh et al., 2014), there was enough PAW to support transpiration. Within all the treatments, soils of all depths were rarely depleted of PAW (i.e., below θ_{wp}), with the exception of the 0–0.1 m that was dry mainly during the growing season (**Figure 7**). Variation in water use as a loblolly pine plantation ages may impact these observations (Domec et al., 2012). When comparing two plantations in sandy soils in the lower coastal plain of North Carolina, transpiration of a 5-year-old stand was 125–290 mm less than a 19-year-old stand. At the 19-year-old site, <20% of water was stored in the top 30 cm of soil and soil at 60–140 cm depth contributed a larger amount of water to transpiration relative to 10–60 cm soils during dry periods (Domec et al., 2012). A modeling study manipulating precipitation inputs to a pine stand showed that when annual precipitation input was reduced more than 30%, plants required stored soil water to satisfy transpirational demands and the contribution of deep soil water to transpiration increased as precipitation declined (Qi et al., 2018a). Considering the uncertainty in climate change, deep soil water could play a more vital role to buffer the effects of drought as stands age.

The observed changes in VWC did not result in reduction of growth (Bartkowiak et al., 2015) or transpiration (**Figure 3**) under the D treatment during the 2013 growing season. However, 2013 had 27% higher precipitation than the 30-year average in this area (http://www.ncdc.noaa.gov). Decreased soil moisture in the F treatment similarly did not have a significant effect on transpiration in 2013 despite increased leaf area due to fertilization. The combined FD treatment did decrease transpiration per ha from 62 to 47 mm/month, but this was not coincident with a significant decrease in aboveground growth (Bartkowiak et al., 2015). By 2015 and 2016, a small decline in height and volume increment was observed under throughfall reduction (Samuelson et al., 2018). The results presented here, however, suggest that, at least, during the 2013 and 2014 growing season soil moisture under throughfall reduction with or without fertilization was sufficient to sustain growth.

Three additional study sites using the same fertilization and throughfall reduction treatment methods were direct companions to this site in Georgia. One companion experiment in a 13-year-old loblolly pine plantation in Florida (30°12′22″ N, 83°52′12″ W) showed similar results with no impact of throughfall reduction (D) on forest productivity or water relations (Wightman et al., 2016). The lack of response at this site was attributed to abundant rainfall and the ability of trees to access a shallow water table (1–2 m depth). In fact, the fertilizer only treatment increased monthly transpiration by 17% in the spring of 2013 and transpiration was not significantly different among treatments during the rest of the year (Wightman et al., 2016). These results suggested that given higher than average precipitation or access to a shallow water table, a ∼30% throughfall reduction may not lower soil moisture enough to stress trees in physiologically significant ways. A second companion research site in a 13-year-old plantation in Virginia (37°27′37″ N, 78°39′50″ W) provided some contrasting results. At this location the throughfall reduction treatment lowered transpiration by 19% during the growing season even when the annual precipitation was 9% higher than the 30-year mean in the research area. Under fertilization, transpiration also declined by 13% during the growing season and under FD transpiration decreased by 29%. Under neither treatment, however, was growth reduced (Ward et al., 2015). Finally, in the Oklahoma site (34°1′47″ N, 94°49′23″ W) between ages 5–7 throughfall reduction in 2013 reduced whole tree water use by 20% and in 2014 by 5% (Maggard et al., 2016, 2017). This reduction reduced stem volume growth by ∼15%. In contrast, fertilization increased stem volume growth by 11% partly by increasing water use efficiency (i.e., stem growth per unit water transpiration). In fact, in all locations growth was enhanced with fertilization even when fertilization was provided under throughfall exclusion (Bracho et al., 2018).

These contrasting results from the Georgia, Florida, Virginia, and Oklahoma studies highlight the critical role of soils in understanding pine plantation responses to drought combined with fertilization in the Southeast USA. The soil in the Georgia site is a very deep (>3 m) and well drained Kanhapludult with

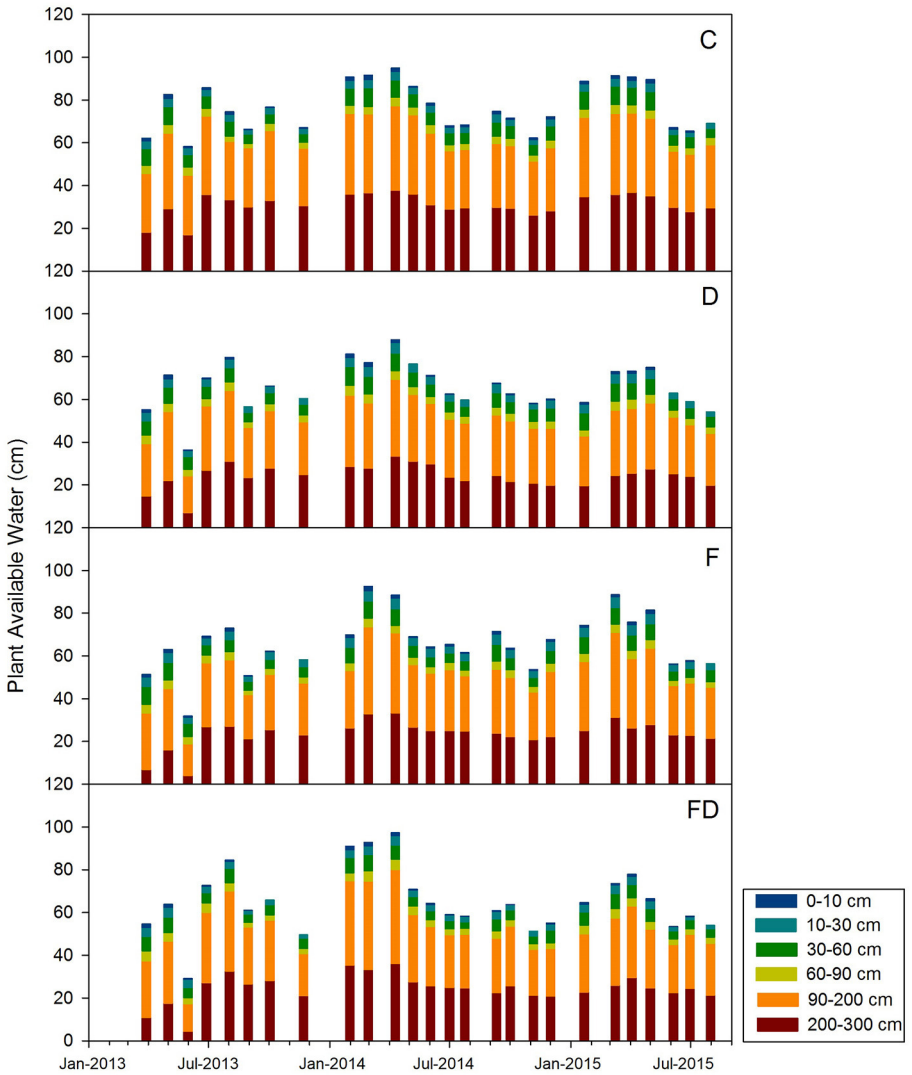

FIGURE 7 | Seasonal trends in plant available water for control (C), fertilization (F), throughfall reduction (D) and combined treatment of FD for March 2013 to July 2015. Stacked bars represent plant available water storage of 0–0.1, 0.1–0.3, 0.3–0.6, 0.6–0.9, 0.9–2.0, and 2.0–3.0 m.

>30% clay from 0.10–2.5 m. These clays are accessible to plants (i.e., rootable) and at saturation may contain up to 0.8 m of PAW. Although at this site, after 3 years of exclusion some impacts on growth were evident (Samuelson et al., 2018). In Florida, soils are a complex of Spodosols and Alfisols with all being somewhat poorly drained and possessing a thick cap of fine sand (Qi et al., 2018b). All these Florida soils, however, also possess a high water table. As such, outside of consecutive years of severe drought we would expect little water limitation at these sites and no impacts on growth were evident (Wightman et al., 2016). At the Virginia site soil is a Hapludult with a silt loam overlying a silty clay loam subsoil but is shallow (~1.5 m) to a paralithic contact (i.e., weathered rock). Soils at the Virginia site are limited in both the depth of rooting and the soil moisture storage capacity. Stands at this site had lower tree densities then the other locations and, although no treatment effects on growth were measured stand productivity was lower at this location (Ward et al., 2015; Bracho et al., 2018). Finally, in Oklahoma, soils are a deep, well-drained Paleudult, although are bisequel such that at ~80 cm the subsoil texture and structure changes, which may limit rooting depth in this younger aged stand. Oklahoma is also the western edge of the range of loblolly pine in the USA experiencing higher growing season temperatures and vapor pressure deficits than the rest of the southeastern USA creating a region more apt to experience water stress. Throughfall exclusion reduced growth at this location (Maggard et al., 2017). Overall, the soil conditions at these four sites provide unique rooting environments and supplies of PAW, thus different reactions to throughfall reduction x fertilization should be expected.

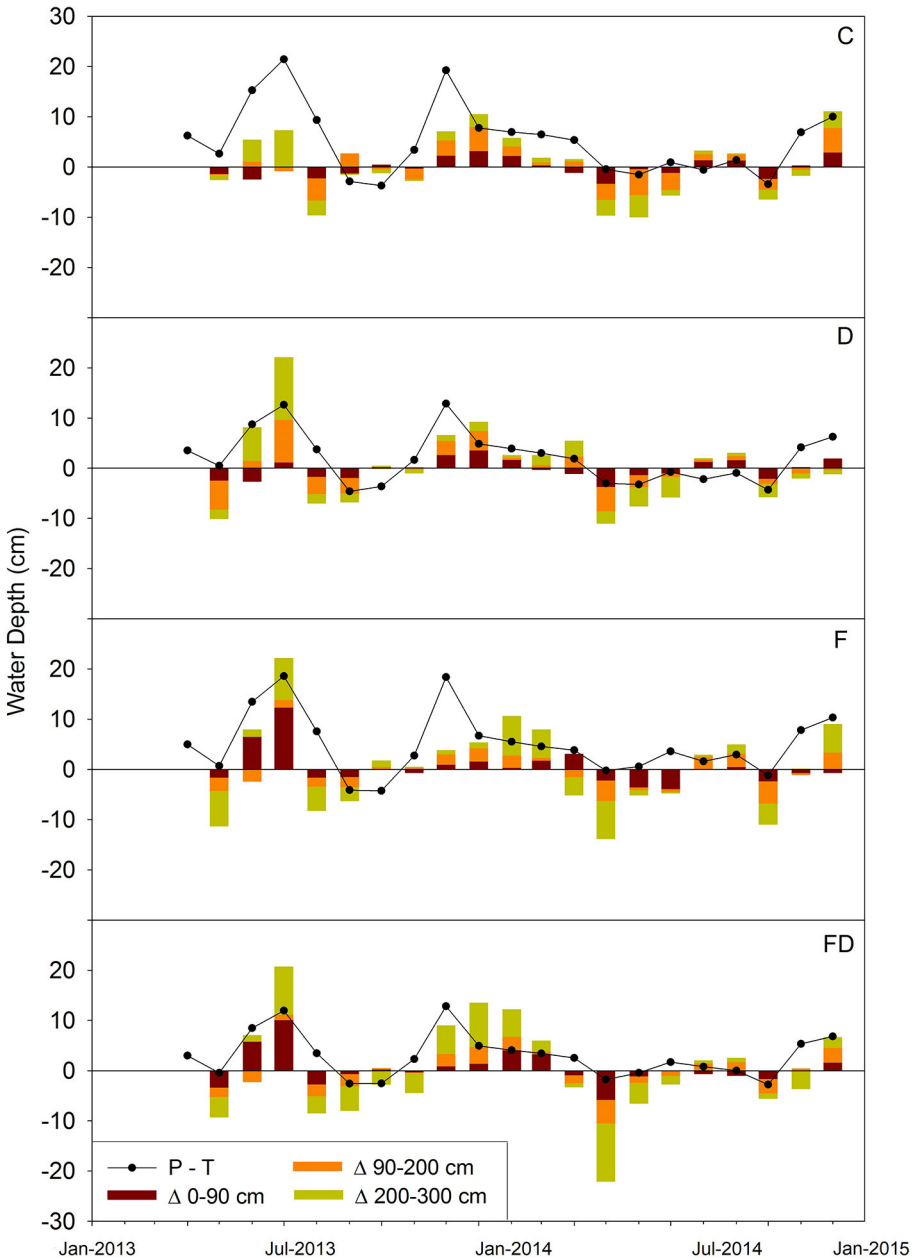

FIGURE 8 | Water mass balance for April 2013 to December 2014. Solid lines are water depth of precipitation—transpiration (P-T). Stacked bars are plant available water storage change by depth. Error bars representing ±1 SE were too small to show ($n = 4$). Treatments are control (C), fertilization (F), throughfall reduction (D), and combined treatment of FD.

The ability of pine stands at the Georgia site to sustain transpiration despite decreased water input (Bartkowiak et al., 2015) may have trickledown effects on other key ecosystem services such as providing a stable water source under a future drier climate (Sun and Liu, 2013). The highest observed transpiration across all treatments was ∼700 mm/year (**Figure 3**), while the 30-year average precipitation is ∼1,120 mm (www.ncdc.noaa.gov). Assuming 30% precipitation reduction, drainage or water yield might decline from 420 to 80 mm impacting drainage to groundwater recharge or limiting stream flows.

The uptake of deep soil water by the root system has been indicated to be sufficient to maintain transpiration in several other forest ecosystems, including a temperate Eucalyptus forest, a tropical wet/dry savanna in Australia (Leuning et al., 2005), scrub oak and pine flatwoods ecosystems in Florida (Bracho et al., 2008), and Amazonian evergreen forests and

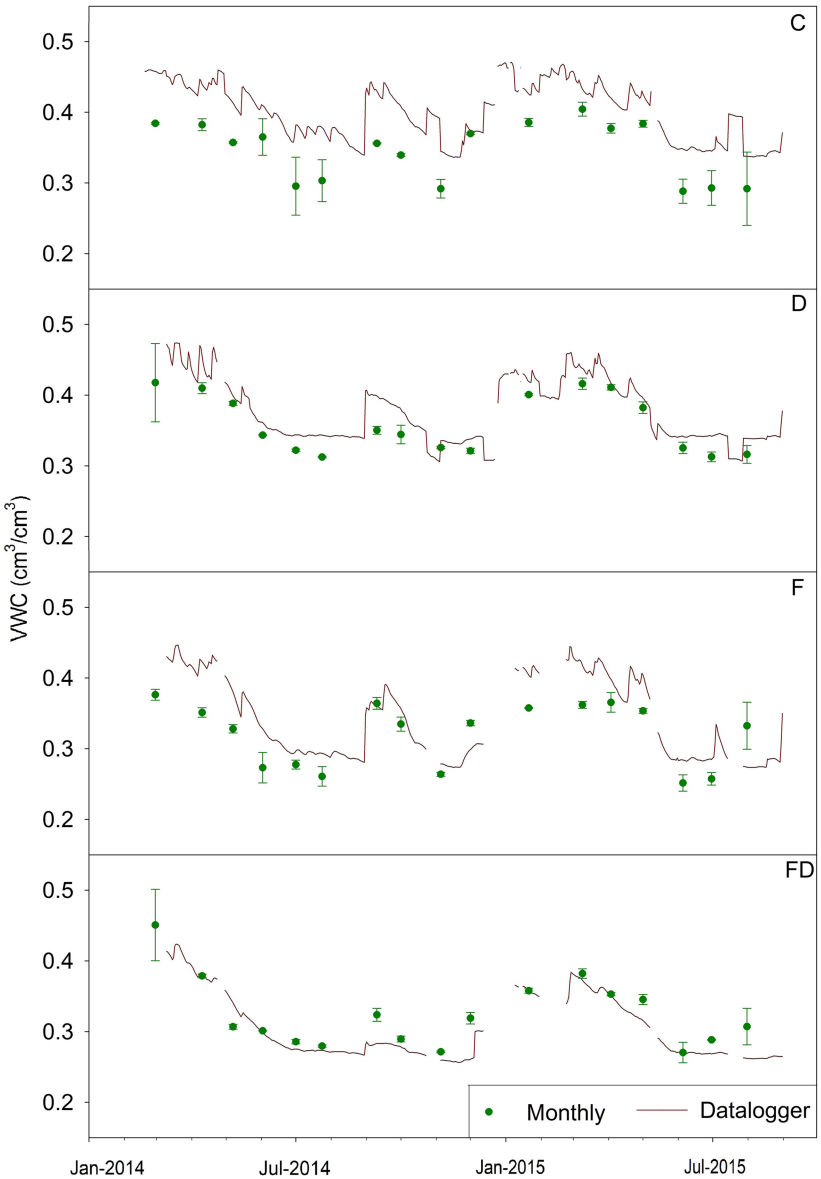

FIGURE 9 | Average daily soil volumetric water content (VWC) at 0.6 m based on 30-min readings of soil moisture probes (red line) and monthly point samples of VWC (mean ± 1 SE) ($n = 4$). Treatments are control (C), fertilization (F), throughfall reduction (D), and combined treatment of FD.

nearby pasture ecosystems (Nepstad et al., 1994; Markewitz et al., 2010). The results from this current research specifically demonstrate the importance of deep soil water in maintaining transpiration in loblolly pine plantations on deep clay rich Ultisols in the Southeast USA, especially in the face of a changing climate.

CONCLUSION

Throughfall reduction and fertilization both lowered soil moisture for all depths (0–3 m) and the combined treatment yielded lower soil moisture than either treatment alone. Even with ∼30% throughfall reduction, soils of all depths were rarely depleted of plant available water, with the exception of the top 10 cm of soil during the growing season. During the months that transpiration exceeded precipitation (i.e., when plant root uptake is depleting plant available water in soil), soil below 0.9 m always contributed to the observed change in plant available water storage. Under throughfall reduction treatment, soil below 0.9 m consistently accounted for more than half of the change in plant available water storage. In this 3 m deep, clay rich Piedmont soil under ∼30% throughfall reduction, soil water storage was able to satisfy plant demand for transpiration. Within Southeast USA loblolly pine plantations, deep soil water (>0.9 m) will be important in maintaining transpiration on deep, clay rich Ultisols.

DATA AVAILABILITY STATEMENT

Soil volumetric water content data can be found in **Supplementary Material**. Other datasets generated for this study are available on request to the corresponding author.

AUTHOR CONTRIBUTIONS

JQ and DM led the research design and implementation, analysis, and manuscript writing. MM contributed to the research implementation and manuscript writing. LS and EW contributed to the research design and manuscript writing.

FUNDING

This research was supported by the Pine Integrated Network: Education, Mitigation, and Adaptation project (PINEMAP) funded by the United States Department of Agriculture National Institute of Food and Agriculture Award #2011-68002-30185.

ACKNOWLEDGMENTS

The authors would like to thank Madison Akers, Dr. Lawrence Morris, and Dr. Robert Teskey for their intellectual and labor input. Thanks to Plum Creek Timber Co. for providing property access.

SUPPLEMENTARY MATERIAL

The Supplementary Material for this article can be found online at: https://www.frontiersin.org/articles/10.3389/ffgc.2019.00093/full#supplementary-material

REFERENCES

Abrahamson, D. A., Dougherty, P. M., and Zarnoch, S. J. (1998). Hydrological components of a young loblolly pine plantation on a sandy soil with estimates of water use and loss. *Water Resour. Res.* 34, 3503–3513. doi: 10.1029/98WR02363

Bartkowiak, S. M., Samuelson, L. J., McGuire, M. A., and Teskey, R. O. (2015). Fertilization increases sensitivity of canopy stomatal conductance and transpiration to throughfall reduction in an 8-year-old loblolly pine plantation. *For. Ecol. Manag.* 354, 87–96. doi: 10.1016/j.foreco.2015.06.033

Belk, E. L., Markewitz, D., Rasmussen, T. C., Maklouf Carvalho, E. J., Nepstad, D. C., and Davidson, E. A. (2007). Modeling the effects of throughfall reduction on soil water content in a Brazilian Oxisol under a moist tropical forest. *Water Resour. Res.* 43:14. doi: 10.1029/2006WR005493

Bell, D. M., Ward, E. J., Oishi, A. C., Oren, R., Flikkema, P. G., and Clarke, J. S. (2015). A state-space modeling approach to estimating canopy conductance and associated uncertainties from sap flux density data. *Tree Physiol.* 35, 792–802. doi: 10.1093/treephys/tpv041

Borken, W., and Matzner, E. (2009). Reappraisal of drying and wetting effects on C and N mineralization and fluxes in soils. *Glob. Change Biol.* 15, 808–824. doi: 10.1111/j.1365-2486.2008.01681.x

Bracho, R., Powell, T. L., Dore, S., Li, J., Hinkle, C. R., and Drake, B. G. (2008). Environmental and biological controls on water and energy exchange in Florida scrub oak and pine flatwoods ecosystems. *J. Geophys. Res. Biogeosci.* 113:G02004. doi: 10.1029/2007JG000469

Bracho, R., Vogel, J. G., Will, R. E., Noormets, A., Samuelson, L. J., Jokela, E. J., et al. (2018). Carbon accumulation in loblolly pine plantations is increased by fertilization across a soil moisture availability gradient. *Forest Ecol. Manag.* 424, 39–52. doi: 10.1016/j.foreco.2018.04.029

Bremner, J. M. (1996). Nitrogen - total. Methods of Soil Analysis Part *3—Chem. Methods sssabookseries*, 1085–1121.

Bryant, M. L., Bhat, S., and Jacobs, J. M. (2005). Measurements and modeling of throughfall variability for five forest communities in the southeastern US. *J. Hydrol.* 312, 95–108. doi: 10.1016/j.jhydrol.2005.02.012

Collins, M., Knutti, R., Arblaster, J., Dufresne, J.-L., Fichefet, T., Friedlingstein, P., Gao, X., et al. (2013). "Long-term climate change: projections, commitments and irreversibility," in *Climate Change 2013: The Physical Science Basis. Contribution of Working Group I to the Fifth Assessment Report of the Intergovernmental Panel on Climate Change*, eds T. F. Stocker, D. Qin, G.-K. Plattner, M. Tignor, S. K. Allen, J. Boschung, et al. (Cambridge; New York, NY: Cambridge University Press), 1029–1136.

Domec, J. C., Sun, G., Noormets, A., Gavazzi, M. J., Treasure, E. A., Cohen, E., et al. (2012). A comparison of three methods to estimate evapotranspiration in two contrasting loblolly pine plantations: age-related changes in water use and drought sensitivity of evapotranspiration components. *For. Sci.* 58, 497–512. doi: 10.5849/forsci.11-051

Evett, S. R., and Ruthardt, B. B. (2005). *A primer on TDR probe construction*. Agricultural Research Service, United States Department of Agriculture. Available online at: http://www.cprl.ars.usda.gov/TDR/MAKE_TDR_PRB.PDF.

Fensham, R. J., and Fairfax, R. J. (2007). Drought-related tree death of savanna eucalypts: species susceptibility, soil conditions and root architecture. *J. Veg. Sci.* 18, 71–80. doi: 10.1111/j.1654-1103.2007.tb02517.x

Fox, T. R., Jokela, E. J., and Allen, H. L. (2007). The development of pine plantation silviculture in the southern United States. *J. For.* 105, 337–347. doi: 10.1093/jof/105.7.337

Gee, G. W., and Or, D. (2002). "2.4 Particle-size analysis," in *Methods of Soil Analysis, Part 4, Physical Methods, SSSA Book Series 5*, eds J. H. Dane and G. C. Topp (Madison, WI: Soil Science Society of America), 255–293.

Goldstein, G., Bucci, S. J., and Scholz, F. G. (2013). Why do trees adjust water relations and hydraulic architecture in response to nutrient availability? *Tree Physiol.* 33, 238–240. doi: 10.1093/treephys/tpt007

Greco, R., and Guida, A. (2008). Field measurements of topsoil moisture profiles by vertical TDR probes. *J. Hydrol.* 348, 442–451. doi: 10.1016/j.jhydrol.2007.10.013

Hanson, P. J., Todd, D. E., Huston, M. A., Joslin, J. D., Croker, J. L., and Augé, R. M. (1998). *Description and Field Performance of the Walker Branch Throughfall Displacement Experiment: 1993–1996 (No. ORNL/TM-13586)*. Oak Ridge National Lab., Environmental Sciences Div., Tennessee, United States.

Harper, R. J., and Tibbett, M. (2013). The hidden organic carbon in deep mineral soils. *Plant Soil* 368, 641–648. doi: 10.1007/s11104-013-1600-9

Jian, S., Zhao, C., Fang, S., and Yu, K. (2014). Characteristics of Caragana korshinskii and Hippophae rhamnoides stemflow and their significance in soil moisture enhancement in Loess Plateau, China. *J. Arid Land* 6, 105–116. doi: 10.1007/s40333-013-0189-4

Jokela, E. J., Allen, H. L., and McFee, W. W. (1991). Fertilization of southern pines at establishment. *For. Regen. Man.* 36, 263–277. doi: 10.1007/978-94-011-3800-0_14

Kunkel, K. E., Stevens, L. E., Stevens, S. E., Sun, L., Janssen, E., Wuebbles, D., et al. (2013). Regional Climate Trends and Scenarios for the U.S. National Climate Assessment: Part 2. Climate of the Southeast U.S. NOAA Technical Report 142-2, National Oceanic and Atmospheric Administration, National Environmental Satellite, Data, and Information Service, Washington DC.

Kyle, K. H., Andrews, L. J., Fox, T. R., Aust, W. M., Burger, J. A., and Hansen, G. H. (2005). Long-term effects of drainage, bedding, and fertilization on growth of loblolly pine (*Pinus taeda* L.) in the coastal plain of Virginia. *South. J. Appl. For.* 29, 205–214. doi: 10.1093/sjaf/29.4.205

Leuning, R., Cleugh, H. A., Zegelin, S. J., and Hughes, D. (2005). Carbon and water fluxes over a temperate Eucalyptus forest and a tropical wet/dry savanna in Australia: measurements and comparison with MODIS remote sensing estimates. *Agric. For. Meteorol.* 129, 151–173. doi: 10.1016/j.agrformet.2004.12.004

Levia, D. F., and Germer, S. (2015). A review of stemflow generation dynamics and stemflow-environment interactions in forests and shrublands. *Rev. Geophys.* 53, 673–714. doi: 10.1002/2015RG000479

Maeght, J. L., Rewald, B., and Pierret, A. (2013). How to study deep roots - and why it matters. *Front. Plant Sci.* 4, 1–14. doi: 10.3389/fpls.2013.00299

Maggard, A. O., Will, R. E., Wilson, D. S., Meek, C. R., and Vogel, J. G. (2016). Fertilization reduced stomatal conductance but not photosynthesis of Pinus taeda which compensated for lower water availability in regards to growth. *For. Ecol. Manag.* 381, 37–47. doi: 10.1016/j.foreco.2016.08.046

Maggard, A. O., Will, R. E., Wilson, D. S., Meek, C. R., and Vogel, J. G. (2017). Fertilization can compensate for decreased water availability by increasing the efficiency of stem volume production per unit of leaf area for loblolly pine (*Pinus taeda*) stands. *Can. J. For. Res.* 47, 445–457. doi: 10.1139/cjfr-2016-0422

Markewitz, D., Devine, S., Davidson, E. A., Brando, P., and Nepstad, D. C. (2010). Soil moisture depletion under simulated drought in the Amazon: impacts on deep root uptake. *New Phytol.* 187, 592–607. doi: 10.1111/j.1469-8137.2010.03391.x

McNulty, S. G., Vose, J. M., and Swank, W. T. (1996). Loblolly pine hydrology and productivity across the southern United States. *For. Ecol. Manag.* 86, 241–251. doi: 10.1016/S0378-1127(96)03744-9

Meehl, G. A., Tebaldi, C., Teng, H., Peterson, T. C., (2007). Current future U.S. weather extremes El Nino. *Geophys. Res. Lett.* 34. doi: 10.1029/2007GL031027

Nepstad, D. C., Decarvalho, C. R., Davidson, E. A., Jipp, P. H., Lefebvre, P. A., Negreiros, G. H., et al. (1994). The role of deep roots in the hydrological and carbon cycles of Amazonian forests and pastures. *Nature* 372, 666–669. doi: 10.1038/372666a0

Nepstad, D. C., Moutinho, P., Dias-Filho, M. B., Davidson, E. A., Cardinot, G., Markewitz, D., et al. (2002). The effects of rainfall exclusion on canopy processes and biogeochemistry of an Amazon forest. *J. Geophys. Res.* 107, 53-1–53-18. doi: 10.1029/2001JD000360

Padilla, F. M., and Pugnaire, F. I. (2007). Rooting depth and soil moisture control Mediterranean woody seedling survival during drought. *Funct. Ecol.* 21, 489–495. doi: 10.1111/j.1365-2435.2007.01267.x

Qi, J., Markewitz, D., Foroughi, M., Jokela, E., Strahm, B., and Vogel, J. (2018b). Drying-wetting cycles: effect on deep soil carbon. *Soil Syst.* 2:3. doi: 10.3390/soils2010003

Qi,. J., Markewitz, D., and Radcliffe, D. (2018a). Modelling the effect of changing precipitation inputs on deep soil water utilization. *Hydrol. Processes* 32, 672–686. doi: 10.1002/hyp.11452

Radcliffe, D. E., and Šimunek, J. (2010). *Soil Physics With HYDRUS: Modeling and Applications*. Boca Raton, FL: CRC Press.

Samuelson, L. J., Kane, M. B., Markewitz, D., Teskey, R. O., Akers, M. K., Stokes, T. A., et al. (2018). Fertilization increased leaf water use efficiency and growth of Pinus taeda subjected to five years of throughfall reduction. *Can. J. For. Res.* 48, 227–236. doi: 10.1139/cjfr-2017-0357

Samuelson, L. J., Pell, C. J., Stokes, T. A., Bartkowiak, S. M., Akers, M. K., Kane, M., et al. (2014). Two-year throughfall and fertilization effects on leaf physiology and growth of loblolly pine in the Georgia Piedmont. *For. Ecol. Manag.* 330, 29–37. doi: 10.1016/j.foreco.2014.06.030

Schenk, H. J., and Jackson, R. B. (2002). The global biogeography of roots. *Ecol. Monographs* 72, 311–328. doi: 10.1890/0012-9615(2002)072[0311:TGBOR]2.0.CO;2

Schwärzel, K., Ebermann, S., and Schalling, N. (2012). Evidence of double-funneling effect of beech trees by visualization of flow pathways using dye tracer. *J. Hydrol.* 470, 184–192. doi: 10.1016/j.jhydrol.2012.08.048

Sun, G. (2013). "Impacts of climate change and variability on water resources in the Southeast USA," in *Climate of the Southeast United States: Variability, Change, Impacts, and Vulnerability*, eds K. T. Ingram, K. Dow, L. Carter, and J. Anderson (Washington, DC: Island Press/Center for Resource Economics), 210–236.

Sun, G., and Liu, Y. (2013). "Forest influences on climate and water resources at the landscape to regional scale," in *Landscape Ecology for Sustainable Environment and Culture* (Dordrecht: Springer), 309–334.

Swank, W. T. (1972). Interception loss in loblolly pine stands of the South Carolina Piedmont. *J. Soil Water Conserv.* 27, 160–164.

Tang, Z. M., Sayer, M. A., Chambers, J. L., and Barnett, J. P. (2004). Interactive effects of fertilization and throughfall exclusion on the physiological responses and whole-tree carbon uptake of mature loblolly pine. *Can. J. Bot. Rev.* 82, 850–861. doi: 10.1139/b04-064

Teskey, R. O., and Sheriff, D. W. (1996). Water use by *Pinus radiata* trees in a plantation. *Tree Physiol.* 16, 273–279. doi: 10.1093/treephys/16.1-2.273

Thomas, G. W. (1996). "Soil pH and soil acidity," *Methods of Soil Analysis Part 3: Chemical Methods, SSSA Book Series 5*, ed Sparks, D. L. (Madison, WI: Soil Science Society of America), 475–490.

Torreano, S. J., and Morris, L. A. (1998). Loblolly pine root growth and distribution under water stress. *Soil Sci. Soc. Am. J.* 62, 818–827. doi: 10.2136/sssaj1998.03615995006200030040x

Van Genuchten, M. T. (1980). A closed form equation for predicting the hydraulic conductivity of unsaturated soils. *Soil Sci. Soc. Am. J.* 44, 892–898. doi: 10.2136/sssaj1980.03615995004400050002x

Walsh, J., Wuebbles, D., Hayhoe, K., Kossin, J., Kunkel, K., Stephens, G., et al. (2014). "Ch. 2: Our changing climate" in *Climate Change Impacts in the United States: The Third National Climate Assessment*, J. M. Melillo, T. C. Richmond, and G. W. Yohe (Washington, DC: U.S. Global Change Research Program), 19–67.

Ward, E. J. J.-,Domec, C., Laviner, M. A., Fox, T. R., Sun, G., McNulty, S., King, J., et al. (2015). Fertilization intensifies drought stress: water use and stomatal conductance of *Pinus taeda* in a midrotation fertilization and throughfall reduction experiment. *For. Ecol. Manag.* 355, 72–82. doi: 10.1016/j.foreco.2015.04.009

Wertin, T. M., McGuire, M. A., and Teskey, R. O. (2010). The influence of elevated temperature, elevated atmospheric CO_2 concentration and water stress on net photosynthesis of loblolly pine (*Pinus taeda* L.) at northern, central and southern sites in its native range. *Glob. Change Biol.* 16, 2089–2103. doi: 10.1111/j.1365-2486.2009.02053.x

Wightman, M. G., Martin, T. A., Gonzalez-Benecke, C. A., Jokela, E. J., Cropper, W. P., and Ward, E. J. Jr. (2016). Loblolly pine productivity and water relations in response to throughfall reduction and fertilizer application on a poorly drained site in Northern Florida. *Forests* 7:214. doi: 10.3390/f7100214

Will, R. E., Fox, T., Akers, M., Domec, J. C., Gonzalez-Benecke, C., Jokela, E. J., et al. (2015). A range-wide experiment to investigate nutrient and soil moisture interactions in loblolly pine plantations. *Forests* 6, 2014–2028. doi: 10.3390/f6062014

Zarnoch, S. J., Abrahamson, D. A., and Dougherty, P. M. (2002). "Sampling throughfall and stemflow in young loblolly pine plantations," *Research Paper SRS-27*. Asheville, NC: US Department of Agriculture, Forest Service, Southern Research Station, 6.

Zimmermann, B., Zimmermann, A., Lark, R. M., and Elsenbeer, H. (2010). Sampling procedures for throughfall monitoring: a simulation study. *Water Resour. Res.* 46:1. doi: 10.1029/2009WR007776

Disclaimer: Any use of trade, firm, or product names is for descriptive purposes only and does not imply endorsement by the U.S. Government.

Conflict of Interest: The authors declare that the research was conducted in the absence of any commercial or financial relationships that could be construed as a potential conflict of interest.

frontiers in Forests and Global Change

ORIGINAL RESEARCH
published: 26 February 2020
doi: 10.3389/ffgc.2020.00017

Climate Change May Increase the Drought Stress of Mesophytic Trees Downslope With Ongoing Forest Mesophication Under a History of Fire Suppression

Taehee Hwang[1], Lawrence E. Band[2,3], Chelcy F. Miniat[4], James M. Vose[5], Jennifer D. Knoepp[4], Conghe Song[6] and Paul V. Bolstad[7]*

[1] Department of Geography, Indiana University Bloomington, Bloomington, IN, United States, [2] Department of Environmental Science, University of Virginia, Charlottesville, VA, United States, [3] Department of Engineering Systems and Environment, University of Virginia, Charlottesville, VA, United States, [4] Coweeta Hydrologic Laboratory, Southern Research Station, U.S. Forest Service, Otto, NC, United States, [5] Center for Integrated Forest Science, Southern Research Station, U.S. Forest Service, Raleigh, NC, United States, [6] Department of Geography, The University of North Carolina at Chapel Hill, Chapel Hill, NC, United States, [7] Department of Forest Resources, University of Minnesota, Saint Paul, MN, United States

OPEN ACCESS

Edited by:
Anthony Parolari, Marquette University, United States

Reviewed by:
Phong V. V. Le, Vietnam National University, Vietnam
John T. Van Stan, Georgia Southern University, United States

***Correspondence:**
Taehee Hwang
taehee@indiana.edu

Specialty section:
This article was submitted to Forest Hydrology, a section of the journal Frontiers in Forests and Global Change

Received: *28 October 2019*
Accepted: *04 February 2020*
Published: *26 February 2020*

Citation:
Hwang T, Band LE, Miniat CF, Vose JM, Knoepp JD, Song C and Bolstad PV (2020) Climate Change May Increase the Drought Stress of Mesophytic Trees Downslope With Ongoing Forest Mesophication Under a History of Fire Suppression. Front. For. Glob. Change 3:17. doi: 10.3389/ffgc.2020.00017

In mountainous headwater catchments, downslope flow of subsurface water could buffer downslope forest communities from soil moisture stress during drought. Here we investigated changes in landscape-scale vegetation patterns at five forested headwater catchments in the Coweeta Hydrologic Laboratory in the southern Appalachians. We used a *ca.* 30-year Landsat Thematic Mapper (TM) image record of normalized difference vegetation index (NDVI), spanning a period of recorded warming since the mid-1970. We then, related spatial and temporal canopy patterns to seasonal water balance, streamflow recession behavior, and low flow dynamics from the long-term hydrologic records. All hydrologic metrics indicated increasing evapotranspiration, decreasing streamflow given precipitation, and potentially decreasing downslope subsidy at the watershed scale over time, especially during low-flow periods. Contrary to expectations, leaf area index (LAI) and basal area increased more upslope compared to downslope over time, coincident with warming. Trends in the ratio of NDVI in upslope and downslope topographic positions were also supported by long-term tree basal area increment, litterfall, and sap flux data in one of the reference watersheds. Mesophytic trees downslope appeared to respond more to frequent droughts and experience lower growth than xerophytic trees upslope, closely mediated by the isohydric/anisohydric continuum along hydrologic flow paths. Considering ongoing forest "mesophication" under a history of fire suppression across the eastern United States deciduous forests, this study suggests that mesophytic trees downslope may be more vulnerable than xerophytic trees upslope under ongoing climate change due to an apparent dependence on upslope water subsidy.

Keywords: forest mesophication, fire suppression, isohydricity and anisohydricity, forest hydrology, drought

INTRODUCTION

Climate change is expected to bring warmer temperatures and increased hydrologic extremes including more frequent droughts and longer inter-storm periods (e.g., Seager et al., 2009; Pachauri et al., 2014). Although warming-induced lengthening of the growing season and increased atmospheric CO_2 concentrations have generally facilitated vegetation growth (e.g., Keeling et al., 1996; Myneni et al., 1997; Keenan et al., 2014), enhanced hydroclimate variability has often led to increased periods of plant water stress (Anderegg et al., 2012), species-specific drought responses (Clark et al., 2011; Brzostek et al., 2014), xylem cavitation (Hoffmann et al., 2011), and subsequent widespread tree mortality (Adams et al., 2009; Klos et al., 2009; McDowell and Allen, 2015). For these reasons, water availability has become more widely recognized as a key driver of ecosystem response to climate change than before, in terms of carbon cycling (van der Molen et al., 2011), vegetation water use (Wullschleger and Hanson, 2006), and species distributions (Stephenson, 1990; Crimmins et al., 2011; VanDerWal et al., 2013) across different scales.

In addition to regional climate variability, topography provides variation in hydroclimate through topoclimate variation, lateral soil water redistribution, and differences in soil depth and storage. The interaction of climate and topography supports a wide range of microclimate and soil moisture conditions for both xeric and mesic tree species (Dobrowski, 2011; McLaughlin et al., 2017), and promotes high productivity and biodiversity especially in mountain forest ecosystems (Davis and Goetz, 1990; Beckage and Clark, 2003; Emanuel et al., 2011; Clark et al., 2014). In mountainous forested catchments, water consumption by vegetation downslope (green water) usually depends on water flow generation from upslope (blue water). Hillslope-riparian-stream connectivity by dominant subsurface hydrologic flow processes plays a key role in runoff generation (Jencso et al., 2009; Detty and McGuire, 2010; McGuire and McDonnell, 2010) and soil moisture organization at the watershed scale (Western et al., 1999; Ali and Roy, 2010). Downslope flows can mitigate the impact of droughts in convergent topographic areas (e.g., Hawthorne and Miniat, 2018). Therefore, topography-mediated soil moisture conditions provide an important control on the patterns of forest water use (Tromp-van Meerveld and McDonnell, 2006; Mackay et al., 2010), periodic water stress (Vicente-Serrano et al., 2008; Ford et al., 2011), tree growth (Clark et al., 2014; Elliott et al., 2015; Martin-Benito et al., 2015), mortality (Berdanier and Clark, 2016; Tai et al., 2017), and species distribution (Day et al., 1988; Crimmins et al., 2011). It is therefore important to understand climate-vegetation-topography-hydrology interactions and feedbacks to predict landscape-scale responses of forest ecosystems to ongoing climate change (e.g., Hoylman et al., 2018).

Forest vegetation often adjusts leaf area amount and duration in response to water and nutrient availability (e.g., Nemani and Running, 1989), which is mediated by lateral hydrologic flows along topographic gradients (Hwang et al., 2009). Hydrologic partitioning between localized water use and drainage often influences emergent vegetation dynamics in space and time (Thompson et al., 2011), which can be used as a simple diagnostic to infer underlying water balance patterns along hydrologic flow paths (Brooks et al., 2011; Voepel et al., 2011; Hwang et al., 2012; Hoylman et al., 2018). Furthermore, close interactions between hydroclimate variability and vegetation dynamics (e.g., large-scale mortality, growing season duration, etc.) have been demonstrated by measurable shifts in seasonal streamflow dynamics and forest water yield at the watershed scale (Adams et al., 2012; Bearup et al., 2014; Hwang et al., 2014, 2018; Creed et al., 2015; Kim et al., 2017, 2018). However, there have been few studies on feedbacks between climate change, lateral soil moisture distribution, and long-term forest canopy patterns at the watershed scale.

Following decades of active fire suppression in the eastern United States, fire-intolerant, mesophytic tree species (e.g., red maple and tulip poplar) have increased in southern Appalachian forests compared to fire-tolerant, xerophytic oak and hickory, often called as forest "mesophication" (Nowacki and Abrams, 2008, 2015). These long-term forest mesophication trends also have a great implication in understanding forest responses to frequent droughts under climate change. Red maple and tulip poplar typically exhibit as isohydric stomatal responses to declining soil water potentials, while oaks are typically anisohydric (Choat et al., 2012; Klein, 2014; Roman et al., 2015; Hwang et al., 2017). Anisohydric trees allow leaf water potential to drop as soil dries, so they maintain greater stomatal conductance to continue gas exchange under moderate droughts (Martínez-Vilalta et al., 2014). In contrast, trees that do not allow leaf water potential to drop as soil dries are known as isohydric, which close stomata to maintain a stable leaf water potential at the expense of CO_2 uptake. For this reason, forest mesophication under fire suppression has been suggested to lead to greater sensitivity to frequent droughts under changing climate and reduced C sink across the eastern deciduous forests (Brzostek et al., 2014; Roman et al., 2015). However, this argument does not sufficiently consider changes in water balance patterns along hillslope gradients although mesophytic trees are usually found more at downslope topographic positions (Day et al., 1988).

Working in humid, mountainous, forest catchments, we hypothesize that climate-vegetation-topography-hydrology interactions will manifest in the following ways over time with warming:

(1) Increasing local evapotranspiration and decreasing downslope hydrologic flow at the watershed scale,
(2) Therefore, more frequently occurring drought stress for mesophytic trees at downslope topographic positions mediated by isohydric/anisohydric transition, and
(3) Lower growth of vegetation downslope than upslope due to potentially decreasing downslope subsidy from upslope ecosystems.

To test these hypotheses, we combined several long-term data sets to examine the role of topography, lateral hydrologic flows, and localized water use and growth at

forested headwater catchments in the southern Appalachian Mountains, United States.

MATERIALS AND METHODS

Study Site

This research was conducted at the U.S. Forest Service, Coweeta Hydrologic Laboratory in the southern Appalachian Mountains, North Carolina, United States (**Figure 1**), also a part of Long-Term Ecological Research (LTER) network. This area is characterized by steep topography with elevation ranging from 660 to 1590 m, providing highly variable yet distinct hydroclimate regimes within a relatively small area (about 20 km^2). The climate is classified as marine, humid temperate. Long-term mean annual temperature is 12.6°C, and annual precipitation increases about 5% with each 100-m elevation increase (Swift et al., 1988); 1870 mm at 685 m elevation to 2500 mm at 1430 m. Precipitation is relatively evenly distributed throughout the year, characterized by small, low-intensity rainfall events with less-than 2% falling as snow (Laseter et al., 2012), but also subject to periodic tropical storms in late summer and fall. The dominant canopy tree species are *Quercus* spp. (oaks), *Carya* spp. (hickory), *Nyssa sylvatica* (black gum), *Acer rubrum* (red maple), and *Liriodendron tulipifera* (yellow poplar). Northern hardwood forests occur at the highest elevations (about 1200 m above), and are dominated by *Betula alleghaniensis* (yellow birch), *Tilia heterophylla* (basswood), *Aesculus flava* (yellow buckeye), and *Acer saccharum* (sugar maple) (Day et al., 1988). At low elevations in the study site, isohydric trees (e.g., tulip poplar, birch, and maple) are common in downslope forest community, while trees that allow leaf water potential to drop as soil dries (anisohydric) are more dominant in upslope community (e.g., oaks) (**Supplementary Figure S8**).

Soils are relatively uniform, described as coarse sandyloam Inceptisols and Ultisols, typically residual with colluvial material in the coves, and areas of deeper, more organic rich soils in toe slope positions (Knoepp and Swank, 1998; Knoepp et al., 2018). Although the research was conducted at five reference watersheds (WS02, WS14, WS18, WS27, and WS36 - 3 low- and 2 high-elevation), due to limitations on data availability and access all five watersheds were used for remote sensing analyses; three watersheds for hydrologic analyses (WS14, WS18, and WS27); and one watershed (WS18) for detailed analyses of vegetation growth and sap flow (**Table 1**). The study watersheds are mostly composed of second succession forests (at least 90–110 years old). The age and stand dynamics reflect logging in the early 1900s, chestnut blight in the 1930s that eliminated most of the American chestnut (Vose and Elliott, 2016), and multiple droughts in the 1980s and 2000s that caused high mortality in

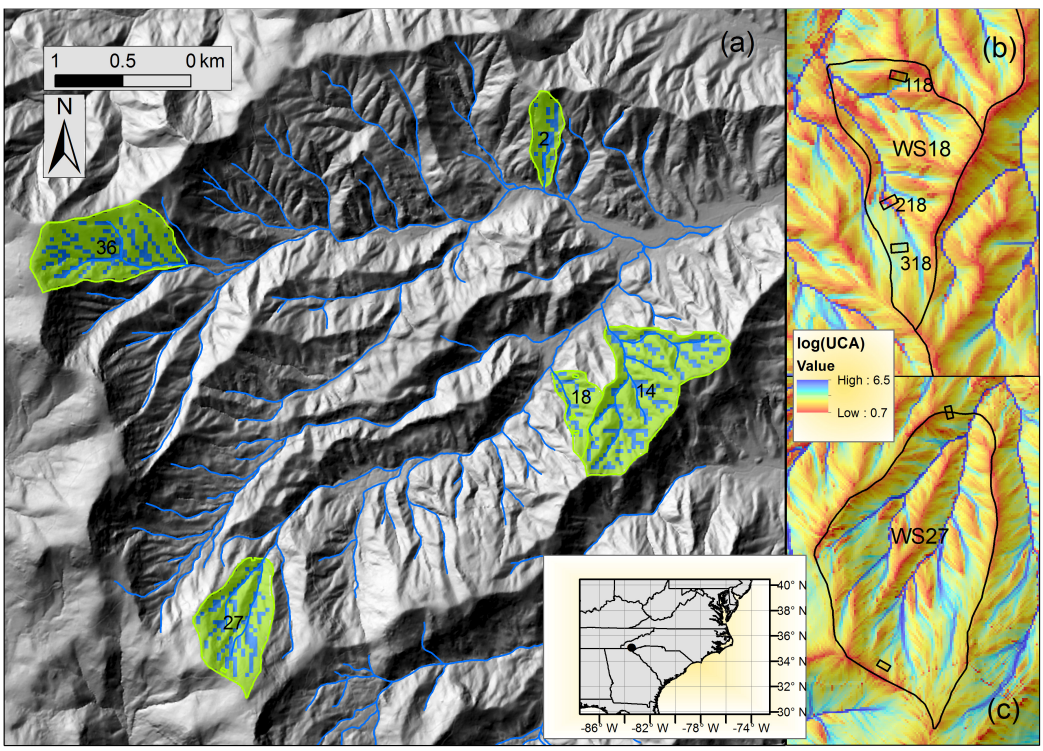

FIGURE 1 | (a) Five reference headwater catchments (WS02, WS14, WS18, WS27, and WS36) in the study site (Coweeta Hydrologic Lab., North Carolina, United States). Green and blue-colored regions represent the pixels classified as upslope and downslope at a 30-m Landsat scale at each catchment, based on the distribution of upslope contributing area (UCA). Detailed UCA maps were generated from the original LiDAR (6.1-m scale) for **(b)** WS18 and **(c)** WS27, calculated from a *D*-infinity method (Tarboton, 1997). Three 80 by 80 m gradient plots (SITE 118, 218, 318) are located in WS18. Detailed explanations of the gradient plots are available in **Supplementary Table S1**.

red oak group at middle elevations (Clinton et al., 2003). Long-term Forest Inventory and Analysis data showed consistent forest mesophication trends since 1930s with increasing the basal area compositions of maples and tulip poplar while decreasing oaks, across the unmanaged forests in the study site (Elliott and Vose, 2011) and at the two of study watersheds (WS14 and WS18) (Caldwell et al., 2016).

Long-Term Climate and Hydrologic Records

We used the long-term climate records at the base (CS01; RG06) and high-elevation (RG31) climate stations (**Supplementary Figure S1**) in the study site (Miniat et al., 2017). We used universal kriging with an elevation trend from seven rain gauges from 1991 to 1995 developing a long-term isohyet to scale daily precipitation over the terrain (Hwang et al., 2012). Three water balance based metrics were calculated from observed daily precipitation (P) and stream discharge (Q) records at three reference headwater catchments (WS14, WS18, and WS27; **Figure 1**) (Miniat et al., 2016): (1) evapotranspiration (ET estimated as $P - Q$), (2) runoff ratio (RR; Q/P), and (3) Horton index (HI; ET/W), which represents the ratio of evapotranspiration (ET) to catchment wetting (W) (Troch et al., 2009). Note that relatively wet condition of the study site without permanent snowpack actually minimizes the effect of dormant-season precipitation in these mass balanced based approach based on the vegetation year (see Figure 2 in Hwang et al., 2014). Catchment wetting (W; $P - S$) is the precipitation retained in the catchment and potentially available to vegetation, calculated by removing quick flow component (stormflow, S) from precipitation. HI has been suggested to remove the precipitation variation and better represent water available for vegetation use at the catchment scale (Brooks et al., 2011; Voepel et al., 2011). We used the Web-based Hydrograph Analysis Tool (Lim et al., 2005) to separate base flow from daily streamflow records using the two-parameter digital filtering method (Eckhardt, 2005). The three hydrologic metrics above were calculated during the peak growing-season period (June–August) annually from all available daily precipitation and streamflow data (**Table 1**). Note that the ET estimates implicitly include seasonal storage changes, and thus effectively represent dryness of watershed systems (Hwang et al., 2018).

We also performed a recession slope analysis from the long-term daily streamflow to characterize the recession behavior of hydrographs (Brutsaert and Nieber, 1977). The observed recession slopes ($-dQ/dt$) were plotted with the daily stream discharge (Q) using a power function (**Supplementary Figure S2**) as follows:

$$-\frac{dQ}{dt} = aQ^b$$

These two recession parameters (a and b) represent the steepness and non-linearity of the recession curve, reflecting hydraulic properties and connectivity of draining aquifers (Rupp and Selker, 2006b). We applied the recession slope analyses for days of decreasing flows without precipitation during the peak growing season. We also applied the recession analyses with 3-year moving windows to ensure a sufficient number of recession periods for the analyses. In this study, the "scaled-dt" recession slope analysis was used, which allows time intervals (dt) adjusted based on -dQ values (Rupp and Selker, 2006a). To characterize low flow regimes, we also employed the widely-used low-flow index, n-day m-year low flow ($_nQ_m$), defined as the lowest average flows that occur for a consecutive n-day period at the recurrence interval of m years (Smakhtin, 2001). We performed both Mann-Kendall and Spearman's rho tests with the null hypothesis of trend absence in all time-series data. We also adjusted the sample sizes when we found significant first-order positive autocorrelation ($p < 0.05$), based on Dawdy and Matalas (1964).

Landsat Thematic Mapper (TM) Dataset

To estimate long-term vegetation patterns at the watershed scale, we analyzed fifty-seven cloud-free summer Landsat Thematic Mapper (TM) images (June–August) at the five reference headwater catchments (WS02, WS14, WS18, WS27, and WS36;

TABLE 1 | Summary of five study headwater catchments and datasets used in this study.

Watershed ID	WS02	WS14	WS18	WS27	WS36
Topographic characteristics					
Area (ha)	13.1	62.4	12.3	39.8	48.7
Elevation (m)	856	878	823	1256	1289
Slope (degree)	27.2	25.7	28.1	28.5	30.5
Aspect	S	NW	NW	NE	SE
Mean downslope flowpath length (m)	129.0	90.9	141.4	146.4	189.3
Forest types	Oak-hickory mixed	Oak-hickory mixed	Oak-hickory mixed	Northern hardwoods	Northern hardwoods
Datasets					
Daily streamflow	NA	1937–2014	1947–2014	1972–2014	NA
Daily soil moisture*	NA	NA	1999–2014	1999–2014	NA
Daily canopy conductance*	NA	NA	2004–2006	NA	NA
Tree basal area (2-year interval)*	NA	NA	1998–2014	1998–2014	NA
Annual litterfall*	NA	NA	1992–2013	1992–2013	NA

Measured at three 80 m-by-80 m gradient plots were established in WS18 (SITE 118, 218, and 318; **Figure 1 and **Supplementary Figure S3**).*

Figure 1 and **Table 1**) between 1984 and 2011. Landsat TM, initially launched in 1984, provides a nearly three-decade multispectral image record, and was used to estimate changes in landscape vegetation pattern at a 30 m resolution. All images were standard level-1, terrain-corrected (L1T) products and checked manually for cloud contamination due to frequent rain events in the study site. A modified dark object subtraction (DOS) method with the effect of Rayleigh scattering was applied to correct atmospheric effects on surface reflectance (Song et al., 2001). Normalized Difference Vegetation Index (NDVI) was calculated as follows:

$$NDVI = \frac{R_{NIR} - R_{RED}}{R_{NIR} + R_{RED}}$$

where R_{NIR} and R_{RED} are near-infrared (NIR) and red band reflectance. NDVI values tend to be non-linearly correlated with leaf area index values (Nemani et al., 1993; Chen and Cihlar, 1996), also observed in the study site (see Figure 4 in Hwang et al., 2009). NDVI is closely correlated to various vegetation biophysical parameters (e.g., leaf area, aboveground biomass, etc.) across different ecosystems (Tucker, 1979; Asrar et al., 1984; Sellers, 1985), and effectively removes much of the multiplicative noise by illumination differences and topographic variation in complex terrain (Huete et al., 2002). Although NDVI is not a direct measure of ecosystem water use or carbon uptake, it is linearly related to the fraction of absorbed photosynthetically active radiation, and thus the energy input into the system (e.g., Song et al., 2015).

Characterization of Watershed-Scale Vegetation Dynamics

We used the NDVI data to estimate long-term vegetation dynamics at all reference (i.e., not harvested or manipulated since the 1920s) headwater catchments in the study site, located at different combinations of aspect and elevation (**Figure 1** and **Table 1**). We first calculated mean values of NDVI separately at upslope and downslope positions of each study watershed. Upslope and downslope positions were determined based on upslope contributing area (UCA) (Erskine et al., 2006). We calculated UCA from 6.1-m (20 ft) LiDAR elevation data with a *D*-infinity method (Whitebox Geospatial Analysis Tools)[1], allowing flow to be proportioned between two downslope pixels to the steepest topographic gradient under the assumption of the same hydraulic gradient (Tarboton, 1997). This UCA map was later aggregated to 30-m Landsat resolution, and the 75th percentile of the UCA distribution was applied to classify upslope and downslope pixels for each watershed (**Figure 1**).

Although the objective of atmospheric correction is to align multi-temporal images on the same radiometric scale, it is almost impossible to consider the full vertical profiles of atmospheric transmissivity in the study site as scene-based atmospheric correction cannot consider small-scale topoclimate variations in rugged terrain, often featured by mountain fogs and aerosol conditions (Song et al., 2001). Therefore, another spatial normalization was performed between upslope and downslope NDVI values at each watershed to effectively cancel out most of the remnant atmospheric effects assuming that atmospheric conditions between downslope and upslope within a catchment are not different. We calculated the ratio of normalized difference vegetation index (*NDVI*) between each catchment's downslope and upslope components ($NDVI_{downslope}/NDVI_{upslope}$) to characterize the vegetation patterns along the hydrologic flow paths as ratio values are less sensitive to inter-image differences in atmospheric corrections.

Long-Term Tree Basal Area and Leaf Litter Data

Long-term soil water content is a core dataset in the Coweeta Long-Term Ecological Research (LTER) program (Data ID 1046), measured in three 80-by-80 m gradient plots established along an elevation gradient in 1991. These plots are classified as upslope (SITE 118), midslope (SITE 318), and downslope (SITE 218) based on the topography in the field (**Figure 1**). Volumetric soil moisture was continuously measured every 15 min at two locations and two depths (0–30 cm and 30–60 cm) in these plots by time domain reflectometer (TDR) probes (CS615; Campbell Scientific, Logan, UT, United States) (Coweeta LTER Data ID 1023). The 60-cm depth of measurements is slightly less than the measured rooting depth in the study site (Hales et al., 2009). The cumulative distributions of long-term observed volumetric water content are consistent with classification of these plots as up-, down-, and midslope, as they show clear differences in soil moisture dynamics at shallow soils (0–60 cm) (**Supplementary Figure S7**). Note that SITE 318 (midslope) is generally classified as an upslope topographic position in the remote sensing analyses above (see **Figure 1**).

There are clear transitions in vegetation community types along these gradient plots, mixed oak/pine upslope, mixed oak/hickory at midslope, and cove hardwood species downslope (**Supplementary Table S1** and **Figure S8**), which represent three typical forest community types at low- to mid-elevation ranges in the study site (Day et al., 1988; Bolstad et al., 1998). At these three gradient plots, tree census was performed approximately every 2 years since 1991 in smaller sub-plots (40 by 20 m). A whole tree census within the plots has been conducted since 1998. Diameter at breast height (DBH) of all trees (over 2 m height), and all new and dead trees were recorded at each census, although shrubs species (e.g., *Rhododendron maximum*) were excluded. Annual basal area increment rates were calculated for all measured trees, and aggregated into the plot scale only for live trees. To compare with the catchment-scale vegetation metrics above, the ratio of downslope to upslope total basal area was computed for each census measurement.

Leaf litter was collected from ten 0.92-m by 0.92-m leaf collectors in each gradient plot since 1992 (Sites 118, 218, and 318; n = 30 total). Collectors were located near the middle of each plot along two 40 m transects that follow the contour of the slope. Litter was collected on a quarterly basis and monthly in the autumn. Leaf litter was oven dried at 65°C until a constant mass was obtained, and then weighed to the nearest 0.01 g. Annual litterfall was estimated as the sum of dried leaf litter from ten

[1]http://www.geomorphometry.org/

collectors during April to March. Litter mass was converted to leaf area index (LAI; m^2 m^{-2}) using specific leaf area (SLA; m^2 kg^{-1}) values at each plot. Mean plot SLA values were from the weighted SLA values with species basal area information at each site (**Supplementary Table S2**). We calculated the mean litterfall and leaf area values at plot ($n = 10$) and watershed scales ($n = 30$), as well as the litterfall change rates at each collector using a simple linear regression (**Supplementary Figure S9**). Lastly, the ratios of leaf area downslope to upslope and watershed-scale standard deviations were computed each year to compare with the catchment-scale vegetation metrics above. More details on plot establishment, basal area, and litterfall sampling can be found in Knoepp et al. (2018).

Canopy Conductance Data From Sap Flux Measurements

To examine soil moisture control on stomatal dynamics at different topographic positions between dry and wet years, we reanalyzed the published data of Ford et al. (2011) in the context of soil moisture deficit (**Supplementary Figure S3**). Canopy conductance (G_c, mmol H_2O m^{-2} s^{-1}) of 30 hardwood trees was estimated from sap flux measurements for four dominant hardwood species, including *Liriodendron tulipifera* (tulip poplar), *Carya* spp. (hickory), *Q. montata* (chestnut oak), and *Q. rubra* (northern red oak), over 3 years (2004–2006) (**Supplementary Figure S3**). These trees were located adjacent to the midslope (SITE 318; $n = 15$ trees) and downslope (SITE 218; $n = 15$ trees) plots within WS18. More details of field methods and post-processing are available in Ford et al. (2011) and Hawthorne and Miniat (2018).

We classified the 3 years into normal (2004), wet (2005), and dry (2006) years, based on total precipitation amount and its seasonal patterns (**Supplementary Figure S3**) and observed soil moisture ranges between days of year (DOY) 130 and 280 (**Supplementary Figure S7**). We converted volumetric soil moisture (SM) to a normalized soil moisture deficit (SMD; dimensionless) each year based on max and min ranges to align relative values seasonally.

$$SMD = \frac{SM_{max} - SM}{SM_{max} - SM_{min}}$$

We regressed the mean daytime G_c values with SMD separately at the mid- and downslope positions each year.

RESULTS

Long-Term Climate and Hydrology

Long-term temperature data showed that this study site has experienced increases both in mean annual and growing-season air temperature since the mid-1970s (**Figure 2**; $p < 0.005$). Since 1977 and 1973, mean annual and growing-season temperatures have been increasing at rates of 0.42 and 0.48°C per decade, respectively. Prior to the increases, slight cooling trends dominated for both series since early 1940s. Total annual and growing-season precipitation had no trend over time (**Figure 2**), however, inter-annual and seasonal variability has been increasing, featured by more frequent and severe growing season droughts (**Figure 2**). Coincident with the start of increasing air temperature trends, the year 1973 was henceforth used as a starting point for time-series analyses of growing-season hydrologic metrics from the long-term streamflow records.

Temperature patterns were paralleled by long-term trends in three hydrologic metrics during the growing season. ET and HI increased over time, while RR decreased (**Figure 3**). In general, the temporal trends were more pronounced at the two low-elevation catchments (WS18 and WS14; $p < 0.05$) than at the high-elevation catchment (WS27), while the direction of the trends remained the same. Note that the similar temporal patterns were also reported in other two catchments (WS02 and WS36) (Figure 3 in Caldwell et al., 2016). The observed recession slopes ($-dQ/dt$) given the discharge (Q) also got steepened and became more linear over the same period, featured by significant trends in two recession parameters (a and b; **Supplementary Figure S4**) for the two low-elevation catchments. Like the three hydrologic metrics above (**Figure 3**), these trends were significant in the two-low elevation catchments ($p < 0.05$), while trends were the same across all catchments. This indicates that, over time, these watersheds had a more linear storage-discharge relationship during low flow periods. Coinciding with the recent increases in temperatures, there are also lower and more frequent 10-day average low flow periods (**Supplementary Figure S5**). The level of low flow dynamics was log-linearly correlated with observed root zone soil moisture (0–60 cm) patterns in the two reference catchments (WS18 and WS27; **Supplementary Figure S6**). All these long-term hydrologic metrics are generally following the long-term temperature trends, slight cooling until early 1970s and warming afterward.

Vegetation Patterns Between Upslope and Downslope

Average NDVI values at the upslope, downslope, and catchment scales did not show any significant trends over time (not shown here), even after the scene-based atmospheric correction. This might be due to the difficulty of atmospheric corrections in complex terrain, or saturation of NDVI at higher LAI in the study site (Myneni et al., 2002). The study site is featured by frequent fogs and localized mists, which could make atmospheric correction difficult. However, the NDVI ratio of down- to upslope topographic positions decreased over time for all catchments, approaching unity over the study period (**Figure 4A**). The standard deviation of NDVI decreased over time at three low-elevation catchments (WS02, WS14, and WS18; **Figure 4B**). These patterns were generally more pronounced in the low-elevation catchments, compared with the high-elevation catchments (WS27 and WS36) (**Figure 1**).

These remotely-sensed canopy patterns at the watershed scale generally coincided with the long-term plot measurements in WS18. Leaf area index (LAI) significantly increased over time

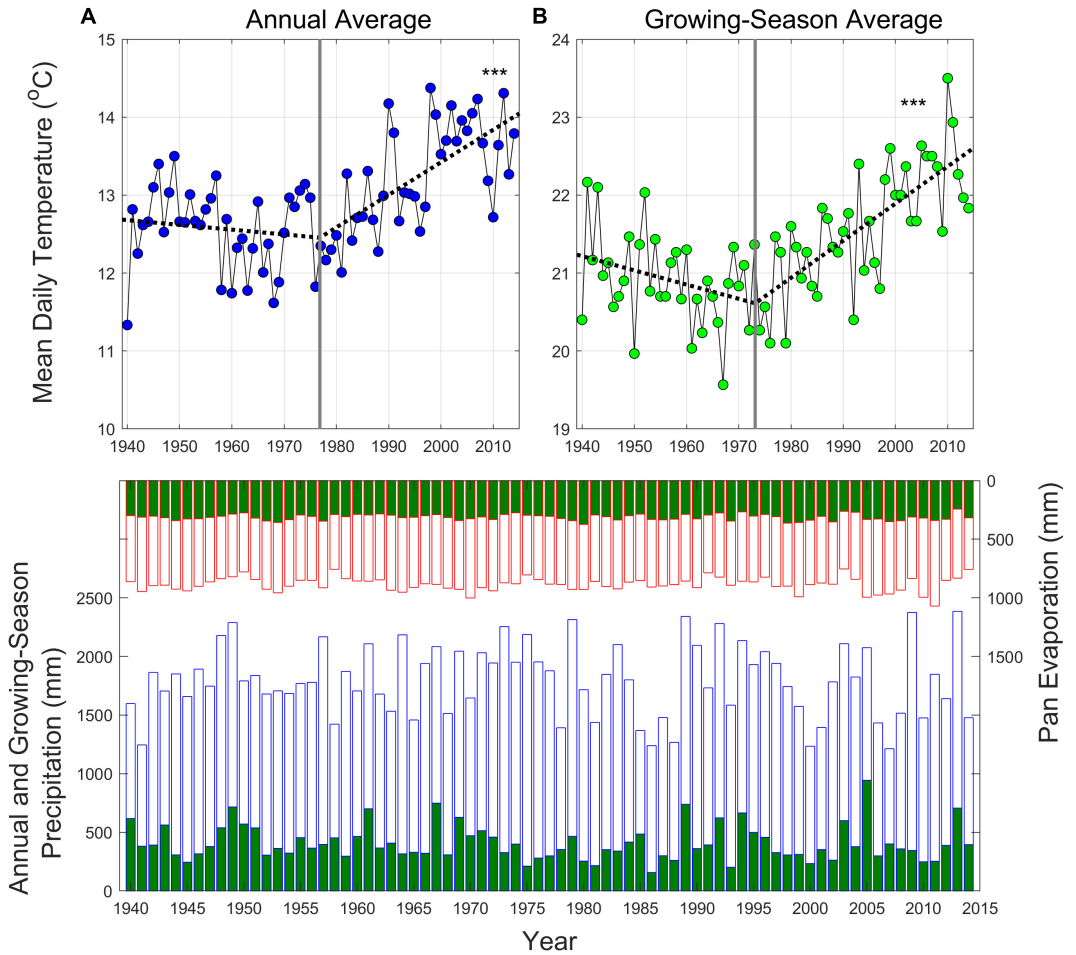

FIGURE 2 | Upper panel: observed mean annual **(A)** and growing-season **(B)** temperatures at the base climate station (CS01) in the study site, calculated from mean daily temperature data. Growing season is defined as a period from June to August. Dashed lines correspond to a piecewise regression model, where vertical lines represent the break points. **Bottom panel:** annual (blue bars) and growing-season (green) precipitation and pan evaporation (reverse *y*-axis; red bars) at the base climate station (RG06; 685 m) in the study site. ***$p < 0.005$.

only at the upslope topographic position since the early 1990s (**Figure 5A**; $p < 0.01$), with a general convergence in LAI among slope positions toward the end of the measurement period. Live tree basal area at the plot scale also generally increased over time in the up- and midslope positions, relative to downslope (**Figure 5B**); therefore, basal area increment rates monotonically decreased from upslope to downslope topographic positions (**Figure 6A**). Interestingly, inter-annual variation in basal area increment rates increased from up- to downslope plots (**Figure 6A**). Litterfall also increased over time more in the upslope than in midslope and downslope plots (**Figure 6B** and **Supplementary Figure S9**). Species-level basal area data showed that these divergent growth patterns between upslope and downslope have largely been driven by greater growth of oak and pine trees upslope/midslope and lesser growth of maple and birch trees downslope (**Figure 5C**). As a result, the down- to upslope ratios of leaf and basal areas also decreased (**Figure 6C**; $p < 0.05$ and $p < 0.005$, respectively), as well as the standard deviations of leaf area within the catchment ($p < 0.005$). Note that higher interannual variations of litterfall-based metrics were from wind conditions, and we removed 2003 data from the original data because the large wind blowouts were reported.

Canopy Conductance

Soil moisture deficit (SMD) affected daytime G_c (**Figure 7**), but varied among species and between years and sites. As reported in Ford et al. (2011) and in Hawthorne and Miniat (2018), daytime G_c of more mesophytic tree species (e.g., tulip poplar) was far greater than that of more xerophytic trees (e.g., oaks) consistently across the sites and years (**Figure 7**). This indicates that the mesophytic trees downslope use much more water for daytime evapotranspiration than the xerophytic trees upslope (**Supplementary Figure S3**), also featured by greater daily soil moisture amplitudes from soil TDR measurements (Hawthorne and Miniat, 2018). However, shallow soils remained consistently wetter downslope than upslope even in dry years

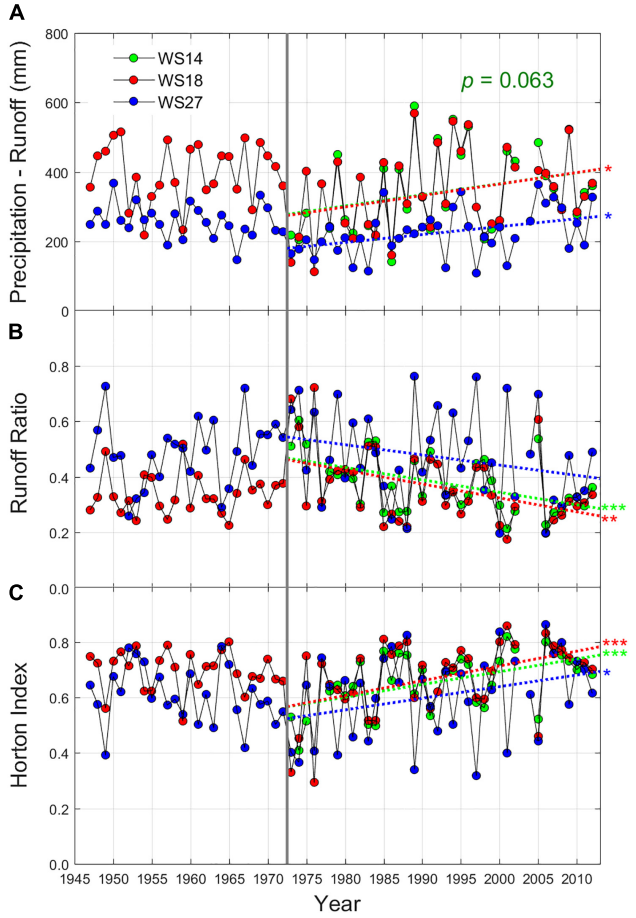

FIGURE 3 | Long-term patterns of growing season **(A)** evapotranspiration (*P*–*Q*), **(B)** runoff ratio (*Q*/*P*), and **(C)** Horton index [(*P*–*Q*)/(*P*–*S*)] at three headwater catchments in the study site (WS14 – green, WS18 – red, and WS27 – blue). Peak growing season is defined as the period from June through September at two low elevation catchments (WS14 and WS18), but from June through August for a high elevation catchment (WS27). These linear fits were analyzed from 1973, which break point was estimated from the long-term growing season temperature trend (**Figure 2**). The significance levels were determined from linear regressions while the similar significances were found in Spearman's rho tests with the null hypothesis of trend absence. *P*: precipitation, *Q*: runoff, and *S*: storm runoff. ***$p < 0.005$, **$p < 0.01$, and *$p < 0.05$.

(**Supplementary Figure S7**) due to higher nighttime recharge (Hawthorne and Miniat, 2018).

The sensitivity of G_c to SMD was greater in normal and dry years (2004 and 2006), compared to a wet year (2005). Interestingly, mesophytic tree species downslope showed greater sensitivity to SMD than xerophytic tree species upslope despite the downslope site having a consistently higher water content than midslope. G_c responded to SMD only at the downslope plot in a normal year (2004) (**Figure 7A**), while this effect was observed at both downslope and midslope in a dry year (2006). In addition, tulip poplar and hickory showed greater declines in G_c with increasing SMD than oak species (mostly $p < 0.005$), which indicates typical isohydric behavior.

DISCUSSION AND CONCLUSION

In this study, we first show that the evapotranspiration has increased, and streamflow yield given precipitation has decreased in the three reference catchments during the growing season using mass balance-based hydrologic metrics (ET, RR and HI; **Figure 3**). Significance levels were greater for the two normalized hydrologic metrics, RR and HI, than ET, suggesting that these two metrics may better capture vegetation water use patterns with normalizing precipitation variability. These long-term trends in three hydrologic metrics effectively represent increasing localized forest water use and decreasing runoff generation given precipitation over the period. Second, we show that hydrograph declines are becoming steeper and more linear over time through empirical recession slope analyses (**Supplementary Figure S4**). The late recession behavior is mostly contributed by slow response units of the catchment (mostly upslope portions with longer flow path) (Woods and Sivapalan, 1997; Li and Sivapalan, 2011), and shallow subsurface flow is a main source of sustained base flow in the study site (Hewlett and Hibbert, 1963). Therefore, steeper declines and more linear responses in hydrograph recession suggest that the upslope regions are potentially less hydrologically connected to streams over time (Harman et al., 2009; McGuire and McDonnell, 2010; Hwang et al., 2012). Third, low streamflow dynamics also showed more frequent and prolonged drought periods during the growing season over time, which closely corresponded with root zone soil moisture patterns in the study watersheds. This suggests that despite relatively high annual precipitation (*ca.* 1,800 mm at low elevations), the study watersheds are moving toward seasonally-drier conditions with greater canopy water use, lower runoff production given precipitation, and potentially lower downslope subsidy.

More frequent and prolonged dry periods could be also partially explained by the increased seasonal and interannual precipitation variability over time. This site has been characterized by an increasing length of inter-storm periods and total rainfall amounts per storm over the period of warming (Laseter et al., 2012; Burt et al., 2018). However, changing precipitation patterns cannot fully explain the increasing ET signals in that more frequent and less intense rainfall usually provides optimal conditions for vegetation water use (both transpiration and interception), and our site is experiencing the opposite. In addition, stormflow dynamics in the study watersheds are characterized by threshold behavior that is a combined function of antecedent soil moisture and storm precipitation (Scaife and Band, 2017); therefore, greater rainfall amounts per storm could lead to higher streamflow generation by subsurface stormflow. Furthermore, pan evaporation has not increased in the study site with warming (**Figure 2C**), thus atmospheric forcing cannot explain the increasing ET trends in hydrologic records (Roderick and Farquhar, 2002). Therefore, increasing ET signals may be better explained by vegetation responses to changing climate and ongoing forest mesophication (Creed et al., 2014; Caldwell et al., 2016; Hwang et al., 2018; Kim et al., 2018) rather than directly driven by climate forcing variables.

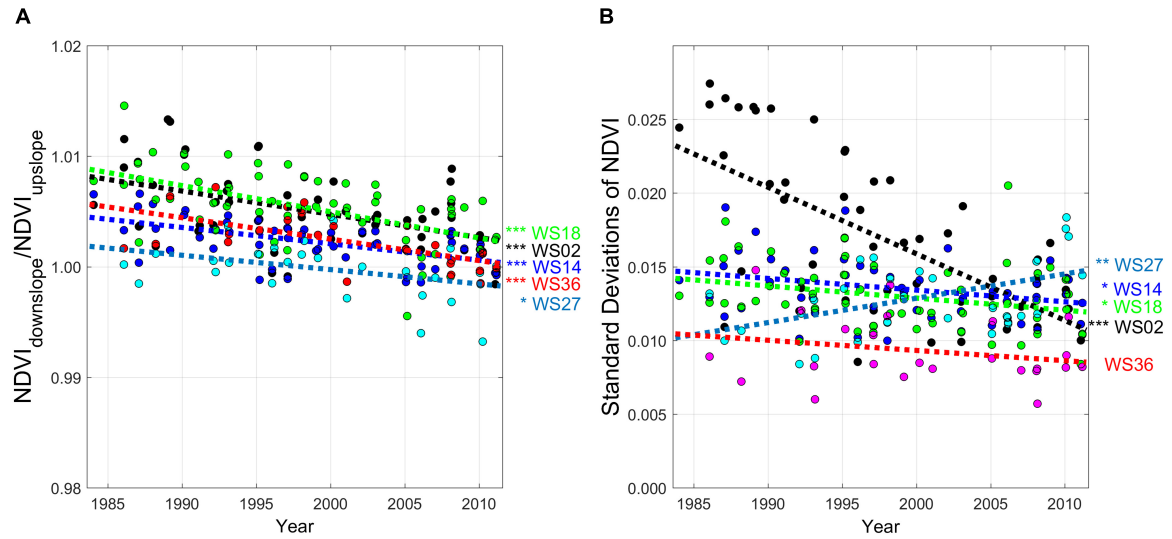

FIGURE 4 | (A) Time-series of the ratios of Normalized Difference Vegetation Index (NDVI) downslope to upslope ($NDVI_{down}/NDVI_{up}$), and **(B)** their standard deviations at a watershed scale. NDVI values were from Landsat Thematic Mapper (TM) images from 1984 to 2011 at five preserved headwater catchments (WS02 - black, WS14 - blue, WS18 - green, WS27 - cyan, and WS36 - red) in the study site (Coweeta Hydrologic Lab, North Carolina, United States). Each watershed was divided into upslope (75%) and downslope (25%) regions at the same resolution with Landsat TM based on the distribution of upslope contributing area (see **Figure 1**). The detailed site information is available in **Table 1**. ***$p < 0.005$, **$p < 0.01$, and *$p < 0.05$.

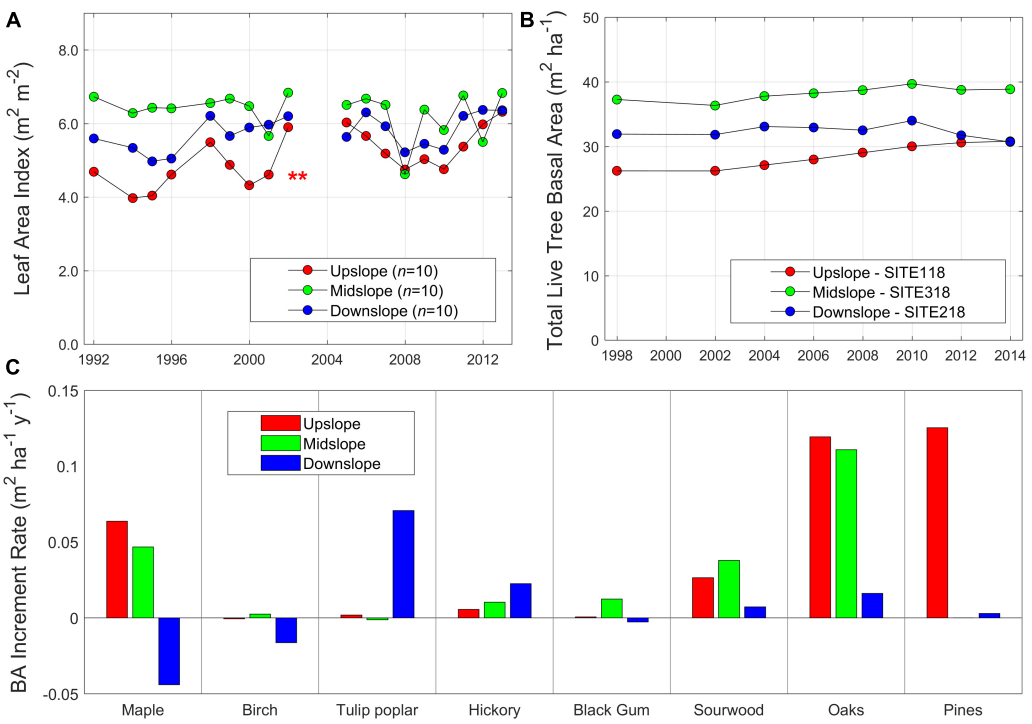

FIGURE 5 | (A) Time series of leaf are index (LAI; m^2 m^{-2}) values (n = 10 each) and **(B)** total basal area (BA) (m^2 ha^{-1}) of all live trees from three gradient plots (upslope - SITE 118, midslope - SITE 318, and downslope - SITE 218; 80-by-80 m size) in the study site (WS18), and **(C)** total basal area change rates (m^2 ha^{-1} y^{-1}) of live trees. LAI values were calculated from total dried litter weight (**Supplementary Figure S9**) and site averaged specific leaf area values (**Supplementary Table S2**). Dry litter fall weights have been measured from 10 litter baskets at each plot every year since 1992 (except for 1993 and 1997). Total basal area has been measured since 1998 with roughly 2-year intervals (except for 2000). Scientific names are available in **Supplementary Table S2**. **$p < 0.01$.

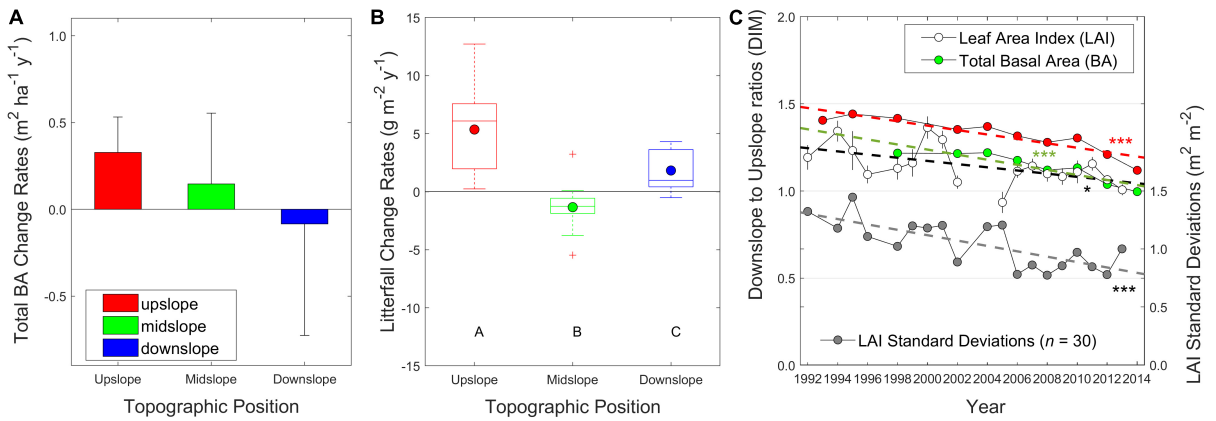

FIGURE 6 | (A) Total basal area (BA) increment rates per year (m^2 ha^{-1} y^{-1}) from 1998 to 2014, and **(B)** Boxplots of litterfall increment rates (g m^{-2} y^{-1}; n = 10 each; **Supplementary Figure S9**) at three 80-by-80 m gradient plots (upslope - red, midslope - green, and downslope - blue) in the watershed 18 (1992 to 2013) (**Supplementary Table S1**). Circles are mean values, while black crosses are outliers. **(C)** Ratios of downslope to upslope in total BA (green and red) and leaf area index (LAI – blank) values, and their standard deviations (gray). Basal area ratio values with red color were calculated from the 40-by-20 m subplots since 1992. Litterfall was collected from ten baskets at each plot, dried, weighted, and converted to LAI using site-averaged specific leaf area values and basal area information (**Supplementary Table S2**). Different letters (A–C) denote significant differences in the group means using an analysis of variance (ANOVA) test ($p < 0.01$). Note that error bars in the BA change rates represent interannual variability at the plot scale, while boxplots for litterfall and error bars of LAI values are from the ten sample plots at each landscape position. ***$p < 0.005$, **$p < 0.01$, and *$p < 0.05$.

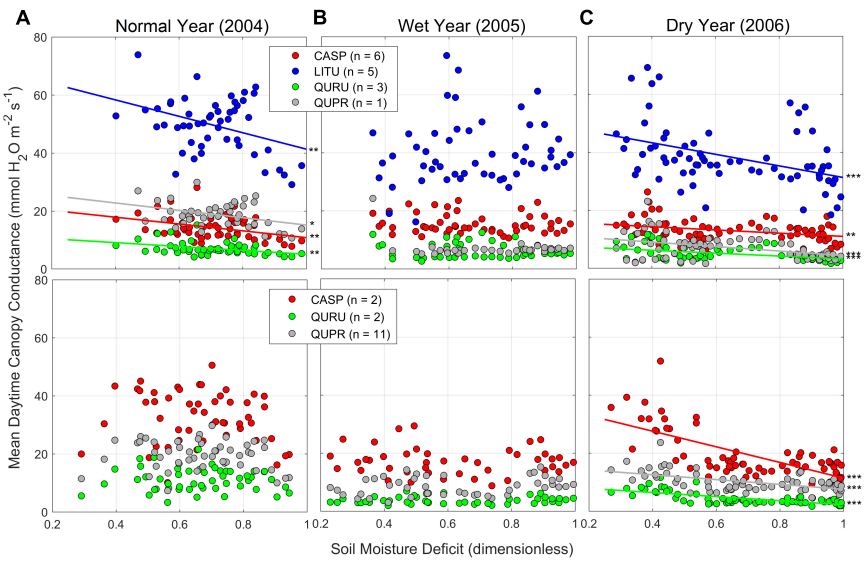

FIGURE 7 | Mean daytime canopy conductance (G_c, mmol H_2O m^{-2} s^{-1}, left axis; **Supplementary Figure S3**) for trees in downslope (218: upper panel) and mid-slope (318: upper panel) plots in WS18 (85-year old low-elevation reference watershed) during **(A)** 2004 (normal year), **(B)** 2005 (wet year), and **(c)** 2006 (dry year) growing season. Soil moisture was measured at two locations and two depths (0–30 and 30–60 cm) in each plot on site (**Supplementary Figure S7**), used to calculate soil moisture deficit (SMD) each year [$(SM_{max}–SM)/(SM_{max}–SM_{min})$]. Different species denoted with different colored symbols and lines: *Liriodendron tulipifera* (LITU), blue; *Carya* spp. (CASP), red; *Quercus prinus* (QUPR), gray; *Q. rubra* (QURU), green. For details, see Ford et al. (2011). ***$p < 0.005$, **$p < 0.01$, and *$p < 0.05$.

Leaf area patterns have been homogenized along hydrologic flow paths over time (approaching the unity) in all the study catchments, as shown in the long-term remote sensing (**Figure 4**) and supported by long-term field data in one catchment (**Figure 5**). Although the ratios of NDVI values decreased <1% over time, there are two main reasons why these signals are not trivial. First, the NDVI metrics from Landsat imagery were from aggregated greenness signals at a 30-m resolution (Hwang et al., 2011a), which may provide inaccurate representations both in topographic and vegetation classifications between upslope and downslope positions (**Figure 1**). Second, the percent changes in NDVI values should be interpreted as greater changes in LAI values due to the non-linear relationship between NDVI and LAI values in the study site (see Figure 4 in Hwang et al., 2009).

Our field-based basal area increment and leaf area index data also showed that the vegetation upslope has grown more than downslope vegetation at least 20% in the similar ratio metrics in the basal area and LAI datasets (**Figure 6C**), as well as the standard deviations. The homogenization patterns were also more statistically significant at the drier low elevation catchments (WS02, WS14, and WS18; **Figure 4**) where we also had more significant seasonal drying signals in streamflow dynamics (**Figure 3**), compared to the wetter high elevation catchments (WS27 and WS36). WS27 might show slightly different patterns both in the NDVI ratios and standard deviations (**Figure 4**) possibly due to the damage by an ice storm in 2006 at high elevations (>1200 m), reflected in long-term basal area and litterfall data (not shown here).

The xerophytic trees upslope showed greater and more consistent growth over time, while mesophytic trees downslope showed lower growth with larger inter-annual variation (**Figure 6**). The canopy conductance of the trees downslope also showed greater declines and sensitivity to relative soil moisture deficit than the trees upslope (**Figure 7**). In other words, mesophytic trees downslope behaved more isohydrically, while xerophytic trees upslope showed typical anisohydric behavior under the moderate drought condition. Although shallow soils remained consistently wetter downslope than upslope, even in dry years (**Supplementary Figure S7**), vegetation downslope was more responsive to mild drought stress than upslope. This suggests that trees downslope may be experiencing more frequent drought stress and subsequent lower growth due to combined effect of frequent droughts, more water use by vegetation upslope, and potentially lower downslope subsidy over time.

A recent study also showed the strong dependency of vegetation downslope on upslope water subsidy in the study site. Hawthorne and Miniat (2018) showed that despite greater transpiration, there was greater overnight recharge of soil moisture in the downslope plot, driven by downslope flow or hydraulic redistribution. This may indicate the strong dependency of vegetation downslope on upslope water subsidy through lateral hydrologic redistribution, shown to have been potentially decreasing over time in long-term hydrologic records above. This also suggests that emergent decreases in hydrologic subsidy to downslope areas over time might be driven by both changing precipitation patterns, forest mesophication (more mesophytic trees), and subsequent increased ET mostly by up- and midslope tree communities, which occupy major portions of watershed landscapes (Day et al., 1988). Recently, Caldwell et al. (2016) also attributed declining water yield to a shift toward mesophytic dominance in the study site that uses more water than xerophytic oak species (**Figure 7**).

The divergent growth responses of trees between up- and downslope may be explained by stomatal responses to mild drought stress across the forest landscape (Meinzer et al., 2016). A recent study in the study site also demonstrated that anisohydric oaks in the upslope plot could maintain relatively high transpiration rates in the spring until presumably hydraulic adjustments (embolism) were incurred following the first major dry period (Hawthorne and Miniat, 2018). Meinzer et al. (2013) also showed that water use by maple and poplar trees was twice as sensitive to soil drying compared to oak species, while oaks were relatively insensitive to drying. This may allow trees in the upslope plots to take advantage of warmer springs with earlier greenup (Hwang et al., 2018; Kim et al., 2018; Oishi et al., 2018) and increasing atmospheric CO_2 concentrations. Although CO_2 fertilization can decrease transpiration by improving water use efficiency especially during dry periods (Warren et al., 2011), we did not see any decreasing vegetation water use signals from the long-term hydrologic records (**Figure 3**). Similar increasing trends of ET were also recently reported at other undisturbed forested watersheds in the southern Appalachians (Hwang et al., 2018). This suggests that the potential CO_2-driven reduction in transpiration might be outweighed by other factors, such as lengthened growing season (Hwang et al., 2011b, 2014) and greater vegetation growth by CO_2 fertilization (**Figure 5**; Frank et al., 2015; Ward et al., 2018).

However, with increasing ET upslope and frequent droughts, water subsidies to downslope vegetation would decline over time as indicated in the long-term hydrologic records (**Figure 3** and **Supplementary Figures S4**, **S5**). Mesophytic, isohydric trees downslope appeared to respond more to increased hydroclimate variability due to their dependence on downslope flows and subsidy (**Figure 8**). A recent tree-ring study in the study site showed that downslope tree species were more sensitive to hydroclimate variability than trees upslope with larger inter-annual variation (Elliott et al., 2015). They demonstrated that radial growth of oaks was greater than maple, birch and tulip poplar on upslope sites in dry years, while the latter species had higher basal increments than oaks on downslope sites in wet years. This pattern has also been confirmed across the eastern deciduous forests using Forest Inventory and Analysis data (Brzostek et al., 2014). This suggests that the isohydric/anisohydric continuum along hillslope gradients will play an important role in forest ecosystem responses to climate change, which would be closely mediated by changes in partitioning between localized water use and lateral hydrologic flows.

The divergent responses of vegetation to soil moisture deficit are not likely attributed to differences in vertical root structures between up- and downslope communities. In this study, we found that trees downslope showed a greater response to mild drought than those upslope, even within the same tree species in a normal year (**Figure 7**). Recent studies in the study site reported rooting depth and vertical distribution from 27 soil pits across different topographic positions and vegetation types (Hales et al., 2009; Hwang et al., 2015; Hales and Miniat, 2017). They found that roots were distributed deeper and more evenly in wet, hollow (areas of convergent topography) locations, compared to drier, nose (divergent topography) landscape positions. However, maximum rooting depth (around 1 m), total root biomass, and root frequency did not vary systematically between dry/nose and wet/hollow topographic positions and among different tree species. They did report observing distinct tap root structures around the depth of saprolite at several nose pits. Although many studies reported that deep tap roots play an important role in vegetation water use via hydraulic lift during dry periods (Nepstad et al., 1994; Canadell et al., 1996; Caldwell et al., 1998; Siqueira et al., 2008), the study by Hawthorne and Miniat (2018) reported greater overnight recharge in soil moisture at downslope

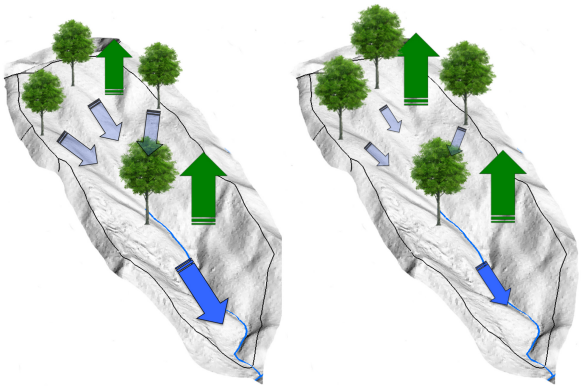

FIGURE 8 | Conceptual models for hydrologic partitioning between localized water use and lateral hydrologic flows between vegetation in up- and downslope positions at the watershed scale. Vegetation water use downslope (green water) partially depends on upslope subsidy (blue water). Therefore, small increases in water use by upland xerophytic species with lengthened growing season and subsequent greater growth would be amplified in downslope topographic positions, where mesophytic tree species has already acclimated to greater soil moisture availability. Note that potential decreases in upslope subsidy may be also driven by more frequent and prolonged drought periods with warming. Green and blue arrows represent evapotranspiration and lateral hydrologic flows, respectively.

rather than at upslope plots. This suggests that stomatal behavior and seasonally high local water use, rather than differences in rooting distributions, may be responsible for greater upslope growth and LAI over time compared to downslope vegetation.

Our study is in contrast with results from drier and colder ecosystems (e.g., Anning et al., 2013). Bunn et al. (2005) showed that tree ring growth patterns of *Pinus balfouriana* in the Sierra Nevada Mountains showed stronger correlations with temperature at wet and high convergence areas (downslope), while they correlated more with precipitation at dry and low convergence areas (upslope). Adams et al. (2014) also reported that tree ring growth of *P. contorta* and *P. ponderosa* at wet downslope areas showed decoupled responses to regional temperature and precipitation patterns, contrary to trees at dry upslope areas. In the western United States, vegetation water use can be usually decoupled from dominant lateral hydrologic flows during the growing season (Brooks et al., 2010) due to a seasonally dry climate (Tague et al., 2008; Tague, 2009). These abiotic factors would lead to less tight coupling between vegetation dynamics and watershed-scale hydrological behavior especially in dry regions (Adams et al., 2012). In the southern Appalachians, hydrologic subsidy by lateral hydrologic flows often leads to a gradient in plant-available water during dry periods (Yeakley et al., 1998), which may indicate strong dependency of downslope vegetation use on upslope water subsidy. This highlights the need to understand landscape-scale ecosystem responses to changing climate as connected systems between upslope and downslope via associated dominant lateral hydrologic flows.

Convergent or downslope topographic areas are often considered to be potential locations of thermal (climatic) microrefugia where local environment conditions may be decoupled from regional climate conditions (e.g., Dobrowski et al., 2009). While this argument has been mostly driven by topographic effects on temperature regimes, such as adiabatic lapse rates with elevation (e.g., Dobrowski et al., 2009; Gollan et al., 2014) and cold air drainage to valley bottoms (Novick et al., 2016), few studies related the changes in topography-mediated water balance patterns with vegetation responses to climate change (but see Crimmins et al., 2011). With an increase in upslope water use and subsequent decreases in hydrologic downslope subsidy, the effect of increased hydroclimate variability with warming should be amplified in downslope topographic positions, where mesophytic trees have already acclimated to greater soil moisture availability through physiological and rooting strategies. Considering ongoing forest "mesophication" under a history of fire suppression across the eastern United States deciduous forests, this study suggests that mesophytic trees downslope may be more vulnerable in terms of growth reduction and enhanced mortality due to the combined effect of frequent droughts and decreased lateral hydrologic flows under changing climate.

CONCLUSION

In this study, we combined long-term streamflow, remote sensing, soil moisture, tree basal area, litterfall, and sap flux datasets to explain long-term changes in vegetation patterns at the hillslope to watershed scales. We showed increasing evapotranspiration, decreasing streamflow yield given precipitation, and potential decreasing upslope subsidy to downslope topographic positions over the period of warming. This led to emergent homogenization of canopy density (leaf area) patterns along the hydrologic flow paths, supported by both long-term remote sensing and field observations. Xerophyric trees upslope showed greater growth over time compared to mesophytic trees downslope, closely mediated by the isohydric/anisohydric continuum along the hydrologic flow paths. This study also suggests that the changes in hydrologic partitioning between localized water use (green water) and lateral hydrologic flows (blue water) mediates the divergent responses of vegetation between upslope and downslope topographic positions. We speculate that with forest growth and more frequent droughts, they may become more hydrologically disconnected and increase the ratio of ET to *Q*, and as a result downslope mesophytic trees become more susceptible to frequent drought due to their strong dependency of green water use on blue water generation upslope. Our findings highlight the need to understand the underlying hydrologic balance along hillslope gradients to predict how forested mountain ecosystems may respond to climate change, possibly reinforced by ongoing forest mesophication under active fire suppression.

DATA AVAILABILITY STATEMENT

The datasets generated for this study can be found in the https://coweeta.uga.edu/dbpublic/dataset_details.asp?accession=1046.

AUTHOR CONTRIBUTIONS

TH, LB, and CM designed the overall research plan, analyzed and interpreted the data, and wrote the manuscript. CM, JV, JK, and PB are in charge of long-term climate, hydrology, soil moisture, and vegetation data, and contributed to writing of the manuscript. CS participated in Landsat TM data analysis and contributed to writing of the manuscript.

FUNDING

This research was supported by the U.S. Forest Service Southern Research Station, and the National Science Foundation (NSF) awards, DEB-0218001, DEB-0823293, DEB-1226983, DEB-1440485, and DEB-1637522 from the Long Term Ecological Research (LTER) Program to the Coweeta LTER. Any opinions, findings, conclusion, or recommendations expressed in the material are those of the authors and do not necessarily reflect the views of the USDA or NSF.

ACKNOWLEDGMENTS

We thank to Brian Kloeppel and Jason P. Love, who coordinated field work, and ensured the quality of field LTER data. We also thank the two reviewers for constructive comments on the manuscript.

SUPPLEMENTARY MATERIAL

The Supplementary Material for this article can be found online at: https://www.frontiersin.org/articles/10.3389/ffgc.2020.00017/full#supplementary-material

REFERENCES

Abrams, M. D. (2003). Where has all the white oak gone? *BioScience* 53, 927–939.

Adams, H. D., Guardiola-Claramonte, M., Barron-Gafford, G. A., Villegas, J. C., Breshears, D. D., Zou, C. B., et al. (2009). Temperature sensitivity of drought-induced tree mortality portends increased regional die-off under global-change-type drought. *Proc. Natl. Acad. Sci. U.S.A.* 106, 7063–7066. doi: 10.1073/pnas.0901438106

Adams, H. D., Luce, C. H., Breshears, D. D., Allen, C. D., Weiler, M., Hale, V. C., et al. (2012). Ecohydrological consequences of drought- and infestation-triggered tree die-off: insights and hypotheses. *Ecohydrology* 5, 145–159. doi: 10.1002/eco.233

Adams, H. R., Barnard, H. R., and Loomis, A. K. (2014). Topography alters tree growth–climate relationships in a semi-arid forested catchment. *Ecosphere* 5:art148. doi: 10.1890/es14-00296.1

Ali, G. A., and Roy, A. G. (2010). Shopping for hydrologically representative connectivity metrics in a humid temperate forested catchment. *Water Resour. Res.* 46:W12544.

Anderegg, W. R., Berry, J. A., Smith, D. D., Sperry, J. S., Anderegg, L. D., and Field, C. B. (2012). The roles of hydraulic and carbon stress in a widespread climate-induced forest die-off. *Proc. Natl. Acad. Sci. U.S.A.* 109, 233–237. doi: 10.1073/pnas.1107891109

Anning, A. K., Rubino, D. L., Sutherland, E. K., and McCarthy, B. C. (2013). Dendrochronological analysis of white oak growth patterns across a topographic moisture gradient in southern Ohio. *Dendrochronologia* 31, 120–128. doi: 10.1016/j.dendro.2012.10.002

Asrar, G., Fuchs, M., Kanemasu, E. T., and Hatfield, J. L. (1984). Estimating absorbed photosynthetic radiation and leaf-area index from spectral reflectance in wheat. *Agron. J.* 76, 300–306. doi: 10.2134/agronj1984.00021962007600020029x

Bearup, L. A., Maxwell, R. M., Clow, D. W., and McCray, J. E. (2014). Hydrological effects of forest transpiration loss in bark beetle-impacted watersheds. *Nat. Clim. Chang.* 4, 481–486. doi: 10.1038/nclimate2198

Beckage, B., and Clark, J. S. (2003). Seedling survival and growth of three forest tree species: the role of spatial heterogeneity. *Ecology* 84, 1849–1861. doi: 10.1890/0012-9658(2003)084%5B1849:ssagot%5D2.0.co;2

Berdanier, A. B., and Clark, J. S. (2016). Multiyear drought−induced morbidity preceding tree death in southeastern US forests. *Ecol. Appl.* 26, 17–23. doi: 10.1890/15-0274

Bolstad, P. V., Swank, W., and Vose, J. (1998). Predicting Southern Appalachian overstory vegetation with digital terrain data. *Landsc. Ecol.* 13, 271–283.

Brooks, J. R., Barnard, H. R., Coulombe, R., and McDonnell, J. J. (2010). Ecohydrologic separation of water between trees and streams in a Mediterranean climate. *Nat. Geosci.* 3, 100–104. doi: 10.1038/ngeo722

Brooks, P. D., Troch, P. A., Durcik, M., Gallo, E., and Schlegel, M. (2011). Quantifying regional scale ecosystem response to changes in precipitation: not all rain is created equal. *Water Resour. Res.* 47:W00J08.

Brutsaert, W., and Nieber, J. L. (1977). Regionalized drought flow hydrographs from a mature glaciated plateau. *Water Resour. Res.* 13, 637–644.

Brzostek, E. R., Dragoni, D., Schmid, H. P., Rahman, A. F., Sims, D., Wayson, C. A., et al. (2014). Chronic water stress reduces tree growth and the carbon sink of deciduous hardwood forests. *Glob. Change Biol.* 20, 2531–2539. doi: 10.1111/gcb.12528

Bunn, A. G., Waggoner, L. A., and Graumlich, L. J. (2005). Topographic mediation of growth in high elevation foxtail pine (*Pinus balfouriana* Grev. et Balf.) forests in the Sierra Nevada, USA. *Glob. Ecol. Biogeogr.* 14, 103–114. doi: 10.1111/j.1466-822x.2005.00141.x

Burt, T. P., Ford Miniat, C., Laseter, S. H., and Swank, W. T. (2018). Changing patterns of daily precipitation totals at the Coweeta Hydrologic Laboratory, North Carolina, USA. *Int. J. Climatol.* 38, 94–104. doi: 10.1002/joc.5163

Caldwell, M. M., Dawson, T. E., and Richards, J. H. (1998). Hydraulic lift: consequences of water efflux from the roots of plants. *Oecologia* 113, 151–161. doi: 10.1007/s004420050363

Caldwell, P. V., Miniat, C. F., Elliott, K. J., Swank, W. T., Brantley, S. T., and Laseter, S. H. (2016). Declining water yield from forested mountain watersheds in response to climate change and forest mesophication. *Glob. Chang. Biol.* 22, 2997–3012. doi: 10.1111/gcb.13309

Canadell, J., Jackson, R. B., Ehleringer, J. R., Mooney, H. A., Sala, O. E., and Schulze, E. D. (1996). Maximum rooting depth of vegetation types at the global scale. *Oecologia* 108, 583–595. doi: 10.1007/BF00329030

Chen, J. M., and Cihlar, J. (1996). Retrieving leaf area index of boreal conifer forests using Landsat TM images. *Remote Sens. Environ.* 55, 153–162. doi: 10.1016/0034-4257(95)00195-6

Choat, B., Jansen, S., Brodribb, T. J., Cochard, H., Delzon, S., Bhaskar, R., et al. (2012). Global convergence in the vulnerability of forests to drought. *Nature* 491, 752–755. doi: 10.1038/nature11688

Clark, J. S., Bell, D. M., Hersh, M. H., and Nichols, L. (2011). Climate change vulnerability of forest biodiversity: climate and competition tracking of demographic rates. *Glob. Chang. Biol.* 17, 1834–1849. doi: 10.1111/j.1365-2486.2010.02380.x

Clark, J. S., Bell, D. M., Kwit, M. C., and Zhu, K. (2014). Competition-interaction landscapes for the joint response of forests to climate change. *Glob. Chang. Biol.* 20, 1979–1991. doi: 10.1111/gcb.12425

Clinton, B. D., Yeakley, J. A., and Apsley, D. K. (2003). Tree growth and mortality in a Southern Appalachian deciduous forest following extended wet and dry periods. *Castanea* 68, 189–200.

Creed, I. F., Hwang, T., Lutz, B., and Way, D. (2015). Climate warming causes intensification of the hydrological cycle, resulting in changes to the vernal and autumnal windows in a northern temperate forest. *Hydrol. Process.* 29, 3519–3534. doi: 10.1002/hyp.10450

Creed, I. F., Spargo, A. T., Jones, J. A., Buttle, J. M., Adams, M. B., Beall, F. D., et al. (2014). Changing forest water yields in response to climate warming: results from long-term experimental watershed sites across North America. *Glob. Chang. Biol.* 20, 3191–3208. doi: 10.1111/gcb.12615

Crimmins, S. M., Dobrowski, S. Z., Greenberg, J. A., Abatzoglou, J. T., and Mynsberge, A. R. (2011). Changes in climatic water balance drive downhill shifts in plant species' optimum elevations. *Science* 331, 324–327. doi: 10.1126/science.1199040

Davis, F. W., and Goetz, S. (1990). Modeling vegetation pattern using digital terrain data. *Landsc. Ecol.* 4, 69–80. doi: 10.1007/bf02573952

Dawdy, D., and Matalas, N. (1964). "Statistical and probability analysis of hydrologic data, part III: analysis of variance, covariance and time series," in *Handbook of Applied Hydrology: A Compendium of Water-Resources Technology*, ed. V. T. Chow, (New York, NY: McGraw-Hill Education), 68–90.

Day, F. P., Philips, D. L., and Monk, C. D. (1988). "Forest communities and patterns," in *Forest Hydrology and Ecology at Coweeta*, eds W. T. Swank, and J. D. A. Crossley, (New York, NY: Springer-Verlag), 141–149. doi: 10.1007/978-1-4612-3732-7_10

Detty, J. M., and McGuire, K. J. (2010). Topographic controls on shallow groundwater dynamics: implications of hydrologic connectivity between hillslopes and riparian zones in a till mantled catchment. *Hydrol. Process.* 24, 2222–2236. doi: 10.1002/hyp.7656

Dobrowski, S. Z. (2011). A climatic basis for microrefugia: the influence of terrain on climate. *Glob. Chang. Biol.* 17, 1022–1035. doi: 10.1111/j.1365-2486.2010.02263.x

Dobrowski, S. Z., Abatzoglou, J. T., Greenberg, J. A., and Schladow, S. G. (2009). How much influence does landscape-scale physiography have on air temperature in a mountain environment? *Agric. For. Meteorol.* 149, 1751–1758. doi: 10.1016/j.agrformet.2009.06.006

Eckhardt, K. (2005). How to construct recursive digital filters for baseflow separation. *Hydrol. Process.* 19, 507–515. doi: 10.1002/hyp.5675

Elliott, K. J., Miniat, C. F., Pederson, N., and Laseter, S. H. (2015). Forest tree growth response to hydroclimate variability in the southern Appalachians. *Glob. Chang. Biol.* 21, 4627–4641. doi: 10.1111/gcb.13045

Elliott, K. J., and Vose, J. M. (2011). The contribution of the Coweeta Hydrologic Laboratory to developing an understanding of long-term (1934–2008) changes in managed and unmanaged forests. *For. Ecol. Manage.* 261, 900–910. doi: 10.1016/j.foreco.2010.03.010

Emanuel, R. E., Riveros-Iregui, D. A., McGlynn, B. L., and Epstein, H. E. (2011). On the spatial heterogeneity of net ecosystem productivity in complex landscapes. *Ecosphere* 2, 1–13.

Erskine, R. H., Green, T. R., Ramirez, J. A., and MacDonald, L. H. (2006). Comparison of grid−based algorithms for computing upslope contributing area. *Water Resour. Res.* 42:W09416.

Ford, C. R., Hubbard, R. M., and Vose, J. M. (2011). Quantifying structural and physiological controls on variation in canopy transpiration among planted pine and hardwood species in the southern Appalachians. *Ecohydrology* 4, 183–195. doi: 10.1002/eco.136

Frank, D., Poulter, B., Saurer, M., Esper, J., Huntingford, C., Helle, G., et al. (2015). Water-use efficiency and transpiration across European forests during the Anthropocene. *Nat. Clim. Chang.* 5, 579–584.

Gollan, J. R., Ramp, D., and Ashcroft, M. B. (2014). Assessing the distribution and protection status of two types of cool environment to facilitate their conservation under climate change. *Conserv. Biol.* 28, 456–466. doi: 10.1111/cobi.12212

Hales, T. C., Ford, C. R., Hwang, T., Vose, J. M., and Band, L. E. (2009). Topographic and ecologic controls on root reinforcement. *J. Geophys. Res. Earth Surf.* 114:F03013.

Hales, T. C., and Miniat, C. F. (2017). Soil moisture causes dynamic adjustments to root reinforcement that reduce slope stability. *Earth Surf. Process. Landf.* 42, 803–813. doi: 10.1002/esp.4039

Harman, C. J., Sivapalan, M., and Kumar, P. (2009). Power law catchment-scale recessions arising from heterogeneous linear small-scale dynamics. *Water Resour. Res.* 45:W09404.

Hawthorne, S., and Miniat, C. F. (2018). Topography may mitigate drought effects on vegetation along a hillslope gradient. *Ecohydrology* 11:e1825. doi: 10.1002/eco.1825

Hewlett, J. D., and Hibbert, A. R. (1963). Moisture and energy conditions within a sloping soil mass during drainage. *J. Geophys. Res.* 68, 1081–1087. doi: 10.1029/jz068i004p01081

Hoffmann, W. A., Marchin, R. M., Abit, P., and Lau, O. L. (2011). Hydraulic failure and tree dieback are associated with high wood density in a temperate forest under extreme drought. *Glob. Chang. Biol.* 17, 2731–2742. doi: 10.1111/j.1365-2486.2011.02401.x

Hoylman, Z. H., Jencso, K. G., Hu, J., Martin, J. T., Holden, Z. A., Seielstad, C. A., et al. (2018). Hillslope topography mediates spatial patterns of ecosystem sensitivity to climate. *J. Geophys. Res. Biogeosci.* 123, 1–19.

Huete, A., Didan, K., Miura, T., Rodriguez, E. P., Gao, X., and Ferreira, L. G. (2002). Overview of the radiometric and biophysical performance of the MODIS vegetation indices. *Remote Sens. Environ.* 83, 195–213. doi: 10.1016/s0034-4257(02)00096-2

Hwang, T., Band, L. E., and Hales, T. C. (2009). Ecosystem processes at the watershed scale: extending optimality theory from plot to catchment. *Water Resour. Res.* 45:W11425.

Hwang, T., Band, L. E., Hales, T. C., Miniat, C. F., Vose, J. M., Bolstad, P. V., et al. (2015). Simulating vegetation controls on hurricane-induced shallow landslides with a distributed ecohydrological model. *J. Geophys. Res. Biogeosci.* 120, 361–378. doi: 10.1002/2014jg002824

Hwang, T., Band, L. E., Miniat, C. F., Song, C., Bolstad, P. V., Vose, J. M., et al. (2014). Divergent phenological response to hydroclimate variability in forested mountain watersheds. *Glob. Chang. Biol.* 20, 2580–2595. doi: 10.1111/gcb.12556

Hwang, T., Band, L. E., Vose, J. M., and Tague, C. (2012). Ecosystem processes at the watershed scale: hydrologic vegetation gradient as an indicator for lateral hydrologic connectivity of headwater catchments. *Water Resour. Res.* 48:W06514.

Hwang, T., Gholizadeh, H., Sims, D. A., Novick, K. A., Brzostek, E. R., Phillips, R. P., et al. (2017). Capturing species-level drought responses in a temperate deciduous forest using ratios of photochemical reflectance indices between sunlit and shaded canopies. *Remote Sens. Environ.* 199, 350–359. doi: 10.1016/j.rse.2017.07.033

Hwang, T., Martin, K. L., Vose, J. M., Wear, D., Miles, B., Kim, Y., et al. (2018). Non−stationary hydrologic behavior in forested watersheds is mediated by climate−induced changes in growing season length and subsequent vegetation growth. *Water Resour. Res.* 54, 5359–5375. doi: 10.1029/2017wr022279

Hwang, T., Song, C., Bolstad, P. V., and Band, L. E. (2011a). Downscaling real-time vegetation dynamics by fusing multi-temporal MODIS and Landsat NDVI in topographically complex terrain. *Remote Sens. Environ.* 115, 2499–2512. doi: 10.1016/j.rse.2011.05.010

Hwang, T., Song, C., Vose, J. M., and Band, L. E. (2011b). Topography-mediated controls on local vegetation phenology estimated from MODIS vegetation index. *Landsc. Ecol.* 26, 541–556. doi: 10.1007/s10980-011-9580-8

Jencso, K. G., McGlynn, B. L., Gooseff, M. N., Wondzell, S. M., Bencala, K. E., and Marshall, L. A. (2009). Hydrologic connectivity between landscapes and streams: transferring reach-and plot-scale understanding to the catchment scale. *Water Resour. Res.* 45:W04428.

Keeling, C. D., Chin, J. F. S., and Whorf, T. P. (1996). Increased activity of northern vegetation inferred from atmospheric CO2 measurements. *Nature* 382, 146–149. doi: 10.1038/382146a0

Keenan, T. F., Gray, J., Friedl, M. A., Toomey, M., Bohrer, G., Hollinger, D. Y., et al. (2014). Net carbon uptake has increased through warming-induced changes in temperate forest phenology. *Nat. Clim. Chang.* 4, 598–604. doi: 10.1038/nclimate2253

Kim, J., Hwang, T., Schaaf, C. L., Orwig, D. A., Boose, E., and Munger, J. W. (2017). Increased water yield due to the hemlock woolly adelgid infestation in New England. *Geophys. Res. Lett.* 44, 2327–2335. doi: 10.1002/2016gl072327

Kim, J. H., Hwang, T., Yang, Y., Schaaf, C. L., Boose, E., and William Munger, J. (2018). Warming−induced earlier greenup leads to reduced stream discharge in a temperate mixed forest catchment. *J. Geophys. Res. Biogeosci.* 123, 1960–1975. doi: 10.1029/2018jg004438

Klein, T. (2014). The variability of stomatal sensitivity to leaf water potential across tree species indicates a continuum between isohydric and anisohydric behaviours. *Funct. Ecol.* 28, 1313–1320. doi: 10.1111/1365-2435.12289

Klos, R. J., Wang, G. G., Bauerle, W. L., and Rieck, J. R. (2009). Drought impact on forest growth and mortality in the southeast USA: an analysis using forest health and monitoring data. *Ecol. Appl.* 19, 699–708. doi: 10.1890/08-0330.1

Knoepp, J. D., See, C. R., Vose, J. M., Miniat, C. F., and Clark, J. S. (2018). Total C and N pools and fluxes vary with time, soil temperature, and moisture along an elevation, precipitation, and vegetation gradient in southern appalachian forests. *Ecosystems* 21, 1623–1638. doi: 10.1007/s10021-018-0244-2

Knoepp, J. D., and Swank, W. T. (1998). Rates of nitrogen mineralization across an elevation and vegetation gradient in the southern Appalachians. *Plant Soil* 204, 235–241.

Laseter, S. H., Ford, C. R., Vose, J. M., and Swift, L. W. (2012). Long-term temperature and precipitation trends at the Coweeta Hydrologic Laboratory, Otto, North Carolina, USA. *Hydrol. Res.* 43, 890–901. doi: 10.2166/nh.2012.067

Li, H., and Sivapalan, M. (2011). Effect of spatial heterogeneity of runoff generation mechanisms on the scaling behavior of event runoff responses in a natural river basin. *Water Resour. Res.* 47:W00H08.

Lim, K. J., Engel, B. A., Tang, Z. X., Choi, J., Kim, K. S., Muthukrishnan, S., et al. (2005). Automated web Gis based hydrograph analysis tool, what. *J. Am. Water Resour. Assoc.* 41, 1407–1416. doi: 10.1016/j.scitotenv.2018.09.225

Mackay, D. S., Ewers, B. E., Loranty, M. M., and Kruger, E. L. (2010). On the representativeness of plot size and location for scaling transpiration from trees to a stand. *J. Geophys. Res. Biogeosci.* 115:G02016.

Martin-Benito, D., Pederson, N., and Svenning, J.-C. (2015). Convergence in drought stress, but a divergence of climatic drivers across a latitudinal gradient in a temperate broadleaf forest. *J. Biogeogr.* 42, 925–937. doi: 10.1111/jbi.12462

Martínez-Vilalta, J., Poyatos, R., Aguadé, D., Retana, J., and Mencuccini, M. (2014). A new look at water transport regulation in plants. *New Phytol.* 204, 105–115. doi: 10.1111/nph.12912

McDowell, N. G., and Allen, C. D. (2015). Darcy's law predicts widespread forest mortality under climate warming. *Nat. Clim. Chang.* 5, 669–672. doi: 10.1038/nclimate2641

McGuire, K. J., and McDonnell, J. J. (2010). Hydrological connectivity of hillslopes and streams: characteristic time scales and nonlinearities. *Water Resour. Res.* 46:W10543.

McLaughlin, B. C., Ackerly, D. D., Klos, P. Z., Natali, J., Dawson, T. E., and Thompson, S. E. (2017). Hydrologic refugia, plants, and climate change. *Glob. Chang. Biol.* 23, 2941–2961. doi: 10.1111/gcb.13629

Meinzer, F. C., Woodruff, D. R., Eissenstat, D. M., Lin, H. S., Adams, T. S., and McCulloh, K. A. (2013). Above-and belowground controls on water use by trees of different wood types in an eastern US deciduous forest. *Tree Physiol.* 33, 345–356. doi: 10.1093/treephys/tpt012

Meinzer, F. C., Woodruff, D. R., Marias, D. E., Smith, D. D., McCulloh, K. A., Howard, A. R., et al. (2016). Mapping 'hydroscapes' along the iso- to anisohydric continuum of stomatal regulation of plant water status. *Ecol. Lett.* 19, 1343–1352. doi: 10.1111/ele.12670

Miniat, C. F., Laseter, S. H., Swank, W. T., and Swift, L. W. J. (2017). *Daily Precipitation Data from Recording Rain Gages (RRG) at Coweeta Hydrologic Lab, North Carolina*. Fort Collins, CO: Forest Service Research Data Archive.

Miniat, C. F., Laseter, S. H., Swank, W. T., and Vose, J. M. (2016). *Daily Streamflow Data for Watersheds at Coweeta Hydrologic Lab, North Carolina*. Fort Collins, CO: Forest Service Research Data Archive.

Myneni, R. B., Hoffman, S., Knyazikhin, Y., Privette, J. L., Glassy, J., Tian, Y., et al. (2002). Global products of vegetation leaf area and fraction absorbed PAR from year one of MODIS data. *Remote Sens. Environ.* 83, 214–231. doi: 10.1016/s0034-4257(02)00074-3

Myneni, R. B., Keeling, C. D., Tucker, C. J., Asrar, G., and Nemani, R. R. (1997). Increased plant growth in the northern high latitudes from 1981 to 1991. *Nature* 386, 698–702. doi: 10.1038/386698a0

Nemani, R., Pierce, L., Running, S., and Band, L. (1993). Forest ecosystem processes at the watershed scale: sensitivity to remotely-sensed leaf area index estimates. *Int. J. Remote Sens.* 14, 2519–2534. doi: 10.1080/01431169308904290

Nemani, R. R., and Running, S. W. (1989). Testing a theoretical climate soil leaf-area hydrologic equilibrium of forests using satellite data and ecosystem simulation. *Agric. For. Meteorol.* 44, 245–260. doi: 10.1016/0168-1923(89)90020-8

Nepstad, D. C., Decarvalho, C. R., Davidson, E. A., Jipp, P. H., Lefebvre, P. A., Negreiros, G. H., et al. (1994). The role of deep roots in the hydrological and carbon cycles of amazonian forests and pastures. *Nature* 372, 666–669. doi: 10.1038/372666a0

Novick, K. A., Oishi, A. C., and Miniat, C. F. (2016). Cold air drainage flows subsidize montane valley ecosystem productivity. *Glob. Chang. Biol.* 22, 4014–4027. doi: 10.1111/gcb.13320

Nowacki, G. J., and Abrams, M. D. (2008). The demise of fire and "mesophication" of forests in the eastern United States. *BioScience* 58, 123–138. doi: 10.1641/b580207

Nowacki, G. J., and Abrams, M. D. (2015). Is climate an important driver of post−European vegetation change in the Eastern United States? *Glob. Chang. Biol.* 21, 314–334. doi: 10.1111/gcb.12663

Oishi, A. C., Miniat, C. F., Novick, K. A., Brantley, S. T., Vose, J. M., and Walker, J. T. (2018). Warmer temperatures reduce net carbon uptake, but do not affect water use, in a mature southern Appalachian forest. *Agric. For. Meteorol.* 252, 269–282. doi: 10.1016/j.agrformet.2018.01.011

Pachauri, R. K., Allen, M., Barros, V., Broome, J., Cramer, W., Christ, R., et al. (2014). *Climate Change 2014: Synthesis Report. Contribution of Working Groups I, II and III to the Fifth Assessment Report of the Intergovernmental Panel on Climate Change*. Geneva: Intergovernmental Panel on Climate Change.

Roderick, M. L., and Farquhar, G. D. (2002). The cause of decreased pan evaporation over the past 50 years. *Science* 298, 1410–1411.

Roman, D., Novick, K., Brzostek, E., Dragoni, D., Rahman, F., and Phillips, R. (2015). The role of isohydric and anisohydric species in determining ecosystem-scale response to severe drought. *Oecologia* 179, 641–654. doi: 10.1007/s00442-015-3380-9

Rupp, D. E., and Selker, J. S. (2006a). Information, artifacts, and noise in dQ/dt-Q recession analysis. *Adv. Water Resour.* 29, 154–160. doi: 10.1016/j.advwatres.2005.03.019

Rupp, D. E., and Selker, J. S. (2006b). On the use of the Boussinesq equation for interpreting recession hydrographs from sloping aquifers. *Water Resour. Res.* 42:W12421.

Scaife, C. I., and Band, L. E. (2017). Nonstationarity in threshold response of stormflow in southern Appalachian headwater catchments. *Water Resour. Res.* 53, 6579–6596. doi: 10.1002/2017wr020376

Seager, R., Tzanova, A., and Nakamura, J. (2009). Drought in the Southeastern United States: causes, variability over the last millennium, and the potential for future hydroclimate change. *J. Clim.* 22, 5021–5045. doi: 10.1175/2009jcli2683.1

Sellers, P. J. (1985). Canopy reflectance, photosynthesis and transpiration. *Int. J. Remote Sens.* 6, 1335–1372. doi: 10.1080/01431168508948283

Siqueira, M., Katul, G., and Porporato, A. (2008). Onset of water stress, hysteresis in plant conductance, and hydraulic lift: scaling soil water dynamics from millimeters to meters. *Water Resour. Res.* 44:W01432.

Smakhtin, V. U. (2001). Low flow hydrology: a review. *J. Hydrol.* 240, 147–186. doi: 10.1016/s0022-1694(00)00340-1

Song, C., Chen, J. M., Hwang, T., Gonsamo, A., Croft, H., Zhang, Q., et al. (2015). "Ecological characterization of vegetation using multisensor remote sensing in the solar reflective spectrum," in *Land Resources Monitoring, Modeling, and Mapping with Remote Sensing*, ed. P. S. Thenkabail, (Boca Raton, FL: CRC Press), 533–575.

Song, C., Woodcock, C. E., Seto, K. C., Lenney, M. P., and Macomber, S. A. (2001). Classification and change detection using Landsat TM data: when and how to correct atmospheric effects? *Remote Sens. Environ.* 75, 230–244. doi: 10.1016/s0034-4257(00)00169-3

Stephenson, N. L. (1990). Climatic control of vegetation distribution: the role of the water balance. *Am. Nat.* 135, 649–670. doi: 10.1086/285067

Swift, L. W., Cunningham, J. G. B., and Douglass, J. E. (1988). "Climatology and hydrology," in *Forest Hydrology and Ecology at Coweeta*, eds W. T. Swank, and J. D. A. Crossley, (New York, NY: Springer-Verlag), 35–55.

Tague, C., Grant, G., Farrell, M., Choate, J., and Jefferson, A. (2008). Deep groundwater mediates streamflow response to climate warming in the Oregon Cascades. *Clim. Chang.* 86, 189–210. doi: 10.1007/s10584-007-9294-8

Tague, C. L. (2009). Assessing climate change impacts on alpine stream-flow and vegetation water use: mining the linkages with subsurface hydrologic processes. *Hydrol. Process.* 23, 1815–1819. doi: 10.1002/hyp.7288

Tai, X., Mackay, D. S., Anderegg, W. R., Sperry, J. S., and Brooks, P. D. (2017). Plant hydraulics improves and topography mediates prediction of aspen

mortality in southwestern USA. *New Phytol.* 213, 113–127. doi: 10.1111/nph.14098

Tarboton, D. G. (1997). A new method for the determination of flow directions and upslope areas in grid digital elevation models. *Water Resour. Res.* 33, 309–319. doi: 10.1029/96wr03137

Thompson, S. E., Harman, C. J., Troch, P. A., Brooks, P. D., and Sivapalan, M. (2011). Spatial scale dependence of ecohydrologically mediated water balance partitioning: a synthesis framework for catchment ecohydrology. *Water Resour. Res.* 47:W00J03.

Troch, P. A., Martinez, G. F., Pauwels, V. R. N., Durcik, M., Sivapalan, M., Harman, C., et al. (2009). Climate and vegetation water use efficiency at catchment scales. *Hydrol. Process.* 23, 2409–2414. doi: 10.1002/hyp.7358

Tromp-van Meerveld, H. J., and McDonnell, J. J. (2006). On the interrelations between topography, soil depth, soil moisture, transpiration rates and species distribution at the hillslope scale. *Adv. Water Resour.* 29, 293–310. doi: 10.1016/j.advwatres.2005.02.016

Tucker, C. J. (1979). Red and photographic infrared linear combinations for monitoring vegetation. *Remote Sens. Environ.* 8, 127–150. doi: 10.1016/0034-4257(79)90013-0

van der Molen, M. K., Dolman, A. J., Ciais, P., Eglin, T., Gobron, N., Law, B. E., et al. (2011). Drought and ecosystem carbon cycling. *Agric. For. Meteorol.* 151, 765–773.

VanDerWal, J., Murphy, H. T., Kutt, A. S., Perkins, G. C., Bateman, B. L., Perry, J. J., et al. (2013). Focus on poleward shifts in species' distribution underestimates the fingerprint of climate change. *Nat. Clim. Chang.* 3, 239–243. doi: 10.1038/nclimate1688

Vicente-Serrano, S. M., Perez-Cabello, F., and Lasanta, T. (2008). Assessment of radiometric correction techniques in analyzing vegetation variability and change using time series of Landsat images. *Remote Sens. Environ.* 112, 3916–3934. doi: 10.1016/j.rse.2008.06.011

Voepel, H., Ruddell, B., Schumer, R., Troch, P. A., Brooks, P. D., Neal, A., et al. (2011). Quantifying the role of climate and landscape characteristics on hydrologic partitioning and vegetation response. *Water Resour. Res.* 47:W00J09.

Vose, J. M., and Elliott, K. (2016). Oak, fire, and global change in the eastern USA: what might the future hold? *Fire Ecol.* 12, 160–178.

Ward, E. J., Oren, R., Kim, H. S., Kim, D., Tor−ngern, P., Ewers, B. E., et al. (2018). Evapotranspiration and water yield of a pine−broadleaf forest are not altered by long−term atmospheric [CO2] enrichment under native or enhanced soil fertility. *Glob. Chang. Biol.* 24, 4841–4856. doi: 10.1111/gcb.14363

Warren, J. M., Pötzelsberger, E., Wullschleger, S. D., Thornton, P. E., Hasenauer, H., and Norby, R. J. (2011). Ecohydrologic impact of reduced stomatal conductance in forests exposed to elevated CO2. *Ecohydrology* 4, 196–210. doi: 10.1002/eco.173

Western, A. W., Grayson, R. B., Bloschl, G., Willgoose, G. R., and McMahon, T. A. (1999). Observed spatial organization of soil moisture and its relation to terrain indices. *Water Resour. Res.* 35, 797–810. doi: 10.1029/1998wr900065

Woods, R. A., and Sivapalan, M. (1997). A connection between topographically driven runoff generation and channel network structure. *Water Resour. Res.* 33, 2939–2950. doi: 10.1029/97wr01880

Wullschleger, S. D., and Hanson, P. J. (2006). Sensitivity of canopy transpiration to altered precipitation in an upland oak forest: evidence from a long−term field manipulation study. *Glob. Chang. Biol.* 12, 97–109. doi: 10.1111/j.1365-2486.2005.001082.x

Yeakley, J. A., Swank, W. T., Swift, L. W., Hornberger, G. M., and Shugart, H. H. (1998). Soil moisture gradients and controls on a southern Appalachian hillslope from drought through recharge. *Hydrol. Earth Syst. Sci.* 2, 41–49. doi: 10.5194/hess-2-41-1998

Conflict of Interest: The authors declare that the research was conducted in the absence of any commercial or financial relationships that could be construed as a potential conflict of interest.

frontiers in Forests and Global Change

ORIGINAL RESEARCH
published: 13 March 2020
doi: 10.3389/ffgc.2020.00023

Southern Pines Are Resistant to Mortality From an Exceptional Drought in East Texas

Paul A. Klockow[1,2]*, *Christopher B. Edgar*[2], *Georgianne W. Moore*[1] and *Jason G. Vogel*[3]

[1] Department of Ecosystem Science and Management, Texas A&M University, College Station, TX, United States, [2] Department of Forest Resources, University of Minnesota, St. Paul, MN, United States, [3] School of Forest Resources and Conservation, University of Florida, Gainesville, FL, United States

In 2011, the state of Texas experienced its worst drought ever recorded, breaking statewide temperature, and precipitation records. With climate predictions suggesting increases in the severity and extent of future droughts in this region, forest managers will need to plan for such events to minimize tree mortality. In east Texas, pine species are economically and ecologically important and are often managed, providing an opportunity to examine silvicultural strategies for mitigating exceptional drought mortality. We used U.S. Forest Service Forest Inventory and Analysis data and Bayesian, logistic, mixed effects regression to model individual tree mortality and the effect of stand structure (i.e., tree size, relative density, and species dominance) on three major pine groups, planted (PL) and naturally-regenerated (NL) loblolly pine (*Pinus taeda* L.) and all shortleaf pine (SL, *Pinus echinata* Mill.), under pre-drought and drought periods in east Texas. These groups represent a spectrum of management intensity with PL generally intensively managed and NL and SL relatively unmanaged. Moreover, loblolly pine tends to be production-oriented while shortleaf pine has perceived drought tolerance. Surprisingly, pine mortality did not increase significantly from pre-drought to drought periods in spite of the record drought conditions. However, mortality differed between pine groups and in response to stand structure for loblolly pine. Planted loblolly was least affected as mortality rate increased 9.8%. In contrast, NL and SL pine mortality rates were significantly higher than PL and increased 26.3 and 20.0%, respectively. The smallest and largest stems experienced elevated mortality under both periods, notably PL under exceptional drought. As expected, higher densities of loblolly pine exacerbated exceptional drought mortality. Surprisingly, greater overstory diversity for NL reduced mortality under exceptional drought. Despite the unprecedented hot and dry conditions of the 2011 drought, our results suggest that current practices in PL that manage relative density and tree size for non-drought conditions confers mortality resistance under exceptional drought. In NL stands, mortality resistance could be increased through active thinning and promoting greater overstory diversity. These results offer critical knowledge for managers tasked with providing continued forest resources in the face of future exceptional droughts.

Keywords: Bayesian multi-level model, exceptional drought, Forest Inventory and Analysis (FIA), loblolly pine, natural regeneration, plantation, shortleaf pine, tree mortality

OPEN ACCESS

Edited by:
Matthew D. Hurteau, University of New Mexico, United States

Reviewed by:
Taehee Hwang, Indiana University Bloomington, United States
Lucy Penn Kerhoulas, Humboldt State University, United States

***Correspondence:**
Paul A. Klockow
pklockow@umn.edu

Specialty section:
This article was submitted to Forest Hydrology, a section of the journal Frontiers in Forests and Global Change

Received: *31 October 2019*
Accepted: *24 February 2020*
Published: *13 March 2020*

Citation:
Klockow PA, Edgar CB, Moore GW and Vogel JG (2020) Southern Pines Are Resistant to Mortality From an Exceptional Drought in East Texas. Front. For. Glob. Change 3:23. doi: 10.3389/ffgc.2020.00023

INTRODUCTION

Future climate is predicted to become hotter and increase the extent and severity of future droughts worldwide [Intergovernmental Panel on Climate Change (IPCC), 2013]. Forests may already be responding to climatic changes (van Mantgem et al., 2009; Peng et al., 2011) in part through increases in drought-related tree mortality (Allen et al., 2015). Elevated mortality and possible tree die-offs from future exceptional droughts could have profound ramifications on forested systems (Anderegg et al., 2013) and represent a major challenge to resource managers tasked with maintaining healthy, productive forests in an uncertain future (Clark et al., 2016; Vose et al., 2016). Manipulating stand structure and composition through silvicultural practices could mitigate stressful conditions and provide resistance to mortality from future disturbances (Puettmann, 2011). However, knowledge of whether such tools could be effective for increasing forest resistance to mortality from future exceptional droughts remains virtually non-existent.

Forests of the southeastern U.S. are highly productive and economically important generating more timber volume than any other region in the country (Oswalt et al., 2014). Nearly 20% of all pine-dominated forest in the southeastern U.S. is comprised of intensively managed plantations (Chen et al., 2017) often receiving competition control, fertilization, and planting of genetically improved seedlings at calculated densities (Fox et al., 2007). In east Texas, this paradigm holds true for loblolly pine (*Pinus taeda* L.) which occurs largely as both heavily managed planted pine and unmanaged or minimally-managed, naturally-regenerated pine (Edgar and Zehnder, 2017). This dichotomy in loblolly pine condition has led to questions about the functionality of plantations compared to naturally-regenerated stands of this species under extreme drought conditions. Evidence from a comparison of physiological characteristics (i.e., root hydraulic conductivity, root:shoot ratios) suggested that plantation loblolly pine should be more drought-sensitive than naturally-regenerated pine in terms of productivity (Domec et al., 2015) possibly driven by fertilization inputs affecting transpiration and root production (Ward et al., 2015). However, fertilized plantation pine at the western edge of its range increased water use efficiency and sustained productivity under water-limited conditions (Maggard et al., 2017; Bracho et al., 2018) suggesting intensively managed pine could better cope with drought. Still, these studies focused on productivity response under more moderate drought conditions. Knowledge of the mortality response of these pine groups to exceptional drought remains virtually non-existent and the implications could have cascading economic impacts throughout the most productive forests in the U.S.

Species selection for planting may play a critical role in the mortality response of forests to future exceptional droughts. In the southeastern U.S., shortleaf pine (*Pinus echinata* Mill.) has a perceived potential to withstand elevated water stress given its historical occurrence across a range of site conditions including xeric sites and rocky outcrops (Mattoon, 1915). Under non-drought conditions, mature shortleaf pine sustained higher mortality and lower productivity than loblolly pine in southeastern Oklahoma (Dipesh et al., 2015). However, no study has compared the mortality response of mature shortleaf pine to more commonly occurring southern pine species under drought conditions, moderate, or exceptional. Shortleaf pine has seen drastically reduced dominance because of logging and subsequent fire suppression (Barrett, 1995) leading to widespread restoration initiatives to increase its prevalence in the southeastern U.S. (e.g., Shortleaf Pine Initiative). East Texas is one region in which this species could be targeted for restoration efforts. Yet, very little information exists on growth and mortality responses of shortleaf pine to drought, and none under exceptional drought. Ultimately, this gap in knowledge hinders management efforts aimed at successfully restoring this declining species in an uncertain climate future.

Stand structure (e.g., tree size, stem density, and species composition) represents one set of conditions most easily manipulated by managers for mitigating negative drought effects (Clark et al., 2016). The smallest and largest trees tend to experience higher mortality rates under non-drought conditions, often termed "U-shaped" or "J-shaped" mortality curves (Lines et al., 2010; Dietze and Moorcroft, 2011). Small stems typically comprise the regenerating component of early-successional forests and drought-related increases in mortality in this group could alter future forest composition (Thrippleton et al., 2018). Large trees play important ecological roles in forested ecosystems (Lindenmayer et al., 2012) yet, recent evidence suggests that they may be most susceptible to extreme drought conditions and are suffering disproportionate mortality worldwide (Lindenmayer et al., 2012; Bennett et al., 2015). However, these patterns in large tree drought mortality have been variable and difficult to confirm (Floyd et al., 2009; Klos et al., 2009; Ganey and Vojta, 2011). Additionally, alleviating competition for limited resources by reducing stand density and basal area (cross-sectional stem area at 1.37 m height) has long been utilized by practitioners to improve growth and productivity. Recent evidence highlights that, reducing competition through silvicultural thinning has improved growth response to water stress (D'Amato et al., 2013; Bottero et al., 2017; Gleason et al., 2017). However, unprecedented exceptional drought conditions that drive very low soil water potentials may negate any benefits gained from reduced competition resulting in increased tree mortality regardless of density (Floyd et al., 2009). Finally, stand species composition can be an important factor in affecting drought mortality (Klos et al., 2009; Cavin et al., 2013) as interactions with water and nutrient pools may differ among species (Forrester, 2014). Neighboring trees of different species may show facilitation via hydraulic lift more than competition (Pretzsch et al., 2013) or access different resource pools alleviating stressful conditions (Kramer and Holscher, 2010) which may be exacerbated in single-species-dominated stands. However, despite the wealth of knowledge on controlling stand structure to achieve desired outcomes, critical knowledge gaps exist in understanding whether common management practices remain effective for increasing pine resistance to future exceptional drought mortality.

From October 2010 to September 2011, the state of Texas experienced its worst drought on record with over 80% of

the land area under the most severe (i.e., exceptional) drought classification (Nielsen-Gammon, 2012). The heavily forested region of east Texas suffered similarly exceptional hot and dry temperature and precipitation patterns seen statewide, having the hottest summer temperature deviation (+3.1°C) and lowest 12-month precipitation (619 mm; 47% lower than twentieth century average of 1,162 mm) ever recorded [National Oceanic and Atmospheric Administration (NOAA), 2018] Within east Texas, *Pinus* mortality was lower than other common genera such as *Quercus* and *Liquidambar* yet still experienced elevated levels of mortality from the harsh conditions (Moore et al., 2016; Klockow et al., 2018). The record exceptional drought of 2011 provides a critical opportunity to examine more closely southern pine vulnerability to exceptional drought and to identify specific aspects of stand structure that could be manipulated to develop adaptive management strategies for increasing resistance to exceptional drought mortality. Using national forest inventory plots with complete and systematic coverage of east Texas, we addressed the following objectives: (1) examine mortality rates of three common pine species groups (i.e., planted loblolly pine, naturally-regenerated loblolly pine, and shortleaf pine) under exceptional drought conditions and pre-drought (i.e., non-exceptional drought) conditions, (2) determine how stand structure (i.e., tree size, stem density, and species composition) affected individual tree mortality in the same pine species groups under exceptional drought conditions and pre-drought conditions, and (3) provide targeted management suggestions based on predicted mortality trends for mitigating exceptional drought mortality in southern pine. We address these objectives at the individual tree scale using extensive re-measurements of pine throughout the region.

For objective 1, we hypothesized that pre-drought group mortality rates would be lowest in planted loblolly pine, given the extensive competition control and management actions in this group, and highest in the shortleaf pine group, given past evidence from Dipesh et al. (2015) under non-drought conditions. Regarding objective 2, we hypothesized for each group that, under pre-drought conditions, smaller trees would have higher mortality given their limited rooting depth and access to deeper water. Larger trees would have higher mortality potentially due to greater hydraulic stress, increased crown exposure, and preference by bark beetles (Bennett et al., 2015). Furthermore, under pre-drought conditions, the highest stem densities would show higher mortality following expected patterns of competition and the lowest stem densities would show higher mortality due to possible increased individual tree risk from maintenance of greater leaf area and root systems (Clark et al., 2016). Finally, pure species mixtures (i.e., plantations) would show higher mortality possibly through increased intra-specific competition (Klos et al., 2009). We generally expected that mortality increased from pre-drought to drought period for each group and each stand structure factor. However, given the dearth of knowledge regarding southern pine mortality to exceptional drought conditions, as experienced in Texas in 2011, it was difficult to speculate on the magnitude of the mortality response and whether any particular groups or aspects of stand structure fared better or worse than others.

MATERIALS AND METHODS

Study Area

This study was located in eastern Texas (29° 17′ to 33° 57′ N and 93° 30′ to 96° 27′ W; **Figure 1**), comprising the western extent of West Gulf Coastal Plain forests. Forests in this region are composed of a diverse species mix yet are heavily dominated by pine species, namely loblolly pine (*Pinus taeda* L.) followed by shortleaf pine (*Pinus echinata* Mill.). Hardwood species tend to comprise much of the mid- and under-story and include a diverse mix of oaks (e.g., *Quercus stellata* Wangenh., *Quercus nigra* L., etc.), sweetgum (*Liquidambar styraciflua* L.), and elm species (e.g., *Ulmus alata* Michx.). Climate is generally humid sub-tropical with hot, humid summers and mild, wet winters. During the study period (2003–2016), mean annual precipitation and temperature ranged between 769–1737 mm and 18.1–20.1°C, respectively (twentieth century averages of 1,162 mm and 18.6°C, respectively) with the lowest precipitation (769 mm) and second highest temperature (19.9°C) during this period occurring in 2011 [National Oceanic and Atmospheric Administration (NOAA), 2018]. Variation in topography is minimal with flat to rolling elevation changes ranging from sea-level near the coast to nearly 200 m above sea level. Soils are variable, ranging from poorly-drained to well-drained conditions predominantly comprised of loamy to clayey Alfisols and Ultisols [US Department of Agriculture Natural Resources Conservation Service (USDANRCS), 2006].

Dataset

Data were taken from the U.S. Forest Service Forest Inventory and Analysis (FIA) program for the region of east Texas. The full dataset consisted of 1,640 forested plots (>10% tree cover) measured across the range of ownerships and conditions existing within east Texas. A plot consists of four subplots each covering 168.1 m^2 (∼672.5 m^2 total plot area) with one central subplot and the three remaining subplots oriented ∼36.6 m distance (central subplot-center to outer subplot-center) at 0, 120, and 240 degrees. Trees were classified as stems ≥2.54 cm diameter at breast height (DBH; 1.37 m stem height). Trees with DBH ≥ 2.54 cm and <12.7 cm were measured on four microplots (13.5 m^2 each, ∼54.0 m^2 total) located within subplots while trees with DBH > 12.7 cm were measured on each full subplot. Species, DBH, and status (live or dead) were all recorded at each plot measurement and used in this study.

We categorized trees within the dataset as planted loblolly pine (PL), naturally-regenerated loblolly pine (NL), and all shortleaf pine (SL). Planted loblolly was identified by selecting plots originating from planted seedlings of loblolly pine and NL was identified by selecting plots of non-planted origin. The FIA dataset does not include information on genetic source of planted seedlings given challenges with spatial and temporal scales of sampling and the variety of ownerships across the landscape. However, these groups (i.e., PL and NL) provide a regional, fundamental comparison between trees of differing origins and management paradigms. There existed a few instances where a plot straddled both PL and NL conditions. We excluded these plots from our dataset to avoid the confounding effects of active

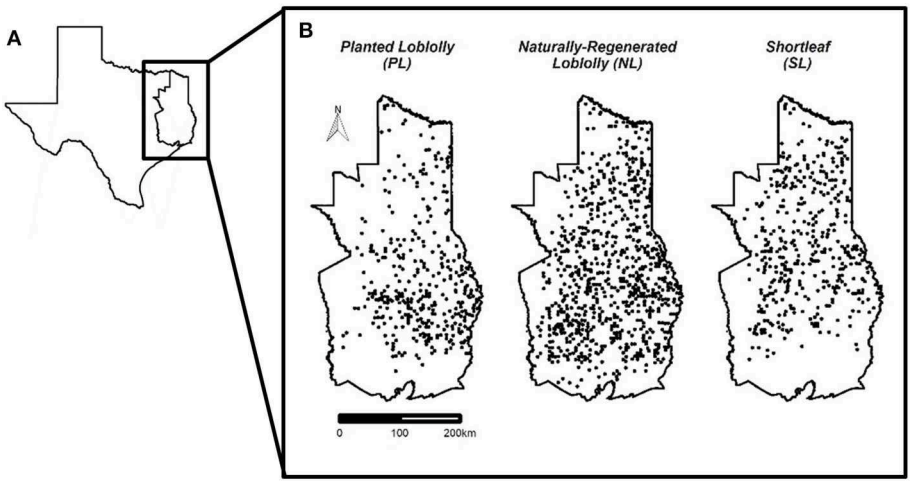

FIGURE 1 | State of Texas map with **(A)** study area of east Texas as inset and **(B)** Forest Inventory and Analysis plot locations used for each pine group.

or non-management at the interface of PL and NL conditions. Given the rare occurrence of shortleaf pine plantations coupled with their relatively low numbers in the dataset, shortleaf pine was categorized as one group (i.e., comprising both naturally-regenerated and any planted stems). All harvested/salvaged trees were excluded from the dataset to avoid confounding effects of silvicultural activity on mortality.

We classified trees into two measurement periods, pre-drought and drought. The pre-drought period consisted of trees initially measured as being alive and subsequently re-measured as alive or dead prior to 2011 (i.e., 2003–2010). Thus, the mortality response of pre-drought trees was not affected by the exceptional conditions of the 2011 drought. Drought period trees were initially measured as alive prior to 2011 and subsequently re-measured as alive or dead after 2011 (i.e., re-measurements between 2012 and 2016). Thus, the mortality response of drought period trees reflect exposure to the 2011 drought conditions assuming any individual tree did not die after initial measurement and prior to the onset of the drought. All plots were re-measured over approximately a 5-year period and differences in plot re-measurement intervals were addressed in our modeling approach described below. Preliminary analyses for spatial autocorrelation of plot-level mortality via Mantel tests confirmed that no significant ($\alpha = 0.05$) spatial autocorrelation existed among individual or all pine groups for both pre-drought and drought period plots.

We selected and calculated the following stand structural variables prior to any analysis: DBH to describe tree size, plot relative density (RD; calculated via DBH and wood specific gravity after Ducey and Knapp (2010), see their Equation 16) to describe competition among all trees within each plot, and plot species group dominance (SPD; basal area of a focal species group in a plot divided by total basal area of the plot) to describe the contribution of each pine group to the relative species diversity of plots. Variable selections were chosen based on their importance in describing individual tree size/age and local inter- and intra-specific competitive interactions. Moreover, the variables included in our analyses represent common metrics used by managers for manipulating forest conditions to achieve desired management objectives, offering operational relevance for potentially improving pine resistance to future exceptional droughts. All data were summarized and presented in **Table 1**.

Analysis

We analyzed the data for each objective using Bayesian, logistic, mixed-effects regression models. In all cases, the response variable was binary tree status at re-measurement (live = 1, dead = 0) modeled as a Bernoulli-distributed variable constrained by a probability of survival.

$$y_{ij} \sim Bernoulli(p_{Sij}) \tag{1}$$

Where, y_{ij} is the response for tree i in plot j and p_{Sij} is the probability of survival for tree i in plot j. To account for variability in plot re-measurement time intervals, we used an approach first presented by Hamilton and Edwards (1976) and incorporated a random effect component.

$$p_{Sij} = \left[\frac{1}{1 + e^{-\left(X_{ij}^T \beta_k + \mu_j\right)}} \right]^{L_j} \tag{2}$$

Where, p_{Sij} is the same as described in Equation (1), X_{ij}^T is the transposed matrix of covariates for tree i in plot j, β_k is the vector of length k of parameters to be estimated, u_j is the random effect of plot j, and L_j is the re-measurement interval for plot j. Using this approach, the estimated β_k's describe the annual log odds of survival for each tree as opposed to the log odds of survival for the specific re-measurement interval L_j. We included the random effect in each model to account for plot-level variability from site differences. Random effects were modeled as a normally-distributed variable with mean of zero and common variance.

$$\mu_j \sim Normal(0, \sigma^2) \tag{3}$$

TABLE 1 | Summary information for the pine groups analyzed in the study.

Pine group	Period	Plot count	Tree count	DBH (cm)	Relative density (RD)	Species dominance (SPD)
Planted loblolly (PL)	Pre	173	3,347	17.0 (4.6, 31.6)	0.37 (0.03, 0.95)	0.88 (0.16, 1.00)
	Drought	282	5,855	17.3 (4.8, 32.8)	0.38 (0.03, 1.00)	0.87 (0.11, 1.00)
Naturally-regenerated loblolly (NL)	Pre	444	3,992	18.0 (3.3, 54.6)	0.53 (0.03, 1.09)	0.40 (0.03, 0.95)
	Drought	612	5,489	19.8 (3.3, 58.9)	0.57 (0.07 1.10)	0.40 (0.02, 0.96)
Shortleaf (SL)	Pre	231	871	22.6 (5.1, 50.0)	0.58 (0.14, 0.98)	0.12 (0.01, 0.69)
	Drought	316	1,175	24.9 (6.9, 53.2)	0.59 (0.11, 1.10)	0.12 (0.01, 0.71)

Pre-drought period (Pre) trees were measured and re-measured from 2003 to 2010 and drought period (Drought) trees were initially measured prior to 2011 and re-measured 2012–2016. Diameter at breast height (DBH) is summarized across individual trees while relative density (RD) and species dominance (SPD) are plot-level metrics. Median values and 2.5th and 97.5th quantiles are presented in parentheses.

Where, μ_j is the mean effect in log odds for plot j and σ^2 is the variance of the distribution of plot mean effects. For objective 1, a single model was constructed and explanatory variables included the three pine groups (PG: PL, NL, SL), two measurement periods (MP: pre-drought, drought), and their interaction.

$$X = PG + MP + PG * MP \quad (4)$$

Where, X is the matrix of covariates from Equation (2). For objective 2, separate models were constructed for each pine group and measurement period (six total). Explanatory variables for each model included the three stand structural variables of DBH, RD, and SPD. All the explanatory variables were modeled as having a quadratic effect on predicted survival response to account for higher hypothesized mortality in the smallest and largest stems, lowest and highest density plots, etc.

$$X = DBH + DBH^2 + RD + RD^2 + SPD + SPD^2 \quad (5)$$

Where, X is the matrix of covariates from Equation (2). Variables for objective 2 were mean-centered and standardized to allow for more meaningful comparison of the effect sizes of each variable on predicted mortality within each model. For the presentation of results, we converted survival probabilities to mortality probabilities via $p_{Mij} = 1 - p_{Sij}$.

All models were fit using Hamiltonian Monte Carlo simulations implemented in the RStan package (Stan Development Team, 2017) accessed via R software (R Core Team, 2016). Vague priors were chosen for the estimated parameters. Specifically, priors for β_k followed a normal distribution of mean zero and standard deviation of 10^4 and μ_j followed a uniform distribution with mean zero and range 10^4. Use of vague priors meant that results of these analyses should be close to estimations from a maximum likelihood analysis. Chains were run for 100 k iterations with a 50 k warm-up and were thinned by 1/20 to reduce autocorrelation. Chain convergence to the posterior distribution was assessed visually using traceplots and by the R-hat statistic (Gelman and Rubin, 1992). To evaluate the performance of our models, we used a mixed posterior predictive assessment developed by Green et al. (2009) as employed by Masuda and Stone (2015). Broadly, posterior predictive model checking involves simulating replicated data under its modeled distribution using each MCMC simulated value of the estimated model parameters and comparing these new data with the observed data set (Hobbs and Hooten, 2015). In particular, the mixed posterior predictive assessment provides a more conservative assessment of model performance, being similar to the widely-accepted cross-validation technique, than a full posterior predictive assessment, particularly for hierarchical models (e.g., containing a random effect) (Green et al., 2009). This is accomplished by first drawing a new random effect for each group from its modeled distribution, adding the new mean effect to the estimated linear model component, and using the resulting value to draw a new observation from its modeled distribution. In contrast, the fixed posterior predictive assessment uses the estimated random effect rather than drawing a new one which consistently results in a deceptively better fit between observed data and replicated data (Green et al., 2009).

We used common management metrics to produce mortality curves from our resulting models and identified particular areas of concern where management actions could be implemented to potentially reduce exceptional drought mortality. Specifically, we produced mortality curves for 35 and 65% relative densities, which represent the range of fully-stocked stands, and for merchantable breast height stem diameters of 15, 25, and 35 cm, representing common pulpwood, small sawtimber, and large sawtimber stem sizes, respectively, in the study area.

RESULTS

Pine Group Mortality

As expected, drought period mortality increased relative to pre-drought mortality for all pine groups increasing 9.8, 20.0, and 26.3% for PL, SL, and NL, respectively. Surprisingly, none of the drought period mortality responses differed significantly from the pre-drought period (**Figure 2**, **Supplementary Table 1**). Notably, PL had significantly lower overall group mortality for both periods than NL and SL. Naturally-regenerated loblolly pine had the greatest increase in mean mortality response between periods suggesting it was the most sensitive to the drought conditions of the three pine groups. Shortleaf pine had the highest mean mortality for both periods and the greatest variability in mortality response.

Stand Structure

Stand structure was most important for describing mortality in loblolly pine with differing effects across PL, NL, and measurement periods (**Table 2**). Interestingly, stand structure

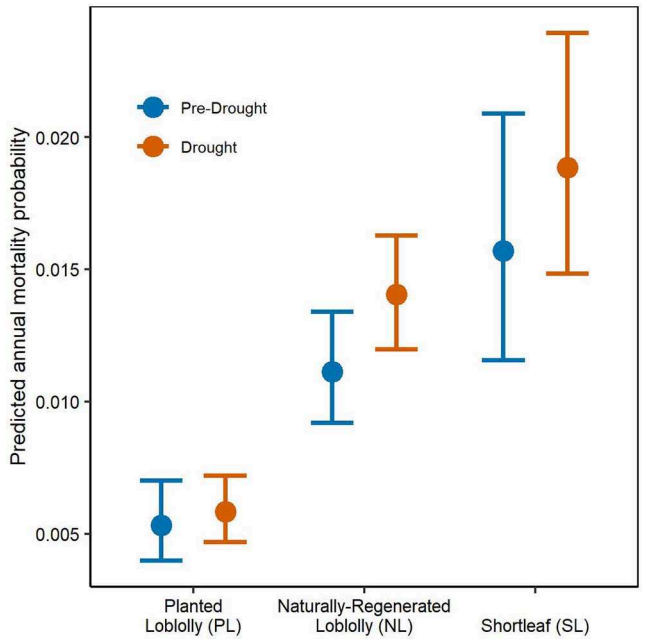

FIGURE 2 | Mortality probabilities for each pine group and measurement period with 95% credible intervals. Pre-drought period trees were measured and re-measured from 2003 to 2010 while drought period trees were initially measured prior to 2011 and re-measured 2012–2016. The R^2 for the mixed predictive assessment was 0.09. Prediction accuracy of live and dead trees was 0.999 and 0.132 for observed vs. predicted responses and 0.916 and 0.097 for replicated vs. predicted responses, respectively.

did not describe mortality in SL under either period. Diameter at breast height followed the hypothesized "U-shaped" or "J-shaped" pattern, reflecting higher mortality in the smallest and largest stems, when examined in relation to mortality for both PL and NL in both periods (**Table 2**). Notably, exceptional drought accentuated this mortality effect in the smallest and largest stems of PL but did not for NL. Plot relative density significantly increased mortality in loblolly pine primarily causing greater mortality with increasing density, being most pronounced in PL under drought (**Table 2**). The effects of relative density on pre-drought NL mortality leveled off at the highest densities but under exceptional drought, increased significantly at higher densities. In contrast to our hypothesis, lower relative densities did not result in elevated loblolly mortality for either period (**Table 2**). Interestingly, plot species dominance, describing the relative mixture of each pine group to all other species in a plot, significantly affected mortality among drought-period NL which experienced higher mortality with increasing NL dominance while pre-drought PL experienced lower mortality under increasing PL dominance (**Table 2**).

Management-Based Mortality Curves

Planted loblolly mortality curves for DBH highlight the increased vulnerability of the smallest and largest stem sizes exposed to the exceptional drought conditions (DBH of < 20 cm and > 40 cm; **Figures 3A,B**). This effect was most pronounced in the largest stems at higher stand densities (65% RD; **Figure 3B**). Merchantable stems of PL had very low mortality with very low variability regardless of period (**Figures 3A,B**). Interestingly, smaller stems under pre-drought conditions did not significantly differ in mortality at 35 or 65% RD (**Figure 3C**). However, smaller stems under exceptional drought had significantly higher mortality at 65% RD than at 35% RD (**Figure 3D**). For reference, PL mortality curves for RD and SPD can be found in **Supplementary Figures 1, 2**, respectively but are not discussed here.

Naturally-regenerated loblolly pine had higher mortality in the smallest and largest stems however, this effect did not differ between pre-drought and drought periods (**Figures 4A,B**). As with PL, merchantable stems of NL had very low mortality with very low variability (**Figures 4A,B**). However, merchantable stem mortality was significantly higher under exceptional drought at 35% RD (**Figure 4C**) whereas, at 65% RD, mortality did not differ between periods but was higher overall than at 35% RD (**Figure 4D**). Interestingly, SPD mortality curves for NL indicated that drought period mortality was significantly higher than pre-drought above ∼50% NL dominance for all merchantable stem sizes (**Figures 5A–C**). However, mortality was lower overall and did not differ significantly when NL dominance was below ∼50% (**Figures 5A–C**). For reference, the NL mortality curve for RD can be found in **Supplementary Figure 3** but is not discussed here.

Model Assessment

The mixed predictive assessment for the model based on Equation (4) (i.e., pine groups and measurement periods) suggested that live trees were predicted accurately and mortality responses were not predicted as well (**Table 2**). This is likely attributable to the limited number of dead trees in the dataset for PL as it had low mortality during both periods and may also be attributable to the similarity in mortality estimates for NL and SL making differentiation between groups difficult. The mixed predictive assessment for the models based on Equation (5) (i.e., stand structure) shows that the PL and NL models performed fairly well while the SL models performed poorly (**Table 2**). In all cases, live trees were predicted well while dead trees were predicted fairly (NL, PL) to poorly (SL). Since essentially none of the stand structural variables for SL significantly differed from zero and most were different from zero for PL and NL, it is not surprising that the SL models performed poorly and the PL and NL models provided better explanatory power for describing pre-drought and drought period mortality.

DISCUSSION

Pine Group Mortality

Climate projections indicate future increases in the extent and severity of droughts with possible substantial and widespread increases in tree mortality (Allen et al., 2015). Given the potential economic and ecological ramifications to the timber industry and forest ecosystem function, adaptive management strategies for coping with future exceptional droughts in forests need to be developed yet are critically lacking in the scientific

TABLE 2 | Model results for the effects of stand structure on pine group mortality for each measurement period with 95% credible intervals (DBH, diameter at breast height; RD, plot relative density; SPD, plot species dominance; Plot RE SD, estimated standard deviation from the random effect of plots).

Estimated parameters	Planted loblolly (PL)		Naturally-regenerated loblolly (NL)		Shortleaf (SL)	
Log odds mortality	**Pre**	**Drought**	**Pre**	**Drought**	**Pre**	**Drought**
Intercept	−5.617 (−6.183, −5.127)	−5.947 (−6.450, −5.498)	−4.924 (−5.291, −4.591)	−4.716 (−5.020, −4.417)	−4.848 (−5.789, −4.080)	−4.133 (−4.601, −3.705)
DBH	**−0.958 (−1.178, −0.748)**	**−1.082 (−1.234, −0.936)**	**−1.421 (−1.617, −1.239)**	**−1.130 (−1.272, −0.990)**	**−0.422 (−0.756, −0.098)**	−0.040 (−0.246, 0.173)
DBH^2	**0.188 (0.124, 0.249)**	**0.330 (0.274, 0.384)**	**0.451 (0.384, 0.517)**	**0.396 (0.341, 0.452)**	0.145 (−0.009, 0.286)	0.089 (−0.022, 0.192)
RD	**0.350 (0.031, 0.678)**	**0.831 (0.521, 1.169)**	**0.449 (0.251, 0.650)**	**0.233 (0.057, 0.414)**	0.257 (−0.096, 0.643)	0.098 (−0.106, 0.309)
RD^2	−0.128 (−0.357, 0.103)	0.017 (−0.191, 0.221)	**−0.160 (−0.312, −0.014)**	−0.037 (−0.161, 0.078)	0.024 (−0.260, 0.273)	0.075 (−0.037, 0.187)
SPD	**−0.587 (−1.075, −0.107)**	−0.071 (−0.520, 0.379)	0.130 (−0.064, 0.328)	**0.266 (0.074, 0.464)**	−0.094 (−0.567, 0.382)	0.061 (−0.186, 0.317)
SPD^2	**−0.221 (−0.439, −0.025)**	−0.176 (−0.383, 0.005)	0.006 (−0.162, 0.168)	−0.066 (−0.221, 0.086)	−0.016 (−0.484, 0.410)	0.037 (−0.231, 0.302)
Plot RE SD	−1.352 (−1.755, −1.016)	−1.715 (−2.087, −1.399)	−1.008 (−1.279, −0.762)	−1.458 (−1.657, −1.273)	−1.813 (−2.594, −1.205)	−1.067 (−1.417, −0.761)
R^2 MPA	0.38	0.25	0.71	0.20	0.07	0.07
Observed Pred. Acc. (live/dead)	0.999/0.014	0.997/0.330	0.996/0.144	0.991/0.315	1/0.144	0.997/0.070
Replicated Pred. Acc. (live/dead)	0.953/0.111	0.925/0.211	0.902/0.262	0.858/0.226	0.870/0.145	0.851/0.156

Pre-drought period (Pre) trees were measured and re-measured from 2003 to 2010 while drought period (Drought) trees were initially measured prior to 2011 and re-measured 2012–2016. Bold estimates, intercepts, and Plot RE SDs are significantly different from zero. The bottom three rows provide metrics from model assessment including, proportion of explained variance from the mixed predictive assessment on observed vs. replicated data (R^2 MPA), accuracy of observed vs. predicted live and dead trees, and accuracy of replicated vs. predicted live and dead trees.

literature (Kemp et al., 2015; Nagel et al., 2017). In this study, we provide an assessment of drought mortality in east Texas by examining the dominant species, loblolly pine, under its two primary silvicultural strategies, planted and naturally-regenerated, which broadly represent managed plantations and unmanaged/minimally-managed stands, respectively. These two conditions occur extensively throughout east Texas across a variety of ownerships (Edgar and Zehnder, 2017) and generally reflect conditions throughout the southeastern U.S., the most productive forested region in the country (Oswalt et al., 2014). Moreover, we examined shortleaf pine, currently a common species throughout the West Gulf Coastal Plain, which is targeted for restoration throughout its extensive historic range. Shortleaf pine is often perceived as drought-tolerant, given its wide historical range which included occurring on xeric sites (Mattoon, 1915), yet has received little attention in the literature regarding its drought mortality response. Here we show these predominant pine species groups are resistant to mortality from the historic exceptional drought conditions experienced in 2011 throughout east Texas.

Notably, we found that intensively managed stands (i.e., PL) appear to be most resistant to drought mortality. This finding was especially notable given that this region represents the westernmost extent of loblolly pine. Planted loblolly mortality was lowest of the three pine groups for both pre-drought and drought conditions, providing support for our hypothesis that pre-drought PL had the lowest mortality of the pine groups examined. Interestingly, exceptional drought exposure did not result in disproportionate mortality vulnerability in PL as has been hypothesized (Domec et al., 2015). Klos et al. (2009) observed higher drought sensitivity (growth and mortality) in pine species of Alabama, Georgia, and Virginia; however, they did not separate out PL from NL. Also, pines in the Klos et al. (2009) study occur in the central reaches of their geographical distribution, whereas east Texas represents the western range margin of loblolly pine. As mentioned in the methods, we were unable to explicitly account for PL seedling source. Yet in general, it is possible that loblolly pine genotypes in Texas are better adapted to drier, more variable climate than those genotypes found further east (Eckert et al., 2010; McNulty et al., 2014; Rehm et al., 2015). Recent examination of PL growth in the West Gulf Coastal Plain suggests that, even under water-limited conditions (albeit not as extreme as the 2011 drought), trees remained productive particularly when given fertilizer inputs (Maggard et al., 2017), suggesting positive response of water-stressed PL under management. However, that study addressed growth and not mortality response of PL to increased water stress. Critically, it appears the broad management actions associated with PL likely allowed these stands to resist mortality from the harsh, hot and dry conditions of the exceptional 2011 drought.

Of the groups examined, NL appeared the most vulnerable to exceptional drought having the highest increase in mean mortality response (26.3% increase). However, NL was still quite resistant given the lack of a significant increase in mortality

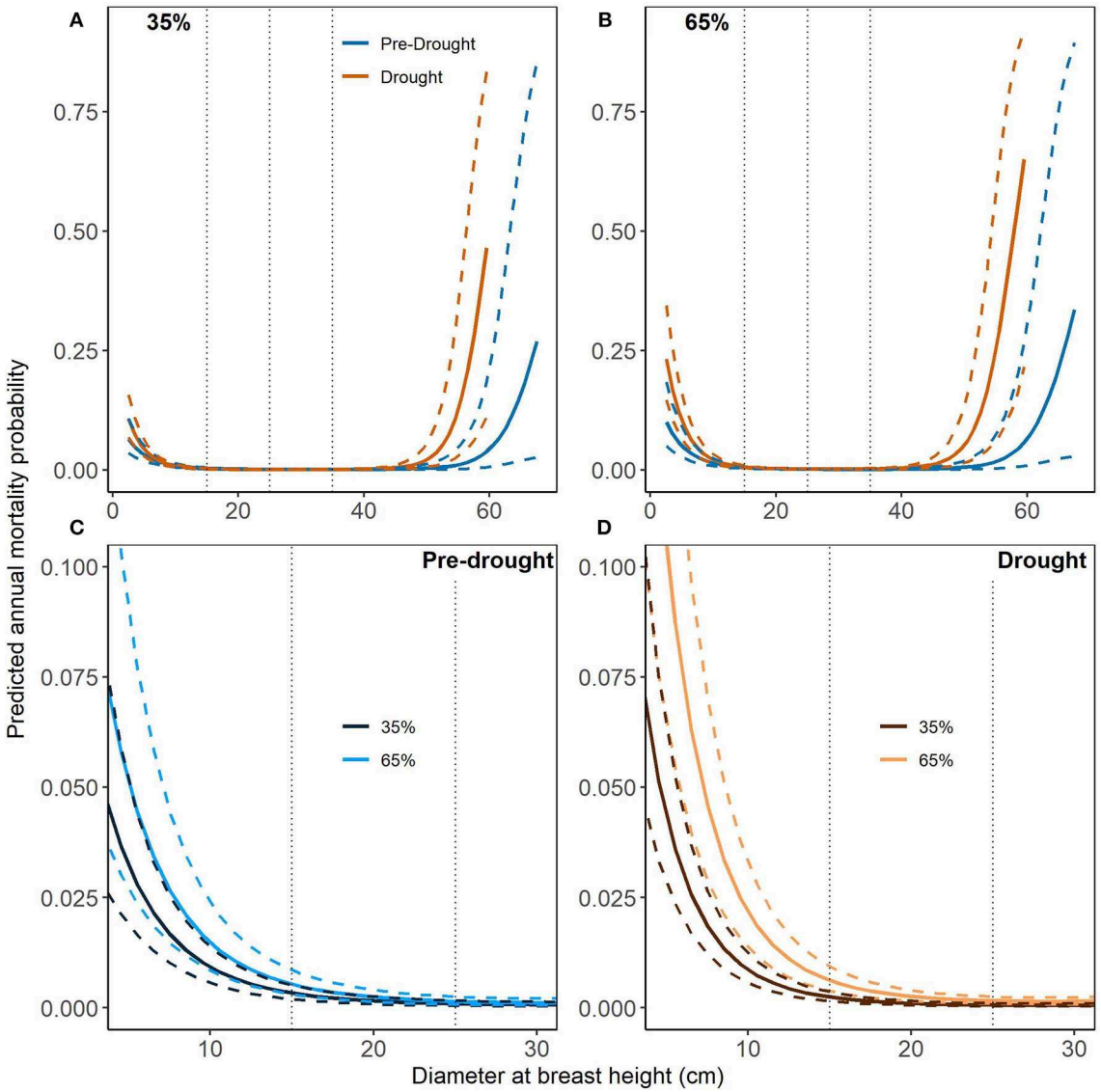

FIGURE 3 | Mortality curves (solid lines) for planted loblolly pine (PL) and diameter at breast height (DBH) with 95% credible intervals (dashed lines). Relative density (RD) is held constant at the lower (35%) and upper (65%) limits of fully-stocked conditions while species dominance (SPD) is held constant at its median values (∼90%, see **Table 1**). Pre-drought period trees were measured and re-measured from 2003 to 2010 while drought period trees were initially measured prior to 2011 and re-measured 2012–2016. Dotted vertical lines highlight merchantable size classes of 15, 25, and 35 cm DBH. **(A,B)** show mortality curves across the full range of DBH values while **(C,D)** display notable differences which occur at smaller DBH values.

between periods. A challenge with examining this group as a whole across the region of east Texas is disentangling the multiple factors driving this increased drought mortality response. Some NL stands remain unmanaged until harvest, however, many stands of NL have active competition control to improve productivity (Nelson and Bragg, 2016) providing an advantage when exposed to water stress. The existence of some management activity in a portion of NL stands may have muted the drought mortality response of unmanaged stands. Regardless, our data highlight that NL stands, as a whole, typically have higher densities across east Texas than PL (**Table 1**) suggesting that density-dependent competition may be the key factor driving the higher exceptional drought mortality response in this group.

Shortleaf pine maintained the highest mean group mortality rates under both pre-drought and drought periods. This result provides some support for the hypothesis that this species experienced the highest pre-drought mortality of the pine groups examined. This agrees with a recent study conducted in forests of southeastern Oklahoma, which reported higher mortality in SL compared to PL (Dipesh et al., 2015). The high variability in mortality estimates for SL can be attributed to the relatively small sample size in our dataset. Ultimately, SL is a relatively minor component of east Texas forests (∼3% of all species measured

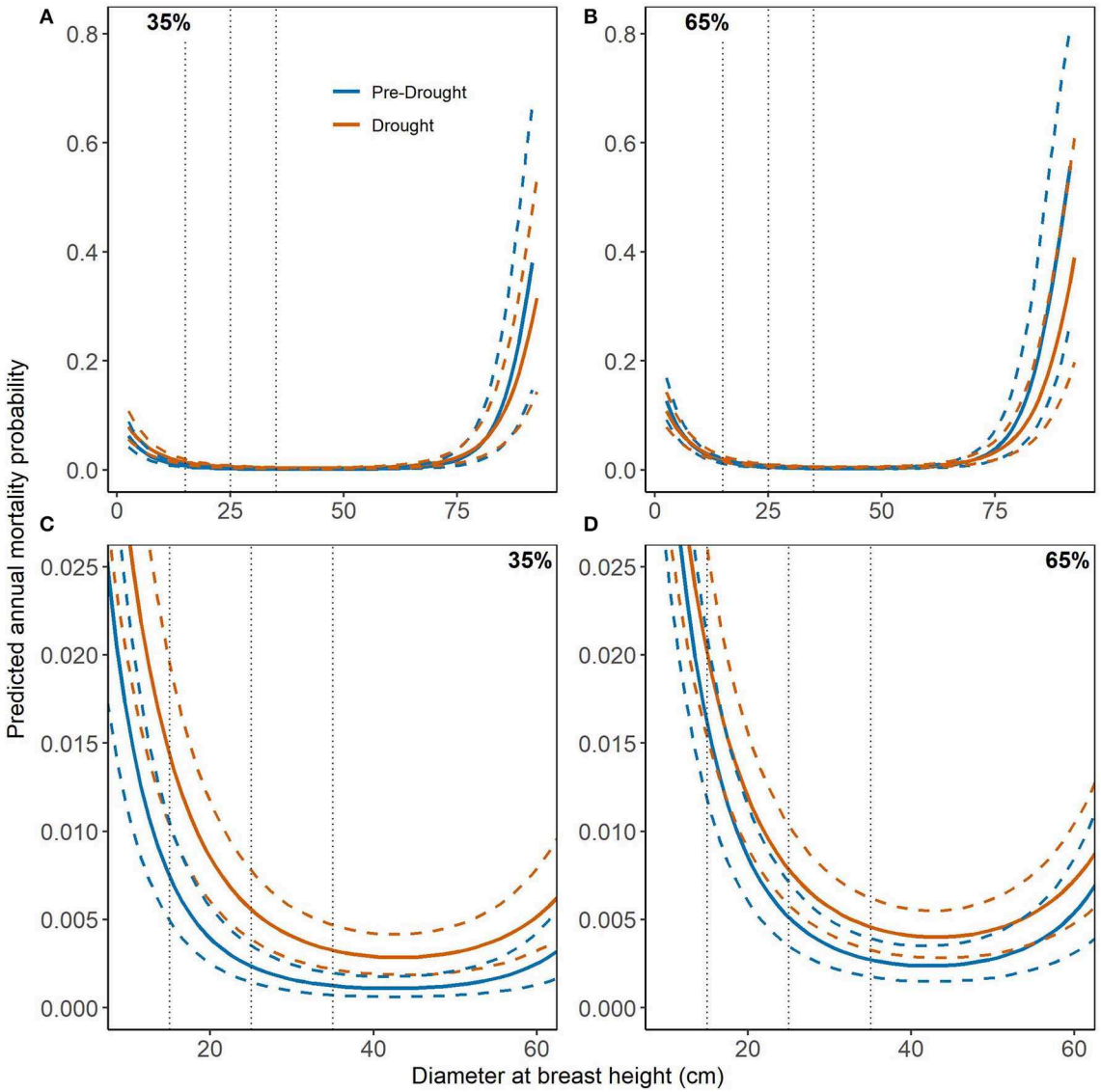

FIGURE 4 | Mortality curves (solid lines) for naturally-regenerated loblolly pine (NL) and diameter at breast height (DBH) with 95% credible intervals (dashed lines). Relative density (RD) is held constant at the lower (35%) and upper (65%) limits of fully-stocked conditions while species dominance (SPD) is held constant at its median values (~60%, see **Table 1**). Pre-drought period trees were measured and re-measured from 2003 to 2010 while drought period trees were initially measured prior to 2011 and re-measured 2012–2016. Dotted lines highlight merchantable size classes of 15, 25, and 35 cm DBH. **(A,B)** show mortality curves across the full range of DBH values in the dataset while **(C,D)** display notable differences which occur at small and mid-range DBH values.

by FIA) possibly occurring on sites less suitable for loblolly production. Thus, these higher mean group mortality rates may be more reflective of inherent site conditions than any particular physiological adaptations suited for drought.

Stand Structure

Despite the exceptional conditions of the 2011 drought, loblolly pine still followed hypothesized trends of mortality with tree size. Specifically, both PL and NL had low mortality in moderately-sized (e.g., merchantable) stems and higher mortality in the smallest and largest stems. Higher mortality in smaller stems is most likely driven by inter- and intra-specific competitive effects before reaching maturity. Increased mortality in larger stems could be driven by multiple effects including senescence, preference by pests (Pfeifer et al., 2011), windthrow (Harcombe et al., 2009), and increased susceptibility to hydraulic failure (Zhang et al., 2009). Interestingly, the exceptional drought conditions significantly elevated mortality in the smallest and largest PL stems compared to pre-drought conditions yet, did not have the same effect in NL. D'Amato et al. (2013) found that pine plantations thinned at a young age and maintained at a low density exhibited lower growth resistance and resilience to drought at later ages likely due to difficulty maintaining high leaf area-to-sapwood ratios developed over time in the

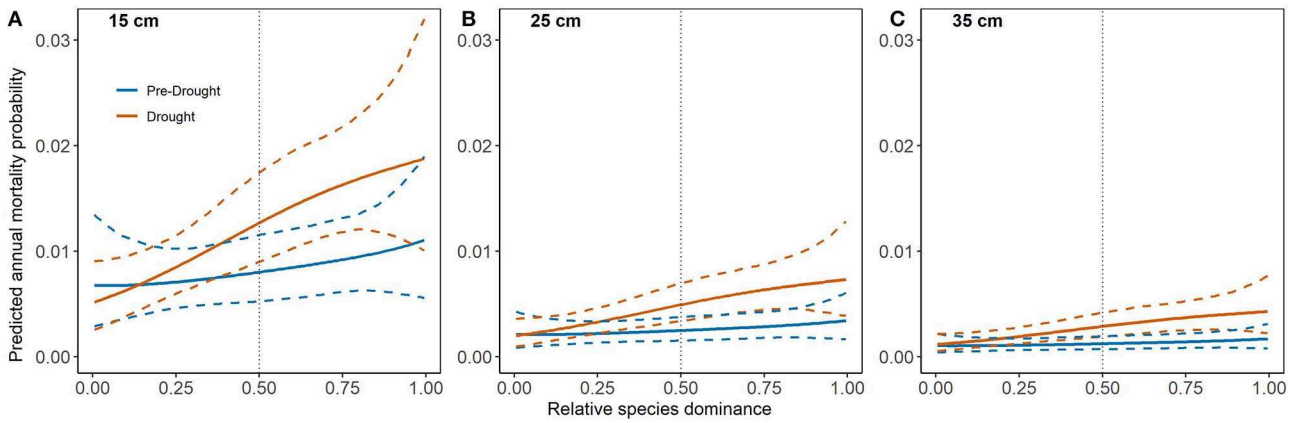

FIGURE 5 | Mortality curves (solid lines) for naturally-regenerated loblolly pine (NL) and species dominance (SPD) with 95% credible intervals (dashed lines). Diameter at breast height (DBH) is held constant at merchantable size classes, **(A)** 15, **(B)** 25, and **(C)** 35 cm, while relative density (RD) is held constant at the lower limit of fully-stocked conditions (35%). Pre-drought period trees were measured and re-measured from 2003 to 2010 while drought period trees were initially measured prior to 2011 and re-measured 2012–2016. Dotted vertical lines highlight 50% dominance by naturally-regenerated loblolly pine (NL).

low-density conditions. It is possible this effect is occurring in intensively managed loblolly pine plantations in east Texas which were thinned and maintained at low densities and slated for harvest beyond a typical rotation age (e.g., >25 years) but were later abandoned.

Density-dependent mortality in PL and NL still followed expected linear trends of increasing mortality with increasing density despite the historic drought conditions. A growing body of literature has found density-dependent mortality occurs in prevalent North American pine species under increasingly water-limited conditions across temperature and precipitation gradients (D'Amato et al., 2013; Bottero et al., 2017; Gleason et al., 2017). Resources inherently become limited as the number of trees occupying the potential growing space in a stand increases and this appeared to be exacerbated under exceptional drought conditions for PL. Interestingly, exceptional drought caused elevated mortality in lower densities of NL compared to the pre-drought period. Naturally-regenerated loblolly trees growing at low densities over time may have greater canopy area and root architecture than denser stands, given the increased growing space and access to resources (D'Amato et al., 2013), and may be more prone to hydraulic failure possibly causing the elevated drought mortality in low density NL stands compared to pre-drought.

Under exceptional drought, species dominance (i.e., relative species mixtures in a plot) became a significant factor in describing NL mortality. Interestingly, intra-specific competition significantly increased mortality in NL-dominated stands under exceptional drought compared to pre-drought. This suggests that more overstory diversity in NL stands (i.e., lower NL basal area) allows for resource partitioning or facilitative effects between mature NL and other species, an effect also noted by Klos et al. (2009). Species dominance affected PL differently, being important pre-drought but having no significant effect under exceptional drought. Planted loblolly pine predominantly occurs in monocultures and ∼85% of all PL plots in this study had >50% of basal area as PL. In fact, mortality decreased as PL dominance increased under pre-drought conditions. This likely reflects that, as PL dominance reaches 100%, these plots occur in the most intensively managed plantations on the landscape where competition control was most prevalent. Thus, pure stands of PL may be more buffered against mortality if they are primarily occurring in actively managed plantations.

Management Implications

The exceptional 2011 drought that occurred in Texas was the worst ever recorded for the state and represents the type of event that could become commonplace in the next few decades (Klepzig et al., 2014). Given that over half of the land area in east Texas is economically productive timberland (Edgar and Zehnder, 2017), it is imperative to develop adaptive management strategies for coping with the stressful conditions of exceptional drought. A critical finding of this study was that, broadly, under current management practices PL stands were more resistant to mortality from exceptional drought stress than NL stands, a finding that, to our knowledge, has not been shown before. In general, PL stands were maintained at lower densities (i.e., within the range of fully-stocked conditions) and at smaller stem sizes compared to NL. These typical management-related effects may have provided the important buffer needed to keep exceptional drought mortality low in PL. Management suggestions for reducing exceptional drought mortality in NL stands are comparable to those for PL with relative density of NL stems being a key driver of mortality risk. Maintaining stands in fully-stocked conditions and even understocked conditions could reduce overall mortality, particularly from exceptional drought. Importantly, promoting other species (i.e., maintaining ≤50% NL basal area), where possible, could provide a crucial advantage for reducing exceptional drought mortality in NL stands, particularly at lower densities. Finally, it remains unclear from this study as to what management strategies could benefit SL under exceptional drought. Further research

into the response of SL to exceptional drought conditions is warranted as initiatives continue to seek strategies to restore this species throughout the southeastern U.S. Overall, the suggestions presented here are based on broad-scale modeling results from West Gulf Coastal Plain forests. Reduction of mortality risk depends on local conditions and, critically, overarching management objectives. However, these suggestions provide straightforward management strategies that could be implemented relatively easily by resource managers concerned with exceptional drought mortality.

DATA AVAILABILITY STATEMENT

The datasets analyzed for this study can be found in the U.S. Forest Service Forest Inventory and Analysis program FIA Datamart (https://apps.fs.usda.gov/fia/datamart/datamart.html).

AUTHOR CONTRIBUTIONS

PK, CE, GM, and JV conceived the ideas. PK designed the methodology, analyzed the data, and led the writing of the manuscript. JV, GM, and CE revised the manuscript for important intellectual content. All authors contributed critically to the drafts and gave final approval for publication.

FUNDING

Funding for this study was provided in part by a Texas A&M University Merit Fellowship and the National Aeronautics and Space Administration Rapid Response and Novel Research in Earth Science program (Grant number NNX14AN99G). The contents of this study are solely the responsibility and creation of the authors and do not necessarily represent the official views of the National Aeronautics and Space Administration.

ACKNOWLEDGMENTS

We thank the U.S. Forest Service FIA program and the Texas A&M Forest Service for collecting, organizing, and making available data used in this study. We also thank Dr. Denis Valle for early assistance with the analysis and Dr. Michelle Masuda for providing valuable insight into the mixed posterior predictive model assessment.

SUPPLEMENTARY MATERIAL

The Supplementary Material for this article can be found online at: https://www.frontiersin.org/articles/10.3389/ffgc.2020.00023/full#supplementary-material

REFERENCES

Allen, C. D., Breshears, D. D., and McDowell, N. G. (2015). On underestimation of global vulnerability to tree mortality and forest die-off from hotter drought in the Anthropocene. *Ecosphere* 6, 1–55. doi: 10.1890/ES15-00203.1

Anderegg, W. R. L., Kane, J. M., and Anderegg, L. D. L. (2013). Consequences of widespread tree mortality triggered by drought and temperature stress. *Nat. Clim. Chang.* 3, 30–36. doi: 10.1038/nclimate1635

Barrett, J. W. (1995). *Regional Silviculture of the United States.* New York, NY: John Wiley & Sons.

Bennett, A. C., McDowell, N. G., Allen, C. D., and Anderson-Teixeira, K. J. (2015). Larger trees suffer most during drought in forests worldwide. *Nat. Plants* 1:15139. doi: 10.1038/nplants.2015.139

Bottero, A., D'Amato, A. W., Palik, B. J., Bradford, J. B., Fraver, S., Battaglia, M. A., et al. (2017). Density-dependent vulnerability of forest ecosystems to drought. *J. Appl. Ecol.* 54, 1605–1614. doi: 10.1111/1365-2664.12847

Bracho, R., Vogel, J. G., Will, R. E., Noormets, A., Samuelson, L. J., Jokela, E. J., et al. (2018). Carbon accumulation in loblolly pine plantations is increased by fertilization across a soil moisture availability gradient. *For. Ecol. Manage.* 424, 39–52. doi: 10.1016/j.foreco.2018.04.029

Cavin, L., Mountford, E. P., Peterken, G. F., and Jump, A. S. (2013). Extreme drought alters competitive dominance within and between tree species in a mixed forest stand. *Funct. Ecol.* 27, 1424–1435. doi: 10.1111/1365-2435.12126

Chen, G., Pan, S., Hayes, D. J., and Tian, H. (2017). Spatial and temporal patterns of plantation forests in the United States since the 1930s: an annual and gridded data set for regional Earth system modeling. *Earth Syst.Sci. Data* 9, 545–556. doi: 10.5194/essd-9-545-2017

Clark, J. S., Iverson, L., Woodall, C. W., Allen, C. D., Bell, D. M., Bragg, D. C., et al. (2016). The impacts of increasing drought on forest dynamics, structure, and biodiversity in the United States. *Glob. Change Biol.* 22, 1–24. doi: 10.1111/gcb.13160

D'Amato, A. W., Bradford, J. B., Fraver, S., and Palik, B. J. (2013). Effects of thinning on drought vulnerability and climate response in north temperate forest ecosystems. *Ecol. Appl.* 23, 1735–1742. doi: 10.1890/13-0677.1

Dietze, M. C., and Moorcroft, P. R. (2011). Tree mortality in the eastern and central United States: patterns and drivers. *Glob. Chang. Biol.* 17, 3312–3326. doi: 10.1111/j.1365-2486.2011.02477.x

Dipesh, K., Will, R. E., Lynch, T. B., Heinemann, R., and Holeman, R. (2015). Comparison of loblolly, shortleaf, and pitch X loblolly pine plantations growing in Oklahoma. *For. Sci.* 61, 540–547. doi: 10.5849/forsci.14-004

Domec, J.-C., King, J. S., Ward, E., Oishi, A. C., Palmroth, S., Radecki, A., et al. (2015). Conversion of natural forests to managed forest plantations decreases tree resistance to prolonged droughts. *For. Ecol. Manage.* 355, 58–71. doi: 10.1016/j.foreco.2015.04.012

Ducey, M. J., and Knapp, R. A. (2010). A stand density index for complex mixed species forests in the northeastern United States. *For. Ecol. Manage.* 260, 1613–1622. doi: 10.1016/j.foreco.2010.08.014

Eckert, A. J., van Heerwaarden, J., Wegrzyn, J. L., Nelson, C. D., Ross-Ibarra, J., Gonzalez-Martinez, S. C., et al. (2010). Patterns of population structure and environmental associations to aridity across the range of loblolly pine (*Pinus taeda* L., Pinaceae). *Genetics* 185, 969–982. doi: 10.1534/genetics.110.115543

Edgar, C. B., and Zehnder, R. (2017). "East Texas Forestlands, 2015," in *Forest Resource Reports* (College Station, TX: Texas A&M Forest Service), 6.

Floyd, M. L., Clifford, M., Cobb, N. S., Hanna, D., Delph, R., Ford, P., et al. (2009). Relationship of stand characteristics to drought-induced mortality in three Southwestern piñon - Juniper woodlands. *Ecol. Appl.* 19, 1223–1230. doi: 10.1890/08-1265.1

Forrester, D. I. (2014). The spatial and temporal dynamics of species interactions in mixed-species forests: from pattern to process. *For. Ecol. Manage.* 312, 282–292. doi: 10.1016/j.foreco.2013.10.003

Fox, T. R., Jokela, E. J., and Allen, H. L. (2007). The development of pine plantation silviculture in the southern United States. *J. For.* 105, 337–347. doi: 10.1093/jof/105.7.337

Ganey, J. L., and Vojta, S. C. (2011). Tree mortality in drought-stressed mixed-conifer and ponderosa pine forests, Arizona, USA. *For. Ecol. Manage.* 261, 162–168. doi: 10.1016/j.foreco.2010.09.048

Gelman, A., and Rubin, D. B. (1992). Inference from iterative simulation using multiple sequences. *Stat. Sci.* 7, 457–472. doi: 10.1214/ss/1177011136

Gleason, K. E., Bradford, J. B., Bottero, A., D'Amato, A. W., Fraver, S., Palik, B. J., et al. (2017). Competition amplifies drought stress in forests across broad climatic and compositional gradients. *Ecosphere* 8, 1–16. doi: 10.1002/ecs2.1849

Green, M. J., Medley, G. F., and Browne, W. J. (2009). Use of posterior predictive assessments to evaluate model fit in multilevel logistic regression. *Vet. Res.* 40:10. doi: 10.1051/vetres/2009013

Hamilton, D. A. Jr., and Edwards, B. M. (1976). "Modeling the probability of individual tree mortality," in *USDA Forest Service Intermountain Research Station Research Paper INT-185* (Ogden, UT), 22. doi: 10.5962/bhl.title.68792

Harcombe, P. A., Leipzig, L. E. M., and Elsik, I. S. (2009). Effects of Hurricane Rita on three long-term forest study plots in east Texas, USA. *Wetlands* 29, 88–100. doi: 10.1672/08-64.1

Hobbs, N. T., and Hooten, M. B. (2015). *Bayesian Models: A Statistical Primer for Ecologists*. Princeton, NJ: Princeton University Press.

Intergovernmental Panel on Climate Change (IPCC) (2013). *Change 2013: The Physical Science Basis*. Cambridge, New York, NY: Contribution of Working Group I to the Fifth Assessment Report of the Intergovernmental Panel on Climate Change.

Kemp, K. B., Blades, J. J., Klos, P. Z., and Hall, T. E. (2015). Managing for climate change on federal lands of the western United States: perceived usefulness of climate science, effectiveness of adaptation strategies, and barriers to implementation. *Ecol. Soc.* 20:14. doi: 10.5751/ES-07522-200217

Klepzig, K., Shelfer, R., and Choice, Z. (2014). *Outlook for Coastal Plain Forests: A Subregional Report From the Southern Forest Futures Project*. Genral Technical Report SRS-196. U.S. Department of Agriculture Forest Service, Southern Research Station, Asheville, NC.

Klockow, P. A., Vogel, J. G., Edgar, C. B., and Moore, G. W. (2018). Lagged mortality among tree species four years after an exceptional drought in east Texas. *Ecosphere* 9:e02455. doi: 10.1002/ecs2.2455

Klos, R. J., Wang, G. G., Bauerle, W. L., and Rieck, J. R. (2009). Drought impact on forest growth and mortality in the southeast USA: an analysis using forest health and monitoring data. *Ecol. Appl.* 19, 699–708. doi: 10.1890/08-0330.1

Kramer, I., and Holscher, D. (2010). Soil water dynamics along a tree diversity gradient in a deciduous forest in Central Germany. *Ecohydrology* 3, 262–271. doi: 10.1002/eco.103

Lindenmayer, D. B., Laurance, W. F., and Franklin, J. F. (2012). Global decline in large old trees. *Science* 338, 1305–1306. doi: 10.1126/science.1231070

Lines, E. R., Coomes, D. A., and Purves, D. W. (2010). Influences of forest structure, climate and species composition on tree mortality across the eastern US. *PLoS ONE* 5:e13212. doi: 10.1371/journal.pone.0013212

Maggard, A. O., Will, R. E., Wilson, D. S., Meek, C. R., and Vogel, J. G. (2017). Fertilization can compensate for decreased water availability by increasing the efficiency of stem volume production per unit of leaf area for loblolly pine (*Pinus taeda*) stands. *Can. J. For. Res.* 47, 445–457. doi: 10.1139/cjfr-2016-0422

Masuda, M. M., and Stone, R. P. (2015). Bayesian logistic mixed-effects modelling of transect data: relating red tree coral presence to habitat characteristics. *ICES J. Mar. Sci.* 72, 2674–2683. doi: 10.1093/icesjms/fsv163

Mattoon, W. R. (1915). *Life History of Shortleaf Pine*. Washington, DC: US Department of Agriculture.

McNulty, S. G., Boggs, J. L., and Sun, G. (2014). The rise of the mediocre forest: why chronically stressed trees may better survive extreme episodic climate variability. *New For.* 45, 403–415. doi: 10.1007/s11056-014-9410-3

Moore, G. W., Edgar, C. B., Vogel, J. G., Washington-Allen, R. A., March, R. G., and Zehnder, R. (2016). Tree mortality from an exceptional drought spanning mesic to semiarid ecoregions. *Ecol. Appl.* 26, 602–611. doi: 10.1890/15-0330

Nagel, L. M., Palik, B. J., Battaglia, M. A., D'Amato, A. W., Guldin, J. M., Swanston, C. W., et al. (2017). Adaptive silviculture for climate change: a national experiment in manager-scientist partnerships to apply an adaptation framework. *J. For.* 115, 167–178. doi: 10.5849/jof.16-039

National Oceanic and Atmospheric Administration (NOAA) (2018). *National Centers for Environmental Information, Climate at a Glance: Divisional Time Series*. Available online at: https://www.ncdc.noaa.gov/cag/ (accessed July 26, 2018).

Nelson, A. S., and Bragg, D. C. (2016). Multidecadal response of naturally regenerated southern pine to early competition control and commercial thinning. *For. Sci.* 62, 115–124. doi: 10.5849/forsci.15-056

Nielsen-Gammon, J. W. (2012). The 2011 texas drought. *Texas Water J.* 3, 59–95.

Oswalt, S. N., Smith, W. B., Miles, P. D., and Pugh, S. A. (2014). *Forest Resources of the United States, 2012: A Technical Document Supporting the Forest Service 2010 Update of the RPA Assessment*. Washington, DC: Gen. Tech. Rep. WO-91. U.S. Department of Agriculture, Forest Service. doi: 10.2737/WO-GTR-91

Peng, C., Ma, Z., Lei, X., Zhu, Q., Chen, H., Wang, W., et al. (2011). A drought-induced pervasive increase in tree mortality across Canada's boreal forests. *Nat. Climate Change* 1, 467–471. doi: 10.1038/nclimate1293

Pfeifer, E. M., Hicke, J. A., and Meddens, A. J. H. (2011). Observations and modeling of aboveground tree carbon stocks and fluxes following a bark beetle outbreak in the western United States. *Global Change Biol.* 17, 339–350. doi: 10.1111/j.1365-2486.2010.02226.x

Pretzsch, H., Schutze, G., and Uhl, E. (2013). Resistance of European tree species to drought stress in mixed versus pure forests: evidence of stress release by inter-specific facilitation. *Plant Biol.* 15, 483–495. doi: 10.1111/j.1438-8677.2012.00670.x

Puettmann, K. J. (2011). Silvicultural challenges and options in the context of global change: "simple" fixes and opportunities for new management approaches. *J. For.* 109, 321–331. doi: 10.1093/jof/109.6.321

R Core Team (2016). *R: A Langauge and Environment for Statistical Computing*. Vienna: R Foundation for Statistical Computing. Available online at: https://www.R-project.org/

Rehm, E. M., Olivas, P., Stroud, J., and Feeley, K. J. (2015). Losing your edge: climate change and the conservation value of range-edge populations. *Ecol. Evol.* 5, 4315–4326. doi: 10.1002/ece3.1645

Stan Development Team (2017). *RStan: The R Interface to Stan*. R package version 2.16.2. Available online at: http://mc-stan.org

Thrippleton, T., Bugmann, H., Folini, M., and Snell, R. S. (2018). Overstorey-understorey interactions intensify after drought-induced forest die-off: long-term effects for forest structure and composition. *Ecosystems* 21, 723–739. doi: 10.1007/s10021-017-0181-5

US Department of Agriculture Natural Resources Conservation Service (USDANRCS) (2006). *Land Resource Regions and Major Land Resource Areas of the United States, the Caribbean, and the Pacific Basin*. Washington, DC: U.S. Department of Agriculture Handbook 296.

van Mantgem, P. J., Stephenson, N. L., Byrne, J. C., Daniels, L. D., Franklin, J. F., Fulé, P. Z., et al. (2009). Widespread increase of tree mortality rates in the western United States. *Science* 323, 521–524. doi: 10.1126/science.1165000

Vose, J. M., Clark, J. S., Luce, C. H., and Patel-Weynand, T. (2016). *Effects of Drought on Forests and Rangelands in the United States: A Comprehensive Science Synthesis*. Genral Technical Report WO-93b. U.S. Department of Agriculture, Forest Service, Washington Office, Washington, DC.

Ward, E. J., Domec, J.-C., Laviner, M. A., Fox, T. R., Sun, G., McNulty, S., et al. (2015). Fertilization intensifies drought stress: water use and stomatal conductance of *Pinus taeda* in a midrotation fertilization and throughfall reduction experiment. *For. Ecol. Manage.* 355, 72–82. doi: 10.1016/j.foreco.2015.04.009

Zhang, Y. J., Meinzer, F. C., Hao, G. Y., Scholz, F. G., Bucci, S. J., Takahashi, F. S. C., et al. (2009). Size-dependent mortality in a Neotropical savanna tree: the role of height-related adjustments in hydraulic architecture and carbon allocation. *Plant Cell Environ.* 32, 1456–1466. doi: 10.1111/j.1365-3040.2009.02012.x

Conflict of Interest: The authors declare that the research was conducted in the absence of any commercial or financial relationships that could be construed as a potential conflict of interest.

frontiers in Forests and Global Change

ORIGINAL RESEARCH
published: 20 March 2020
doi: 10.3389/ffgc.2020.00021

Using Process Based Snow Modeling and Lidar to Predict the Effects of Forest Thinning on the Northern Sierra Nevada Snowpack

Sebastian A. Krogh[1,2]*, *Patrick D. Broxton*[3], *Patricia N. Manley*[4] *and Adrian A. Harpold*[1,2]

[1] Department of Natural Resources and Environmental Science, University of Nevada, Reno, NV, United States, [2] Global Water Center, University of Nevada, Reno, NV, United States, [3] School of Natural Resources and the Environment, University of Arizona, Tucson, AZ, United States, [4] U.S. Forest Service, Pacific Southwest Research Station, Placerville, CA, United States

Reductions in snow accumulation and melt in headwater basins are increasing the water stress on forest ecosystems across the western US. Forest thinning has the potential to reduce water stress by decreasing sublimation losses from canopy interception; however, it can also increase snowpack exposure to sun and wind. We used the high-resolution (1 m) energy and mass balance Snow Physics and Lidar Mapping (SnowPALM) model to investigate the effect of two virtual forest thinning scenarios on the snowpack of two adjacent watersheds (54 km^2 total) in the Lake Tahoe Basin, California, where forest thinning is being planned. SnowPALM realistically represents small-scale snow-forest interactions to simulate the impact of virtual thinning experiments in which trees <10 and <20 m are removed. In general, thinning results in an overall increase in peak snow water equivalent and snowmelt. Areas around sheltered tree clusters have the largest increases of snowmelt due to decreases of canopy sublimation, while more open and exposed areas show a small decrease due to increases in snowpack sublimation. At the 30-m forest stand scale, existing forest structure controls the efficacy of thinning, where forest stands with mean leaf area index (LAI) >3 m^2/m^2 and 5–15-m tall show the largest increases in snow accumulation (up to 450 mm) and melt volume (up to 650 mm). Despite the role of tree- and stand-scale thinning on snowmelt, macroscale effects were limited to slightly larger increases in melt volumes at mid to low elevation slopes (<2,300 masl) and south facing areas per unit of LAI removed. A decision support tool using machine learning (random forest) was developed to synthesize SnowPALM results, and was applied to neighboring watersheds. These results will inform ongoing forest management practices in California, and improve our understanding of the effects of snow-forest interactions at scales relevant to water management.

Keywords: snow hydrology, modeling, lidar, forest, forest management, restoration

OPEN ACCESS

Edited by:
Steven George Mcnulty, USDA Southeast Climate Hubs, United States

Reviewed by:
John L. Campbell, Northern Research Station, Forest Service (USDA), United States
Fengjing Liu, Michigan Technological University, United States

***Correspondence:**
Sebastian A. Krogh
skrogh@cabnr.unr.edu;
sebakrogh@gmail.com

Specialty section:
This article was submitted to Forest Hydrology, a section of the journal Frontiers in Forests and Global Change

Received: *27 November 2019*
Accepted: *24 February 2020*
Published: *20 March 2020*

Citation:
Krogh SA, Broxton PD, Manley PN and Harpold AA (2020) Using Process Based Snow Modeling and Lidar to Predict the Effects of Forest Thinning on the Northern Sierra Nevada Snowpack. Front. For. Glob. Change 3:21. doi: 10.3389/ffgc.2020.00021

INTRODUCTION

Upland snowmelt is a vital water resource for downstream populations and local ecological systems. Snow is particularly important in regions with Mediterranean climates, such as the Sierra Nevada in the western US, where snowmelt provides the majority of the water supply. Increasing temperatures in such regions are shortening the snow accumulation season, increasing

the frequency of mid-winter snowmelt events and producing earlier snowmelt runoff (López-Moreno et al., 2013; Musselman et al., 2017a; Harpold and Brooks, 2018; Mote et al., 2018), with significant ecological and economic impacts (Sturm et al., 2017). Tree removal, and particularly targeted forest thinning, has the potential to increase snow accumulation and melt through a reduction in snowfall that is intercepted and sublimated from forest canopy (Varhola et al., 2010; Tague et al., 2019). However, there is significant regional variability in the snowpack response to tree removal due to differences in climate, topography, forest species, and the spatial distribution of trees on the landscape (Varhola et al., 2010). Key snow processes are highly sensitive to forest canopy, such as snowpack sublimation, blowing snow redistribution, incoming radiation, and turbulent energy fluxes (Anderson et al., 1976; Troendle and Leaf, 1980; Golding and Swanson, 1986; Toews and Gluns, 1986; Pomeroy and Granger, 1997; Pomeroy et al., 2002; Winkler et al., 2005; Bewley et al., 2010). Early studies in the Sierra Nevada, California, have shown that forest patches with glades accumulate more snow than dense forest patches (Church, 1933; Anderson, 1956, 1963), consistent with the idea that tree removal increases snowmelt volume. However, it remains challenging to quantify the response of the snowpack's mass and energy budgets to tree removal over relatively large domains (e.g., >10 km^2). Large domain simulations that capture key fine-scale processes are needed to predict hydrologic responses to forest restoration efforts, which span substantial gradients of climate, topography, and vegetation removal.

Paired watershed experiments and studies comparing canopy clearings with under canopy locations have provided insights into the effect of forest removal on snow processes (Anderson et al., 1976; Troendle and Leaf, 1980; Alexander et al., 1985; Golding and Swanson, 1986; Toews and Gluns, 1986; Pomeroy et al., 2002; Woods et al., 2006). However, many of these studies are constrained by relatively small domains (e.g., Goodell, 1952) that limit their scalability and representativeness for larger domains with more variable vegetation and topographic conditions. Model predictions of snowpack response typically use spatially-averaged parameters to represent snow-forest interactions (Essery et al., 2009; Rutter et al., 2009) that fail to represent the spatial heterogeneity of forests. A lack of model fidelity can be problematic because snow processes do not vary linearly across spatial scales (Blöschl, 1999). Current modeling approaches are likely to provide biased estimates of the effect of forest thinning on snowpack at large scales. For example, Broxton et al. (2015) found that coarsening the spatial resolution of a process-based snow model from 1 to 100 m reduced peak snow water equivalent (SWE) between 14 and 24% due to the simplification of radiation transfer processes. These types of studies demonstrate the importance of tree-scale processes to make accurate snowpack predictions of heterogeneous forest change.

Increasing availability of aerial light detection and ranging (lidar) datasets from snow-covered forests, combined with improved computational resources, has the potential to revolutionize model representations of small-scale snow-forest interactions (Moeser et al., 2014, 2015; Musselman et al., 2015, 2017b). Very high spatial resolution models (e.g., 1 m) allow a spatially explicit representation of heterogeneous forest canopy and associated snowpack processes (Broxton et al., 2015; Moeser et al., 2015). However, applications of these models using lidar are rare due to computational requirements and issues related to model development, calibration, and validation. One of the first efforts to develop a full energy budget snowmelt model at high resolution was Broxton et al. (2015), who created the Snow Physics and Lidar Mapping (SnowPALM) model, which uses lidar data to parameterize vegetation structure. Broxton et al. (2015) successfully validated SnowPALM using both snow pillow data and lidar-derived snow depths at two sites in the central and southern Rocky Mountains. Harpold et al. (2020) extended the application of SnowPALM to the Sierra Nevada, California, and developed new validation datasets of snow depth and surface temperature across different forest structures. Their study investigated the effects of a "virtual thinning" on snow mass and energy fluxes over a relatively small domain (1,200 $\times$ 1,200 m), and showed which forest and topographic conditions had the greatest increases in snowmelt volume after removing trees of different heights. However, there remains uncertainty about snowpack response to forest thinning over large areas and a lack of detailed recommendations needed for ongoing forest restoration efforts.

Building upon this recent work, we extend this high-resolution SnowPALM modeling to a much larger domain encompassing two medium sized ($\sim$25 km^2 each) mountain watersheds on the west shore of Lake Tahoe, California. These watersheds are part of the Lake Tahoe West Restoration Partnership, which aims to develop a landscape restoration strategy that increases the resiliency of this region to drought, climate change, and extreme fire. Tree (fuel) removal is a common fire suppression practice in this region; however, its impact on snow accumulation and melt volumes are not considered as part of the thinning strategies. This study was developed as an effort to provide actionable scientific information to forest and water managers in the region, along with a decision support tool that can be readily deployed with relatively few computational resources. For this purpose, we parameterized the SnowPALM model to predict snowpack response to two "virtual thinning" scenarios where all trees below 10 and 20-m tall were removed. We then used these simulations to train a machine-learning algorithm that informs a decision support tool for forest managers to determine where thinning should be performed. These simulations were used to answer four questions: (1) which tree removal scenario provides the largest increases in snow accumulation and melt volumes? (2) what are the characteristics of forest stands that yield the greatest water benefits from thinning and what is their topographic distribution? (3) what are the physical mechanisms that explain this variation in snow water benefits from thinning and how do they vary over topography? and (4) can we develop a decision support tool that synthesizes high resolution modeling to extract more information from the models about best thinning practices within and outside of the study area?

Study Site

Two mountainous watersheds along the west shore of Lake Tahoe (**Figure 1**) in California were chosen for this study because they represent a large variation in topography and vegetation, and have detailed hydrological observations: Ward Creek (24.9 km^2) and Blackwood Creek (28.9 km^2). Elevation ranges from roughly 1,900 masl at the shore of Lake Tahoe, which has gentle slopes and tall and dense forest, to 2,700 masl where much steeper and sparsely vegetated slopes exist. These two watersheds have high resolution (1 m) lidar estimates of vegetation height and density (Xu et al., 2018), as well as snow depth and SWE measurements from Snow Telemetry (SNOTEL) stations within and nearby these watersheds. This region has a Mediterranean-type climate with dry, hot summers and wet winters. The 30-year climate normal (1980–2010) from the nearby Tahoe City weather station (from the US National Weather Service) shows a mean annual air temperature of 6.4°C and a maximum and minimum mean monthly air temperature of about 16 and −7°C in July and January, respectively. Mean annual precipitation for the same period is estimated to be 870 mm, from which about 78% falls during November and March. Snow accumulation at the SNOTEL station in Ward Creek (**Figure 1**) typically starts in early November and lasts until mid-May. Tree species in the Tahoe Basin consist predominantly of Jeffrey Pine (*pinus Jeffrey balf.*), Ponderosa Pine (*pinus pondersa*), Red Fir (*abies magnifica*), Lodgepole Pine (*pinus contorta*), and White Fir (*abies concolor*) (van Gunst, 2012).

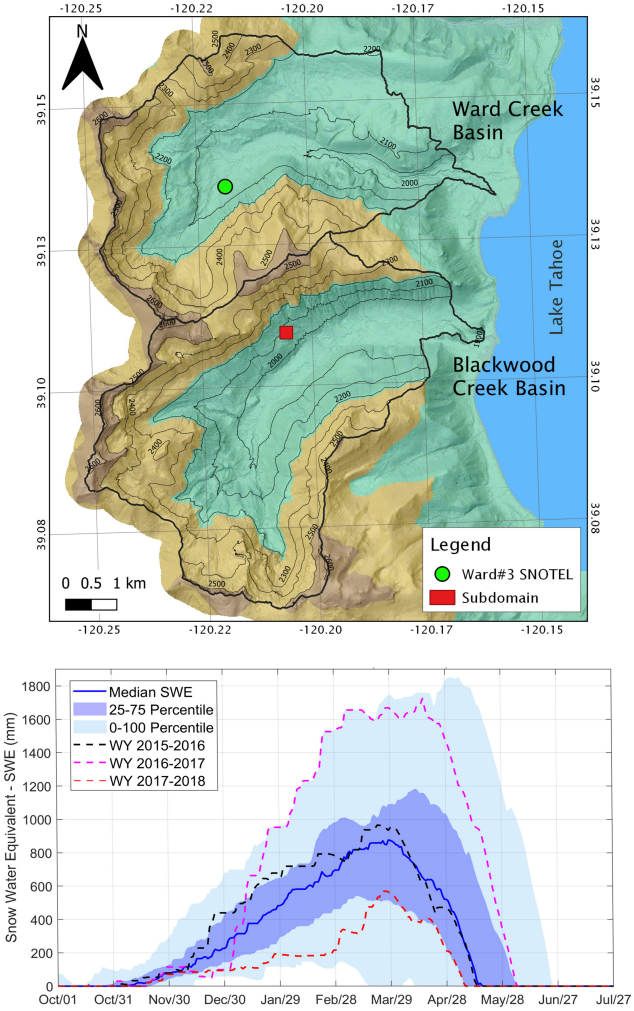

FIGURE 1 | Upper panel: Relief map showing the modeled basins along the west shore of Lake Tahoe, California (contour interval = 100 m). The red rectangle shows the subdomain (150 × 150 m) presented in **Figure 4**. **Lower panel:** Observed snow water equivalent (SWE) climatology at the Ward #3 SNOTEL station, including the observed SWE for the three water years simulated in this study (dashed lines).

METHODS

Snow Modeling

The Snow Physics and Lidar Mapping (SnowPALM; Broxton et al., 2015) model was used to simulate the mass and energy budgets of snow in forested areas with complex topography. Broxton et al. (2015) describes SnowPALM parameterization and model development; however, key features are also presented here. SnowPALM simulates snow processes at a high spatial (1 m) and temporal (1 h) resolution, which is particularly important for applications in regions with complex terrain and heterogeneous forest structure, as it improves the model's fidelity to simulate snow-forest interactions. SnowPALM simulates snowpack using a one-layer snow energy and mass balance whose skin temperature is calculated separately through an energy balance between net radiation, sensible heat and heat conduction to the middle of the snowpack and a one-layer soil to compute ground heat exchange. SnowPALM also simulates wind distribution of snowfall (Winstral and Marks, 2002), canopy interception and evaporation/sublimation of rainfall/snowfall, canopy unloading of rain/snow (Deardorff, 1978; Pomeroy et al., 1998), attenuation of shortwave radiation by the canopy (Mahat and Tarboton, 2012), longwave radiation from the forest (whose skin temperature is calculated balancing net radiation with turbulent fluxes assuming a snow-free canopy albedo), and albedo decay as a function of time. The liquid water that falls on top of the snowpack, either from rain passing through the canopy or canopy drip, can either freeze to the snowpack or pass through the snowpack and infiltrate into the soil. Hereafter, we will refer to the sum of this infiltrated water and snowmelt as "net water input," or the total water emanating from the snowpack that is available for infiltration and runoff.

The meteorological data used in this study are from phase 2 of the North American Land Data Assimilation System (NLDAS-2; Xia et al., 2012), which provides hourly precipitation, air temperature, wind speed and direction, air pressure, downward shortwave and longwave radiation, and specific humidity at 1/8 of degree spatial resolution. These data were downscaled using SnowPALM's built-in downscaling procedures, using a combination of linear interpolation (for some variables) and relationships with elevation derived from the Parameter-elevation Regressions on Independent Slopes Model (PRISM) monthly maximum/minimum temperature and precipitation

data. Three water years (starting in October 1) were simulated in this study: 2015–2016, 2016–2017, and 2017–2018, hereafter referred as WY16, WY17, and WY18, respectively. These years represent a wide range of historical conditions, ranging from relatively dry (WY18), normal (WY16), and wet (WY17) conditions (lower panel **Figure 1**).

The model parameterization used in this study is the same as the one presented by Harpold et al. (2020), who used data from three different SNOTEL stations: Rubicon#2 (ID: 724, about 15 km south of Ward Creek), Ward Creek#3 (ID: 848) and Tahoe City Cross (ID: 809, about four km north of Ward Creek) for calibration and validation. The idea behind this cross-site calibration/validation was to produce a model capable of representing the snowpack at more than a single location to reduce the uncertainty of parameter estimation. However, emphasis was given to representing snowpack conditions at the Rubicon#2 SNOTEL station, which is located within their study domain. Key parameters adjusted in SnowPALM during calibration relate to reduction of biases in the gridded forcing data and a parameter describing the leaf area index (LAI) of fully dense canopy. For a detailed description of the parameterization used in the model, the readers are referred to Harpold et al. (2020).

Lidar Datasets and Virtual Thinning Experiments

Airborne lidar was collected for an area surrounding Lake Tahoe from August 11 and 24, 2010 (Romsos, 2011). The average first return point density was 11.82 point/m^2, the average ground point density was 2.26 point/m^2, and the vertical accuracy (RMSE) was estimated to be 3.5 cm. The point cloud dataset was downloaded from OpenTopography.org (http://opentopo.sdsc.edu/datasetMetadata?otCollectionID=OT.032011.26910.1, accessed October 1, 2019) in LAS 1.4 format. Vegetation height, density, and leaf area index (LAI) were derived from the lidar point cloud and a bare-earth model (from OpenTopography) to parameterize SnowPALM. Vegetation height was calculated as the difference between the canopy height model and the bare-earth model at 1 m resolution. Canopy density was computed as the ratio between non-ground return (>2 m above the ground surface) and total returns per square meter. LAI at 1-m resolution was defined as the product of vegetation density and an estimated maximum LAI of 4 m^2/m^2, based on the local observation presented by van Gunst (2012).

Two virtual thinning scenarios were created, following the thinning experiment presented by Harpold et al. (2020). These scenarios consist of removing all trees <10 and 20-m tall, which are considered to be scenarios of moderate and significant forest disturbance, respectively. These were created by changing LAI and vegetation height to zero for all the pixels with vegetation height below 10 and 20 m using the tree-delineated dataset from Xu et al. (2018). This type of forest disturbance was selected to mimic forest management strategies in the region, which are primarily design to reduce the risk of severe forest fires while maintaining the recreational and aesthetic value of the forest. SnowPALM was run for the Ward Creek and Blackwood Creek Basins, using maps generated for these two thinning scenarios (10 and 20 m removal simulations) and those representing the current forest conditions (control run).

To understand the impact of the two virtual thinning experiments on the snowpack across a large topographic gradient, the modeling domain was divided into five ∼160-m elevation bands (low, mid-low, mid, mid-high, and high), and north and south facing aspects, resulting in 10 regions that we termed "Snow Zones." The high elevation Snow Zones are steeper (average slope ∼40%) than those at lower elevations (average slope ∼20%, **Figure 2**). Low elevation Snow Zones also have denser and taller trees than high elevation Snow Zones (**Figure 2**), where mean tree height and density include non-vegetated areas. Peak SWE at low elevations is less than half of that at high elevations and the snow lasts about 45 days longer at high elevations (**Figure 2**). Snow disappearance is 2–3 weeks later on the north-facing Snow Zones compared to south-facing Snow Zones with the same elevation (**Figure 2**). The 1-m SnowPALM simulations were averaged to 30-m grids to investigate the effect of forest thinning on the snowpack at a meaningful scale for forest managers.

Random Forest (RF) Decision Support Tool

The goal of the decision support tool is to extend our findings to areas outside the SnowPALM modeling domain and to identify priority management areas where forest thinning is likely to have the most positive benefits for water supply. We used a regression-type of Random Forest (Breiman, 2001) (RF) algorithm to learn from the SnowPALM simulations. The RF was developed to predict how changes in forest structure affect snowpack under a wide range of topographic (e.g., north vs. south facing slopes) and climatic (e.g., warm and cold) conditions. RF models have a strong track record in snow hydrology and have been previously used to understand the spatial distribution of the snowpack using lidar (Tinkham et al., 2014) and fractional snow cover (Petersky et al., 2018). In this application, RF is used to predict 30-m changes to total net water input using the following predictors: elevation, aspect, slope, existing forest height and LAI, and changes to forest LAI (between the existing forest and the virtual thinning scenarios). It was implemented using the function TreeBagger in Matlab®. This function uses a bootstrapping algorithm to sample the data and train each tree. At each decision split or "branch," the algorithm selects a random subset of predictors to be used in the regression tree. Ultimately, it combines the results of all decision trees to predict a response, reducing problems with overfitting the training dataset. We used 50 trees in the RF as this converged to a minimum "out-of-bag" error. The out-of-bag error is the error when using the dataset not selected by the bootstrapping algorithm to run the RF, similar to a cross-validation. An importance metric for each predictor was calculated using the out-of-bag dataset, where each predictor (e.g., elevation) was randomly permuted (one at a time) and used to run the RF. The predictions from these runs were then compared to those using the original out-of-bag dataset to compute the importance metric. Predictors with higher errors after the random permutation were the most "important" (i.e., sensitive) in the RF.

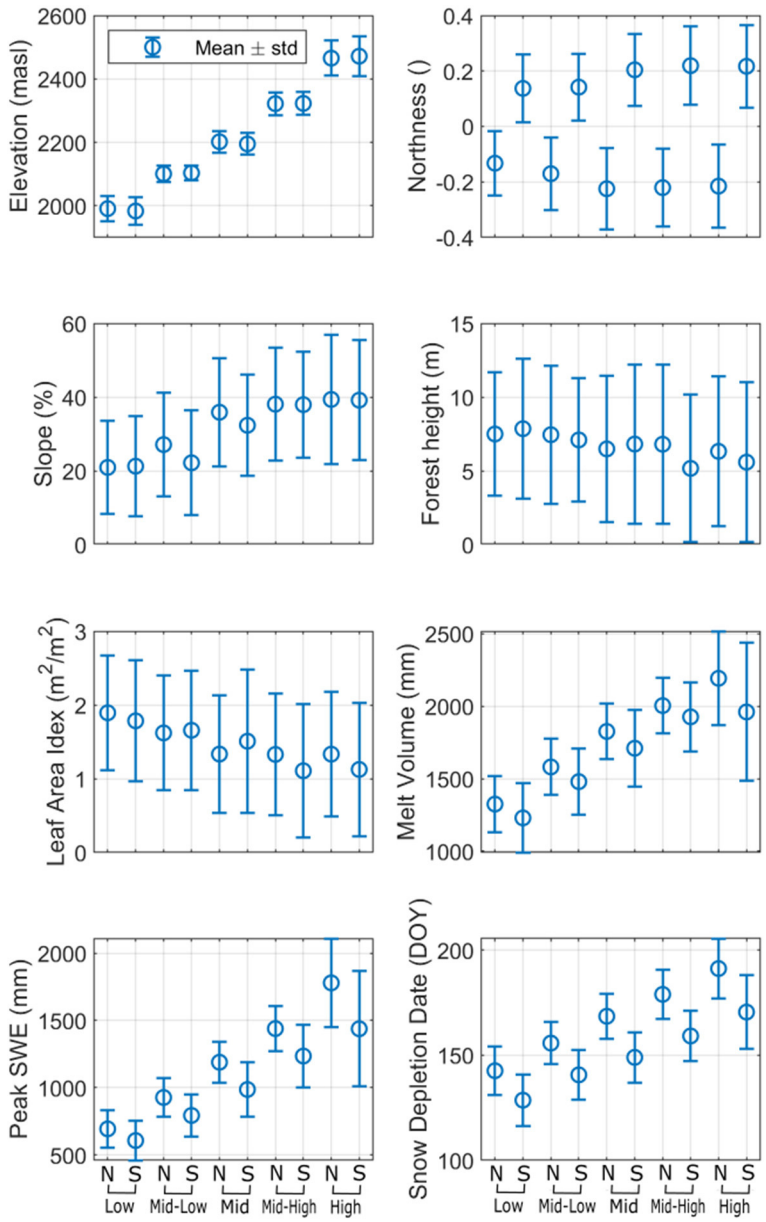

FIGURE 2 | Mean (± standard deviation) Snow Zones' topography, vegetation and snow conditions for the water years 2016–2018 as simulated by SnowPALM. Values for forest LAI and height include non-vegetated areas within each Snow Zone. "N" and "S" on the x-axis represent north- and south-facing Snow Zones.

RESULTS

SnowPALM Validation

Harpold et al. (2020) showed SnowPALM's good performance against observed SWE and snow depth at the Rubicon #2 SNOTEL, consisting of a snow pillow in a forest clearing. They also showed the model's adequate performance against snow surface temperature and depth under different canopy conditions. Here, we compare snow observations from the other two SNOTEL sites in the region (Tahoe City Cross and Ward Creek SNOTELs) against SnowPALM simulations. The SWE comparison is at the snow pillow scale, where the 1-m SWE simulations are averaged to match the extent of the snow pillow on the ground. The model generally captures the accumulation season relatively well for the different water years and across sites. However, during the wet WY17, peak SWE at Ward Creek #3 is overestimated by 350 mm (20%), whereas at Tahoe City Cross, it is underestimated by 156 mm (25%). These differences are related to difficulties representing how air temperature influences precipitation phase at each SNOTEL site using the NLDAS-2 (and PRISM) data. For example, at Ward Creek #3, air temperature during the period of peak SWE was underestimated

(**Figure 3**), resulting in some rainfall events being simulated as snowfall, leading to an overestimation of peak SWE. Despite the imperfect match against SNOTEL data, the validation is strong and consistent with previous studies (Harpold et al., 2020). Although this study lacks of detailed *in situ* measurements to validate SnowPALM, Harpold et al. (2020) validated SnowPALM using snow depth and snow surface temperature observations in open and under canopy environments on a nearby site (15 km south) with similar physiographic conditions, showing an adequate model performance. Furthermore, Broxton et al. (2015)

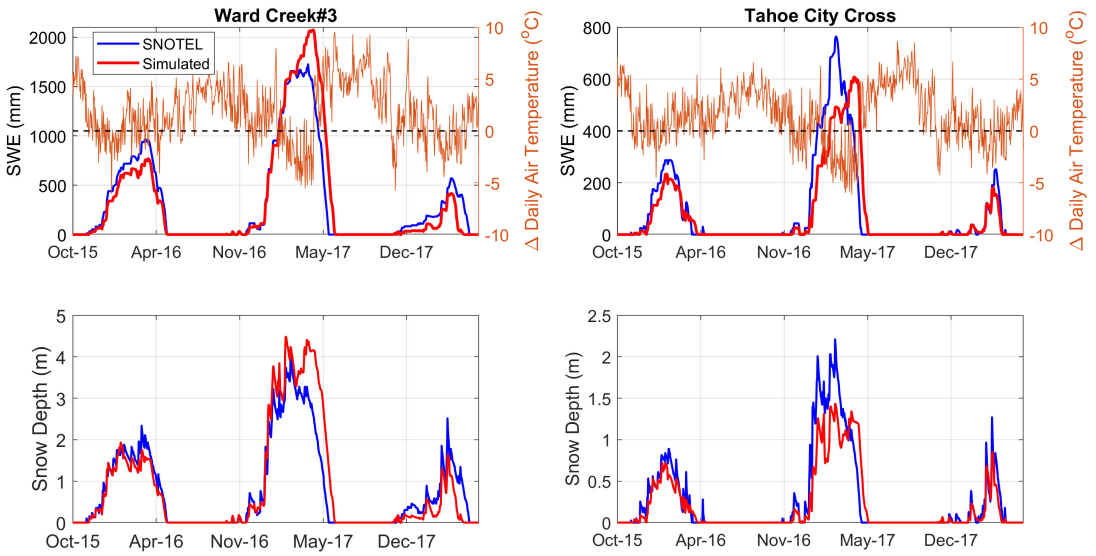

FIGURE 3 | Model validation of snow water equivalent (SWE) and snow depth for Ward #3 **(Left)** and Tahoe City Cross **(Right)** SNOTEL stations. Upper panels include the difference between simulated and observed mean daily air temperature, with positive values indicating a model overestimation.

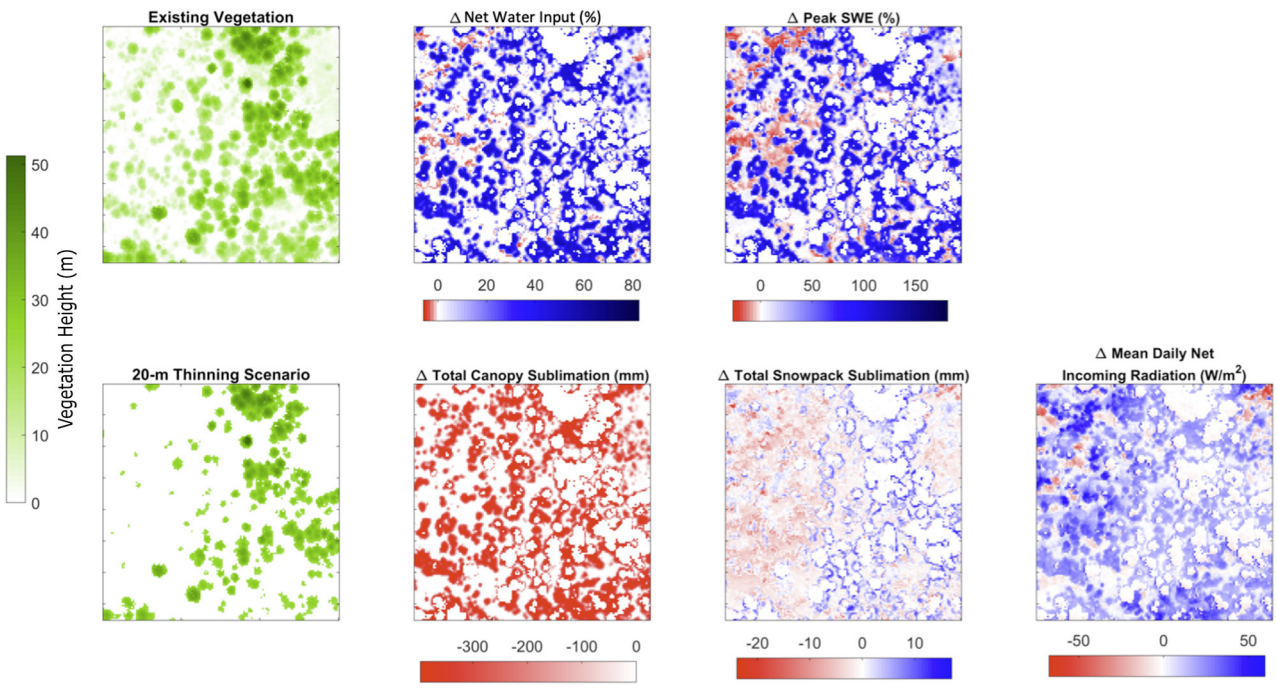

FIGURE 4 | Subdomain (150 × 150 m; see red box in **Figure 1**) example at 1-m resolution for the 20-m thinning scenario in the WY16. Left panels show pre- and post-thinning vegetation height, and the remaining panels show changes (thinning scenario—control run) in net water input, peak SWE, total canopy sublimation, total snowpack sublimation, and average incoming solar radiation during the snow covered season.

showed a detailed lidar-based validation of SnowPALM in the mountains of Colorado and New Mexico under different degrees of canopy cover, demonstrating its ability to reproduce the effect of canopy on snow accumulation and melt. Moreover, this study does not require a perfect match at all sites because it analyzes the relative differences of snowpack between the modeling scenarios.

Example of Forest Thinning at 1-m Spatial Resolution

Figure 4 shows 1-m differences between snowpack simulations for the 20-m thinning scenario and the control run at a relatively low elevation and north-facing subdomain (150 × 150 m, **Figure 1**). Overall, across this subdomain, melt volume increases by 14% on average, with substantial variability. Some areas show increases up to 80%, while other areas with little tree cover show a decrease in melt volume and peak SWE. Thinning decreased the total canopy sublimation by 130 mm on average (including areas without changes), with some decreases ranging up to 400 mm. Changes to snowpack sublimation, which depend on changes to the incoming net radiation (shortwave and longwave radiation), the wind regime, and the duration of the snowpack, are relatively small and variable across the domain. Net incoming radiation increased in most places where trees were removed due to increased solar exposure after thinning; however, some areas near previously existing (but removed) warm trees that emitted large amounts of longwave radiation show a decrease. Areas showing decreases in net radiation are found at the south edges of existing tree stands in relatively open areas (upper left and right areas of the subdomain). Overall, changes to peak SWE and net water input reflect complex interactions between mass and energy fluxes.

Impacts of Forest Thinning Across Snow Zones on Mass and Energy Fluxes

When thinning results are aggregated to the 30-m scale (forest patch) to better match scales where management decision are made, there is a strong positive linear relationship between changes of LAI and changes of net water input for all Snow Zones (**Figure 5**; r^2 from 0.76 to 0.95 and RMSE from 16 to 42 mm). The slopes of the linear relationships suggest that melt volume changes in mid to mid-low elevation Snow Zones are most sensitive to changes in canopy cover (slopes between 121 and 125 $mm/m^2 m^{-2}$), whereas at high elevations, net water input changes are about 10% less sensitive (slope <107 mm/m^2 m^{-2}). Scatter plots between canopy cover changes and peak SWE are similar to those for net water input (**Supplementary Figure 1**); however, lower correlations and steeper slopes are found in mid- to high-elevation Snow Zones. These relationships not only show the importance of absolute forest removal to changes in melt volume and peak SWE (i.e., strength of linear relationships), but also that forest thinning of the same magnitude may have uneven results (note the scatter in **Figure 5** and **Supplementary Figure 1**).

To identify which 30-m forest patches have the largest increases in net water input and peak SWE in response to forest thinning, we investigate these changes in relation to their forest structure prior to thinning (**Figures 6**, **7**). Snow Zones that show the largest increases in net water input (i.e., >500 mm) are the Low North, Low South, Mid-Low South, and Mid South Snow Zones (**Figure 6** and **Supplementary Figure 11**). Forest patches that have the largest increase in net water input from tree removal are those that are relatively dense (LAI $>$ 3 m^2/m^2) with an average forest height of 5–15 m (**Figure 6**). Forest patches with those characteristics typically have many trees (stem density >50) with mean height up to roughly 30 m (**Supplementary Figure 2**), resulting in scattered tall trees after thinning. Forest patches with this vegetation structure provide the largest decrease of canopy sublimation (**Supplementary Figure 3**) and relatively low increase in incoming net radiation (**Supplementary Figure 4**), resulting in the largest increase in melt volume. Large net water input increases (>500 mm) also occur for a few forest patches with low LAI (<2 m^2/m^2) and canopy height (<5 m) in the High North Snow Zone. These increases are not caused by changes to canopy sublimation (**Supplementary Figure 3**) or snowpack sublimation (**Supplementary Figure 6**), but rather by changes to snow redistribution by wind, which blows snow from these exposed patches to more sheltered forest patches. Redistributed snowfall causes an increase in peak SWE in forest patches that act as a deposition area for snow redistribution in the thinning scenario (**Figure 7**, High North Snow Zone) and a decrease in the forest patches that lose preferential snow deposition after thinning (**Supplementary Figure 7**, High North Snow Zone).

Changes to peak SWE (**Figure 7**) show similar patterns to net water input (**Figure 6** and **Supplementary Figure 12**), with relatively dense (LAI >3 m^2/m^2) and between 5 and 15 m tall pre-existing forest patches showing the largest SWE increases (>350 mm). However, unlike changes in net water input, some relatively dense (LAI $>$ 3 m^2/m^2) forest patches with large peak SWE changes are also found at high elevations. Both positive and negative changes to mean daily incoming net radiation during snow covered days can be found across Snow Zones (**Supplementary Figures 4, 5**), due to the spatially uneven increase in solar radiation and decrease in longwave radiation produced by thinning. Forest patches that experience the largest decrease in incoming net radiation are those with low initial LAI (<2 m^2/m^2) and relatively short heights (<5 m) (**Supplementary Figure 5**). These areas are already significantly exposed to solar radiation and, therefore, the decrease in longwave radiation from removing warm trees outweighs the relatively smaller increase in shortwave radiation.

Changes to Mass and Energy Fluxes

Figure 8 shows changes of mass and energy fluxes, normalized by changes in LAI (**Supplementary Table 1**) for both thinning scenarios and the control run. Results from the 10 and 20-m thinning scenarios are aggregated to create an average normalized response to thinning. Changes to canopy sublimation drive the majority of changes to peak SWE and snowmelt. Snowmelt is separated from rain falling through snowpack in this analysis to adequately account for changes to the mass balance due to forest thinning. On average, melt volume changes are about 100 $mm/m^2 m^{-2}$ for all Snow Zones, when averaging data for all water years and for both thinning scenarios. However, there are differences in melt volume changes across years, where the wet and normal (WY17 and WY16, respectively) years are more sensitivity to LAI

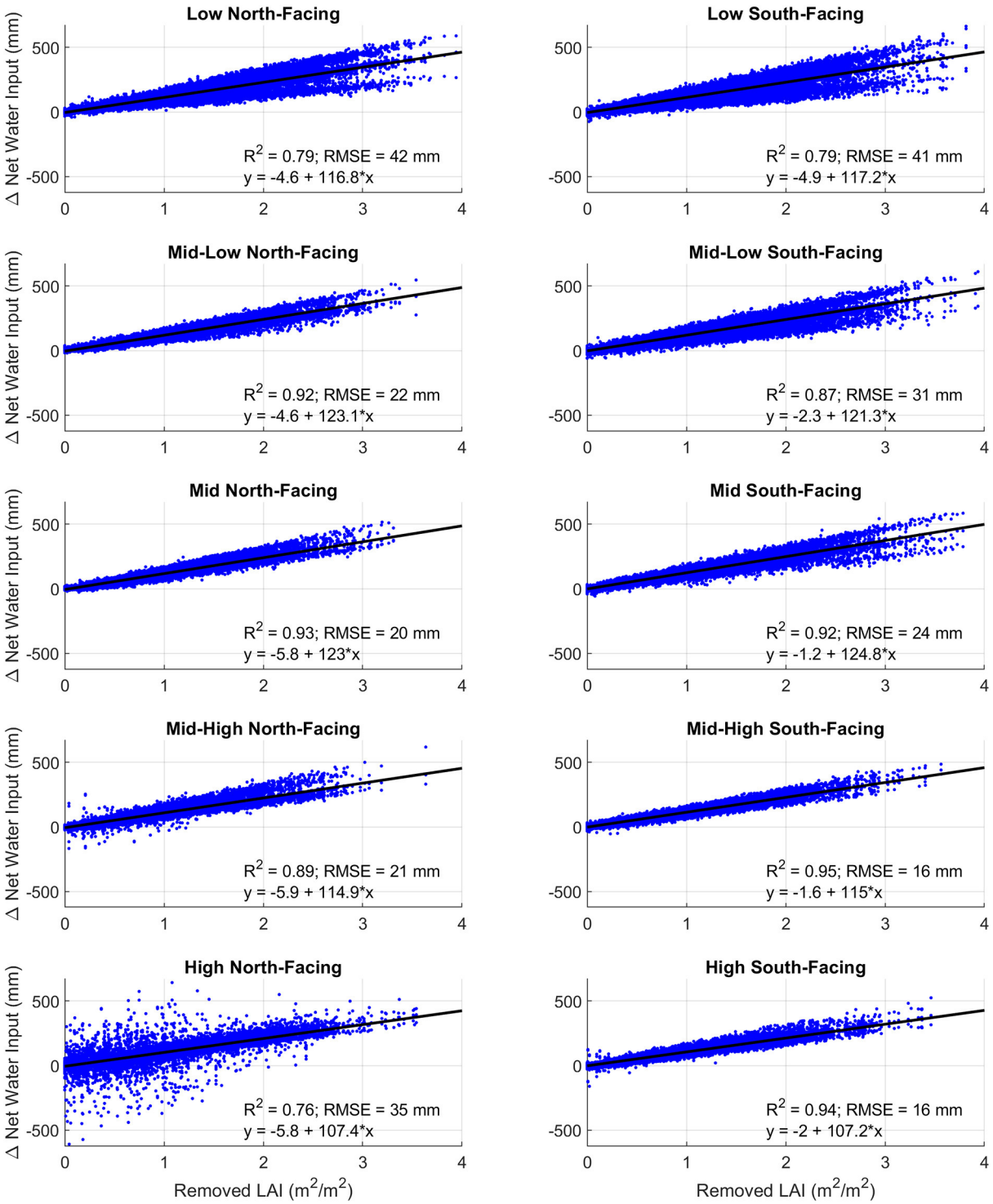

FIGURE 5 | Forest patch (30 m) relationships between changes in net water input and removed LAI for the two thinning scenarios and the three water years across Snow Zones.

changes (uniformly 100–150 mm/m^2m^{-2} across all snow zones), and the dry year (WY18) shows smaller sensitivity to LAI changes and more variability among Snow Zones. In WY18, increasing melt volume and peak SWE were smaller at lower elevations with more rain-on-snow occurring at lower elevations. This is explained by the fact that the

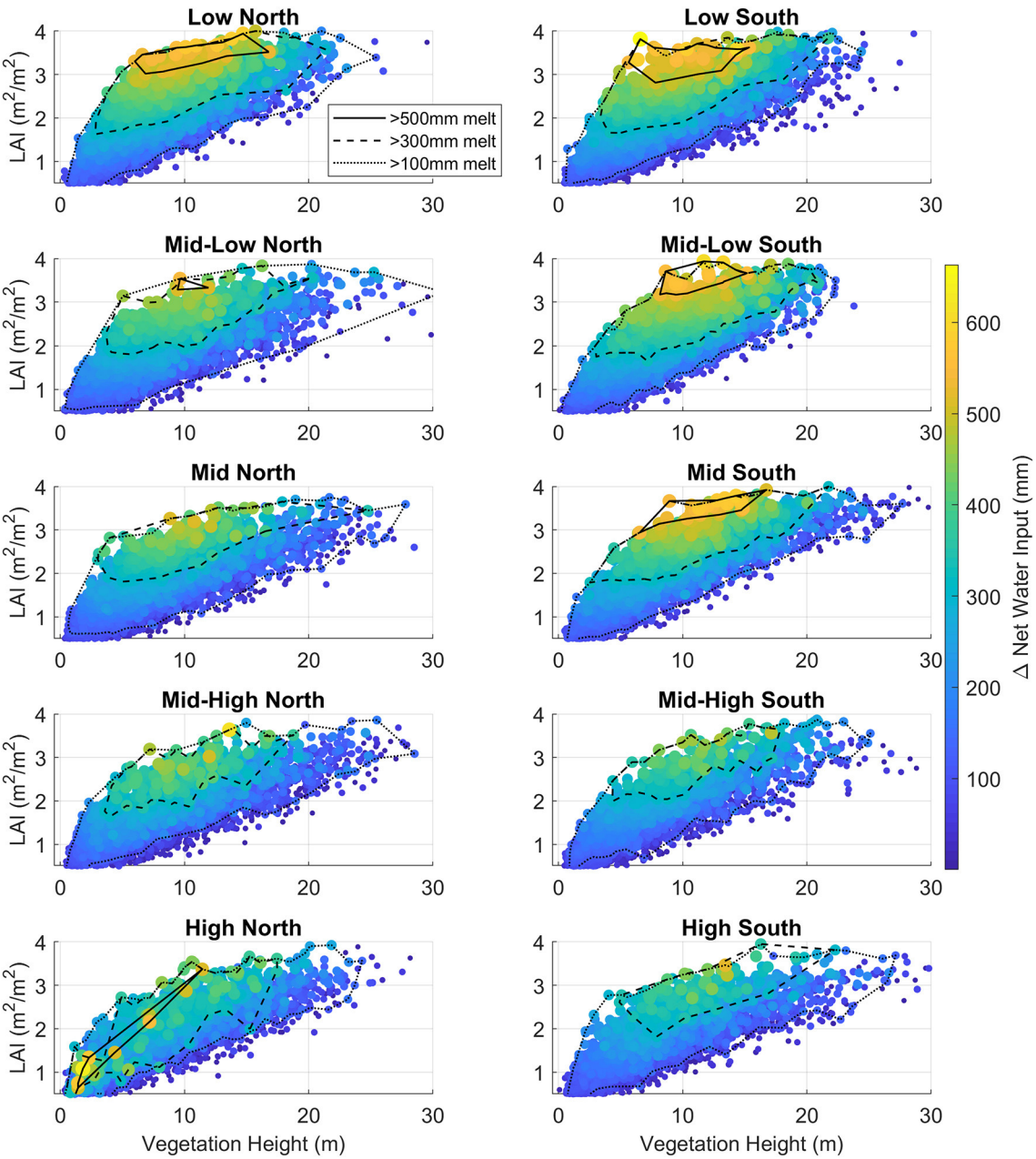

FIGURE 6 | Forest patch (30 m) increase in total net water input across Snow Zones for both thinning scenarios and organized by existing vegetation LAI and height. Dots are colored and sized according to changes to net water input. Continuous, dashed and pointed lines show the boundary of points with changes in melt volume >500, 300, and 100 mm, respectively.

snow season was lengthened on average by about a week at lower elevations following tree removal, which allowed later rainfall events to be added to the remaining snowpack. Overall, normalized changes to snowmelt range from about 50 mm/m^2m^{-2} for the dry year (WY18) up to about 150 mm/m^2m^{-2} for the wet year (WY17) at mid to low elevations. Normalized changes to snowpack sublimation (both increasing and decreasing) are relatively small, due to the compensating effects between increasing incoming shortwave radiation and decreasing incoming longwave radiation following tree removal (lower panels **Figure 8**).

Relatively little inter annual variability was found across Snow Zones for the energy flux changes (lower panel **Figure 8**). The largest changes to the energy fluxes are from increasing incoming shortwave radiation and decreasing incoming longwave radiation. Normalized changes to incoming shortwave radiation increase with elevation, opposite to the decrease of incoming longwave radiation with elevation. The net result of

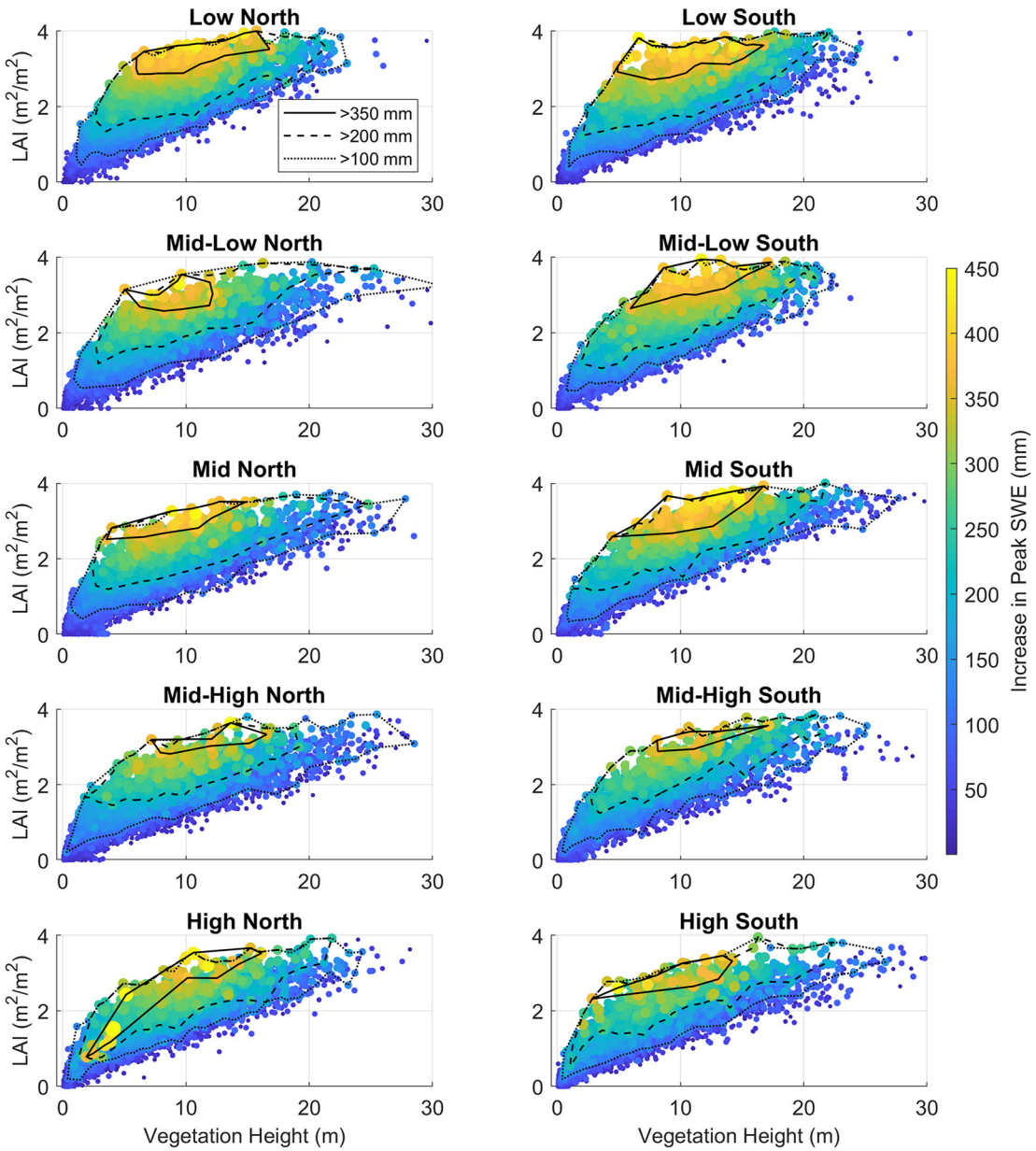

FIGURE 7 | Forest patch (30 m) increase in peak SWE across Snow Zones for both thinning scenarios and organized by existing vegetation LAI and height. Dots are colored and sized according to increases in peak SWE. Continuous, dashed and pointed lines show the boundary of points with changes in melt volume >350, 200, and 100 mm, respectively.

these compensating factors is that average changes to incoming net radiation are relatively small. The relationship between changes to incoming radiation with elevation is a result of the correlation between elevation, forest cover and slope, where higher elevations have sparser forest and steeper slopes (**Figure 2**). Steeper slopes mean that at times of low solar angles (winter and early melt season), more incoming solar radiation is available on south-facing slopes; therefore, after thinning, relatively more incoming solar radiation reaches the snowpack on higher-elevation south-facing slopes. Moreover, in sparser forests (typically found at high elevations), there are relatively fewer trees remaining after thinning to provide shelter from the sun. The opposite is true of denser forests, such as those found at lower elevations. Incoming longwave radiation shows the opposite pattern, where high elevation and south-facing Snow Zones have the largest decrease due to removal of warm trees emitting longwave.

Figure 9 presents time series of cumulative mass flux and SWE changes between the 20-m thinning scenario and the control run. This scenario is selected to analyze the largest

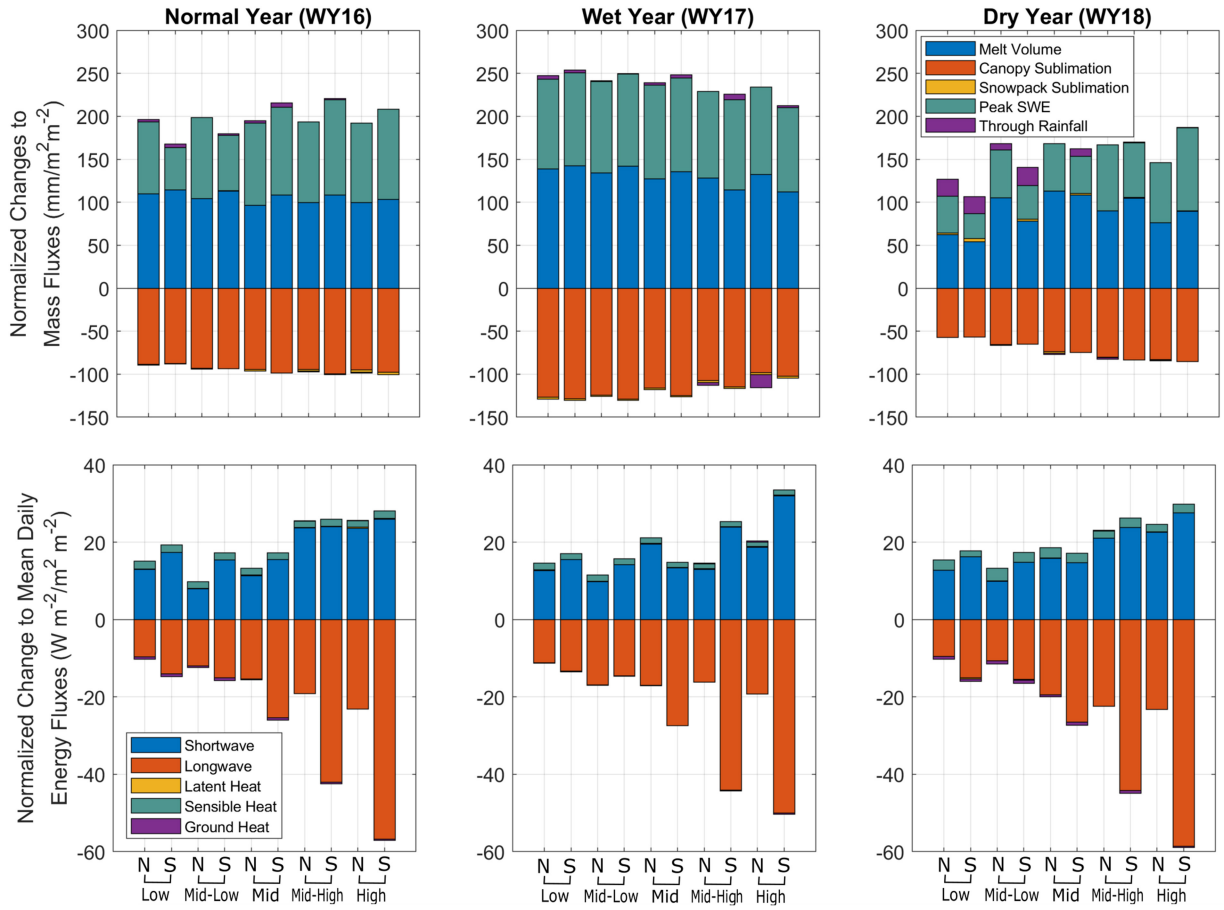

FIGURE 8 | Upper panels: changes to the mean total mass fluxes normalized by LAI changes between the thinning scenarios and the control run. **Lower panels:** changes to the mean daily energy fluxes normalized by LAI changes. Values from both thinning scenarios are used.

expected changes to the timing of mass flux changes. Net water input shows that more early- and mid-winter events occur at lower elevations, producing earlier snowmelt than in the control run. Changes to SWE show that for the higher Snow Zones, there is a larger negative change (i.e., control run has higher SWE) before it reaches zero, suggesting a faster melting rate and an average earlier date of snow depletion after thinning (**Figure 10**). On average, at the High North-Facing Snow Zone, snow does not disappear during the wet WY17 (**Figure 9**), as SWE changes stay below zero (more snow in the control run) until end of WY17, due to significant snowfall that year. Changes to snowpack sublimation are minimal ($< \pm 3$ mm), particularly when compared to changes to the other mass fluxes. Changes in the number of snow-covered days and the date of snow disappearance after thinning are inconsistent across water years (**Figure 10**). However, the wet WY17 nearly always has a decrease in both snow-covered days and earlier date of snow disappearance following thinning, up to about 8 and 4.5 days, respectively (for the Mid to High North-Facing Snow Zones). The other water years showed a more variable response that generally reflects more snow-covered days and later snow disappearance following tree removal at lower elevation that shifts to less snow-covered days at higher elevations and north-facing Snow Zones (**Figure 10**).

Decision Support Tool: Random Forest (RF) Model

SnowPALM results are used to train the RF models to synthetize results and expand the analysis to neighboring watersheds. The out-of-bag RMSE and correlation coefficient of the RF models for each Snow Zone show overall good model performance (left panel **Figure 11**). RMSEs are similar to those found for the linear relationship between changes of LAI and total melt volume (**Figure 5**), and the correlation coefficients are consistently high ($r^2 > 0.8$). Out-of-bag mean bias was also calculated and it was below 0.1% for all the models, suggesting that the RF models are skillful and can be used to predict changes to net water input. The RF analysis shows that, not surprisingly, LAI change is the key driving variable for predicting changes to net water input across Snow Zones, followed by the LAI and height of existing vegetation (right panel **Figure 11**). Topographic variables have relatively little impact on the model; however, Snow Zones are already classified by topographic variability, reducing the relative

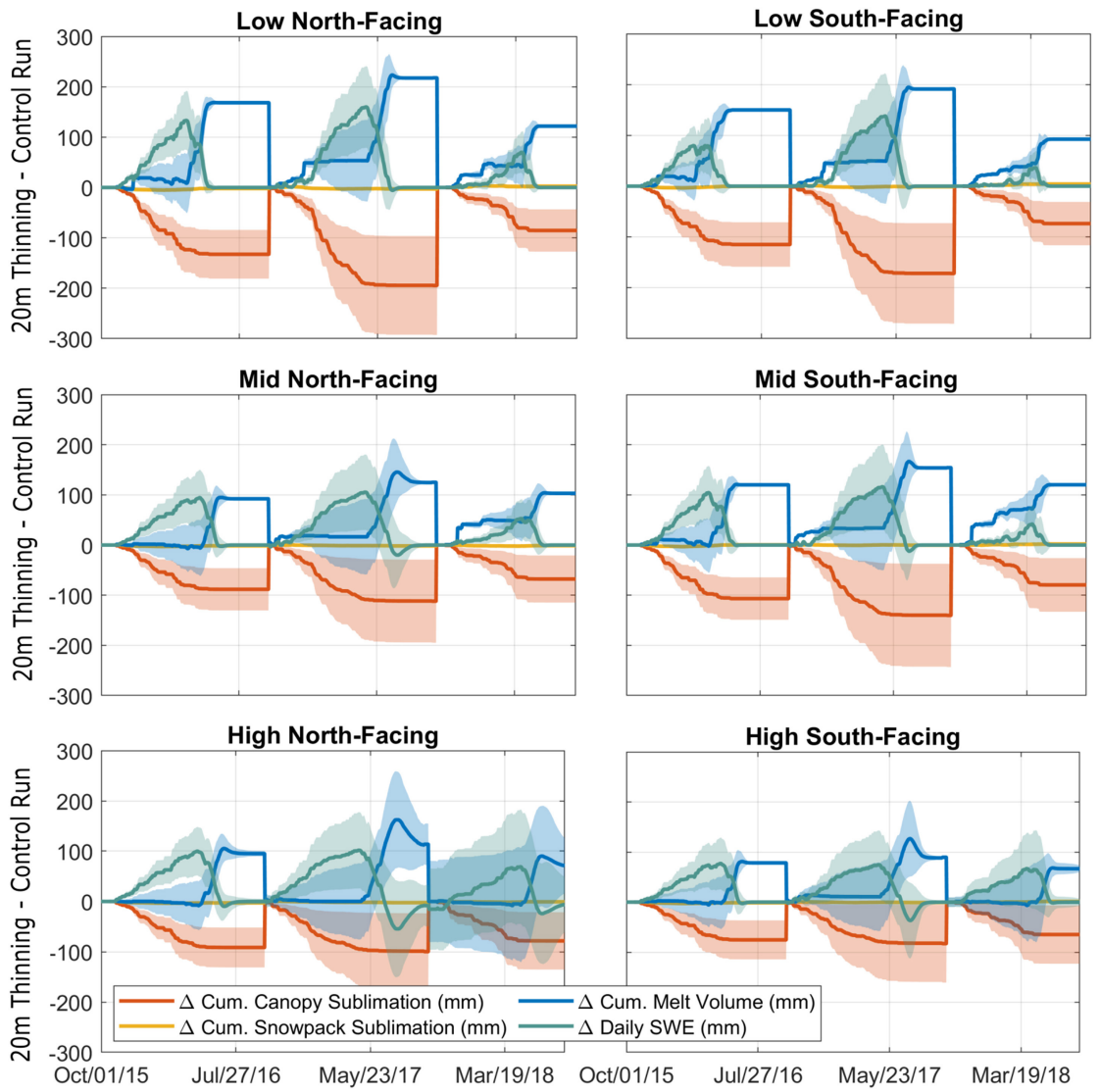

FIGURE 9 | Time series of changes to cumulative mass fluxes and daily SWE for six representative Snow Zones between the 20-m thinning scenario and the control run.

importance of these variables. We also trained a Random Forest model using all the data, without classifying by Snow Zones, and that analysis shows a similar pattern, as variables associated with vegetation structure explain more than 90% of the changes to snowmelt volume.

Figure 12 shows the simulated impacts of two forest thinning scenarios (0.6 and 2.4 mm^2/mm^2 removal) using the trained RF model on the net water input of relatively dense (LAI = 3 m^2/m^2) and 10-m tall forest patches across different topographic conditions. We show these two scenarios as they represent a moderate and a severe thinning, which can be qualitatively associated with the 10 and 20-m thinning scenarios implemented in SnowPALM. The severe forest removal scenario increases melt volume three times more than the moderate scenario, with a maximum change of 310 mm for south-facing (northness >0) and mid-elevation (∼2,200 masl) slopes. In both scenarios, thinning above ∼2,300 masl produces lower melt volume increases than lower elevations. Similarly, thinning of low elevation (<2,100 m) areas also produce lower melt volume increases, particularly for the severe forest thinning scenario, compared to those between 2,100 and 2,300 m. Changes in elevation were associated with larger differences than changes in aspect (**Figure 12**); however, south-facing slopes generally benefitted more from thinning, especially at elevations <2,200 m. These results generally agree with those presented in the previous section, where thinning mid-elevation and south-facing Snow Zones produce the largest changes to net water input (**Figure 5**).

We applied the RF model to 12 watersheds across the west shore of Lake Tahoe (**Supplementary Figure 8**), as an example

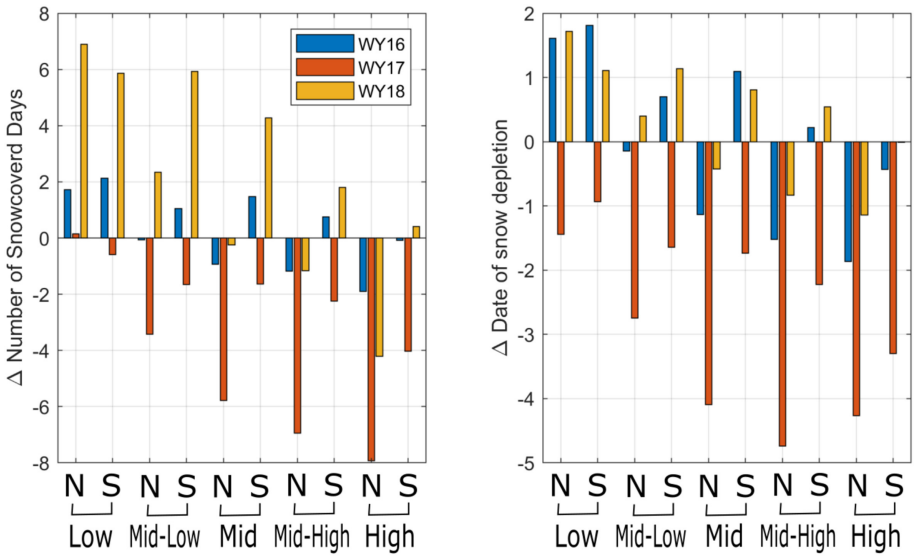

FIGURE 10 | Mean changes in the number of snow-covered days and the date of snow depletion across Snow Zones between the two thinning scenarios and the control run.

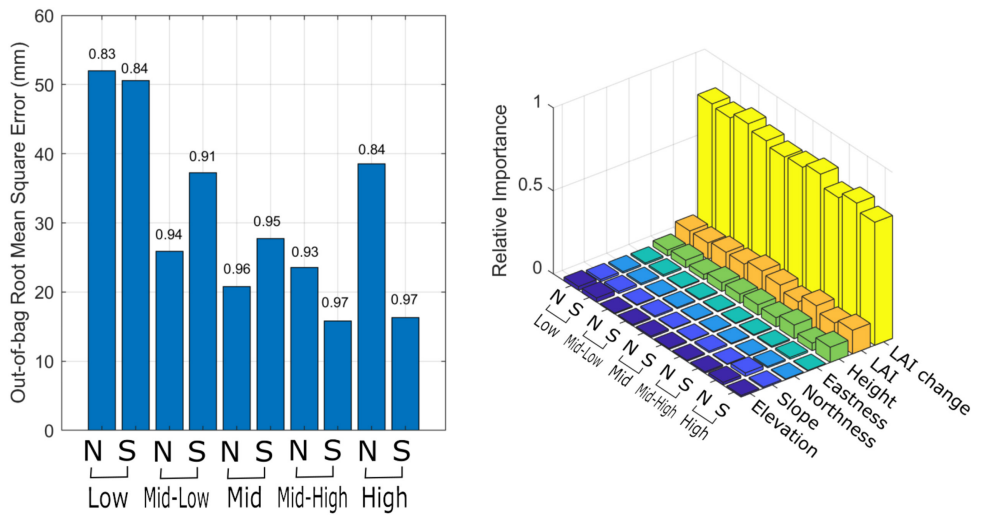

FIGURE 11 | Left panel: out-of-bag root mean square error (y-axis) and correlation (numbers on top of bars) for the Random Forest models at each Snow Zone. **Right panel:** relative importance factors of the predictor variables used in the Random Forest model.

of an application of the decision support tool. These watersheds span from Burton Creek in the North to Cascade Creek to the South of Lake Tahoe. Drainage area varies from about 29 km^2 for Blackwood Creek to about 1.7 km^2 for the Little Rubicon Creek. These watersheds have different degrees of vegetation cover and topographic gradients. The RF model was applied only to forest patches with LAI >3 m^2/m^2 and height between 5 and 15 m, which are the most sensitive to forest removal (**Figure 7**). Five thinning scenarios of 0.7, 1.4, 2.1, 2.8, and 3.5 m^2/m^2 LAI removal in each 30-m forest patch scale were investigated, representing scenarios of minimal to severe intervention. The watersheds with the largest number of targeted forest patches per km^2 are Burton Creek and Little Rubicon at about 120 km^{-2}. The average impact on melt volume is 80–380 mm for the 0.7 and 3.5 m^2/m^2 LAI removal, respectively (center panel **Figure 13**). The normalized change in melt volume suggests that there is not much variability in the sensitivity of these watersheds to forest thinning. The Little Rubicon Creek Watershed is the most sensitive (120 mm/m^2m^2) to forest removal and Eagle Creek watershed the least sensitive (107 mm/m^2m^2) to changes in melt volume, a difference of only 11%. These minor differences across watersheds are consistent with their similar topography and the dominant role of vegetation structure.

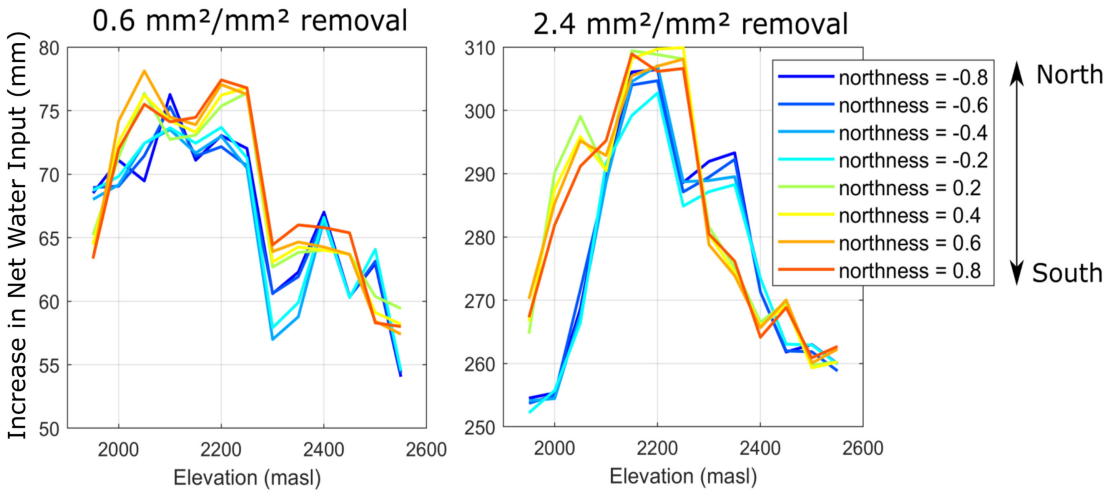

FIGURE 12 | Predicted increase in the total melt volume by the Random Forest model for a dense forest patch with mean LAI and height of 3 m^2/m^2 and 10 m, respectively, and two thinning scenarios: moderate (0.6 m^2/m^2) and significant (2.4 m^2/m^2) thinning. A negative northness index represents a more north oriented slope, with−1 representing a completely north-facing slope.

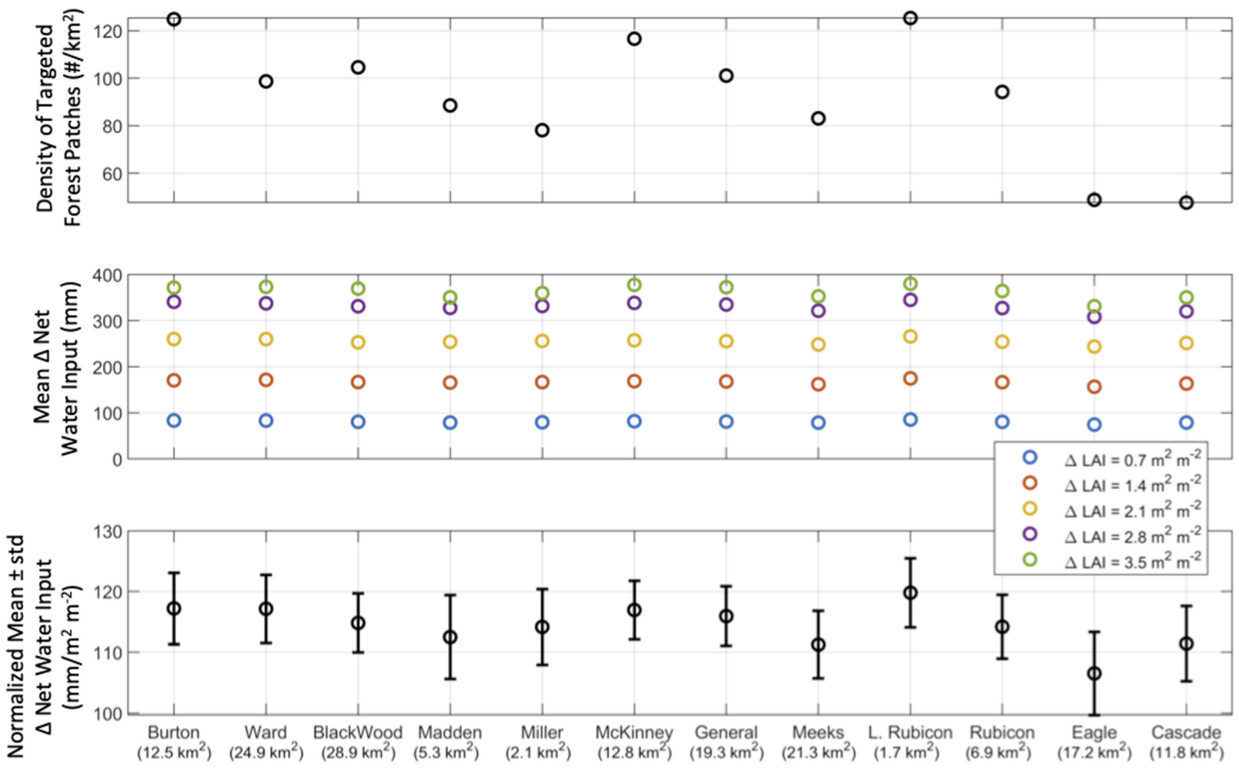

FIGURE 13 | Upper panel: density of targeted forest patches (LAI > 3 m^2/m^2 and height between 5 and 15 m) across 12 watersheds on the west shore of Lake Tahoe. Center panel: expected change to net water input for the targeted forest patches and each thinning scenario. **Lower panel:** mean and standard deviation of the expected normalized changes to net water input. Watersheds in the X-axis are sorted from north to south (left to right) and the drainage area is also presented for comparison.

DISCUSSION

In this study, we use high resolution (1 m) and large-extent (>50 km^2) spatially explicit snow modeling to predict the impact that landscape-scale forest thinning will have on snowpack along the west shore of Lake Tahoe. We find that in general, forest thinning decreases canopy sublimation, resulting in greater peak SWE and melt volumes (**Figure 8**). Because of this, the

20-m thinning scenario (most aggressive) produced the largest increases in snow accumulation and melt. Changes in incoming net radiation are relatively small due to compensating effects of decreasing incoming longwave radiation and increasing incoming shortwave radiation that accompany the forest cover changes (**Supplementary Figure 9**). This results in relatively small changes to snowpack sublimation, which only reach values up to about 25 mm (**Supplementary Figure 6**). Despite broad increases in melt volumes following tree removal, the snowpack response of any given 30-m forest patch depends on topographic position, existing vegetation structure and the seasonal climate variability. Our implications are consistent with those from Harpold et al. (2020), suggesting that relatively dense and shorter forest patches produce the largest increase in melt volume. However, the significantly larger domain and more variable climatic conditions used in the study, allowed insight into the transferability across topographic conditions (e.g., aspect and elevation) and identified watersheds where melt volumes would benefit most from thinning.

Our results help to place previous field observations of forest cover effects on snow accumulation and ablation into context. The model results show that decreasing forest cover tends to increase snow accumulation and increase ablation rates, in general agreement with a meta-analysis of 33 studies (Varhola et al., 2010) (**Figure 14**). In particular, our results agree with those from the nearby Central Sierra Snow Laboratory in the 1950's (Anderson and Gleason, 1960; Anderson et al., 1976) (green dots, **Figure 14**), in which their variability falls within the inter-patch variability found in our study (blue dashed lines, **Figure 14**). The sensitivity of snow ablation (melt volume + snowpack sublimation) to changes in forest cover in Lake Tahoe are somewhat smaller than the Varhola et al. (2010) dataset. Future pre- and post-thinning observations will be challenged to account for inter-annual climate variability and the effects of topography, which may cause substantial variability in stand-scale analyses (e.g., Varhola et al., 2010) limiting out ability to provide generalized inferences and recommendations across regions.

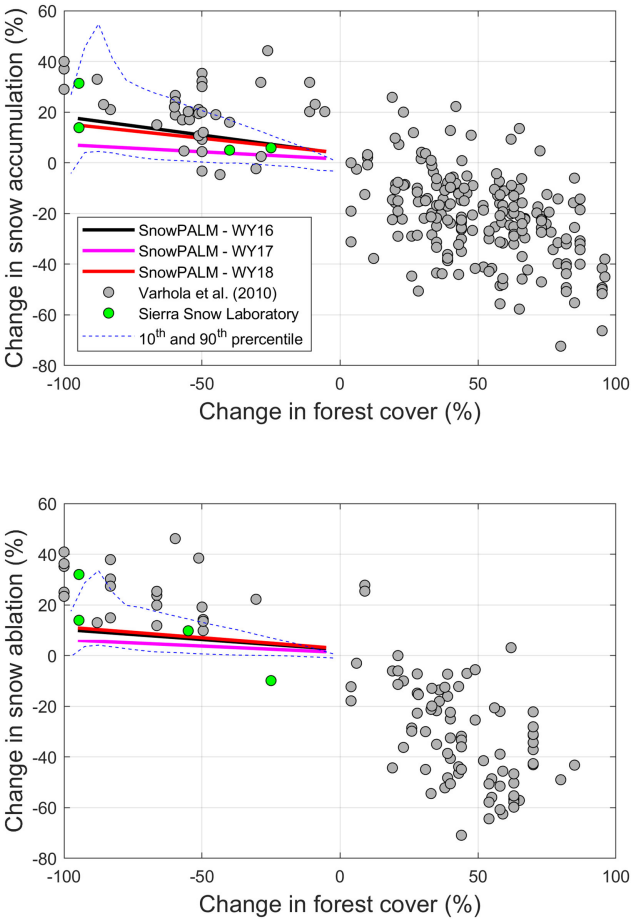

FIGURE 14 | Changes in peak snow accumulation (upper) and snow ablation (melt + snowpack sublimation) (lower) against changes in forest cover comparing the data from Varhola et al. (2010, Figure 8) meta-analysis and linear regressions for the three water years and both thinning scenarios simulated by SnowPALM at a 30-m forest stand scale. Dashed lines show the 10th and 90th percentile of all the 30-m forest stands used in the regression lines. Green dots highlight those points from Varhola et al. (2010) that are the closest to our study domain.

We find that differences due to forest thinning are highly dependent on the spatial distribution of trees. For example, the largest changes to canopy sublimation and snow accumulation are found in stands that are dense (LAI > 3 m^2/m^2) and between 5 and 15-m tall (**Figures 6**, **7**). These most responsive forest stands can increase peak SWE by about 400–450 mm (**Figure 7**) or more than 60% in the 20-m thinning scenario. Spatial patterns of increases and decreases of snowpack sublimation are also highly dependent on forest geometry and its change (**Supplementary Figure 6**). Relatively open areas exhibit decreasing snowpack sublimation, while areas around tree clusters increase snowpack sublimation (**Figure 4**). However, limitations associated with the representation of wind fields and turbulent fluxes remain one of the key uncertainties in modeling forest environments, where current approaches can lead to compensating modeling errors (Conway et al., 2018). Forest thinning also increases and decreases net incoming radiation, due to tradeoffs between increasing incoming shortwave and decreasing incoming longwave radiation by removing warm trees that shade nearby snowpack. Open areas on the south edges of trees removed by thinning show a decrease in net incoming radiation leading to relatively small snowpack changes (**Figure 4**). Conversely, areas with denser forest cover have an increase in net incoming radiation; however, changes to snowpack in these places are mostly controlled by changes in canopy sublimation.

Pre- and post-thinning forest structure and climate are the primary controls on snow accumulation and melt, with large-scale topography having a secondary effect that is likely related to the co-dependence between forests structure and topography. For example, we find that lower elevation Snow Zones have the largest absolute snowpack changes (**Supplementary Figure 6**),

and the lowest snowfall, because low elevation forests are generally denser (**Figure 2**). The impact of forest thinning on the high north-facing Snow Zone is somewhat distinct, as thinning enhances wind speed and increases snow redistribution by wind, which produces areas of preferential snow accumulation that are not found in other Snow Zones (**Figure 7**). Inter-annual climate variability is a more important control than topography in terms of the relative impact of thinning on the snowpack. For example, relative changes to net water input for the 20-m thinning scenario are larger during dry years (16% of the control run) than wet years (7% of the control run) (**Supplementary Figure 10**). This suggests that positive effects of thinning on net water input are greatest when water is needed the most (dry years), representing an important and positive co-benefit for forest health and water supply.

We use these model results to train a novel decision support tool to predict the greatest potential to increase water yields and identify co-benefits to other resources from forest thinning. The goal of the tool is to provide guidance to resource managers on how to incorporate hydrologic interests, such as increasing water yield, snow melt volumes and snow duration, into landscape restoration strategies that seek to achieve multiple benefits. In general, retaining snow longer on the landscape delays the timing of water inputs, which leads to a shorter period of soil water stress (Harpold, 2016) and reduces severe fire risk (Westerling et al., 2006). Historically in the Sierra Nevada, montane conifer forests were dominated by tall, large diameter trees that were variably distributed across the landscape (North et al., 2009). Fire suppression and timber harvest over the past 100 years has resulted in much higher densities of smaller diameter trees occurring consistently across large areas, particularly at low to moderate elevations. Forest restoration efforts intended to promote habitat in Sierra Nevada forests are designed to decrease the density of shorter, smaller diameter trees, increase the occurrence of larger trees, and increase the heterogeneity of their spatial distribution across the landscape toward an array of tree clumps and gaps (North et al., 2009). These ideal forest characteristics are more closely matched to our synthetically thinned forest than the existing forest (**Figure 4**). High density stands are more likely to carry high intensity fire (Collins et al., 2011), and topography can have a substantial effect on fire intensity as well (e.g., Harris and Taylor, 2015). South-facing slopes are less likely to carry high intensity fire because they tend to have lower tree densities compared to north-facing slopes, but they also experience greater solar radiation, so high tree densities are more likely to experience drought stress (Underwood et al., 2010). Therefore, targeting high density forest patches in south-facing slopes is a high priority that is further supported by this study (**Figures 6**, **12**). North-facing slopes, alternatively, are typically cooler and can be more suitable for supporting forests with higher canopy density and associated forest plants and wildlife. Thus, forest restoration, fire risk management, and wildlife habitat conservation can be reconciled with forest thinning effects on net water input, and in fact can have positive feedbacks that promote co-benefits for water availability during dry periods (Boisramé et al., 2018).

SUMMARY AND CONCLUSION

Changes to LAI in 30-m forest patches with specific pre-existing vegetation structure (LAI $>$ 3 m^2/m^2 and between 5 and 15-m tall) produce the largest increase in snow accumulation and melt volume. Macro-topography has a secondary role in predicting changes to snowpack following tree removal. Mid to low elevation ($<$2,300 masl) and south-facing areas were found to produce the largest increase in snow accumulation and melt after thinning. Forest thinning strategies in those forest patches are informed by a decision-support tool that recommends slightly different tree removal strategies in different topographic positions. We found that these recommendations are generally consistent with co-management for multiple resource goals, such as fire suppression, wildlife habitat conservation and water conservation, which is a key to maximizing resources invested into expanding forest restoration efforts.

In this study, we take an early step to develop a computationally efficient tool that is easy to implement for forest managers to predict changes to snowpack after thinning that resolves tree-scale processes. Given the lack of high-resolution models like SnowPALM, our simulations and the decision support tool derived from them are a novel means to translate information to nearby watersheds and different conditions. Challenges remain, however, in refining and verifying models like SnowPALM and implementing them in domains large enough to resolve primary snow forest controls across a range of vegetation and climate conditions. For example, the east shore of Lake Tahoe has a much different climate and dominant tree species that may not coincide with the recommendations made here. Another area where current forest planning is lacking is understanding the long-term impact of forest thinning on the water budgets. Processes such as compensating tree water use, under story, and tree regrowth may impact the long term efficiency of thinning. The scale of forest restoration needed for fuel management is significant in the Sierra Nevada (Kirwan et al., 2014), and represents one of the few ways that humans can manage their upland water supply systems. Given this societal need, continued work at the interface of basic process research and large-scale forest restoration applications are an avenue that could yield important advances.

DATA AVAILABILITY STATEMENT

The datasets generated for this study are available on request to the corresponding author.

AUTHOR CONTRIBUTIONS

SK, AH, and PB designed the study. SK and PB conducted snow simulation with SnowPALM. SK analyzed SnowPALM outputs with help from AH and PB. SK, AH, PB, and PM contributed to writing and overall discussion of results.

FUNDING

Financial support for this study was provided by the USFS via the Tahoe West Project and the State of California Wildlife Conservation Board.

ACKNOWLEDGMENTS

Authors thank A. Varhola for providing some of the data used in **Figure 14**. We thank Jonathan Greenberg for developing the tree segmentation data used. SnowPALM simulations were run at the Arizona Remote Sensing Center and at the University of Nevada, Reno, using computing resources from the Nevada Mountain Ecohydrology Lab. Comments from two reviewers are greatly appreciated.

SUPPLEMENTARY MATERIAL

The Supplementary Material for this article can be found online at: https://www.frontiersin.org/articles/10.3389/ffgc.2020.00021/full#supplementary-material

REFERENCES

Alexander, R. R., Troendle, C. A. A., Kaufmann, M. R., Shepperd, W. D., Crouch, G. L., and Watkins, R. K. (1985). The fraser experimental forest colorado: research program and published research 1937-1985. *Fort Collins: U.S. Dept. of agriculture, Forest Service, Rocky Mountain Forest and Range Experiment Station*. Available online at: https://www.fs.fed.us/rm/pubs_rm/rm_gtr118.pdf (accessed March 03, 2020).

Anderson, H. W. (1956). Forest-cover effects on snowpack accumulation and melt, central sierra snow laboratory. *Eos Trans. Am. Geophys. Union* 37, 307–312. doi: 10.1029/TR037i003p00307

Anderson, H. W. (1963). *Managing California's Snow Zone Lands For Water*. Available online at: http://citeseerx.ist.psu.edu/viewdoc/download?doi=10.1.1.224.4871&rep=rep1&type=pdf (accessed March 03, 2020).

Anderson, H. W., and Gleason, C. H. (1960). Effects of logging and brush removal on snow water runoff. *Int. Assoc. Hydrol. Sci. Publ.* 51, 478–489.

Anderson, H. W., Hoover, M., and Reinhart, K. G. (1976). *Forests and Water: Effects of Forest Management on Floods, Sedimentation, and Water Supply*. Berkley, CA. Available online at: https://www.fs.usda.gov/treesearch/pubs/24048 (accessed March 03, 2020).

Bewley, D., Alila, Y., and Varhola, A. (2010). Variability of snow water equivalent and snow energetics across a large catchment subject to mountain pine beetle infestation and rapid salvage logging. *J. Hydrol.* 388, 464–479. doi: 10.1016/j.jhydrol.2010.05.031

Blöschl, G. (1999). Scaling issues in snow hydrology. *Hydrol. Process.* 13, 2149–2175. doi: 10.1002/(SICI)1099-1085(199910)13:14/15<2149::AID-HYP847>3.0.CO;2-8

Boisramé, G., Thompson, S., and Stephens, S. (2018). Hydrologic responses to restored wildfire regimes revealed by soil moisture-vegetation relationships. *Adv. Water Resour.* 112, 124–146. doi: 10.1016/j.advwatres.2017.12.009

Breiman, L. (2001). Random Forest. *Mach. Learn.* 45, 5–32. doi: 10.1023/A:1010933404324

Broxton, P. D., Harpold, A. A., Biederman, J. A., Troch, P. A., Molotch, N. P., and Brooks, P. D. (2015). Quantifying the effects of vegetation structure on snow accumulation and ablation in mixed-conifer forests. *Ecohydrology* 8, 1073–1094. doi: 10.1002/eco.1565

Church, J. E. (1933). Snow surveying: its principles and possibilities. *Geogr. Rev.* 23, 529–563. doi: 10.2307/209242

Collins, B. M., Everett, R. G., and Stephens, S. L. (2011). Impacts of fire exclusion and recent managed fire on forest structure in old growth Sierra Nevada mixed-conifer forests. *Ecosphere* 2, 1–4. doi: 10.1890/ES11-00026.1

Conway, J. P., Pomeroy, J. W., Helgason, W. D., and Kinar, N. J. (2018). Challenges in modeling turbulent heat fluxes to snowpacks in forest clearings. *J. Hydrometeorol.* 19, 1599–1616. doi: 10.1175/JHM-D-18-0050.1

Deardorff, J. W. (1978). Efficient prediction of ground surface temperature and moisture, with inclusion of a layer of vegetation. *J. Geophys. Res.* 83:1889–1903. doi: 10.1029/JC083iC04p01889

Essery, R., Rutter, N., Pomeroy, J., Baxter, R., Stähli, M., Gustafsson, D., et al. (2009). SNOWMIP2: An evaluation of forest snow process simulations. *Bull. Am. Meteorol. Soc.* 90, 1120–1136. doi: 10.1175/2009BAMS2629.1

Golding, D. L., and Swanson, R. H. (1986). Snow distribution patterns in clearings and adjacent forest. *Water Resour. Res.* 22, 1931–1940. doi: 10.1029/WR022i013p01931

Goodell, B. (1952). Watershed-management aspects of thinned young lodgepole pine stands. *J. For.* 50, 374–378. doi: 10.1093/jof/50.5.374

Harpold, A. A. (2016). Diverging sensitivity of soil water stress to changing snowmelt timing in the Western U.S. *Adv. Water Resour.* 92, 116–129. doi: 10.1016/j.advwatres.2016.03.017

Harpold, A. A., and Brooks, P. D. (2018). Humidity determines snowpack ablation under a warming climate. *Proc. Natl. Acad. Sci.U. S. A.* 115, 1215–1220. doi: 10.1073/pnas.1716789115

Harpold, A. A., Krogh, S. A., Kohler, M., Eckberg, D., Greenberg, J., Sterle, G. (2020). "Increasing the efficacy of forest thinning for snow using high-resolution modeling: a proof of concept in The Lake Tahoe Basin, California, USA" in *Ecohydrology*. doi: 10.1002/eco.2203

Harris, L., and Taylor, A. H. (2015). Topography, fuels, and fire exclusion drive fire severity of the rim fire in an old-growth mixed-conifer forest, yosemite national park, USA. *Ecosystems* 18, 1192–1208. doi: 10.1007/s10021-015-9890-9

Kirwan, B. J., Branham, J., and Keegan, J. (2014). *The State of The Sierra Nevada's Forests*. Available online at: https://sierranevada.ca.gov/wp-content/uploads/sites/236/attachments/StateOfSierraForestsRptWeb.pdf (accessed March 03, 2020).

López-Moreno, J. I., Pomeroy, J. W., Revuelto, J., and Vicente-Serrano, S. M. (2013). Response of snow processes to climate change: spatial variability in a small basin in the spanish pyrenees. *Hydrol. Process.* 27, 2637–2650. doi: 10.1002/hyp.9408

Mahat, V., and Tarboton, D. G. (2012). Canopy radiation transmission for an energy balance snowmelt model. *Water Resour. Res.* 48, 1–16. doi: 10.1029/2011WR010438

Moeser, D., Roubinek, J., Schleppi, P., Morsdorf, F., and Jonas, T. (2014). Canopy closure, LAI and radiation transfer from airborne LiDAR synthetic images. *Agric. For. Meteorol.* 197, 158–168. doi: 10.1016/j.agrformet.2014.06.008

Moeser, D., Stahli, M., Jonas, T., Stähli, M., Jonas, T., Stahli, M., et al. (2015). Improved snow interception modeling using canopy parameters derived from airborne LIDAR data. *Water Resour. Res.* 51, 5041–5059. doi: 10.1002/2014WR016724

Mote, P. W., Li, S., Lettenmaier, D. P., Xiao, M., and Engel, R. (2018). Dramatic declines in snowpack in the western US. *npj Clim. Atmos. Sci.* 1:2. doi: 10.1038/s41612-018-0012-1

Musselman, K. N., Clark, M. P., Liu, C., Ikeda, K., and Rasmussen, R. (2017a). Slower snowmelt in a warmer world. *Nat. Clim. Chang.* 7, 214–219. doi: 10.1038/nclimate3225

Musselman, K. N., Pomeroy, J. W., Centre, O., Musselman, K. N., and Pomeroy, J. W. (2017b). Estimation of needleleaf canopy and trunk temperatures and longwave contribution to melting snow. *J. Hydrometeorol.* 18, 555–572. doi: 10.1175/JHM-D-16-0111.1

Musselman, K. N., Pomeroy, J. W., and Link, T. E. (2015). Variability in shortwave irradiance caused by forest gaps: measurements, modelling, and implications for snow energetics. *Agric. For. Meteorol.* 207, 69–82. doi: 10.1016/j.agrformet.2015.03.014

North, M., Stine, P., O'Hara, K., Zielinski, W., and Stephens, S. (2009). *An Ecosystem Management Strategy For Sierran Mixed- Conifer Forests*. Available online at: https://www.fs.fed.us/psw/publications/documents/psw_gtr220/psw_gtr220.pdf (accessed March 03, 2020).

Petersky, R. S., Shoemaker, K. T., Weisberg, P. J., and Harpold, A. A. (2018). The sensitivity of snow ephemerality to warming climate across an arid to montane vegetation gradient. *Ecohydrology* 12, 1–14. doi: 10.1002/eco.2060

Pomeroy, J. W., and Granger, R. J. (1997). "Sustainability of the western canadian boreal forest under changing hydrological conditions. I. snow accumulation and ablation," in *Sustainability of Water Resources under Increasing Uncertainty,* eds. D. Rosjberg, N. Boutayeb, A. Gustard, Z. Kundzewicz, and P. Rasmussen (Wallingford: International Association of Hydrological Sciences) (IAHS Publ. No. 240), 237–242.

Pomeroy, J. W., Gray, D. M., Hedstrom, N. R., and Janowicz, J. R. (2002). Prediction of seasonal snow accumulation in cold climate forests. *Hydrol. Process.* 16, 3543–3558. doi: 10.1002/hyp.1228

Pomeroy, J. W., Parviainen, J., Hedstrom, N., and Gray, D. M. (1998). Coupled modelling of forest snow interception and sublimation. *Hydrol. Process.* 12, 2317–2337. doi: 10.1002/(SICI)1099-1085(199812)12:15<2317::AID-HYP799>3.0.CO;2-X

Romsos, S. (2011). *LiDAR Remote Sensing, Lake Tahoe Watershed.*

Rutter, N., Essery, R., Pomeroy, J., Altimir, N., Andreadis, K., Baker, I., et al. (2009). Evaluation of forest snow processes models (SnowMIP2). *J. Geophys. Res.* 114:D06111. doi: 10.1029/2008JD011063

Sturm, M., Goldstein, M. A., and Parr, C. (2017). Water and life from snow: a trillion dollar science question. *Water Resour. Res.* 53, 3534–3544. doi: 10.1002/2017WR020840

Tague, C. L., Moritz, M., and Hanan, E. (2019). The changing water cycle: the eco-hydrologic impacts of forest density reduction in Mediterranean (seasonally dry) regions. *Wiley Interdiscip. Rev. Water* 6:e1350. doi: 10.1002/wat2.1350

Tinkham, W. T., Smith, A. M. S., Marshall, H. P., Link, T. E., Falkowski, M. J., and Winstral, A. H. (2014). Quantifying spatial distribution of snow depth errors from LiDAR using random forest. *Remote Sens. Environ.* 141, 105–115. doi: 10.1016/j.rse.2013.10.021

Toews, D. A. A., and Gluns, D. R. D. R. (1986). "Snow accumulation and ablation on adjacent forested and clearcut sites in southeastern British Columbia," in *54th Western Snow Conference* (Phoenix, AZ), 12.

Troendle, C. A., and Leaf, C. F. (1980). "Hydrology," in *An Apporach to Water Resources Evaluation of Non-Point Silvicultural Sources: (A Procedural Handbook)*, Washington, DC: U.S. Environmental Protection Agency.

Underwood, E. C., Viers, J. H., Quinn, J. F., and North, M. (2010). Using topography to meet wildlife and fuels treatment objectives in fire-suppressed landscapes. *Environ. Manage.* 46, 809–819. doi: 10.1007/s00267-010-9556-5

van Gunst, K. J. (2012). *Forest mortality in Lake Tahoe Basin from 1985-2010: influences of forest type, stand density, topography and climate* (Master's degree thesis). Department of Natural Resources and Environmental Science, University of Nevada, Reno, NV, USA. Available online at: https://scholarworks.unr.edu/handle/11714/3773 (accessed March 03, 2020).

Varhola, A., Coops, N. C., Weiler, M., and Moore, R. D. (2010). Forest canopy effects on snow accumulation and ablation: an integrative review of empirical results. *J. Hydrol.* 392, 219–233. doi: 10.1016/j.jhydrol.2010.08.009

Westerling, A. L., Hidalgo, H. G., Cayan, D. R., and Swetnam, T. W. (2006). Warming and earlier spring increase western U.S. forest wildfire activity. *Science* 313, 940–943. doi: 10.1126/science.1128834

Winkler, R. D., Spittlehouse, D. L., and Golding, D. L. (2005). Measured differences in snow accumulation and melt among clearcut, juvenile, and mature forests in southern British Columbia. *Hydrol. Process.* 19, 51–62. doi: 10.1002/hyp.5757

Winstral, A., and Marks, D. (2002). Simulating wind fields and snow redistribution using terrain-based parameters to model snow accumulation and melt over a semi-arid mountain catchment. *Hydrol. Process.* 16, 3585–3603. doi: 10.1002/hyp.1238

Woods, S. W., Ahl, R., Sappington, J., and McCaughey, W. (2006). Snow accumulation in thinned lodgepole pine stands, Montana, USA. *For. Ecol. Manage.* 235, 202–211. doi: 10.1016/j.foreco.2006.08.013

Xia, Y., Mitchell, K., Ek, M., Sheffield, J., Cosgrove, B., Wood, E., et al. (2012). Continental-scale water and energy flux analysis and validation for the North American land data assimilation system project phase 2 (NLDAS-2): 1. Intercomparison and application of model products. *J. Geophys. Res. Atmos.* 117, 1–27. doi: 10.1029/2011JD016051

Xu, Q., Man, A., Fredrickson, M., Hou, Z., Pitkänen, J., Wing, B., et al. (2018). Quantification of uncertainty in aboveground biomass estimates derived from small-footprint airborne LiDAR. *Remote Sens. Environ.* 216, 514–528. doi: 10.1016/j.rse.2018.07.022

Conflict of Interest: The authors declare that the research was conducted in the absence of any commercial or financial relationships that could be construed as a potential conflict of interest.

frontiers in Forests and Global Change

ORIGINAL RESEARCH
published: 02 April 2020
doi: 10.3389/ffgc.2020.00034

Effects of Temperature and Water Availability on Northern European Boreal Forests

Guiomar Ruiz-Pérez and Giulia Vico*

Department of Crop Production Ecology, Swedish University of Agricultural Sciences, Uppsala, Sweden

Boreal forests are warming faster than the rest of the planet. Do the benefits of higher temperatures and longer growing seasons for forest productivity exceed the negative effects of more frequent dry spells and heat waves, shifting precipitation patterns, and higher evaporative demands? And are the effects uniformly distributed geographically? To answer to these questions, the relationship between climatic variables and NDVI—a proxy of forest productivity at regional scale—was explored via Partial Least Square (PLS) regression analyses. We focused on Northern Europe, where contrasting findings on the effects of warming have been reported and that has so far been overlooked by systematic large-scale explorations of the linkages between boreal forest productivity and climatic conditions. The results show that the effects of warmer temperatures on boreal forest productivity are not uniformly positive and that water stress is already negatively affecting these forests. Indeed, increased temperatures appear beneficial in northern and wetter regions, while warmer temperatures mostly reduce forest productivity in southern and drier areas. These results are suggestive of already existing limitations due to water availability and warm temperatures, even in mesic regions like Northern Europe. These conditions are expected to become more frequent and intense in the future, potentially reducing the ability of boreal forests to provide their essential ecosystem services unless forest management practices are adapted to the new conditions.

Keywords: boreal forest, temperature, precipitation, water stress, NDVI, Northern Europe

OPEN ACCESS

Edited by:
Matthew D. Hurteau, University of New Mexico, United States

Reviewed by:
Tanya Doody, Commonwealth Scientific and Industrial Research Organisation (CSIRO), Australia
Courtney M. Siegert, Mississippi State University, United States

****Correspondence:***
Guiomar Ruiz-Pérez
guiomar.ruiz.perez@slu.se

Specialty section:
This article was submitted to Forest Hydrology, a section of the journal Frontiers in Forests and Global Change

Received: *28 October 2019*
Accepted: *06 March 2020*
Published: *02 April 2020*

Citation:
Ruiz-Pérez G and Vico G (2020) Effects of Temperature and Water Availability on Northern European Boreal Forests. Front. For. Glob. Change 3:34. doi: 10.3389/ffgc.2020.00034

INTRODUCTION

Global warming is more pronounced in boreal forests than elsewhere, with temperatures increasing twice as fast as the rest of the planet (Intergovernmental Panel on Climate Change, 2014). They are considered largely unaffected by or even benefitting from climate change (Boisvenue and Running, 2006), particularly if compared to ecosystems experiencing drier or more variable conditions (Allen et al., 2010; Anderegg et al., 2013). So far, rising temperatures have mostly enhanced boreal forest productivity and some forests might still be able to cope with further temperature increases (Myneni et al., 1997; Kauppi et al., 2014). Nevertheless, there is increasing evidence that boreal ecosystems are also negatively affected by climate change (Martin-Benito and Pederson, 2015), suggesting that their vulnerability to future conditions is currently severely underestimated (Allen et al., 2015). Indeed, future climates can lead to more frequent stress events, including longer periods without precipitation (hereafter "dry spells") and potentially damaging high temperatures, which can cause widespread reduction in productivity and enhance mortality (Anderegg et al., 2013; Buermann et al., 2014). Dry spells can also cancel out the beneficial effects of higher temperatures (Belyazid and Zanchi, 2019).

Based on remotely sensed data, a prolonged and extensive regional decline in forest productivity [termed "browning trend" by Goetz et al. (2005), Lloyd and Bunn (2007)] has already been observed in eastern Alaska and western Canada (Beck and Goetz, 2011), western central Eurasia and western North America (Buermann et al., 2014). Additionally, tree rings and wood density measurements suggest that in recent decades there has been a divergence between warming and tree growth, with localized shifts to a negative correlation between temperature and growth (D'Arrigo et al., 2008; Porter and Pisaric, 2011). Moreover, boreal forests appear increasingly vulnerable to indirect effects of rising temperatures, including temperature-induced drought stress (Barber et al., 2000; Beck and Goetz, 2011), increased frequency of fires (Kasischke and Turetsky, 2006; Rubtsov et al., 2011), increased risk of insect outbreaks (Kurz et al., 2008) and more frequent climate extremes (Mulder et al., 2019). Nevertheless, in Northern Europe, the effects of rising temperatures are still largely unclear and partially contrasting. For example, positive correlations emerged between tree growth and monthly mean temperature in June and July of the year prior to the ring formation at latitudes higher than ∼65°N, whereas correlations were negative at lower latitudes (Babst et al., 2012). Reports of forest growing stocks showed that forest productivity has been increasing in the region (Gauthier et al., 2015), whereas analysis based on remotely-sensed variables found mostly stable productivity in boreal forests (Bjerke et al., 2014). Northern Europe is also not exempt from indirect damaging effects of rising temperatures, with recent reports of detrimental effects of dry spells and high temperatures on forest productivity in southern Sweden, symptoms of drought-induced top dieback in southern Norway, several drought-affected sites over Finland, and reductions in the carbon (C) sequestration potential of forests (Muukkonen et al., 2015; Rosner et al., 2018; Belyazid and Zanchi, 2019).

These partially contrasting observations regarding the effects of changing climatic conditions on Northern European forests can be due to differences in the proxy of forest productivity being used in each study—from remotely sensed vegetation indices such as NDVI (Olofsson et al., 2008) to *in-situ* measures such as tree-rings (Babst et al., 2012); the extent and diversity of the study site(s)—from specific species (Rosner et al., 2018) to mixed forests (Piao et al., 2017); the spatial resolution and coverage—from images at different spatial resolutions (Olofsson et al., 2008 and Sulla-Menashe et al., 2018) to experimental plots (Rosner et al., 2018); the temporal resolution of observations and the length of the period analyzed—from analyses based on monthly averages (Babst et al., 2012) to seasonal and annual averages (Beck and Goetz, 2011). These discrepancies call for an updated analysis extending over the entire region, in order to elucidate the key drivers of forest productivity and hence how future conditions can affect these forests and where management should focus on climate adaptation. Ensuring continued forest productivity in Northern Europe in the future is key for European climate mitigation actions and economy. Indeed, one of the pathways toward the reduction of CO_2 stipulated in the Paris Agreement of the United Nations Framework Convention on Climate Change (UNFCCC) is the use of harvested biomass to substitute fossil fuel (Kallio et al., 2013; Smyth et al., 2017). Northern European forests are the main source of biomass in Europe and hence they are necessary for the achievement of the European targets for CO_2 emission reduction in energy and climate policies (Rytter et al., 2015, 2016). Already today, 40% of energy used in the Nordic countries is obtained from renewable sources, mostly from forest biomass (∼60% of the total renewable energy; Nordic Statistics, 2017). In Sweden and Finland, the consumption of wood-based energy by the rural population is more than five times the European average (Köhl et al., 2011). Northern European forests act as a C sink in the global C cycle, with an estimated annual C gain around 20,000 Gg [the highest proportion of European forests; United Nations Framework Convention on Climate Change (2011)]. Moreover, Northern European forests are also a key economic resource, especially in Finland and Sweden, constituting around 5.5 and 3.5% of national GDP, respectively. The pressure to produce biomass already clashes with the provision of other ecosystem services, such as those linked to soil and water quality (Koskiaho et al., 2003), mental and physical health (Grahn and Stigsdotter, 2003), and opportunities for recreational activities and tourism (Hall et al., 2009; Tangeland et al., 2013). Aside from their importance for climate actions and economy, investigating the effects of Northern European forests is interesting because of the intrinsic differences between these forests and other boreal regions. From the management standpoint, Northern European forests differ from other boreal forests in species composition and use. Scots pine, Norway spruce, mountain birch and downy birch dominate the boreal forest of Europe, with a minor component of European aspen ({Boonstra et al., 2016 #128}). Furthermore, forests in Northern European have been harvested for longer periods and more intensively than in North America and Russia, so that there is considerably less primary forest left (Ruckstuhl et al., 2008; Elbakidze et al., 2013). Climatically, Northern Europe is subject generally to milder and wetter conditions when compared to similar latitudes in Asia and North America (mostly characterized by continental climates). These conspicuous differences prevent the direct extrapolation of results and conclusions obtained elsewhere (Kong et al., 2017).

Because of the importance of boreal forests in Northern Europe for the delivery of the aforementioned ecosystem services, there is the need to quantify the forest sensitivity to climatic conditions at regional scale and identify which climatic conditions are beneficial and which are detrimental for these forests. Future climates are expected to result in a substantial increase in temperatures, in particular at high latitudes. The projected changes in precipitation are less clear, but an increase in winter precipitation and a decrease during the summers is expected (Ruosteenoja et al., 2018). Even if the amount of precipitation remained unaltered, the expected increase in temperature will enhance losses via evapotranspiration and result in more frequent periods of low water availability (Ruosteenoja et al., 2018). As such, extreme conditions in terms of heat and drought like the ones observed in summer 2018 are expected to become common in the next few decades (Toreti et al., 2019). Therefore, the importance of water availability for forest productivity on Northern Europe is expected to increase;

and management approaches should consider this aspect in increasing detail at least in more vulnerable regions. With a focus on the interplay between warmer temperatures and water availability, the following hypotheses were tested:

- Even though classified as temperature- and light-limited, the productivity of Northern European forests is also affected by water availability;
- The effects of warmer temperature on forest productivity are not homogeneously positive over Northern Europe;
- The correlation between temperature and forest productivity is positive in cold and moist locations while shifting to negative in warm and dry ones;
- By driving vegetation water availability, the timing of precipitation plays a more important role than the total precipitation amount.

To this aim, we explore the relationship between the MODIS-derived Normalized Difference Vegetation Index (NDVI)—a measure of vegetation activity and a proxy of forest productivity—and high-resolution gridded meteorological data (E-OBS) across Northern Europe for the period 2000–2015. Such large-scale study allows going beyond site-specific observations, potentially providing explanations for existing conflicting findings on Norther European forest responses to climate change. In particular, the response of forests to variations in climatic drivers within this period is examined and regions where forest productivity is positively and negatively affected by warming are identified. The potential mechanisms behind different responses are discussed, with special focus on the joint role of temperatures and water availability. The results have implications in the face of climate change because boreal regions are predicted to shift from short, cool summers toward longer, warmer summers. It will also serve to identify the most problematic hotspots where specific management strategies—species choices, planting density, rules of thinning and final felling, harvest intensities (e.g., Baul et al., 2017)—should be implemented.

DATA AND METHODS

Study Area

Northern Europe has a heterogeneous landscape, characterized by extensive forests, agricultural lands mostly in the southernmost regions and sparsely vegetated areas at higher elevations and in the northernmost areas. Here the focus is forested areas extending from latitude 55° to 70°N in Norway, Sweden and Finland (**Figure 1**—Denmark and Baltic countries were not included).

The forested areas were identified based on the CORINE land cover dataset (version 2012, 100 × 100 m of resolution, provided by the European Environment Agency). CORINE land cover is widely used for environmental modeling and land cover/land use change analyses in Europe (Büttner, 2014). CORINE land cover is widely used for environmental modeling and land cover/land use change analyses in Europe (Büttner, 2014). Two European validation studies have shown that the achieved accuracy is above the 85%, lending support to the use of this product (Soukup et al., 2016). The analyses were extended to all pixels identified in CORINE as dominated by coniferous, broadleaf or mixed forests. More than 90% of those pixels were classified as coniferous. This approach allowed excluding the non-vegetated or sparsely vegetated areas, grasslands, croplands, water bodies and urban areas.

Source of Data

Moderate Resolution Imaging Spectroradiometer (MODIS)—Normalized Difference Vegetation Index (NDVI)

To explore the entire study area, the Normalized Difference Vegetation Index (NDVI) was used as a proxy of forest productivity. NDVI is a radiometric measure of the amount of photosynthetically active radiation (∼400–700 nm) absorbed by vegetation and provides an indirect measure of vegetation photosynthetic activity, among other ecosystems, also in boreal forests (Park et al., 2016). Even though some aspects of productivity are not well-captured by this index (Fernández-Martínez et al., 2019; Tei et al., 2019), NDVI is often used as proxy of forest productivity (Olofsson et al., 2008; Sulla-Menashe et al., 2018) because it is well-correlated with tree growth, according to several independent validations against tree rings (Beck and Goetz, 2011; Berner et al., 2011). Further, NDVI has some advantages with respect to other remotely-sensed products. For example, Enhanced Vegetation Index (EVI) is often more sensitive than NDVI to variations in the viewing geometry, surface albedo, and sun elevation angle across variable terrain (Matsushita et al., 2007; Sesnie et al., 2012). These factors are particularly relevant at middle-to-high latitudes (Walther et al., 2016). Similarly, even though promising, other recent products such as the Solar Induced Fluorescence (SIF) and/or the Photochemical Reflectance Index (PRI) appear to be negatively affected by atmospheric effects and random noises (Walther et al., 2016). On these bases, and similar to other recent studies (Sulla-Menashe et al., 2018; Mulder et al., 2019), NDVI was selected as the most suitable variable to perform a regional analysis of how boreal forest is affected by climate conditions.

NDVI data for the period 2000–2015 were extracted from tiles h18v02, h18v03, and h19v03 of the level 3 MOD13Q1 and MYD13Q1 provided by the Terra and Aqua satellites, respectively (NASA Land Processes Distributed Active Archive Center), at 16 day temporal resolution and 250 × 250 m spatial resolution. In these products, NDVI is retrieved from daily, atmosphere-corrected, bidirectional surface reflectance, via a MODIS-specific compositing procedure that discards low quality pixels. This product provides the maximum NDVI observed over the 16-day period, so that most of the effects of clouds and other atmospheric noises are effectively removed [see Didan (2015) for details]. Because the MODIS sensors aboard Terra and Aqua satellites are identical and, for each one, the maximum NDVI observed over the 16-day period is computed 8 days apart from one another, we combined both products so that, in practical terms, the temporal resolution of the NDVI dataset used here was 8 days.

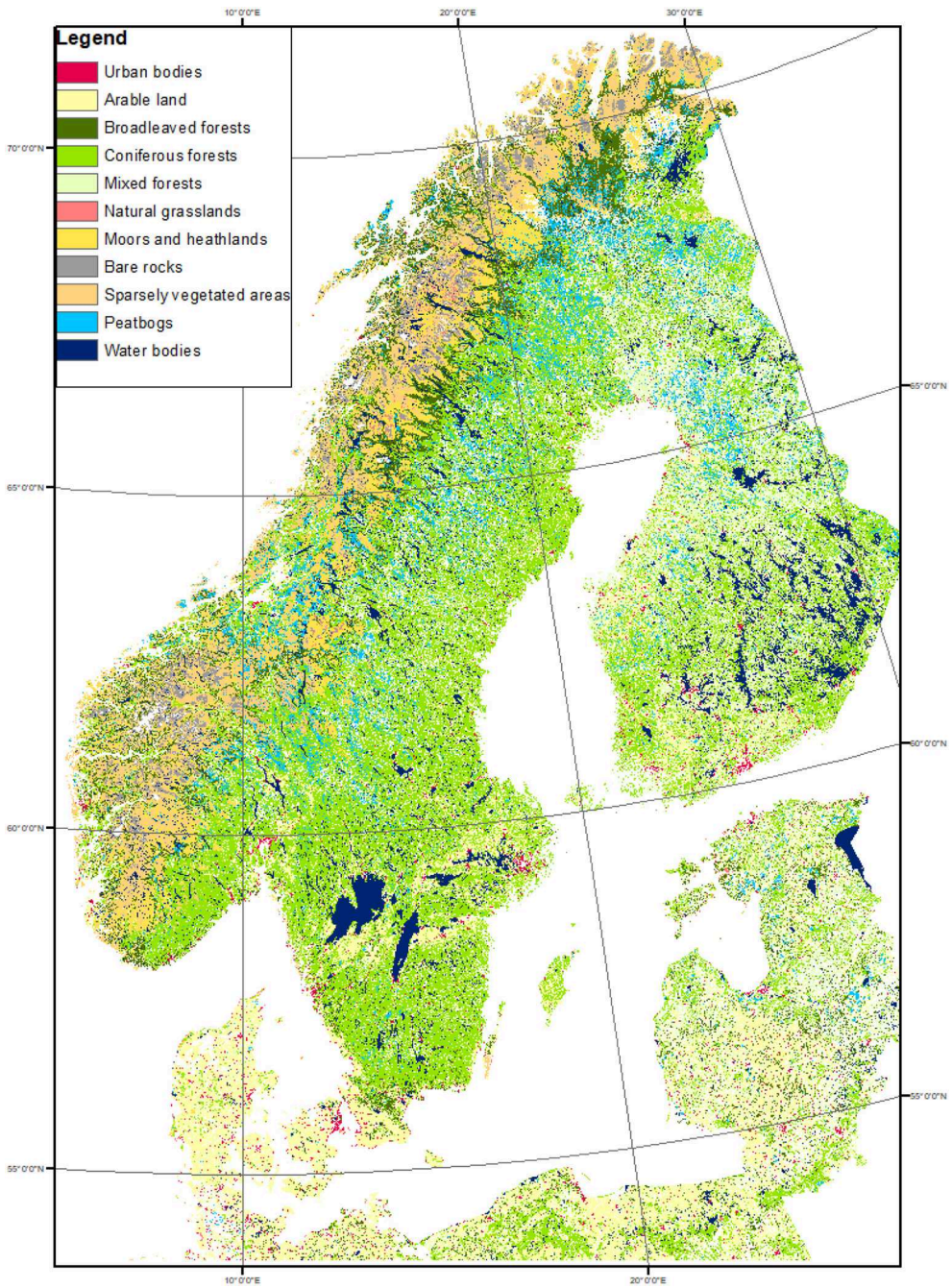

FIGURE 1 | Scandinavian land-use map extracted from CORINE (2012). The statistical analyses were performed in all pixels classified as forest (broad-leaved, coniferous, and mixed forests; green shades).

Meteorological Data: The E-OBS Dataset

Meteorological data for the study region for the period 2000–2015 were obtained from the E-OBS dataset. E-OBS is a high-resolution gridded dataset providing daily precipitation, minimum, maximum, and mean temperatures from 1950 (Haylock et al., 2008). This dataset was generated via innovative interpolation techniques combined with an accurate pre-processing of the raw data retrieved from meteorological stations [see Haylock et al. (2008) for details]. The accuracy of E-OBS meteorological data depends on the number of meteorological stations and their spatial distribution. The station list updated to November 2016 reported more than 11,000 stations, of which over 1,900 were located in the region of interest.

This particular product was selected mainly because of its high spatial resolution (0.25° × 0.25°)—higher than most of the current available gridded dataset of climatic variables. To our knowledge, there are only two precipitation products with finer resolution (CHIRPS and GSMap-MVK with 0.05° and 0.10°, respectively), but they do not cover high latitudes. E-OBS has been previously used with satisfactory results (Kysely and Plavcova, 2010; Nikulin et al., 2011) and recently tested explicitly for Sweden (Ledesma and Futter, 2017).

Data Preparation

NDVI Data

The NDVI data were prepared for the analyses following a three-step approach. First, NDVI data were filtered based on their quality, exploiting the pixel reliability map included in each MOD13 file. This layer contains a flag describing the overall pixel quality at each time step [−1: No data; 0: Good data, 1: Marginal data (useful); 2: Snow/Ice and 3: Cloudy]. For each pixel, only NDVI values with reliability level of 0 or 1 were considered. The NDVI values with reliability 1 were further contrasted against the previous and subsequent value. Differences between the current NDVI and previous or subsequent values higher than the long-term mean NDVI in each pixel were considered as indicative of potential inconsistencies and the corresponding value discarded. Areas with sparse vegetation were masked out, by completely excluding pixels with long-term mean NDVI below 0.12, as recommended by Bjerke et al. (2014). Indeed, according to NASA providers, NDVI values between −0 and 0.12 correspond to scarce vegetation cover or bare soil.

Second, for each pixel, NDVI values were averaged over the growing season (see definition of growing season in the following sub-section). Finally, following Buermann et al. (2014), the data were aggregated to a 0.25° × 0.25° spatial grid to match the spatial resolution of the gridded meteorological data (details on the resampling approach can be found in section Spatial resampling). In this way, we obtained a proxy of annual vegetation productivity, to be analyzed for its interannual variability and linked to observed meteorological conditions. These spatial aggregation and seasonal averaging have also the advantage of decreasing the effect of low quality pixels, mostly caused by long cloudy periods.

Definition of the Climatic Variables of Interest

To capture different mechanisms, we considered six climatic variables, and their values relative to both the whole year and the growing season only (subscript A and GS, respectively). Among the basic meteorological variables, we selected the annual and seasonal precipitation totals (PPT_A, PPT_{GS}), daily average temperature (T, T_{GS}) and daily maximum temperature ($T_{MAX,A}$, $T_{MAX.GS}$). Totals of reference evapotranspiration ($ET_{0,A}$ and $ET_{0,GS}$) were used as a measure of the ecosystem water demand; they include the role of temperature and solar radiation (and hence, indirectly, day length). Further, two additional variables were considered: (1) the $ET_{0,A}$ /PPT_A ratio ($ET_{0,GS}$/PPT_{GS} ratio) describing the potential for annual (seasonal) water imbalances; and (2) the maximum number of consecutive days without precipitation (DWP_A, DWP_{GS}), characterizing the length of dry spells. These additional indicators allow exploring the potential effects of water shortage. The ET_0/PPT ratios quantify the water available in comparison to the evapotranspiration demand, thus summarizing the combined effects of precipitation, temperature and day length (i.e., warm temperatures and long days lead to high ET_0). The ratio ET_0/PPT allows distinguishing between water-limited and energy-limited ecosystems (Budyko, 1964). DWP was suggested by the World Meteorological Organization Expert Team of Climate Change Detection and Indices as one indicator of extremes in climate and also by the Swedish Commission on Climate and Vulnerability for similar purposes (Persson et al., 2007). DWP informs about the precipitation timing and an increase in DWP indicates that rainfall is clustering more strongly into wet and dry periods, which will affect soil moisture dynamics (Folwell et al., 2016). All the climatic variables are summarized in **Table 1**, along with their definitions, symbols, and units.

TABLE 1 | Symbols, definitions, and units of the climatic variables considered in this research.

Climatic variables	Definition	Units
PPT_A	Annual mean daily precipitation	mm
PPT_{GS}	Mean daily precipitation within the growing season	mm
T_A	Annual mean daily temperature	°C
T_{GS}	Mean daily temperature within the growing season	°C
T_{MAX}	Annual mean of the maximum daily temperatures	°C
T_{MAX-GS}	Mean of the maximum daily temperatures within the growing season	°C
$ET_{0,A}$	Annual mean reference evapotranspiration	mm
$ET_{0,GS}$	Mean reference evapotranspiration within the growing season	mm
$ET_{0,A}/PPT_A$ ratio	Ratio of annual cumulative ET_0 to annual cumulative PPT	–
$ET_{0,GS}/PPT_{GS}$ ratio	Ratio of cumulative ET_0 within the growing season to cumulative PPT within the growing season	–
DWP_A	Maximum number of consecutive days without precipitation within the year	day
DWP_{GS}	Maximum number of consecutive days without precipitation within the growing season	day

Annual values are defined with reference to the period from November to October of the following year; the growing season is defined as the days with a mean daily temperature higher than 5°C.

The climatic variables of interest were extracted from the meteorological data for every forested pixel in Northern Europe from 55 to 70° N and for each year over the period for which both NDVI and E-OBS data were available (2000–2015). Annual values (subscript A) are means or totals relative to the months from November of 1 year to October of the following year, i.e., they are relative to the period from the approximate beginning of winter dormancy to the end of the growing season during the following calendar year. Growing season values (subscript GS) refer to those observed within the thermal growing season (Ruosteenoja et al., 2016). Here, the thermal growing season was defined as the period with daily mean air temperature above 5°C for two or more consecutive days (Skaugen and Tveito, 2004; Kauppi et al., 2014; Peichl et al., 2014). The 5°C threshold

is commonly employed in temperate and boreal ecosystems; it emerged also by comparing the thermal growing season with the actual onset of the growing season as inferred from satellite observations in Fennoscandia (Karlsen et al., 2007).

$ET_{0,A}$ and $ET_{0,GS}$ were determined as totals of daily reference evapotranspiration values determined according to the Hargreaves and Samani formula (Hargreaves, 1983). This approach has the advantage of requiring only the maximum, minimum and mean daily temperatures, and an estimate of the potential solar radiation.

Spatial Resampling

The spatial resolution of the E-OBS meteorological data is 0.25°, whereas the CORINE land cover data and the NDVI data have spatial resolutions of 100 and 250 m, respectively. Therefore, both the land use and the NDVI data were resampled to the 0.25° spatial resolution for consistency. In the case of the discrete land use data from CORINE, the spatial aggregation scheme could affect the prevalence of the different classes and the spatial coherence of each land use class within the aggregated product. Here, to assign the prevailing land cover class, a majority approach was adopted, as proposed by de Jong et al. (2013), among others.

Conversely, NDVI data were aggregated to 0.25° using the cubic convolution method (ArcGis 10.4.2, ESRI, Redlands, CA, USA). This method was deemed more appropriate than bilinear interpolation when using satellite data because it reduces potential noises and it does not have the disjointed appearance of the nearest neighbor interpolation (Wu et al., 2008). It is important to note that the NDVI resampling was performed on the pre-processed maps (i.e., the steps detailed in section NDVI data were carried out at the original resolution).

Once all the datasets were resampled at the same spatial resolution, the pixels classified as forest were identified based on the resampled CORINE. These pixels-−7,020 in total—were retained for the analyses detailed below.

Data Analyses: Partial Least Square (PLS) Regression and Their Rationale

NDVI and meteorological data for all pixels classified as forest were analyzed by Partial Least Square (PLS) regression. The goal was to assess the role played by each climatic driver and whether such role varied with location (and hence climatic conditions). PLS is a generalization of the Principal Components Regression (PCR) analysis (Geladi and Kowalski, 1986; Wold et al., 2001). Similar to PCR, PLS is used to analyze the relationship between a set of dependent (y-variables: in our case, $NDVI_{GS}$) and independent variables (x-variables: the climatic variables reported in **Table 1**). It extracts from the x-variables the set of new components with the best explanatory power of the y-variable. Different from simple regression techniques, both PCR and PLS can handle collinear predictors (Gunst and Mason, 1979), thus making these techniques suitable when considering multiple, potentially partially correlated, climatic indicators. This advantage makes PLS and/or PCR appropriate for our aims, since we expect that some of the climatic variables involved (**Table 2**) are correlated (Zscheischler and Seneviratne, 2017). The main difference between PCR and PLS is that with PCR, the principal components are determined solely based on the data values of the x-variables, whereas with PLS the data values of both the x and y-variables influence the construction of the components. Thus, PLS is particularly useful when considering a high number of x-variables in comparison with the number of y-variables (Abdi, 2010)—as it is the case in this study. A similar approach was used by Peichl et al. (2014) to investigate the combined effect of temperature and water table level on the net CO_2 exchange of a boreal fen. We apply the PLS analyses over a substantially larger area, i.e., Northern European forests within 55 and 70°N.

To better understand the role of the climatic variables, in each pixel, we performed nine different PLS analyses with different choices of climatic (explanatory) variables (**Table 2**). Each analysis considered five to six climatic variables, chosen as discussed next and listed in **Table 2**. In summary, this choice of climatic variables led to the six PLS analyses (referred to as 1–6) listed and justified below. Further analyses complemented this set, by considering the same set of climatic variables of analyses 1, 4 and 5, but by focusing just on the growing season (Analysis 1_{GS}) or on the values of the climatic variables pertaining the previous year (Analyses 4 and 5 lag). The second-order Akaike Information Criterion (AIC) allowed the estimate of the relative quality of each statistical model. The AIC measures the relative model fit and it is proportional to the likelihood of the model and the number of parameters used to generate it (Burnham et al., 2011). A set of climatic variables with high explanatory power and low AIC value are suggestive of those variables being adequate to explain the changes in NDVI.

The explanatory variables were chosen as follows. The first two PLS analyses aimed at quantifying the explanatory power of the climatic variables when considering only their annual means [Analysis 1, as e.g., in Ichii et al. (2002) and Yuan et al. (2009)] or within growing season means (Analysis 1_{GS}, as e.g., in Zhao et al., 2018).

Analysis 2 involved only the basic meteorological variables: PPT, T and T_{MAX} for the whole year and within the growing season. As such, Analysis 2 represents the baseline for comparison to other choices of the explanatory variables. Comparison of the results of Analysis 2 and those of Analyses 1 and 1_{GS} shows whether annual and seasonal variables need to be combined to explain the observed patterns of NDVI.

Four additional sets of explanatory variables were considered, based on the following rationale. Since the maximum temperature is likely to occur during the growing season, we only considered T_{MAX} within the growing season ($T_{MAX,GS}$), while keeping annual T (T_A), while keeping annual T, including thus both climatic variables but computed over different periods. Further, ET_0 and both the water stress indicators (ET_0/PPT ratio and DWP) likely have a higher explanatory power of forest productivity when computed within the growing season rather than over the whole year. Hence, the basic climatic variables were complemented by $ET_{0,GS}$ in Analysis 3, $ET_{0,GS}/PPT_{GS}$ ratio in Analysis 4, and DWP_{GS} in Analysis 5. Analysis 6 included a water stress index but it did not consider $ET_{0,GS}$. When compared to the results of Analysis 5, Analysis 6 allowed assessing the relative importance of including a water stress indicator in lieu of $ET_{0,GS}$.

TABLE 2 | Combinations of climatic variables considered in each PLS analysis and median, maximum, and minimum AIC score attached to each combination of climatic variables over the study site.

Climatic variables	1	1_{GS}	2	3	4	5	6	4 lag	5 lag
PPT_A	X		X	X	X	X	X	X	X
PPT_{GS}		X	X	X	X	X	X	X	X
T_A	X		X	X	X	X	X	X	X
T_{GS}		X	X						
$T_{MAX,A}$	X		X						
$T_{MAX,GS}$		X	X	X	X	X	X	X	X
$ET_{0,A}$	X								
$ET_{0,GS}$		X		X	X	X		X	X
$ET_{0,A}/PPT_A$ ratio	X								
$ET_{0,GS}/PPT_{GS}$ ratio		X			X				
$ET_{0,GS}/PPT_{GS}$ ratio (lag)								X	
DWP_A	X								
DWP_{GS}		X				X	X		
DWP_{GS} (lag)									X
AIC	$13.25^{17.66}_{13.01}$	$12.78^{18.02}_{12.46}$	$11.72^{12.42}_{10.42}$	$16.68^{18.23}_{15.52}$	$11.26^{11.92}_{11.01}$	$7.26^{10.58}_{3.36}$	$13.70^{15.46}_{9.43}$	$11.44^{16.68}_{11.44}$	$11.46^{14.3}_{7.95}$
ΔAIC	5.99	5.52	4.46	9.46	4	0	6.44	4.18	4.2

ΔAIC is the difference between AIC of each analysis and the minimum AIC (corresponding to Analysis 5).

TABLE 3 | Long-term and study-period annual average temperature, precipitation, and length of the growing season.

		LONG-TERM			STUDY PERIOD		
		Average	Period	Source	Average	Period	Source
TEMPERATURE (°C)	Norway	1.1	1960–2013	CRU	1.6	2000–2015	E-OBS
	Sweden	4.8	1960–2013	SMHI	5.3	2000–2015	E-OBS
	Finland	2.0	1960–2013	FMI	4.1	2000–2015	E-OBS
PRECIPITATION (mm)	Norway	960	1960–2013	CRU	1030	2000–2015	E-OBS
	Sweden	600	1960–2013	SMHI	620	2000–2015	E-OBS
	Finland	620	1960–2013	FMI	648	2000–2015	E-OBS

The sources of data are: CRU, Climatic Research Unit; UEA, University of East Anglia; SMHI, Swedish Meteorological and Hydrological Institute; FMI, Finnish Meteorological Institute.

All the analyses mentioned above were based on the climatic and vegetation data of the same year in which the NDVI was observed, as in Buermann et al. (2014). Indeed, no apparent lag effect longer than 1–2 months, i.e., no lag effect beyond the current year, emerged in previous analyses of NDVI data at higher northern latitudes (Wu et al., 2015). However, other studies showed that climatic conditions during the previous growing season can affect vegetation activities and NDVI in some locations over the northern high latitude region (<20% of Northern Europe) (Tei and Sugimoto, 2018). Moreover, a 1 year-long lag effect of droughts (or periods with low water availability) emerged in some regions located in northern latitudes (Vicente-Serrano et al., 2013). To explore the possibility of a lag effect of water scarcity, two additional PLS analyses were performed, with the same configuration as Analyses 4 and 5, but considering $ET_{0,GS}/PPT_{GS}$ ratio and DWP_{GS} relative to the previous growing season (Analyses 4 and 5 lag).

Moreover, the non-parametric Kruskal-Wallis test (Kruskal, 1952) was used to test whether the median cumulated explanatory power of the PLS were significantly (at 5%) different among the nine analyses performed. When the Kruskal-Wallis test indicated that there were significant differences among the medians, multiple pairwise comparisons based on the Dunn's test (Dunn, 1964) allowed identifying which specific groups of analyses led to significantly different results from the others.

Finally, we computed the correlation coefficient between $NDVI_{GS}$ and each climatic variable (**Table 2**) in each pixel and we extracted the 90th and 10th percentile of those values. Aiming to focus on those locations where the response of $NDVI_{GS}$ to the climatic variables was the strongest, the pixels with the highest correlation (i.e., above the 90th percentile) and the lowest correlation (i.e., below the 10th percentile) were singled out. Then, the median and variability of the mean annual temperature and total precipitation for each group were compared. To ensure that values higher/lower than these extremes corresponded to highly positive/negative correlations between the variables and $NDVI_{GS}$, we tested that both percentiles were significantly (at 5%) different from zero.

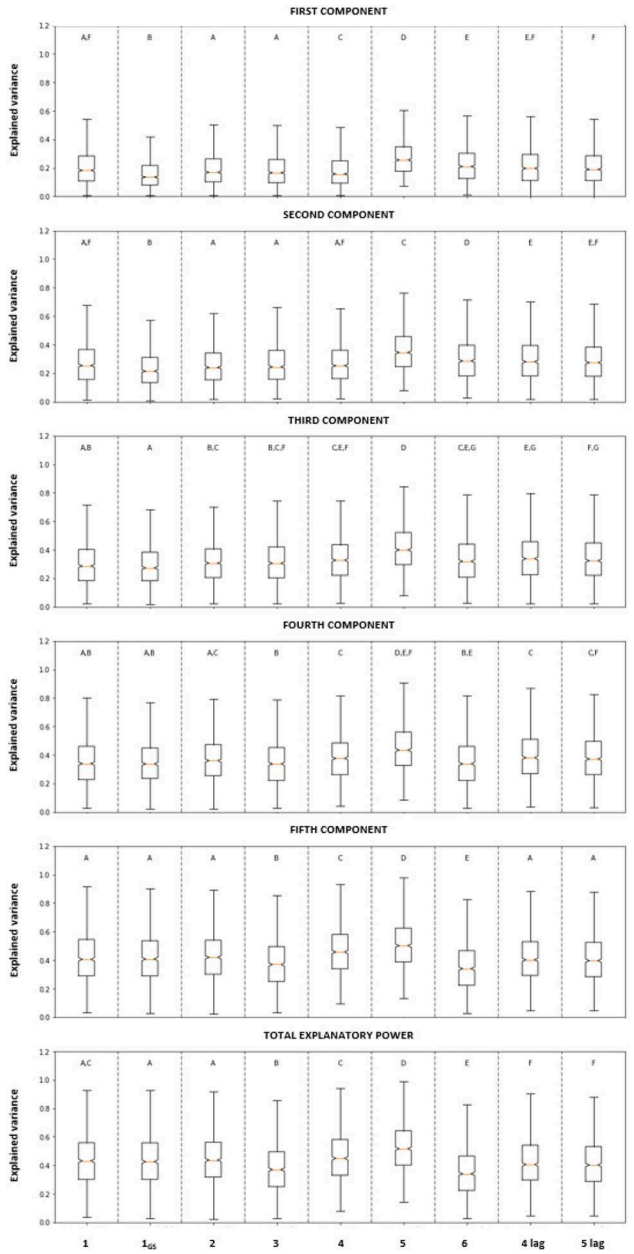

FIGURE 2 | Fraction of cumulated variance of $NDVI_{GS}$ explained by the components 1 to 5 (rows 1–5) and total explanatory power (bottom panel) of the combination of the climatic variables considered in each PLS analysis (details in **Table 2**). For the analyses involving just 5 climatic variables, the content of the last two panels is the same. The boxes extend from the first and the third quartile, the end of the whiskers are computed as 1.5*IQR (Interquantile Range). The median values are indicated by the orange line. The notches extend over the 95% confidence intervals of the median, as determined by bootstrapping. Bars with the same letter are not significantly different at $p = 5\%$ (as determined by the Kruskal-Wallis and Dunn tests).

RESULTS

Climatic Conditions

The long-term average annual temperature for the period 1960–2013 was 4.8°C in Sweden, 1°C in Norway, and 2°C in Finland. Among the 15 study years (2000–2015), all years except 2010 were warmer than these long-term averages (**Table 3**). As expected, the average annual temperature decreased with latitude.

The length of the growing season decreased with latitude along with temperature. In the northernmost regions, the average growing season length over the period 1960–2013 was <170 days in all years, while it was around 210 days in southern Sweden. A substantial increase of the duration of the growing season has been observed from 1960 to 2014 in Sweden as a consequence of warming (Kauppi et al., 2014).

Regarding precipitation, the long-term average annual total for the period 1960–2013 was 960 mm in Norway, 600 mm in Sweden, and 620 mm in Finland. All the years within the study period had annual average precipitation similar to the long-term precipitation averages (**Table 3**).

In summary, over the period 2000–2015, the study region experienced warmer temperatures and longer growing seasons without significant changes in precipitation, when compared to the long-term averages (**Table 3**). This combination can lead to more frequent temperature-induced water stress.

Abiotic Controls on $NDVI_{GS}$: PLS Analysis

A PLS analysis was performed for each set of explanatory variables (**Table 2**) and pixel. For our purposes, the key outputs of the PLS analyses are (1) the variance explained by each component; and (2) the correlation coefficients, the sign of which allows distinguishing negative and positive correlations between the climatic conditions and the $NDVI_{GS}$ (x and y-variables, respectively). Due to the large area analyzed, the results of the PLS analyses can differ from pixel to pixel. The results are presented mostly in an aggregated form, i.e., as distributions of values across pixels, to facilitate the comparison among locations and the different combinations of explanatory variables.

Variance Explained by the Components

Figure 2 summarizes the distribution of the cumulated explanatory power for the component 1 to 5, and its variability across pixels, for the components 1–5. The bottom panel reports the total explanatory power for each set of predictor variables.

Analyses 1 and 1_{GS} had a low median explanatory power (**Figure 2**; median total explanatory power of 43.7 and 42.5%, respectively), despite the inclusion of all the climatic variables for the whole year and the growing season, respectively. The variables included in Analysis 1 (i.e., variations within the whole year) provided a small but significantly (at 5%) higher explanatory power in the first two components than Analysis 1_{GS} (top two plots) but there was no difference between these two analyses when considering their total explanatory power (bottom plot).

Analysis 2 combined the basic meteorological variables for both the whole year and the growing season (T_A, $T_{MAX,A}$ and PPT_A and T_{GS}, $T_{MAX,GS}$ and PPT_{GS}, **Table 2**). The median explanatory power of the first three components was 27.2%, while the median total explanatory power was 42.5%. There was no significant difference in the total explanatory power between Analysis 2 and those considering the annual and growing season variables in isolation (Analyses 1 and 1_{GS}).

Analysis 3 was designed to quantify the importance of $ET_{0,GS}$ (and hence, indirectly day-length and potential solar radiation) to explain the observed patterns in $NDVI_{GS}$. Thus, it considered the basic meteorological variables plus $ET_{0,GS}$ (**Table 2**) but neglected $T_{MAX,GS}$ and T_{GS}. The median explanatory power of the three first components was not significantly different from those of the previously discussed choices of explanatory variables (**Figure 2**, three first panels).

Analyses 4 and 5 were designed to better understand the effects of water availability on the observed NDVI. By including either the $ET_{0,GS}/PPT_{GS}$ ratio or the days without precipitation (DWP_{GS}), the total explained variance of $NDVI_{GS}$ significantly (at 5%) increased with respect to the analyses not considering any proxy of water availability. Between the two water availability proxies, the explanatory power was significantly (at 5%) higher when considering DWP_{GS} (Analysis 5) than that including $ET_{0,GS}/PPT_{GS}$ ratio (Analysis 4).

Analyses 3 and 6, which involved the same number of explanatory variables (5 in total), presented similar results regarding the first three components with a median explanatory power of 30.5 and 31.8%, respectively (**Figure 2**). However, the total explanatory power of Analysis 3 was significantly (at 5%) higher than Analysis 6 (**Figure 2**), pointing to the importance of including $ET_{0,GS}$ as predictor of the $NDVI_{GS}$.

Finally, Analyses 4-lag and 5-lag were designed to evaluate the potential lag effect of the climatic conditions on plant productivity. In both cases, considering the climatic variables during the same growing season in which $NDVI_{GS}$ was measured (i.e., Analyses 4 and 5) resulted in a significantly (at 5%) higher explanatory power than those based on lagged climatic variables.

In summary, despite having the same number of climatic variables as Analysis 1, 1_{GS}, 2, and 4, Analysis 5 (which included PPT_A, PPT_{GS}, T_A, $T_{MAX,GS}$, $ET_{0,GS}$, and DWP_{GS}) had a significantly higher explanatory power than any other choice of climatic variables investigated here, both in each component and in total. Analysis 5 emerged as the best fitting model also based on the AIC (**Table 2**). It should be noted that, in practical terms, models with AIC differing from the minimum AIC (corresponding to the best fitting model) of <2 all have plausible support, i.e., no differences between models (Burnham and Anderson, 2002). The differences obtained in our analyses were higher than that threshold in all cases, showing that there were significant differences between the models and Analysis 5 had the highest performance (**Table 2**).

Correlation Coefficients

Focusing on the set of climatic variables with the highest explanatory power (Analysis 5), we considered the sign of the correlation coefficients between the climatic (x-)variables and $NDVI_{GS}$ (y-variable), and whether positive or negative correlations were co-occurring with specific mean annual temperature and precipitation total. Positive correlations imply that higher values of the climatic variable result in higher values of $NDVI_{GS}$; and, *vice versa*, negative correlations imply that higher values of the variable results in lower $NDVI_{GS}$.

To focus on the locations where the response of $NDVI_{GS}$ to the climatic conditions was strongest, the pixels with the highest (above the 90th percentile) and lowest (below the 10^{th} percentile) correlation coefficients between $NDVI_{GS}$ and each climatic variable were singled out. All the correlation coefficients above the 90th percentile were positive, while all the ones below the 10th percentile were negative. The values of these percentiles for each climatic variable are reported in **Table 4**. Both percentiles for all climatic variables are significantly (at 5%) different from zero, indicating that values higher/lower than these extremes correspond to high correlations between the variables and $NDVI_{GS}$. **Figure 3** summarizes the median and variability of mean annual temperature (top panel) and precipitation (bottom panel) of the pixels with the highest (green) and lowest (brown) correlation coefficients between $NDVI_{GS}$ and each climatic variable.

TABLE 4 | Values of the percentile 90th and 10th of the correlation coefficient between $NDVI_{GS}$ and each climatic variable included in Analysis 5.

Climatic variables	Percentile 90th	Percentile 10th
PPT_A	0.487	−0.347
PPT_{GS}	0.481	−0.418
T_A	0.521	−0.315
$T_{MAX,GS}$	0.462	−0.493
$ET_{0,GS}$	0.483	−0.115
DWR_{GS}	0.419	−0.372

The highest (and positive) and lowest (and negative) correlation coefficients were found in a wide range of thermal regimes (**Figure 3**, top panel). However, focusing on the medians, pixels with extremely negative correlation coefficients between $NDVI_{GS}$ and any of the climatic variables (except PPT_{GS} and T_A) were located in significantly (at 5%) warmer regions (**Figure 3** top panel and **Figure 4**). The same pattern holds also for T_A, but the difference between the median correlation coefficients is not significant at 5%. This general pattern is suggestive that higher $ET_{0,GS}$, T_A, $T_{MAX,GS}$, PPT_A, and DWP_{GS} result in lower values of $NDVI_{GS}$ in warmer places. Regarding mean annual PPT (**Figure 3**, bottom panel), median correlations between $T_{MAX,GS}$ and $NDVI_{GS}$ where significantly (at 5%) higher in wetter than drier pixels. Also extremely positive correlations between T_A and DWP_{GS} with $NDVI_{GS}$ were more common in wetter pixels. Hence, higher temperatures and higher number of days without precipitation appear more beneficial when precipitation totals are higher. Conversely, extremely positive correlations between $NDVI_{GS}$ and PPT_A and $ET_{0,GS}$ occurs significantly (at 5%) more in pixels with lower mean PPT_A.

DISCUSSION

Drivers of Boreal Forest Productivity in Northern Europe: the Key Role of Water Availability

A set of PLS analyses was performed to identify the main drivers of boreal forest productivity. While statistical analyses such as the one presented here cannot reveal the mechanistic cause of the observed patterns, the comparison of different choices of

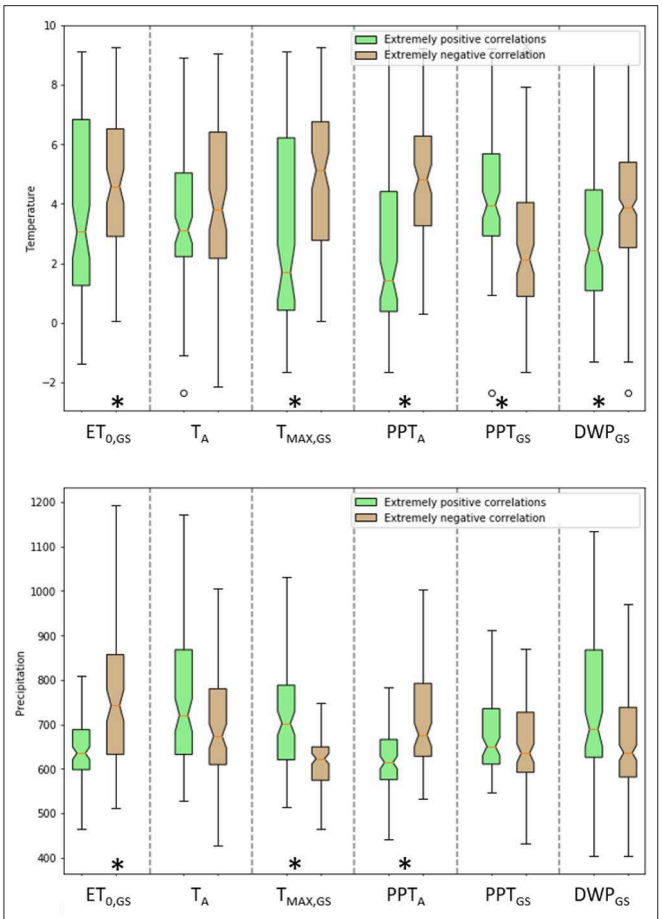

FIGURE 3 | Box plot of annual mean temperature (T_A–top panel) and annual mean PPT (PPT_A–bottom panel) of cells with correlations between each climatic variable and $NDVI_{GS}$ below 10th percentile (negative correlations, in brown) and above 90th percentile (positive correlations, in green). The orange line represents the median, the ends of the whiskers are computed as 1.5* IQR and the bottom and the top of the boxes correspond to the first and third quartile, respectively. The notches extend over the 95% confidence intervals of the median, as determined by bootstrapping. Stars at the bottom of each pair of bars denotes significant (at 5%) differences in the median values of mean T_A (top) or mean PPT_A (bottom) between pixels when the correlations with the corresponding climatic variable are extremely positive and extremely negative.

explanatory variables allows identifying the key drivers and is suggestive of the mechanisms at play. Our pairwise comparison of the seven analyses without time lags highlighted that considering proxies of water availability markedly increases the explanatory power of the climatic variables. Indeed, even though Analyses 1, 1_{GS}, 2, 4, and 5 included the same number of climatic variables (**Table 2**), the total explanatory power of Analysis 5 was significantly higher than that of the other analyses (**Figure 2**). Analysis 5 is also ranked as the best model based on AIC, followed by Analysis 4 (**Table 2**). Altogether, these findings support our first hypothesis, suggesting that water availability can limit plant productivity also across boreal forests in Northern Europe—an ecosystem so far considered as light- and temperature-limited, but not water-limited (Allen et al., 2010).

It has long been recognized that water availability can affect plant photosynthetic capacity, growth, and physiological stress responses (Hsiao, 1973). Nevertheless, so far the response of boreal forests to reduced soil water availability has been seldom considered (Solberg, 2004; Grossiord et al., 2014). A decrease in aboveground growth rates as a consequence of water limitation and a clear interaction between biodiversity and water availability emerged in a boreal forest stand located in Finland (Grossiord et al., 2014). In southeastern Norway, dry and warm summers led to defoliation, yellowing, scarce cone formation and high mortality in Norway spruce (Solberg, 2004; Andreassen et al., 2006). However, these results are based on specific sites and conditions, while our analyses show that the sensitivity of boreal forest to water limitations is common in most of Northern Europe.

Finally, the potential lag effect of water scarcity on forest productivity was explored by Analysis 4-lag and 5-lag. Regional dendroclimatological studies have shown that tree growth is better correlated to the conditions during the previous growing season than those of the current one (Carrer et al., 2010; Babst et al., 2012). Nevertheless, while lag effects in tree-rings and autocorrelation in ring width measurements are well-established (Berner et al., 2011), lag effects in NDVI measurements have not been widely examined. Further, a high correlation between tree rings and NDVI does not imply that tree rings adjust immediately to changes in NDVI (Kaufmann et al., 2008). As such, even though a lagged effect of growing conditions on tree ring formation has been observed, a similar delay might not emerge when considering NDVI (Wu et al., 2015; Tei and Sugimoto, 2018). Indeed, our results show that current year conditions have a higher explanatory power than those of the previous year, suggesting that $NDVI_{GS}$ mostly responds to current conditions. This result is consistent with previous analyses showing that conditions of the previous year are dominant in <20% of high latitude study sites in Europe (Wu et al., 2015; Tei and Sugimoto, 2018).

Effects of Temperature on Boreal Forest Productivity: From Positive to Negative

To disentangle the role of different climatic variables on $NDVI_{GS}$, we considered the combination of climatic variables with the highest explanatory power (Analysis 5) and explored the sign and level of correlation between the different climatic variables and $NDVI_{GS}$ across locations and climatic conditions. Special attention was devoted to temperature in an attempt to unravel the potentially opposite effects of the predicted increase in temperatures on boreal forest productivity. On the one hand, warmer temperatures reduce the constraints on productivity imposed by low temperature and growing season length typical of higher latitudes; on the other hand, warmer temperatures can lead to more frequent and severe heat stress but also to water stress, even if not associated to reductions in precipitation (Ruiz-Pérez et al., 2019). Temperature was included in Analysis 5, directly through T_A and $T_{MAX,GS}$, indirectly through $ET_{0,GS}$. Temperature plays a key role on boreal forest productivity regardless of latitude—a conclusion consistent with

previous results on boreal ecosystems and their dependency on temperatures (e.g., Bonan and Shugart, 1989). Nevertheless, our results show that the correlations between T_A (and $T_{MAX,GS}$) and $NDVI_{GS}$ were far from uniformly positive across the study region (**Figure 4**). In other words, the expectation that an increase in temperatures is beneficial for boreal forests does not always hold.

Patterns emerged when comparing the climatic conditions under which the extremely negative (below the 10th percentile) and the extremely positive (above the 90th percentile) correlations occurred (**Figures 3**, **4**). Regardless of the temperature-related climatic variable considered, extremely positive correlations occurred mostly in locations with lower annual mean temperature. A similar divergence between increased temperatures and tree-ring formation was observed in the southernmost regions of Scandinavia [Babst et al. (2012) and Trahan and Schubert (2016)]. Nevertheless, being based on satellite data and standard meteorological data, our approach permits analyses at regional scale, thus facilitating the identification of regions that are potentially more sensitive to specific climatic conditions.

Geographically, the effects of warming temperatures on forest productivity depend on the mean annual temperature (as apparent in **Figure 3**, top panel) and hence substantially on latitude. The majority of pixels with extremely positive correlation between temperature-related climatic variables and $NDVI_{GS}$ are located in northern/colder regions. Conversely, the pixels with extremely negative correlation are mostly located at lower latitudes. An example of this geographical distribution is reported in **Figure 4**, which refers to the case of the correlation between $T_{MAX,GS}$ and $NDVI_{GS}$. 65°N emerges as the latitudinal threshold at which the correlation between $T_{MAX,GS}$ and $NDVI_{GS}$ shifts from extremely positive at higher latitudes to extremely negative at lower ones. Only one pixel with extremely negative correlation is located north of 65°N, while 65.9% of those with extremely positive correlation are. This latitudinal threshold is consistent with the one emerging from analyses based on the European Tree Ring Width (TRW) network, suggesting that Northern Europe can be divided into two regions according to similarities in the annual growth variability (Babst et al., 2012). A similar threshold emerges also outside Northern Europe. In Eurasia, the correlation between summer temperatures and tree ring increments increases linearly with latitude from negative to positive values, with positive correlations at latitudes above 65°N, and negative elsewhere (Hellmann et al., 2016). Across the whole circumboreal region such emerging latitudinal threshold was 67°N (Tei and Sugimoto, 2018). Due to the clear link between temperature and latitude in these regions, the latitudinal threshold is most likely to be interpreted as a threshold in terms of temperature. In other words, at latitudes below 65°N, the air temperature might have already exceeded a limit above which boreal forests do not benefit from increases in air temperature. As apparent from **Figure 4**, this temperature threshold ranges from 14.5 to 17.8°C (average maximum air temperature within the growing season). Future warmer temperatures could shift this geographic boundary farther north.

Hence, these results confirm the hypothesis that the effects of warmer temperature of forest productivity are not uniformly positive over Northern Europe. Rather, an increase in temperature is currently beneficial (as indicated by a positive correlation) mainly in the coldest (i.e., northernmost) regions, while negative correlations were observed in warmer regions (i.e., southernmost regions). Further, the emerging patterns are suggestive of a threshold-like pattern in the correlation between temperature and forest productivity. However, some exceptions emerged, i.e., some pixels with extremely positive correlations were located in southern regions and *vice versa*. These exceptions might be driven by local features such as soil properties or wind patterns. In particular, deeper soils and higher water retention capacity can reduce the effects of low precipitation amount in general and dry spells in particular, buffering dry, and warm periods.

Interplay Between Temperature and Water Availability

In most circumstances, plants are able to cope well with high temperatures for short periods as long as they have access to sufficient water resources. Under well-watered conditions, plants can maintain their stomata fully open, ensuring not only a high net CO_2 uptake, but also leaf evaporative cooling. Conversely, low soil water availability reduces not only stomatal aperture, CO_2 uptake via photosynthesis and thus potentially plant growth (Hsiao, 1973), but also evaporative cooling, so that water limitations can exacerbate the negative effects of warm temperatures. If air temperature and solar radiation are high, then leaf temperature can become such that net CO_2 assimilation rate is reduced (Yamori et al., 2014) and permanent damage could occur (O'Sullivan et al., 2017).

This role of the water availability on the response of tree growth to warmer temperatures has already been observed also in boreal regions. Indeed, one key consequence of global warming in boreal North America has been regional drought stress leading to reduced tree growth (Verbyla, 2015) and even enhanced tree mortality [(e.g., Williams et al. (2013)]. In Norway, tree-ring formation of Norway spruce was shown to respond negatively to warm summers in dry locations, while the response was positive in moist regions Solberg, 2004; Andreassen et al., 2006. Our results point to a similar pattern, but over a larger region and species set: most of the pixels with extremely negative correlations between $NDVI_{GS}$ and T_A and $T_{MAX,GS}$ are located in places with lower annual mean precipitation (**Figure 3**, bottom panel). These findings support our initial hypothesis, suggesting that the correlation between temperature and forest productivity varies not only according to a thermal gradient but also according to a moisture one, being positive in cold and moist regions and negative in warm and dry ones.

The analysis of the correlation coefficients between $NDVI_{GS}$ and DWP_{GS} also shows the influence of water availability on boreal forest productivity. Extremely negative correlations between $NDVI_{GS}$ and DWP_{GS} coefficients were more common in drier and warmer conditions, while extremely positive correlation coefficients occurred mostly in well-watered and cooler pixels (**Figure 3**). These results suggest that the effect of temperature is mediated by water availability and its timing.

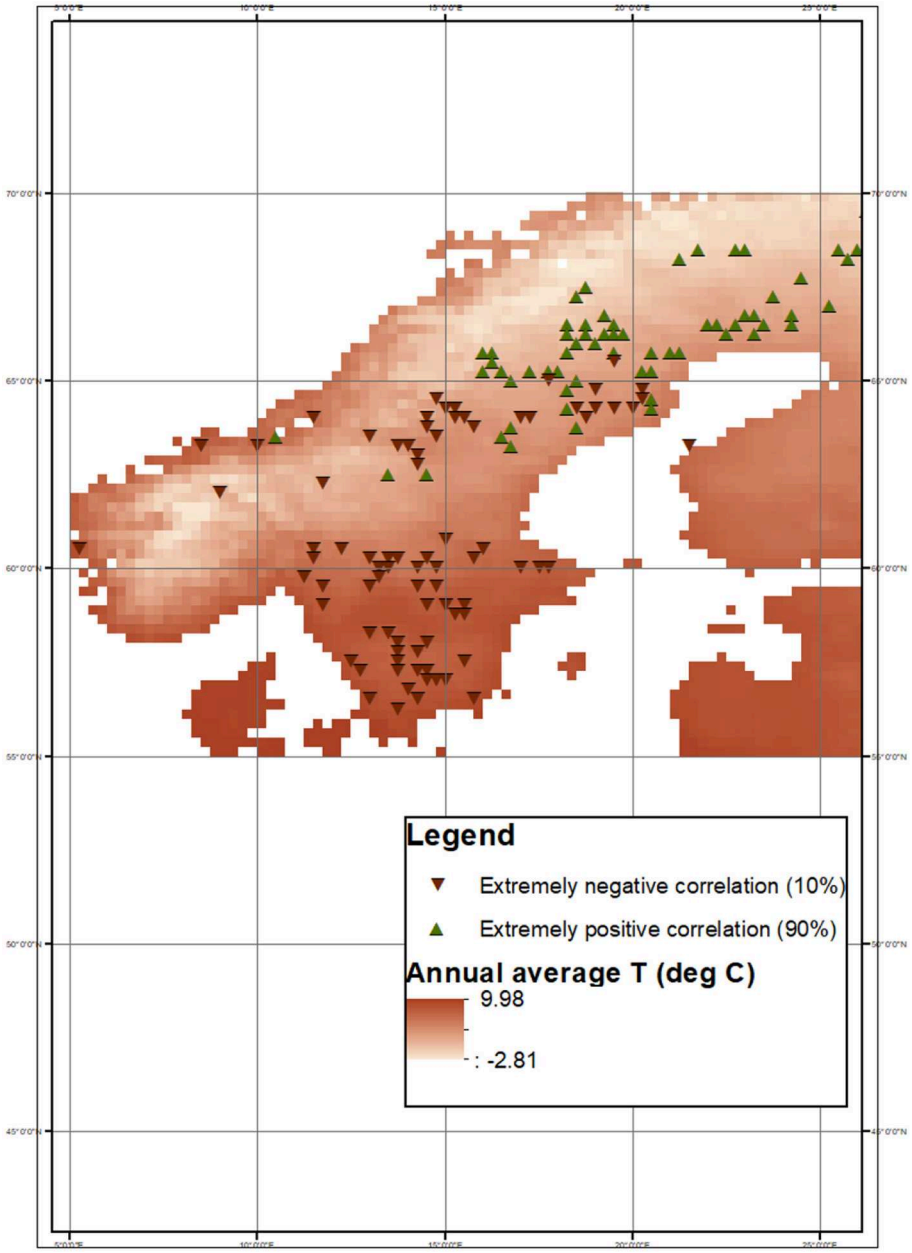

FIGURE 4 | Pixels where extremely positive (90th percentile) and negative (10th percentile) correlation between $NDVI_{GS}$ and T_{MAX-GS} occur. The annual average T_A map was obtained from E-OBS gridded dataset.

Hence, a (direct or indirect) role of water stress is to be expected not only in dry regions (Anderegg et al., 2013), but also in the relatively mesic Northern European boreal forests. Furthermore, most of the extremely negative correlations between $T_{MAX,GS}$ and $NDVI_{GS}$ are located over southern Sweden.

Geographically, similarly to temperature-related climatic variables, most pixels with extremely positive correlation between DWP_{GS} and $NDVI_{GS}$ are located in northern/colder regions, whereas the pixels with extremely negative correlation are at lower latitudes (**Figure 5**). Moreover, even though less evident, this dichotomy between north and south was also observed when comparing "less extreme" correlation coefficients (corresponding to the 80th−20th and 70th−30th percentiles) as shown in the **Supplementary Material**.

Importance of Precipitation Timing

As shown by the Kruskall-Wallis and Dunne's tests, significant differences in the explanatory power emerged between the two proxies of water stress explored here (the $ET_{0,GS}/PPT_{GS}$ ratio and DWP_{GS}). The inclusion of DWP_{GS} (i.e., Analysis 5) led

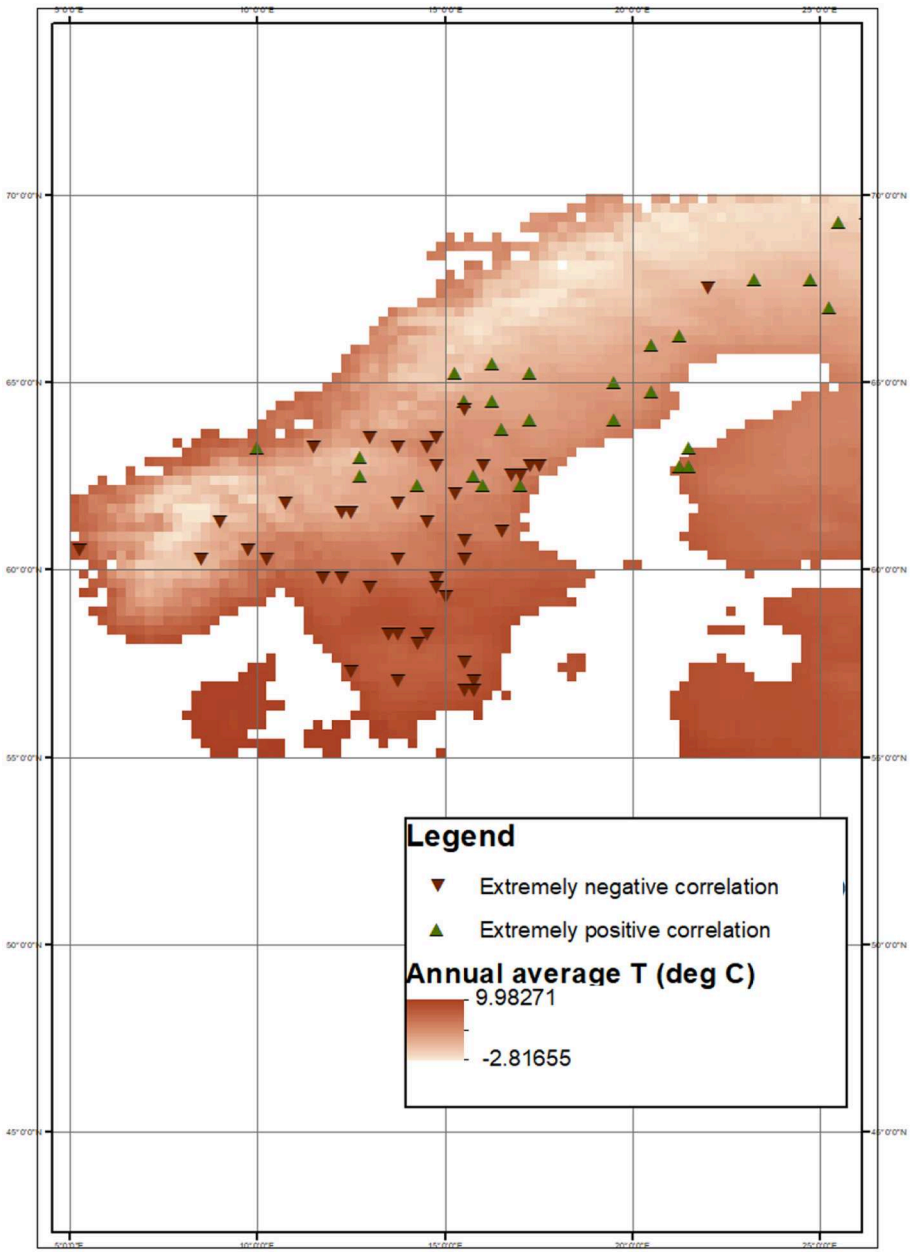

FIGURE 5 | Pixels where extremely positive (90th percentile) and negative (10th percentile) correlation between $NDVI_{GS}$ and DWP_{GS} occur. The annual average T_A map was obtained from E-OBS gridded dataset.

to the highest total explanatory power (**Figure 2**). PPT and ET_0 are the key drivers of the water balance. Their ratio, ET_0/PPT, represents the water available for evapotranspiration and allows distinguishing between water-limited and energy-limited ecosystems (Budyko, 1964). This ratio is based on the precipitation and transpiration totals over the growing season or whole year. Cumulative values can mask fluctuations, so that wet periods can compensate dry periods. Conversely, the maximum number of consecutive days without precipitation, DWP, does not depend on the total amount of the precipitation but on its timing. The higher explanatory power of DWP_{GS} supports our hypothesis that changes in the distribution in time of the precipitation have a larger effect on the inter-annual variability of $NDVI_{GS}$ than variations in precipitation totals. Indeed, several previous studies showed that DWP is well-correlated with ecosystem functions in different pedoclimatic conditions. For example, the radial growth of six deciduous species in southern Appalachia (Eastern USA) were more sensitive to the number of storms and the number of dry days than to the total precipitation (Elliott et al., 2015). Moreover, in the Northern

Hemisphere forests, DWP correlates well with the C turnover rate—a measure of the net effect of several ecosystem processes, including background mortality, mortality by disturbances, and forest management (Thurner et al., 2016). These results have potential implications under future climates. Predictions of no change or even increase in the annual mean precipitation do not imply that Northern European forest productivity will not be affected by such changes, as the timing of precipitation will be critical.

DWP highlights periods when soil water availability could become low, as a result of an extended lack of precipitation. While the actual water stress level during a dry spell also depends on the soil water availability at the beginning of the dry period and the evapotranspiration rate during the period, periods without precipitation are often associated with high solar irradiance and potentially high temperature and low air humidity, i.e., conditions that enhance losses via evapotranspiration. It follows that even relatively short precipitation-free periods can lead to marked water losses (Folwell et al., 2016). A simple model representing the land surface energy and water balance applied over Europe showed that evapotranspiration rates decline (i.e., the surface shifts to a water-limited regime) after only four consecutive days without precipitation, given initial soil moisture conditions ∼ 20% above the minimum soil water conditions that do not limit transpiration rates (i.e., well-watered conditions) (Folwell et al., 2016). This estimated length of the period before the decline in evapotranspiration rates study is shorter or comparable to the DWP_{GS} observed over Northern Europe during our study period (12 days average length; range 5–20 days). Hence, even though the effects of a period without precipitation depend on the actual properties of the system and the atmospheric conditions, the DWP_{GS} occurring in Northern Europe are already long enough to be associated with reduced evapotranspiration rates, suggesting the occurrence of water stressed conditions. Thus, the explanatory power of DWP emerging from our analyses is suggestive of an effect of water stress in Northern European boreal forests—an ecosystem generally considered light- or energy-limited.

The analysis of the correlation coefficients of the combination of climatic variables with the highest explanatory power (Analysis 5) allows assessing the effects on $NDVI_{GS}$ of precipitation and its timing in further detail. As apparent in **Figure 3**, higher PPT_A and PPT_{GS} (i.e., annual and seasonal daily mean precipitation, respectively) have opposite effects on $NDVI_{GS}$. In other words, the response of the Northern European forests to variations in precipitation totals depends on whether precipitation increases within the growing season or during the rest of the year. Extremely positive correlations between $NDVI_{GS}$ and PPT_{GS} are apparent in warmer locations. There, higher temperatures enhance soil water depletion via evapotranspiration, so that higher precipitation amounts might be key to maintain well-watered conditions. In colder places, where the evaporative atmospheric demand is lower, the correlation between $NDVI_{GS}$ and PPT_{GS} was negative. This is likely the result of reduced solar radiation with increasing precipitation, which could exceed the benefits of increasing water availability (Churkina and Running, 1998; Mulder et al., 2019). Conversely, extremely positive correlations between $NDVI_{GS}$ and PPT_A were found in colder and drier locations, while they were negative in warmer and wetter ones. Unlike precipitation within the growing season, precipitation outside the growing season can occur as snow in Northern Europe. Winter snow accumulation affects forest productivity in different and potentially opposite ways. On the one hand, reduced winter snow accumulation is generally related to earlier complete snowmelt, in turn leading to earlier leaf onset (Korner, 2003; Inouye, 2008; Ernakovich et al., 2014). As such, reduced snow accumulation could be beneficial for forest productivity by extending the growing season (Piao et al., 2017). On the other hand, larger snow accumulation can have positive effects on soil water availability during a large part of the growing season. Moreover, an earlier onset of the spring could also lead to drier soils later in the growing season, unless the larger water losses due to extended periods with non-negligible evapotranspiration are compensated by larger precipitation amounts (Buermann et al., 2013). Which of these opposite effects of snow is dominant depends on the location and climate. A multivariate analyses based on remotely-sensed snow water equivalent and NDVI showed that in Northern Europe snow accumulation primarily affects the date of leaf onset rather than soil water availability during the growing season (Wang et al., 2018). Nevertheless, in the northernmost regions, spring leaf onset did not prove to be well-synchronized with snowmelt date, due to other environmental constraints preventing trees from taking full advantage of earlier snowmelt (e.g., insufficient heat accumulation after snowmelt and light limitation) (Basler and Körner, 2012; Zohner and Renner, 2015). Therefore, in this region, reduced snow accumulation was not related to earlier spring onset, while it still affected soil water availability. This might explain why in our analyses extremely positive correlation between PPT_A and $NDVI_{GS}$ emerged in cold and dry places. Conversely, in the southernmost regions, earlier snowmelt allows earlier spring onset, longer growing seasons and potentially higher average $NDVI_{GS}$, when the growing season precipitation ensures well-watered conditions, leading to extremely negative correlations between PPT_A and $NDVI_{GS}$ in warm and wet locations.

CONCLUSIONS

Understanding the links between climatic variables and boreal forest productivity is considered one of the grand challenges for global change scientists (Williams et al., 2011). This is a stepping stone for robust projections of the response of boreal forests to shifts in climatic conditions, their role in the global C balance, and their ability to provide a number of ecosystem and socioeconomic services. Yet, systematic large-scale studies that explore the linkages between vegetation dynamics and climatic variability in the boreal region are still limited (Buermann et al., 2014) and have provided contradictory results for Northern Europe (Babst et al., 2012; Bjerke et al., 2014; Gauthier et al., 2015). It is thus still unknown whether the negative effects of global warming on forest productivity

will exceed the positive ones and whether such effects are uniformly distributed in this region. To address this knowledge gap, we used high-resolution gridded meteorological data and satellite NDVI data—a proxy of forest productivity—to explore how boreal forests in Northern Europe respond to variation in climatic drivers.

Our results are suggestive of the main drivers of boreal forest productivity and they provide essential and innovative information about the general response of the Northern European forest. Indeed, while only few studies have focused on the response of boreal forests to water availability, our results show that soil water availability does play a key role in boreal forest productivity, even in a relatively mesic region as Northern Europe. Further exploration of the correlation coefficients between $NDVI_{GS}$ and several climatic variables highlighted that boreal forests may indeed be negatively affected by water stress, in particular in southern and warmer regions. Further, the correlation between forest productivity and temperature is not uniformly positive over the region, rather it varies according to a thermal and moisture gradient. Indeed, warmer temperatures appears beneficial mainly in the northernmost (cooler) and wetter locations, whereas their effects appear negative in the southern (warmer) and drier ones. These different responses can partially explain the conflicting findings reported so far regarding the effects of increasing temperatures. Moreover, the timing of precipitation has a higher explanatory power for boreal forest productivity than precipitation totals, because of its role on the occurrence of water stress. These results and their interpretation are suggestive of likely mechanisms driving the interplay between climatic conditions and forest productivity in Northern Europe. We acknowledge that statistical analyses as the one performed here do not inform about the actual processes and depend on the temporal and spatial resolution of both meteorological and forest productivity data. As such, further testing via specific experiments is needed.

Our results have implications in the face of climate change and management for climate adaptation. Boreal regions are predicted to shift from short, cool summers to longer, warmer summers (Jylha et al., 2010). Even under unaltered precipitation patterns, warmer and longer summers can result in more frequent occurrence of periods with low water availability, potentially transitioning Northern Europe forests from "greening" to "browning," as already observed in North America. Regarding climate adaptation, our large scale analysis supports the identifications of regions where the projected future conditions will most likely have negative rather than positive effects, thus allowing the prioritization of management actions. Furthermore, unequivocal scientific evidence of the already occurring effects of climatic conditions on boreal forests can facilitate management decisions toward better adapted ecosystems, now currently mostly based on subjective factors (Vulturius et al., 2018).

This large scale analysis shows that the expected benefits of rising temperatures are reduced or even reversed by water shortage and that there are regions or hot spots over Northern Europe particularly vulnerable to the projected changes in climatic conditions. Synergetic efforts via *in-situ* experiments and the implementation of physically-based models should thus focus on those likely most vulnerable regions, in order to understand the actual mechanisms, make predictions under a changing climate, and potentially even identify suitable management approaches to reduce the vulnerability.

DATA AVAILABILITY STATEMENT

The datasets generated for this study are available on request to the corresponding author.

AUTHOR CONTRIBUTIONS

GR-P and GV have contributed equally to the conception and design of the work and the interpretation of the data. GR-P acquired and performed the data analysis and led the drafting of the manuscript. GV revised it critically and guided all the analysis process and design.

FUNDING

This research was supported by Trees and Crops for the Future (TC4F)—a co-operative project between established research environments at the Swedish University of Agriculture (SLU), Umeå University and Skogforsk. Partial support was also received by the Swedish Research Council for Sustainable Development (FORMAS), through grants 2018-01820 and 2018-00968, and the European Commission and Swedish Research Council for Sustainable Development (FORMAS), in the frame of the collaborative international consortium WaterWorks 2017 ERA-NET Joint Programming Initiative Water challenges for a changing world, under cofound grant 2018-02787 (iAqueduct).

ACKNOWLEDGMENTS

We acknowledge the E-OBS dataset from the EU-FP6 project ENSEMBLES (http://ensembles-eu.metoffice.com) and the data providers in the ECA&D project (http://www.ecad.eu). The MODIS data were obtained through the online Data Pool at the NASA Land Processes Distributed Active Archive Center (LP DAAC), USGS/Earth Resources Observation and Science (EROS) Center, Sioux Falls, South Dakota (https://lpdaac.usgs.gov/get_data). All the data used in this work are freely available from the above-mentioned sources.

SUPPLEMENTARY MATERIAL

The Supplementary Material for this article can be found online at: https://www.frontiersin.org/articles/10.3389/ffgc.2020.00034/full#supplementary-material

REFERENCES

Abdi, H. (2010). Partial least squares regression and projection on latent structure regression (PLS Regression). *Wiley Interdiscip. Rev. Comput. Stat.* 2, 97–106. doi: 10.1002/wics.51

Allen, C. D., Breshears, D. D., and McDowell, N. G. (2015). On underestimation of global vulnerability to tree mortality and forest die-off from hotter drought in the Anthropocene. *Ecosphere* 6, 1–55. doi: 10.1890/ES15-00203.1

Allen, C. D., Macalady, A. K., Chenchouni, H., Bachelet, D., McDowell, N., Vennetier, M., et al. (2010). A global overview of drought and heat-induced tree mortality reveals emerging climate change risks for forests. *For. Ecol. Manage.* 259, 660–684. doi: 10.1016/j.foreco.2009.09.001

Anderegg, W. R. L., Kane, J. M., and Anderegg, L. D. L. (2013). Consequences of widespread tree Mortality triggered by drought and temperature stress. *Nat. Clim. Chang.* 3, 30–36. doi: 10.1038/nclimate1635

Andreassen, K., Solberg, S., Tveito, O. E., and Lystad, S. L. (2006). Regional differences in climatic responses of Norway spruce (Picea abies L. Karst*)* growth in Norway. *For. Ecol. Manage.* 222, 211–221. doi: 10.1016/j.foreco.2005.10.029

Babst, F., Carrer, M., Poulter, B., Urbinati, C., Neuwirth, B., and Frank, D. (2012). 500 years of regional forest growth variability and links to climatic extreme events in Europe. *Environ. Res. Lett.* 7, 45705–45711. doi: 10.1088/1748-9326/7/4/045705

Barber, V. A., Juday, G. P., and Finney, B. P. (2000). Reduced growth of Alaskan white spruce in the twentieth century from temperature-induced drought stress. *Nature* 405, 668–673. doi: 10.1038/35015049

Basler, D., and Körner, C. (2012). Photoperiod sensitivity of bud burst in 14 temperate forest tree species. *Agric. For. Meteorol.* 165, 73–81. doi: 10.1016/j.agrformet.2012.06.001

Baul, T., Alam, A., Ikonen, A., Strandman, H., Asikainen, A., Peltola, H., et al. (2017). Climate change mitigation potential in boreal forests: impacts of management, harvest intensity and use of forest biomass to substitute fossil resources. *Forests* 8:455. doi: 10.3390/f8110455

Beck, P. S. A., and Goetz, S. J. (2011). Satellite observations of high northern latitude vegetation productivity changes between 1982 and 2008: ecological variability and regional differences. *Environ. Res. Lett.* 6:045501. doi: 10.1088/1748-3182/6/4/049501

Belyazid, S., and Zanchi, G. (2019). Water limitation can negate the effect of higher temperatures on forest carbon sequestration. *Eur. J. For. Res.* 138, 287–297. doi: 10.1007/s10342-019-01168-4

Berner, L. T., Beck, P. S. A., Bunn, A. G., Lloyd, A. H., and Goetz, S. J. (2011). High-latitude tree growth and satellite vegetation indices: correlations and trends in Russia and Canada (1982-2008). *J. Geophys. Res. Biogeo.* 116:G01015. doi: 10.1029/2010JG001475

Bjerke, J. W., Karlsen, S. R., Hogda, K. A., Malnes, E., Jepsen, J. U., Lovibond, S., et al. (2014). Record-low primary productivity and high plant damage in the nordic arctic region in 2012 caused by multiple weather events and pest outbreaks. *Environ. Res. Lett.* 9:084006. doi: 10.1088/1748-9326/9/8/084006

Boisvenue, C., and Running, S. W. (2006). Impacts of climate change on natural forest productivity–evidence since the middle of the 20th century. *Glob. Chang. Biol.* 12, 862–882. doi: 10.1111/j.1365-2486.2006.01134.x

Bonan, G. B., and Shugart, H. H. (1989). Environmental-factors and ecological processes in boreal forests. *Annu. Rev. Ecol. Syst.* 20, 1–28. doi: 10.1146/annurev.es.20.110189.000245

Boonstra, R., Andreassen, H. P., Boutin, S., Husek, J., Ims, R. A., Krebs, C. J., et al. (2016). Why do the boreal forest ecosystems of northwestern europe differ from those of Western North America? *Bioscience* 66, 722–734. doi: 10.1093/biosci/biw080

Budyko, M. I. (1964). Contribution to theory explaining influence of climatic factors on photosynthesis. Doklady Akademii Nauk Sssr 158, 331.

Buermann, W., Bikash, P. R., Jung, M., Burn, D. H., and Reichstein, M. (2013). Earlier springs decrease peak summer productivity in North American boreal forests. *Environ. Res. Lett.* 8:024027. doi: 10.1088/1748-9326/8/2/024027

Buermann, W., Parida, B., Jung, M., MacDonald, G. M., Tucker, C. J., and Reichstein, M. (2014). Recent shift in Eurasian boreal forest greening response may be associated with warmer and drier summers. *Geophys. Res. Lett.* 41, 1995–2002. doi: 10.1002/2014GL059450

Burnham, K. P., and Anderson, D. R. (2002). *A Practical Information Theoretic Approach. Model Selection and Multimodel Inference,* 2nd Edn. New York, NY: Springer.

Burnham, K. P., Anderson, D. R., and Huyvaert, K. P. (2011). AIC model selection and multimodel inference in behavioral ecology: some background, observations, and comparisons. *Behav. Ecol. Sociobiol.* 65, 23–35. doi: 10.1007/s00265-010-1029-6

Büttner, G. (2014). "CORINE land cover and land cover change products," in *Land Use and Land Cover Mapping in Europe. Remote Sensing and Digital Image Processing*, *Vol. 18,* 55–74. eds I. Manakos, M. Braun (Springer: Dordrecht).

Carrer, M., Nola, P., Motta, R., and Urbinati, C. (2010). Contrasting tree-ring growth to climate responses of *Abies alba* toward the southern limit of its distribution area. *Oikos* 119, 1515–1525. doi: 10.1111/j.1600-0706.2010.18293.x

Churkina, G., and Running, S. W. (1998). Contrasting climatic controls on the estimated productivity of global terrestrial biomes. *Ecosystems* 1, 206–215. doi: 10.1007/s100219900016

D'Arrigo, R., Wilson, R., Liepert, B., and Cherubini, P. (2008). On the 'Divergence Problem' in northern forests: a review of the tree-ring evidence and possible causes. *Glob. Planet. Change* 60, 289–305. doi: 10.1016/j.gloplacha.2007.03.004

de Jong, R., Schaepman, M. E., Furrer, R., De Bruin, S., and Verburg, P. H. (2013). Spatial relationship between climatologies and changes in global vegetation activity. *Glob. Chang. Biol.* 19, 1953–1964. doi: 10.1111/gcb.12193

Didan, K. (2015). *MOD13Q1 MODIS/Terra Vegetation Indices 16-Day L3 Global 250m SIN Grid V006 [Data set]*. NASA EOSDIS LP DAAC.

Dunn, O. J. (1964). Multiple comparisons using rank sums. *Technometrics* 6, 241–252. doi: 10.1080/00401706.1964.10490181

Elbakidze, M., Andersson, K., Angelstam, P., Armstrong, G. W., Axelsson, R., Doyon, F., et al. (2013). Sustained yield forestry in Sweden and Russia: how does it correspond to sustainable forest management policy? *Ambio* 42, 160–173. doi: 10.1007/s13280-012-0370-6

Elliott, K. J., Miniat, C. F., Pederson, N., and Laseter, S. H. (2015). Forest tree growth response to hydroclimate variability in the southern Appalachians. *Glob. Chang. Biol.* 21, 4627–4641. doi: 10.1111/gcb.13045

Ernakovich, J. G., Hopping, K. A., Berdanier, A. B., Simpson, R. T., Kachergis, E. J., Steltzer, H., et al. (2014). Predicted responses of arctic and alpine ecosystems to altered seasonality under climate change. *Glob. Chang. Biol.* 20, 3256–3269. doi: 10.1111/gcb.12568

Fernández-Martínez, M., Yu, R., Gamon, J., Hmimina, G., Filella, I., Balzarolo, M., et al. (2019). Monitoring spatial and temporal variabilities of gross primary production using MAIAC MODIS data. *Remote Sens.* 11:874. doi: 10.3390/rs11070874

Folwell, S. S., Harris, P. P., and Taylor, C. M. (2016). Large-Scale surface responses during european dry spells diagnosed from land surface temperature. *J. Hydrometeorol.* 17, 975–993. doi: 10.1175/JHM-D-15-0064.1

Gauthier, S., Bernier, P., Kuuluvainen, T., Shvidenko, A. Z., and Schepaschenko, D. G. (2015). Boreal forest health and global change. *Science* 349, 819–822. doi: 10.1126/science.aaa9092

Geladi, P., and Kowalski, B. R. (1986). Partial least-squares regression - a tutorial. *Anal. Chim. Acta* 185, 1–17. doi: 10.1016/0003-2670(86)80028-9

Goetz, S. J., Bunn, A. G., Fiske, G. J., and Houghton, R. A. (2005). Satellite-observed photosynthetic trends across boreal North America associated with climate and fire disturbance. *Proc. Natl. Acad. Sci. U.S.A.* 102, 13521–13525. doi: 10.1073/pnas.0506179102

Grahn, P., and Stigsdotter, U. (2003). Landscape planning and stress. *Urban For. Urban Green.* 2, 1–18. doi: 10.1078/1618-8667-00019

Grossiord, C., Granier, A., Gessler, A., Jucker, T., and Bonal, D. (2014). Does drought influence the relationship between biodiversity and ecosystem functioning in boreal forests? *Ecosystems* 17, 394–404. doi: 10.1007/s10021-013-9729-1

Gunst, R. F., and Mason, R. L. (1979). Some considerations in the evaluation of alternate prediction equations. *Technometrics* 21, 55–63. doi: 10.1080/00401706.1979.10489722

Hall, C. M., Muller, D. K., and Saarinen, J. (2009). "Nature based tourism in Northern Wilderness," in *Nordic Tourism - Issues and Cases* (Bristol: Channel View Publications).

Hargreaves, G. H. (1983). Estimating potential evapotranspiration - closure. *J. Irrig. Drain. Eng -Asce* 109, 343–344. doi: 10.1061/(ASCE)0733-9437(1983)109:3(343)

Haylock, M. R., Hofstra, N., Tank, A. M. G. K., Klok, E. J., Jones, P. D., and New, M. (2008). A European daily high-resolution gridded data set of surface temperature and precipitation for 1950–2006. *J. Geophys. Res-Atmos.* 113:D20119. doi: 10.1029/2008JD010201

Hellmann, L., Agafonov, L., Ljungqvist, F. C., Churakova, O., Duthorn, E., Esper, J., et al. (2016). Diverse growth trends and climate responses across Eurasia's boreal forest. *Environ. Res. Lett.* 11:074021. doi: 10.1088/1748-9326/11/7/074021

Hsiao, T. C. (1973). Plant responses to water stress. *Annu. Rev. Plant Physiol. Plant Mol. Biol.* 24, 519–570. doi: 10.1146/annurev.pp.24.060173.002511

Ichii, K., Kawabata, A., and Yamaguchi, Y. (2002). Global correlation analysis for NDVI and climatic variables and NDVI trends: 1982-1990. *Int. J. Remote Sens.* 23, 3873–3878. doi: 10.1080/01431160110119416

Inouye, D. W. (2008). Effects of climate change on phenology, frost damage, and floral abundance of montane wildflowers. *Ecology* 89, 353–362. doi: 10.1890/06-2128.1

Intergovernmental Panel on Climate Change (2014). *Climate Change 2014–Impacts, Adaptation and Vulnerability: Regional Aspects*. Cambridge: Cambridge University Press. doi: 10.1017/CBO9781107415416

Jylha, K., Tuomenvirta, H., Ruosteenoja, K., Niemi-Hugaerts, H., Keisu, K., and Karhu, J. A. (2010). Observed and projected future shifts of climatic zones in Europe and their use to visualize climate change information. *Weather Clim. Soc.* 2, 148–167. doi: 10.1175/2010WCAS1010.1

Kallio, A. M. I., Salminen, O., and Sievanen, R. (2013). Sequester or substitute-consequences of increased production of wood based energy on the carbon balance in Finland. *J. For. Econ.* 19, 402–415. doi: 10.1016/j.jfe.2013.05.001

Karlsen, S. R., Solheim, I., Beck, P. S. A., Hogda, K. A., Wielgolaski, F. E., and Tommervik, H. (2007). Variability of the start of the growing season in Fennoscandia, 1982-2002. *Int. J. Biometeorol.* 51, 513–524. doi: 10.1007/s00484-007-0091-x

Kasischke, E. S., and Turetsky, M. R. (2006). Recent changes in the fire regime across the North American boreal region - Spatial and temporal patterns of burning across Canada and Alaska. *Geophys. Res. Lett.* 33:L09703. doi: 10.1029/2006GL025677

Kaufmann, R. K., D'Arrigo, R. D., Paletta, L. F., Tian, H. Q., Jolly, W. M., and Myneni, R. B. (2008). Identifying climatic controls on ring width: the timing of correlations between tree rings and NDVI. *Earth Interact.* 12, 1–14. doi: 10.1175/2008EI263.1

Kauppi, P. E., Posch, M., and Pirinen, P. (2014). Large impacts of climatic warming on growth of boreal forests since 1960. *PLoS ONE* 9:e111340. doi: 10.1371/journal.pone.0111340

Köhl, M., Bastup-Birk, A., Marchetti, M., Cimini, D., Corona, P., Thorsen, B., et al. (2011). "Criterion 3: Maintenance and encouragement of productive functions of forest," in *FOREST EUROPE, UNECE and FAO 2011: State of Europe's Forests 2011* (Oslo: Status and Trends in Sustainable Forest Management in Europe).

Kong, D., Zhang, Q., Singh, V. P., and Shi, P. (2017). Seasonal vegetation response to climate change in the Northern Hemisphere (1982–2013). *Glob. Planetar. Change* 148, 1–8. doi: 10.1016/j.gloplacha.2016.10.020

Korner, C. (2003). Carbon limitation in trees. *J. Ecol.* 91, 4–17. doi: 10.1046/j.1365-2745.2003.00742.x

Koskiaho, J., Ekholm, P., Raty, M., Riihimaki, J., and Puustinen, M. (2003). Retaining agricultural nutrients in constructed wetlands - experiences under boreal conditions. *Ecol. Eng.* 20, 89–103. doi: 10.1016/S0925-8574(03)00006-5

Kruskal, W. H. (1952). A nonparametric test for the several sample problem. *Ann. Math. Stat.* 23, 525–540. doi: 10.1214/aoms/1177729332

Kurz, W. A., Stinson, G., Rampley, G. J., Dymond, C. C., and Neilson, E. T. (2008). Risk of natural disturbances makes future contribution of Canada's forests to the global carbon cycle highly uncertain. *Proc. Natl. Acad. Sci. U.S.A.* 105, 1551–1555. doi: 10.1073/pnas.0708133105

Kysely, J., and Plavcova, E. (2010). A critical remark on the applicability of E-OBS European gridded temperature data set for validating control climate simulations. *J. Geophys. Res-Atmos.* 115:D23118. doi: 10.1029/2010JD014123

Ledesma, J. L. J., and Futter, M. N. (2017). Gridded climate data products are an alternative to instrumental measurements as inputs to rainfall-runoff models. *Hydrol. Process.* 31, 3283–3293. doi: 10.1002/hyp.11269

Lloyd, A. H., and Bunn, A. G. (2007). Responses of the circumpolar boreal forest to 20th century climate variability. *Environ. Res. Lett.* 2:045013. doi: 10.1088/1748-9326/2/4/045013

Martin-Benito, D., and Pederson, N. (2015). Convergence in drought stress, but a divergence of climatic drivers across a latitudinal gradient in a temperate broadleaf forest. *J. Biogeogr.* 42, 925–937. doi: 10.1111/jbi.12462

Matsushita, B., Yang, W., Chen, J., Onda, Y., and Qiu, G. Y. (2007). Sensitivity of the enhanced vegetation index (EVI) and Normalized difference vegetation index (NDVI) to topographic effects: a case study in high-density cypress forest. *Sensors* 7, 2636–2651. doi: 10.3390/s7112636

Mulder, V. L., van Eck, C. M., Friedlingstein, P., Arrouays, D., and Regnier, P. (2019). Controlling factors for land productivity under extreme climatic events in continental Europe and the Mediterranean Basin. *CATENA* 182:104124. doi: 10.1016/j.catena.2019.104124

Muukkonen, P., Nevalainen, S., Lindgren, M., and Peltoniemi, M. (2015). Spatial occurrence of drought-associated damages in Finnish boreal forests: results from forest condition monitoring and GIS analysis. *Boreal Environ. Res.* 20, 172–180.

Myneni, R. B., Keeling, C. D., Tucker, C. J., Asrar, G., and Nemani, R. R. (1997). Increased plant growth in the northern high latitudes from 1981 to 1991. *Nature* 386, 698–702. doi: 10.1038/386698a0

Nikulin, G., Kjellstrom, E., Hansson, U., Strandberg, G., and Ullerstig, A. (2011). Evaluation and future projections of temperature, precipitation and wind extremes over Europe in an ensemble of regional climate simulations. *Tellus* 63, 41–55. doi: 10.1111/j.1600-0870.2010.00466.x

Nordic Statistics (2017). *Nordic Statistics 2017*. Nordic Co-operation Nordiska ministerrådets sekretariat, Nordic Council of Ministers, Oslo.

Olofsson, P., Lagergren, F., Lindroth, A., Lindström, J., Klemedtsson, L., Kutsch, W., et al. (2008). Towards operational remote sensing of forest carbon balance across Northern Europe. *Biogeosciences* 5, 817–832. doi: 10.5194/bg-5-817-2008

O'Sullivan, O. S., Heskel, M. A., Reich, P. B., Tjoelker, M. G., Weerasinghe, L. K., Penillard, A., et al. (2017). Thermal limits of leaf metabolism across biomes. *Glob. Chang. Biol.* 23, 209–223. doi: 10.1111/gcb.13477

Park, T., Ganguly, S., Tommervik, H., Euskirchen, E. S., Hogda, K. A., Karlsen, S. R., et al. (2016). Changes in growing season duration and productivity of northern vegetation inferred from long-term remote sensing data. *Environ. Res. Lett.* 11:084001. doi: 10.1088/1748-9326/11/8/084001

Peichl, M., Oquist, M., Lofvenius, M. O., Ilstedt, U., Sagerfors, J., Grelle, A., et al. (2014). A 12-year record reveals pre-growing season temperature and water table level threshold effects on the net carbon dioxide exchange in a boreal fen. *Environ. Res. Lett.* 9:055006. doi: 10.1088/1748-9326/9/5/055006

Persson, G., Bärring, L., Kjellström, E., Strandberg, G., and Rummukainen, M. (2007). *Climate Indices for Vulnerability Assessments*. Norrköpping: SMHI.

Piao, S. L., Liu, Z., Wang, T., Peng, S. S., Ciais, P., Huang, M. T., et al. (2017). Weakening temperature control on the interannual variations of spring carbon uptake across northern lands. *Nat. Clim. Change* 7, 359–363. doi: 10.1038/nclimate3277

Porter, T. J., and Pisaric, M. F. J. (2011). Temperature-growth divergence in white spruce forests of old crow flats, Yukon Territory, and adjacent regions of northwestern North America. *Glob. Chang. Biol.* 17, 3418–3430. doi: 10.1111/j.1365-2486.2011.02507.x

Rosner, S., Gierlinger, N., Klepsch, M., Karlsson, B., Evans, R., Lundqvist, S. O., et al. (2018). Hydraulic and mechanical dysfunction of Norway spruce sapwood due to extreme summer drought in Scandinavia. *For. Ecol. Manage.* 409, 527–540. doi: 10.1016/j.foreco.2017.11.051

Rubtsov, A. V., Sukhinin, A. I., and Vaganov, E. A. (2011). System analysis of weather fire danger in predicting large fires in Siberian forests. *Izv. Atmos. Ocean. Phys.* 47, 1049–1056. doi: 10.1134/S0001433811090143

Ruckstuhl, K. E., Johnson, E. A., and Miyanishi, K. (2008). Introduction. The boreal forest and global change. *Philos. Trans. R. Soc. B-Biol. Sci.* 363, 2245–2249. doi: 10.1098/rstb.2007.2196

Ruiz-Pérez, G., Launiainen, S., and Vico, G. (2019). Role of plant traits in photosynthesis and thermal damage avoidance under warmer and drier climates in boreal forests. *Forests* 10:398. doi: 10.3390/f10050398

Ruosteenoja, K., Markkanen, T., Venalainen, A., Raisanen, P., and Peltola, H. (2018). Seasonal soil moisture and drought occurrence in Europe

in CMIP5 projections for the 21st century. *Clim. Dyn.* 50, 1177–1192. doi: 10.1007/s00382-017-3671-4

Ruosteenoja, K., Raisanen, J., Venalainen, A., and Kamarainen, M. (2016). Projections for the duration and degree days of the thermal growing season in Europe derived from CMIP5 model output. *Int. J. Climatol.* 36, 3039–3055. doi: 10.1002/joc.4535

Rytter, L., Andreassen, K., Bergh, J., Eko, P. M., Gronholm, T., Kilpelainen, A., et al. (2015). Availability of biomass for energy purposes in nordic and baltic countries: land areas and biomass amounts. *Balt. For.* 21, 375–390.

Rytter, L., Ingerslev, M., Kilpelainen, A., Torssonen, P., Lazdina, D., Lof, M., et al. (2016). Increased forest biomass production in the Nordic and Baltic countries - a review on current and future opportunities. *Silva Fenn.* 50:1660. doi: 10.14214/sf.1660

Sesnie, S. E., Dickson, B. G., Rosenstock, S. S., and Rundall, J. M. (2012). A comparison of Landsat TM and MODIS vegetation indices for estimating forage phenology in desert bighorn sheep (*Ovis canadensis nelsoni*) habitat in the Sonoran Desert, USA. *Int. J. Remote Sens.* 33, 276–286. doi: 10.1080/01431161.2011.592865

Skaugen, T. E., and Tveito, O. E. (2004). Growing-season and degree-day scenario in Norway for 2021-2050. *Clim. Res.* 26, 221–232. doi: 10.3354/cr026221

Smyth, C., Kurz, W. A., Rampley, G., Lempriere, T. C., and Schwab, O. (2017). Climate change mitigation potential of local use of harvest residues for bioenergy in Canada. *Glob. Change Biol. Bioenergy* 9, 817–832. doi: 10.1111/gcbb.12387

Solberg, S. (2004). Summer drought: a driver for crown condition and mortality of Norway spruce in Norway. *For. Pathol.* 34, 93–104. doi: 10.1111/j.1439-0329.2004.00351.x

Soukup, T., Büttner, G., Feranec, J., Hazeu, G., Jaffrain, G., Jindrova, M., et al. (2016). CORINE Land Cover 2006–2012 changes: analysis and assessment. *Eur. Landscape Dyn.* 1, 111–119. doi: 10.1201/9781315372860-17

Sulla-Menashe, D., Woodcock, C. E., and Friedl, M. A. (2018). Canadian boreal forest greening and browning trends: an analysis of biogeographic patterns and the relative roles of disturbance versus climate drivers. *Environ. Res. Lett.* 13:014007. doi: 10.1088/1748-9326/aa9b88

Tangeland, T., Aas, O., and Odden, A. (2013). The socio- demographic influence on participation in outdoor recreation activities - implications for the norwegian domestic market for nature-based tourism. *Scand. J. Hosp. Tour.* 13, 190–207. doi: 10.1080/15022250.2013.819171

Tei, S., and Sugimoto, A. (2018). Time lag and negative responses of forest greenness and tree growth to warming over circumboreal forests. *Glob. Change Biol.* 24, 1–13. doi: 10.1111/gcb.14135

Tei, S., Sugimoto, A., Kotani, A., Ohta, T., Morozumi, T., Saito, S., et al. (2019). Strong and stable relationships between tree-ring parameters and forest-level carbon fluxes in a Siberian larch forest. *Polar Sci.* 21, 146–157. doi: 10.1016/j.polar.2019.02.001

Thurner, M., Beer, C., Carvalhais, N., Forkel, M., Santoro, M., Tum, M., et al. (2016). Large-scale variation in boreal and temperate forest carbon turnover rate related to climate. *Geophys. Res. Lett.* 43, 4576–4585. doi: 10.1002/2016GL068794

Toreti, A., Belward, A., Perez-Dominguez, I., Naumann, G., Luterbacher, J., Cronie, O., et al. (2019). The exceptional 2018 European water seesaw calls for action on adaptation. *Earth's Fut.* 7, 652–663. doi: 10.1029/2019EF001170

Trahan, M. W., and Schubert, B. A. (2016). Temperature-induced water stress in high-latitude forests in response to natural and anthropogenic warming. *Glob. Chang. Biol.* 22, 782–791. doi: 10.1111/gcb.13121

United Nations Framework Convention on Climate Change (2011). *Report of the United Nations Climate Change Conference, Durban, South Africa*.

Verbyla, D. (2015). Remote sensing of interannual boreal forest NDVI in relation to climatic conditions in interior Alaska. *Environ. Res. Lett.* 10:125016. doi: 10.1088/1748-9326/10/12/125016

Vicente-Serrano, S. M., Gouveia, C., Camarero, J. J., Begueria, S., Trigo, R., Lopez-Moreno, J. I., et al. (2013). Response of vegetation to drought time-scales across global land biomes. *Proc. Natl. Acad. Sci. U.S.A.* 110, 52–57. doi: 10.1073/pnas.1207068110

Vulturius, G., André, K., Swartling, Å. G., Brown, C., Rounsevell, M. D. A., and Blanco, V. (2018). The relative importance of subjective and structural factors for individual adaptation to climate change by forest owners in Sweden. *Reg. Environ. Change* 18, 511–520. doi: 10.1007/s10113-017-1218-1

Walther, S., Voigt, M., Thum, T., Gonsamo, A., Zhang, Y. G., Kohler, P., et al. (2016). Satellite chlorophyll fluorescence measurements reveal large-scale decoupling of photosynthesis and greenness dynamics in boreal evergreen forests. *Glob. Change Biol.* 22, 2979–2996. doi: 10.1111/gcb.13200

Wang, X. Y., Wang, T., Guo, H., Liu, D., Zhao, Y. T., Zhang, T. T., et al. (2018). Disentangling the mechanisms behind winter snow impact on vegetation activity in northern ecosystems. *Glob. Chang. Biol.* 24, 1651–1662. doi: 10.1111/gcb.13930

Williams, A. P., Allen, C. D., Macalady, A. K., Griffin, D., Woodhouse, C. A., Meko, D. M., et al. (2013). Temperature as a potent driver of regional forest drought stress and tree mortality. *Nat. Clim. Chang.* 3, 292–297. doi: 10.1038/nclimate1693

Williams, J., Crowley, J., Fischer, H., Harder, H., Martinez, M., Petaja, T., et al. (2011). The summertime Boreal forest field measurement intensive (HUMPPA-COPEC-2010): an overview of meteorological and chemical influences. *Atmos. Chem. Phys.* 11, 10599–10618. doi: 10.5194/acp-11-10599-2011

Wold, S., Sjostrom, M., and Eriksson, L. (2001). PLS-regression: a basic tool of chemometrics. *Chemometr. Intell. Lab. Syst.* 58, 109–130. doi: 10.1016/S0169-7439(01)00155-1

Wu, D. H., Zhao, X., Liang, S. L., Zhou, T., Huang, K. C., Tang, B. J., et al. (2015). Time-lag effects of global vegetation responses to climate change. *Glob. Chang. Biol.* 21, 3520–3531. doi: 10.1111/gcb.12945

Wu, S., Li, J., and Huang, G. H. (2008). A study on DEM-derived primary topographic attributes for hydrologic applications: sensitivity to elevation data resolution. *Appl. Geogr.* 28, 210–223. doi: 10.1016/j.apgeog.2008.02.006

Yamori, W., Hikosaka, K., and Way, D. A. (2014). Temperature response of photosynthesis in C-3, C-4, and CAM plants: temperature acclimation and temperature adaptation. *Photosyn. Res.* 119, 101–117. doi: 10.1007/s11120-013-9874-6

Yuan, W. P., Luo, Y. Q., Richardson, A. D., Oren, R., Luyssaert, S., Janssens, I. A., et al. (2009). Latitudinal patterns of magnitude and interannual variability in net ecosystem exchange regulated by biological and environmental variables. *Glob. Chang. Biol.* 15, 2905–2920. doi: 10.1111/j.1365-2486.2009.01870.x

Zhao, L., Dai, A. G., and Dong, B. (2018). Changes in global vegetation activity and its driving factors during 1982-2013. *Agric. For. Meteorol.* 249, 198–209. doi: 10.1016/j.agrformet.2017.11.013

Zohner, C. M., and Renner, S. S. (2015). Perception of photoperiod in individual buds of mature trees regulates leaf-out. *N. Phytol.* 208, 1023–1030. doi: 10.1111/nph.13510

Zscheischler, J., and Seneviratne, S. I. (2017). Dependence of drivers affects risks associated with compound events. *Sci. Adv.* 3:e1700263. doi: 10.1126/sciadv.1700263

Conflict of Interest: The authors declare that the research was conducted in the absence of any commercial or financial relationships that could be construed as a potential conflict of interest.

frontiers in Forests and Global Change

MINI REVIEW
published: 15 April 2020
doi: 10.3389/ffgc.2020.00041

Tree-Ring Evidence of Forest Management Moderating Drought Responses: Implications for Dry, Coniferous Forests in the Southwestern United States

Phillip J. van Mantgem[1], Lucy P. Kerhoulas[2], Rosemary L. Sherriff[3] and Zachary J. Wenderott[1,3]*

[1] U.S. Geological Survey, Western Ecological Research Center, Arcata, CA, United States, [2] Department of Forestry and Wildland Resources, Humboldt State University, Arcata, CA, United States, [3] Department of Geography, Environment, and Spatial Analysis, Humboldt State University, Arcata, CA, United States

OPEN ACCESS

Edited by:
Julia Annick Schwarz, University of Freiburg, Germany

Reviewed by:
Peter Fule, Northern Arizona University, United States
Jesús Julio Camarero, Spanish National Research Council, Spain

***Correspondence:**
Phillip J. van Mantgem
pvanmantgem@usgs.gov

Specialty section:
This article was submitted to Forest Hydrology, a section of the journal Frontiers in Forests and Global Change

Received: *21 December 2019*
Accepted: *20 March 2020*
Published: *15 April 2020*

Citation:
van Mantgem PJ, Kerhoulas LP, Sherriff RL and Wenderott ZJ (2020) Tree-Ring Evidence of Forest Management Moderating Drought Responses: Implications for Dry, Coniferous Forests in the Southwestern United States. Front. For. Glob. Change 3:41. doi: 10.3389/ffgc.2020.00041

Drought, coupled with rising temperatures, is an emerging threat to many forest types across the globe. At least to a degree, we expect management actions that reduce competition (e.g., thinning, prescribed fire, or both) to improve growth of residual trees during drought. The influences of management actions and drought on individual tree growth may be measured with high precision using tree-rings. Here, we summarize tree-ring-based assessments of the effectiveness of thinning and prescribed fire as drought adaptation tools, with special consideration for how these findings might apply to dry coniferous forests in the southwestern United States. The existing literature suggests that thinning treatments generally improve individual tree growth responses to drought, though the literature specific to southwestern coniferous forests is sparse. Assessments from studies beyond the southwestern United States indicate treatment effectiveness varies by thinning intensity, timing of the drought relative to treatments, and individualistic species responses. Several large-scale studies appear to conflict on specifics of how site aridity influences sensitivity to drought following thinning. Prescribed fire effects in the absence of thinning has received much less attention in terms of subsequent drought response. There are limitations for using tree-ring data to estimate drought responses (e.g., difficulties scaling up observations to stand- and landscape-levels). However, tree-rings describe an important dimension of drought effects for individual trees, and when coupled with additional information, such as stable isotopes, aid our understanding of key physiological mechanisms that underlie forest drought response.

Keywords: dendrochronology, ecosystems, fire effects, fuel treatments, thinning

INTRODUCTION

Periodic droughts are occurring against a backdrop of increasing temperatures, so that drought effects are exacerbated by greater evaporative demand. These "hotter droughts" have been linked to vegetation stress and complete forest diebacks (Allen et al., 2015). In response, forest managers are developing strategies to adapt to these changing conditions (Millar and Stephenson, 2015).

The need to develop forest management tools is particularly urgent in the dry coniferous forests of the southwestern United States (here defined as dry forest types in Arizona, California, New Mexico, Nevada, and Utah). In this region, a history of fire exclusion has resulted in many forest types experiencing changes in forest structure, increased accumulation of forest fuels, and increased fire activity with changing climatic conditions (Hurteau et al., 2014). Simultaneously, this region has experienced drought-induced forest diebacks (Allen et al., 2015).

Managers have two primary tools for large-scale forest restoration: mechanical thinning and prescribed fire (with both treatments sometimes applied sequentially to the same stand). Mechanical thinning removes competing vegetation to promote growth of residual trees, and has a long history of use that includes conservation applications (e.g., Kolb et al., 2007). Prescribed fire, where fire is intentionally ignited or let burn under conditions that encourage moderate fire effects, is used to remove surface fuels and continuity of live fuels (shrubs, small trees and low branches) (Ryan et al., 2013). It is less clear if prescribed fire leads to negative or positive growth responses in residual trees. Fire often injures surviving trees, and prescribed fire is typically designed to only remove surface and ladder fuels (i.e., small trees), so that large reductions in stand basal area are uncommon (Schwilk et al., 2009). Managers have much greater control over treatment outcomes with thinning operations relative to prescribed fire, but both types of treatments can be designed to be more or less "aggressive," with varying numbers of surviving trees.

Tree-ring measurements have been used to provide evidence for the effectiveness of thinning and prescribed fire treatments in terms of drought adaptation. These observations have intuitive appeal for these applications, as tree-rings can be used to measure response to environmental stress and construct indices of drought response. Here, we briefly review the use of tree-ring evidence to support or refute the efficacy of thinning and prescribed fire as a drought adaptation strategy, with a focus on how these results may apply to drought-sensitive, coniferous forest types in the southwestern United States.

TREE-RING INDICES OF DROUGHT RESPONSE

Drought stress and competition lower photosynthetic capacity, and as a consequence trees may reduce carbon allocation to non-critical functions such as stem growth (Waring, 1987). Therefore, tree-ring records of growth may be an early indicator of stress on individual trees. Drought response as measured by tree-rings can be decomposed into the following elements (Lloret et al., 2011): drought resistance, quantified as growth insensitivity to stress (growth during drought/pre-drought growth); growth recovery, considered as the growth rate following drought relative to growth during drought (post-drought growth/growth during drought); and drought resilience, measured as the magnitude of return to pre-drought growth (post-drought growth/pre-drought growth) (**Figure 1**). These indices have been used to measure drought response and effects of management in a wide variety of forest types (Sohn et al., 2016). Problematically, indices of drought resistance, recovery, and resilience appear to be correlated (Gazol et al., 2017a,b, 2018). These indices are also sensitive to the measurements of growth that are used (e.g., radial versus basal area increment), and suffer from potential biases arising from length and growth conditions of the pre-drought reference period, lack of standardization in defining drought severity and duration, variation in post-drought conditions, and differential species responses (Schwarz et al., 2019). These shortcomings complicate comparisons of drought and thinning effects across studies.

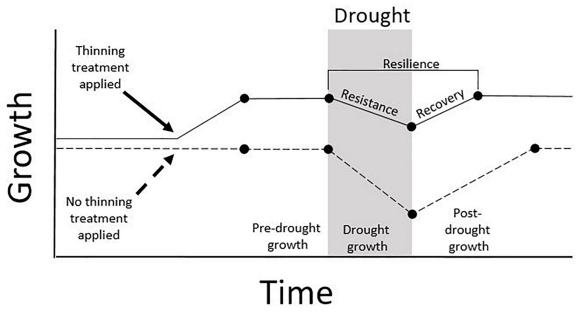

FIGURE 1 | Hypothetical growth responses of individual trees to drought (shaded area) following thinning treatment. The solid line depicts a tree that responds to treatment with higher growth, relatively little loss in growth during drought (high resistance), and a relatively rapid return to pre-drought growth rate (high resilience). The dashed line depicts a tree in an untreated stand that subsequently experiences greater loss of growth during drought (low resistance) and requires longer to recover the pre-drought growth rate (low resilience).

WHAT IS THE EVIDENCE?

There are surprisingly few published tree-ring-based studies of management effects on drought resistance and resilience in coniferous forests of the southwestern United States, a region known for its vulnerability to drought-induced tree mortality (Adams et al., 2009; Williams et al., 2013; **Table 1**). Field studies from outside of this region using tree-ring evidence support the use of thinning treatments to promote resistance and resilience to drought (**Figure 1**) for conifers (Kohler et al., 2010; Sohn et al., 2016), with the magnitude of response positively related to thinning intensity (Laurent et al., 2003), and negatively related to stand age (D'Amato et al., 2013). Time-since-thinning is also expected to influence outcomes, with treatment effectiveness becoming increasingly muted over time as vegetation regrows (Sohn et al., 2016). However, it is unclear how site aridity influences thinning responses to drought, a critical consideration for forests in the southwestern United States.

Large-scale analyses using tree-ring drought response indices (**Figure 1**) provide somewhat conflicting results concerning the effects of site aridity. Across North America (including the southwestern United States) and Europe, Gazol et al. (2017a) found trees in arid sites had less resistance but greater recovery relative to mesic sites, although they did not consider thinning

TABLE 1 | Studies using tree-ring evidence to assess thinning and prescribed burning effectiveness in moderating drought response in dry coniferous forests of the southwestern United States.

Study	Species	Location	Treatment type	Number of treatments	Years between last thinning treatment and drought	Response		
						Resistance	Recovery	Resilience
Bottero et al., 2017	ponderosa pine	Arizona	Thinning	5	0	+	NA	+
Erickson and Waring, 2014	ponderosa pine	Arizona	Thinning and burning	1	1	+	NA	+
Gleason et al., 2017	ponderosa pine	Arizona	Thinning	6	0	NA	NA	NA
Kerhoulas et al., 2013	ponderosa pine	Arizona	Thinning and burning	1	1	+	NA	NA
Kolb et al., 2007	ponderosa pine	Arizona	Thinning, Thinning & burning	1	9	−	+	NA
McDowell et al., 2006	ponderosa pine	Arizona	Thinning	4	4	NA	NA	NA
Skov et al., 2005	ponderosa pine	Arizona	Thinning and burning	1	2	0/+	NA	NA
Thomas and Waring, 2015	ponderosa pine	New Mexico	Thinning, Thinning & burning	1	3	+	NA	+
Vernon et al., 2018	Douglas-fir	California	Thinning	1	2	+	NA	NA
	ponderosa pine		Thinning	1	2	+	NA	NA

effects. They speculated that the faster recovery in arid sites may be attributable to species differences, with arid regions containing species better able to recover from drought. Gazol et al. (2017b) and Gazol et al. (2018) found the same drought response pattern with site aridity in intensive studies of sites across Spain. In contrast, a meta-analysis of drought effects and thinning including data from the southwestern United States found radial growth drought resistance (**Figure 1**) increased with site aridity, at least for unthinned and heavily thinned stands (Sohn et al., 2016). After drought Sohn et al. (2016) found this relationship with site aridity and drought response indices reversed, with aridity generally associated with decreased drought recovery and resilience. The authors hypothesized that trees adapted to drier environments invest more resources in non-structural carbohydrates, allowing them to maintain growth during initial drought stress, but then following drought it may be difficult to replace these resources and recover growth. Another large-scale study of growth response to drought and stand density in North America (using data from similar southwestern United States sites) found drought and competition reduced growth across all observed forest types, but that at arid sites growth was highly sensitive to drought stress and less sensitive to stand density (Gleason et al., 2017). The authors did not employ the drought response indices outlined in **Figure 1**, instead determining drought response from the relationship between drought severity and stand-level basal area increment based on tree-rings. The findings of Gleason et al. (2017) suggest that thinning can be used as a drought adaptation tool in dry coniferous forests of the United States Southwest, but that these treatments might be less effective relative to mesic forest types.

Specific to forests in the southwestern United States, the few existing reports have generally shown improved growth responses following thinning and drought (**Table 1**), but with differences among specific drought indices (**Figure 1**). Building on results from Feeney et al. (1998), Kolb et al. (2007) showed that thinning with and without prescribed fire resulted in lower resistance to severe drought for large (> 40 cm DBH, diameter at breast height, 1.37 m) ponderosa pine (*Pinus ponderosa* Douglas ex C. Lawson), although growth recovery appeared to be enhanced for trees in treated stands. Skov et al. (2005) found that small (≤ 39 cm DBH) ponderosa pine in northern Arizona had greater drought resistance with increasing thinning intensity across two years of drought, although larger individuals (≤ 55 cm DBH) did not show this response. Erickson and Waring (2014) and Thomas and Waring (2015) found that thinning increased drought resistance and resilience following severe drought for ponderosa pine in New Mexico and Arizona. Bottero et al. (2017) considered stand-level basal area increment based on tree-rings from ponderosa pine in northern Arizona (among other sites), finding that drought resistance and resilience were negatively related to stand density both in early- and late-stage drought. Kerhoulas et al. (2013) found that highly aggressive fuel treatments enhanced radial growth rates in large residual ponderosa pine in northern Arizona, potentially improving resistance to short-duration droughts. However, the resulting changes in tree architecture (i.e., greater leaf-to-sapwood area ratios) may commit residual trees to high transpirational demands, perhaps making them more vulnerable to droughts over the long term (McDowell et al., 2006). In a mixed-conifer forest in northern California, thinning improved drought resistance, but tree size, competition and species identity influenced this response (Vernon et al., 2018). Analyses of prescribed fire effects without mechanical thinning on drought response are far less common. Using repeated stem diameter measurements (not tree-ring data) in a Sierra Nevada mixed conifer forest, Collins et al. (2014) found that prescribed fire did not create growth conditions that reduced vulnerability for most common species.

The large-scale studies outlined above, as well as other studies (e.g., Zang et al., 2014), indicate that species are expected to respond individualistically to drought. For example, within the dry coniferous forests in northern California, Vernon et al. (2018) found that drought-tolerant ponderosa pine responded more positively to thinning treatments during drought relative to less drought-tolerant Douglas-fir [*Pseudotsuga menziesii* (Mirbel) Franco]. Responses of angiosperms to thinning and drought are less well studied than conifers (Sohn et al., 2016), a pattern that

also holds in the southwestern United States. Gazol et al. (2017a, 2018) suggest gymnosperms and angiosperms may have different drought resistance and recovery responses that may be partially determined by species-specific physiological drought responses and adaptive capacities. As such, drought-related mortality risk tends to be associated with lower drought resistance in angiosperms, while in gymnosperms this risk is often associated with lower drought recovery (DeSoto et al., 2020). Further tree-ring-based assessments of hardwood responses to drought and how management may influence these responses are needed. Note that the studies using drought resistance, recovery, and resilience metrics (**Figure 1**) are subject to important biases outlined by Schwarz et al. (2019), making it challenging to generalize across studies. Also note that many of these studies set in the southwestern United States occurred at similar sites in northern Arizona and focused on ponderosa pine (**Table 1**).

LIMITATIONS OF TREE-RING EVIDENCE

There are several limitations to the use of tree-rings to assess forest adaptation strategies. Tree-rings integrate a wide variety of signals; outside of extreme environments (e.g., high altitude, high latitude, or ecotonal forests) it is difficult to assign causes of growth variability without additional information (Speer, 2010). Typical sampling strategies can be problematic, with tree-ring samples often limited to large living or recently dead trees (i.e., the "fading record" problem) (Swetnam et al., 1999), complicating assessments of long-term growth patterns (Bowman et al., 2013). Tree-rings represent samples from individual trees and growth variability is affected by tree species, age, and size so that samples restricted to large trees cannot be reliably scaled up to stand- and landscape-level growth patterns (Clark et al., 2016). In recognition of this problem, some studies have sampled across a range of tree sizes (Bottero et al., 2017; Gleason et al., 2017).

Tree growth is only one possible measure of drought response. Other important metrics include tree mortality, reproduction, and vulnerability to further disturbances (e.g., wildfires, pests, and diseases). Several large-scale studies in the southwestern United States have demonstrated that competition is directly related to mortality during drought (Bradford and Bell, 2017; Young et al., 2017), so that thinning treatments may lower drought-related mortality (Restaino et al., 2019).

BEYOND GROWTH: COMPLEMENTARY EVIDENCE FOR UNDERSTANDING FOREST DROUGHT RESPONSE

Tree-ring data can be combined with other data sources to provide a better understanding of the patterns and mechanisms underlying forest drought responses. We briefly describe some of these complementary data sources and how they may enhance our understanding of drought responses in dry coniferous forests of the southwestern United States.

Stable Isotopes – Evidence of Physiological Mechanisms Underlying Forest Responses

To better understand forest drought responses, tree-ring stable isotopes can provide insights on possible physiological mechanisms that may vary in response to management with annual and even sub-annual resolution. Examples of such mechanisms include water stress, intrinsic water use efficiency (iWUE, carbon assimilated per water transpired), and source water use. Despite this potential, tree-ring stable isotopes seem relatively underutilized, likely due to the fact that analyses of stable isotope ratios (e.g., $\delta^{13}C$ and $\delta^{18}O$) and discrimination rates ($\Delta^{13}C$) generally require skilled expertise in sample preparation methods and data interpretation and costs can be high at commercial isotope laboratories.

Increasing resources for growth (e.g., water, light, and nutrients) by reducing competition seems an obvious result of thinning (and perhaps of prescribed fire), but these treatments can also potentially decrease water availability via increased evapotranspirational losses. Thus, tree-ring based analyses of stable isotopes at inter- and intra-annual timescales provide insights regarding the mechanisms of tree response to stand manipulations and drought. Across a range of environments many tree-ring $\delta^{13}C$ analyses suggest that iWUE is a relatively homeostatic trait largely unresponsive to changes in competition (e.g., Fernández-de-Uña et al., 2016), while other studies indicate that the magnitude of change in rates of carbon assimilation and stomatal conductance of water vapor can differ in response to reductions in competition via thinning (McDowell et al., 2003; Giuggiola et al., 2016; Rezaie et al., 2018). Specific to arid southwestern United States coniferous forests, McDowell et al. (2006) found that following thinning treatments, increases in stomatal conductance of water vapor (largely driven by increased water availability) were higher than increases in carbon assimilation rates (largely driven by light and nitrogen availability), such that iWUE can decrease in response to management actions. Although iWUE responses to thinning are variable, the majority of tree-ring stable isotope analyses demonstrate that reductions in competition can increase tree water availability, stomatal conductance, and carbon assimilation, potentially decreasing forest vulnerability to drought, particularly via increased resilience (**Figure 1**; Sohn et al., 2013). In arid southwestern coniferous forests, tree-ring stable isotopes indicate that heavy thinning treatments can reduce tree water stress (McDowell et al., 2006; Sohn et al., 2014); this finding corroborates growth-based findings that management has the potential to decrease drought vulnerability in these forest types.

Forest Pests and Inducible Defenses

As noted above, drought response can be measured in terms of tree mortality. As in other forest types, mortality in southwestern United States forests may go beyond direct effects of drought stress (e.g., loss of hydraulic function and carbon starvation) (Adams et al., 2017), to include secondary attacks by forest pests. In the southwestern United States, important forest pests include bark beetles (*Dendroctonus* spp., *Ips* spp., and *Scolytus* spp.).

Dense stands may be more susceptible to bark beetle attacks and subsequent tree mortality in association with drought (Negrón et al., 2009; Fettig et al., 2019). While drought stress may presage bark beetle attack in southwestern forests, severe drought may lead to bark beetle outbreaks where otherwise vigorous trees (as measured by stem growth rate) are killed (Stephenson et al., 2019). Under these circumstances forest management may be less effective.

In southwestern United States pines, tree-ring-based measurements of resin duct size and area can supplement annual growth data or be used alone to predict successful bark beetle attack and subsequent mortality (Kane and Kolb, 2010). In coniferous forests outside of the United States Southwest, thinning and prescribed fire may stimulate trees to increase resin flow and develop resin duct defenses against bark beetles (Hood et al., 2015, 2016). The increase in resin defenses may be related to improved growth in residual trees or in response to wounding (Hood and Sala, 2015). Thus far, the role of forest management on inducible defenses is not well defined for southwestern United States forests.

Linking Tree-Ring Data With Remotely Sensed Information

Linking tree-ring information with remotely sensed imagery provides a potential method to scale up observations. Gazol et al. (2018) found that tree-ring drought indices (**Figure 1**) and the Normalized Difference Vegetation Index (NDVI) showed similar responses to drought across several species in Spain. A similar comparison found trends in both records of declining forest productivity (NDVI) and growth (tree-rings) in interior Alaska associated with drought-induced climate changes between 1982 and 2008 (Beck et al., 2011). Expanding such analyses to directly consider the role of management in drought response in southwestern United States forests would help generalize findings based on tree-ring information alone to broader spatial scales.

DISCUSSION

There are surprisingly few tree-ring-based studies of drought response following management treatments in dry coniferous forests of the southwestern United States, a heavily managed region particularly vulnerable to widespread drought-induced forest mortality. Currently published studies in the southwestern United States have focused on a forest type at a particular location (ponderosa pine forests in northern Arizona). These results can be thought of as a model system that anticipate responses in similar southwestern forests and allow analyses across aridity gradients (Sohn et al., 2016; Gleason et al., 2017). The evidence to date suggests we should expect other water limited coniferous forests in the southwestern United States to be highly sensitive to drought, and that growth responses to drought can be improved by stand management. How these responses vary by treatment type (mechanical thinning, prescribed fire, or both), treatment intensity, taxa (particularly for Douglas-fir and common *Abies* and *Quercus* spp.), and across elevation and topoclimate (e.g., aspect) remain key unanswered questions in the United States Southwest.

Tree-rings provide one well-studied way to critically evaluate the effectiveness of management treatments, in spite of some well-known limitations. Cross-study comparisons using tree-ring drought response metrics (**Figure 1**) can be improved with standardization (Schwarz et al., 2019) or using alternate response indices (e.g., Gleason et al., 2017). Tree-ring data can be especially powerful when coupled with additional observations, such as stable isotopes, providing key insights as to how management can shape drought response. The appraisal of management activities is crucially important to develop and refine strategies to respond to rapidly changing environments.

AUTHOR CONTRIBUTIONS

All authors developed the study and assembled available literature. PM, LK, and ZW wrote the manuscript with contributions from RS.

FUNDING

This project was supported by the U.S. Geological Survey's Ecosystems Mission Area, the National Park Service, and the National Science Foundation (Grant # BCS-1853903).

ACKNOWLEDGMENTS

We thank Jeff Kane, Tom Kolb and two reviewers who provided helpful comments on the manuscript. Any use of trade, firm, or product names is for descriptive purposes only and does not imply endorsement by the United States Government.

REFERENCES

Adams, H. D., Guardioloa-Claramonte, M., Barron-Gafford, G. A., Villegas, J. C., Breshears, D. D., Zou, C. B., et al. (2009). Temperature sensitivity of drought-induced tree mortality portends increased regional die-off under global-change-type drought. *Proc. Natl. Acad. Sci. U.S.A.* 106, 7063–7066. doi: 10.1073/pnas.0901438106

Adams, H. D., Zeppel, M. J., Anderegg, W. R., Hartmann, H., Landhäusser, S. M., Tissue, D. T., et al. (2017). A multi-species synthesis of physiological mechanisms in drought-induced tree mortality. *Na. Ecol. Evol.* 1, 1285–1291.

Allen, C. D., Breshears, D. D., and McDowell, N. G. (2015). On underestimation of global vulnerability to tree mortality and forest die-off from hotter drought in the Anthropocene. *Ecosphere* 6:art129. doi: 10.1890/es15-00203.1

Beck, P. S. A., Juday, G. P., Alix, C., Barber, V. A., Winslow, S. E., Sousa, E. E., et al. (2011). Changes in forest productivity across Alaska consistent with biome shift. *Ecol. Lett.* 14, 373–379. doi: 10.1111/j.1461-0248.2011.01598.x

Bottero, A., D'Amato, A. W., Palik, B. J., Bradford, J. B., Fraver, S., Battaglia, M. A., et al. (2017). Density-dependent vulnerability of forest ecosystems to drought. *J. Appl. Ecol.* 54, 1605–1614. doi: 10.1111/1365-2664.12847

Bowman, D. M. J. S., Brienen, R. J. W., Gloor, E., Phillips, O. L., and Prior, L. D. (2013). Detecting trends in tree growth: not so simple. *Trends Plant Sci.* 18, 11–17. doi: 10.1016/j.tplants.2012.08.005

Bradford, J. B., and Bell, D. M. (2017). A window of opportunity for climate-change adaptation: easing tree mortality by reducing forest basal area. *Front. Ecol. Environ.* 15, 11–17. doi: 10.1002/fee.1445

Clark, J. S., Iverson, L., Woodall, C. W., Allen, C. D., Bell, D. M., Bragg, D. C., et al. (2016). The impacts of increasing drought on forest dynamics, structure, and biodiversity in the United States. *Global Change Biol.* 22, 2329–2352. doi: 10.1111/gcb.13160

Collins, B. M., Das, A. J., Battles, J. J., Fry, D. L., Krasnow, K. D., and Stephens, S. L. (2014). Beyond reducing fire hazard: fuel treatment impacts on overstory tree survival. *Ecol. Appl.* 24, 1879–1886. doi: 10.1890/14-0971.1

D'Amato, A. W., Bradford, J. B., Fraver, S., and Palik, B. J. (2013). Effects of thinning on drought vulnerability and climate response in north temperate forest ecosystems. *Ecol. Appl.* 23, 1735–1742. doi: 10.1890/13-0677.1

DeSoto, L., Cailleret, M., Sterck, F., Jansen, S., Kramer, K., Robert, E., et al. (2020). Low growth resilience to drought is related to future mortality risk in trees. *Nat. Commun.* 11:545.

Erickson, C. C., and Waring, K. M. (2014). Old *Pinus ponderosa* growth responses to restoration treatments, climate and drought in a southwestern US landscape. *Appl. Vegetation Sci.* 17, 97–108. doi: 10.1111/avsc.12056

Feeney, S. R., Kolb, T. E., Covington, W. W., and Wagner, M. R. (1998). Influence of thinning and burning restoration treatments on presettlement ponderosa pines at the Gus Pearson Natural Area. *Can. J. For. Res.* 28, 1295–1306. doi: 10.1139/x98-103

Fernández-de-Uña, L., McDowell, N. G., Cañellas, I., and Gea-Izquierdo, G. (2016). Disentangling the effect of competition, CO_2 and climate on intrinsic water-use efficiency and tree growth. *J. Ecol.* 104, 678–690. doi: 10.1111/1365-2745.12544

Fettig, C. J., Mortenson, L. A., Bulaon, B. M., and Foulk, P. B. (2019). Tree mortality following drought in the central and southern Sierra Nevada. *Calif. U.S. For. Ecol. Manag.* 432, 164–178. doi: 10.1016/j.foreco.2018.09.006

Gazol, A., Camarero, J. J., Vicente-Serrano, S. M., Sánchez-Salguero, R., Gutiérrez, E., de Luis, M., et al. (2018). Forest resilience to drought varies across biomes. *Global Change Biol.* 24, 2143–2158. doi: 10.1111/gcb.14082

Gazol, A., Camarero, J. J., Anderegg, W. R. L., and Vicente-Serrano, S. M. (2017a). Impacts of droughts on the growth resilience of Northern Hemisphere forests: forest growth resilience to drought. *Global Ecol. Biogeogr.* 26, 166–176. doi: 10.1111/geb.12526

Gazol, A., Ribas, M., Gutiérrez, E., and Camarero, J. J. (2017b). Aleppo pine forests from across Spain show drought-induced growth decline and partial recovery. *Agric. For. Meteorol.* 232, 186–194. doi: 10.1016/j.agrformet.2016.08.014

Giuggiola, A., Ogée, J., Rigling, A., Gessler, A., Bugmann, H., and Treydte, K. (2016). Improvement of water and light availability after thinning at a xeric site: which matters more? A dual isotope approach. *New Phytol.* 210, 108–121. doi: 10.1111/nph.13748

Gleason, K. E., Bradford, J. B., Bottero, A., D'Amato, A. W., Fraver, S., Palik, B. J., et al. (2017). Competition amplifies drought stress in forests across broad climatic and compositional gradients. *Ecosphere* 8:e01849. doi: 10.1002/ecs2.1849

Hood, S., and Sala, A. (2015). Ponderosa pine resin defenses and growth: metrics matter. *Tree Physiol.* 35, 1223–1235.

Hood, S., Sala, A., Heyerdahl, E. K., and Boutin, M. (2015). Low-severity fire increases tree defense against bark beetle attacks. *Ecology* 96, 1846–1855. doi: 10.1890/14-0487.1

Hood, S. M., Baker, S., and Sala, A. (2016). Fortifying the forest: thinning and burning increase resistance to a bark beetle outbreak and promote forest resilience. *Ecol. Appl.* 26, 1984–2000. doi: 10.1002/eap.1363

Hurteau, M. D., Bradford, J. B., Fulé, P. Z., Taylor, A. H., and Martin, K. L. (2014). Climate change, fire management, and ecological services in the southwestern US. *For. Ecol. Manag.* 327, 280–289. doi: 10.1016/j.foreco.2013.08.007

Kane, J. M., and Kolb, T. E. (2010). Importance of resin ducts in reducing ponderosa pine mortality from bark beetle attack. *Oecologia* 164, 601–609. doi: 10.1007/s00442-010-1683-4

Kerhoulas, L. P., Kolb, T. E., Hurteau, M. D., and Koch, G. W. (2013). Managing climate change adaptation in forests: a case study from the U.S. Southwest. *J. Appl. Ecol.* 50, 1311–1320.

Kohler, M., Sohn, J., Nägele, G., and Bauhus, J. (2010). Can drought tolerance of Norway spruce (*Picea abies* (L.) Karst.) be increased through thinning?. *Eur. J. For. Res.* 129, 1109–1118. doi: 10.1007/s10342-010-0397-9

Kolb, T. E., Agee, J. K., Fulé, P. Z., McDowell, N. G., Pearson, K., Sala, A., et al. (2007). Perpetuating old ponderosa pine. *For. Ecol. Manag.* 249, 141–157. doi: 10.1016/j.foreco.2007.06.002

Laurent, M., Antoine, N., and Joël, G. (2003). Effects of different thinning intensities on drought response in Norway spruce (*Picea abies* (L.) Karst.). *For. Ecol. Manag.* 183, 47–60. doi: 10.1016/s0378-1127(03)00098-7

Lloret, F., Keeling, E. G., and Sala, A. (2011). Components of tree resilience: effects of successive low-growth episodes in old ponderosa pine forests. *Oikos* 120, 1909–1920. doi: 10.1111/j.1600-0706.2011.19372.x

McDowell, N. G., Adams, H. D., Bailey, J. D., Hess, M., and Kolb, T. E. (2006). Homeostatic maintenance of ponderosa pine gas exchange in response to stand density changes. *Ecol. Appl.* 16, 1164–1182. doi: 10.1890/1051-0761(2006)016%5B1164:hmoppg%5D2.0.co;2

McDowell, N. G., Brooks, J. R., Fitzgerald, S. A., and Bond, B. J. (2003). Carbon isotope discrimination and growth response of old *Pinus ponderosa* trees to stand density reductions. *Plant Cell Environ.* 26, 631–644. doi: 10.1046/j.1365-3040.2003.00999.x

Millar, C. I., and Stephenson, N. L. (2015). Temperate forest health in an era of emerging megadisturbance. *Science* 349, 823–826. doi: 10.1126/science.aaa9933

Negrón, J. F., McMillin, J. D., Anhold, J. A., and Coulson, D. (2009). Bark beetle-caused mortality in a drought-affected ponderosa pine landscape in Arizona. USA. *For. Ecol. Manag.* 257, 1353–1362. doi: 10.1016/j.foreco.2008.12.002

Restaino, C., Young, D. J., Estes, B., Gross, S., Wuenschel, A., Meyer, M., et al. (2019). Forest structure and climate mediate drought-induced tree mortality in forests of the Sierra Nevada. USA. *Ecol. Appl.* 29:e01902. doi: 10.1002/eap.1902

Rezaie, N., D'Andrea, E., Bräuning, A., Matteucci, G., Bombi, P., and Lauteri, M. (2018). Do atmospheric CO_2 concentration increase, climate and forest management affect iWUE of common beech? Evidences from carbon isotope analyses in tree rings. *Tree Physiol.* 38, 1110–1126. doi: 10.1093/treephys/tpy025

Ryan, K. C., Knapp, E. E., and Varner, J. M. (2013). Prescribed fire in North American forests and woodlands: history, current practice, and challenges. *Front. Ecol. Environ.* 11:e15–e24. doi: 10.1890/120329

Schwarz, J. A., Skiadaresis, G., Kohler, M., Kunz, J., Schnabel, F., Vitali, V., et al. (2019). Quantifying growth responses of trees to drought - a critique of the Lloret-indicators and recommendations for future studies. *EcoEvoRxiv* [Preprint]. doi: 10.32942/osf.io/5ke4f

Schwilk, D. W., Keeley, J. E., Knapp, E. E., McIver, J., Bailey, J. D., Fettig, C. J., et al. (2009). The national Fire and Fire Surrogate study: effects of fuel reduction methods on forest vegetation structure and fuels. *Ecol. Appl.* 19, 285–304. doi: 10.1890/07-1747.1

Skov, K. R., Kolb, T. E., and Wallin, K. F. (2005). Difference in radial growth response to restoration thinning and burning treatments between young and old ponderosa pine in Arizona. *Western J. Appl. For.* 20, 36–43. doi: 10.1093/wjaf/20.1.36

Sohn, J. A., Brooks, J. R., Bauhus, J., Kohler, M., Kolb, T. E., and McDowell, N. G. (2014). Unthinned slow-growing ponderosa pine (*Pinus ponderosa*) trees contain muted isotopic signals in tree rings as compared to thinned trees. *Trees* 28, 1035–1051. doi: 10.1007/s00468-014-1016-z

Sohn, J. A., Gebhardt, T., Ammer, C., Bauhus, J., Häberle, K.-H., Matyssek, R., et al. (2013). Mitigation of drought by thinning: short-term and long-term effects on growth and physiological performance of Norway spruce (Picea abies). *For. Ecol. Manag.* 308, 188–197. doi: 10.1016/j.foreco.2013.07.048

Sohn, J. A., Saha, S., and Bauhus, J. (2016). Potential of forest thinning to mitigate drought stress: a meta-analysis. *For. Ecol. Manag.* 380, 261–273. doi: 10.1016/j.foreco.2016.07.046

Speer, J. H. (2010). *Fundamentals of Tree-Ring Research*. Tucson: University of Arizona Press.

Stephenson, N. L., Das, A. J., Ampersee, N. J., Bulaon, B. M., and Yee, J. L. (2019). Which trees die during drought? The key role of insect host-tree selection. *J. Ecol.* 107, 2383–2401. doi: 10.1111/1365-2745.13176

Swetnam, T. W., Allen, C. D., and Betancourt, J. L. (1999). Applied historical ecology: using the past to manage for the future. *Ecol. Appl.* 9, 1189–1206. doi: 10.1890/1051-0761(1999)009%5B1189:aheutp%5D2.0.co;2

Thomas, Z., and Waring, K. M. (2015). Enhancing resiliency and restoring ecological attributes in second-growth ponderosa pine stands in northern New Mexico, USA. *For. Sci.* 61, 93–104. doi: 10.5849/forsci.13-085

Vernon, M. J., Sherriff, R. L., van Mantgem, P., and Kane, J. M. (2018). Thinning, tree-growth, and resistance to multi-year drought in a mixed-conifer forest of northern California. *For. Ecol. Manag.* 422, 190–198. doi: 10.1016/j.foreco.2018.03.043

Waring, R. H. (1987). Characteristics of trees predisposed to die. *Bioscience* 37, 569–574. doi: 10.2307/1310667

Williams, A. P., Allen, C. D., Macalady, A. K., Griffin, D., Woodhouse, C. A., Meko, D. M., et al. (2013). Temperature as a potent driver of regional forest drought stress and tree mortality. *Nat. Clim. Change* 3, 292–297. doi: 10.1038/nclimate1693

Young, D. J. N., Stevens, J. T., Earles, J. M., Moore, J., Ellis, A., Jirka, A. L., et al. (2017). Long-term climate and competition explain forest mortality patterns under extreme drought. *Ecol. Lett.* 20, 78–86. doi: 10.1111/ele.12711

Zang, C., Hartl-Meier, C., Dittmar, C., Rothe, A., and Menzel, A. (2014). Patterns of drought tolerance in major European temperate forest trees: climatic drivers and levels of variability. *Global Change Biol.* 20, 3767–3779. doi: 10.1111/gcb.12637

Conflict of Interest: The authors declare that the research was conducted in the absence of any commercial or financial relationships that could be construed as a potential conflict of interest.

frontiers in Forests and Global Change

ORIGINAL RESEARCH
published: 27 May 2020
doi: 10.3389/ffgc.2020.00062

Recovering the Metabolic, Self-Thinning, and Constant Final Yield Rules in Mono-Specific Stands

Assaad Mrad[1], Stefano Manzoni[2,3], Ram Oren[1,4], Giulia Vico[5], Magnus Lindh[2] and Gabriel Katul[1,6]*

[1] Nicholas School of the Environment, Duke University, Durham, NC, United States, [2] Department of Physical Geography, Stockholm University, Stockholm, Sweden, [3] Bolin Centre for Climate Research, Stockholm University, Stockholm, Sweden, [4] Department of Forest Science, University of Helsinki, Helsinki, Finland, [5] Department of Crop Production Ecology, Swedish University of Agricultural Sciences (SLU), Uppsala, Sweden, [6] Department of Civil and Environmental Engineering, Duke University, Durham, NC, United States

OPEN ACCESS

Edited by:
Anthony Parolari, Marquette University, United States

Reviewed by:
Yun Yang, United States Department of Agriculture, United States
Christina Tague, University of California, Santa Barbara, United States

***Correspondence:**
Assaad Mrad
mradassaad2@gmail.com

Specialty section:
This article was submitted to Forest Hydrology, a section of the journal Frontiers in Forests and Global Change

Received: *09 October 2019*
Accepted: *29 April 2020*
Published: *27 May 2020*

Citation:
Mrad A, Manzoni S, Oren R, Vico G, Lindh M and Katul G (2020) Recovering the Metabolic, Self-Thinning, and Constant Final Yield Rules in Mono-Specific Stands. Front. For. Glob. Change 3:62. doi: 10.3389/ffgc.2020.00062

Competition among plants of the same species often results in power-law relations between measures of crowding, such as plant density, and average size, such as individual biomass. Yoda's self-thinning rule, the constant final yield rule, and metabolic scaling, all link individual plant biomass to plant density and are widely applied in crop, forest, and ecosystem management. These dictate how plant biomass increases with decreasing plant density following a given power-law exponent and a constant of proportionality. While the exponent has been proposed to be universal and thus independent of species, age, environmental, and edaphic conditions, different theoretical mechanisms yield absolute values ranging from less than 1 to nearly 2. Here, eight hypothetical mechanisms linking the exponent to constraints imposed on plant competition are featured and contrasted. Using dimensional considerations applied to plants growing isometrically, the predicted exponent is −3/2 (Yoda's rule). Other theories based on metabolic arguments and network transport predict an exponent of −4/3. These rules, which describe stand dynamics over time, differ from the "rule of constant final yield" that predicts an exponent of −1 between the initial planting density and the final yield attained across stands. The latter can be recovered from statistical arguments applied at the time scale in which the site carrying capacity is approached. Numerical models of plant competition produce plant biomass-density scaling relations with an exponent between −0.9 and −1.8 depending on the mechanism and strength of plant-plant interaction. These different mechanisms are framed here as a generic dynamical system describing the scaled-up carbon economy of all plants in an ecosystem subject to differing constraints. The implications of these mechanisms for forest management under a changing climate are discussed and recent research on the effects of changing aridity and site "quality" on self-thinning are highlighted.

Keywords: constant final yield, mono-specific stand, plant biomass, plant competition, plant density, power-law, self-thinning

1. INTRODUCTION

Power-law relations in ecology remain a subject of fascination and research interest given their simultaneous ubiquity and practical significance (Thompson, 1942; Vogel, 1988; Niklas, 1994; Brown and West, 2000; Farrior et al., 2016; West, 2017). That a complex phenomenon such as competition among plants may be succinctly summarized by a power-law expression between measures of plant size (e.g., biomass) and crowding (e.g., density) is arguably one of the most important examples prominently featured in ecological textbooks and research articles alike (Perry et al., 2008). In terrestrial ecology, two power-law relations have emerged between biomass and density, both developed for dense mono-specific stands (Shinozaki and Kira, 1956; Yoda, 1963): the self-thinning or Yoda's rule and the constant final yield rule. The usage of the term "rule" reflects the extensive experimental evidence supporting the universal character of the exponents of the size-density relations. The significance of these power-law relations to crop production, forestry and ecosystem management is rarely in dispute and has been reviewed elsewhere (Willey and Heath, 1969; Drew and Flewelling, 1977, 1979; White, 1981; Westoby, 1984; Peet and Christensen, 1987; Friedman, 2016). However, the ecological mechanisms responsible for their apparent universal character remains a subject of inquiry and debate since their inception in 1864 (Spencer, 1864). This debate frames the scope of this review.

1.1. The Self-Thinning Rule

Self-thinning, depicted in **Figure 1A**, describes a natural process in a single stand whereby the number of plants per unit area (p) decreases as average plant (or mean individual) above-ground weight (w) increases as time t progresses. That is, the relation between $w(t)$ and $p(t)$ is associated with *transient* dynamics initiated when $p(t)$ begins to decline from its initial value with increasing time due to overcrowding. Self-thinning is, by definition, a process arising from space-filling where vegetation has covered the whole area under consideration. Self-thinning is presumed to be a process intrinsic to many managed and unmanaged terrestrial plant communities, whose composition and structure are influenced by competition for resources available proportionally to space—whether above-ground (e.g., photosynthetically active radiation) or below-ground (e.g., water and nutrients) (Zhang et al., 2011; Hecht et al., 2016). Therefore, w-p temporal trajectories of self-thinning have considerable implications for forest management practices (Ge et al., 2017; Zhang et al., 2019). It is to be noted, however, that $p(t)$ reductions due to ice storms, hurricanes, fires, diseases, or other disturbances are not considered in the $w-p$ relations described by self-thinning.

As shown in **Figure 1A**, self-thinning does not describe the entire temporal trajectory of $w-p$ and only "kicks in" when the $w(t)$ is large enough for a given initial density to initiate intense resource competition (i.e., space-filling). At the early stage of stand establishment, $w(t)$ may increase rapidly while the density remains at its maximum $p(t) = p_0$, where $p_0 = p(0)$ is the initial (or planting) density, until the space-filling requirement is reached.

Quantitative studies on a possible occurrence of universal $w-p$ scaling emerged from data in the early 1930s in forestry (Reineke, 1933). Using measurements collected in many overstocked forests in California (USA), presumed to be experiencing self-thinning, p was empirically linked to the mean diameter at breast height D using

$$\log\left(p\right) = C_R - 1.605\log\left(D\right), \tag{1}$$

where C_R is a species specific constant. This equation states that plant density decreases as size increases across forest stands. Equation (1) is commonly referred to as Reineke's rule or Reineke's stand density index in forestry. Contrary to initial expectations by Reineke, the coefficient -1.605 appeared invariant across many species (12 out of 14 studied), age and environmental conditions. Thus, Reineke concluded that determining density of stocking in even-aged stands using Equation (1) has the advantages of freedom from correlation with age and site quality, and thus offers simplicity and general applicability.

Reineke's rule can be recast as a power-law of the form $p = e^{C_R}D^{-1.605}$. It is evident that when linking w to D using a power-law expression derived from allometry, Reineke's rule can also be formulated as a relation between plant biomass and crowding instead of plant size and crowding. Yoda (1963) and others later popularized similar power-law expressions extending the range downward from mature forest stands to seedlings of herbaceous plants,

$$w\left(t\right) = Cp\left(t\right)^{-\alpha}, \tag{2}$$

where both $w(t)$ and $p(t)$ are time-dependent (**Figure 2**). Equation 2 is hereafter referred to as Yoda's self-thinning rule when setting the exponent $\alpha = 3/2$.

The generality of this expression and the limited variability of the exponent α imply that annual and perennial crops, herbaceous plants, and trees are expected to respond to crowding in a surprisingly similar manner (White and Harper, 1970; Gorham, 1979; Antonovics and Levin, 1980). Moreover, density manipulation experiments seem to yield $\alpha = 3/2$, yet C varies (Dean and Long, 1985). An $\alpha \approx 3/2$ was reported even in mixtures of *Sinapis alba* and *Lepidium sativum*, sown together at high densities, after having undergone collective self-thinning as described elsewhere (Bazzaz and Harper, 1976) (see **Table S1**). Nevertheless, some variability in α has been found (typically between 1 to 3/2), based on both theoretical arguments (reviewed in section 2) and empirical evidence, motivating this review.

1.2. The Constant Final Yield Rule

Equation (2) relates trends of $w(t)$ and $p(t)$ with time t in a single stand, but these two quantities can also be multiplied to calculate the biomass per unit area $y(t) = w(t)p(t)$. The constant final yield rule applies when stands sown at different initial densities p_0 all achieve the same biomass per unit area or yield y_c at a fixed time after sowing (i.e., $y_c \neq f(p_0)$; **Figures 1B,C**, **2**). To illustrate how this rule can be obtained, relations between initial planting density and stand-level yield of the following form are

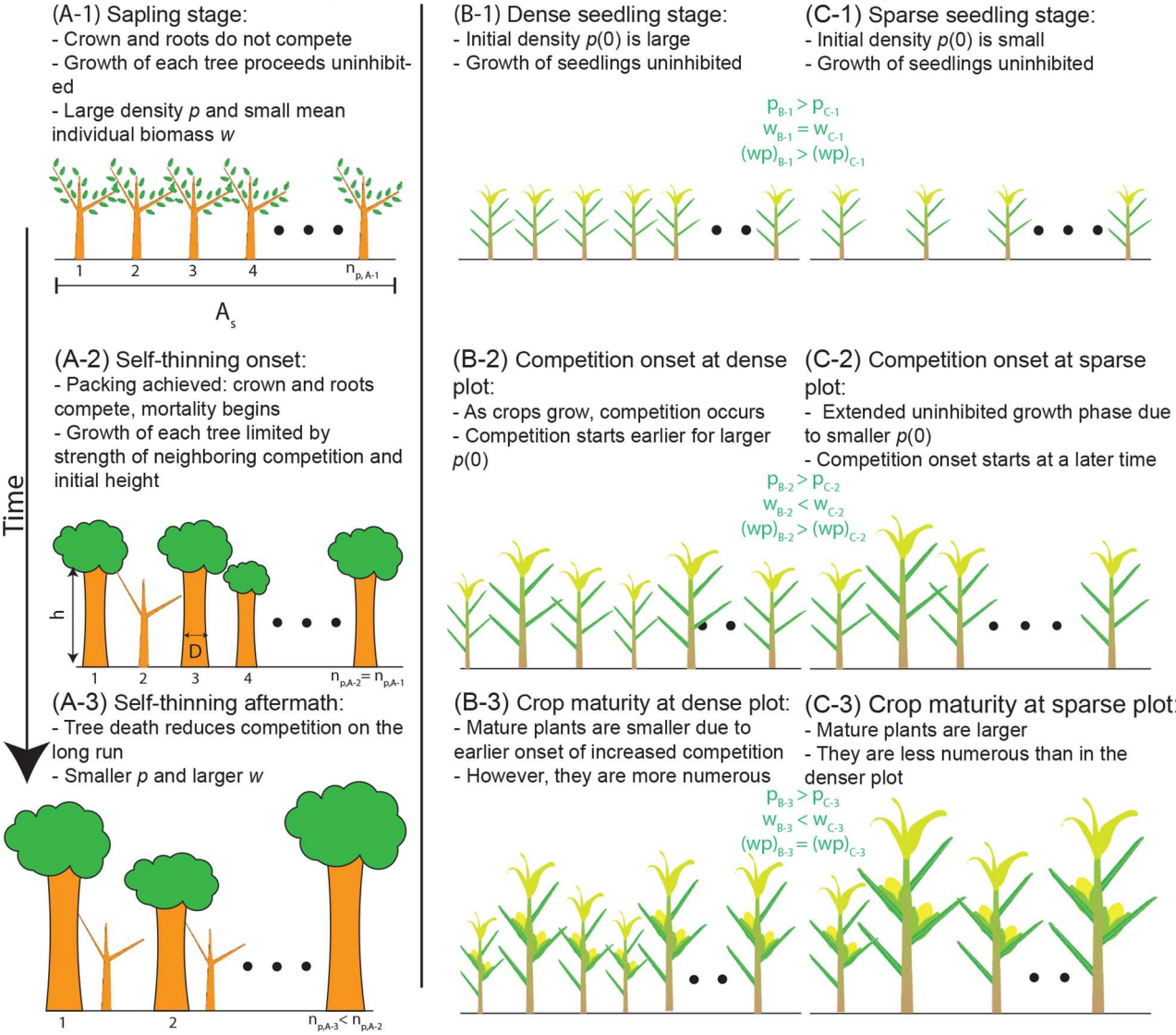

FIGURE 1 | Conceptual representations of **(A)** self-thinning and **(B,C)** the constant final yield rule. **(A)** Self-thinning is initiated after crowding occurs, resulting in decreasing plant density $p(t)$ with time t. **(B)** A high initial planting density p_0 is compensated for by poor growth conditions for each individual resulting in a small individual biomass w at harvest after an initial growth time period **(B-3)**. **(C)** Conversely, a small p_0 allows for improved growth conditions leading to higher w at harvest after the same growth time period **(C-3)**. The choice of a woody species in column **(A)** and a herbaceous species in columns **(B,C)** is to highlight the wide applicability of the self-thinning and constant final yield rules. Symbols: n_p refers to the number of plants in a plot, A_s is the plot ground area, D is the stem diameter, h is the plant height, $p = n_p/A_s$ is the plant density, w is the mean individual biomass, and the product wp is the total biomass per unit ground area at time t. Subscripts refer to the different scenarios shown.

considered (Shinozaki and Kira, 1956; Holliday, 1960; Willey and Heath, 1969; Watkinson, 1980)

$$\frac{1}{y(p_0|t)} = \frac{C_{f,1}(t)}{p_0} + C_{f,2}(t), \tag{3}$$

where y is a function of p_0 across stands at a fixed time t after sowing. In Equation (3), $C_{f,1}$ and $C_{f,2}$ are species-specific parameters that change with time (Kikuzawa, 1999). When intense resource competition has had long enough time to appreciably affect stand structure ($t >> 0$ where $t = 0$ is sowing time), the constant final yield rule dictates that $C_{f,1}\, p_0^{-1}$ becomes small compared to $C_{f,2}$ and $y(p_0|t) = y_c(t) = C_{f,2}^{-1}(t)$ (**Figure 1**).

When density-driven mortality or self-thinning is absent (i.e., $p(t) = p_0$), this rule leads to an exponent -1 between $w(p_0|t)$ and p_0, as it can be shown by multiplying both sides of Equation (3) by p_0, and recalling that $y(t) = w(t)p(t)$. This gives a relation between mean individual plant mass at steady-state and initial density,

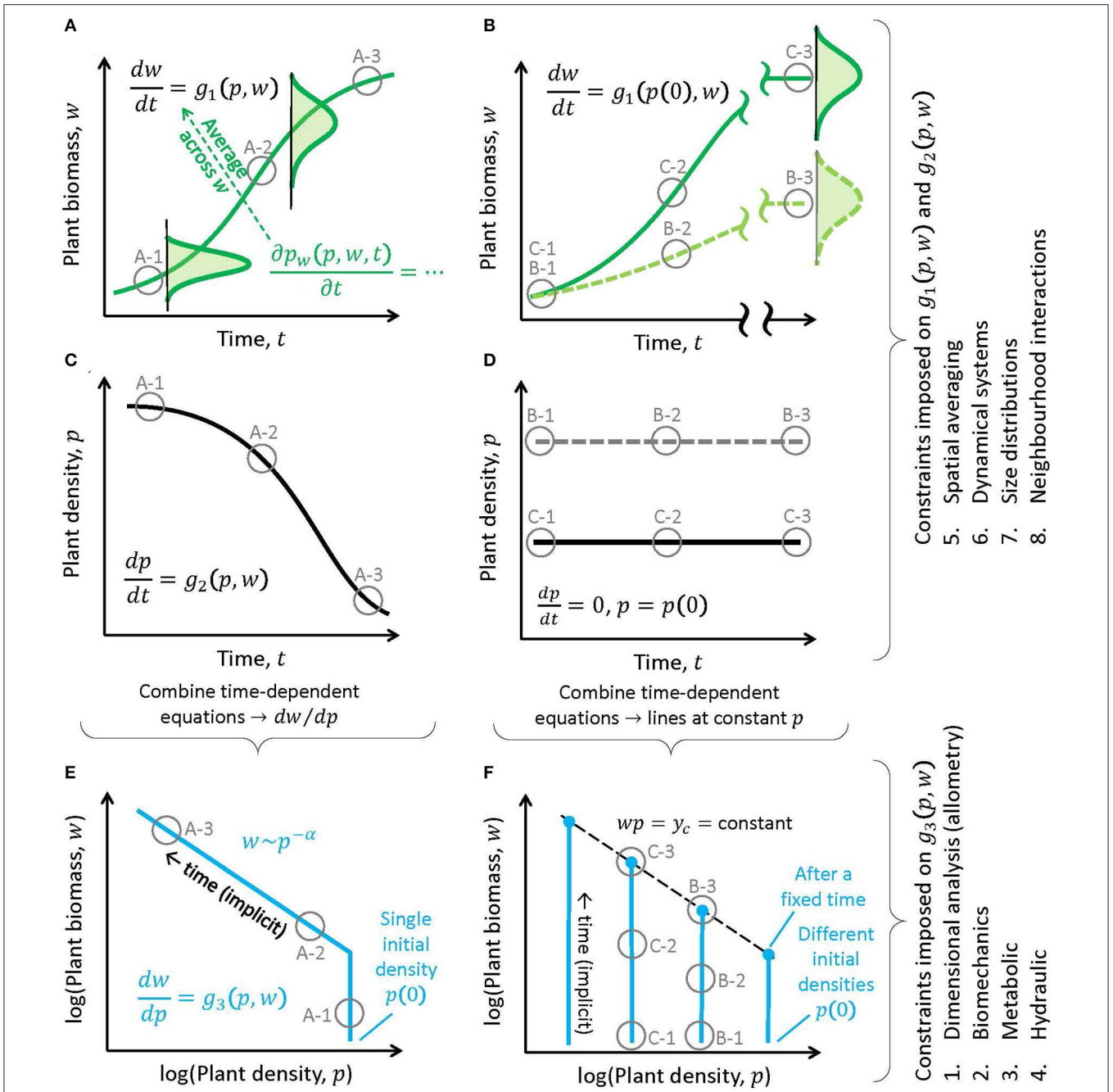

FIGURE 2 | Linkages between dynamic equations for individual plant biomass (w) and density (p; Equation 5) for the self-thinning rule ($w = Cp^{-\alpha}$; left panels) and the constant final yield rule ($y_c = wp$; right panels). **(A,B)** Illustration of the time evolution of w (green curves: mean biomass; green curves with shaded area: probability densities of individual biomass in size-structured models). **(C,D)** Illustration of the time evolution of p. Combining the dynamic equations in subplots **(A–C)** and **(B–D)**, respectively, leads to a single equation describing trajectories in the $w - p$ phase space (Equation 6): **(E)** when starting from a single initial density, different experiments and arguments show that α could vary from 1 to 3/2, or **(F)** multiple stands starting from different sowing densities achieve the same biomass per unit area y at a fixed point in time after sowing. Brackets right of the subplots: how constraints are imposed on the functions $g_{1(.)}$, $g_{2(.)}$, and $g_{3(.)}$ of Equations (5) and (6); constraint numbering refers to the model categories discussed in the text (see also Figure 3). Gray circles and labels correspond to the scenarios depicted in **Figure 1**.

$$\frac{1}{w(p_0|t)} = C_{f,1}(t) + C_{f,2}(t)\, p_0, \tag{4}$$

or $w(p_0|t) = C_{f,2}(t)\, p_0^{-1}$ when $C_{f,1}$ is negligible compared to $C_{f,2}\ p_0$ as noted earlier. Equation (4) describes how w varies with p_0 at a fixed time after sowing (comparing different stands)

TABLE 1 | Summary of the studied mechanisms leading to a different exponent α (Equation 2) along with the most pertinent equations and assumptions used.

Mechanism	α	Assumptions
1. Dimensional and allometric	1 to 3/2	1, 2 or 3-D growth; closed canopy
2. Structural and biomechanical	4/3	Elastic buckling; closed canopy
3. Metabolic and translocation network theories	4/3 or 3/2	2 or 3-D growth; volume-filling branching; imposed resource supply
4. Growth-hydraulic	4/3	Equal resource demand and supply; leaf area proportional to stem area
5. Spatial averaging	1 or α(CUE)	Carrying capacity of total biomass; coupled equation for total biomass and plant number; intrinsic growth rate∼NPP; mortality rate proportional to plant number
6. Dynamical systems	3/2, 4/3 or α(CUE)	Coupled equations for plant carbon and plant number; biomass feedback on NPP; mortality rate proportional to plant number
7. Size distribution	3/2	Equation for the evolution of plant size distribution; canopy closure under the perfect plasticity approximation; different α depending on assumptions
8. Neighborhood interactions	1 to 3/2	Equation for individual plant biomass; size asymmetry in competition; crowding effects; mortality when biomass balance < 0; different α depending on the mechanism and strength of competition

A complete list of symbols can be found in ***Table 2****.*

whereas Equation (2) describes temporal changes in w on the same stand.

In contrast to Equation (4), Equation (3) also applies with the presence of mortality. In other words, the constant final yield rule and density-driven mortality, or self-thinning, are not mutually exclusive. Constant final yield has received experimental support in crops (Shinozaki and Kira, 1956; Holliday, 1960) and in a number of tree species in forest stands (Pacala and Weiner, 1991; Xue and Hagihara, 1998; Kikuzawa, 1999) (**Table S1**).

1.3. Interpreting Self-Thinning Exponents

A range of α values can be derived from contrasting theoretical arguments suggesting that $\alpha = 3/2$ (for the self-thinning rule) and $\alpha = 1$ (for constant, time-independent yield $y \neq f(t)$) are not universal values, but rather that α may be context-dependent. On the one hand, if indeed different constraints lead to specific exponents, it might be possible to infer which processes shape forest development from observed α values. For example, different types of plant-plant interactions lead to contrasting exponents in individual-based models (as shown later in section 2.8). In turn, knowledge of the constraints at play would allow predicting how α shifts in response to changing conditions (e.g., climate and land use). On the other hand, as shown in the following, several arguments lead to similar α values, making it difficult to establish which one is dominant (**Table 1**).

An obvious question to pursue is how the exponent α reflects constraints or mechanisms controlling competition among mono-specific plants. The multiple mechanisms covered in this review are summarized in **Table 1** and relations between them are featured in **Figure 3**. That multiple mechanisms can result in the same α is not new (Pickard, 1983). What is original here is the establishment of a link between the constraint(s) on competition, the transient dynamics leading to power-law relations between w and p, and the numerical value of α. Extensions proposed here are distinguished from published arguments in subsections labeled "*Extended Analysis*" (some of which are expanded in the **Supplementary Material**). This effort is motivated both by the lack of a synthesis of the mathematical foundations of the self-thinning and constant final yield rules, and by the need to quantify how the scaling exponents may vary under future conditions, with implications for agricultural and forest management.

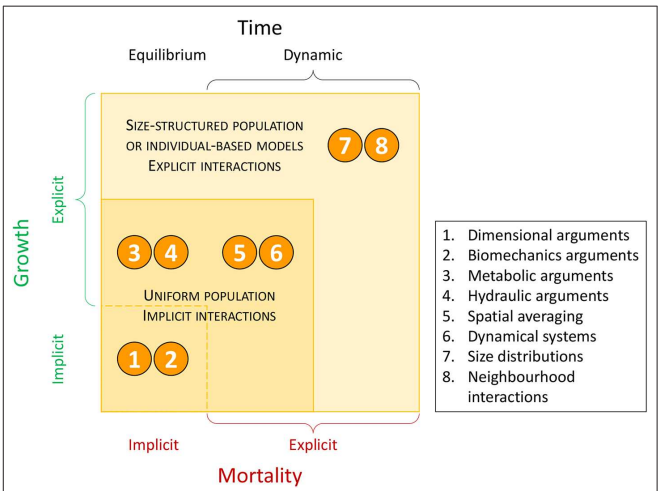

FIGURE 3 | The various mechanisms leading to the power-law relation $w(t) = C[\rho(t)]^{-\alpha}$ reviewed here. The mechanisms are grouped based on how growth and mortality are treated and whether time, age class, and resource competition among individuals are explicitly considered. Note: in all temporally dynamic mechanisms, mortality is explicit. However, an explicit account of growth does not preclude an implicit account of mortality.

2. THEORY

Additional definitions are now introduced: l is a characteristic dimension of the plant, the one most sensitive to growth, V is the whole plant volume (product of projected crown area and height), ρ is the whole plant density, i.e., the individual plant mass over the entire individual plant volume, and s is the mean ground area covered by an individual plant or tree. From these

definitions, $w = \rho V$ and crown radius is defined as $r = \sqrt{s}$. The symbols and definitions are listed in **Table 2**.

Mechanistic studies, the subject of this review, typically begin with the carbon balance of the individual plant, where the carbon gains and costs as well as their constraints must be considered. Mortality and its associated effects on stand density must also be parameterized. Hence, these studies lead to a dynamical system coupling the individual scale (e.g., the single plant weight) with the plot or ecosystem scale (e.g., the density). This two-scale system may be represented by the general expression

$$\begin{aligned} \frac{dw}{dt} &= g_1(p, w); \\ \frac{dp}{dt} &= g_2(p, w), \end{aligned} \tag{5}$$

where $g_1(.)$ and $g_2(.)$ are functions that do not explicitly vary in time (i.e., the system of equations is autonomous) and must be determined from structural, hydraulic, energetic, and physiological constraints on competition. In this two-equation system, t can be eliminated to yield

$$\frac{dw}{dp} = \frac{g_1(p, w)}{g_2(p, w)} = g_3(p, w). \tag{6}$$

Depending on the choices made for $g_1(.)$ and $g_2(.)$ [and thus for $g_3(.)$] or their constraints, a solution of the form $w = Cp^{-\alpha}$ can be recovered under certain conditions. The focus here is on the connection between the exponent α and the constraints imposed on $g_1(.)$, $g_2(.)$, or $g_3(.)$. The tactics explored to solve Equation (6) for the various constraints include (**Figure 3**) (1) allometric constraints and dimensional analysis (Shinozaki and Kira, 1956; White and Harper, 1970; Miyanishi et al., 1979; Kikuzawa, 1999), (2) structural constraints and other biomechanical arguments (McMahon, 1973; Givnish, 1986), (3) energetic constraints, metabolic arguments, and network transport theories (West et al., 1997; Enquist et al., 1998), (4) hydraulic constraints (Niklas and Spatz, 2004), (5) spatial averaging arguments at extended lifespans (Roderick and Barnes, 2004), (6) dynamical systems theory (von Bertalanffy, 1957) where $g_1(.)$ and $g_2(.)$ are specified (Hozumi, 1977; Hara, 1984; Perry, 1984; Pahor, 1985; Dewar, 1993), and (7-8) models with local interactions for resources among individuals of different sizes, or where p is linked to the dynamics of w via neighborhood interactions shaping the competition for resources (Aikman and Watkinson, 1980; Adler, 1996; Li et al., 2000; Chu et al., 2010; Coomes et al., 2011; Deng et al., 2012; Lin et al., 2013). In short, these approaches differ based on how growth and mortality are treated, and whether time, size class, and resource competition among individuals are explicit in the model. The essential elements of these approaches are briefly reviewed and connections between them highlighted.

2.1. Mechanism 1: Dimensional Analysis and Allometric Constraints

The "Principle of Similitude" is a statement about the dimensional consistency of any mathematical expression relating

TABLE 2 | List of symbols with definitions, equation where they are first used, and dimensions.

Symbol	Definition	Equation	Dimension
Common symbols			
C	Constant of the power-law between p and w	2	$ML^{2\alpha}$
C_R	Reineke's rule species-specific constant	1	-
$C_{f,1}$,$C_{f,2}$	Coefficients for final yield relation	3	M^{-1}, L^2M^{-1}
D	Mean stand diameter at breast height	1	L
g_1, g_2, g_3	Generic functions describing the dynamics of w and p	5	MT^{-1}
h	Canopy height	15	L
l	Plant characteristic dimension	-	varies
p	Plant area density (number of plants per ground area)	1	L^{-2}
s	Mean ground area covered by a plant	-	L^2
r	Crown radius ($= \sqrt{s}$)	15	L
V	Whole plant volume	-	L^3
w	Mean plant weight	2	M
y	Weight per unit area ($= wp$)	3	ML^{-2}
y_c	Constant final yield	-	ML^{-2}
α	Scaling exponent of the $p - w$ relation	2	-
ρ	Whole plant density	8	ML^{-3}
1. Dimensional and allometric arguments			
A_d	Integration constant	9	M
m	Scaling exponent between projected canopy area and l	14	-
n	Scaling exponent between V and l	14	-
E_{env}	Environmental supply of resources (e.g., energy)	12	MT^{-3}
R_p	Metabolic rate per plant	12	ML^2T^{-3}
α'_1, α'_2	Dimensionless constants/exponents	8, 10	-
β_a (β_b)	Power-law exponent between h (D) and r	16	-
λ_1, λ_2	Exponents for application of the Principle of Similitude	7	-
2. Structural and biomechanical arguments			
E	Modulus of elasticity of wood	18	$ML^{-1}T^{-2}$
h_{crit}	Height at self-buckling	18	L
ρ_W	Wood density	18	ML^{-3}
3. Metabolic arguments and translocation network theories			
D_i	Dimension of space-filling network	21	-
l_n	Linear scale of space-filling network	-	varies
R_E	Metabolic rate per unit ground area	20	MT^{-3}
V_f	Moving fluid volume	-	L^3
4. Growth-hydraulic arguments			
g_{11}, g_{22}	Constants linked to k_0, k_1, k_2, k_3, and k_4	-	-
k_0	Constant relating growth rate to w_L	23	T^{-1}
k_1	Constant relating growth rate to total biomass	23	$M^{1/4}T^{-1}$
k_2	Constant relating w_L to D	25	ML^{-2}
k_3	Constant relating w_R to w_S	26	-
$k_4 = \rho_W$	Constant relating w_S to D and h	26	ML^{-3}
w_L, w_S, w_R	Leaf, stem, root biomass	23, 24	M
5. Spatial averaging arguments			
A_s	Crop or stand area	29	L^2
C_s	Integration constant	34	M^{-1}

(Continued)

TABLE 2 | Continued

Symbol	Definition	Equation	Dimension
CUE	Plant carbon use efficiency	36	-
GPP	Gross primary productivity	-	MT^{-1}
K_c	Carrying capacity (or final yield) per ground area	30	ML^{-2}
n_p	Number of plants within A_s	32	-
NPP	Net primary productivity	36	MT^{-1}
R_A	Autotrophic respiration	36	MT^{-1}
r_c	Intrinsic specific growth rate ($\sim NPP/w$)	31	T^{-1}
w_i ($\overline{w}$)	Weight of an individual plant (arithmetic mean)	35	M
W_T	Total stand plant biomass	32	M
Y_0	Parameter group	35	varies
α_m	Mortality inverse time constant ($\sim R_A/w$)	32	T^{-1}
6. Dynamical systems theory for plant carbon balance			
a_{ag}	Fraction of P_m allocated to above-ground biomass	37	-
B_p	Constant relating P_m to p	39	varies
C_f	Constant relating LAP to w	39	varies
k_m	Maintenance respiration rate	37	T^{-1}
LAP	Leaf area of a plant	37	L^2
m_a	Exponent relating LAP to w	39	-
m_b	Exponent relating P_m to p	39	-
P_m ($P_{m,max}$)	Photosynthetic rate per leaf area (and maximum)	37, 39	ML^{-2}
7. Size distribution arguments			
a_c	Canopy area per unit ground area over D^2	43	L^{-2}
D_0	Diameter at breast height at $t = 0$	43	L
G	Plant growth rate	42	LT^{-1}
$p_D(D\|t)$	Distribution of individual sizes	42	L^{-1}
p_0	Initial plant density	43	L^{-2}
t^*	Canopy closure time	44	T
μ	Plant mortality rate	42	T^{-1}
8. Individual-based models for neighborhood interactions			
a_i	Growth rate per unit area	47	$MT^{-1}L^{-2}$
b_i	$a_i(w_{max})^{-4/3}(k_g)^{-2/3}$	47	$M^{-1}T^{-1}$
k_g	Constant relating the zone of influence s to w	48	ML^{-3}
s_i	Ground area covered by plant i	47	L^2
w_{max}	Maximum plant weight	-	M
ϕ_1	Crowding exponent describing competition	49	-
ϕ_2	Asymmetry exponent describing competition	49	-
T_p	Integration period	-	T
α_{CD}	Power-law exponent of the competition-density relation	50	-

In the far right column, L refers to generic units of length, M to mass and T to time. If an equation number is not listed, the symbol is used in the text.

physical quantities to each other, such as mass, length, and time as described in Equation (5) (Spencer, 1864). It states, simply, that terms on both sides of an equation describing a physical state need to have the same dimension. Although evident, its consequences, first pointed out by Fourier (in 1822), allow for significant results to be derived (Lemons, 2018). The "Principle of Similitude" is now invoked in the context of w-p power-law relations.

2.1.1. Extended Analysis: Applying the Principle of Similitude

The dimensions needed to describe dw/dp are mass ($[M]$) and length ($[L]$), where $[M]$ and $[L]$ signify units of mass and length. An expression for $g_3(.)$ is sought by inspecting a list of variables it might depend on such as w, p, ρ, s, r, and then combining these variables in groups that preserve the dimensions of dw/dp. The analysis is focused only on the period where self-thinning occurs, i.e., $p(t) < p_0$, not the entire trajectory linking w to p at all times. Self-thinning only commences when the length scales associated with plant position in a stand (but not necessarily plant height) are related to p. This means that p must be retained to carry $[L]$ into the equation for $g_3(.)$. If $g_3(.)$ is assumed to be independent of w, then the only mass unit available in this list of variables is ρ. Dimensional considerations of w and p alone (having dimensions of mass $[M]$ and the inverse of surface area $[L]^{-2}$, respectively) result in

$$\frac{dw}{dp} = \frac{[M]}{[L]^{-2}} \propto p^{\lambda_1}\rho^{\lambda_2} \propto \left(\frac{1}{[L]^2}\right)^{\lambda_1}\left(\frac{[M]}{[L]^3}\right)^{\lambda_2}. \quad (7)$$

Matching the units on the most left-hand side to the most right-hand side requires $\lambda_2 = 1$, and $2\lambda_1 + 3\lambda_2 = -2$, or $\lambda_1 = -5/2$. Hence, $g_3(\rho, p) \propto \rho\, p^{-5/2}$ (a power-law as expected from such dimensional analysis). Replacing the proportionality symbol with a dimensionless constant α_1' results in

$$\frac{dw}{dp} = \alpha_1'\, \rho\, p^{-5/2}. \quad (8)$$

Provided ρ is not impacted by p, although it can vary in time, the ordinary differential Equation (8) can be solved to yield

$$w = A_d - (2/3)\,\alpha_1'\, p^{-3/2}, \quad (9)$$

where A_d is an integration constant that must be determined from other considerations. This argument apparently recovers Yoda's rule without any explicit considerations to p declining with increasing t as necessary for self-thinning. However, assuming that the length scales are all related to p implicitly means that crowding has occurred.

Likewise, if w replaces ρ, then dimensional considerations alone result in

$$\frac{dw}{dp} = \alpha_2'\frac{w}{p}, \quad (10)$$

where α_2' is a dimensionless constant. Solving this equation leads to $w = A_d p^{\alpha_2'}$, which again is a power-law. In this case, dimensional analysis fails to determine the numerical value of the exponent α_2', but it still predicts a power-law relation between w and p. Clearly, the choice of variables impacting $g_3(.)$ or the constraints imposed on it affects the value of the exponent α. For

example, if the constraint is a constant total mass in time (i.e., $dy/dt = 0$), then it directly follows that

$$\frac{d(wp)}{dt} = w\frac{dp}{dt} + p\frac{dw}{dt} = 0 \Rightarrow \frac{dw}{dp} = -1\frac{w}{p}. \quad (11)$$

That is, the constant total mass in time acts as a new constraint, allowing the determination of $\alpha_2' = -1$ and the achievement of a constant yield y_c.

The main constraint on the outcome of competition may be a constant energy (or limiting resource) per unit area supplied by the environment R_{env}. When this constant (in time) supply satisfies the ecosystem metabolic demands per unit area, $R_{env} = p\,R_p$, where R_p is basal metabolic rate per individual plant, then

$$\frac{dR_{env}}{dt} = 0 = \frac{d(p\,R_p)}{dt} \Rightarrow \frac{dp}{p} = -1\frac{dR_p}{R_p}. \quad (12)$$

This system yields $p \sim R_p^{-1}$. In metabolic theory, R_p is uniquely determined by w and the temperature of the environment (Brown et al., 2004). Employing Kleiber's law (Kleiber, 1932)

$$R_p \sim w^{3/4} \quad (13)$$

and inserting this result into $p \sim R_p^{-1}$, directly recovers the exponent $\alpha = 4/3$ (i.e., the metabolic argument).

2.1.2. Allometry and Growth Habits as Constraints

Self-thinning is initiated when packing is achieved: the ground area is entirely covered by the plants or trees as discussed elsewhere (Miyanishi et al., 1979). It is emphasized that the probability that some local densities will achieve packing before the majority does is neglected, because p is a property that pertains to the whole ground area. If plant growth is three-dimensional (i.e., height and crown diameter are increasing proportionally with increasing individual biomass) and ρ is constant, then $V \sim l^3$, $w \sim \rho l^3$, $s \sim l^2$. Self-thinning occurs when $s \sim p^{-1}$. When this point is reached, $l \sim s^{1/2} \sim p^{-1/2}$. Thus, all length scales are now linked to p as foreshadowed earlier. Yoda's rule is directly recovered by noting that $w \sim \rho l^3 \sim \rho p^{-3/2}$, which is the key result in Equation (9). This argument assumes that the increment of plant size is isometric and proportional in all three dimensions (Miyanishi et al., 1979). Linking w to l, and all length scales to p, is akin to setting $g_3(.)$ of Equation (6) to uniquely depend on the density (p) over the course of self-thinning.

Other growth habits may now be analyzed, and two limiting cases are illustrated: prostrate ground cover plants (i.e., 2-D growth) to etiolated seedlings (i.e., 1-D growth). To place these growth habits in a framework that employs allometric scaling, it is assumed that $V \sim l^m$ and $s \sim l^n$. Hence, $w \sim \rho l^m$ and at the incipient point of self-thinning, the condition $s \sim p^{-1}$ must be maintained. These assumptions lead to

$$w = Cp^{-m/n}, \quad (14)$$

where $m = 3$ (i.e., 3-D growth) and $n = 2$ recovers Yoda's rule, and C is a proportionality constant. For prostrate ground cover plants, $m = 2$ and $n = 2$ resulting in $w \sim p^{-1}$. For etiolated seedlings, the cross-sectional area is assumed constant and growth only occurs in the vertical (a race to harvest light). Hence, $m = 1$ and, with mean ground area covered by a plant being constant, requires s to be constant and thus $n = 0$. Hence, $w \sim p^{-1/0}$ yields infinite exponent, or stated differently, no self-thinning is to be expected (Miyanishi et al., 1979).

2.1.3. Extended Analysis: Reineke's vs. Yoda's Rules

Having covered the growth habits, it is now instructive to distinguish between a vertical dimension (canopy height h) and a horizontal dimension (canopy radius r), which allow recasting Equation (14) as

$$\log(p) = \frac{n}{m}\log(C) - \frac{n}{m}\log\left[\rho(r^2 h)\right], \quad (15)$$

where $w = \rho(r^2 h)$. When Equation (15) is combined with an allometric expression linking h to r of the form $h \sim r^{\beta_a}$, and when relating r to stem diameter D of the form $r \sim D^{\beta_b}$ (Enquist et al., 2009), the outcome is

$$\log(p) = \frac{n}{m}\log\left(\frac{C}{\rho}\right) - \beta_b(2+\beta_a)\frac{n}{m}\log(D). \quad (16)$$

Comparing Equation (16) with Reineke's Equation (1) suggests that the exponents of the height-to-canopy radius (β_a) and canopy radius-to-stem diameter (β_b) allometries must be constrained by

$$1.605\frac{m}{n} = \beta_b\,(2+\beta_a)\,. \quad (17)$$

For $m = 3$ and $n = 2$ (i.e., Yoda's rule), $\beta_b(2+\beta_a) \approx 2.4$. The immediate consequence of this combination is that $V \sim (r^2 h) \sim D^{2.4}$. Conversion of D to a characteristic scale $l \sim r$, results in $V \sim l^{\frac{2.4}{\beta_b}}$ and not $V \sim l^3$. Notably, scaling relations discussed elsewhere (Enquist et al., 2009) provide $\beta_a = 1.14$ and $\beta_b = 0.684$ so that $\beta_b\,(2+\beta_a) \approx 2.2$, lower than the 2.4 value obtained above. Therefore, only for particular choices of the coefficient in Reineke's Equation (1) and of the scaling exponents β_a and β_b, can the relation $V \sim l^3$ be recovered. In fact, this corroborates the point made by the incisive analysis of Weller (1987) that Yoda's exponent $\alpha = \frac{3}{2}$ may be the exception rather than the rule.

As the stand becomes crowded, more individuals are suppressed. Acclimation allows suppressed individuals to survive longer by decreasing the carbon investment in diameter relative to height and maintaining smaller crowns closer to the top of the canopy. These adjustments decrease β_b of the entire stand. A reduction in β_b is expected to reduce the slope of the $p - w$ scaling (e.g., m/n in Equation 17). The reduction in crown size of suppressed individuals reduces the wind-induced drag force, allowing these trees to maintain structural integrity despite the lower taper.

2.2. Mechanism 2: Structural and Biomechanical Constraints

Relations between height and diameter can be derived to further constrain allometric scaling based on self-buckling or structural

considerations. The key observation regarding self-buckling for trees is that the critical height for buckling (h_{crit}) plotted against tree base diameter (D) follows a power-law of the form $h_{crit} \sim D^{2/3}$ for nearly every American tree species (McMahon, 1973) (**Table S1**). This $h - D$ scaling was consistent with the incipient point of buckling of tall columns (due to their own weight) given by the elastic buckling criterion (or Euler-Greenhill formula)

$$h_{crit} \propto \frac{E}{\rho_W} D^{2/3}, \tag{18}$$

where E is the modulus of elasticity, ρ_W is the density of wood. If Equation (18) describes an allometric scaling law, then for 3-D growth, $l \sim D$, $V \sim D^2 h_{crit} \sim D^{8/3}$, and $s \sim D^2$. Employing once more the allometric scaling framework presented previously, $w \sim (\rho) l^{m=8/3}$, and $s \sim l^{n=2}$. Inserting these estimates of m and n in Equation (14) result in (McMahon, 1973)

$$w \sim p^{-4/3}. \tag{19}$$

This scaling is intermediate between a steady state biomass per individual ($\alpha = 1$) and Yoda's rule ($\alpha = 3/2$). Connections between the aforementioned scaling law in Equation (19) and metabolic arguments (i.e., Kleiber's law) have already been noted (McMahon, 1973). However, the scaling law in Equation (19) can also be derived without resorting to self-buckling, using a variant of the growth-hydraulic constraint (Niklas and Spatz, 2004), as well as metabolic constraints, as described later on. Additional implications of self-buckling are explored in the **Supplementary Material**.

2.3. Mechanism 3: Metabolic Limitations

Metabolic arguments and their connection to the exponent α have been popularized by the work of West, Enquist, and Brown (West et al., 1997; Enquist et al., 1998; Brown et al., 2004). To sustain a total biomass per unit ground area wp requires a rate of energy (or other limiting resource) supply from the environment per unit area of at least $R_E = pR_p$, where R_p is the metabolic rate per plant (energy or resource use per time per plant). In living organisms, the basal metabolic rate R_p varies with size and is given by Kleiber's law (Equation 13) (Kleiber, 1932; Banavar et al., 1999). Hence, $R_E = pR_p \sim pw^{3/4}$.

2.3.1. A Steady State Resource Balance

The case of a limiting essential resource is first considered. When the external environmental supply of this resource ($= E_{env}$) is balanced, or fully exploited, by the stand (or ecosystem) metabolic demand R_E, then

$$E_{env} = R_E \sim pw^{3/4}, \tag{20}$$

resulting in $w \sim p^{-4/3}$ when E_{env} is set to a constant (e.g., a given annual shortwave radiation or precipitation rate). For all practical purposes, Equation (20) is an equilibrium argument (constant resource supply) with a constraint shaping $g_1(.)$ in Equation (5) at a given supply E_{env}. It is also interesting to note that Equation (20) suggests a link between the constant C in Equation (2) and environmental conditions, as $C \sim E_{env}^{4/3}$. The debate on the difference between the 4/3 and the 3/2 exponents are highlighted as they offer a new perspective on links between the scaling exponent α and the constraints. The $\alpha = 4/3$ exponent has experimental support when average "mature" plant weight is plotted against p_0 for different species spanning nine orders of magnitude by weight (Enquist et al., 1998) and appears consistent with a number of spatially explicit simulation studies discussed elsewhere (Deng et al., 2012) (**Table S1**). Such an inter-species comparison, however, fundamentally differs from plotting $w(t)$ against $p(t)$ for a single stand across time (Yoda, 1963).

2.3.2. Extended Analysis: Constraints on the Trans-location Network Distribution

It has been argued that distributed trans-location networks evolved from a need for effective connectivity with increased size (i.e., analogous to the economy of scale in microeconomics). Distributed trans-location networks occur in biological systems (including respiratory networks) and in inanimate systems alike (e.g., river networks). The flow rate in an arbitrary trans-location network can be derived as a function of the local connectivity as discussed elsewhere (Banavar et al., 1999). For the problem at hand, this trans-location network may represent the phloem, where metabolic products derived from photosynthesis (mainly carbohydrates) are being translocated from leaves, or the xylem, where water is transported to the leaves. In this network derivation, a moving fluid volume filling the network is assumed to be V_f. The V_f scales with the product of the number of links in the network and the distance between nodes. In a D_i-dimensional space-filling network (i.e., a network that can deliver fluid to all the domain), the number of links is proportional to $l_n^{D_i}$, where l_n is a linear scale of the network. The distance among links is also proportional to l_n. Hence, $V_f \sim l_n^{D_i} \times l_n = l_n^{D_i+1}$, or $l_n \sim V_f^{1/(D_i+1)}$. For a constant fluid density, $w \sim V_f$ and $R_p \sim l_n^{D_i}$. It directly follows that the metabolic rate for an individual is given by

$$R_p \sim w^{D_i/(1+D_i)}. \tag{21}$$

For $R_E = pR_p = E_{env} = constant$, it follows that $R_p \sim p^{-1}$ as before. As a result, Equation (21) is used to obtain

$$w \sim p^{-(1+1/D_i)}. \tag{22}$$

For $D_i = 3$, the 3/4 metabolic scaling exponent is recovered from Equation (21), and $\alpha = 4/3$ is now recovered from Equation (22) in a manner that is compatible with Kleiber's law without resorting to critical height and self-buckling. Interestingly, the analysis here also suggests that Yoda's 3/2 scaling exponent is recovered for $D_i = 2$ (i.e., $R_p \sim w^{2/3}$). A 2-D translocation network may be incompatible with Yoda's original assumption of proportional growth in all three dimensions. This incompatibility is one of the salient features of the aforementioned controversy surrounding the 4/3 vs. the 3/2 self-thinning scaling exponent.

2.4. Mechanism 4: Hydraulic Constraints on Growth

In addition to structural and energy supply constraints discussed as mechanisms 2 and 3, a hydraulic constraint can be formulated

by imposing a steady-state transpiration rate from the roots to the leaves. This constraint may be viewed as a "network-on-network" supply constraint. There are three networks that must be coordinated: a root network that must harvest water and nutrients from the soil, a xylem network that must deliver water to leaves, and distributed end-nodes for water loss through leaves. It is assumed that these three networks are sufficiently coordinated so that no severe "bottleneck" in one network routinely impairs the function of the other two networks (Thompson and Katul, 2012; Huang et al., 2018). Based on this view, a simplified version of a growth-hydraulic constraint (Niklas and Spatz, 2004) is now reviewed. In this mechanism, it is assumed that the annual increment of dry matter per plant scales (i) linearly with standing leaf biomass w_L that provides metabolic products and (ii) with $w^{3/4}$ as in Kleiber's law. Hence, equating these two assumptions results in

$$k_0 w_L = k_1 w^{3/4}, \tag{23}$$

where k_0 and k_1 denote allometric constants. With w defined by the sum of leaf, stem, and root mass (i.e., $w = w_L + w_S + w_R$) results in

$$k_0 w_L = k_1 \left(w_L + w_S + w_R\right)^{3/4}. \tag{24}$$

The hydraulic component of this argument is framed as follows (Niklas and Spatz, 2004): the amount of water absorbed by roots per unit time must pass through stems, experience a phase transition and then exit through the stomata distributed on leaf surfaces. Because this amount of water loss is conserved throughout the plant (i.e., no storage or capacitive effects on time scales commensurate with stand development), w_L must scale with the hydraulically functional cross-sectional area of stems and roots (sapwood area). The key assumption is that the sapwood area is proportional to the square of the stem diameter (i.e., D^2). The assumption need not imply that the diameter of the water transporting vessels is proportional to D, but that D reflects the total number of vessels of fixed diameter. Viewed from this perspective, this assumption may also be interpreted as another expression of the so-called da Vinci rule, or the pipe flow model of Shinozaki (Shinozaki et al., 1964; Horn, 2000), and leads to $w_L = k_2 D^2$. Substituting w_L in Equation 24 and rearranging the terms lead to

$$\left(\frac{k_0}{k_1} k_2 D^2\right)^{4/3} - k_2 D^2 = w_S + w_R. \tag{25}$$

Two additional assumptions are required (Niklas and Spatz, 2004): an allometric relation between root and stem biomass ($w_R = k_3 w_S$) and a relation between stem biomass and stem volume (i.e., $w_S = k_4(D^2 h)$), where $k_4 = \rho_W$, but the notation of Niklas and Spatz (2004) is maintained in the following. Hence, Equation (25) can be formulated as

$$\left(\frac{k_0}{k_1} k_2 D^2\right)^{4/3} - k_2 D^2 = \left(1 + k_3\right) k_4 (D^2 h), \tag{26}$$

from which it follows that $h \propto D^{2/3}$ and $w_S \propto D^{8/3}$. Upon comparison with the Euler-Greenhill formula (Equation 18), the same $h \propto D^{2/3}$ scaling has been recovered from metabolic and hydraulic constraints acting in concert (i.e., in coordination), not from mechanical limits on tree height, nor from energy supply by the environment. Combining these outcomes with $w \propto (D^2 h) = D^{8/3}$, $s \sim D^2$, and $s \sim p^{-1}$ (or $D \propto p^{-1/2}$) at the point where self-thinning commences, recovers the metabolic formulation $w \sim p^{-4/3}$. Here, geometric packing (i.e., $s \sim p^{-1}$) leading to self-thinning is necessary to arrive at $\alpha = 4/3$, which was not the case in the metabolic arguments.

2.4.1. Extended Analysis: An Alternative Hydraulic Link to Stem Diameter

The aforementioned arguments may be generalized to include other linkages between sapwood area and stem diameter. One such linkage is the so-called Hess-Murray law that predicts the optimal blood vessel tapering in cardiovascular systems. This linkage leads to $w_L \propto D^3$ (Murray, 1926; McCulloh et al., 2003) instead of D^2. Starting again from Equation (24), the aforementioned argument leads to

$$\frac{\left(\frac{k_0}{k_1} k_2 D^2\right)^{4/3} - k_2 D^3}{D^2\left(1 + k_3\right) k_4} = h, \tag{27}$$

or $h \sim D^{2/3}$ for small D only, not for any D as it was the case for the Da Vinci rule. For intermediate or large D, $h \sim g_{11} D^{2/3} - g_{22} D$ (g_{11} and g_{22} are constants linked to k_0, k_1, k_2, k_3, k_4), which does not exhibit a unique exponent provided $D < (g_{11}/g_{22})^3$. The connection between the da Vinci rule (along with the pipe flow model) and water transport has been the subject of debate outside the scope of the present work (Bohrer et al., 2005), with some arguing that the da Vinci rule is compatible with structural, rather than water transport theories (Eloy, 2011).

2.5. Mechanism 5: Spatial Averaging Arguments

This approach explicitly considers that stands generally comprise individuals of different sizes, even in even-aged mono-cultures, owing to small genetic variability as well as variations in site micro-environmental factors, impacting growth potential and access to resources. It is thus necessary to consider the effect of spatial averaging over individuals within the crop or stand area A_s. By definition, $p = n_p/A_s$ where n_p is the number of individual plants within area A_s. Also, the arithmetic mean weight of all individuals within A_s is defined as

$$\overline{w} = \frac{1}{n_p} \sum_{i=1}^{i=n_p} w_i, \tag{28}$$

where w_i is the weight of each individual plant. Equation (28) can be rearranged to yield (Roderick and Barnes, 2004)

$$\overline{w} = \left(\frac{A_s}{n_p}\right) \frac{1}{A_s} \sum_{i=1}^{i=n_p} w_i = \left(p^{-1}\right) \frac{1}{A_s} \sum_{i=1}^{i=n_p} w_i. \tag{29}$$

It was suggested that over an extended life span, the total stand biomass dynamics eventually reaches a steady-state such

as in the experiments of Shinozaki and Kira (1956) on soybean, a herbaceous species, where mortality was absent (**Table S1**). If such steady-state conditions are attained within a single stand, then

$$\frac{1}{A_s}\sum_{i=1}^{i=n_p} w_i = K_c, \tag{30}$$

where K_c is a constant carrying capacity determined by the available resources supporting maximum biomass per unit area. Equation (30) implies that $\alpha = 1$ because $w = K_c p^{-1}$ as long as K_c is constant. The derivation of Equation (30) makes no assumption about p_0, $p(t)$ or $w(t)$, or that $y(t)$ follows logistic growth as in the competition-density effect (Shinozaki and Kira, 1956; Xue and Hagihara, 1998). Equation (30) was also shown to apply for a pine stand (Xue and Hagihara, 1998).

For prostrate ground cover plant growth, the emergent scaling law was already shown to be $w(t) \sim p(t)^{-1}$ using an entirely different set of assumptions. Evidently, the $\alpha = 1$ scaling exponent can be recovered from multiple mechanisms. It is demonstrated next that (i) $w(t) \sim p(t)^{-1}$ may still reflect a correct minimum exponent under weak self-thinning style competition and (ii) novel links can be established between the newly derived exponent here and other "conservative" ratios describing stand carbon dynamics.

2.5.1. Extended Analysis: Recovering the $\alpha = -1$ Exponent From a Dynamical System

The previous argument can be extended by relaxing the assumption of steady state, showing that the same result is obtained in a more general case. As a point of departure from prior work (Roderick and Barnes, 2004), the $\alpha = 1$ exponent is now analyzed using the framework of Equation (5). To facilitate this analysis, the total stand weight $W_T = n_p\overline{w}$ is assumed to vary logistically in time using (Verhulst, 1838)

$$\frac{dW_T}{dt} = r_c W_T\left(1 - \frac{W_T}{A_s K_c}\right), \tag{31}$$

where r_c is the intrinsic growth rate. This assumption has been used in the original work of Shinozaki and Kira (1956) at the individual level and generalized by others at the stand level (e.g., Xue and Hagihara, 1998). Such assumption is equivalent to prescribing $g_1(.)$ and $g_2(.)$ of Equation (5). Instead of analyzing the dynamics at an equilibrium point $W_T/A_s = K_c$ being constant, it is instructive to explore the transient dynamics where $n_p = pA_s$ begins to decline in time. This type of competition is intended to resemble some but not all aspects of self-thinning (i.e., being a transient and operating when $dn_p/dt < 0$) while maintaining a density-dependent logistic form for total biomass (instead of constant K_c) used by Shinozaki and Kira (1956). In particular, we ask under what conditions such a "stylized competition" remains compatible with scaling laws associated with a steady state yield or the self-thinning rule (or intermediates). A minimal model describing the n_p decline is

$$\frac{dn_p}{dt} = A_s\frac{dp}{dt} = A_s g_2(p) = -\alpha_m n_p, \tag{32}$$

where α_m is a mortality inverse time constant. Equation (32) specifies the reduction in the number of plants through mortality as proportional to the number of plants n_p thus making n_p an exponential function of time. Again, viewed from the perspective of Equations (5), these approximations are equivalent to specifying $g_2(p)$ and $g_1(w, p)$ via Equation (31) when recalling that $W_T = n_p w$. By eliminating time t in Equations (31) and (32) (as before, to obtain Equation 6), an ordinary differential equation describing the variations of w with n_p can be explicitly derived,

$$\frac{dw}{dn_p} + \frac{w}{n_p}\left[1 + \frac{r_c}{\alpha_m}\left(1 - \frac{n_p w}{K_c A_s}\right)\right] = 0. \tag{33}$$

The general solution of Equation (33) is given by

$$w(t) = \frac{A_s}{n_p(t)}K_c\left[\frac{1}{1 + C_s K_c A_s n_p(t)^{(r_c/\alpha_m)}}\right], \tag{34}$$

where C_s is an integration constant. Noting again that $p^{-1} = A_s/n_p$, Equation (34) can be expressed as

$$w(t) = K_c p(t)^{-1}\left[\frac{1}{1 + Y_0 p(t)^{(r_c/\alpha_m)}}\right], \tag{35}$$

where $Y_0 = C_s K_c A_s^{(r_c/\alpha_m + 1)}$. Equation (35) recovers $w(t) = K_c p(t)^{-1}$ when $Y_0 p^{(r_c/\alpha_m)} << 1$. When $Y_0 p^{(r_c/\alpha_m)} >> 1$, Equation (35) predicts a $w \sim p^{-[1+(r_c/\alpha_m)]}$. For $Y_0 p^{(r_c/\alpha_m)}$ of the order of unity, no unique scaling exponent exists, although any power-law approximation to this solution must yield exponents exceeding unity in magnitude, which is the sought result. This finding offers an explanation as to why the exponent α varies between 1 and 2 across many data sets *a priori* conditioned on $dn_p/dt < 0$ (i.e., when mortality begins to play a role).

2.5.2. Extended Analysis: the Effects of Invariant Carbon-Use Efficiency on Self-Thinning

The quantity r_c/α_m reflects the ratio of two time scales: one associated with net carbon gain of an individual plant ($1/r_c$) and another associated with its mortality ($1/\alpha_m$). The time scale for carbon gain may be associated with the net primary productivity (NPP) of an individual plant, so that $r_c \sim NPP/w$ (Thurner et al., 2016). In self-thinning stands where carbon loss in respiration is not compensated by photosynthesis in highly suppressed individuals (under light competition), it may be (simplistically) assumed that carbon starvation is the causal mechanism of mortality. Thus, the mortality time scale is associated with autotrophic respiration R_A, so that $\alpha_m \sim R_A/w$ and

$$\frac{r_c}{\alpha_m} = \frac{\text{NPP}}{R_A} = \frac{\text{CUE}}{1 - \text{CUE}}, \tag{36}$$

where NPP=CUE×GPP, GPP is the gross primary productivity, R_A=GPP-NPP=(1-CUE) GPP, and CUE is the plant carbon use efficiency ($0 < \text{CUE} < 1$). Therefore, this link between r_c/α_m and CUE offers a new perspective about α and carbon use efficiency; i.e., $\alpha = 1 + (r_c/\alpha_m) = (1 - \text{CUE})^{-1}$. This estimate

of α is expected to be an upper limit, because α_m is likely to be underestimated when mortality time scale is estimated from R_A.

The value of plant CUE typically ranges between 0.4 and 0.8 depending on species, plant age, and growing conditions, with values even lower than 0.4 in mature trees and generally higher values in rapidly growing crop species (Manzoni et al., 2018). For an intermediate CUE=0.47 (typical in forests; Waring et al., 1998), large scaling exponents are obtained, $w \sim p^{-1.88}$ as already foreshadowed. For relatively inefficient plants with CUE=1/3, $w \sim p^{-3/2}$, recovering Yoda's rule. The metabolic argument $w \sim p^{-4/3}$ can only be recovered for CUE=1/4. This argument is prone to large uncertainties due to both the qualitative link between parameters r_c and α_m, and CUE, and the uncertainties in CUE estimates. Nevertheless, plants that are more effective in converting resources to biomass are expected to exhibit steeper $w-p$ scaling relations, a conjecture to be explored in future studies.

Up to this point, it was assumed that at the individual plant scale, the entire biomass captured in w is alive and contributes to respiration. However, for a preset total biomass, lower initial density may lead to greater live crown ratio at the incipient point of self-thinning. Hanging onto large branches at the bottom of long crowns contributes little to annual photosynthesis (Oren et al., 1986), but requires investment in maintaining active sapwood, cambium, and phloem. Thus, the initial planting density can play a role in determining the fraction of live to total biomass at the start of self-thinning. At that point, despite similarities in stand density, mean total individual tree biomass (Peet and Christensen, 1987), and leaf area (Dean and Long, 1985), stands characterized by individuals with a higher fraction of live to total biomass may exhibit higher whole-tree respiration rates per unit of leaf area and, therefore, reduced CUE and α.

2.6. Mechanism 6: Dynamical Systems Theories for Plant Carbon Balance

A number of approaches have been proposed that recover the self-thinning rule from a mechanistic representation of the plant carbon balance (Hozumi, 1977; Pickard, 1983; Hara, 1984; Perry, 1984; Pahor, 1985; Voit, 1988). Common to all these approaches is the so-called von Bertalanffy equation (von Bertalanffy, 1957; Perry, 1984) or a variant of it that applies to individual plants as discussed in **Figure 3**. Using the framework of Equation (5), this equation represents $g_1(w,p)$ as

$$\frac{dw}{dt} = g_1(w,p) = a_{ag}P_m(p)\mathrm{LAP}(w) - k_m w, \tag{37}$$

where a_{ag} is the fraction of photosynthesis allocated to biomass, LAP is the leaf area of an individual plant, assumed to vary with w, P_m is the photosynthetic rate per unit leaf area, varying with p (e.g.,due to light competition), and k_m is the rate of maintenance respiration (whereas mortality is described by Equation 32). The overarching assumption of von Bertalanffy equation is that resource acquisition must traverse a limiting surface area (here LAP; scales as $\sim l^2$) whereas respiratory and maintenance costs vary with plant size (or mass, w; scales as $\sim l^3$). Variants to Equation (37) include complex expressions for photosynthetic gains, respiratory losses, connections between P_m and p (such connections are the subject of spatially explicit models discussed later), and the partitioning of w into metabolically active and inactive parts.

The goal of this section is not to review all of them but to offer links between the von Bertalanffy equation and the general framework set in Equation (5). Equation (37) is coupled to Equation (32) after eliminating time t and substituting $n_p = A_s p$ to yield

$$\frac{dw}{dp} - \frac{k_m}{\alpha_m}\frac{w}{p} = -\frac{1}{p}\frac{a_{ag}P_m\mathrm{LAP}}{\alpha_m}. \tag{38}$$

Mechanistic models link LAP to w using allometric rules and P_m to p assuming that increases in p reduces the main resource driving photosynthesis such as photosynthetically active radiation (Perry, 1984). For example, LAP and P_m may be expressed as

$$\begin{aligned} \mathrm{LAP} &= C_f w^{m_a}; \\ \frac{P_m}{P_{m,max}} &= 1 - \exp\left[-B_p p^{m_b}\right]. \end{aligned} \tag{39}$$

Here, $m_a \approx 0.81$ and $C_f \approx 0.011$ when LAP is treated as all sided (in m^2) and w is expressed in grams (determined for a wide range of species), whereas $B_p = 4.61$ and m_b was varied as a control parameter (plausible values for most species in Perry, 1984). The representation in Equation (39) preserves the autonomous nature of Equation (38) thereby linking the phase-space of the $p-w$ trajectories directly to model parameters. It also provides a complete description of $g_3(w,p)$ in Equation (6). However, a unique power-law solution of the form $w = Cp^{-\alpha}$ is not apparent even though model calculations suggest an approximate power-law with exponent $\alpha = 1.0 - 1.8$ for plausible parameter combinations. We now seek to clarify the connection between the von Bertalanffy equation and the exponent α for certain approximations revising the mathematical form of $g_3(.)$.

2.6.1. Extended Analysis: Power-Laws From the von Bertalanffy Equation

To extract power-law features from the von Bertalanffy equation and place them in the framework of Equation (5), it is assumed again that individual GPP$= a_{ag}P_m\mathrm{LAP} = R_A/(1-\mathrm{CUE})$ and $R_A \approx k_m w$, resulting in an estimate of $a_{ag}P_m\mathrm{LAP} = k_m w/(1-\mathrm{CUE})$. Hence, Equation (38) reduces to

$$\frac{dw}{dp} - \frac{w}{p}\frac{k_m}{\alpha_m}\frac{\mathrm{CUE}}{\mathrm{CUE}-1} = 0. \tag{40}$$

The solution to Equation (40) is now a power-law of the form

$$w \sim p^{-\frac{k_m}{\alpha_m}\frac{\mathrm{CUE}}{1-\mathrm{CUE}}}. \tag{41}$$

Yoda's rule is recovered when $(k_m/\alpha_m) = (3/2)(\mathrm{CUE}^{-1}-1)$ whereas the metabolic exponent is recovered when $k_m/\alpha_m = (4/3)(\mathrm{CUE}^{-1}-1)$. Because CUE $\approx$ 0.5 (Waring et al., 1998; Manzoni et al., 2018), this analysis leads to a unique relation

between respiratory and mortality time scales, and the exponent α given by $k_m/\alpha_m \approx 3/2$, 4/3, or 1. That is, the exponent α may be related to the ratio of the two aforementioned time scales.

2.6.2. Phase Space Trajectories Constraints on α

Dynamical systems theory has been used to explore self-thinning empirically by modeling the $w - p$ time-course in crowded plant populations (Hara, 1984). The dynamical system can be expressed in terms of relative quantities, namely (relative) mortality rate (i.e., $p^{-1}\frac{dp}{dt}$) and relative growth rate (i.e., $w^{-1}\frac{dw}{dt}$). Among the choices of the functions linking p and w to relative mortality and growth rate, generalized Gompertz functions are empirically well-supported (Hara, 1984; Tsoularis and Wallace, 2002). With such choices, the dynamical systems theory can establish explicit dependencies of the empirical coefficients and the exponent α and plausibility constraints. Such a plausibility constraint is the imposition that equilibrium points are stable fixed points (as expected in self-thinning). A key result is that several combinations of the empirical parameters of the Gompertz function lead to exponents commensurate with the "rule of constant yield" or Yoda's thinning rule, while other exponents are possible with other empirical parameter combinations. The details are illustrated in the **Supplementary Material**.

2.7. Mechanism 7: Size Distribution Arguments

The self-thinning rule can also be obtained by following the temporal evolution of a population of individuals characterized by a certain size, which is interpreted as a stochastic variable. Without loss of generality, stem diameter D can be considered as the relevant size and can be linked to plant height and mass using allometric relations. For size-structured populations, it can be shown that the distribution of individuals of size D conditioned at time t, $p_D(D|t)$, is determined by the von Foerster equation (von Foerster, 1959; Hara, 1988; Kohyama, 1992; Strigul et al., 2008)

$$\frac{\partial p_D(D|t)}{\partial t} = \frac{\partial\left[G(D,t)\,p_D(D|t)\right]}{\partial D} - \mu(D,t)\,p_D(D|t), \quad (42)$$

where G is the growth rate (i.e., $G = dD/dt$) and μ is a mortality rate applied to plant density. In addition, a boundary condition $p_D(D_0|t=0)$ (i.e., where D_0 is the diameter at birth) must be specified. In principle, the self-thinning and constant yield laws could be obtained from the solution $p_D(D|t)$ of Equation (42) for specific choices of the functions G and μ, and the allometric relations between D and w. Here, a simplified approach is followed using the perfect crown plasticity rationale by Strigul et al. (2008) though by no means is this approach unique (Kohyama, 1992). As before, the focus is on a mono-specific, even-aged stand with negligible mortality until canopy closure, a constant growth rate (so that $D(t) = D_0 + Gt$), small but finite initial stem diameter and diameter variance ($D_0 \ll Gt$), and constant allometric coefficient linking canopy area per unit ground area to stem diameter (here a_c =canopy area per unit ground area over D^2). With these conditions and assumptions, integrating the distribution $p_D(D|t)$ over all initial sizes, the total canopy area per unit ground area is calculated as,

$$\int_0^\infty p_D(D_0|t=0)\,a_c\,(D_0+Gt)^2\;\mathrm{d}D_0 \approx a_c p_0 G^2 t^2, \quad (43)$$

where $(D_0+Gt)^2 \approx (Gt)^2$ is the canopy area per unit area and p_0 is, as before, the initial plant density. When canopy closure occurs, the canopy area per unit ground area reaches 1. Hence, the canopy closure time t^* can be calculated as

$$1 = a_c p_0 G^2 t^2 \Rightarrow t^* = \left(G\sqrt{a_c p_0}\right)^{-1}. \quad (44)$$

Upon canopy closure ($t > t^*$), plant growth must adjust to maintain a closed canopy as time progresses, which requires lowering plant density through the death of suppressed, shaded plants according to,

$$Gt = \left(a_c p_0\right)^{-\frac{1}{2}}. \quad (45)$$

These constraints allow finding the scaling relation between plant biomass and density in the two regimes - before ($t < t^*$) and after ($t > t^*$) canopy closure. For $t < t^*$, plant biomass $w \sim D^2 h$, where h is the plant height as before. However, neither D nor h depend on plant density because they only depend on time before canopy closure. As a consequence, plant biomass $w \sim p^0$ when $t < t^*$. In contrast, for $t > t^*$, plant biomass depends on plant density because after canopy closure Equation (45) yields,

$$w \sim D^2 h = G^2 t^2 h = h\left(a_c p\right)^{-1} \sim \left(a_c p\right)^{-\frac{3}{2}}, \quad (46)$$

where isometric scaling of height and diameter (i.e., $h \sim D$) was assumed to recover Yoda's rule (last term).

2.8. Mechanism 8: Neighborhood Interaction Arguments

As a bridge to the general framework in Equation (5), the equations specifying $g_1(w_i)$ for an individual i must now include interaction terms with adjacent individuals to explicitly account for competition. Upon specifying mortality and solving w_i for each individual, the solution yields the mean biomass w and $g_2(p)$ by aggregating over all surviving individuals (i.e., the stand-scale). Hence, $w(t) - p(t)$ trajectories are constructed thereby allowing the determination of α. The previously discussed carbon balance approaches only accounted for competition indirectly by varying the average individual's photosynthetic rate with p. Also, size-structured population approaches accounted for interactions among individuals implicitly. Individual-based models (Aikman and Watkinson, 1980; Westoby, 1982; Hara, 1988; Thomas and Weiner, 1989; Adler, 1996; Li et al., 2000; Stoll et al., 2002; Strigul et al., 2008; Chu et al., 2010; Coomes et al., 2011; Deng et al., 2012; Rivoire and Le Moguedec, 2012; Rüger and Condit, 2012; Lin et al., 2013) are often characterized as either spatially explicit, where plant spatial coordinates are specified, or spatially implicit, where only the zone of influence of each plant is tracked assuming equal spacing among individuals. Such models recover the 3/2 or 4/3 exponents for a wide range of mortality conditions

or metabolic thresholds, while others exhibit greater sensitivity to competition between adjacent plants. These models follow a continuum of competition modes bounded by two limiting cases: size asymmetric competition where the largest plants acquire all the resources in overlapping areas to size symmetric competition where resources in overlapping areas are divided equally among interacting individuals regardless of their size (Weiner, 1990; DeMalach et al., 2016). Obviously, the degree of competition among individuals increases in all such models when the plot area A_s available for growth is diminished. These models can recover increased variability, skewness, or bi-modality in the histograms of individual plant biomass w_i as self-thinning is initiated at the stand level. A parsimonious, spatially implicit model is now considered to explore how different competition modes, initial densities, and experimental durations result in different α values. While some spatially explicit, more complex models are more realistic, the spatially implicit model explored here strikes a balance between simplicity and the ability to grasp all the proposed power-law exponents.

2.8.1. Competition and Mortality in Spatially Implicit Models

In this model, the growth rate of an individual plant i is assumed to be (Aikman and Watkinson, 1980)

$$\frac{dw_i}{dt} = a_i s_i f(s_i) - b_i w_i^2, \tag{47}$$

where a_i and b_i are constants for a given stand, reflecting growth rate per unit area and the need for more resources as individual plant biomass increases, b_i depends on the maximum individual biomass w_{max}, and s_i measures the space occupied by plant i, which is linked to its size by a prescribed allometric relation

$$s_i = \left(\frac{w_i}{k_g}\right)^{2/3}, \tag{48}$$

where k_g is a constant relating the area or zone of influence s to plant weight w. The 2/3 exponent is derived from dimensional considerations for isometric growth as discussed in section 2.1. The function $f(s_i)$ encodes all of the spatial competition on the growth rate of plant i. To represent the space limitation and the two end-members of symmetric vs. asymmetric size-based competition, $f(s_i)$ was represented as (Aikman and Watkinson, 1980)

$$f(s_i) = \left[1 + \left(\frac{\sum_j s_j}{A_s}\right)^{\phi_1} \left(\frac{\bar{s}}{s_i}\right)^{\phi_2}\right]^{-1}, \tag{49}$$

where the term $\frac{\sum_j s_j}{A_s}$ describes the space availability for resource acquisition (i.e., a measure of crowding) and $\frac{\bar{s}}{s_i}$ measures the relative size of plant i compared to the mean size $\bar{s}$. The two exponents ϕ_1 and ϕ_2 describe the importance of each mode of competition, representing respectively the roles of crowding and size asymmetry. The plot size A_s sets the spatial domain for competition. The initial number of uniformly distributed plants within A_s defines p_0. By varying ϕ_1 and ϕ_2, various modes of competition can be explored and their effect on α tracked. Mortality of plant i occurs when its carbon balance first becomes negative (i.e., $dw_i/dt < 0$). Needless to say, mortality need not occur when $dw_i/dt < 0$ (at least not on short time scales) though a negative carbon balance at the individual level implies a progressive competitive disadvantage and an increasing likelihood of mortality. Two related issues are addressed: The effect of $f(s_i)$ on (i) the value of the self-thinning exponent α and (ii) the emergence of constant final yield when varying p_0 across multiple stands, waiting for a fixed duration, and observing w and p at each stand separately as shown in **Figure 1** (Weiner and Freckleton, 2010).

Because growth and mortality in Equations (47) and (48) are proportional to powers of biomass (w_i) without distinguishing live and dead parts, this model is more appropriate for herbaceous species rather than forests. The individual tree biomass in high density forests may consist of a considerable proportion of dead biomass, reducing respiration costs. To avert this complexity, large initial densities and growth rates are used as is the case in crops. In fact, the range of parameter values used here (**Table S3**) are within the range used in Aikman and Watkinson (1980) and which were shown to agree with stand structure observations in even-aged monoculture competition experiments (Ford, 1975).

2.8.2. Effects of Competition Type on α and the Emergence of Constant Final Yield

For the first set of model runs, the power-law relation between individual biomass $w(p_0|T_p)$ at a fixed time after sowing T_p and initial density p_0 is examined, where T_p is the integration period of the simulation (**Figure 4**). A constant integration period of $T_p = 50$ days is maintained for these runs during which no mortality occurs as is the case in the seminal work of Shinozaki and Kira (1956). Here,

$$w(p_0|T_p) \sim p_0^{-\alpha_{CD}}, \tag{50}$$

where the subscript CD stands for competition-density. The model runs here compare different plots at different p_0 and at a fixed period after sowing. Clearly, $\alpha_{CD} = 1$ corresponds to the constant final yield rule as in Equation (3). In **Figure 4A**, for small p_0, normalized biomass per individual at the end of the simulation $w(p_0|T_p)/w_{max}$ appears to be insensitive to p_0. As p_0 increases, variations in α_{CD} occur depending on choices made about ϕ_1 and ϕ_2. **Figure 4B** shows that at relatively low crowding exponent ($\phi_1 = 5$) and relatively large size asymmetry exponent ($\phi_2 = 5$), $\alpha_{CD} = 1$, corresponding to invariant biomass per ground area $y(p_0|T_p) = y_c$ regardless of the initial sowing density. This is therefore a manifestation of the constant final yield rule but not of self-thinning since mortality is absent. As the crowding exponent becomes large ($\phi_1 \to 10$), α_{CD} becomes bounded between 4/3 and 3/2, and insensitive to variations in the size asymmetry exponent ϕ_2. These cases are compatible with neither the constant final yield rule nor the self-thinning rule.

The temporal patterns of $y(t) = w(t)p(t)$ associated with various choices of p_0 and ϕ_2 are shown in **Figure 5** for different

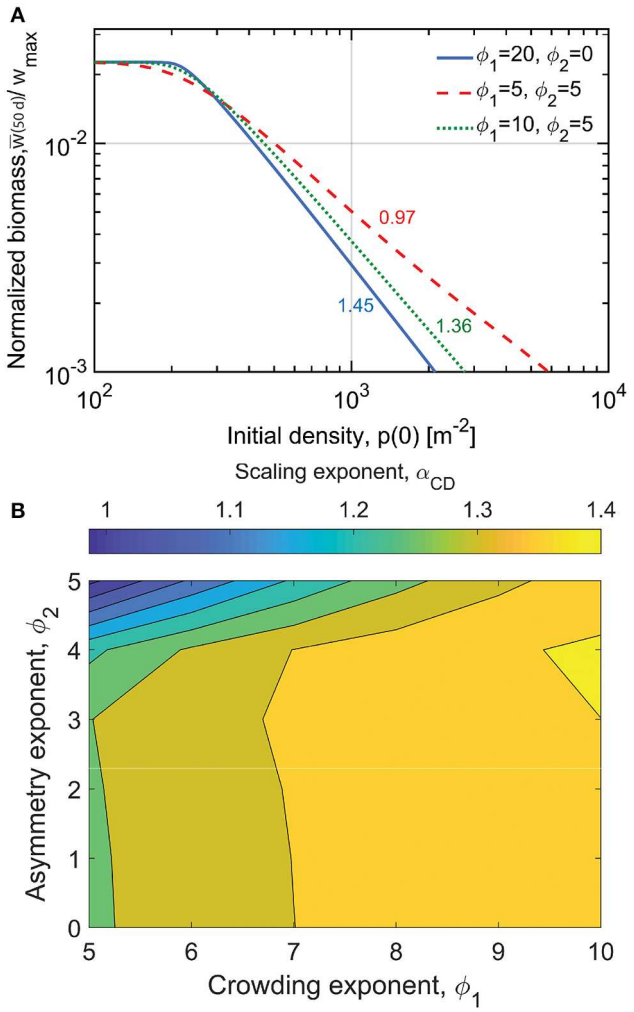

FIGURE 4 | (A) Each line represents modeled normalized biomass per individual for multiple simulations of different initial density p_0 after a fixed integration period of 50 days. The lines correspond to the three competition scenarios indicated in the legend. The corresponding scaling exponent α_{CD} is displayed next to each plotted line. **(B)** Variation in α_{CD} driven by different competition scenarios for crops (as determined by high initial plant densities and growth rates). Model parameters are found in **Table S3**.

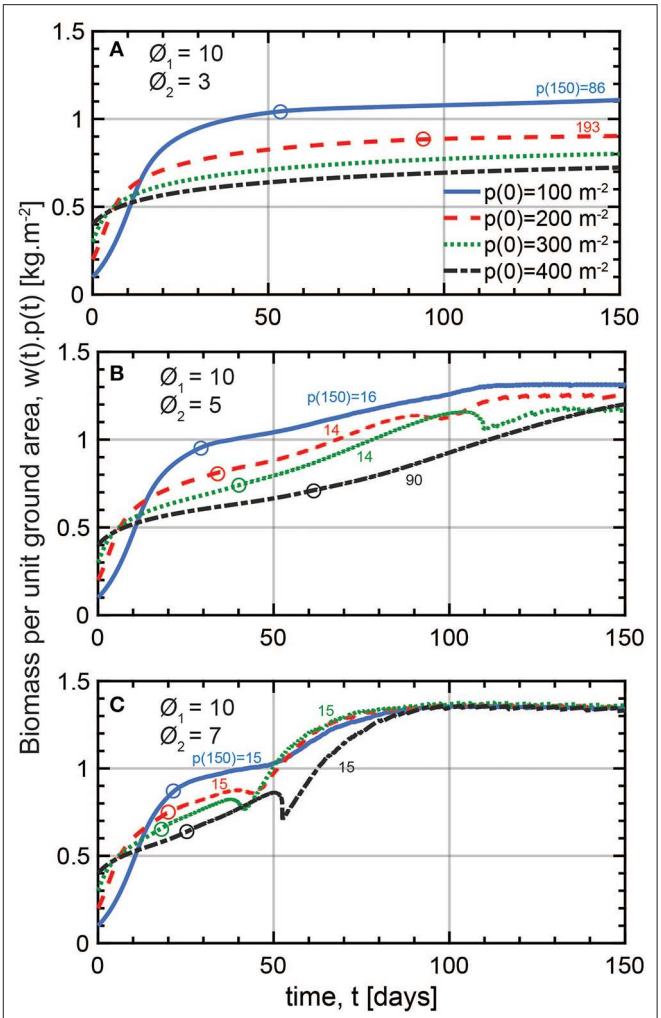

FIGURE 5 | Modeled temporal variations of biomass per unit ground area with time for three competition types with less and more prominent size asymmetry effect (respectively smaller and larger ϕ_2). **(A)** At low ϕ_2, model runs with different initial densities p_0 (m^{-2}) result in divergent final yields. Mortality only occurs in the low density plots as indicated by the circles. The final densities [p(150) in m^{-2}] as indicated by the color-coded numbers on their corresponding curves are not very different from p_0. **(B)** At medium size asymmetry, final yields are closer than in **(A)**, but differences still occur after 150 days. Mortality is present in all four plots. **(C)** At high size asymmetry, final yields are the same regardless of p_0 90 days into the simulation which corresponds to the constant final yield rule. All plots reach the same low final density of 15 m^{-2}. Model parameters are found in **Table S3**. Circles designate the onset of mortality in time and color-coded numbers are the final densities at the end of the 150 days corresponding to each simulation.

plant properties and a longer integration period of $T_p = 150$ days to assess the robustness of the results (see **Table S2**). The longer period allows for the presence of mortality whose onset in time is depicted using circles in **Figure 5** ($p(t) < p_0$). Here, an intermediate crowding exponent $\phi_1 = 10$ is kept as a constant. Biomass per ground area reaches an equilibrium that is sensitive to p_0 for low ϕ_2 values of 3 and 5 (**Figures 5A,B**). This does not conform to the constant final yield rule. For the highly size asymmetric mode of competition set by $\phi_2 = 7$, the steady state biomass becomes independent of p_0 (**Figure 5C**), consistent with the constant final yield rule as presented by Xue and Hagihara (1998) when density-driven mortality occurs. The fact that a constant biomass is achieved for large ϕ_2 underscores that the phenomenon of the constant final yield only applies to certain types of plants competing for certain limited resources.

Self-thinning is shown in **Figure 6** and **Figure S1**. The differences between experiments conducted at a single stand experiencing self-thinning sampled through time (Equation 2), and multiple stands with varying p_0 at a fixed period after sowing (Equations 4 and 50) is seen by comparing **Figure 6B** and **Figure 4B**. The discrepancy in the contour plots underscores the fact that the meaning of the scaling exponent α and α_{CD}

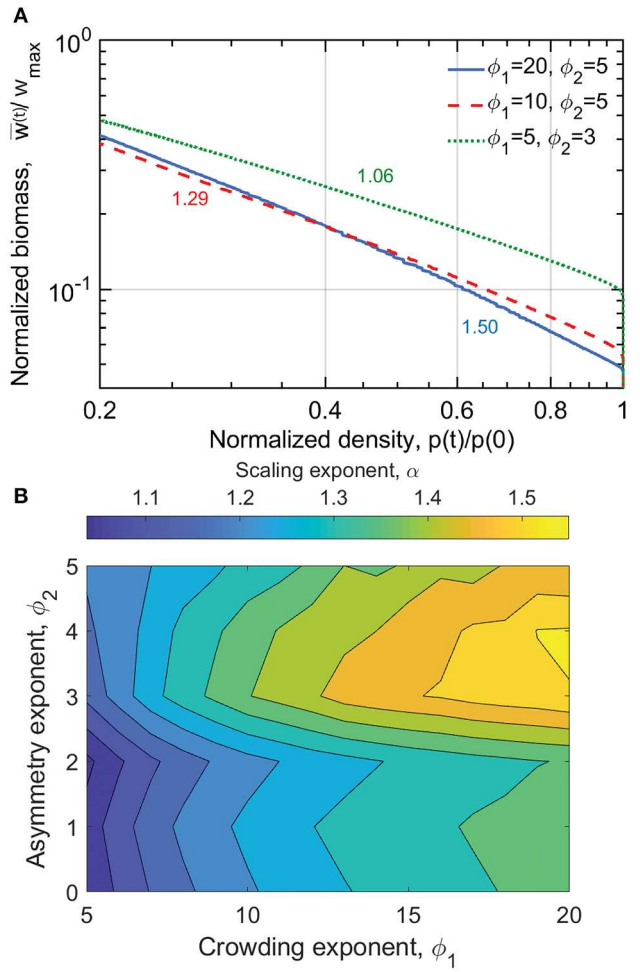

FIGURE 6 | (A) Modeled normalized biomass per individual as a function of normalized plant density for the three competition scenarios indicated in the legend; time progresses from right to left as plants grow and density decreases. The corresponding scaling exponents α are written next to the plotted lines. **(B)** Variation in α driven by different competition scenarios. Model parameters are found in **Table S3**.

is not equivalent. As earlier noted, one of the highly cited critiques on the universality of the self-thinning exponent was an empirical analysis by Weller (1987). Weller noted that when analyzing multiple stands with different p_0, exponents differing from those tracking self-thinning in a single stand were obtained. The differences between these two experimental setups have been discussed elsewhere (Weiner and Freckleton, 2010), but are quantified here using the same spatially implicit model (as well as a range of ϕ_1 and ϕ_2).

In **Figure 6**, it is seen that the stronger the influence of space availability on competition (ϕ_1), the steeper the power-law relation between $w(t)$ and $p(t)$. The effect of size asymmetry on the α is more nuanced (**Figure 6B**). It is therefore seen that Yoda's definition of self-thinning, where $\alpha = 3/2$ is achieved only when competition for space is high ($\phi_1 > 15$) and size asymmetry is moderate to high ($\phi_2 > 3$; **Figure 6B**). The green dashed line of **Figure 6A** where $\alpha = 1.06$ is equivalent to the scenario in **Figure 5C** where the biomass per ground area is invariant with respect to p_0. **Figure 6B** shows that all 3 aforementioned exponents ($\alpha \approx 1, 4/3, 3/2$) can be recovered from the same zonal model, depending on choices of ϕ_1 and ϕ_2.

3. IMPACTS ON FOREST MANAGEMENT, FUTURE OUTLOOK, AND CONCLUSIONS

Competition for resources among same-species individuals sharing the same resource niche can be as complex as interactions among individuals of different species (Perry et al., 2008). That such competition among individuals of the same species results in power-law relations between the mean weight of an individual w and plant density p remains scientifically challenging to explain. Yet, such power-law relations are appealing to agricultural and forestry practitioners and have routinely been used in crop and forest management. In this context, mortality is only due to resource competition between individual plants, neglecting mortality due to external factors such as ice storms, hurricanes, forest fires, extended droughts, insect outbreaks, and human thinning of forests for management. As such, they set an "upper bound" on mean individual size for a given stocking (or planting) density (Luyssaert et al., 2011). In the case of crop management, initial planting density emerges as a key determinant of individual biomass and elapsed time when the steady state yield is reached; whereas in the case of forest management the $w - p$ trajectories serve as a guide to when, and how much and often stands must be thinned to either maximize profitability or to mitigate hazards such as forest fires, insect outbreaks, or drought-induced mortality.

As already alluded to by Reineke (1933), forest density management utilizes size-density indices because they are presumably independent of site quality and stand age and the self-thinning line has taken center stage in determining management regimes (Begin et al., 2001). Such a presumably time-invariant power-law relation between w and p enables forest managers to also compare levels of growing stock regardless of differences in site quality or stand age. A particular set of management objectives resulting in an ideal p value can be projected forward or backward in time to a different development stage using the aforementioned $w - p$ trajectories if the power-law exponent is known (e.g., $\alpha = 3/2$). The self-thinning rule is a particularly powerful tool in combination (or as a part of) growth models to inform managers when the stands reach a particular management regime (Landsberg and Waring, 1997).

This review has focused on the many hypothetical mechanisms generating power-law relations between w and p due to the constraints imposed on resource competition in monospecific plots. Depending on the resource constraints (e.g., structural, allometric, hydraulic, supply of energy) and the type of competition imposed, multiple arguments suggest that the exponent of the power-law solution to $dw/dp = g_3(w, p)$ converges toward one of the three α values: 1, 4/3, 3/2 (**Table 1**). The different α values reflect the numerous environmental influences and physiological factors and the

degree of asymmetry of the competitive interaction (e.g., light interception is dominated by the tallest trees; Craine and Dybzinski, 2013). Therefore, for foresters aiming to optimize productivity, they should manage tree density based on the specific resource constraints shaping inter-plant competition. Often, the cultivation strategy maximizing plant density also minimizes resource availability such as soil water, i.e., the tragedy of the commons (Hardin, 1968). However, forest managers may be able to avoid this risky strategy by balancing resource use and plant density. This may be increasingly relevant in a changing climate where frequent and extended droughts are becoming a reality in many parts of the world. If storm intensities and inter-arrival times change in relatively short time-scales, then rooting profiles that successfully harnessed soil water in the past might become less effective (Farooq et al., 2009).

The theoretical results presented can be used to generate hypotheses on what controls α, to be tested in specific experiments or simulation studies. For example, species characterized by contrasting growth patterns or hydraulic traits could be grown under the same conditions to test predicted patterns of α. Similarly, trends in α could be assessed along climatic and edaphic gradients to test predicted deviations from the 3/2 or 4/3 values. The focus was purposely restricted to monospecific stands, but self-thinning also occurs in diverse communities, though niche complementarity and facilitation effects can become important drivers of the plant mass-density relations (Loreau and Hector, 2001). It is possible that denser communities containing a greater number of small individuals (belonging to more than one species) emerge when these effects are at play compared to monospecific stands. To tackle this problem, models describing a multitude of species (or functional traits), or capturing differences across individuals, should be used, which we expect will require a broader range of scaling exponents as the communities become more diverse.

The finding that the self-thinning exponent is not invariant has several consequences for forest managers designing their thinning regimes based on an invariant self-thinning rule (Drew and Flewelling, 1977). Time variance has been attributed to stand aging, canopy closure and environmental change, including increasing aridity in many parts of the world. Several amendments to the size-density indices presented in this text have been proposed elsewhere to take these effects into account (Zeide, 2001; Ge et al., 2017; Aguirre et al., 2018; Bravo-Oviedo et al., 2018; Zhang et al., 2019). Forest managers may expect a given self-thinning slope based on data from space-for-time substitution and, thus, set their thinning or harvest operations based on this expectation (Drew and Flewelling, 1979). For example, the self-thinning rule can be used to characterize "reference" conditions and, based on that, define indicators of the degree of land use intensity (Luyssaert et al., 2011). Such indicators quantify how far a given stand is from either a pristine forest or a stand following the self-thinning rule. However, as shown here, the shape of the self-thinning rule may vary depending on growth conditions and therefore indicators based on this curve may be sensitive to the chosen exponent and intercept.

A line of inquiry of increasing relevance to crops and plantation forestry alike is the effect of environmental change (e.g., elevated atmospheric CO_2, or air temperature) on C or α. Do the $w - p$ trajectories remain the same or are they altered with these changes? Does elevated atmospheric CO_2 simply speed up the trajectories in the $w - p$ phase plane? Does α remain constant but C likely to vary due to changes in leaf area index or other ecosystem properties? These are but a few of the questions that could motivate future work (Brunet-Navarro et al., 2016; Jump et al., 2017; Bravo-Oviedo et al., 2018). The implications of these answers to forest management cannot be overstated. If C or α vary under future conditions, management tactics will need to be adjusted accordingly. Even if the parameters of the self-thinning rule do not change, higher CO_2 and air temperature may promote growth (in absence of other limitations), resulting in faster movements along the $w - p$ trajectory. This alone would require adjusting the thinning schedule. Modeling studies suggest that maintaining under-stocked stands (below the self-thinning curve) by more frequent or intense thinning could compensate negative impacts of future environmental conditions on the tree C balance (Collalti et al., 2018). However, for new thinning approaches to be effective, they will need to be based on a self-thinning rule that accounts for future growth conditions. For example, Equation (41) suggests that lower values of α can be expected if autotrophic respiration increases more than GPP in a warmer world, or if stands become nutrient-limited or age faster, resulting in lower CUE (Collalti et al., 2018). The use of such power-law expressions in forest management map onto the famous quote by the great Russian physicist Lev Landau:

> Money is in the exponent. And exponent needs to be calculated precisely.

Power law relations between measures of biomass and density have been the subject of over a century of experimentation and theoretical analysis. They not only describe biomass development as a function of density for a single stand but also steady-state biomass as a function of maximum density for species ranging nine orders of magnitude by weight. The ubiquity and relative invariance of these power law relations makes them a research breeding ground to uncover the underlying mechanisms of inter-plant competition and develop effective management strategies for forests and croplands increasingly suffering from aridity in a changing climate.

DATA AVAILABILITY STATEMENT

All sources of data used in this study are included in the article/ **Supplementary Material**.

AUTHOR CONTRIBUTIONS

GK, RO, and SM conceived the initial ideas and design of the manuscript. AM and SM designed all the figures and illustrations and were responsible for ideas in the extended analysis. ML and GV contributed to the literature review and checked derivations

and dimensional consistencies. AM and GK developed and conducted all model simulations. All authors contributed to the writing of the manuscript and provided their consent to publish this work.

FUNDING

GK and AM acknowledge support from the National Science Foundation (NSF-DGE-1068871, NSF-EAR-1344703, NSF-AGS-1644382, and NSF-IOS-1754893). SM and ML were partly supported by the Swedish Research Council Formas (2016-00998). GV acknowledges support from the Swedish Research Council Formas (2018-01820) and Trees and Crops for the Future (TC4F)—a co-operative project between established research environments at the Swedish University of Agriculture (SLU), Umeå University and Skogforsk. RO acknowledges support from the Erkko Visiting Professor Programme of the Jane and Aatos Erkko 375th Anniversary Fund through University of Helsinki, Finland.

ACKNOWLEDGMENTS

The authors thank N. Christensen, the editor CT, and the two reviewers for their helpful comments and suggestions.

SUPPLEMENTARY MATERIAL

The Supplementary Material for this article can be found online at: https://www.frontiersin.org/articles/10.3389/ffgc.2020.00062/full#supplementary-material

REFERENCES

Adler, F. R. (1996). A model of self-thinning through local competition. Proceedings of the National Academy of Sciences 93, 9980–9984. doi: 10.1073/pnas.93.18.9980

Aguirre, A., del Río, M., and Condés, S. (2018). Intra-and inter-specific variation of the maximum size-density relationship along an aridity gradient in Iberian pinewoods. *Forest Ecol. Manage.* 411, 90–100. doi: 10.1016/j.foreco.2018.01.017

Aikman, D., and Watkinson, A. (1980). A model for growth and self-thinning in even-aged monocultures of plants. *Ann. Bot.* 45, 419–427. doi: 10.1093/oxfordjournals.aob.a085840

Antonovics, J., and Levin, D. A. (1980). The ecological and genetic consequences of density-dependent regulation in plants. *Annu. Rev. Ecol. Syst.* 11, 411–452. doi: 10.1146/annurev.es.11.110180.002211

Banavar, J. R., Maritan, A., and Rinaldo, A. (1999). Size and form in efficient transportation networks. *Nature* 399:130. doi: 10.1038/20144

Bazzaz, F., and Harper, J. (1976). Relationship between plant weight and numbers in mixed populations of *Sinapsis alba* (L.) *rabenh*., and *Lepidium sativum* L. *J. Appl. Ecol.* 13, 211–216. doi: 10.2307/2401940

Begin, E., Begin, J., Belanger, L., Rivest, L.-P., and Tremblay, S. (2001). Balsam fir self-thinning relationship and its constancy among different ecological regions. *Can. J. Forest Res.* 31, 950–959. doi: 10.1139/x01-026

Bohrer, G., Mourad, H., Laursen, T. A., Drewry, D., Avissar, R., Poggi, D., et al. (2005). Finite element tree crown hydrodynamics model (Fetch) using porous media flow within branching elements: a new representation of tree hydrodynamics. *Water Resour. Res.* 41:W11404. doi: 10.1029/2005WR004181

Bravo-Oviedo, A., Condés, S., del Río, M., Pretzsch, H., and Ducey, M. J. (2018). Maximum stand density strongly depends on species-specific wood stability, shade and drought tolerance. *Forest. Int. J. Forest Res.* 91, 459–469. doi: 10.1093/forestry/cpy006

Brown, J. H., Gillooly, J. F., Allen, A. P., Savage, V. M., and West, G. B. (2004). Toward a metabolic theory of ecology. *Ecology* 85, 1771–1789. doi: 10.1890/03-9000

Brown, J. H., and West, G. B. (2000). *Scaling in Biology*. Oxford University Press.

Brunet-Navarro, P., Sterck, F. J., Vayreda, J., Martinez-Vilalta, J., and Mohren, G. M. (2016). Self-thinning in four pine species: an evaluation of potential climate impacts. *Ann. Forest Sci.* 73, 1025–1034. doi: 10.1007/s13595-016-0585-y

Chu, C.-J., Weiner, J., Maestre, F. T., Wang, Y.-S., Morris, C., Xiao, S., et al. (2010). Effects of positive interactions, size symmetry of competition and abiotic stress on self-thinning in simulated plant populations. *Ann. Bot.* 106, 647–652. doi: 10.1093/aob/mcq145

Collalti, A., Trotta, C., Keenan, T. F., Ibrom, A., Bond-Lamberty, B., Grote, R., et al. (2018). Thinning can reduce losses in carbon use efficiency and carbon stocks in managed forests under warmer climate. *J. Adv. Model. Earth Syst.* 10, 2427–2452. doi: 10.1029/2018MS001275

Coomes, D. A., Lines, E. R., and Allen, R. B. (2011). Moving on from metabolic scaling theory: hierarchical models of tree growth and asymmetric competition for light. *J. Ecol.* 99, 748–756. doi: 10.1111/j.1365-2745.2011.01811.x

Craine, J. M., and Dybzinski, R. (2013). Mechanisms of plant competition for nutrients, water and light. Functional Ecology 27, 833–840. doi: 10.1111/1365-2435.12081

Dean, T., and Long, J. N. (1985). Response of self-thinning to artificially reduced levels of leaf area in monocultures of *Trifolium pratense*. *Ann. Bot.* 55, 361–366. doi: 10.1093/oxfordjournals.aob.a086913

DeMalach, N., Zaady, E., Weiner, J., and Kadmon, R. (2016). Size asymmetry of resource competition and the structure of plant communities. *J. Ecol.* 104, 899–910. doi: 10.1111/1365-2745.12557

Deng, J., Ran, J., Wang, Z., Fan, Z., Wang, G., Ji, M., et al. (2012). Models and tests of optimal density and maximal yield for crop plants. *Proc. Natl. Acad. Sci. U.S.A.* 109, 15823–15828. doi: 10.1073/pnas.1210955109

Dewar, R. C. (1993). A mechanistic analysis of self-thinning in terms of the carbon balance of trees. *Ann. Bot.* 71, 147–159. doi: 10.1006/anbo.1993.1019

Drew, T. J., and Flewelling, J. W. (1977). Some recent Japanese theories of yield-density relationships and their application to monterey pine plantations. *Forest Sci.* 23, 517–534.

Drew, T. J., and Flewelling, J. W. (1979). Stand density management: an alternative approach and its application to Douglas-fir plantations. *Forest Sci.* 25, 518–532.

Eloy, C. (2011). Leonardo's rule, self-similarity, and wind-induced stresses in trees. *Phys. Rev. Lett.* 107:258101. doi: 10.1103/PhysRevLett.107.258101

Enquist, B. J., Brown, J. H., and West, G. B. (1998). Allometric scaling of plant energetics and population density. *Nature* 395:163. doi: 10.1038/25977

Enquist, B. J., West, G. B., and Brown, J. H. (2009). Extensions and evaluations of a general quantitative theory of forest structure and dynamics. *Proc. Natl. Acad. Sci. U.S.A.* 106, 7046–7051. doi: 10.1073/pnas.0812303106

Farooq, M., Wahid, A., Kobayashi, N., Fujita, D., and Basra, S. M. A. (2009). Plant drought stress: effects, mechanisms and management. *Agron. Sustain. Dev.* 29, 185–212. doi: 10.1051/agro:2008021

Farrior, C., Bohlman, S., Hubbell, S., and Pacala, S. W. (2016). Dominance of the suppressed: power-law size structure in tropical forests. *Science* 351, 155–157. doi: 10.1126/science.aad0592

Ford, E. (1975). Competition and stand structure in some even-aged plant monocultures. *J. Ecol.* 63, 311–333. doi: 10.2307/2258857

Friedman, S. P. (2016). Evaluating the role of water availability in determining the yield-plant population density relationship. *Soil Sci. Soc. Am. J.* 80, 563–578. doi: 10.2136/sssaj2015.11.0395

Ge, F., Zeng, W., Ma, W., and Meng, J. (2017). Does the slope of the self-thinning line remain a constant value across different site qualities?–An implication for plantation density management. *Forests* 8:355. doi: 10.3390/f8100355

Givnish, T. J. (1986). Biomechanical constraints on self-thinning in plant populations. *J. Theor. Biol.* 119, 139–146. doi: 10.1016/S0022-5193(86)80069-8

Gorham, E. (1979). Shoot height, weight and standing crop in relation to density of monospecific plant stands. *Nature* 279:148. doi: 10.1038/279148a0

Hara, T. (1984). Modelling the time course of self-thinning in crowded plant populations. *Ann. Bot.* 53, 181–188. doi: 10.1093/oxfordjournals.aob.a086679

Hara, T. (1988). Dynamics of size structure in plant populations. *Trends Ecol. Evol.* 3, 129–133. doi: 10.1016/0169-5347(88)90175-9

Hardin, G. (1968). The tragedy of the commons. *Science* 162, 1243–1248. doi: 10.1126/science.162.3859.1243

Hecht, V. L., Temperton, V. M., Nagel, K. A., Rascher, U., and Postma, J. A. (2016). Sowing density: a neglected factor fundamentally affecting root distribution and biomass allocation of field grown spring barley (*Hordeum vulgare* L.). *Front. Plant Sci.* 7:944. doi: 10.3389/fpls.2016.00944

Holliday, R. (1960). Plant population and crop yield. *Nature* 186, 22–24. doi: 10.1038/186022b0

Horn, H. S. (2000). "Twigs, trees, and the dynamics of carbon in the landscape," in *Scaling in Biology, 199–220. Santa Fe Institute Studies on the Sciences of Complexity*. Oxford: Oxford University Press.

Hozumi, K. (1977). Ecological and mathematical considerations on self-thinning in even-aged pure stands. *Bot. Mag.* 90, 165–179. doi: 10.1007/BF02488355

Huang, C.-W., Domec, J.-C., Palmroth, S., Pockman, W. T., Litvak, M. E., and Katul, G. G. (2018). Transport in a coordinated soil-root-xylem-phloem leaf system. *Adv. Water Resour.* 119, 1–16. doi: 10.1016/j.advwatres.2018.06.002

Jump, A. S., Ruiz-Benito, P., Greenwood, S., Allen, C. D., Kitzberger, T., Fensham, R., et al. (2017). Structural overshoot of tree growth with climate variability and the global spectrum of drought-induced forest dieback. *Glob. Change Biol.* 23, 3742–3757. doi: 10.1111/gcb.13636

Kikuzawa, K. (1999). Theoretical relationships between mean plant size, size distribution and self thinning under one-sided competition. *Ann. Bot.* 83, 11–18. doi: 10.1006/anbo.1998.0782

Kleiber, M. (1932). Body size and metabolism. *Hilgardia* 6, 315–353. doi: 10.3733/hilg.v06n11p315

Kohyama, T. (1992). Density-size dynamics of trees simulated by a one-sided competition multi-species model of rain forest stands. *Ann. Bot.* 70, 451–460. doi: 10.1093/oxfordjournals.aob.a088502

Landsberg, J., and Waring, R. (1997). A generalised model of forest productivity using simplified concepts of radiation-use efficiency, carbon balance and partitioning. *Forest Ecol. Manage.* 95, 209–228. doi: 10.1016/S0378-1127(97)00026-1

Lemons, D. S. (2018). *Dimensional Analysis for Curious Undergraduates: A Student's Guide to Dimensional Analysis*. Cambridge, MA: Cambridge University Press.

Li, B.-L., Wu, H.-I., and Zou, G. (2000). Self-thinning rule: a causal interpretation from ecological field theory. *Ecol. Modell.* 132, 167–173. doi: 10.1016/S0304-3800(00)00313-6

Lin, Y., Berger, U., Grimm, V., Huth, F., and Weiner, J. (2013). Plant interactions alter the predictions of metabolic scaling theory. *PLoS ONE* 8:e57612. doi: 10.1371/journal.pone.0057612

Loreau, M., and Hector, A. (2001). Partitioning selection and complementarity in biodiversity experiments. *Nature* 412, 72–76. doi: 10.1038/35083573

Luyssaert, S., Hessenmöller, D., Von Lüpke, N., Kaiser, S., and Schulze, E. (2011). Quantifying land use and disturbance intensity in forestry, based on the self-thinning relationship. *Ecol. Appl.* 21, 3272–3284. doi: 10.1890/10-2395.1

Manzoni, S., Čapek, P., Porada, P., Thurner, M., Winterdahl, M., Beer, C., et al. (2018). Reviews and syntheses: carbon use efficiency from organisms to ecosystems-definitions, theories, and empirical evidence. *Biogeosciences* 15, 5929–5949. doi: 10.5194/bg-15-5929-2018

McCulloh, K. A., Sperry, J. S., and Adler, F. R. (2003). Water transport in plants obeys Murray's law. *Nature* 421, 939–942. doi: 10.1038/nature01444

McMahon, T. (1973). Size and shape in biology: elastic criteria impose limits on biological proportions, and consequently on metabolic rates. *Science* 179, 1201–1204. doi: 10.1126/science.179.4079.1201

Miyanishi, K., Hoy, A., and Cavers, P. (1979). A generalized law of self-thinning in plant populations (self-thinning in plant populations). *J. Theor. Biol.* 78, 439–442. doi: 10.1016/0022-5193(79)90342-4

Murray, C. D. (1926). The physiological principle of minimum work: I. the vascular system and the cost of blood volume. *Proc. Natl. Acad. Sci. U.S.A.* 12:207. doi: 10.1073/pnas.12.3.207

Niklas, K. J. (1994). *Plant Allometry: The Scaling of Form and Process*. Chicago, IL: University of Chicago Press.

Niklas, K. J., and Spatz, H.-C. (2004). Growth and hydraulic (not mechanical) constraints govern the scaling of tree height and mass. *Proc. Natl. Acad. Sci. U.S.A.* 101, 15661–15663. doi: 10.1073/pnas.0405857101

Oren, R., Schulze, E.-D., Matyssek, R., and Zimmermann, R. (1986). Estimating photosynthetic rate and annual carbon gain in conifers from specific leaf weight and leaf biomass. *Oecologia* 70, 187–193. doi: 10.1007/BF00379238

Pacala, S., and Weiner, J. (1991). Effects of competitive asymmetry on a local density model of plant interference. *J. Theor. Biol.* 149, 165–179. doi: 10.1016/S0022-5193(05)80275-9

Pahor, S. (1985). On the -3/2 power thinning law in plant ecology. *J. Theor. Biol.* 112, 535–537. doi: 10.1016/S0022-5193(85)80020-5

Peet, R. K., and Christensen, N. L. (1987). Competition and tree death. *Bioscience* 37, 586–595. doi: 10.2307/1310669

Perry, D. A. (1984). A model of physiological and allometric factors in the self-thinning curve. *J. Theor. Biol.* 106, 383–401. doi: 10.1016/0022-5193(84)90037-7

Perry, D. A., Oren, R., and Hart, S. C. (2008). *Forest Ecosystems*. Baltimore, MD: JHU Press.

Pickard, W. (1983). Three interpretations of the self-thinning rule. *Ann. Bot.* 51, 749–757. doi: 10.1093/oxfordjournals.aob.a086526

Reineke, L. H. (1933). Perfecting a stand-density index for even-aged forests. *J. Agric. Res.* 46, 627–630.

Rivoire, M., and Le Moguedec, G. (2012). A generalized self-thinning relationship for multi-species and mixed-size forests. *Ann. Forest Sci.* 69, 207–219. doi: 10.1007/s13595-011-0158-z

Roderick, M., and Barnes, B. (2004). Self-thinning of plant populations from a dynamic viewpoint. *Func. Ecol.* 18, 197–203. doi: 10.1111/j.0269-8463.2004.00832.x

Rüger, N., and Condit, R. (2012). Testing metabolic theory with models of tree growth that include light competition. *Func. Ecol.* 26, 759–765. doi: 10.1111/j.1365-2435.2012.01981.x

Shinozaki, K., and Kira, T. (1956). Intraspecific competition among higher plants. VII. Logistic theory of the CD effect. *J. Inst. Polytech. Osaka City Univ. Ser.* 7, 35–72.

Shinozaki, K., Yoda, K., Hozumi, K., and Kira, T. (1964). A quantitative analysis of plant form-the pipe model theory: I. Basic analyses. *Jpn. J. Ecol.* 14, 97–105.

Spencer, H. (1864). *The Principles of Biology*. London, UK: Williams and Norgate.

Stoll, P., Weiner, J., Muller-Landau, H., Müller, E., and Hara, T. (2002). Size symmetry of competition alters biomass-density relationships. *Proc. R. Soc. Lond. B Biol. Sci.* 269, 2191–2195. doi: 10.1098/rspb.2002.2137

Strigul, N., Pristinski, D., Purves, D., Dushoff, J., and Pacala, S. (2008). Scaling from trees to forests: tractable macroscopic equations for forest dynamics. *Ecol. Monogr.* 78, 523–545. doi: 10.1890/08-0082.1

Thomas, S. C., and Weiner, J. (1989). Including competitive asymmetry in measures of local interference in plant populations. *Oecologia* 80, 349–355. doi: 10.1007/BF00379036

Thompson, D. W. (1942). *On Growth and Form*. Cambridge, UK: Cambridge University Press.

Thompson, S. E., and Katul, G. G. (2012). Hydraulic determinism as a constraint on the evolution of organisms and ecosystems. *J. Hydraul. Res.* 50, 547–557. doi: 10.1080/00221686.2012.732969

Thurner, M., Beer, C., Carvalhais, N., Forkel, M., Santoro, M., Tum, M., et al. (2016). Large-scale variation in boreal and temperate forest carbon turnover rate related to climate. *Geophys. Res. Lett.* 43, 4576–4585. doi: 10.1002/2016GL068794

Tsoularis, A., and Wallace, J. (2002). Analysis of logistic growth models. *Math. Biosci.* 179, 21–55. doi: 10.1016/S0025-5564(02)00096-2

Verhulst, P.-F. (1838). Notice sur la loi que la population suit dans son accroissement. Correspondance mathématique et physique publiée par a. *Quetelet* 10, 113–121.

Vogel, S. (1988). *Life's Devices: The Physical World of Animals and Plants*. Princeton, NJ: Princeton University Press.

Voit, E. (1988). Dynamics of self-thinning plant stands. *Ann. Bot.* 62, 67–78. doi: 10.1093/oxfordjournals.aob.a087637

von Bertalanffy, L. (1957). Quantitative laws in metabolism and growth. *Q. Rev. Biol.* 32, 217–231. doi: 10.1086/401873

von Foerster, H. (1959). "Some remarks on changing populations," in *The Kinetics of Cellular Proliferation*, ed J. F. Stohlman (New York, NY: Grune and Stratton), 382–407.

Waring, R., Landsberg, J., and Williams, M. (1998). Net primary production of forests: a constant fraction of gross primary production? *Tree Physiol*. 18, 129–134. doi: 10.1093/treephys/18.2.129

Watkinson, A. (1980). Density-dependence in single-species populations of plants. *J. Theor. Biol*. 83, 345–357. doi: 10.1016/0022-5193(80)90297-0

Weiner, J. (1990). Asymmetric competition in plant populations. *Trends Ecol. Evol*. 5, 360–364. doi: 10.1016/0169-5347(90)90095-U

Weiner, J., and Freckleton, R. P. (2010). Constant final yield. *Annu. Rev. Ecol. Evol. Syst*. 41, 173–192. doi: 10.1146/annurev-ecolsys-102209-144642

Weller, D. E. (1987). A reevaluation of the -3/2 power rule of plant self-thinning. *Ecol. Monogr*. 57, 23–43. doi: 10.2307/1942637

West, G. (2017). *Scale: The Universal Laws of Growth, Innovation, Sustainability, and the Pace of Life in Organisms, Cities, Economies, and Companies*. New York, NY: Penguin.

West, G. B., Brown, J. H., and Enquist, B. J. (1997). A general model for the origin of allometric scaling laws in biology. *Science* 276, 122–126. doi: 10.1126/science.276.5309.122

Westoby, M. (1982). Frequency distributions of plant size during competitive growth of stands: the operation of distribution-modifying functions. *Ann. Bot*. 50, 733–735. doi: 10.1093/oxfordjournals.aob.a086416

Westoby, M. (1984). The self-thinning rule. *Adv. Ecol. Res.* 14, 167–225. doi: 10.1016/S0065-2504(08)60171-3

White, J. (1981). The allometric interpretation of the self-thinning rule. *J. Theor. Biol*. 89, 475–500. doi: 10.1016/0022-5193(81)90363-5

White, J., and Harper, J. (1970). Correlated changes in plant size and number in plant populations. *J. Ecol*. 58,467–485. doi: 10.2307/2258284

Willey, R. W., and Heath, S. B. (1969). The quantitative relationships between plant population and crop yield. *Adv. Agron*. 21, 281–321. doi: 10.1016/S0065-2113(08)60100-5

Xue, L., and Hagihara, A. (1998). Growth analysis of the self-thinning stands of *Pinus densiflora Sieb. et Zucc. Ecol. Res*. 13, 183–191. doi: 10.1046/j.1440-1703.1998.00256.x

Yoda, K. (1963). Self-thinning in overcrowded pure stands under cultivated and natural conditions (intraspecific competition among higher plants. *J. Biol. Osaka City Univers*. 14, 107–129.

Zeide, B. (2001). Natural thinning and environmental change: an ecological process model. *Forest Ecol. Manage*. 154, 165–177. doi: 10.1016/S0378-1127(00)00621-6

Zhang, W.-P., Jia, X., Bai, Y.-Y., and Wang, G.-X. (2011). The difference between above- and below-ground self-thinning lines in forest communities. *Ecol. Res*. 26, 819–825. doi: 10.1007/s11284-011-0843-2

Zhang, X., Cao, Q. V., Lu, L., Wang, H., Duan, A., and Zhang, J. (2019). Use of modified Reineke's stand density index in predicting growth and survival of Chinese fir plantations. *Forest Sci*. 65, 1–8. doi: 10.1093/forsci/fxz033

Conflict of Interest: The authors declare that the research was conducted in the absence of any commercial or financial relationships that could be construed as a potential conflict of interest.

frontiers in Forests and Global Change

ORIGINAL RESEARCH
published: 30 June 2020
doi: 10.3389/ffgc.2020.00069

Evapotranspiration Mapping for Forest Management in California's Sierra Nevada

James W. Roche[1], *Qin Ma*[2,3], *Joseph Rungee*[3] *and Roger C. Bales*[3,4]*

[1] National Park Service, Torrey, UT, United States, [2] Department of Forestry, Mississippi State University, Starkville, MS, United States, [3] Sierra Nevada Research Institute, University of California, Merced, Merced, CA, United States, [4] School of Engineering, University of California, Merced, Merced, CA, United States

We assessed the response of densely forested watersheds with little apparent annual water limitation to forest disturbance and climate variability, by studying how past wildfires changed forest evapotranspiration and what past evapotranspiration patterns imply for the availability of subsurface water storage for drought resistance. We determined annual spatial patterns of evapotranspiration using a top–down statistical model, correlating measured annual evapotranspiration from eddy-covariance towers across California with normalized difference vegetation index (NDVI) measured by satellite and with annual precipitation. The study area was the Yuba and American River watersheds, two densely forested watersheds in the northern Sierra Nevada. Wildfires in the 1985–2015 period resulted in significant post-fire reductions in evapotranspiration for at least 5 years and in some cases for more than 20 years. The levels of biomass removed in medium-intensity fires (25–75% basal area loss), similar to magnitudes expected from forest treatments for fuel reduction and forest health, reduced evapotranspiration by as much 150–200 mm year^{-1} for the first 5 years. Rates of recovery in post-wildfire evapotranspiration confirm the need for follow-up forest treatments at intervals of 5–20 years to sustain lower evapotranspiration, depending on local landscape attributes and interannual climate. Using the metric of cumulative precipitation minus evapotranspiration (P-ET) during multiyear dry periods, we found that forests in the study area showed little evidence of moisture stress during the 1985–2018 period of our analysis, owing to relatively small reliance on interannual subsurface water storage to meet dry-year evapotranspiration needs of vegetation. However, more severe or sustained drought periods will push some lower-elevation forests in the area studied toward the cumulative P-ET thresholds previously associated with widespread forest mortality in the southern Sierra Nevada.

Keywords: evapotranspiration, drought, wildfire, forest, Sierra Nevada (CA), California

OPEN ACCESS

Edited by:
Christina (Naomi) Tague, University of California, Santa Barbara, United States

Reviewed by:
Gabrielle F. S. Boisrame, Desert Research Institute (DRI), United States
Cate Macinnis-Ng, The University of Auckland, New Zealand

***Correspondence:**
Roger C. Bales
rbales@ucmerced.edu

Specialty section:
This article was submitted to Forest Hydrology, a section of the journal Frontiers in Forests and Global Change

Received: *08 March 2020*
Accepted: *12 May 2020*
Published: *30 June 2020*

Citation:
Roche JW, Ma Q, Rungee J and Bales RC (2020) Evapotranspiration Mapping for Forest Management in California's Sierra Nevada. Front. For. Glob. Change 3:69. doi: 10.3389/ffgc.2020.00069

INTRODUCTION

Understanding and predicting how forests respond to disturbance is important for managing source-water areas, particularly in semiarid climates, which have a high ratio of evapotranspiration to precipitation. This is an immediate concern where a combination of a warming climate and past management has contributed to: (i) high wildfire extent and intensity (McKenzie et al., 2004; Westerling, 2006; North et al., 2015a), (ii) drought-related forest mortality

(Allen et al., 2010; Anderegg et al., 2013, 2015; Bales et al., 2018), and (iii) reduced runoff (Barnett et al., 2005; Goulden and Bales, 2014). The response of evapotranspiration to disturbance and interannual changes in temperature and precipitation is relatively muted compared to runoff, making it a potentially convenient metric for changes in water balance from forest management. Thus, it is urgent to improve our understanding and accurate mapping of evapotranspiration response to changes in forest vegetation, which dominates that response (Bosch and Hewlett, 1982; Naudts et al., 2016; Saksa et al., 2017).

As forests are dynamic systems, water use by forests can respond in multiple ways to reductions in biomass (Tague et al., 2018). For example, Saksa et al. (2019) reported a significant reduction in evapotranspiration following fuel treatment in a densely forested central Sierra Nevada area but no significant reduction in a comparable but more water-limited southern Sierra area. In the southern site, reductions in forest biomass apparently stimulated growth of remaining vegetation. Forest regrowth following disturbance is also quite variable (Tague et al., 2013; Roche et al., 2018; Tague and Moritz, 2019).

While multiple interacting and non-linear factors affect evapotranspiration, as reflected in physics-based models (Running et al., 1987; Chen et al., 2005) and bottom–up modeling blended with remote-sensing data (Mu et al., 2011; Baldocchi et al., 2019), it is also possible to consider their net effects in top–down approaches, particularly over multiyear timescales (Sivapalan et al., 2003). With the advent of high-confidence spatial-evapotranspiration estimates driven by a robust empirical relation between satellite-derived estimates of vegetation greenness, represented by normalized difference vegetation index (NDVI), and point measurements of evapotranspiration in a variety of ecosystems (Goulden et al., 2012; Goulden and Bales, 2019), it is possible to estimate the water balance with high spatial resolution across forested mountain landscapes. In the context of forest management, this tool permits estimation of evapotranspiration change resulting from past fuel treatments and wildfire (Roche et al., 2018), and projecting changes from future treatments and disturbance. This data-driven, top–down statistical approach complements more-detailed bottom–up hydrologic modeling, which generally uses precipitation and streamflow as the main state variables to infer changes in evapotranspiration as forest vegetation changes (Zierl et al., 2007). The empirical–statistical approach is also attractive for basin-scale or smaller studies, where remote-sensing-based evapotranspiration products that were largely designed for global and large regional applications perform poorly (Goulden et al., 2012).

Furthermore, extending the work of Fellows and Goulden (2017), it is possible to map the spatial variability in the amount of subsurface water storage required to sustain evapotranspiration during both dry seasons and during multiyear droughts, thereby identifying areas with greater or lesser drought resistance and/or potential benefit from thinning treatments (Klos et al., 2018; Rungee et al., 2019).

Forest management for fuel treatments in the Sierra Nevada and other overstocked forests is widely regarded as a necessary step to reduce the probability of high-intensity wildfire, restore forest health, and return forests to a more-sustainable condition following a century of fire suppression (Miller et al., 2012; North et al., 2015a). While fuels and forest-health concerns may be the primary drivers for fuel treatments, other benefits can be important contributors to the collaborations needed to implement forest-restoration projects. Valuing and monetizing water-related benefits requires credible, accessible metrics for both planning and verification.

The aim of the research reported here is to assess the response of densely forested mountain watersheds with little apparent annual water limitation to forest disturbance and climate variability. Two questions motivated this work. First, what changes in evapotranspiration and water balance across these densely forested areas have occurred from historical disturbances by wildfire and post-fire regrowth. Second, what magnitude of subsurface water storage have these forests historically used to continue growth during seasonally and multiyear dry periods, and what future vulnerabilities do the spatial patterns of these water balances reveal.

METHODS

In the analysis of water-balance changes from wildfire, we focused on evapotranspiration (ET) patterns in the Yuba and American River watersheds (**Figure 1**), two densely forested basins with significant annual runoff and multiple downstream services that depend on that runoff, yet high potential for severe wildfire and disruption of those services. Vegetation in the study area goes from grassland and oak savannah at lower elevations, through pine-oak forest, mixed-conifer forest, and subalpine at higher elevations. The 4,825 km^2 American basin experienced five wildfires over 4,000 ha (9,884 ac) in area during our 1985–2018 study period, with the largest being the 2014 King Fire (37,315 ha) (**Tables S1, S2**). Much of the area burned in these large fires was in dense, productive mixed-conifer forests, with overall wildfire elevations spanning 600–2,200 m. Only one fire over 4,000 ha occurred in the 2,870 km^2 Yuba, the 1999 Pendola Fire (4,408 ha, 467–1,028 m elevation). There were several smaller fires in both watersheds. Using California Wildlife Habitat Relationship System data (https://wildlife.ca.gov/Data/CWHR), 77% of burned area may be classed as mixed conifer (Sierra mixed conifer, white fir, Jeffrey pine, ponderosa pine, montane-hardwood-conifer, montane chaparral), 15% is montane hardwood, and 3% is perennial grasslands (**Figure 1**).

We determined annual spatial patterns of evapotranspiration using a top–down statistical model (Goulden and Bales, 2014, 2019) and used published gridded data for precipitation (P). Using a pixel-by-pixel annual water balance ($P = ET + Q - \Delta S$), we evaluated spatial values of $P - ET$ to estimate gridded runoff (Q) and change in annual subsurface storage (ΔS) following Bales et al. (2018). We evaluated the basin-scale water balance by summing $P - ET$ across each basin and comparing with published values of whole-basin runoff.

We examined the impact that wildfire has had on evapotranspiration using the methods of Roche et al. (2018) and estimated the spatial patterns of subsurface

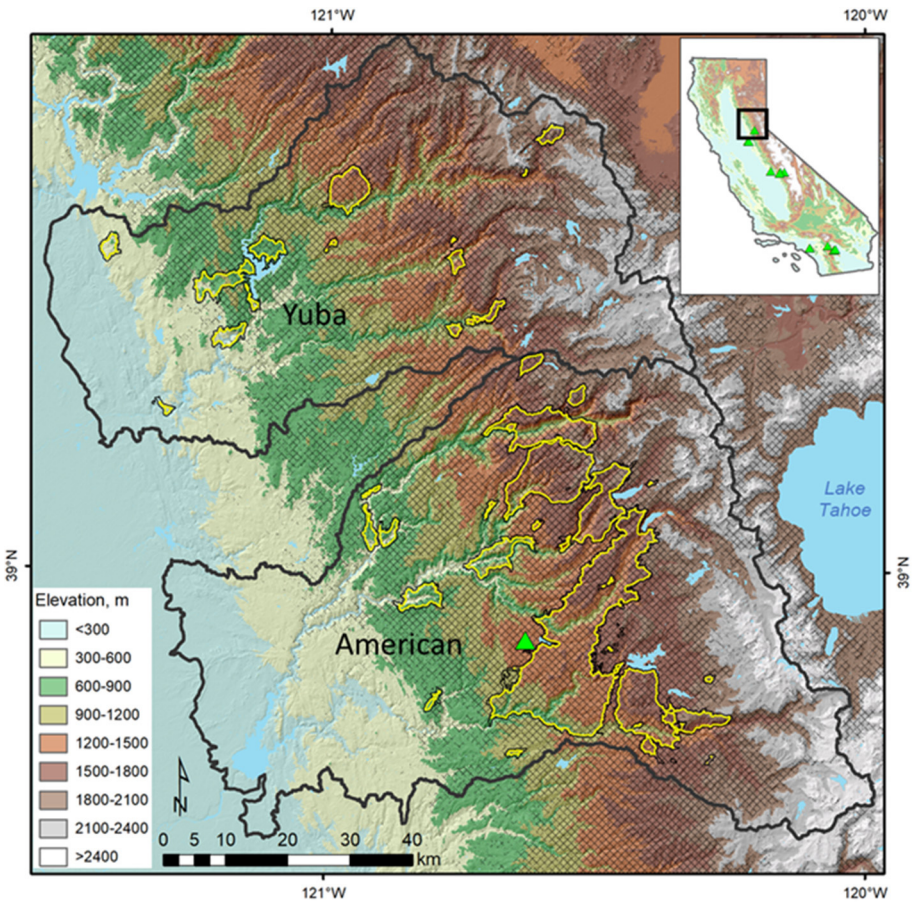

FIGURE 1 | Study area shaded by 300-m elevation bands. Fire perimeters (yellow–black outlines) are all fires to occur in the Yuba and American watersheds >50 ha (1985–2017). Cross-hatching indicates the extent of mixed conifer forest. Inset depicts the study location within the state of California, USA. Green triangles on insert and main map show locations of flux towers used in this study.

water demand using the methods of Fellows and Goulden (2017). Finally, we show how this approach can be used to project potential evapotranspiration reductions for the level of fuel treatments proposed to restore forests to a more-sustainable state.

Gridded Evapotranspiration

To prepare components of the water balance for the Yuba-American region, we first assembled water-year (October–September) annual means of NDVI from Landsat data for 1985–2018. Annual means incorporated US Geological Survey (USGS) Landsat Collection 1 Tier 1 surface-reflectance data (30-m resolution) from Landsat 5 (1985–2011), Landsat 7 (2012–2013), and Landsat 8 (2014–2018) missions, filtered for clouds, cloud shadows, water, and snow. Additional filtering for shadows was accomplished by masking pixels for which values in the red, shortwave infrared 1, and shortwave infrared 2 bands were <1%, and values in the infrared band were <5% reflectance. All NDVI grids derived from Landsat 7 ($L7_{ETM+}$) and Landsat 8 ($L8_{OLI}$) were then homogenized to Landsat 5 Thematic Mapper ($L5_{TM}$) using the methods of Su et al. (2017), by the following equations:

$$L5_{TM} \times 100 = 0.9883 \times L7_{ETM+} \times 100 - 3.6652 \quad (1)$$

$$L5_{TM} \times 100 = 0.8212773 \times L8_{OLI} \times 100 + 4.0277188 \quad (2)$$

Assembling the NDVI means and homogenization was completed in the Google Earth Engine cloud-computing environment (Gorelick et al., 2017), and products were exported for further processing as described below.

Annual mean NDVI raster datasets were converted to estimates of annual evapotranspiration building on the methods of Goulden et al., who provide rationale for using a statistical vs. energy-balance approach to extrapolate ET in complex terrain like that found in the Sierra Nevada (Goulden et al., 2012). They note that previous investigators have shown that in semiarid regions, a site's water balance, leaf area index (LAI), primary production, and annual ET are tightly correlated through a series of feedbacks, with a high LAI both driving a high annual ET and symptomatic of a location with a high ET (Grier and Running, 1977; Gholz, 1982). They also note that LAI has been shown to be well-correlated with NDVI (Carlson and Ripley, 1997), creating

a tight relationship between NDVI and ET, with previous studies confirming a strong correlation between annual ET and NDVI across semiarid landscapes (Groeneveld et al., 2007). Goulden et al. (2012) further note that, alternatively, physically based approaches to scaling ET require spatially resolved radiation, temperature, humidity, wind speed, and other attributes that vary markedly over small distances, making extrapolation of montane meteorological conditions to fine scale highly uncertain. We thus use their simpler approach of regressing ET against a vegetation index.

Because our focus is on wetter regions than most of the calibration data used in previous studies, we extended the calibration to include three sites with higher precipitation that are in or near the study area (see **Supplement Material** for details). Specifically, we evaluated two calibrations: (i) an extension of the two-parameter exponential regression used previously (Bales et al., 2018; Roche et al., 2018) that has been applied previously for disturbance analysis and (ii) a multiple regression using NDVI and precipitation aimed at better representing basin-wide water balance. Using leave-one-out cross-validation to assess the model temporal sensitivity, we found that most predictions fall within ± 100 mm year^{-1} of measurements, with the main exceptions being points at high NDVI where saturation is an issue (see **Figures S1**, **S2** for data and calibrations).

Eddy covariance is a well-accepted measurement method, yet it remains important to consider uncertainties. Analysis of cumulative ET and carbon dioxide (CO_2) fluxes shows that there is no single definition or single cause of uncertainty (Goulden, 1996). The uncertainty in ET fluxes, estimated to be up to 10%, is driven by uncertainty in the assumption that the Bowen ratio is correct, uncertainty in soil and other heat-storage terms, and to a lesser extent, net radiation. Sampling uncertainty should be ~5%, similar to that estimated for CO_2. Thus, the uncertainty of annual ET from an individual tower is as much as 15%. This uncertainty should be random from tower to tower and, to a lesser extent, year to year, so the overall uncertainty should be less for the full dataset. Calibration with NDVI may introduce another 5%, leading to an overall uncertainty in the model of at least 10% but <20%.

Fire Effects on Evapotranspiration

Using the estimate of annual *ET* derived above, we estimated the elevational and cumulative *ET* effects of large fires, >50 ha, as assembled by Region 5 of the US Forest Service (1990–2017; https://www.fs.usda.gov/Internet/FSE_DOCUMENTS/fseprd596284.zip) in these watersheds using the methods of Roche et al. (2018). Fire statistics are shown in **Tables S1, S2**. We chose to examine the impacts of fires for 1990–2013 in order to incorporate a 5-years-before-fire estimate of *ET* from the Landsat record, which begins in 1985, and similarly estimate the 5-years-post-fire mean *ET* (up to the year 2018). Given that overlapping fire perimeters accounted for <2% of the area burned, we combined all fire polygons into a single layer, attributing overlap areas with information pertaining to the earliest fire to occur in the 1985–2017 period. This layer was overlain with a 100-m grid that was buffered from the fire perimeters by 75 m to minimize the influence of partially burned grid cells. Each grid cell was additionally attributed with the year of the fire, mean elevation, mean percent change in basal area 1-year post-fire using Miller et al. (2009) and Miller and Quayle (2015) (https://www.fs.usda.gov/Internet/FSE_DOCUMENTS/fseprd596279.zip), and mean estimated *ET* for each water year. We created a similar database of unburned 100 × 100 m polygons that comprised 20% of forested area in each watershed over the period 1985–2018. A polygon was designated "forested" if the majority of 30-m grid cells intersected by the polygon were classified as forest (deciduous, evergreen, or mixed-forest classes) in the 2011 USGS National Land Cover Database (Homer et al., 2015). The actual change in ET for each grid cell was estimated for each year post-fire until post-fire ET equaled or exceeded pre-fire ET, or until 2018:

$$\begin{aligned}&\text{Annual ET reduction}\\&= \mathrm{ET}_{\text{burned, 5-years-pre-fire-mean}} - \mathrm{ET}_{\text{burned, post-fire}}\\&\quad -(\mathrm{ET}_{\text{unburned, 5-years-pre-fire-mean}} - \mathrm{ET}_{\text{unburned, post-fire}})\end{aligned} \tag{3}$$

Estimates of the unburned control ET were a mean of all unburned polygons in a 500-m elevation band centered on each burned grid cell in each major watershed.

Using this dataset, we then estimated changes in evapotranspiration by forest basal area reduction (burn severity) class (0–25%, 25–50%, 50–75%, and 75–100%) and elevation (by 100-m elevation band) by comparing the 5-year post-fire mean ET with the 5-year pre-fire mean ET. We also estimated net annual evapotranspiration change across all burned areas for the period 1990–2018 as well as recovery rates by burn-severity class as reported by the US Forest Service (USFS).

Subsurface Water Balance

In order to estimate the amount of soil water extracted from storage each year, we used the methods of Fellows and Goulden (2017), which follows methods outlined by Lutz et al. (2010). The steps are as follows: (i) estimate monthly water input to the soil water index using monthly 800-m parameter-elevation relationships on independent slopes model (PRISM Climate Group, 2019) precipitation data and an estimate of snowmelt (see Lutz et al., 2010), (ii) calculate monthly potential evaporation (PET) using monthly mean temperature from PRISM and the modified Hamon (1963) method employed by Lutz et al. (2010), and (3) combining estimates of actual evapotranspiration from NDVI regression with water indices and PET, by subtracting the annual sum of monthly minimums of water indices and PET from ET values. All calculations were done at 30-m resolution. We used the time series of PRISM precipitation data at a resolution of 800 m for the study period. We downsampled these layers to 30 m by nearest-neighbor interpolation, summed by water year, and aligned the resulting grids with the above ET raster. We averaged daily minimum and maximum temperature using 800-m PRISM data, then created monthly means, and finally downsampled the monthly temperature layers to 30 m by nearest-neighbor interpolation. Estimates of PET using the method of Hamon as outlined in Dingman (2002) were modified

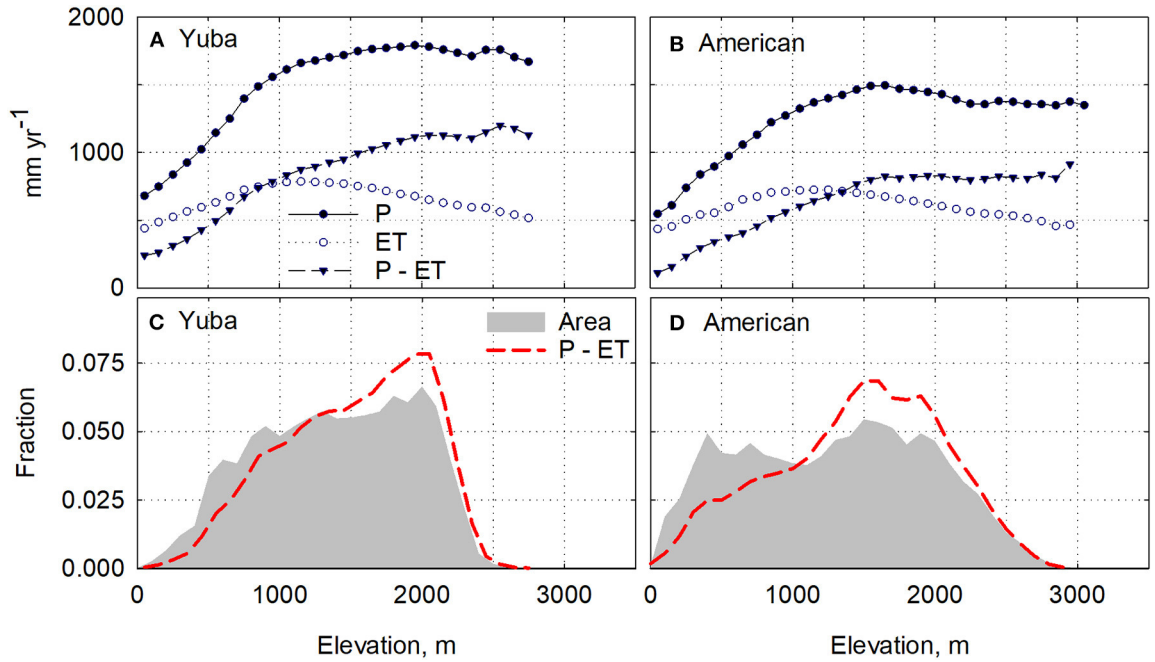

FIGURE 2 | Elevational distribution of mean precipitation (*P*) and evapotranspiration (ET), and P-ET in the **(A)** Yuba and **(B)** American River watersheds by 100-m elevation bin for the period 1985–2018. Basin-area fraction and volume fraction of P-ET in each 100-m band are shown on **(C,D)**. Volume fraction was calculated from depth and area fractions on **(A,B)** see **Figure S5** for annual values for an average, wet, and dry year.

as follows:

$$\mathrm{PET} = 1.265 \times \mathrm{PET_{Hamon}} \quad (4)$$

where 1.265 is a tuning factor used by Fellows and Goulden (2017) to minimize bias between PET and ET datasets. Snowpack was set to zero each year, i.e., no year-to-year carryover of snowpack storage. Finally, we determined the maximum withdrawal from storage for each grid cell over the 1985–2018 period, which may be considered the minimum amount of subsurface water-storage capacity.

Basin-Scale Annual and Interannual Water Balance

We derived annual rasters of P-ET, an estimate of the amount of water available for runoff or storage recharge (excess) or the amount of water required from storage (deficit) to maintain estimated annual ET. Starting with the 1985 P-ET grid, we then tracked interannual use of water in storage by summing P-ET in each cell year by year. Negative values of P-ET, which indicate withdrawal from storage, were retained in any given year, and positive values, indicating no withdrawal, were set to zero. In order to estimate a maximum amount of storage water used in any pixel during the 1985–2018 period, we extracted the lowest negative P-ET value from all storage-water-use grids.

We compared water-balance components using the above grids with full natural flow for the Yuba (Yuba River at Smartville, ID=YRS, California Data Exchange Center, 2019) and American (American River at Folsom, ID=AMF, California Data Exchange Center, 2019) River watersheds using the methods of Bales et al. (2018). For each watershed, we extracted annual *P*, ET, and depth of water extracted from soil storage (ΔS). The latter was determined as the mean of all grid cells where P-ET was negative. These components were compared to full natural flow (Q), using the annual water balance: $P = \mathrm{ET} + Q - S$.

RESULTS

ET and Precipitation by Elevation Band

Evapotranspiration values peak in the Yuba and American at 700–800 mm year^{-1} around the 1,100–1,200 m elevation, whereas precipitation peaks at elevations closer to 1,600–2,000 m (**Figure 2**). Average precipitation (±stdev) is higher in the Yuba (1,479 ± 500), peaking near 1,800 mm year^{-1} at 2,000 m elevation, compared to the American (1,228 ± 430 mm year^{-1}), peaking near 1,500 mm year^{-1} at 1,700 m elevation. Volumetric runoff was calculated based on area per elevation band times runoff depth and comes mainly from 800 to 2,100 m elevation in the Yuba and 500–2,100 m in the American (**Figure 2**). Evapotranspiration varied little between wet vs. dry years, averaging about 675 ± 57 mm across the Yuba and 619 ± 54 mm in the American. The large interannual differences in precipitation, indicated by the coefficient of variation (CV) were amplified to give even larger relative interannual differences in P-ET. CV averaged 0.35 for precipitation and 0.63 for P-ET across the two basins, whereas ET is similar in wet vs. dry years (CV = 0.09) (see also **Figures S4, S5**).

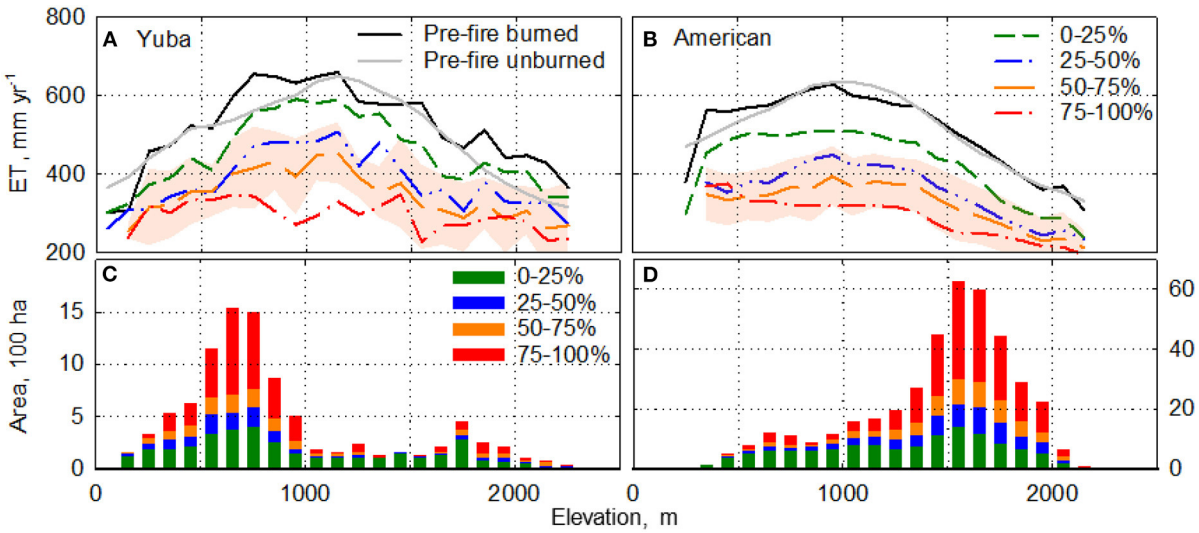

FIGURE 3 | Elevational dependence of 5-year mean evapotranspiration (ET) post-forest fire, for fires in the period 1990–2013, categorized by basal area reduction (fire-severity class): **(A)** Yuba and **(B)** American watersheds. Solid black line is pre-fire ET, and solid gray line is control (unburned) area. Shaded area illustrates the standard deviation around the 50–75% basal area reduction line. Other standard deviations are similar. Panels **(C)** Yuba and **(D)** American depict the burned area by basal area reduction quartile class (note the different ordinate scales).

Effect of Fire on ET

Reduced evapotranspiration due to all forest fires in the study area between 1990 and 2013 varied with respect to elevation and basal area change (**Figure 3**). The mean annual ET during the 5 years post-fire was reduced approximately 30–100 mm year^{-1} for each additional 25% reduction in basal area, between 750 and 2,100 m elevation. This is most apparent in the American watershed, which had over four times the area burned as did the Yuba (42,299 vs. 9,850 ha) during this period (**Tables S1, S2**). Note that ET reduction varies within each burn-severity class, as illustrated for the 50–75% basal area reduction class.

Post-fire recovery rates of ET were most rapid in the first 5 years, with approximate rates of 7–10 mm year^{-1}, 7–13 mm year^{-1}, and 9–13 mm year^{-1} for 0–25, 25–75, and 75–100% basal area reduction, respectively (**Figure 4**). Evapotranspiration rates stabilized after 12 years in the Yuba and 15 years in the American. At 20 years post-fire, there remained 50–90 mm year^{-1} ET reduction in the higher burn-severity classes in the American, while little post-fire effect was evident in the Yuba. Note that this analysis aggregated results over all fires analyzed; and variability in recovery rates within a severity class is quite large.

Differences in evapotranspiration reduction by fire and post-fire recovery between fires are illustrated for four large fires on **Figure 5**. The high severity of the Pendola fire did not translate to above-average ET reduction, which was 50–200 mm year^{-1}, increasing with severity class. The area experienced a moderately long period to recover to pre-fire ET levels, with an average of 10.75 years. The percent area recovered was very high, averaging 78%. The area of the Star Fire had similar ET reduction and has also experienced a high percentage of recovery, averaging 50%. This recovery took an average of 13 years, which is also comparatively high. Of particular note is that these recovery

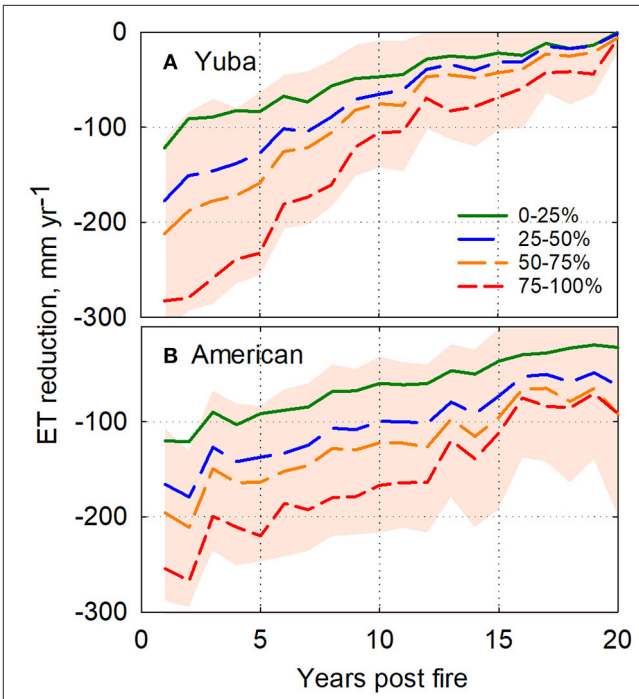

FIGURE 4 | Time series of mean post-fire evapotranspiration (ET) reduction by fire-severity class or post-fire response of ET, for the **(A)** Yuba and **(B)** American, 1990–2018. Plus and minus one standard deviation is shown for the 50–75% basal area-reduction class. Other standard deviations are similar.

metrics are relatively consistent across severity classes, i.e., ET in areas burned at low severity did not recover at a faster rate than did those experiencing higher-severity fire. We hypothesize

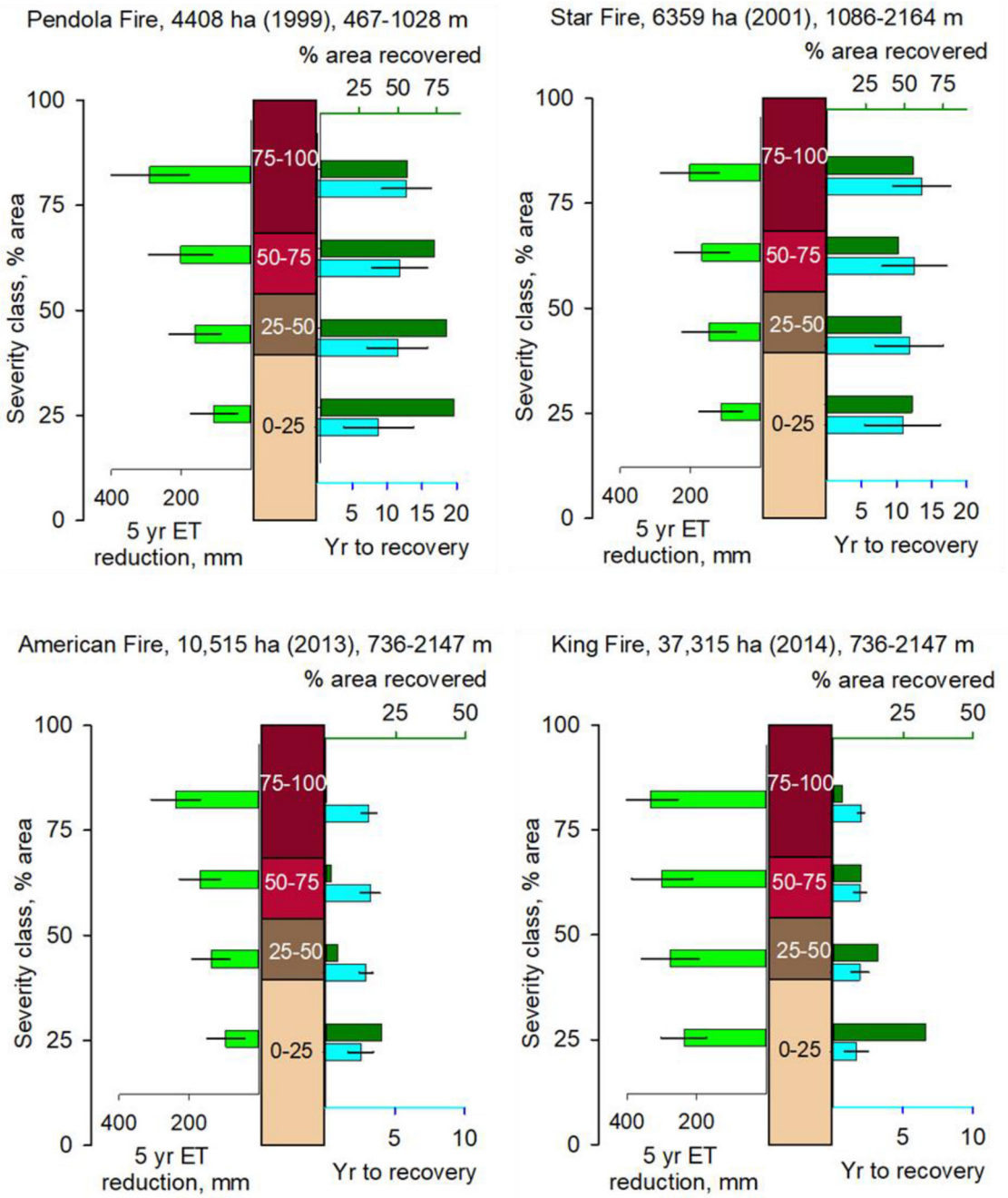

FIGURE 5 | Evapotranspiration (ET) reduction and recovery to pre-fire levels for four large fires that burned with a range of severity classes. Center, vertical bar shows percent area of fire in each of the four severity classes. Bars on the left show ET reduction by fire (mean and standard deviation), averaged over 5 years post-fire, by severity class (highest bar is highest severity class). The four pairs of bars on right also correspond to the four severity classes, with the upper bar being area recovered and lower bar in each pair being years to recovery of pre-fire ET levels (mean and standard deviation); the number of years to recovery refers only to those grid cells where net ET change is greater than or equal to zero relative to pre-fire and unburned grid cell ET values (see Equation 5). The remaining grid cells had not recovered as of 2018. The proportion of mixed conifer for each fire is 73% (Pendola), 80% (Star), 83% (King), and 95% (American).

that this is due to the forest in areas experiencing lower severity being less dense to start with. For the American fire, the ET reduction was similar, and there was a consistently shorter period to recovery, under 5 years across all severity classes. The area recovered is also very low, with a maximum of 12%, and decreases with increasing severity class. The much larger King Fire had a very significant 5-year reduction in evapotranspiration, above 280 mm across all severity classes. It took 2 years to recovery for

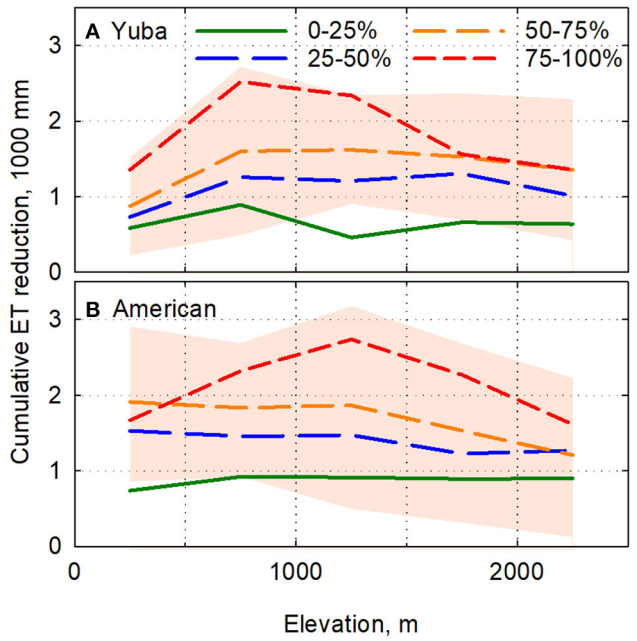

FIGURE 6 | Cumulative evapotranspiration (ET) reduction by fire-severity class and 500-m elevation bins for the **(A)** Yuba and **(B)** American watersheds for fires 1985–2013. Plus and minus one standard deviation is shown for the 50–75% basal area reduction class. Other standard deviations are similar.

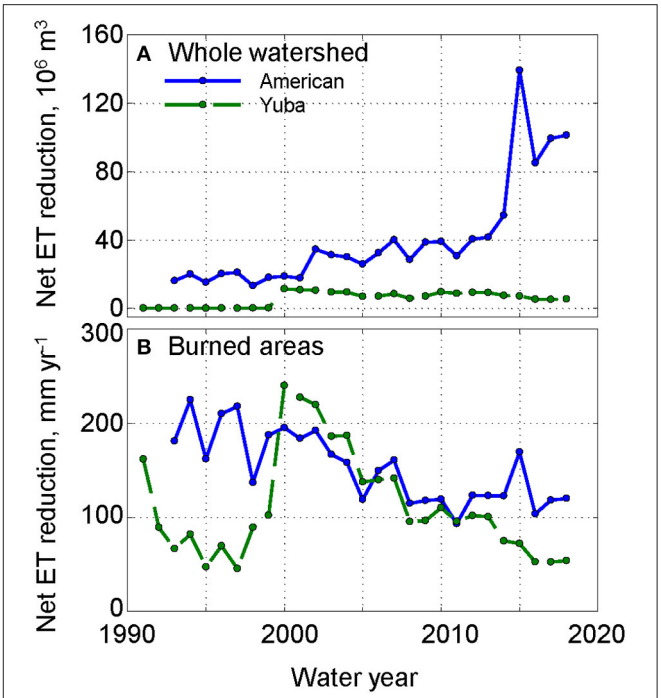

FIGURE 7 | Change in evapotranspiration (ET): **(A)** net whole-basin volumetric change and **(B)** depth of ET reduction in burned areas (1990–2017) for each watershed.

some areas in all severity classes, which is low. The area recovered is relatively high in the 25% severity class and decreases with increasing severity.

Summing total ET reduction from one year post fire until recovery to pre-fire levels, we estimated the cumulative ET reduction for the period 1986–2018 for areas that burned 1985–2013, by fire by severity class. While the data are somewhat noisy, even after aggregating to 500-m elevation bands, given lack of uniform fire coverage by severity class within each basin, it is apparent that cumulative ET reduction generally exceeds 1,200 mm for moderate fire severity (25–75% basal area reduction) in both basins and across a broad elevation range (500–2,200 m) (**Figure 6**). Values are generally higher in the American across all severity classes except in the 750-m band in the highest severity class, which is the result of a single large fire.

Summed over the whole basin, the cumulative volumetric evapotranspiration reduction due to fires in the American watershed is more than 15 times that in the Yuba due to the extensive area burned in the American, particularly since 2013 (**Figure 7A**). Prior to 2013, ET reduction in the American peaked in 2009 at just over 40 million m^3 per year. This number more than tripled by 2015 due several large fires, including the American and King fires. The effect of the 2014 King Fire (largest polygon on **Figure 1**, running SSW to NNE in the center of the basin), is quite visible on the ET and P-ET maps for 2015 (**Figure S4**). The Yuba watershed exhibited about 5–10 million m^3 reduction per year. The net ET reduction for burned areas ranged between 50 and 240 mm $year^{-1}$ depending on the size, basal area reduction, and time since fire in each watershed (**Figure 7B**).

Maximum Annual Soil Water Use for Evapotranspiration

Much of the forested area in the watershed apparently has historically used 450–600 mm $year^{-1}$ of subsurface water during the summer dry season each year to meet annual ET demand (**Figure 8**). Forests in the north Yuba access greater than 600 mm $year^{-1}$, while forests at the highest elevations in both watersheds access less subsurface water due to a limited growing season. Lower values of subsurface water use at lower elevations reflect less vegetation and drier conditions.

Annual and Interannual Water Balance

The maximum cumulative subsurface water accessed for evapotranspiration for any consecutive multiyear period (1985–2018) is depicted in **Figure 9**. A broad belt of substantial interannual subsurface use (200–300 mm $year^{-1}$) is evident in the middle elevations of the American River watershed (~800–1,300 m), which is largely absent in the Yuba. Upper elevations of both watersheds exhibit little subsurface water accessed for evapotranspiration.

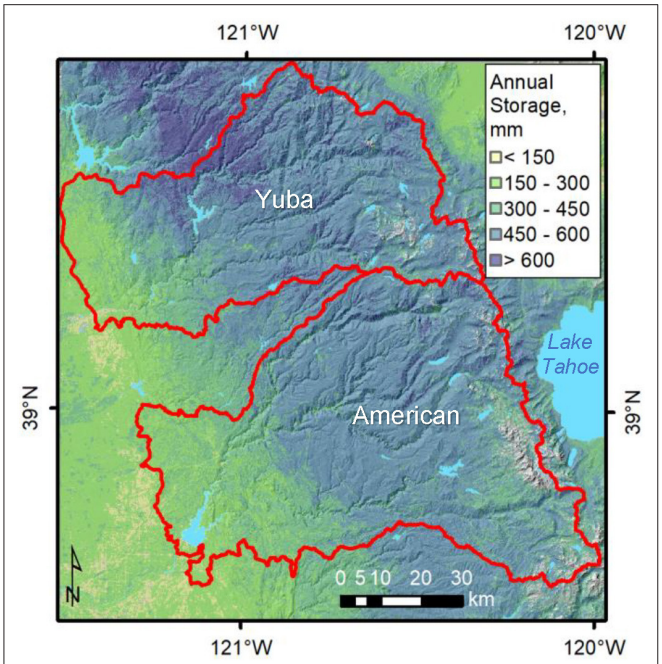

FIGURE 8 | Maximum seasonal amount of subsurface water storage used for evapotranspiration in a single year for the period 1985–2018. Gray area is no data.

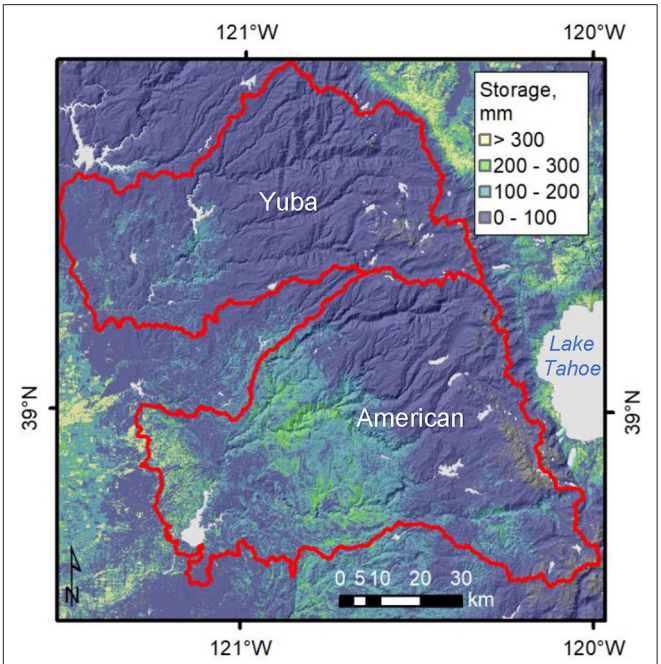

FIGURE 9 | Maximum cumulative (interannual) evapotranspiration supplied by subsurface water storage for the study period (1985–2018), which is the maximum accumulated negative value of annual P-ET. Dark and light gray areas indicate no data and lakes, respectively.

DISCUSSION

Disturbance and Management Effects on Water Balance

Declines in evapotranspiration make a greater fraction of annual precipitation available for runoff from source-water watersheds to downstream users. Disturbance by wildfire, managed fire, or mechanical thinning lowers evaporative demand, which is proportional to biomass amount, i.e., forest density. The amount that evaporative demand decreases, and the rate of growth in demand as vegetation regrows, also depends on the interaction of climate and geology. While reported fire severity, represented by basal area reduction, varies from fire to fire (**Figure 5**); these two densely forested watersheds give 5-year post-fire average values of about 65 ± 32 mm year^{-1} reduction (mean ± standard deviation) in ET for each 25% increase in basal area reduction class (**Figure 3**). The variability around the mean, shown for the 50–75% line, is expected given the heterogeneity in vegetation density, forest structure, species mix, and thus fire response across the basin. Differences in weather between different wildfires, plus landscape attributes, also contribute to the observed variability in wildfire response.

The lowest fire-intensity class, 0–25% reduction in basal area, may be considered equivalent to a relatively light management treatment but one that is realistic for areas where infrastructure or habitat limit actions. A fire in the two medium-intensity classes (25–75%) includes the range considered for restoration treatments. Our data reflect a 5-year mean decrease in *ET* of ∼85 mm year^{-1} for 0–25% basal area removal vs. ∼175 mm year^{-1} for a 25–75% basal area reduction (**Figure 3**). Again, variability across forest stands with different elevations, precipitation, subsurface-water storage, and pre-fire density, plus interannual variability in climate, give a standard deviation of ∼50% of the mean. Still, these values provide planning scenarios rooted in historical data.

For comparison, it is useful to consider some broader assessments of data from other regions that reported changes in evapotranspiration with reductions in forest density. The broad synthesis of data by Zhang et al. (2001), using the Budyko framework, provides an indication of the potential water impacts of forest management. Using Equation 8 in Zhang et al. (2001) with the average annual precipitation for the two basins for the study period (1,479 mm for the Yuba and 1,228 mm for the American), a 50% reduction in forest cover, replaced by grassland vegetation, gives a 167 and 136 mm reduction in annual ET, respectively. Each 25% reduction in forest density provides about a 77-mm reduction in annual ET. These numbers are remarkably similar to the averages apparent in our data (**Figure 3**), which give an average of 68 mm year^{-1} across the study area, and ∼83 mm year^{-1} for the elevations having the most area burned.

The large variability in rates of post-fire recovery of evapotranspiration toward pre-fire levels is also expected, given the variability of wildfire patterns across the different fires aggregated in this analysis, the interannual variability in climate following the different fires, and the heterogeneity of landscape attributes across the steep gradients in mountains such as the Sierra Nevada. While individual wildfires showed a range of ET recovery rates and amounts (**Figure 5**), an overall examination

of post-fire evapotranspiration recovery amounts suggests little influence of precipitation and temperature (elevation), at least for the first 5 years post-fire (data not shown). Nevertheless, the consistency in rates for the two medium-intensity classes, especially in the American, 6.4 mm year^{-1}, provide planning values based on past climate (**Figure 4**). Values in the Yuba were higher, 8.8–10.5 mm year^{-1}, but dominated by one large lower-elevation fire in an area with higher precipitation. The future rate of post-fire recovery will depend on the sequence of wet and dry years, particularly for areas with higher dependence on interannual subsurface water storage (**Figure 9**).

The net observed changes in ET over the two basins, when expressed as changes in P-ET, are relatively small compared to the whole-basin discharge. The net reduction in the American basin for the decade ending in 2013, before the 2014 King Fire, averaged about 40 million m^3 year^{-1} (**Figure 7A**), compared to an average annual basin discharge over that period of 2,849 million m^3 year^{-1}. Even the value of about 100 million m^3 year^{-1} in 2018 is still under 4% and not detectable in flow measured at the basin outlet.

The Yuba and American watersheds have higher *P*, ET, and P-ET values compared to areas further south in the Sierra Nevada (Bales et al., 2018), suggesting that there is significant potential for higher gains in P-ET and thus runoff from forest management. For example, sustained ET reductions at the level shown on **Figure 6**, averaging over 50 mm year^{-1} for 25–75% basal area reduction for the 1985–2013 period, could have a significant impact if extended over a larger areas. Sustaining that amount, over 50% of the American and Yuba basins would reduce evapotranspiration and provide potential runoff by about 121 and 72 million m^3 year^{-1} in the two basins, respectively, or ∼4% of each basin's average discharge over our 1985–2008 study period. Applying the higher average amounts of ET reduction observed in both basins in the 25-year period shown on **Figure 7B**, 131 mm year^{-1}, would give about reductions in ET and potential runoff of ∼10% of the period-average discharge, totaling about 0.5 billion m^3 year^{-1} for the two basins. It is acknowledged, however, that extending treatments over large areas of the Sierra Nevada is constrained by multiple factors (North et al., 2015b).

Subsurface Storage and Resistance to Dry Periods

In California's Mediterranean climate, both snowpack and subsurface water storage provide the water needed to sustain ecosystems during the summer–fall dry period. For higher elevations which are also cold during the wet winter season, the dry period is the main period of growth. Vegetation densities are thus controlled in part by climate, i.e., temperature and precipitation, and also by the interaction of climate with weathered bedrock over geologic time. The vulnerability of forests to drought then occurs with a shortage of precipitation, warmer temperatures, and limited subsurface storage.

In a multiyear drought, precipitation may be less than the level of evapotranspiration needed to sustain a forest, with multiyear subsurface storage making up the difference. However, there is a limit to how many years and how much water deficit can be met from storage before root-zone water storage is depleted (Klos et al., 2018). As temperature warms, the evaporative demand of existing vegetation can increase (Goulden and Bales, 2019). Warmer temperatures also shift precipitation from snow to rain, and melt snow earlier in the year, resulting in longer reliance on subsurface water storage for the growing season. Thus, subsurface storage is expected to support less summer evaporative demand by vegetation as climate warms, vs. in the past.

Broad areas of the upper Yuba appear to have substantial annual subsurface storage (**Figure 8**) and during the period of analysis drew upon minimal interannual (over-year) subsurface storage (**Figure 9**). That is, current forest water use is well within precipitation amounts at all elevations, and forests are able to tap substantial subsurface water storage during warm and dry periods each summer. Interannual storage is more important at lower elevations where there is less rain; however, these areas also have low ET values (**Figure 2** and **Figure S4**).

The main area exhibiting potential vulnerability to multiyear dry periods is the broad middle portion of the American River basin (**Figure 9**), in the 600–1,200 m elevation range (**Figure 1**). A cumulative interannual deficit of 300 mm in subsurface storage should not affect the seasonal demand to sustain summer evapotranspiration, provided root-accessible water is greater than the sum of the interannual deficit and the seasonal ET supported by storage, on the order of 600 mm. As reported for the further-south Kings River basin, the forest at 1,160 m elevation had a P-ET deficit approaching 1,500 mm when tree mortality became widespread (Goulden and Bales, 2019). Indications are that moisture stress may have started when the *P-ET* deficit surpassed 1,000 mm. Thus, the American basin has some additional resilience, but should see greater drought stress for a more-sustained, warmer or drier drought than in the period fall 2011 to fall 2015.

It is also important to emphasize that for projecting drought stress, cumulative P-ET deficit (**Figure 9**) has been shown to be well correlated with indices of drought stress and tree mortality such as satellite-derived normalized difference moisture index (NDMI) and aerial surveys done by the US Forest Service (Goulden and Bales, 2019). Traditional indices such as Standardized Precipitation Index (SPI), Standardized Precipitation Evapotranspiration Index (SPEI), and Palmer Drought Severity Index (PDSI) were not well-correlated with forest stress or mortality in the Sierra Nevada during the recent 4-year drought. When used together with seasonal demand for subsurface water to support evapotranspiration (**Figure 8**), cumulative P-ET deficit (**Figure 9**) can be applied more broadly to anticipate drought stress and focus forest-management priorities.

Water-Balance Uncertainty

As a check on the water balance, we summed total annual runoff (P-ET) per basin, which compared well with full natural flow values from the California Department of Water Resources (**Figure 10**). The P-ET values exhibit a median bias of ∼130 mm for the Yuba and 40 mm for the American. These values, about

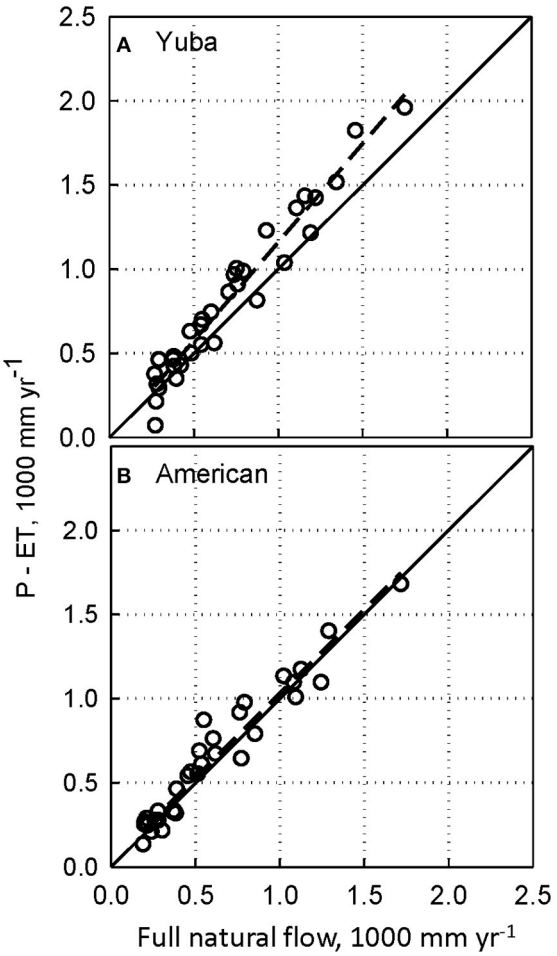

FIGURE 10 | Water balance for the **(A)** Yuba and **(B)** American watersheds (1985–2018). Full natural flow is for the respective USGS stream gage.

5% of precipitation or 10% of full natural flow, are within the expected uncertainty of the analysis. Note that annual values of P-ET do not account for ΔS, which is reflected in dry years having slightly higher runoff than would occur in the absence of multiyear storage to support ET. Conversely, in wet years some precipitation will go to replenishing over-year storage deficits, especially when following multiyear dry periods (Bales et al., 2018). However, in these basins, interannual ΔS during the study period was relatively small (**Figure 9**).

In the current analysis, we used the two-variable model (NDVI and precipitation) for scaling the analysis of drought stress and continue the NDVI-only model for assessing response to disturbance. The two variables in our additive model are weakly correlated in the calibration data ($r^2 = 0.33$). Given the weighting between the additive terms in the two-variable model, the ET response to NDVI changes is muted compared to the one-variable model.

In prior analyses, the NDVI-only model worked well for water balance in the southern Sierra (Bales et al., 2018) and provided an index for projecting forest drought stress (Goulden and Bales, 2019). Yet, in the current water-balance analysis, it underestimates evapotranspiration across higher-precipitation basins, giving median bias values of 300 and 170 mm for P-ET vs. full-natural flow for the Yuba and American, respectively. The two-variable additive model (NDVI and precipitation) gave respective average ET values for the two watersheds of 668 and 610 mm year^{-1} vs. 461 and 432 for the NDVI-only model. These latter values are essentially the same as those from a large-scale blended satellite-data and bottom–up modeling approach, which reported evaporation estimates across California (Baldocchi et al., 2019). Their average ET values for the two watersheds were 460 and 454 mm year^{-1}, respectively. Another difference between the results from Baldocchi et al. (2019) vs. our statistical approach is the pattern of ET. Their results show less difference in modeled ET across areas with different NDVI, precipitation, and temperature compared to our statistical approach.

The basin water balance in **Figure 10** shows that P-ET values during dry years have a relatively small bias compared to flow measured at the basin outlet, reflecting evapotranspiration in drier parts of the basin depending on multiyear subsurface water storage to make up for deficits in precipitation. In wet years, the bias in P-ET relative to full natural flow is larger, part of which should reflect replenishment of subsurface storage that was drawn down in wetter years. Overall, however, there is little evidence for water limitation basin wide. The implication for forest restoration is that reductions in forest density by management actions or wildfire should reduce forest evapotranspiration, as remaining vegetation is not water limited (Saksa et al., 2019). Forest treatments, therefore, will not only increase runoff by reducing ET but also have the potential to increase subsurface storage of water in dry years. This increase should lead to increases in runoff in current or subsequent years, increase minimum flows, and increase forest water availability.

Limitations of Analysis

An interesting result of this work is that net evapotranspiration change due to fire in the American River watershed was ∼20% less than that reported by Roche et al. (2018). This is the result of (i) using the USGS Tier 1 Collection 1 of Landsat data vs. the precollection data, and (ii) using a normalization that is more representative of the entire vegetation range of California than that of Su et al. (2017). While there may be an impact to the annual NDVI average due to variable snow and cloud cover filtering of mid- and high-elevation areas, the improved regression results relative to that used earlier gives us confidence in the current results. Note that the current regression has additional years of data not available for the earlier analysis. Additional work is needed to characterize the difference between an unweighted mean NDVI as used here vs. a smoothed and month-centered NDVI average as used in Roche et al. (2018).

This analysis assumed that all unburned forested polygons represented control conditions even though some proportion had been logged or mechanically thinned during the analysis period. The effect of this known issue would be to reduce the estimate of evapotranspiration reduction due to fire. With respect to these limitations, it can then be stated that the results should

represent conservative estimates of potential ET reductions due to forest thinning through fire.

An additional limitation is the neglect of net lateral subsurface flow between cells. Subsurface redistribution of water would result in some cells having more and some less water for evapotranspiration than indicated by annual precipitation. While a comprehensive spatial analysis of the question has yet to be reported for Sierra Nevada basins, both measurements and modeling point to the effect being relatively small across most of the landscape. This does not rule out local hotspots where lateral redistribution is important, given its importance in sustaining baseflow in streams and dry-season evapotranspiration. In a southern Sierra headwater catchment, Oroza et al. (2018) found topographic wetness index (TWI) to be an explanatory variable for spatial patterns of soil–water storage only during the dry summer period, after drawdown of soil water following the wet winter and spring periods. Similarly, across a broad area of the southern Sierra, Su et al. (2017) found that TWI was not a good predictor of patterns in moisture stress (NDMI) or greenness (NDVI) from Landsat. Using a rich suite of soil–moisture data from headwater catchments in the American and Merced River basins, Saksa et al. (2017) modeled catchment-scale water balances, with no significant lateral redistribution. This is also consistent with extensive subsurface measurements focusing on the 2012–2015 drought in the southern Sierra, which showed limited evidence of lateral redistribution (Bales et al., 2018). Lateral redistribution is an inherent limitation in any hydrologic model that accounts for significant amounts of stored water to meet evaporative demands (see **Figure 8**). Lundquist and Loheide (2011) estimated lateral transfer of subsurface water from high to low elevations to be ∼10% of the water balance for the Upper Merced River watershed in the Central Sierra Nevada Mountains of California. Broader and more-thorough examination of when and where this component of the water balance could be important could build on these several studies, particularly the rich spatial data sets now available in the Sierra Nevada.

Finally, while the findings reported here can be used to predict ET response to wildfire and regrowth in these and nearby watersheds, they represent mean historical behavior across several disturbance events. Averaged over longer times and areas, these predictions can provide useful guides for assessing water-balance response to disturbance and recovery. These top–down modeling results can serve as evaluation data for more process-based, bottom–up modeling. Predictions based on the results presented here also provide important data for resource-management planning and scenario analysis.

CONCLUSIONS

We found that historical wildfire has made significant post-fire reductions in evapotranspiration for at least 5 years in northern Sierra forested watersheds and in some cases for more than 20 years. However, as the areas affected by wildfire were only a fraction of the larger watersheds in which the fires occurred, the effect on runoff in the two basins studied was somewhat limited. Based on the response of evapotranspiration to the levels of biomass removed in medium-intensity fires (25–75% basal area loss), widespread management actions involving mechanical thinning and controlled burns can have significant local effects on evapotranspiration, with reductions as much as 150–200 mm year^{-1} for the first 5 years. For the two basins studies, this represents 25–30% of average annual evapotranspiration in productive forests and has the potential to increase runoff by measurable amounts if extended over as much of the watershed as can be treated. Rates of regrowth in post-wildfire evapotranspiration confirm the need for follow-up forest treatments at intervals of 5–20 years to sustain lower evapotranspiration, depending on local landscape attributes and interannual climate.

The northern Sierra watersheds studied have experienced little moisture stress during the 1985–2018 period of our analysis, owing to relatively small reliance on interannual subsurface water storage to meet dry-year evapotranspiration needs of vegetation. The cumulative interannual deficits that we found were up to 300 mm year^{-1}, which are on the order of 25% of the deficits observed in the southern Sierra before widespread tree mortality occurred. However, longer dry periods will push parts of the American River basin toward the thresholds that resulted in widespread forest mortality in the Southern Sierra Nevada. Use of cumulative precipitation minus evapotranspiration (P-ET) provides a good index for planning and assessment.

DATA AVAILABILITY STATEMENT

All data used in this analysis are included in the **Supplementary Material** or are publicly available. Questions regarding the datasets should be directed to Roger Bales, rbales@ucmerced.edu.

AUTHOR CONTRIBUTIONS

JWR carried out most of the analysis and wrote parts of the manuscript. QM developed the spatial data products. JR developed the datasets used to develop the spatial data. RB supervised the work and prepared the final manuscript. All authors edited the manuscript.

FUNDING

This research was supported by a USDA Small Business Innovation Research grant to Blue Forest Conservation, with supplemental support from the National Science Foundation through the Southern Sierra Critical Zone Observatory (EAR-1331939), from the Nature Conservancy, and from the California Strategic Growth Council through the Innovation Center for Ecosystem Climate Solutions.

ACKNOWLEDGMENTS

The authors wish to acknowledge constructive comments from the reviewers, which guided improvements to the manuscript. Eddy-covariance data are available at https://ameriflux.lbl.gov/. PRISM data are accessible at http://www.prism.oregonstate.

edu/. Landsat data are available at https://www.usgs.gov/land-resources/nli/landsat/landsat-collection-1-surface-reflectance. Unimpaired runoff data are accessible at https://cdec.water.ca.gov/. SRTM data were used for elevations and are available at https://www2.jpl.nasa.gov/srtm/.

SUPPLEMENTARY MATERIAL

The Supplementary Material for this article can be found online at: https://www.frontiersin.org/articles/10.3389/ffgc.2020.00069/full#supplementary-material

REFERENCES

Allen, C. D., Macalady, A. K., Chenchouni, H., Bachelet, D., McDowell, N., Vennetier, M., et al. (2010). A global overview of drought and heat-induced tree mortality reveals emerging climate change risks for forests. *For. Ecol. Manag.* 259, 660–684. doi: 10.1016/j.foreco.2009.09.001

Anderegg, W. R. L., Hicke, J. A., Fisher, R. A., and Allen, C. D. (2015). Tree mortality from drought, insects, and their interactions in a changing climate. *N. Phytol.* 208, 674–683. doi: 10.1111/nph.13477

Anderegg, W. R. L., Kane, J. M., and Anderegg, L. D. L. (2013). Consequences of widespread tree mortality triggered by drought and temperature stress. *Nat. Clim. Change.* 3, 30–36. doi: 10.1038/nclimate1635

Baldocchi, D., Dralle, D., Jiang, C., and Ryu, Y. (2019). How much water is evaporated across California? *A multiyear assessment using a biophysical model forced with satellite remote sensing data. Water Resour. Res.* 55, 2722–2741. doi: 10.1029/2018WR023884

Bales, R. C., Goulden, M. L., Hunsaker, C. T., Conklin, M. H., Hartsough, P. C., O'Geen, A. T., et al. (2018). Mechanisms controlling the impact of multi-year drought on mountain hydrology. *Sci. Rep.* 8:690. doi: 10.1038/s41598-017-19007-0

Barnett, T. P., Adam, J. C., and Lettenmaier, D. P. (2005). Potential impacts of a warming climate on water availability in snow-dominated regions. *Nature* 438, 303–309. doi: 10.1038/nature04141

Bosch, J. M., and Hewlett, J. D. (1982). A review of catchment experiments to determine the effect of vegetation changes on water yield and evapotranspiration. *J. Hydrol.* 55, 3–23. doi: 10.1016/0022-1694(82)90117-2

California Data Exchange Center (2019). Available online at: http://cdec.water.ca.gov/dynamicapp/selectQuery (accessed October 6, 2019).

Carlson, T. N., and Ripley, D. A. (1997), On the relation between NDVI, fractional vegetation cover, and leaf area index. *Remote Sens. Environ.* 62, 241–252. doi: 10.1016/S0034-4257(97)00104-1

Chen, J. M., Chen, X., Ju, W., and Geng, X. (2005). Distributed hydrological model for mapping evapotranspiration using remote sensing inputs. *J. Hydrol.* 305, 15–39. doi: 10.1016/j.jhydrol.2004.08.029

Dingman, S. L. (2002). *Physical Hydrology. 2nd Edn.* Upper Saddle River, NJ: Prentice Hall, 646.

Fellows, A. W., and Goulden, M. L. (2017). Mapping and understanding dry season soil water drawdown by California montane vegetation. *Ecohydrol.* 10:e1772. doi: 10.1002/eco.1772

Gholz, H. L. (1982), Environmental limits on above-ground net primary production, leaf-area, and biomass in vegetation zones of the pacific northwest. *Ecology* 63, 469–481. doi: 10.2307/1938964

Gorelick, N., Hancher, M., Dixon, M., Ilyushchenko, S., Thau, D., and Moore, R. (2017). Google Earth Engine: Planetary-scale geospatial analysis for everyone. *Remote Sens. Environ.* 202, 18–27. doi: 10.1016/j.rse.2017.06.031

Goulden, M. L. (1996). Carbon assimilation and water-use efficiency by neighboring Mediterranean-climate oaks that differ in water access. *Tree Physiol.* 16, 417–424. doi: 10.1093/treephys/16.4.417

Goulden, M. L., Anderson, R. G., Bales, R. C., Kelly, A. E., Meadows, M., and Winston, G. C. (2012). Evapotranspiration along an elevation gradient in California's Sierra Nevada. *J. Geophys. Res. Biogeosci.* 117, 1–13. doi: 10.1029/2012JG002027

Goulden, M. L., and Bales, R. C. (2014). Mountain runoff vulnerability to increased evapotranspiration with vegetation expansion. *Proc. Natl. Acad. Sci. U.S.A.* 111, 14071–14075. doi: 10.1073/pnas.1319316111

Goulden, M. L., and Bales, R. C. (2019). California forest die-off linked to multi-year deep soil drying in 2012–2015 drought. *Nat. Geosci.* 12, 632–637. doi: 10.1038/s41561-019-0388-5

Grier, C. C., and Running, S. W. (1977), Leaf area of mature northwestern coniferous forests - relation to site water-balance. *Ecology* 58, 893–899. doi: 10.2307/1936225

Groeneveld, D. P., Baugh, W. M., Sanderson, J. S., and Cooper, D. J. (2007), Annual groundwater evapotranspiration mapped from single satellite scenes. *J. Hydrol.* 344, 146–156. doi: 10.1016/j.jhydrol.2007.07.002

Hamon, W. R. (1963). Computation of direct runoff amounts from storm rainfall. *Int. Assoc. Sci. Hydrol. Publ.* 63, 52–62.

Homer, C. G., Dewitz, J., Yang, L., Jin, S., Danielson, P., Xian, C. J., et al. (2015). Completion of the 2011 national land cover database for the conterminous united states – representing a decade of land cover change information. *Photogramm. Eng. Remote Sens.* 81, 345–353. doi: 10.14358/PERS.81.5.345

Klos, P. Z., Goulden, M. L., Riebe, C. S., Tague, C. L., O'Geen, A. T., Flinchum, B. A., et al. (2018). Subsurface plant-accessible water in mountain ecosystems with a mediterranean climate. *WIRES Water* 5:e1277. doi: 10.1002/wat2.1277

Lundquist, J. D., and Loheide, S. P. (2011). How evaporative water losses vary between wet and dry water years as a function of elevation in the Sierra Nevada, California, and critical factors for modeling. *Water Resour. Res.* 47:02. doi: 10.1029/2010WR010050

Lutz, J. A., Van Wagtendonk, J. W., and Franklin, J. F. (2010). Climatic water deficit, tree species ranges, and climate change in yosemite national park. *J. Biogeogr.* 37, 936–950. doi: 10.1111/j.1365-2699.2009.02268.x

McKenzie, D., Gedalof, Z., Peterson, D. L., and Mote, P. (2004). Climatic change, wildfire, and conservation. *Conserv. Biol.* 18, 890–902. doi: 10.1111/j.1523-1739.2004.00492.x

Miller, J. D., Collins, B. M., Lutz, J. A., Stephens, S. L., van Wagtendonk, J. W., and Yasuda, D. A. (2012). Differences in wildfires among ecoregions and land management agencies in the Sierra Nevada region, California, USA. *Ecosphere* 3:art80. doi: 10.1890/ES12-00158.1

Miller, J. D., Knapp, E. E., Key, C. H., Skinner, C. N., Isbell, C. J., Creasy, R. M., et al. (2009). Calibration and validation of the relative differenced normalized burn ratio (RdNBR) to three measures of fire severity in the sierra nevada and klamath mountains, California, USA. *Remote Sens. Environ.* 113, 645–656. doi: 10.1016/j.rse.2008.11.009

Miller, J. D., and Quayle, B. (2015). Calibration and validation of immediate post-fire satellite derived data to three severity metrics. *Fire Ecol.* 11, 12–30, doi: 10.4996/fireecology.1102012

Mu, Q., Zhao, M., and Running, S. (2011). Improvements to a MODIS global terrestrial evapotranspiration algorithm. *Remote Sens. Environ.* 115, 1781–1800. doi: 10.1016/j.rse.2011.02.019

Naudts, K., Chen, Y., McGrath, M. J., Ryder, J., Valade, A., Otto, J., et al. (2016). Europes forest management did not mitigate climate warming. *Science* 351, 597–600. doi: 10.1126/science.aad7270

North, M. P., Brough, A., Long, J., Collins, B., Bowden, P., Yasuda, D., et al. (2015b). Constraints on mechanized treatment significantly limit mechanical fuels reduction extent in the Sierra Nevada. *J. Forest.* 113, 40–48. doi: 10.5849/jof.14-058

North, M. P., Stephens, S. L., Collins, B. M., Agee, J. K., Aplet, G., Franklin, J. F., et al. (2015a). Reform forest fire management. *Science* 349, 1280–1281. doi: 10.1126/science.aab2356

Oroza, C. A., Bales, R. C., Stacy, E. M., Zheng, Z., and Glaser, S. D. (2018). Long-term variability of soil moisture in the southern sierra: measurement and prediction. *Vadose Zone J.* 17:170178. doi: 10.2136/vzj2017.10.0178

PRISM Climate Group (2019) *Oregon State University*. Available online at: http://prism.oregonstate.edu (accessed July 2019).

Roche, J. W., Goulden, M. L., and Bales, R. C. (2018). Estimating evapotranspiration change due to forest treatment and fire at the basin scale in the Sierra Nevada, California. *Ecohydrol* 11:e1978. doi: 10.1002/eco.1978

Rungee, J., Ma, Q., Bales, R., and Goulden, M. (2019). Evapotranspiration response to multiyear dry periods in the semiarid western United States. *Hydrol. Process.* 32, 182–194. doi: 10.1002/hyp.13322

Running, S. W., Nemani, R. R., and Hungerford, R. D. (1987). Extrapolation of synoptic meteorological data in mountainous terrain and its use for simulating forest evapotranspiration and photosynthesis. *Can. J. For. Res.* 17, 472–483. doi: 10.1139/x87-081

Saksa, P. C., Bales, R. C., Tague, C. L., Battles, J. J., Tobin, B. W., and Conklin, M. H. (2019). Fuels treatment and wildfire effects on runoff from Sierra Nevada mixed-conifer forests. *Ecohydrol* 13:2151. doi: 10.1002/eco.2151

Saksa, P. C., Conklin, M. H., Battles, J. J., Tague, C. L., and Bales, R. C. (2017). Forest thinning impacts on the water balance of Sierra Nevada mixed-conifer headwater basins. *Water Resour. Res.* 53, 5364–5381. doi: 10.1002/2016WR019240

Sivapalan, M., Blöschl, G., Zhang, L. and Vertessy, R. (2003). Downward approach to hydrological prediction. *Hydrol. Proc.* 17, 2101–2111. doi: 10.1002/hyp.1425

Su, Y., Bales, R. C., Ma, Q., Nydick, K., Ray, R. L., Li, W., et al. (2017). Emerging stress and relative resiliency of giant sequoia groves experiencing multiyear dry periods in a warming climate. *J. Geophys. Res. Biogeosci.* 122, 3063–3075. doi: 10.1002/2017JG004005

Tague, C. L., McDowell, N. G., and Allen, C. D. (2013). An integrated model of environmental effects on growth, carbohydrate balance, and mortality of pinus ponderosa forests in the southern rocky mountains. *PLoS ONE* 8:e80286. doi: 10.1371/journal.pone.0080286

Tague, C. L., and Moritz, M. A. (2019). Plant accessible water storage capacity and tree-scale root interactions determine how forest density reductions alter forest water use and productivity. *Front. For. Glob. Change* 2:36. doi: 10.3389/ffgc.2019.00036

Tague, C. L., Moritz, M. A., and Hanan, E. (2018). The changing water cycle: the eco-hydrologic impacts of forest density reduction in Mediterranean (seasonally dry) regions. *WIRES Water* 6:e1350. doi: 10.1002/wat2.1350

Westerling, A. L. (2006). Warming and earlier spring increase western U.S. *Forest Wildfire Act. Sci.* 313, 940–943. doi: 10.1126/science.1128834

Zhang, L., Dawes, W. R., and Walker, G. R. (2001). Responses of mean annual temperature to vegetation changes at catchment scale. *Water Resour. Res.* 37, 701–708. doi: 10.1029/2000WR900325

Zierl, B., Bugmann, H., and Tague, C. L. (2007). Water and carbon fluxes of European ecosystems: an evaluation of the ecohydrological model RHESSys. *Hydrol. Process.* 21, 3328–3339. doi: 10.1002/hyp.6540

Conflict of Interest: The authors declare that the research was conducted in the absence of any commercial or financial relationships that could be construed as a potential conflict of interest.

frontiers in Forests and Global Change

ORIGINAL RESEARCH
published: 09 September 2020
doi: 10.3389/ffgc.2020.539429

Hydrologic Response of Sierra Nevada Mixed-Conifer Headwater Catchments to Vegetation Treatments and Wildfire in a Warming Climate

Phil C. Saksa[1,2], Martha H. Conklin[1], Christina L. Tague[3] and Roger C. Bales[1]*

[1] Sierra Nevada Research Institute, University of California, Merced, Merced, CA, United States, [2] Now at Blue Forest, Sacramento, CA, United States, [3] Bren School of Environmental Science & Management, University of California, Santa Barbara, Santa Barbara, CA, United States

OPEN ACCESS

Edited by:
Stephen Douglas Sebestyen, United States Forest Service (USDA), United States

Reviewed by:
Timothy Link, University of Idaho, United States
Masanori Katsuyama, Kyoto Prefectural University, Japan

***Correspondence:**
Phil C. Saksa
phil@blueforest.org

Specialty section:
This article was submitted to Forest Hydrology, a section of the journal Frontiers in Forests and Global Change

Received: *01 March 2020*
Accepted: *14 August 2020*
Published: *09 September 2020*

Citation:
Saksa PC, Conklin MH, Tague CL and Bales RC (2020) Hydrologic Response of Sierra Nevada Mixed-Conifer Headwater Catchments to Vegetation Treatments and Wildfire in a Warming Climate. Front. For. Glob. Change 3:539429. doi: 10.3389/ffgc.2020.539429

We used a hydro-ecologic model (RHESSys) constrained by measurements of stream discharge, and spatially distributed snow and soil moisture, to simulate the impacts of operational forest treatments, historical wildfire and climate warming on productive mixed-conifer forests. We compared the response of two headwater catchments at the rain-snow-transition elevation in the wetter central Sierra and more water-limited southern Sierra. The variability of precipitation exerted a greater influence on annual evapotranspiration and runoff than vegetation changes from operational fuels treatment or historical wildfire. The short-term impacts of vegetation changes associated with wildfire, however, did have a greater effect on evapotranspiration and runoff than temperature increases in a warming climate. The average central-Sierra headwater response of evapotranspiration and runoff to fuels treatments (−12%, +12%, respectively) and wildfire (−43%, +46%) were greater than the projected responses to a 4.5°C temperature increase (+2 and −7%). The response in the southern Sierra was limited by lower annual precipitation and showed no response to fuels treatments; but the catchment showed respective changes of −11 and +17% in evapotranspiration and runoff for wildfire, versus +9 and −3% to a 4.5°C temperature increase. These results suggest that in the central Sierra, reductions in vegetation from either fuels treatments or historical wildfire can, temporarily, offset reductions in streamflow from a warming climate. In the southern Sierra, impacts of fuels treatments were small, and only more-extensive vegetation removal as would occur with wildfire, results in significant changes in hydrologic fluxes. Further research is needed to investigate how initial hydrologic changes and climate effects evolve as vegetation adapts and regrows following disturbance.

Keywords: vegetation change, climate variability, simulation, forested watersheds, hydrologic cycle

INTRODUCTION

It has long been known that mountain watersheds such as those on the western slopes of the Sierra Nevada, and the critical water supplies originating in these areas, are sensitive to climate warming (Pupacko, 1993; Jeton et al., 1996). Many of the winter storms that provide the deep seasonal snowpack in the western Sierra occur at temperatures above −3°C (Bales et al., 2006), making precipitation vulnerable to a transition toward a higher rainfall fraction and reduced snowpack storage in a warmer climate (Knowles, 2002; Miller et al., 2003). The frequency of wildfires is also increasing in western U.S. forests as the temperatures warm, and fuel loads remain high, the legacy of a century-long history of suppressing the frequent low-intensity fires that previously kept vegetation densities low (Westerling et al., 2006). Climate warming is changing the timing, amount and quality of mountain water supplies, as demand pressures grow and as policy requires balancing statewide water supply and demand.

Climate projections for California point to a 3.1–5.0°C increase in temperatures by the year 2100, with annual precipitation increasing or decreasing as much as 15% (Pierce et al., 2018). Greater changes in Sierra Nevada precipitation are possible by 2050–2100, as indicated under a high-emissions scenario (Garfin et al., 2013). While confidence in precipitation projections is low to medium, taken together the projected temperature and precipitation reinforce the need to consider climate scenarios that are hotter and drier than even the most-severe droughts of the past 1100 years (Griffin and Anchukaitis, 2014).

One of the impacts from climate warming is an increase in the fraction of precipitation falling as rain versus snow and effects on runoff will depend on both climate and land use attributes (Bales et al., 2018). However, Berghuijs et al. (2014) suggested that catchments with a higher fraction of snowfall have higher streamflow than would otherwise be expected from precipitation and potential evaporation. A number of studies focusing on watershed response to changes in climate have been completed for the western slope of the Sierra Nevada, which has been identified as more sensitive to changes in temperature than the eastern slope due to the larger area of lower elevation (Pupacko, 1993). For projected temperature increases of 2–5°C in the American and Merced river basins, and no change in precipitation amount or timing, Dettinger et al. (2004) reported that average-annual runoff generally remained constant, despite changes in the fraction of precipitation falling as rain and earlier snowmelt. These trends that have already been observed in the last half of the twentieth century (Stewart et al., 2004). An analysis of historical streamflow in the Sacramento River basin found that the interannual variability in precipitation explained 95% of differences in annual streamflow volumes while only 3% was explained by temperature (Risbey and Entekhabi, 1996), consistent with the minimum 80% of streamflow explained by precipitation reported by Duell (1994).

Wildfire is one of the key risks to North American ecosystems from climate change (Romero-Lankao et al., 2014). Westerling et al. (2006) discuss the competing influences of climate and forest management on increasing wildfire occurrence across the western U.S., suggesting that although recent climate change was the primary driver in Northern California, fire exclusion is also an important contributing factor in this region. In response to these changing conditions, Millar et al. (2007) encourage a proactive planning approach for forest management. Fuels treatments are an effective forest-management tool for mitigating wildfire risk in Sierra Nevada forests (Stephens, 1998; Collins et al., 2011; Stephens et al., 2013), and include selective thinning and prescribed burning for promoting fire-resilient landscapes (Agee and Skinner, 2005).

Forest-vegetation density and structure impact the interception of precipitation (Storck et al., 2002; Moeser et al., 2015), evapotranspiration amounts (Dore et al., 2010, 2012; Hawthorne et al., 2013), and the surface energy balance for snowmelt (Essery et al., 2008; Ellis et al., 2011; Mahat and Tarboton, 2012; Lundquist et al., 2013). Molotch and Meromy (2014) found elevation, temperature and precipitation were more influential than vegetation, using regression-tree analysis to rank relative physiographic and climatic influence on snow cover for the major Sierra Nevada watersheds. A modeling study using the Distributed Hydrology Soil Vegetation Model (DHSVM; Wigmosta et al., 1994) suggested that both forest cover and temperature increases will have significant, non-linear effects on snowpack and streamflow in the upper Tuolumne (Cristea et al., 2014). The relative effects of temperature and vegetation may then depend on the specific montane elevation range, vegetation type, and annual precipitation received in a watershed, requiring more-localized analyses to determine the dominant influences on evapotranspiration and runoff.

The specific aim of this study was to project the interacting effects of climate warming with forest treatments and disturbance on the annual water balance of productive Sierra Nevada mixed-conifer forests in the elevation range that transitions from rain- to snow-dominated precipitation (1500–2500 m). We focus on the extent to which reductions in vegetation that are consistent with relatively light thinning prescriptions and historical wildfire versus increasing temperatures will affect the partitioning of precipitation between evapotranspiration versus runoff.

MATERIALS AND METHODS

This study used a hydro-ecologic model, the Regional Hydro-Ecologic Simulation System (RHESSys version 5.14.7; Tague and Band, 2004), to integrate distributed-snow, distributed-soil-moisture and stream-discharge measurements, and to project water-balance response of two Sierra Nevada mixed-conifer headwater catchments to temperature and vegetation perturbations. Extensive catchment and model descriptions are available in Saksa et al. (2017), with the most-relevant information provided here. Two types of vegetation change were simulated, a forest-thinning treatment implemented in 2012, and impacts of wildfires modeled with and without the thinning. Projected temperature increases from two climate scenarios were also simulated, Representative Concentration Pathways (RCP) 4.5 and 8.5, at 2050 and 2100. The climate and

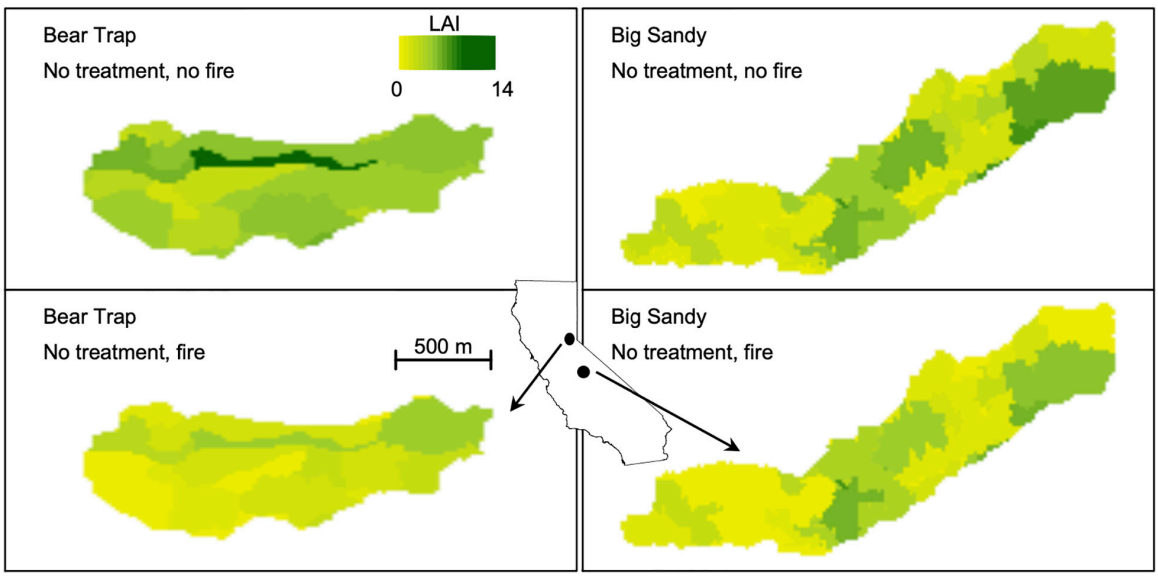

FIGURE 1 | Leaf Area Index (LAI) values in the Bear Trap and Big Sandy catchments in the highest (no treatment, no fire) and lowest (no treatment, fire) vegetation density scenarios.

vegetation scenarios were then simulated together to determine the dominant factors controlling evapotranspiration and runoff, assessed over the range of dry-to-wet precipitation conditions observed during a 4-year period (2010–2013) for which field measurements were carried out.

Study Sites

Two headwater catchments at different latitudes along the western slope of the Sierra Nevada were monitored for climate, stream discharge, distributed snow depth and soil moisture during water years 2010–2013 (**Figure 1**). Bear Trap Creek (1.4 km^2, 1560–1826 m elev) is located in the headwaters of the American River basin, in the central Sierra, and Big Sandy Creek (2.2 km^2, 1776–2475 m elev) is located in the Merced River Basin, in the southern Sierra. Observed discharge was calculated from stream-level data recorded every 15 min, and a stage-discharge relationship developed for each stream. The catchments are dominated by mixed-conifer forests, a forest type covering 13–14% (∼52,500–56,500 km^2) of California (Barbour and Minnich, 2000), and have well-drained soils, classified as loamy-sand in Bear Trap and sandy or sandy-loam in the Big Sandy catchment. The headwaters receive a mix of rain and snow precipitation at the elevation of the catchment outlet, but are snow dominated at the upper elevations, suggesting these basins would be sensitive to lower snowfall and higher rainfall from increases in temperature.

Model Scenarios

Four vegetation scenarios were combined with climate projections to determine dominant influences in forest hydrology: no-treatment, thinning-treatment, no-treatment with wildfire, and thinning-treatment with wildfire. Strategically Placed Landscape Treatments (SPLATs; Finney, 2001), a fuels treatment strategy to lower the risk of high-severity fire by treating part of the landscape, were implemented at the fireshed scale during the summer of 2012. As part of SPLAT implementation on a larger fireshed, the mixed-conifer forest was selectively thinned in 95% of the Bear Trap catchment and in 32% of the Big Sandy catchment. It should be noted that these treatments reflect operational decisions of the local forest managers, which are constrained by topography, wildlife habitat, public input, budgets and other factors (North et al., 2015; Lydersen et al., 2019). LiDAR data, described in Kelly and Guo (2015), was used to determine vegetation-community type, and forest-plot measurements were performed before and after SPLAT implementation. Forest plot data were used to impute forest-structure characteristics into the individual vegetation areas (Su et al., 2016), to capture vegetation changes in both horizontal (canopy cover) and vertical (Leaf Area Index) (Saksa et al., 2017).

Understory-vegetation cover was also estimated using a linear equation developed from forest-plot data relating basal area and canopy cover with shrub-cover fraction (Hopkinson and Battles, 2015). The vegetation densities before and after fuels treatments were used to run the Forest Vegetation Simulator (FVS; Dixon, 2002) with the Fire and Fuels Extension (FFE; Reinhardt and Crookston, 2003) and the Fire Area Simulator (FARSITE; Finney, 2004) to project treatment impacts on wildfire severity and vegetation mortality (Fry et al., 2015). As the fire model was calibrated with recent observations, the post-fire vegetation scenarios reflect fire behavior under current climate conditions. FVS was then used to estimate forest-vegetation regrowth for 10 years after the simulated fire events. Following the 10 years of regrowth, overstory canopy cover was transferred directly from FVS, and LAI was calculated from tree lists using allometric estimates.

The model did not consider changes in surface characteristics such as soil hydrophobicity, reduced soil-infiltration capacity, and diminished litter cover that can occur immediately after fire. While these can be important in more semi-arid regions, the impacts are likely to be small in this region where hydraulic conductivity is quite high in the loamy-sand to sandy-soil textures, and infiltration excess runoff production is relatively rare. Wildfire simulations were based on current 95th percentile weather and fuel moisture conditions, as more extreme weather and wildfire events are expected with climate warming, we consider this a conservative scenario.

The climate scenarios were based on changes projected in the minimum and maximum daily temperatures for RCP 4.5, defined as a 4.5 W m^{-2} increase in radiative forcing relative to pre-industrialization with stabilization by 2100; and for RCP 8.5, which represents an 8.5 W m^{-2} radiative increase by 2100 that continues to rise (van Vuuren et al., 2011). Mean-annual minimum and maximum temperature anomalies were calculated using the 4-year annual mean of 2010–2013 as a baseline. The 4-year baseline period was + 0.4°C (−0.2°C to +0.9°C) and + 0.1°C (−0.8°C to + 0.9°C) of the long-term climate mean for minimum and maximum temperature in the Sierra climate region, respectively (California Climate Tracker; Abatzoglou et al., 2009). A 4-year trailing ensemble mean was calculated using the Coupled Model Intercomparison Project Phase 5 (CMIP5) output for the Community Climate System Model version 4 (CCSM4) and the Model for Interdisciplinary Research on Climate version 5 (MIROC5) (**Figure 2**). These models were chosen because they showed low error in bias analyses (Kattsov et al., 2013), and both were archived in the CMIP5 database with the required daily minimum and maximum temperatures. Using the temperature anomalies to produce a uniform offset in minimum and maximum temperatures on our observed-temperature data set aside the need for downscaling climate projections. Vapor pressure and relative humidity were derived using standard air temperature relationships in the model simulations (Tague and Band, 2004), and respond accordingly with increasing temperatures. Impacts on snowpack from vapor pressure and relative humidity are minor, with greater differences during the ablation period in higher elevations and wetter years (Roche et al., 2018a).

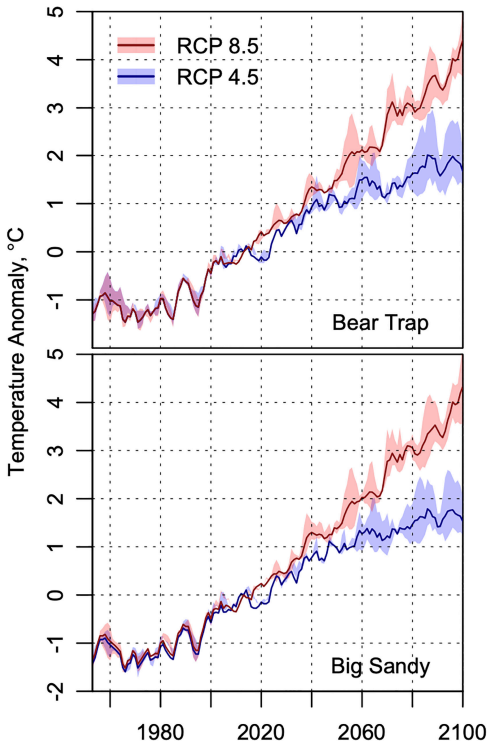

FIGURE 2 | Climate-scenario temperature anomalies based on the 2010–2013 4-year mean. Each line connects data points for annual-mean temperature anomalies calculated as a 4-year trailing mean from 1950 to 2100. Shaded areas note the range of daily minimum and maximum temperature anomalies from the two climate scenarios used to calculate the mean.

Water-Balance Model

RHESSys was used to simulate the hydrologic response to vegetation and climate scenarios. Model calibration was completed for the pre-thinning water years of 2010–2012, during which annual precipitation varied from drier than normal (−39%) to wetter than normal (+60%) conditions in the Sierra Nevada (Saksa et al., 2017). Drainage and subsurface-storage processes were calibrated by comparing simulated and observed streamflow at a daily time step, with precipitation not attributed to evapotranspiration or runoff considered subsurface bypass flow, a comprehensive term to account for all subsurface storage and routing, as in Saksa et al. (2017). Garcia et al. (2013) provides additional details on RHESSys storage and drainage parameters and standard calibration. Monte-Carlo style calibrations were completed by running 5000 sets of random parameters and selecting the parameter sets that conformed to a Nash-Sutcliffe and log-transformed Nash-Sutcliffe statistic higher than 0.60, as well as annual and August streamflow rates within 25% of observed values. Six parameter sets met the criteria for the Bear Trap catchment and 17 sets were acceptable for the Big Sandy catchment, providing a range of modeled responses to temperature and vegetation perturbations.

Increasing temperatures at the elevation range of these catchments will have a significant impact on the amount of precipitation received as snow versus rain, and the persistence of snowpack during the winter and into spring. RHESSys calibration was completed using a separate rain and snow precipitation input, and changes to initial snowfall rates were implemented using the linear transition of snowfall temperatures in the model, from −1 to 3°C. Three inputs contribute to snowmelt rates: temperature, precipitation falling as rain, and radiation. All three components are affected by air temperature, and the relevant top-level equations are listed below from Tague and Band (2004). Melt attributed to temperature is based on an empirical relationship to sensible and latent heat, and is calculated as:

$$M_T = \beta_{MT} T_{air}(1 - 0.8F) \quad (1)$$

where β_{MT} is the temperature-index melt coefficient, calibrated to 0.0005 for Bear Trap and 0.001 for Big Sandy, T_{air} is the

temperature in Celsius and F is the fraction of forest cover. Snowmelt from advection due to rainfall is calculated as:

$$M_v = (\rho_{water} T_{air} TF cp_{water})/\lambda_f \quad (2)$$

where ρ_{water} is the density of water, TF is net throughfall onto the snowpack, cp_{water} is the heat capacity of water, and λ_f is the latent heat of fusion. Lastly, melt due to radiation is calculated as:

$$M_{rad} = (K_{direct} + K_{diffuse} + L)/\lambda_f \rho_{water} \quad (3)$$

where K_{direct} and $K_{diffuse}$ are direct and diffuse net shortwave radiation, and L is net longwave radiation. Melt only occurs when the snowpack is ripe, but snow loss also can occur by sublimation from radiation energy input, calculated by adding the latent heat of vaporization to the latent heat of fusion in Eq. 3 ($\lambda_f + \lambda_v$).

RHESSys was also used to estimate overstory and understory transpiration and evaporation of water intercepted by forest canopy and litter, as well as soil evaporation and snow sublimation. RHESSys simulates vertical infiltration and drainage between surface storage, plant rooting zone, and unsaturated and saturated zones. Lateral redistribution of water follows topography. Previous application of RHESSys in snow-dominated mountain environments demonstrates that the model can capture the impact of climate variation on eco-hydrologic processes such as streamflow (Zierl et al., 2007; Garcia et al., 2013), the impact of increases in atmospheric carbon dioxide concentration on conifer net primary productivity and water use efficiency (Vicente-Serrano et al., 2015), and snowpack (Christensen et al., 2008; Godsey et al., 2013; Morán-Tejeda et al., 2014; Bart et al., 2016). Additional details on RHESSys process representation can be found in these studies, plus Tague and Band (2004), and the open-access code maintained online[1].

RESULTS

Vegetation and Climate Changes

Mean-annual water-balance components of evapotranspiration and runoff were assessed in response to vegetation and climate scenarios over the complete observation period (water years 2010–2013). Mean annual precipitation for this period was 1990 mm in Bear Trap and 1300 mm in Big Sandy. Selective thinning implemented in Bear Trap reduced mean LAI (Canopy Cover) from 9.9 (0.51) to 9.1 (0.49), with reductions from modeled wildfire being 8.8 (0.37) with SPLATs and 7.7 (0.29) without SPLATs. Wildfire in the catchment had a mean flame length of 2.2 m and crowning in 42% of the area without SPLATs, reduced to a mean flame length of 1.2 m and crowning in 19% of the area with SPLATs.

Mean LAI in Big Sandy was 5.0 (0.55 Canopy Cover), and the limited commercial thinning did not reduce the mean catchment LAI substantially (change of < 0.1). A small section of Big Sandy was thinned, with LAI being reduced by as much as 4.0; but the minor amount of area thinned combined with incremental increases in growth elsewhere led to the small changes in basin-scale LAI. Wildfire in Big Sandy reduced LAI to 3.8 (0.47 Canopy Cover), with thinning prior to wildfire having an insignificant effect. Because of the limited catchment-scale thinning impacts on Big Sandy, results are only reported for the no-treatment and post-fire vegetation change. Wildfire in the catchment had a mean flame length of 1.5 m and crowning in 22% of the area.

Observed mean-daily winter temperatures during the months of heaviest precipitation (Nov-Apr), were 4.3°C in both Bear Trap and Big Sandy catchments. Projected increases in mean-annual temperature with RCP 4.5 were 1.2°C by 2050 and 1.6°C by 2100 in Bear Trap, with slightly smaller increases at Big Sandy, 1.0°C by 2050 and 1.4°C by 2100. In the RCP 8.5 projections, temperature increases by 2050 and 2100 are 1.8 and 4.7°C in Bear Trap and 1.6 and 4.4°C in Big Sandy, respectively.

Water-Balance Simulations

Simulations showed that vegetation changes had much greater effects on runoff and evapotranspiration than did the changes in temperature (**Figure 3**). Ninety-five percent confidence intervals were calculated for the 6 Bear Trap and 17 Big Sandy model calibrations, with runoff and evapotranspiration responses reported as fractions of precipitation. Confidence intervals were small for both pre-treatment and post-fire scenarios in Big Sandy. Confidence intervals in Bear Trap increased with decreasing vegetation and resulted in higher uncertainty of water-balance response with greater vegetation disturbance. In Bear Trap, the scenario of greatest vegetation change (no treatment, fire) increased the mean runoff fraction by 0.20 (from 0.44 to 0.64) and decreased the mean fraction of evapotranspiration by 0.20 (from 0.47 to 0.27), in response to the 22% LAI decrease (from 9.9 to 7.7) and 42% canopy decrease (0.51 to 0.29). This is equivalent to a drop in ET of about 398 mm yr^{-1}, from 935 to 537 mm yr^{-1} (**Figure 4**). In comparison, the climate scenario of greatest temperature increases (RCP 8.5, 2100) with no change in vegetation resulted in a smaller reduction in runoff, from 0.44 to 0.41, and smaller evapotranspiration increase, from 0.47 to 0.48. Responses of mean runoff and evapotranspiration fractions in 2050 and 2100 to RCP 4.5 temperature increases were limited to less than 0.03, as was the response to RCP 8.5 in 2050.

In the Big Sandy catchment, the simulated response of evapotranspiration and runoff to the 26% LAI decrease (from 5.0 to 3.7) and 14% canopy decrease (0.55–0.47) from modeled wildfire was more limited than in Bear Trap, increasing the runoff fraction by 0.06 (from 0.35 to 0.41) and decreasing the evapotranspiration fraction by 0.06 (from 0.54 to 0.48). This is equivalent to a drop in ET of about 78 mm yr^{-1}, from 702 to 624 mm yr^{-1} (**Figure 4**). A similar response in the reduction of evapotranspiration of 0.05 (from 0.54 to 0.49) was simulated due to the RCP 8.5 temperature increase by 2100, but the response of runoff was not significant, only increasing from 0.35 to 0.36. Precipitation not accounted for in runoff or evapotranspiration is routed to deeper groundwater storage and thus changes in evapotranspiration do not necessarily translate directly into runoff change in the model. Response to all other climate scenarios also resulted in changes of less than 0.03 in evapotranspiration and runoff fractions, similar to Bear Trap, even though Big Sandy has a higher overall evapotranspiration fraction due to the lower precipitation.

[1] https://github.com/RHESSys/RHESSys

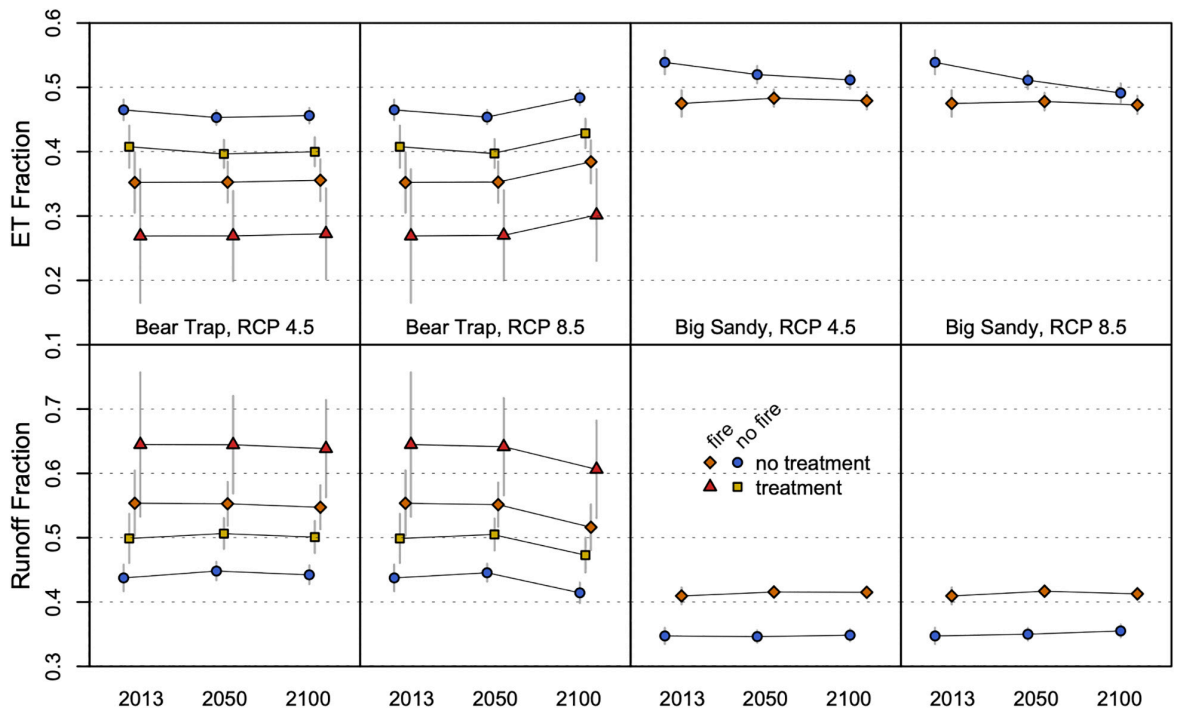

FIGURE 3 | Simulation results of the runoff and evapotranspiration fractions for vegetation scenarios and projected temperature increases in 2050 and 2100. Basin-mean LAI in Big Sandy following treatment, with and without fire, were not different from the no-treatment scenarios and are not shown. Simulations are for water-year 2010–2013 conditions, during which mean precipitation was 1990 mm in Bear Trap and 1300 mm in Big Sandy. Vertical bars indicate the 95% confidence interval based on the multiple parameter sets for each catchment.

Precipitation Variability

Runoff in Bear Trap varied between wet, average, and dry years, and runoff response also varied across vegetation scenarios (fire and treatment). The difference in runoff between wet and dry years exceeded 750 mm while the runoff difference between no treatment/fire runoff and runoff from the most-substantial vegetation disturbance was limited to less than 500 mm (**Figure 4**). Trends of runoff and evapotranspiration response with increasing temperatures were the same in all climate scenarios except for RCP 8.5 in 2100, where evapotranspiration increases were greater in the wet years (<50 mm). In Big Sandy, precipitation variability between wet and dry years had a greater effect on evapotranspiration and runoff than the reductions in vegetation from wildfire (**Figure 4**). The differences in annual precipitation resulted in evapotranspiration differences near 400 mm without treatment or fire, and runoff differences close to 700 mm with post-fire vegetation. Water-balance response to reductions in LAI from wildfire were smaller, with evapotranspiration decreases and runoff increases of <200 mm. Elevated temperatures in 2050 and 2100 increased ET during mean to high precipitation years, offsetting some of the ET decline due to fire.

Hydrologic Timing and Storage

Precipitation falling as rain or snow, along with the accumulation and melt of the seasonal snowpack, determines the timing of soil infiltration, runoff and availability of water in the soil for use by vegetation. Projected temperature increases affected both precipitation phase and melt rate, and changes in vegetation density impacted snowmelt by modifying the surface-energy balance. Simulations of temperature and vegetation impacts on hydrologic storage and timing were assessed for 2010, a mean precipitation year (**Figure 5**).

In Bear Trap, post-fire vegetation losses advanced the snowpack melt-out date by about 3 weeks, while temperature increases by 2100 in RCP 4.5 advanced the melt-out date by about 4 weeks (**Figures 5A,B**). Increases in temperature by 2100 in RCP 8.5 showed no persistent snowpack, with the fraction of precipitation falling as snow decreasing from 0.40 to 0.10 (**Table 1**). The reduced vegetation after fire increased soil-water storage during the dry season from minimal storage to within 150 mm of saturated winter conditions (∼350 mm). Increased temperatures resulted in an earlier start of the soil-water storage recession from wet winter to dry summer conditions by approximately 1.5 weeks, associated with the reduced snowpack. Evapotranspiration with increased temperatures becomes more limited in the early summer because of the earlier soil drying. The reduced post-fire vegetation resulted in evapotranspiration reductions during all seasons and was not limited by soil-water storage. Runoff timing was accelerated with both scenarios of increased temperatures and reduced vegetation, with peak runoff about 8 weeks earlier. Post-fire vegetation resulted in 67% higher annual runoff, with increased peak (+54%) and

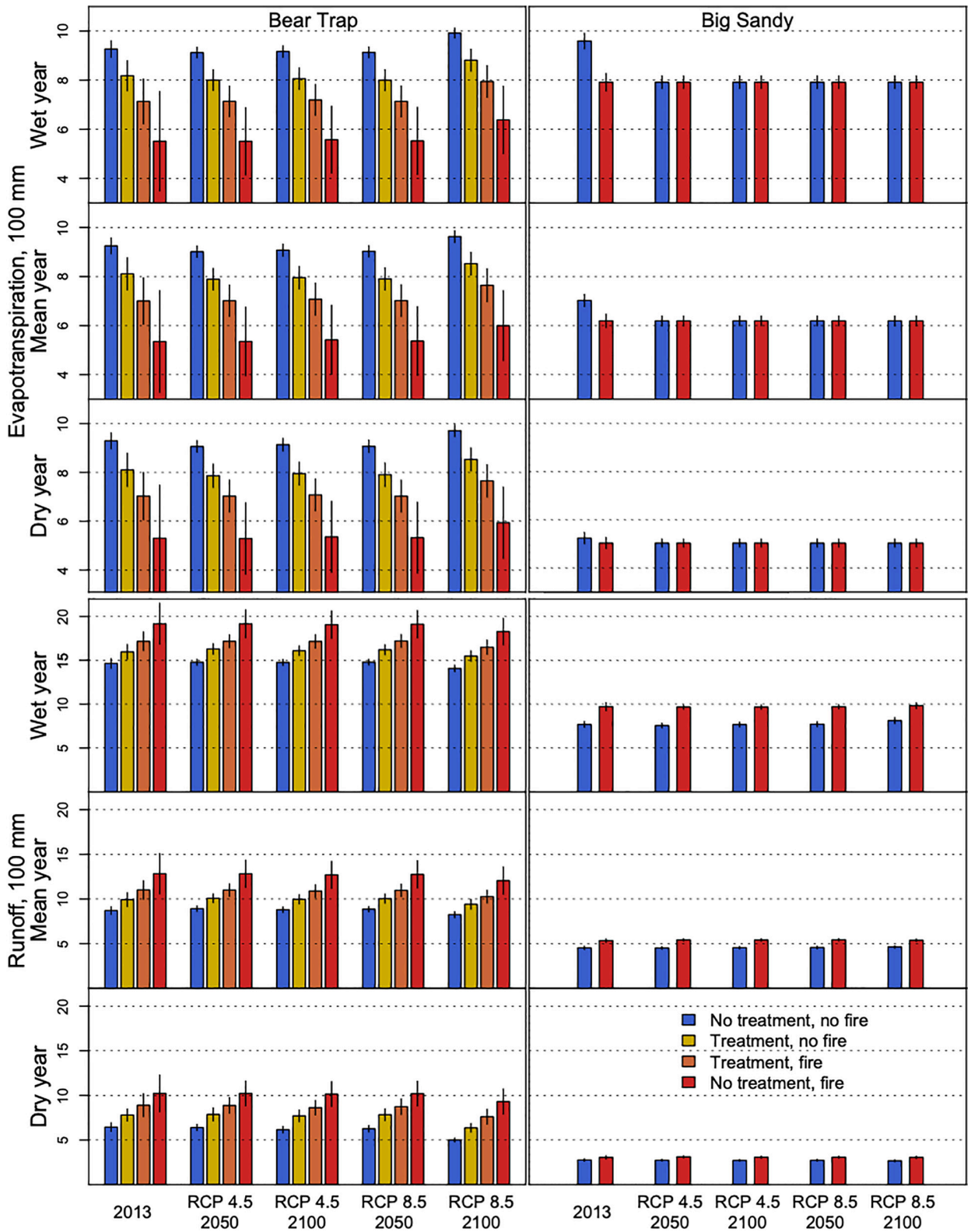

FIGURE 4 | Evapotranspiration (upper 6 panels) and runoff (lower 6 panels) for forest-treatment and disturbance scenarios during dry (2012), mean (all years), and wet (2011) precipitation conditions for current and projected temperatures Vertical bars indicate the 95% confidence interval based on the multiple parameter sets for each catchment. Left column of panels is Bear Trap and right column of panels is Big Sandy. Big Sandy mean basin LAI following treatments were not different than having no treatment and are not shown.

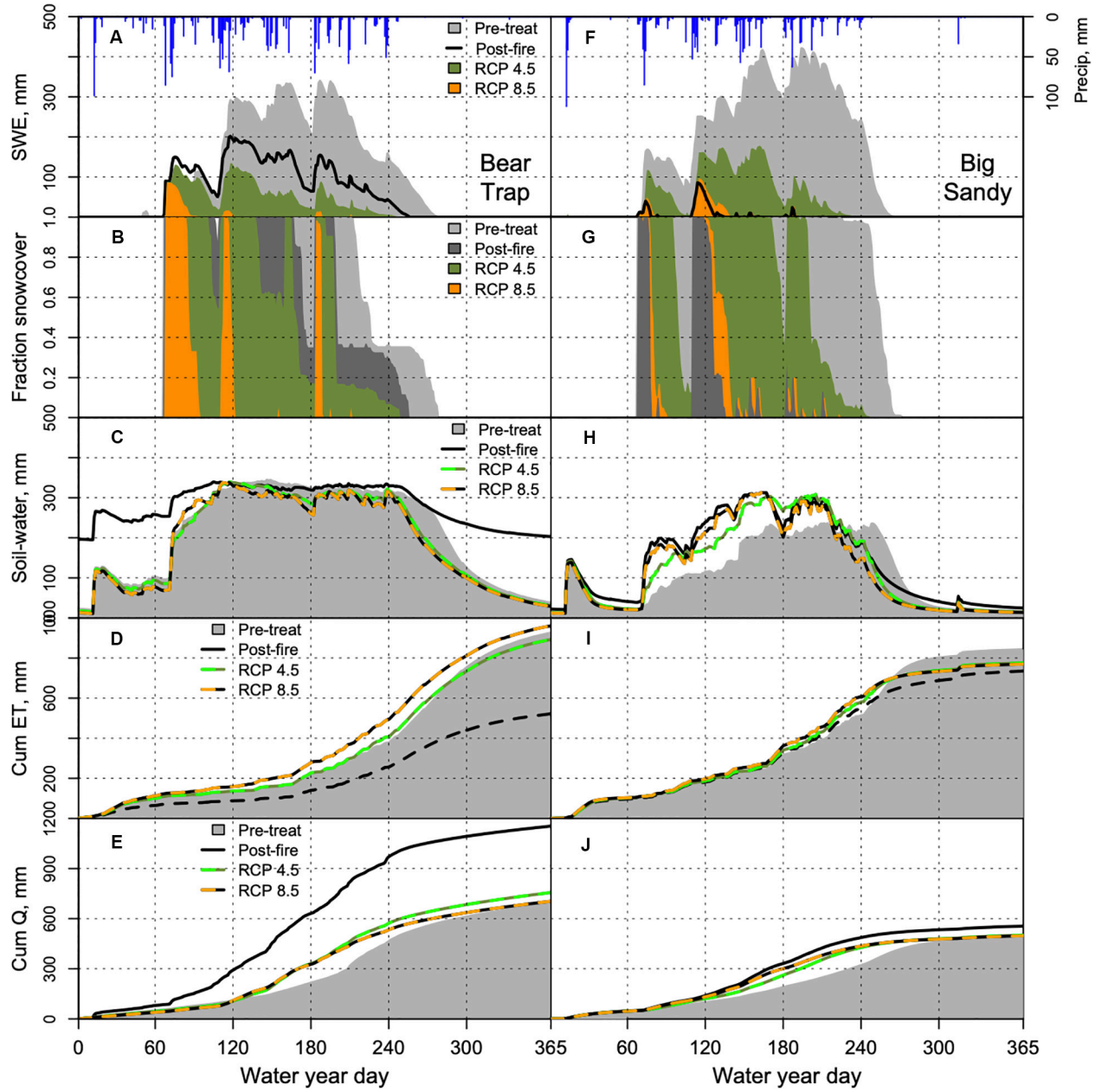

FIGURE 5 | Daily precipitation and snowpack storage **(A,F)**, basin snow-cover fraction **(B,G)**, soil-water storage **(C,H)**, evapotranspiration **(D,I)**, and stream discharge **(E,J)** in the Bear Trap and Big Sandy catchments with vegetation and temperature perturbations. Vegetation densities are from control and post-fire conditions, and temperature increases are from year 2100 projections with RCP 4.5 and 8.5 climate scenarios.

TABLE 1 | Mean daily temperatures for the months of highest precipitation (November–April) and the fraction of precipitation falling as snow under each climate scenario.

		2013	RCP 4.5 2050	RCP 4.5 2100	RCP 8.5 2050	RCP 8.5 2100
Bear Trap (American River)	November–April mean temperature	4.3°*C*	5.5°*C*	5.9°*C*	6.1°*C*	8.8°*C*
	Mean annual snow fraction	0.40	0.33	0.27	0.29	0.10
Big Sandy (Merced River)	November–April mean temperature	4.3°*C*	5.3°*C*	5.7°*C*	5.9°*C*	8.7°*C*
	Mean annual snow fraction	0.60	0.57	0.53	0.54	0.29

frequency (5–14 events) of high-flow events, where increased-temperature scenarios resulted in lower peak flow (−35%) at similar frequency.

In Big Sandy, post-fire vegetation resulted in the loss of a persistent winter snowpack, similar to temperature increases by 2100 with RCP 8.5 (**Figures 5F,G**). Increases in temperature by 2100 with RCP 4.5 and 8.5 reduced the snowfall fraction from 0.60 to 0.53 and 0.29 of precipitation, respectively. Soil-water storage from infiltration increased earlier in the winter and became more saturated with temperature increases (300 mm) than in the control (230 mm), but the dry season recession curve also started about 4 weeks earlier than in the control scenario. Evapotranspiration response to the vegetation reductions was muted, but evapotranspiration was reduced in all vegetation and temperature simulations from the earlier drawdown in soil-water storage. Peak runoff timing was shifted about 12 weeks, from early June to early March, in the post-fire and RCP 8.5 scenarios, with higher peak flow (+29%) in the post-fire vegetation simulation than with projected increases in temperature (−9% to +4%). The earlier peak runoff in the RCP 4.5 scenario was only shifted about 8 weeks, to mid-April.

DISCUSSION

These are highly productive ecosystems compared to other temperate conifer forests (Millar, 1996), where vegetation change from wildfire, and to a lesser extent forest management, impacted evapotranspiration and streamflow more than projected temperature increases from climate warming. On the other hand, impacts from inter-annual climate variation between relatively wet and dry years were greater than the impacts of vegetation change or climate warming. The hydrologic impacts of wildfire were greater than those associated with fuel treatments and the magnitude of vegetation change impacts were greater in the wetter central-Sierra study site. These results are based on two relatively small Sierra Nevada watersheds that enable the incorporation of substantial observation data for constraining a physically based model, but that also limit the ability to fully capture the wide range of geoclimatic variation within the Sierra. Nonetheless, our findings demonstrate how climate and vegetation change effects can interact to produce significant, short term hydrologic changes, but also show why it can be challenging to meaningfully generalize about these impacts in the context of climate and site differences.

Estimated hydrologic responses to vegetation change in this study were relatively high, particularly for the wetter Bear Trap catchment. Boisramé et al. (2019) found streamflow increases of about 20–40 mm as managed fires were allowed to return to the Illilouette Creek Basin, which is lower than the ∼75 mm change in the climatically similar Big Sandy Creek catchment. The difference can likely be attributed to a greater vegetation change from a reduction in forest cover in the Big Sandy headwater simulated wildfire, a single event that burned the entire catchment during 95th percentile weather conditions (e.g., high temperature, low humidity) in which high-severity wildfires are more likely to occur. Vegetation change in the Illilouette Creek catchment is a result of the ongoing managed wildfires that burned portions of the larger Illilouette Creek catchment in various weather conditions over 40 years, and incorporated conversion of forested areas to shrubs and meadows. Bart et al. (2016) showed the potential for water balance changes in the southern Sierra region in excess of 100 mm with reduced vegetation, and changes in vegetation type from forest to shrubs. The greater 400 mm yr^{-1} decline in ET with high-intensity wildfire in the high-precipitation, mixed-conifer region of the central-Sierra American River basin was approximately 70 mm higher than the findings of Roche et al. (2018b) and Roche et al. (2020). For example, the nearby 2014 King Fire resulted in a 330 mm (±80 mm) ET reduction in areas burned by high-severity fire, averaged over 4 years after the fire event. Saksa et al. (2020) also demonstrated the higher response of the water balance to horizontal forest structure changes in RHESSys, as such the 42% reduction in canopy cover contributed substantially to the change in ET.

Water-Balance Simulations

Ficklin and Barnhart (2014) suggest using multiple parameter sets and General Circulation Model outputs, as significant differences in hydrologic projections will occur from uncertainty in model parameterization and climate scenario. In this study, we used the ensemble means from two climate models and two emissions scenarios, with 6 (Bear Trap, American River Basin) and 17 (Big Sandy, Merced River Basin) parameter sets to incorporate some accounting of uncertainty. Additional uncertainties can originate from climate downscaling, which was not done in this study, and model structure (Wilby and Harris, 2006). We simulated a uniform increase in the minimum and maximum daily temperatures, using projected temperature anomalies for 2050 and 2100. Studies often use a single mean-temperature adjustment to project effects of climate warming on Sierra Nevada watersheds (e.g., Young et al., 2009; Meyers et al., 2010), but minimum and maximum temperatures may have periods of non-linear increases, which can modify the diurnal temperature range (Easterling, 1997; Vose et al., 2005).

In the RCP 4.5 projections, minimum and maximum temperatures increased an average of 0.017 and 0.020°C yr^{-1} in the American and 0.016 and 0.019°C yr^{-1} in the Merced between 2013 and 2100, respectively. RCP 8.5 projections of minimum and maximum temperatures resulted in mean increases of 0.044 and 0.055°C yr^{-1} in the American and 0.045 and 0.053°C yr^{-1} in the Merced between 2013 and 2100, respectively. The rate differences of minimum and maximum temperature will impact snow accumulation and melt estimates, along with ecological estimates in RHESSys, such as the estimation of vapor-pressure deficit and the Jarvis-based calculations of stomatal conductance (Jarvis, 1976) used to estimate transpiration in RHESSys, which incorporates functions of mean and minimum daily temperatures to limit maximum conductance.

The simulation results of temperature perturbations generally agree with the findings of Dettinger et al. (2004) that without statistically significant changes in precipitation, annual volumes of streamflow will generally remain steady in the American and Merced River basin areas with increasing temperatures. Dettinger

et al. (2004) did find a general trend of +8% precipitation per year with climate warming, but the effect was small compared to the interannual variation, which was also found to have a large effect on runoff in this study (**Figure 4**). Previous work in the Merced River basin (Christensen et al., 2008) also showed the sensitivity of transpiration to precipitation at an elevation range similar to Big Sandy, with their model extending into higher elevations where transpiration became increasingly sensitive to changes in temperature. The sensitivity to transpiration at higher elevations may also be why Bales et al. (2018) estimated a greater increase in evapotranspiration (+12–15%) with a +1°C temperature increase in the Kings River Basin during the recent California drought, leading to a −5% change in runoff over the basin, calculated as precipitation minus evapotranspiration. Null et al. (2010) used the Water Evaluation and Planning (WEAP21) water-balance model that includes supply, demand, and policy scenario capabilities to project progressively decreasing mean annual flows in all major Sierra Nevada basins with increasing temperature, including a respective −5.6 and −6.3% for the Merced and American with +4°C. Temperature increases in this study were similar for the RCP 8.5 scenario in 2100, resulting in a similar response for projected mean runoff in Bear Trap (American) of −5.3%, but a lesser runoff response in Big Sandy (Merced) of −1.2%. Changes in Water Use Efficiency and evapotranspiration with increasing atmospheric CO_2 concentrations were not considered in this study (De Kauwe et al., 2013).

Precipitation Variability

The strong response of evapotranspiration to vegetation density in Bear Trap, and to annual precipitation in Big Sandy, suggests that within a Budyko (1974) framework of competing water and energy limitations of transpiration, the Big Sandy region tends to be more water limited (**Figure 6**). The difference in energy and water limitations will affect the magnitude of the water-balance response to changes in vegetation and temperature, consistent with Zhang et al. (2001), who showed the potential for increased response of evapotranspiration with reduced forest cover in regions with higher precipitation. In both sites, yearly runoff was influenced by interannual precipitation variability more than temperature, similar to results from previous work in the western Sierra (Duell, 1994; Risbey and Entekhabi, 1996).

The individual years of 2011 and 2012 were selected from the 4 years of simulation (2010–2013) to provide a spectrum of response to climate and vegetation perturbations during a wet and dry year, respectively. Antecedent-moisture conditions can modify watershed response to disturbance, so the progression of dry to wet years may be important. Precipitation in 2010 was close to the long-term mean for both regions, followed by the wet year of 2011, and dry years of 2012 and 2013. Shallow subsurface water-storage capacity and the rates of soil drainage versus evapotranspiration will impact the magnitude of summer-baseflow response in low-precipitation years and where temperature increases lead to earlier snowmelt (Jefferson et al., 2008; Tague and Grant, 2009; Huntington and Niswonger, 2012). The uncertainty associated with the calibrated model parameter sets of subsurface flow increased in Bear Trap Creek with simulated reductions in vegetation (**Figures 3**, **4**). Improved characterization of subsurface properties in Sierra watersheds are needed to enhance our understanding and predictive capability of runoff response to climate (Shaw et al., 2014), which could be used to further constrain the simulation uncertainty of vegetation scenarios in this study. The total subsurface storage capacity, and plant-available water storage (Garcia and Tague, 2015; Tague et al., 2019), could limit the evapotranspiration increases seen in warmer Sierra Nevada watersheds that have been used as a proxy for temperature increases with climate change (Goulden and Bales, 2014).

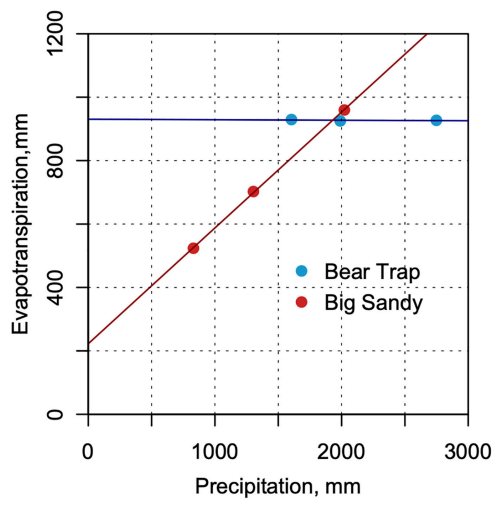

FIGURE 6 | Annual evapotranspiration as a function of dry to wet precipitation conditions in Bear Trap and Big Sandy. Forest vegetation was constant (pre-treatment), with fitted lines highlighting the different trends between the two catchments.

Hydrologic Timing and Storage

Both reduced vegetation and increased temperatures resulted in more energy being absorbed by the snowpack, with persistent snow cover eliminated by 2100 in RCP 8.5 (**Figures 5B,H**). In contrast to results from Berghuijs et al. (2014) that indicated streamflow will generally decrease with decreasing snowfall, these results are consistent with studies such as Tague and Peng (2013) that argue that snowmelt inputs can in some cases support higher rates of evapotranpiration than winter precipitation. In this study, the increased winter (November–April) snowmelt led to higher water storage in the soil and increased streamflow, while evapotranspiration generally remained unchanged. The earlier melt reduced soil-water storage, evapotranspiration and streamflow in May through July in both Bear Trap and Big Sandy (**Figure 5**). These results agree with Tague and Peng (2013), showing that evapotranspiration response to temperature increases will depend on timing of snowmelt. Forrest et al. (2018) also project higher winter flows by 2050 for watersheds supplying California hydropower facilities, a significant source of renewable-power-generation – but noted that due to increased spillage events, higher flows did not necessarily yield additional power generation.

The response of snowmelt to vegetation loss from wildfire in Big Sandy was much greater than in Bear Trap. LAI drives radiation attenuation (Varhola and Coops, 2013), and in RHESSys, radiation transferred through the canopy to the snowpack follows a Beer's Law type of exponential curve. In Bear Trap, LAI was reduced from 9.9 to 7.7 in the post-fire scenario, is within the saturated range of radiation absorption by the canopy, and is similar to previous reported LAI values for ponderosa pine forests in the area (Goldstein and Hultman, 2000; Gersonde et al., 2004; Campbell et al., 2009). In Big Sandy, the LAI was reduced from 5.0 to 3.7, which is similar to previous LiDAR LAI estimates for the Sierra National Forest (Zhao et al., 2012; Tang et al., 2014). The lower LAI in Big Sandy is within the exponential increase of radiation with changes in vegetation, resulting in snowpack patterns more similar to RCP 8.5 in 2100. The combination of reduced vegetation and elevated snowmelt led to the highest peak runoff in the post-fire scenario, compared to the control or climate projections, but will be further influenced by forest gap size and slope orientation (Ellis et al., 2013).

Changes in the timing of snowmelt and runoff also have implications for fish habitat and other aquatic species that rely on summer baseflow. Using the end of the 2010 water year (Sep 30) as an indicator of low flow in this study showed in baseflow reduced more following wildfire (−19%) than temperature increases (−4 to −8%) in Bear Trap Creek. In Big Sandy Creek, however, baseflow was reduced more following temperature increases (−29 to −33%) than wildfire (−25%). Godsey et al. (2013) note than low flows in this region depend on both Snow Water Equivalent level of both current and previous years, and impacts are influenced by subsurface storage capacity and underlying bedrock. Meyers et al. (2010) further extend their temperature warming assessment to winter and spring flooding in the region, which may negatively impact both brook and rainbow trout, but the greater proportion of winter flooding may impact brook trout more severely.

CONCLUSION

The water-balance responses to simulations of temperature and vegetation perturbations in productive mixed-conifer forests with wildfire disturbances showed that vegetation changes from operational fuel treatments and historical wildfire exerted a greater influence on annual evapotranspiration and runoff than did projected temperature increases in a warming climate. However, inter-annual variation in precipitation had a greater influence on runoff than did effects due to either fuels treatments or wildfire. Hydrologic impacts associated with historic wildfire were generally greater than those associated with operational fuel treatments. In the wetter central Sierra, headwater evapotranspiration decreased, and runoff increased 40–50% for a simulated wildfire event. In the more water-limited southern Sierra, the headwaters response was constrained to a respective −11 and +17% change in evapotranspiration and runoff following a simulated wildfire event. In contrast, evapotranspiration increases and runoff decreases to a 4.4°C temperature increase were less than 10% of current values for all headwaters.

Climate warming will eliminate the persistent seasonal snowpack at these elevations (1500–2500 m) by 2100 in the RCP 8.5 projections, becoming rain dominated as the amount of precipitation falling as snow was reduced from the current 40–60% down to 10–29%. The early snowmelt has cascading effects on the rate and timing of soil-water storage, and thus on evapotranspiration and runoff. Increases in temperatures resulted in peak streamflow occurring up to 12 weeks earlier, but post-fire vegetation conditions also increased peak runoff, especially in the American River headwaters of Bear Trap Creek. These results suggest that in the central Sierra, reductions in vegetation from either light thinning and fuels treatment or historical wildfire generate increases in flow, however, only wildfire or more-extensive fuels treatments provide significant increases in the southern Sierra. In both cases, these reductions are premised on vegetation changes that can be sustained. Further work to examine the dynamics of vegetation regrowth following fuels treatments, wildfire, and vegetation adaptation to a warming climate are needed to determine longer-term impacts of vegetation change on runoff and evapotranspiration.

DATA AVAILABILITY STATEMENT

The datasets generated for this study are available on request to the corresponding author.

AUTHOR CONTRIBUTIONS

PS contributed to the study design, data processing, modeling, and drafted the manuscript. MC and RB contributed to the study design, modeling approach, and manuscript revisions. CT contributed to the modeling approach and execution, and manuscript revisions. All authors contributed to the article and approved the submitted version.

FUNDING

This is SNAMP publication #59. The Sierra Nevada Adaptive Management Project (SNAMP) was funded by USDA Forest Service Region 5, USDA Forest Service Pacific Southwest Research Station, U.S. Fish and Wildlife Service, California Department of Water Resources, California Department of Fish and Game, California Department of Forestry and Fire Protection, and the Sierra Nevada Conservancy. This research was also supported by the U.S. National Science Foundation, through the Southern Sierra Critical Zone Observatory (EAR-0725097).

ACKNOWLEDGMENTS

We would like to thank California Department of Water Resources, United States Forest Service, Sierra Nevada Research

Institute, and Sierra Nevada Adaptive Management Project personnel for their support and assistance. We thank Patrick Womble and Sarah Martin for their significant work in field data collection at UC Merced, and to Norm Miller at UC Berkeley for assistance with the climate datasets. We thank John Battles and Danny Fry at UC Berkeley for the forest vegetation and wildfire modeling components incorporated in this study. We acknowledge the World Climate Research Programme's Working Group on Coupled Modelling, which is responsible for CMIP, and we thank the climate modeling groups for producing and making available their model output. For CMIP the U.S. Department of Energy's Program for Climate Model Diagnosis and Intercomparison provides coordinating support and led development of software infrastructure in partnership with the Global Organization for Earth System Science Portals.

REFERENCES

Abatzoglou, J. T., Redmond, K. T., and Edwards, L. M. (2009). Classification of regional climate variability in the state of California. *J. Appl. Meteorol. Climatol.* 48, 1527–1541. doi: 10.1175/2009JAMC2062.1

Agee, J. K., and Skinner, C. N. (2005). Basic principles of forest fuel reduction treatments. *For. Ecol. Manag.* 211, 83–96. doi: 10.1016/j.foreco.2005.01.034

Bales, R. C., Goulden, M. L., Hunsaker, C. T., Conklin, M. H., Hartsough, P. C., O'Geen, A. T., et al. (2018). Mechanisms controlling the impact of multi-year drought on mountain hydrology. *Sci. Rep.* 8:690. doi: 10.1038/s41598-017-19007-19000

Bales, R. C., Molotch, N. P., Painter, T. H., Dettinger, M. D., Rice, R., and Dozier, J. (2006). Mountain hydrology of the western United States. *Water Resour. Res.* 42, 1–13. doi: 10.1029/2005WR004387

Barbour, M., and Minnich, R. (2000). "California upland forests and woodlands," in *North American Terrestrial Vegetation*, eds M. Barbour and W. Billings (Cambridge: Cambridge University Press), 159–200.

Bart, R. R., Tague, C. L., and Moritz, M. A. (2016). Effect of tree-to-shrub type conversion in lower montane forests of the Sierra Nevada (USA) on Streamflow. *PLoS One* 11:e0161805. doi: 10.1371/journal.pone.0161805

Berghuijs, W. R., Woods, R. A., and Hrachowitz, M. (2014). A precipitation shift from snow towards rain leads to a decrease in streamflow. *Nat. Clim. Chang.* 4, 583–586. doi: 10.1038/nclimate2246

Boisramé, G. F. S., Thompson, S. E., Tague, C., Naomi, L., and Stephens, S. L. (2019). Restoring a natural fire regime alters the water balance of a Sierra Nevada catchment. *Water Resour. Res.* 55, 5751–5769. doi: 10.1029/2018WR024098

Budyko, M. (1974). *Climate and Life*. San Diego, CA: Academic Press.

Campbell, J., Alberti, G., Martin, J., and Law, B. E. (2009). Carbon dynamics of a ponderosa pine plantation following a thinning treatment in the northern Sierra Nevada. *For. Ecol. Manag.* 257, 453–463. doi: 10.1016/j.foreco.2008.09.021

Christensen, L., Tague, C. L., and Baron, J. S. (2008). Spatial patterns of simulated transpiration response to climate variability in a snow dominated mountain ecosystem. *Hydrol. Process.* 22, 3576–3588. doi: 10.1002/hyp

Collins, B., Stephens, S., Roller, G., and Battles, J. (2011). Simulating fire and forest dynamics for a landscape fuel treatment project in the Sierra Nevada. *For. Sci.* 57, 77–88. doi: 10.1093/forestscience/57.2.77

Cristea, N. C., Lundquist, J. D., Loheide, S. P., Lowry, C. S., and Moore, C. E. (2014). Modelling how vegetation cover affects climate change impacts on streamflow timing and magnitude in the snowmelt-dominated upper Tuolumne Basin, Sierra Nevada. *Hydrol. Process.* 28, 3896–3918. doi: 10.1002/hyp.9909

De Kauwe, M. G., Medlyn, B. E., Zaehle, S., Walker, A. P., Dietze, M. C., Hickler, T., et al. (2013). Forest water use and water use efficiency at elevated CO_2: a model-data intercomparison at two contrasting temperate forest FACE sites. *Glob. Chang. Biol.* 19, 1759–1779. doi: 10.1111/gcb.12164

Dettinger, M. D., Cayan, D. R., Meyer, M. K., and Jeton, A. E. (2004). Simulated hydrologic responses to climate variations and change in the Merced, Carson, and American River Basins, Sierra Nevada, California, 1900-2099. *Clim. Change* 62, 283–317. doi: 10.1023/B:CLIM.0000013683.13346.4f

Dixon, G. E. (2002). *Essentail FVS: A User's Guide to the Forest Vegetation Simulator*. Collins, CO: U. S. Department of Agriculture.

Dore, S., Kolb, T. E., Eckert, S. E., Sullivan, B. W., Hungate, B. A., Hart, S. C., et al. (2010). Carbon and water fluxes from ponderosa pine forests disturbed by wildfire and thinning. *Ecol. Appl.* 20, 663–683. doi: 10.1890/09-0934.1

Dore, S., Montes-Helu, M., Hart, S. C., Hungate, B. A., Koch, G. W., Moon, J. B., et al. (2012). Recovery of ponderosa pine ecosystem carbon and water fluxes from thinning and stand-replacing fire. *Glob. Chang. Biol.* 18, 3171–3185. doi: 10.1111/j.1365-2486.2012.02775.x

Duell, L. F. W. (1994). The sensitivity of northern Sierra Nevada streamflow to climate change. *J. Am. Water Resour. Assoc.* 30, 841–859. doi: 10.1111/j.1752-1688.1994.tb03333.x

Easterling, D. R. (1997). Maximum and minimum temperature trends for the globe. *Science* 277, 364–367. doi: 10.1126/science.277.5324.364

Ellis, C. R., Pomeroy, J. W., Essery, R. L. H., and Link, T. E. (2011). Effects of needleleaf forest cover on radiation and snowmelt dynamics in the Canadian rocky mountains. *Can. J. For. Res.* 41, 608–620. doi: 10.1139/X10-227

Ellis, C. R., Pomeroy, J. W., and Link, T. E. (2013). Modeling increases in snowmelt yield and desynchronization resulting from forest gap-thinning treatments in a northern mountain headwater basin. *Water Resour. Res.* 49:89. doi: 10.1002/wrcr.20089

Essery, R., Pomeroy, J., Ellis, C., and Link, T. (2008). Modelling longwave radiation to snow beneath forest canopies using hemispherical photography or linear regression. *Hydrol. Process.* 2800, 2788–2800. doi: 10.1002/hyp.6930

Ficklin, D. L., and Barnhart, B. L. (2014). SWAT hydrologic model parameter uncertainty and its implications for hydroclimatic projections in snowmelt-dependent watersheds. *J. Hydrol.* 519, 2081–2090. doi: 10.1016/j.jhydrol.2014.09.082

Finney, M. (2001). Design of regular landscape fuel treatment patterns for modifying fire growth and behavior. *For. Sci.* 47, 219–228. doi: 10.1093/forestscience/47.2.219

Finney, M. (2004). *FARSITE: Fire Area Simulator-Model Development and Evaluation. RMRS-RP-4*. Fort Collins, CO: USDA Forest Service, Rocky Mountain Research Station.

Forrest, K., Tarroja, B., Chiang, F., AghaKouchak, A., and Samuelsen, S. (2018). Assessing climate change impacts on California hydropower generation and ancillary services provision. *Clim. Change* 151, 395–412. doi: 10.1007/s10584-018-2329-5

Fry, D., Battles, J., Collins, B., and Stephens, S. (2015). "Appendix A: fire and forest ecosystem health report," in *Learning How to Apply Adaptive Management in Sierra NEVADA Forests, an Integrated Assessment*, eds P. Hopkinson and J. Battles (Berkeley, CA: Univeristy of California).

Garcia, E. S., and Tague, C. L. (2015). Subsurface storage capacity influences climate-evapotranspiration interactions in three western United States catchments. *Hydrol. Earth Syst. Sci.* 19, 4845–4858. doi: 10.5194/hess-19-4845-2015

Garcia, E. S., Tague, C. L., and Choate, J. S. (2013). Influence of spatial temperature estimation method in ecohydrologic modeling in the Western Oregon Cascades. *Water Resour. Res.* 49, 1611–1624. doi: 10.1002/wrcr.20140

Garfin, G., Jardine, A., Merideth, R., Black, M., and LeRoy, S. (eds) (2013). *Assessment of Climate Change in the Southwest United States: A Report Prepared for the National Climate Assessment*. Washington, DC: Island Press.

Gersonde, R., Battles, J. J., and O'Hara, K. L. (2004). Characterizing the light environment in Sierra Nevada mixed-conifer forests using a spatially explicit light model. *Can. J. For. Res.* 34, 1332–1342. doi: 10.1139/X04-013

Godsey, S. E., Kirchner, J. W., and Tague, C. L. (2013). Effects of changes in winter snowpacks on summer low flows: case studies in the Sierra Nevada, California, USA. *Hydrol. Process.* 28, 5048–5064. doi: 10.1002/hyp.9943

Goldstein, A., and Hultman, N. (2000). Effects of climate variability on the carbon dioxide, water, and sensible heat fluxes above a ponderosa pine plantation in the Sierra Nevada (CA). *Agric. For. Meteorol.* 101, 113–129. doi: 10.1016/S0168-1923(99)00168-169

Goulden, M. L., and Bales, R. C. (2014). Mountain runoff vulnerability to increased evapotranspiration with vegetation expansion. *Proc. Natl. Acad. Sci.* 111, 1–5. doi: 10.1073/pnas.1319316111

Griffin, D., and Anchukaitis, K. J. (2014). How unusual is the 2012 - 2014 California drought? *Geophys. Res. Lett.* 41, 9017–9023. doi: 10.1002/2014GL062433.1

Hawthorne, S. N. D., Lane, P. N. J., Bren, L. J., and Sims, N. C. (2013). The long term effects of thinning treatments on vegetation structure and water yield. *For. Ecol. Manag.* 310, 983–993. doi: 10.1016/j.foreco.2013.09.046

Hopkinson, P., and Battles, J. J. (2015). *Learning How to Apply Adaptive Management in Sierra Nevada forests: An integrated Assessment*. Berkeley, CA: Center for Forestry, University of California.

Huntington, J. L., and Niswonger, R. G. (2012). Role of surface-water and groundwater interactions on projected summertime streamflow in snow dominated regions: an integrated modeling approach. *Water Resour. Res.* 48:319. doi: 10.1029/2012WR012319

Jarvis, P. (1976). The interpretation of the variations in leaf water potential and stomatal conductance found in canopies in the field. *Philos. Trans. R. Soc. Lond.* 273, 593–640. doi: 10.1098/rstb.1976.0035

Jefferson, A., Nolin, A., Lewis, S., and Tague, C. (2008). Hydrogeologic controls on streamflow sensitivity to climate variation. *Hydrol. Process.* 4385, 4371–4385. doi: 10.1002/hyp.7401

Jeton, A. E., Dettinger, M. D., and Smith, J. L. (1996). *Potential Dffects of Climate Change on Streamflow, Eastern and Western Slopes of the Sierra Nevada, California and Nevada*. Sacramento, CA: U. S. Geological Survey Water-Resources Investigations Report.

Kattsov, V., Federation, R., Reason, C., Africa, S., Uk, A. A., Uk, T. A., et al. (2013). "Evaluation of climate models," in *Climate Change 2013 - the Physical Science Basis: Working Group I Contribution to the Fifth Assessment Report of the Intergovernmental Panel on Climate Change*, eds V. Bex and P. M. Midgley (Cambridge: Cambridge University Press), 741–866. doi: 10.1017/CBO9781107415324.020

Kelly, M., and Guo, Q. (2015). "Appendix B: spatial team final report," in *Learning How to Apply Adaptive Management in Sierra Nevada Forests, An Integrated Assessment*, eds P. Hopkinson and J. Battles (Berkeley, CA: Center for Forestry, Univeristy of California).

Knowles, N. (2002). Potential effects of global warming on the Sacramento/San Joaquin watershed and the San Francisco estuary. *Geophys. Res. Lett.* 29, 2–5. doi: 10.1029/2001GL014339

Lundquist, J. D., Dickerson-Lange, S. E., Lutz, J. A., and Cristea, N. C. (2013). Lower forest density enhances snow retention in regions with warmer winters: a global framework developed from plot-scale observations and modeling. *Water Resour. Res.* 49, 6356–6370. doi: 10.1002/wrcr.20504

Lydersen, J. M., Collins, B. M., and Hunsaker, C. T. (2019). Implementation constraints limit benefits of restoration treatments in mixed-conifer forests. *Int. J. Wildl. Fire* 28, 495–511. doi: 10.1071/WF18141

Mahat, V., and Tarboton, D. G. (2012). Canopy radiation transmission for an energy balance snowmelt model. *Water Resour. Res.* 48:W01534. doi: 10.1029/2011WR010438

Meyers, E. M., Dobrowski, B., and Tague, C. L. (2010). Climate change impacts on flood frequency, intensity, and timing may affect trout species in Sagehen Creek, California. *Trans. Am. Fish. Soc.* 62, 1657–1664. doi: 10.1577/T09-192.1

Millar, C. I. (1996). *Sierra Nevada Ecosystem Project, Final Report to Congress, Vol. I, Assessment Summaries and Management Strategies*. Centers for Water and Wildlife Resource, Report No. 36. Davis, CA: University of California.

Millar, C. I., Stephenson, N. L., and Stephens, S. L. (2007). Climate change and forests of the future: managing in the face of uncertainty. *Ecol. Appl.* 17, 2145–2151. doi: 10.1890/06-1715.1

Miller, N. L., Bashford, K. E., and Strem, E. (2003). Potential impacts of climate change on California hydrology. *J. Am. Water Resour. Assoc.* 39, 771–784. doi: 10.1111/j.1752-1688.2003.tb04404.x

Moeser, D., Stahli, M., and Jonas, T. (2015). Improved snow interception modeling using cnaopy parameters derived from airborn LiDAR data. *Water Resour. Res.* 51, 5041–5059. doi: 10.1002/2014WR016724

Molotch, N. P., and Meromy, L. (2014). Physiographic and climatic controls on snow cover persistence in the Sierra Nevada mountains. *Hydrol. Process.* 28, 4573–4586. doi: 10.1002/hyp.10254

Morán-Tejeda, E., Zabalza, J., Rahman, K., Gago-silva, A., López-moreno, J. I., Vicente-serrano, S., et al. (2014). Hydrological impacts of climate and land-use changes in a mountain watershed: uncertainty estimation based on model comparison. *Ecohydrology* 8:1590. doi: 10.1002/eco.1590

North, M., Brough, A., Long, J., Collins, B., Bowden, P., Yasuda, D., et al. (2015). Constraints on mechanized treatment significantly limit mechanical fuels reduction extent in the sierra nevada. *J. For.* 113, 40–48. doi: 10.5849/jof.14-058

Null, S. E., Viers, J. H., and Mount, J. F. (2010). Hydrologic response and watershed sensitivity to climate warming in California's Sierra Nevada. *PLoS One* 5:9932. doi: 10.1371/journal.pone.0009932

Pierce, D. W., Kalansky, J. F., and Cayan, D. R. (2018). *Climate, Drought, and Sea Level Rise Scenarios for the Fourth California Climate Assessment*. Available online at: www.climateassessment.ca.gov

Pupacko, A. (1993). Variations in Northern sierra nevada streamflow: implications of climate change. *J. Am. Water Resour. Assoc.* 29, 283–290. doi: 10.1111/j.1752-1688.1993.tb03208.x

Reinhardt, E., and Crookston, N. (2003). *The Fire and Fuels Extension to the Forest Vegetation Simulator. RMRS-GTR-116*. Ogden, UT: USDA Forest Service Rocky Mountain Research Station.

Risbey, J. S., and Entekhabi, D. (1996). Observed sacramento basin streamflow response to precipitation and temperature changes and its relevance to climate impact studies. *J. Hydrol.* 184, 209–223. doi: 10.1016/0022-1694(95)02984-2982

Roche, J. W., Bales, R. C., Rice, R., and Marks, D. G. (2018a). Management implications of snowpack sensitivity to temperature and atmospheric moisture changes in yosemite National Park, CA†. *J. Am. Water Resour. Assoc.* 54, 724–741. doi: 10.1111/1752-1688.12647

Roche, J. W., Goulden, M. L., and Bales, R. C. (2018b). Estimating evapotranspiration change due to forest treatment and fire at the basin scale in the Sierra Nevada, California. *Ecohydrology* 11:e1978. doi: 10.1002/eco.1978

Roche, J. W., Ma, Q., Rungee, J., and Bales, R. C. (2020). Evapotranspiration Mapping for Forest Management in California's Sierra Nevada. *Front. For. Glob. Chang.* 3:69. doi: 10.3389/ffgc.2020.00069

Romero-Lankao, P., Smith, J. B., Davidson, D. J., Diffenbaugh, N. S., Kinney, P. L., Kirshen, P., et al. (2014). "North America," in *Climate Change 2014: Impacts, Adaptation, and Vulnerability. Part B: Regional Aspects. Contribution of Working Group II to the Fifth Assessment Report of the Intergovernmental Panel on Climate Change*, eds V. R. Barros, C. B. Field, D. J. Dokken, M. D. Mastrandrea, K. J. Mach, and T. E. Bilir (Cambridge: Cambridge University Press), 1439–1498.

Saksa, P., Conklin, M. H., Battles, J. J., Tague, C. L., and Bales, R. C. (2017). Forest thinning impacts on the water balance of Sierra Nevada mixed-conifer headwater basins. *Water Resour. Res.* 53:2016WR019240.

Saksa, P. C., Bales, R. C., Tague, C. L., Battles, J. J., and Conklin, M. H. (2020). Forest fuels treatment and wildfire effects on Sierra Nevada mixed-conifer runoff. *Ecohydrology* 13, 1–16. doi: 10.1002/eco.2151

Shaw, G. D., Conklin, M. H., Nimz, G. J., and Liu, F. (2014). Groundwater and surface water flow to the Merced River, Yosemite Valley, California: 36Cl and Cl- evidence. *Water Resour. Res.* 50, 1943–1959. doi: 10.1002/2013WR014222

Stephens, S. L. (1998). Evaluation of the effects of silvicultural and fuels treatments on potential fire behaviour in Sierra Nevada mixed-conifer forests. *For. Ecol. Manag.* 105, 21–35. doi: 10.1016/S0378-1127(97)00293-294

Stephens, S., Agee, J., Fule, P., North, M. P., Romme, W., Swetnam, T., et al. (2013). Managing forest and fire in changing climates. *Science* 342, 41–42. doi: 10.1126/science.1240294

Stewart, I. T., Cayan, D. R., and Dettinger, M. D. (2004). Changes in snowmelt runoff timing in western North America under a "business as usual" climate change scenario. *Clim. Chang.* 62, 217–232. doi: 10.1023/b:clim.0000013702.22656.e8

Storck, P., Lettenmaier, D. P., and Bolton, S. M. (2002). Measurement of snow interception and canopy effects on snow accumulation and melt in a mountainous maritime climate, Oregon, United States. *Water Resour. Res.* 38:1123. doi: 10.1029/2002WR001281

Su, Y., Guo, Q., Fry, D. L., Collins, B. M., Kelly, M., Flanagan, J. P., et al. (2016). Vegetation mapping strategy for conifer forests by combining airborne lidar data and aerial imagery. *Can. J. Remote Sens.* 42, 1–15. doi: 10.1080/07038992.2016.1131114

Tague, C., and Grant, G. E. (2009). Groundwater dynamics mediate low-flow response to global warming in snow-dominated alpine regions. *Water Resour. Res.* 45, 1–12. doi: 10.1029/2008WR007179

Tague, C., and Peng, H. (2013). The sensitivity of forest water use to the timing of precipitation and snowmelt recharge in the California Sierra: implications for a warming climate. *J. Geophys. Res. Biogeosci.* 118, 875–887. doi: 10.1002/jgrg.20073

Tague, C. L., and Band, L. E. (2004). RHESSys: regional hydro-ecologic simulation system—an object-oriented approach to spatially distributed modeling of carbon, water, and nutrient cycling. *Earth Interact.* 8, 1–42. doi: 10.1175/1087-3562(2004)8<1:rrhsso>2.0.co;2

Tang, H., Brolly, M., Zhao, F., Strahler, A. H., Schaaf, C. L., Ganguly, S., et al. (2014). Deriving and validating Leaf Area Index (LAI) at multiple spatial scales through lidar remote sensing: a case study in Sierra National Forest, CA. *Remote Sens. Environ.* 143, 131–141. doi: 10.1016/j.rse.2013.12.007

Tague, C. L., Moritz, M., and Hanan, E. (2019). The changing water cycle: the eco-hydrologic impacts of forest density reduction in Mediterranean (seasonally dry) regions. *Wiley Interdiscip. Rev. Water* 6:e1350. doi: 10.1002/wat2.1350

van Vuuren, D. P., Edmonds, J., Kainuma, M., Riahi, K., Thomson, A., Hibbard, K., et al. (2011). The representative concentration pathways: an overview. *Clim. Change* 109, 5–31. doi: 10.1007/s10584-011-0148-z

Varhola, A., and Coops, N. C. (2013). Estimation of watershed-level distributed forest structure metrics relevant to hydrologic modeling using LiDAR and Landsat. *J. Hydrol.* 487, 70–86. doi: 10.1016/j.jhydrol.2013.02.032

Vicente-Serrano, S. M., Camarero, J. J., Zabalza, J., Sanguesa-Barreda, G., Lopez-Moreno, J. I., and Tague, C. L. (2015). Evapotranspiration deficit controls net primary production and growth of silver fir: implications for Circum-Mediterranean forests under forecasted warmer and drier conditions. *Agric. For. Meteorol.* 206, 45–54. doi: 10.1016/j.agrformet.2015.02.017

Vose, R. S., Easterling, D. R., and Gleason, B. (2005). Maximum and minimum temperature trends for the globe: an update through 2004. *Geophys. Res. Lett.* 32, 1–5. doi: 10.1029/2005GL024379

Westerling, A. L., Hidalgo, H. G., Cayan, D. R., and Swetnam, T. W. (2006). Warming and earlier spring increase western U.S. forest wildfire activity. *Science* 313, 940–943. doi: 10.1126/science.1128834

Wigmosta, M. S., Vail, L. W., and Lettenmaier, D. P. (1994). A distributed hydrology-vegetation model for complex terrain. *Water Resour. Res.* 30:1665. doi: 10.1029/94WR00436

Wilby, R. L., and Harris, I. (2006). A framework for assessing uncertainties in climate change impacts: low-flow scenarios for the River Thames. *UK. Water Resour. Res.* 42, 1–10. doi: 10.1029/2005WR004065

Young, C., Escobar_Arias, M., Fernandes, M., Joyce, B., Kiparsky, M., Mount, J., et al. (2009). Modeling the hydrology of climate change in California's Sierra Nevada for subwatershed scale adaptation1. *J. Am. Water Resour. Assoc.* 45, 1409–1423. doi: 10.1111/j.1752-1688.2009.00375.x

Zhang, L., Dawes, W. R., and Walker, G. R. (2001). Response of mean annual evapotranspiration to vegetation changes at catchment scale. *Water Resour. Res.* 37, 701–708. doi: 10.1029/2000WR900325

Zhao, F., Strahler, A. H., Schaaf, C. L., Yao, T., Yang, X., Wang, Z., et al. (2012). Measuring gap fraction, element clumping index and LAI in Sierra Forest stands using a full-waveform ground-based lidar. *Remote Sens. Environ.* 125, 73–79. doi: 10.1016/j.rse.2012.07.007

Zierl, B., Bugmann, H., and Tague, C. L. (2007). Water and carbon fluxes of European ecosystems: an evaluation of the ecohydrological model RHESSys. *Hydrol. Process.* 21, 3328–3339. doi: 10.1002/hyp.6540

Conflict of Interest: The authors declare that the research was conducted in the absence of any commercial or financial relationships that could be construed as a potential conflict of interest.

frontiers in Forests and Global Change

ORIGINAL RESEARCH
published: 05 January 2021
doi: 10.3389/ffgc.2020.591162

Understanding How Fuel Treatments Interact With Climate and Biophysical Setting to Affect Fire, Water, and Forest Health: A Process-Based Modeling Approach

William D. Burke[1]*, *Christina Tague*[1], *Maureen C. Kennedy*[2] and *Max A. Moritz*[1,3]

[1] Bren School of Environmental Science and Management, University of California, Santa Barbara, Santa Barbara, CA, United States, [2] School of Interdisciplinary Arts and Sciences Division of Sciences and Mathematics, University of Washington Tacoma, Tacoma, WA, United States, [3] Bren School of Environmental Science and Management, University of California Cooperative Extension, Agriculture and Natural Resources Division, Modesto, CA, United States

OPEN ACCESS

Edited by:
David Findlay Scott,
University of British Columbia Okanagan, Canada

Reviewed by:
Camille Susan Stevens-Rumann,
Colorado State University, United States
John T. Van Stan,
Georgia Southern University, United States

***Correspondence:**
William D. Burke
wburke@ucsb.edu

Specialty section:
This article was submitted to Forest Hydrology, a section of the journal Frontiers in Forests and Global Change

Received: 03 August 2020
Accepted: 30 November 2020
Published: 05 January 2021

Citation:
Burke WD, Tague C, Kennedy MC and Moritz MA (2021) Understanding How Fuel Treatments Interact With Climate and Biophysical Setting to Affect Fire, Water, and Forest Health: A Process-Based Modeling Approach. Front. For. Glob. Change 3:591162. doi: 10.3389/ffgc.2020.591162

Fuel treatments are a key forest management practice used to reduce fire severity, increase water yield, and mitigate drought vulnerability. Climate change exacerbates the need for fuel treatments, with larger and more frequent wildfires, increasing water demand, and more severe drought. The effects of fuel treatments can be inconsistent and uncertain and can be altered by a variety of factors including the type of treatment, the biophysical features of the landscape, and climate. Variation in fuel treatment effects can occur even within forest stands and small watershed management units. Quantifying the likely magnitude of variation in treatment effects and identifying the dominant controls on those effects is needed to support fuel treatment planning directed at achieving specific fire, water, and forest health goals. This research aims to quantify and better understand how local differences in treatment, landscape features, and climate alter those fuel treatment effects. We address these questions using a mechanistic coupled ecohydrologic model—the Regional Hydro-Ecological Simulation System (RHESSys). We ran 13,500 scenarios covering a range of fuel treatment, biophysical, and climate conditions, for the Southern Sierra Nevada of California. Across fuel treatment type, biophysical, and climate parameters, we find nontrivial variation in fuel treatment effects on stand carbon, net primary productivity, evapotranspiration, and fire-related canopy structure variables. Response variable estimates range substantially, from increases (1–48%) to decreases (−13 to −175%) compared to untreated scenarios. The relative importance of parameters differs by response variable; however, fuel treatment method and intensity, plant accessible water storage capacity (PAWSC), and vegetation type consistently demonstrate a large influence across response variables. These parameters interact to produce non-linear effects. Results show that projections of fuel treatment effects based on singular mean parameter values (such as mean PAWSC) provide a limited picture of potential responses. Our findings emphasize the need for a more

complete perspective when assessing expected fuel treatment outcomes, both in their effects and in the interacting biophysical and climatic parameters that drive them. This research also serves as a demonstration of methodology to assess the likely variation in potential effects of fuel treatments for a given planning unit.

Keywords: climate, forest management, modeling, ecohydrology, fuel treatment

INTRODUCTION

Informed forest and vegetation management is progressively more important as both severe drought and wildfire activity are predicted to increase in the Western US (Moritz et al., 2012; Clark et al., 2016). In many Mediterranean fire-prone ecosystems drought is already shaping stand-scale dynamics, shifting habitats, and altering the severity and frequency of disturbances including fire and insects (Clark et al., 2016). Recent droughts, like the 2012-2015 California event and subsequent water stress and mortality (Asner et al., 2016), highlight the magnitude of potential impacts of droughts on forest structure and water resources. At the same time, increasing fire severity in many of these regions has led to unprecedented social and economic costs (Moritz et al., 2014). Given these ecologic and socio-economic costs, fuel treatments are increasingly proposed as a way to reduce risks associated with both droughts and fires. Fuel treatments modify forest structure typically by removing understory and small diameter trees, either through mechanical harvest or controlled burns (Agee and Skinner, 2005). Fuel treatments have a variety of purposes, from timber harvest-oriented practices to increase productivity, to the restoration of historic forest structures and associated habitat. Key among these purposes is the role that fuel treatments can play in reducing wildfire severity (Hessburg et al., 2016; Barros et al., 2019) and mitigating drought impacts on vegetation (Tague et al., 2019). We need to understand more broadly how those treatments are altering our landscapes and affecting resources we care about, both directly and indirectly.

Heterogeneity in forest species and stand structures, along with different goals and available resources for forest management, leads to a wide range of actions that fall under the broad category of fuel treatments. Mechanical thinning is frequently used to reduce fire severity and limit canopy fires by reducing surface fuels, increasing the height to live canopy, and decreasing the density of the canopy (Agee and Skinner, 2005; Evans et al., 2011). Prescribed fire is often paired with mechanical thinning, and in this same context aims to increase forest resilience through reductions in surface fuels and scorching (killing) lower branches of trees, increasing the height to live canopy (Evans et al., 2011; Fernandes, 2015). The size and placement of fuel treatments, however, varies. Treatments, particularly thinning, are expensive and are typically focused on areas where fire threatens residences and communities, or where abnormally high severity fire is expected (Wibbenmeyer et al., 2016; Anderson et al., 2018). Fuel treatments can be effective in reducing fire severity or altering fire regimes, but effectiveness varies with forest type and treatment implementation. Treatments can also have adverse and unintended effects (Omi and Martinson, 2002; Agee and Skinner, 2005; Safford et al., 2012). For instance—the stems removed during thinning, called slash, if left on the forest floor can result in greater surface fuels which then increase fire intensity (Stephens et al., 2012). The long-term efficacy and effects of treatments are linked to regrowth and the presence or absence of new and competing species, leading to uncertainty in the net effects on fire severity (Moritz et al., 2014). The uncertainty in these long-term effects, combined with the (often large) expense of each treatment, make long-term planning for, and prediction of, the effectiveness of fuel treatments for reducing fire severity challenging.

In addition to reducing fire severity, fuel treatments, specifically forest density reductions through thinning, have been used to increase forest productivity and growth as part of silviculture, and more recently, as a forest management tool to reduce drought vulnerability and forest mortality (Spittlehouse and Stewart, 2003; McDowell et al., 2007; Cabon et al., 2018). While there is general agreement on the short-term effectiveness of treatments to reduce drought vulnerability and forest mortality, there is still noteworthy uncertainty in the long-term net effects of treatments. In fact, there is potential for post-treatment scenarios to instead increase vulnerability to future drought (Clark et al., 2016; Tague et al., 2019). Typically, density reduction increases the productivity of remaining trees, and reduces overall water stress, largely by a reduction in tree-scale competition for water (Clark et al., 2016; Sohn et al., 2016). However, in semi-arid regions, increases to productivity may be diminished during dry periods (Sohn et al., 2016). Increased leaf-to-sapwood area ratios and type conversion can also both lead to greater drought vulnerability (Clark et al., 2016). Treatment effects on productivity are further affected by the access of remaining trees to shared subsurface storage and changes to the tree scale radiation environment (Tague et al., 2019; Tsamir et al., 2019). Density reductions both directly and indirectly affect carbon sequestration, and while the short-term effect is straightforward, long term sequestration depends on post-disturbance regrowth (North et al., 2009). The interactions between treatments and forest health are also expected to evolve with climate change, making a priori predictions of treatment success uncertain (Allen et al., 2010).

Fuel treatments can also be used to alter water yield (surface and subsurface water leaving an area). Though paired catchment clear cutting studies show consistent increases in water yield; thinning, particularly in Mediterranean forests, shows variability in the magnitude and direction of effects on water yield (Hewlett and Hibbert, 1967; Brown et al., 2005; Saksa et al., 2017).

Thinning effects on water yield are dependent on a range of factors, including regrowth, access to storage, species changes, and the resulting forest structure, and there remains persistent debate on the dominant controls on the forest cover-water yield relationship (Brown et al., 2005; Ellison et al., 2012; Filoso et al., 2017; Tsamir et al., 2019; Kirchner et al., 2020, Tague and Moritz, 2019).

The wide range of covarying factors that both affect and are affected by fuel treatments combine to make predicting the net effects of a given treatment difficult. Much of this difficulty is associated with the multiple sources of variation including fuel treatment options, species characteristics, landscape, topographic position, climate, and the possible interactions among them. Understanding and ultimately predicting the total impacts of fuel treatments requires considering the interplay between these factors and thinning objectives, such as carbon sequestration, fire management, forest health. Models are key tools that can be used to explore variable interactions and identify particularly important sources of variation even within the same watershed (Fatichi et al., 2016). By identifying which factors matter and when, these tools provide uncertainty bounds on expected outcomes and can guide strategic fuel treatment placement.

Here we use a mechanistic coupled ecohydrologic model to explore the range of fuel treatment scenarios through time and across biophysical sources of variation. We focus on a mid-elevation forest stand within the California Sierra as a representative example of a region where fuel treatments are both likely to occur and may be focused on multiple benefits (Gould, 2019a,b). In the context of existing uncertainty around the effects of treatments, the goals of this work are twofold:

1. To characterize the expected distribution of fuel treatment effects on key response variables (covering the domains of forests, water, and fire), across likely variability in biophysical contexts that would occur within a management unit (e.g., a forest stand within a particular bioclimatic region).
2. To understand how variability in fuel treatment effects is explained by different biophysical, climatic, or fuel treatment parameters. We demonstrate a novel approach, combining modeling and statistical methods, to understand this parameter-driven variability in fuel treatment effects.

In our analysis, we highlight fuel treatment effects on fire severity, carbon sequestration, water yield and forest productivity and examine whether estimates of these effects are similar to commonly held assumptions of treatment outcomes. We typically expect that over short to medium time periods (5–30 years) fuel treatments:

H1. Reduce fire severity – fuel treatments remove fuel and alter canopy structure, limiting the ability of fire to reach the canopy and thus reducing risk of high severity fires (Agee and Skinner, 2005).

H2. Reduce carbon sequestration – fuel treatments are a direct removal of carbon from the landscape, and so lead to lower carbon sequestration, in the short term and in the absence of future fires (North et al., 2009).

H3. Increase water yield – removal of vegetation directly reduces total transpiration. Though more soil is exposed, increasing ET, those increases are typically smaller than decreases to transpiration, and so water yield (or streamflow) is expected to increase overall (Brown et al., 2005).

H4. Increase productivity – remaining vegetation after a fuel treatment will tend to have less competition and greater access to resources (light, water, nutrients) following a treatment, increasing net primary productivity (Clark et al., 2016; Cabon et al., 2018).

Through sensitivity analysis, we assess how biophysical and treatment variation within a given watershed impact these expected outcomes. While the goal of precise prediction of the total long-term effects of fuel treatments on a specific landscape is still in the future, this work demonstrates a watershed scale approach for mapping the fuel treatment-ecohydrologic parameter space. Our approach can be leveraged to assess fuel treatment effects not only at the stand to watershed scale, but regionally. Moreover, understanding the linkages between biophysical parameters and fuel treatment effects can serve to inform future modeling and forest management in similar watersheds.

METHODS

Model Framework

We use the Regional Hydro-Ecological Simulation System (RHESSys) to simulate the effects of thinning (RHESSys 7.1.1). RHESSys captures the relevant range of processes, at scales that support analysis of the hydrologic and vegetation carbon cycling impacts of density reduction. RHESSys is a process-based ecohydrologic model, which in addition to traditional hydrologic modeling, dynamically models plant growth, carbon, and nitrogen cycling, and has successfully been applied to simulate the effects of thinning and climate change impacts on forest growth, carbon cycling, and hydrologic fluxes (Tague et al., 2009; Grant et al., 2013; Saksa et al., 2017; Tague and Moritz, 2019, Tsamir et al., 2019). In particular, Saksa et al. (2017) demonstrated the use of RHESSys to estimate post-thinning water fluxes and vegetation responses. The model has also been used to estimate hydrologic impacts of the restoration of natural fire regimes, including the removal of understory vegetation in Yosemite National Park (Boisramé et al., 2019). RHESSys has recently been coupled with fire spread and fire effects models and coupled model evaluation shows the model can capture spatial and temporal variation in fire regimes (e.g., variation in fire return interval) (Kennedy et al., 2017) and expected relationships in pre- and post-fire forest structure (Bart et al., 2020). Previous work has also evaluated the ability of RHESSys to capture hydrologic and carbon cycling in semi-arid mountain systems (Garcia et al., 2016; Son et al., 2016).

RHESSys accounts for both understory and overstory vegetation. Vegetation ecophysiology parameters can be adjusted to simulate a different plant species. These parameters are set via the RHESSys parameter database (https://github.com/RHESSys/ParamDB), literature derived values, previous

RHESSys implementations, or a combination of these methods. Precipitation, wind, and radiation are attenuated through overstory and then understory canopies. All vegetation grows stems, leaves, and roots dynamically. Downwelling radiation is adjusted by topography following MT-CLIM (Running et al., 1987) and landscape scale topographic shading through horizon angles. Radiation interactions with the ecosystem are modeled separately for direct and diffuse radiation, as radiation is attenuated through the canopy. Leaf scale fluxes differentiate between sunlit and shaded leaves. Gross photosynthesis is estimated using the Farquhar Photosynthesis model (Farquhar et al., 1980), which is driven primarily by the availability of light, water, and nitrogen, as well as growth and maintenance respiration models adapted from Ryan (1991). Net photosynthesis is allocated using the method from Dickinson et al. (1998) as also described in Garcia et al. (2016), and carbon and nitrogen both cycle vertically and can transfer laterally. Water input to RHESSys is driven by precipitation, and the model features vertical and horizonal water fluxes, both above and below-ground. Above-ground there is canopy, litter, and soil evaporation and transpiration [using Penman-Monteith (Monteith, 1965)], as well as overland flow (either Hortonian or saturation) and infiltration. Snow accumulation and melt, and the impact of forest shading on these processes is also simulated. Below-ground water (and nutrient) stores are separated into the root zone, which is dynamically defined by the depth of vegetation roots, the unsaturated zone, and the saturated zone. A groundwater store can also be used both as a sink from the saturated zone and contribution to the stream, and water fluxes occur vertically between these below-ground stores as well as laterally, driven by elevation gradients derived from above ground elevation.

A stochastic fire spread module has been recently added to RHESSys (Kennedy et al., 2017). In the module, spread is iteratively tested against a spread probability that is calculated from the litter load, relative deficit (1-ET/PET), topographic slope, and wind direction relative to the direction of spread. RHESSys also calculates fire effects on forest stand and litter variables for those burned cells (Bart et al., 2020) by using the spread probability as a proxy for surface fire intensity. This, in combination with biomass and the relative heights of the understory and overstory, is used to calculate fire-related changes to the surface, understory, and overstory carbon stores. We use a subset of this functionality for our purposes, not running the full fire spread and effects models but instead components derived from them, which is detailed more in section fuel treatment scenarios.

Previously in RHESSys the patch was the smallest modeling unit both spatially and with respect to nutrient and water routing. Here, we include the use of a new "multiscale routing" method (Burke and Tague, 2019; Tsamir et al., 2019). This approach creates a "patch family" as the smallest spatially explicit model unit and use "aspatial patches" within the patch family to account for within patch heterogeneity (e.g., areas within a spatial stand that comprise thinned, open areas, and remaining trees) without requiring very fine scale (meter) spatially explicit representation that would require computational complexity beyond currently available tools. In this context, the aspatial patch is then the smallest modeling unit for vertical water, energy, and nutrient dynamics. In previous RHESSys applications, RHESSys used only hillslope routing, routing subsurface water between spatially explicit model units (patch families) based only on topography. Within patch family routing or "local" routing occurs not because of topography but rather root access, and at scales smaller than are typically modeled. Crucially for the purposes of this work, we have added RHESSys functionality to capture finer scale density reduction impacts on water availability and growth. These advances account for between vegetation (aspatial patch) exchanges (among gaps, thinned, and unthinned vegetated areas) as well as shading by neighboring trees within a stand (patch family). Thus, RHESSys now supports "multiscale routing" with two scales of water (and nutrient) routing: a) routing due to topography between patch families within a hillslope or watershed and b) a new "local routing" that allows exchanges between aspatial patches and their associated vegetation types, that are typically at scales too small (<30-meter) to characterize as spatially explicit units within a watershed scale model such as RHESSys. Sensitivity of ecophysiological fluxes to the addition of multiscale routing methods is demonstrated by Tsamir et al. and presented by Burke and Tague (2019).

Previous work has shown that this "local" routing between gaps, thinned areas and remaining trees can have a substantial impact on post disturbance (fire or density reduction) hydrology and regrowth (Tague and Moritz, 2019). In this study, local routing (shown conceptually in **Figure 1**), moves water between patches, with the water content of each patch approaching the mean of the patch family, mediated by the sharing coefficient. Water in the rooting zone and unsaturated zone is transferred among aspatial patches in each patch family. A sharing coefficient is defined to modulate the transfer of water between patches. When gaining water, only water up to field capacity is available to the root zone, with excess going to the unsaturated zone. When losing water, only water down to the wilting point is available from the root zone, with the remainder coming from the unsaturated zone. Sharing coefficients will vary primarily with species (which controls root spread and distribution) and gap size distributions (determined by the preexisting forest structure, thinning method, and thinning intensity; Schenk and Jackson, 2002; Clark et al., 2016). Nitrate and dissolved organic carbon (DOC) are transferred along with water following existing approaches in RHESSys for linking water and nutrient transport.

Shading within the patch family is also accounted for as a part of multi-scale routing. Though the multi-scale routing method does not model individual trees explicitly, by modeling thinned and unthinned areas separately, we approximate the effects of shading between neighboring thinned, unthinned and open area patches. Shading is modified by an adjustment to the east/west horizon, which is used to determine total daily incoming shortwave radiation, based on the relative height of the patch compared to the patch family. Shading is adjusted if the shading angle is greater than the existing horizon angle. Note that for each patch, vertical shading or attenuation of radiation through vertical canopy layers remains as in earlier

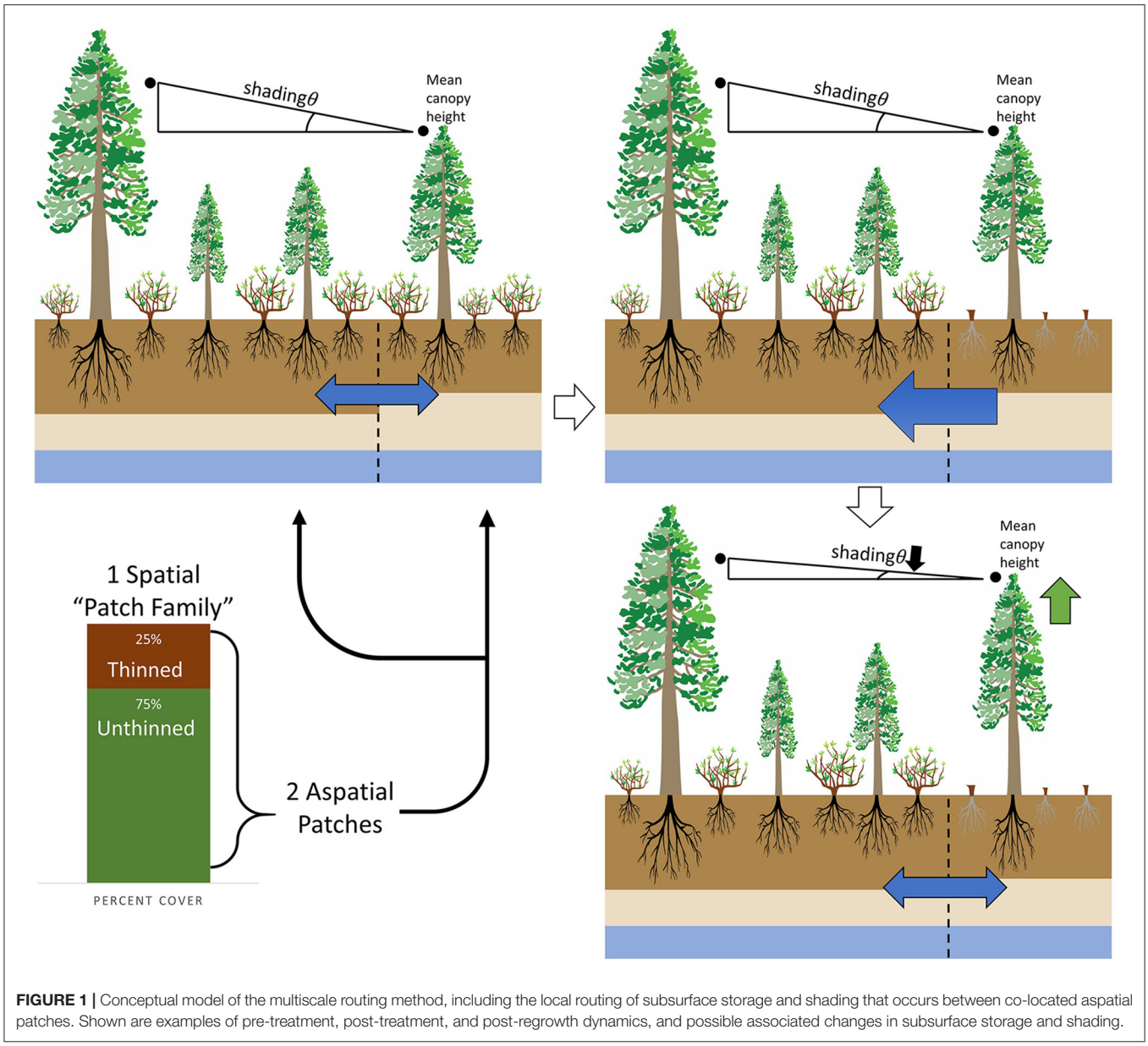

FIGURE 1 | Conceptual model of the multiscale routing method, including the local routing of subsurface storage and shading that occurs between co-located aspatial patches. Shown are examples of pre-treatment, post-treatment, and post-regrowth dynamics, and possible associated changes in subsurface storage and shading.

versions of RHESSys (Tague and Band, 2004). **Figure 1** shows our implementation of shading and how it evolves with changing conifer height.

Site

Our study site is a typical mid-elevation conifer forest in the Southern California Sierra, an area that has been previously identified as a high priority area for fuel treatment (Thompson et al., 2016). For model set up and parameterization we use data from the Kings River Experimental Watersheds (KREW) and the Southern Sierra Nevada Critical Zone Observatory (CZO). Higher elevations at this site maintain a seasonal snowpack but transition to rain dominated at lower elevations (Son et al., 2016). Vegetation cover is mainly mixed-conifer forest, consisting of white fir (*Abies concolor*), ponderosa pine (*Pinus ponderosa*), Jeffery pine (*Pinus jeffreyi*), California black oak (*Quercus kelloggii*), sugar pine (*Pinus lambertiana*), and incense cedar (*Calocedrus*), that transition to sclerophyll shrubs [greenleaf manzanita (*Arctostaphylos patula*), mountain whitehorn (*Ceanothus cordulatus*)] at lower elevations (Bart et al., 2016; Safeeq and Hunsaker, 2016). Soils are coarse sand and sandy loam (Gerle-Cagwin) with high infiltration capacities, and relatively deep storage (Bales et al., 2011). For this study, we build on previous watershed scale RHESSys simulations at this site (Bart et al., 2016; Son et al., 2016). Here we sample forest stand characteristics by selecting from aspect, elevation, subsurface water storage capacity, and vegetation types within the watershed. For our model scenarios, described in

TABLE 1 | Summary of fuel treatment scenario parameters.

Fuel treatment scenarios	
Treatment method and intensity	**10**
Understory thinning + prescribed fire: high, med, low	3
Overstory thinning, with/without slash: high, med, and low	6
Prescribed fire	1
Treatment Frequency: 5, 10, and 30 years	**3**
No treatment	**1**
Site characteristics	**540**
Vegetation: shrub, conifer, and shrub/conifer mix	3
Aspect: north, south	2
Plant accessible water storage capacity: low, med, and high	3
Aridity: dry, variable, and wet	3
Climate warming: baseline, + 2°C	2
Root sharing coefficients: 0, 0.25, 0.5, 0.75, and 1	5
Total (incompatible combinations removed)	**13,500**

Bold values highlight the major subcategories of scenario variation.

more detail in section scenarios, we use data from a local meteorology station (Grant Grove, National Climate Data Center Station, Lat: 36.73603○N, Lon: 118.96122○W, elevation 2,005 m). Historic records (1943–2015) for this station have a mean annual temperature of 8°C and mean annual precipitation of 1,037 mm.

Scenarios

Model simulation scenarios were designed to cover a reasonable range of possible physical conditions and fuel treatment types for mid-elevations in the Southern Sierra Nevada. A synopsis of these scenarios is included in **Table 1**. Given the high computational cost of simultaneous parameter variation with continuous sampling of the parameter space, we use a factorial approach and choose 2-3 end member parameter values encompassing high, medium, and low ranges, that define the expected extremes and, in some cases, mid points for each parameter. All simulations are done for a single location (patch family).

Biophysical Parameters and Climate Scenarios

Three vegetation covers were simulated: shrub, conifer overstory with a shrub understory, and a 50/50 mix of uncovered shrub and conifer over shrub (also referred to subsequently as shrub, conifer+shrub, and conifer+shrub/shrub). For aspect we used north and south. For plant (root) accessible subsurface water storage capacity (PAWSC, included at "low," "medium," and "high" intervals), we used parameters from Tague and Moritz (2019). These parameters span the range of PAWSC for vegetated locations in mid-elevation Sierras. We note that "high" PAWSC is greater than typical soil depth for this site, and acknowledge that plants often access water well below organic soil depths (Klos et al., 2018). We use root sharing coefficients of {0, 0.25, 0.5, 0.75, 1}, where 0 indicates no root sharing (all aspatial patches are isolated) and 1 indicates complete sharing by all vegetation. Climate in each scenario is varied in two ways: the aridity and the presence or lack of climate warming. "Aridity" is defined by the subset of the observed climate record at Grant Grove station over which the simulation is run, with "wet," "variable," and "dry" periods being the maximum, median, and minimum of 30-years moving averages of annual precipitation. The "wet" period is (water years) 1953–1983 (1,103 mm mean annual precipitation), "variable" is 1942–1972 (1,057 mm), and the "dry" period is 1985–2015 (967 mm). Though there is overlap in these periods, importantly the wet and dry periods are mutually exclusive, and the dry period captures the recent Californian droughts which is of particular interest here. Climate warming is included through a uniform shift in the observed climate record, increasing temperature by 2°C, and increasing CO_2 to 450 ppm. Climate warming is applied to the wet, dry, and variable periods to extend the range of climate conditions (e.g., to include the possibility of warmer droughts). We acknowledge that future climate may include a wider range of conditions (such as longer duration or more frequent droughts). However, climate model estimates of precipitation change for this region remain uncertain (Hayhoe et al., 2018). To limit computational and model complexity we focus on our simple set of scenarios that have a high likelihood of occurring in the short-term (next decade).

Model estimates require initial conditions that may vary with the biophysical parameters listed above. To account for this, spin-up to initial conditions was done separately for each vegetation, PAWSC, root sharing coefficient, and aspect, as each of these factors could alter the long-term soil nutrient and above ground biomass supported by the plot. Each instance was initialized with known soil nutrient values for the mid-elevation Southern Sierra site, and then each was run for an additional 140 years (looping the observed climate record) to further initialize the soil nutrients and allow vegetation to grow and reach maturity. Our analysis focuses on mature forest/shrubs, assuming no recent fires as these are likely to be the conditions targeted by fuel treatments.

Fuel Treatment Scenarios

Fuel treatment scenarios were selected to explore the range of possible thinning methods, intensities, and frequencies, while being limited and guided based on reasonable real-world (financial and physical) constraints on area treated and treatment frequency (Calkin and Gebert, 2006; North et al., 2015). Three main categories of treatment were selected: understory thinning (paired with prescribed fire), overstory thinning, and prescribed fire alone. In RHESSys, fuel removal is implemented as removal of a combination of litter and vegetation understory or overstory carbon and nitrogen stores (including stores in leaf, stems, and roots). RHESSys does not currently track individual stems, thus all thinning scenarios remove a given percentage of litter, overstory and/or understory pools, based on the type and intensity of thinning. Understory thinning is meant to approximate a thinning from below strategy, though we limit fuels removed to only the shrub understory. All understory treatments were coupled with a lagged (by 1 month) prescribed fire. Understory thinning was simulated in RHESSys through removal of both carbon and nitrogen from the shrub understory. Prescribed fire following thinning removes litter carbon and nitrogen stores. Overstory thinning is meant to approximate a selection thinning strategy and is limited to removal of overstory vegetation carbon and nitrogen pools. Overstory thinning was

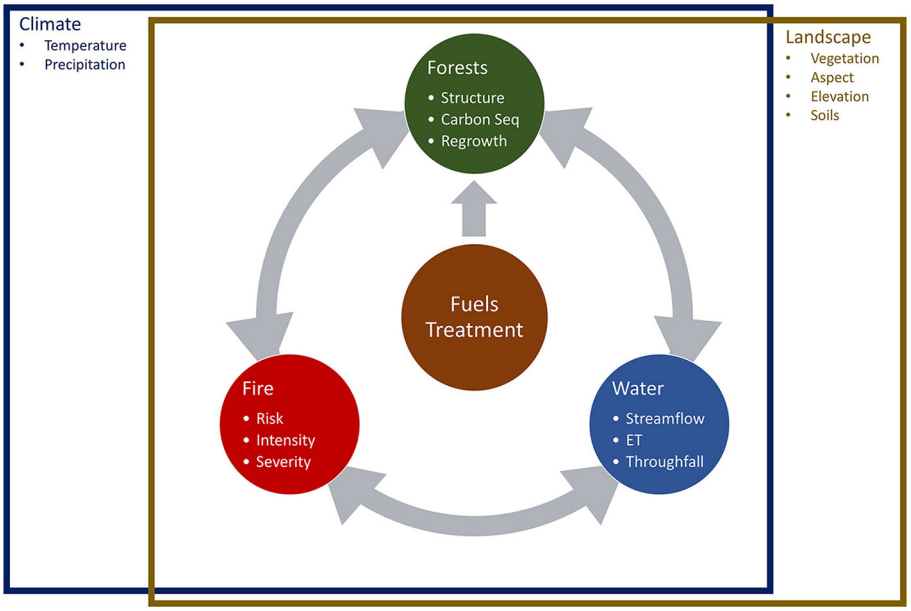

FIGURE 2 | Conceptual model of the domains that underpin and are affected by fuel treatments.

combined with two slash (vegetation removed during thinning) management scenarios. One where slash remains and becomes part of litter pools (potentially increasing future fire spread and severity) and a second where slash is removed. Prescribed fire, both when it follows an understory thinning and when used alone, is simulated by removal of both litter and coarse woody debris.

Understory and overstory treatments were performed at three intensities, implemented in RHESSys through application of the treatment (e.g., removal of vegetation) at fractional area coverages of 0.1, 0.25, and 0.4. For example, a 0.1 intensity understory treatment removes all understory carbon and nitrogen for an aspatial patch with 10% coverage, which for the encompassing patch family, translates to removal of 10% of the total understory (and a smaller reduction in total stand carbon). A treatment of only prescribed fire was also run where 100% of litter and coarse woody debris pools were removed for all aspatial patches. For scenarios with only shrub vegetation cover, where there is no understory, we omit the overstory thinning scenarios (as the single shrub canopy "overstory" is already thinned equivalently by the understory thinning scenarios).

Each of the treatment method and intensity combinations was run at three different temporal frequencies over the 30-years simulation. All treatment scenarios start with a treatment at the simulation start. We then have three different temporal treatment frequencies over the 30-years simulations: no further treatments, treatments every 5 years, and treatments every 10 years. Each of these treatment scenarios were repeated for all combinations of biophysical parameters. A no treatment scenario was also run for each biophysical scenario. A total of 31 treatment scenarios, and 540 biophysical and climatic scenarios were run yielding a total of 13,500 scenarios (with incompatible vegetation type + treatment method scenarios removed). All scenarios were run at a daily timestep for 30 years. For each scenario we output three key biophysical variables: stand carbon, net primary productivity (NPP), and evapotranspiration (ET), and three fire-related variables: fire spread probability (FSP), shrub fuel height (shrub only scenarios), and conifer canopy fuel gap (conifer+shrub scenarios). The three biophysical variables broadly serve as metrics for key functions in the domains included in **Figure 2**. Stand carbon is included as a means of tracking carbon sequestration, NPP is used as a metric of forest health and is further useful as a measure of drought resilience, and ET shows direct effects on the water balance and indirect effects of treatments on water yield.

The fire-related variables: FSP, shrub fuel height, and conifer canopy fuel gap, are indicators of how fire regimes might vary across scenarios and parameters. FSP denotes the likelihood that a location would burn, given ignition (or fire in a neighboring patch), and is broadly an indicator of surface fire occurrence and fire spread. This metric however does not reflect the fire severity or the impact of a fire on stand structure and biomass. We note that for the single patch family implementation used here (without neighboring patch families), we cannot run the full RHESSys-Fire model (Kennedy et al., 2017; Bart et al., 2020) directly. RHESSys, however, does provide fire-related outputs at the patch scale, from which we calculate the metrics included here. Shrub fuel height and conifer canopy fuel gap are direct indicators of stand structure/biomass, and indirectly serve as proxies for potential fire severity. In the shrub only case we use mean annual maximum shrub height (over the simulation period), as it is indicative of available fuels. In conifer+shrub scenarios we use the difference in understory and overstory fuel heights. We use the canopy height gap here as an indicator of the

likelihood that ladder fuels (understory shrubs) would facilitate a crown fire if fire were to spread into this patch. The mixed 50/50 vegetation runs (conifer overstory with shrub understory combined with uncovered shrub alone) were excluded in these analyses as the severity metrics are not comparable. Together the six variables, stand carbon, ET, NPP, FSP, shrub fuel height, and conifer canopy fuel gap, span the range of domains encompassed in **Figure 2**.

Analysis

The number and breadth of simulation outputs presents a challenge in analyzing the simulation results. Each scenario produces a time series of responses to the fuel treatments, that reflects the impact of daily to inter-annual variation in meteorological forcing. **Figure 3** highlights an example of this, illustrating the roles of fuel treatment timing, vegetation regrowth, and seasonally driven trends in stand carbon. There are complex interactions that arise from the layered effects of baseline seasonal trends (in stand carbon) and post-treatment regrowth—**Figure 3** shows just one example of this that illustrates differences between treatments and the baseline "no treatment" case at a monthly time scale. Though these finer-time scale regrowth dynamics certainly merit greater investigation, this work is focused on a broader synthetic perspective. Our goal is to assess the differential role of biophysical and climatic parameters and treatment scenarios on the long-term aggregate effects of fuel treatments. For all response variables, our analyses look at changes in treated scenarios relative to otherwise equivalent untreated scenarios, computed as the percent change of the simulation-long (30-years) annual averages, between each treated scenario and untreated equivalent scenario. Because we average over the 30-years simulation, we provide a longer-term perspective of fuel treatment effects, with less emphasis on the ephemeral and more immediate fuel treatment responses.

As the goal of this research is both to characterize the broader scope of outcomes, while also interrogating specific parameter interactions, we include analyses to facilitate both goals. Histograms are used to capture the range and distribution of fuel treatment effects on each response variable. To illustrate parameter interactions, we also use a series of boxplots, showing response variable distributions subset by parameters. Showing all possible parameter interactions in this way is not feasible, thus we select several particularly salient examples. We also use Random Forests [with the R packages RandomForest and randomForestExplainer; (Liaw and Wiener, 2002; Paluszynska et al., 2019)] to identify the relative importance of biophysical and climatic parameters in predicting the treatment effects. Random forests use a bootstrap of the regression tree combined with random sampling of predictors at each node in the tree. We generated the random forests each with 500 trees (bootstrap runs) and with local importance set to TRUE. We use minimum depth to rank the parameters by importance. The depth in a tree indicates the order in which a parameter is selected. A smaller value for depth indicates higher importance, with typical low values (for our purposes) of ∼1, and high values >3.

RESULTS

The 13,500 scenarios produced by the varied input parameters result in noteworthy range and variability in effects on forests (stand carbon and NPP), water (ET), and fire (FSP, shrub fuel height, and conifer canopy fuel gap). The distribution of effect sizes of the biophysical and fire variables of interest, across expected variability in biophysical, climatic, and fuel treatment parameters, is shown in **Figure 4**. Effect sizes highlight the long-term mean changes in each response variable to a fuel treatment, relative to untreated equivalents. Distributions shown for each response variable are grouped (colored) only by treatment type, and thus results for each treatment type include variation in not only biophysical parameters but also fuel treatment intensities and timing. All four of the expected fuel treatment outcomes (H1–H4) are confirmed to varying degrees by means of simulation distributions, although for NPP mean is not significantly different from 0 (no change). Fire severity (as indicated by shrub fuel height and conifer canopy fuel gap) is reduced, carbon sequestration goes down, and water yield increases. However, for all effects there is substantial variation in the magnitude, and for some scenarios, direction of the outcomes. Most treatment effect distributions are roughly normally distributed, although some variables including ET, shrub fuel height, and conifer canopy fuel gap (**Figures 4C,E,F**) show left tailed skews. The result of this is that, despite fuel treatment effects broadly conforming to expected outcomes (H1–H4), some subset of scenarios will diverge from those expectations. Stand carbon and ET (**Figures 4A,C**) adhere to expected treatment effects (H2, H3) in most cases, with only 23.4 and 22.4% of scenarios showing increases in stand carbon and ET respectively, and those increasing scenarios are weighted toward 0% change. NPP features a large range of treatment effects (-150–50%), with 42% of scenarios leading to decreases, departing from expected treatment effects (H4). FSP has a narrow range, spanning only−13–8%, which is an expected outcome given that fuel treatments are not typically expected to have a strong effect on fire spread rates. Potential fire severity, on the other hand, is expected to be affected by fuel treatments. Shrub fuel height and conifer canopy fuel gap show a substantial range of outcomes,−62–1% for shrubs, and−170–48% for conifer. Treatment effects on shrub fuel height consistently align with expected reductions in fire severity (H1) whereas changes in conifer canopy fuel gap are strongly dependent on treatment type with overstory treatments leading to increases in potential fire severity, diverging from expected effects.

Interactions between fuel treatment and biophysical parameters, and the subsequent impact on fuel treatment effects, are of specific interest in this research. Interactions between treatment type and PAWSC alter fuel treatment effects on NPP, ET, conifer canopy fuel gap, and fire spread probability (subset for only conifer+shrub vegetation scenarios; **Figure 5**). Treatments, of all types, performed on high PAWSC, largely lead to increasing NPP (**Figure 5A**), In contrast, in low PAWSC, overstory thinning produces substantial decreases in NPP (median of−24%), while understory thinning and prescribed fire both have a positive median change of 4%. These

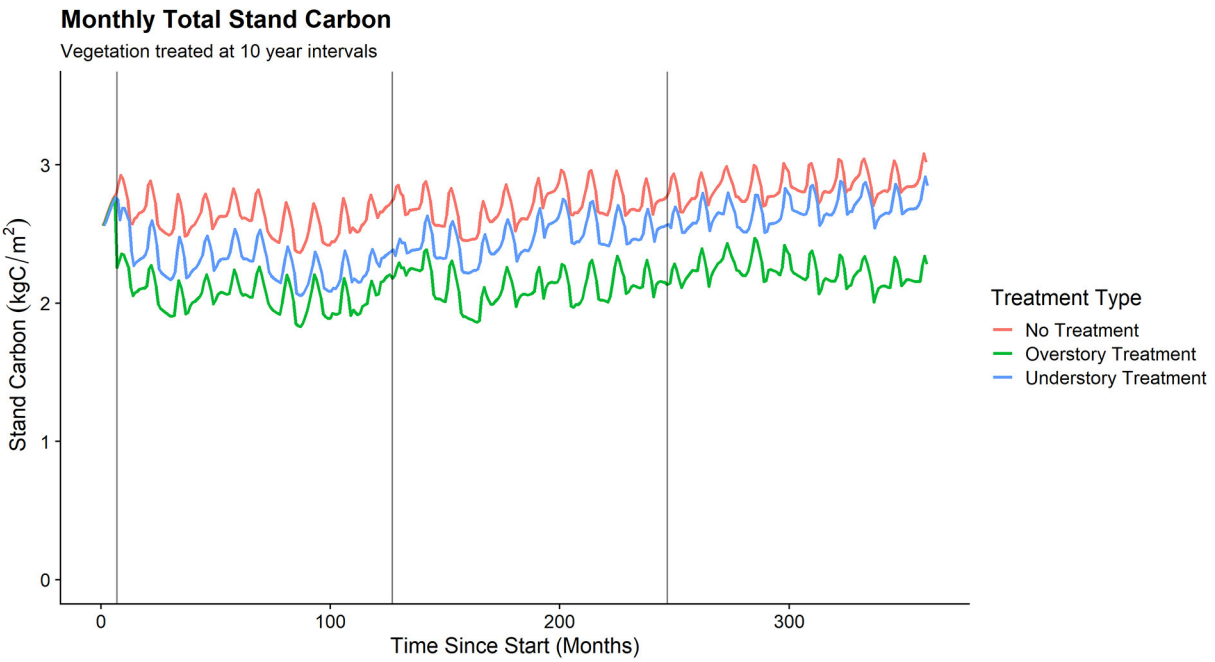

FIGURE 3 | Monthly stand carbon for two treatment scenarios (40% understory removal with following prescribed fire and 40% overstory removal) and a no treatment scenario, performed on conifer overstory with shrub understory, implemented every 10 years (vertical lines), with otherwise identical biophysical and climatic parameters ("wet" aridity, no climate warming, "low" PAWSC, 0.5 root sharing coefficient, North aspect).

varied treatment effects show that for some sites with lower PAWSC (shallow soils), NPP declines may occur and are more likely, while for other sites with high PAWSC, differences in treatment can lead to substantially larger or smaller increases. Treatment effects on ET (**Figure 5B**), by comparison to NPP, tend to be smaller and have less variation, both across PAWSC and treatment type. At medium and low PAWSC, thinning leads to expected reductions in ET, while at high PAWSC and for all prescribed fire scenarios ET increases, deviating from expectations (H3). Conifer canopy fuel gap (**Figure 5C**) shows a more notable difference in treatment effects across treatment type as opposed to PAWSC. Overstory treatment effects on conifer canopy fuel gap are nearly all negative (median−32-−38%), indicating increasing fire severity contrary to expected reductions (H1), while understory treatments and prescribed fire have more moderate, and typically positive effects on conifer canopy fuel gap (median ∼ 0–32%). Fire spread probability (**Figure 5D**) has much smaller magnitude of effects overall than any of the other responses, and shows increasingly negative changes with lower PAWSC, though across all treatments and PAWSC, median changes still only range from 0% (prescribed fire on high PAWSC) to−3% (understory thinning on low PAWSC).

For a subset of parameters, assessed across treatment type, treatment effects on conifer canopy fuel gap vary consistently with fuel treatment type, and inconsistently with the other varied parameters (**Figure 6**). Across all parameters, fuel treatment effects on conifer canopy fuel gap are split, with consistent negligible to moderate increases from understory treatments and prescribed fire, and reductions from overstory treatments. Though treatment type is the strongest determinant of whether treatment effects will lead to expected reductions in potential fire severity (through increases in conifer canopy fuel gap), the other varied parameters alter the magnitude of those changes. Climate warming (**Figure 6A**) and aridity (**Figure 6B**) lead to marginal differences in conifer canopy fuel gap. Increased warming and dry aridity scenarios reduce variability of understory treatments and prescribed fire, though median effects are consistent regardless warming at 9 and 2%, respectively (for both parameters). Treatment intensity (**Figure 6C**) results in progressively larger changes in conifer canopy fuel gap with greater treatment intensities. For intensities of 0.1–0.4, overstory treatments lead to reductions of −12 to −77%, while understory treatments produce the expected increases (H1) from 5 to 11% (prescribed fire does not have an associated intensity). Treatment interval (**Figure 6D**) mirrors treatment intensity somewhat, though with greater variability and smaller median shifts. The shortest treatment interval (most frequent) leads to the largest magnitude changes in conifer canopy fuel gap, increases coming from understory treatments and prescribed fire, and reductions from overstory treatments.

To summarize the influences of all parameters, accounting for their potential interactions we use random forests. Minimum depth distributions, generated from the random forest decision trees for stand carbon, NPP, ET, FSP, shrub fuel height, and conifer canopy fuel gap are shown in **Figure 7**. Climate, treatment scenarios and biophysical parameters (collectively "parameters") are ordered by mean minimal depth. In all cases the predicted metric is the difference between the treated and

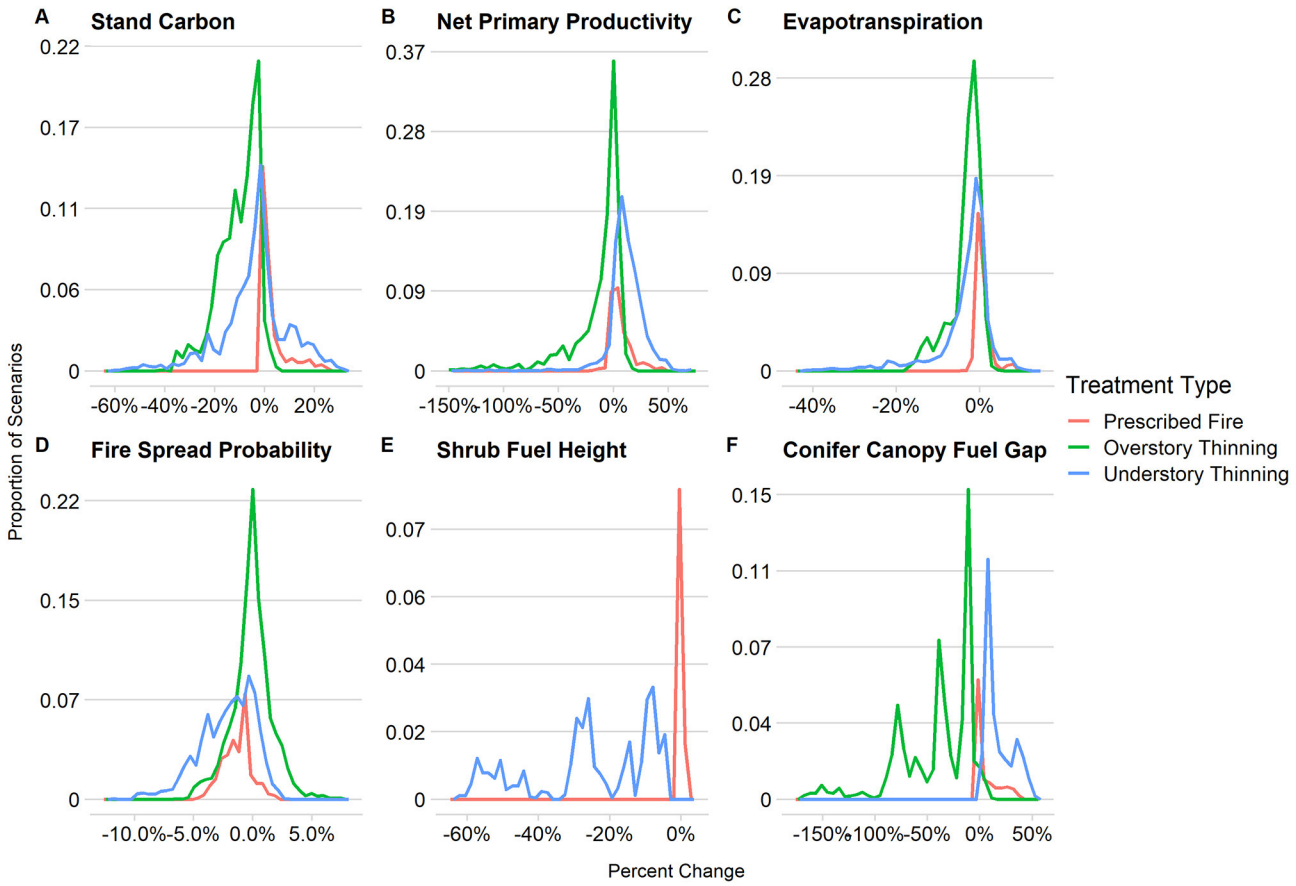

FIGURE 4 | Histograms of fuel treatment effect sizes, in percent change of simulation long (30-years) means relative to untreated equivalent scenarios, for stand carbon **(A)**, net primary productivity **(B)**, evapotranspiration **(C)**, fire spread probability **(D)**, shrub fuel height **(E)**, and conifer canopy fuel gap **(F)**. Colored by treatment type.

untreated paired simulation. The rank order of simulation parameters differs across effects—a parameter is ranked higher (has a lower mean minimum depth) when it has a greater ability to reduce variability in subsets of the variable of interest, with the mean value indicating the mean decision tree level at which that occurs. However, lower ranked parameters may still contribute to explaining variability in effect size, particularly if there are a substantial number of trees (cases) where this parameter is ranked highly (ex. minimal depth <= 3). This variable importance occurs for all parameters to some degree apart from aspect.

Fuel treatment method and intensity rank either first or second for all response variables while treatment interval shows more variation in its contribution to treatment effects and tends to rank lower, ranging from second to fourth. Nonetheless fuel treatment interval is a higher-order control, often ranking higher than biophysical or climate parameters. The most consistent parameter across variables, and least influential is aspect, ranking last for all parameters and with a particularly high mean minimal depth of 3.1–3.4. Both PAWSC and vegetation type are moderately important with a consistently high degree of influence. PAWSC matches or exceeds the mean minimal depth of the treatment parameters for stand carbon and NPP effects.

Aridity and climate warming tend to rank relatively low but still contribute to variation in effect. For stand carbon (**Figure 7A**) these climate parameters have influence that is nearly equal to that of treatment interval. Climate warming, compared to aridity, has a slightly more pronounced effect on NPP and ET (**Figures 7B,C**), and has less influence in the case of FSP (**Figure 7D**), but both the ranking and magnitude of the mean minimal depths (~2–2.7) of climate warming and aridity are very similar. The root sharing coefficient, which determines fine-scale within-stand interaction, ranks low, second to last in general, but both the mean minimal depth values (2.39–2.58) and the distributions of minimal depth are similar to that of climate parameters.

Minimum depths of shrub fuel height (**Figure 7E**) and conifer canopy fuel gap (**Figure 7F**) feature fewer parameters due to already being subset by vegetation type. The mean minimal depth values and distributions for shrub fuel height follow both the form and general order of the mean minimal depths and distributions of the other response variables. The

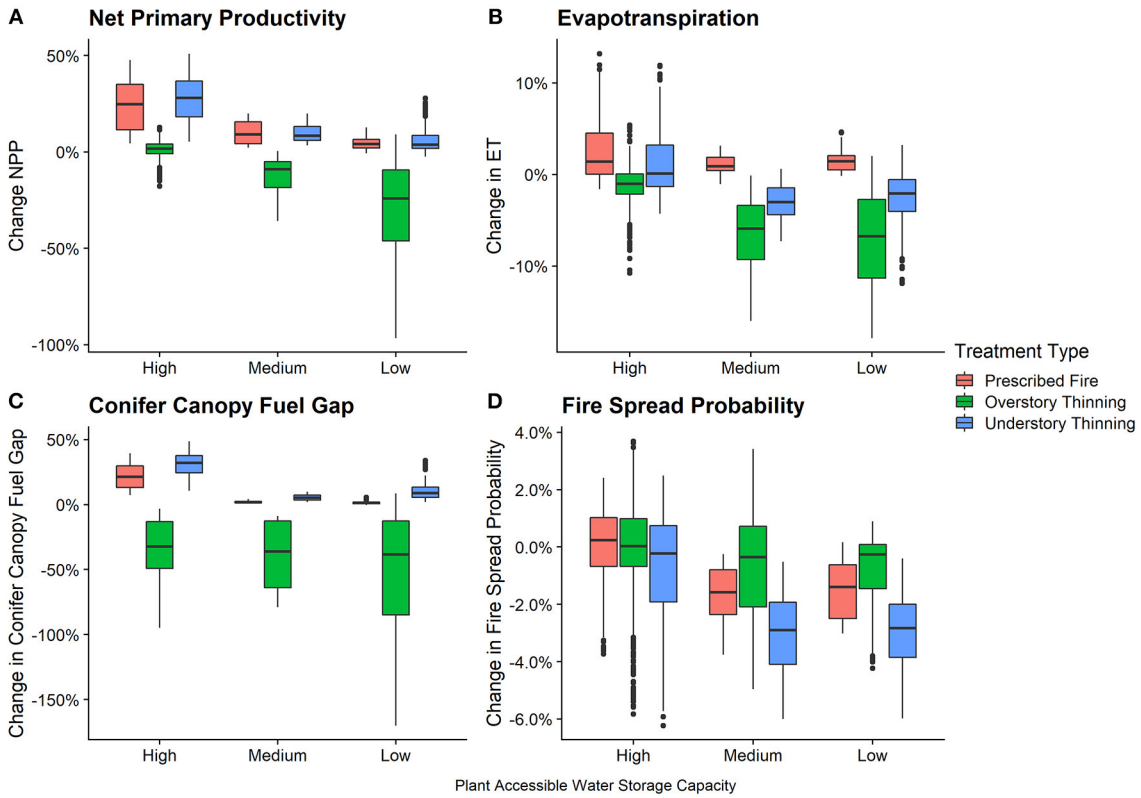

FIGURE 5 | Boxplots of percent change of simulation long (30-years) means relative to untreated equivalent scenarios, for net primary productivity **(A)**, evapotranspiration **(B)**, conifer canopy fuel gap **(C)**, and fire spread probability **(D)**, for only conifer+shrub scenarios, subdivided by PAWSC on the x-axis and colored by treatment type. Upper and lower hinges indicate the 1st and 3rd quartiles (25 and 75th percentiles), and whiskers indicate the greatest/smallest value within 1.5 times the inter-quartile range.

minimal depth distributions for conifer canopy fuel gap have a somewhat different form, with four parameters grouped tightly at mean minimum depths of 1.98–2.08. Root sharing coefficient also stands out in the conifer case, ranking 3rd with a mean minimal depth of 1.98 (ranked 5th at 2.06 for shrub fuel height), indicating a greater influence of this parameter on the effect of thinning on conifer canopy fuel gap, relative to the role of root sharing coefficient for the other response variables.

DISCUSSION

This analysis has improved our understanding of the effects of fuel treatments across a range of biophysical and climate settings with varied fuel treatment practices. Through the simulations and subsequent analysis done here we provide insight toward two goals: (1) understanding the scope and magnitude of expected fuel treatments effects on forests, water, and fire for a mid-elevation Southern Sierra site and (2) understanding how fuel treatments, biophysical parameters, and climate interact and serve to explain responses in fuel treatment effects on forests, water, and fire.

Distribution of Fuel Treatment Effects on Water, Carbon, and Fire

The distributions of fuel treatment effect sizes characterize the range of outcomes across expected biophysical conditions and varying treatments at the Southern Sierra site (**Figure 4**). While simulations reflect results for a particular site, these distributions have broader use in a few main ways: (1) By varying topographic and climate parameter sets used in our simulations, results are likely to be representative of much of the Southern Sierra Nevada region. Thus, these results can support regional-scale questions and goals or be upscaled into multi-region analyses. (2) The distributions of effect sizes serve as a starting point, highlighting potential sources of variation in fuel treatment effects that should be explored by more focused simulations for watershed-specific fuel treatment impact assessments. (3) Our approach demonstrates a method that could be readily applied in other locations.

Our sensitivity analysis found non-trivial differences in fuel treatment impacts on mean annual stand carbon, NPP, ET, FSP, shrub fuel height, and conifer canopy fuel gap across fuel treatment type, biophysical, and climate parameters. This is evident both through the varying parameter relationships, such as effects on NPP resulting from varied fuel treatment type

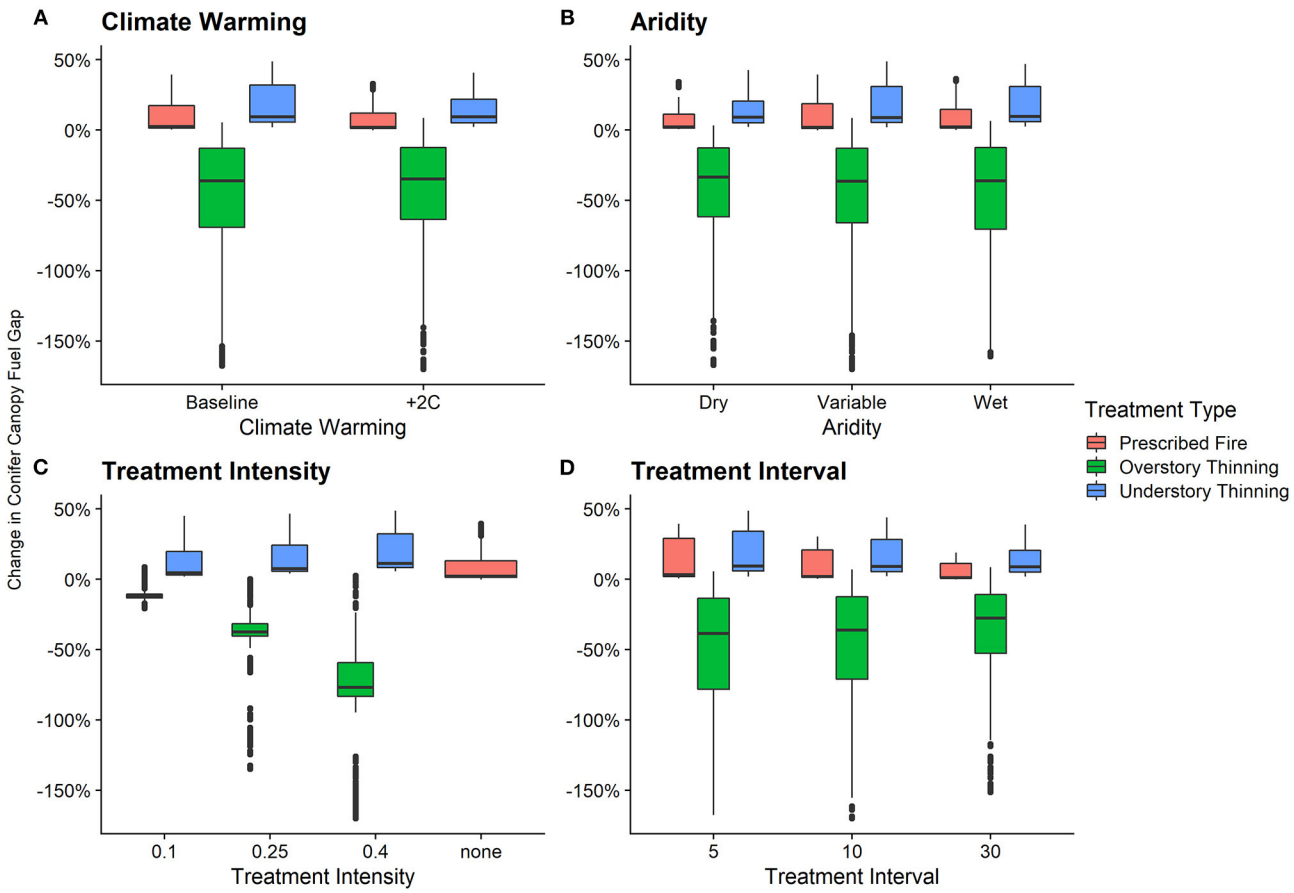

FIGURE 6 | Boxplots of percent change of simulation long (30-years) mean conifer canopy fuel gap, relative to untreated equivalent scenarios, for only conifer+shrub scenarios, subdivided by climate warming **(A)**, aridity **(B)**, treatment intensity **(C)**, and treatment interval **(D)** on the x-axes and colored by treatment type. Upper and lower hinges indicate the 1st and 3rd quartiles (25 and 75th percentiles), and whiskers indicate the greatest/smallest value within 1.5 times the inter-quartile range.

and PAWSC (**Figure 5A**), or effects on conifer canopy fuel gap across fuel treatment type and treatment intensity (**Figure 6C**), and the differences in parameter influence across response variables shown via the random forest analysis (**Figure 7**). These parameter relationships are complex, context dependent, and vary by response variable, but together they emphasize that fuel treatment effects are likely to be highly variable even within the same watershed. Variation is not only in magnitude, but often also in direction with some conditions leading to increases and others decreases in the response variable of interest. We find key instances where fuel treatment effects deviate from expected outcomes (H1–H4), such as increases in carbon sequestration or reductions in water yield. This variation across fuel treatment practices, biophysical conditions, and climate parameters (that could all occur within the same management unit) underline the need for a more comprehensive understanding of the factors affecting fuel treatment effectiveness. Results here can extend to regional planning to meet forest management goals; attempting to balance key regional priorities like fire severity reduction and carbon sequestration will require accounting for the likely variation in fuel treatment effects.

Our results serve as a first-order approximation of possible outcomes resulting from a fuel treatment, as well as distributions indicating likely outcomes. Stand carbon (**Figure 4A**) and ET (**Figure 4C**; showing changes in water yield), are noteworthy here. Both response variables have relatively few scenarios resulting in increases (percent change $>$ 0%), which is indicative both of how often treatments lead to increases in water yield (reduce ET) and the challenge in increasing carbon sequestration through fuel treatments. These results are generally consistent with our expectations (H2, H3) from other modeling and field-based studies. While these results suggest that fuel treatments alone will generally lead to a decline in sequestered carbon, other studies have shown that if fuel treatments effectively reduce fire severity, this could lead to a long term net gain in carbon storage in the Sierra (Liang et al., 2018). In this study, where wildfire is not explicitly included, the scenarios that do show modest increases in carbon (up to 30%), reflect cases where thinning effectively stimulates growth of remaining vegetation (potentially by reducing competition for water or reducing understory shading). These cases are particularly noteworthy given the baseline assumption of decreasing sequestration (H2).

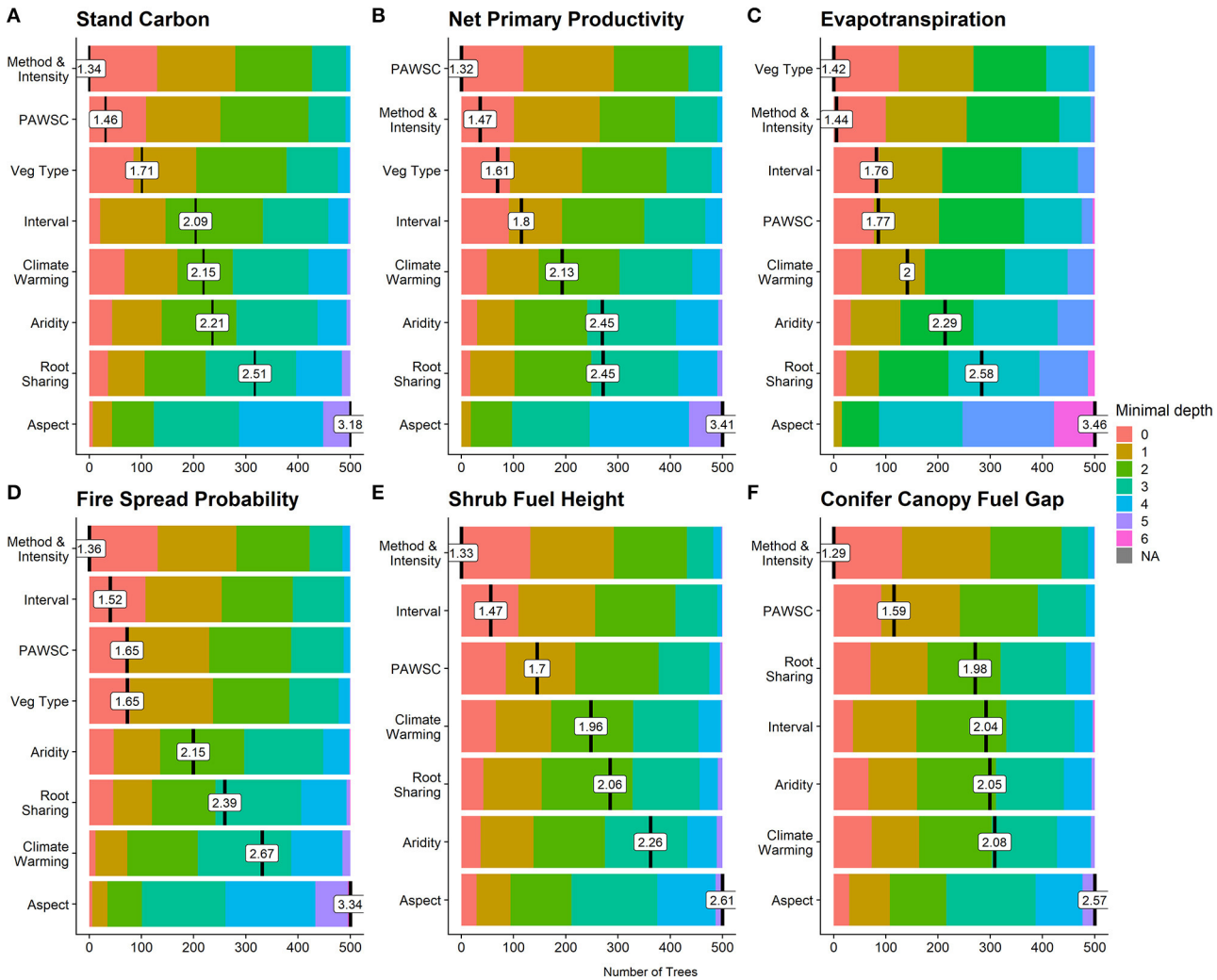

FIGURE 7 | Means and distributions of minimal depths for the random forest decision trees of stand carbon **(A)**, net primary productivity **(B)**, evapotranspiration **(C)**, fire spread probability **(D)**, shrub fuel height **(E)**, and conifer canopy fuel gap **(F)**. Minimal depth indicates, for each random forest, the first decision tree node that a given parameter best grouped (minimized variance) for the output variable.

While large scale biomass removal generally leads to increases in streamflow due to declines in transpiration (Brown et al., 2005), the smaller biomass removal associated with thinning is often compensated for by increases in evaporation, and transpiration of remaining trees (Saksa et al., 2017; Tague and Moritz, 2019). We find similar outcomes in this study where some scenarios have a net decrease in water availability (a net increase in ET), diverging from the typically expected water yield increases (H3). The magnitude of changes resulting from treatment are modest—a positive skew from 0% up to 14% increase in ET. For both stand carbon and ET, understanding the limited, but still present, scenarios that depart from typically expected outcomes (H2 and H3), will be key to forest management planning, but also useful as a basis for further, more focused modeling and analysis.

In considering the distribution of fuel treatment effects on fire related variables we see a dichotomy between the small range of effects on FSP (**Figure 4D**) and the more noteworthy range of effects on shrub fuel height and conifer canopy fuel gap (**Figures 4E,F**). The difference between the fire metrics shown in **Figure 4** underscores the often-small magnitude of effects a fuel treatment is likely to have on fire spread. However, treatments do produce a large range of effects on fire severity, shown in our study particularly when considering the conifer canopy fuel gap, which broadly aligns with expected treatment effects (H1). It should be noted that despite generating metrics assessing potential fire spread and severity, we do not run these simulations dynamically with fires affecting the landscape. Our results emphasize that fuel treatments mostly contribute to reducing potential fire severity, rather than fire spread. We note, however, that our spread indicator does not consider active fire suppression and it is likely that the fire suppression will be more effective at reducing spread when fires are less extreme.

Our results also highlight that reductions in potential fire severity also differ both with biophysical/climatic conditions and the type of fuel treatment. Critically, even when only considering understory treatment followed by prescribed fire, a treatment option supported by the literature in regards to its efficacy in reducing fire severity (Agee and Skinner, 2005), there is still a nontrivial range of effects, with many at or near 0% change. This range of effects is in contrast with the (often assumed) expectation of consistent treatment effects on fire severity (H1), and in turn emphasizes the challenge simply in consistently altering fire severity through fuel treatments. Though more specificity and detail on a fuel treatment scenario may lead to greater certainty on the efficacy of that treatment, the baseline assumption should account for this distribution of outcomes, or at the very least should emphasize the uncertainty inherent in these estimates.

Parameter Interactions

For all types of fuel treatment responses - carbon, water, and fire—our results demonstrate substantial interactions among biophysical, climatic, and fuel treatment parameters. Even when only viewing the influence of two parameters on fuel treatment effects (**Figure 5**), we find that treatment type and PAWSC can interact to produce varied effects across both dimensions. When comparing high and low PAWSC, changes in NPP (**Figure 5A**) are divergent across treatment type. ET (**Figure 5B**) and conifer canopy fuel gap (**Figure 5C**) show similar trends, though it is both the median effect as well as variability that varies across treatment type and PAWSC. This variability arising from parameter interactions is not present for all response variables—fire spread probability (**Figure 5D**) varies little across PAWSC. Similarly, not all parameters interact and lead to variation in effects. Conifer canopy fuel gap (**Figure 6**) responds similarly across some parameter combinations and shows varying or diverging trends across others. Both climate warming and aridity (**Figures 6A,B**), subset by treatment type, show small median impacts on conifer canopy fuel gap, with the primary response being small effects on variability. Treatment intensity and interval (**Figures 6C,D**), on the other hand, show much less consistency, with conifer canopy fuel gap changing in median effect and variability across both parameters. A critical repercussion of the variable responses we demonstrate is that a treatment strategy, or expected outcome of a treatment (e.g., H1–H4), assessed solely across a single parameter, may miss key trends in how that treatment will more broadly affect forests, water, and fire.

When we look at the effects of all parameters simultaneously using the Regression Trees (**Figure 7**), we find that most of the parameters play a nontrivial role in explaining response variability. Some parameters, however, do appear to be consistently more important—treatment method and intensity, for example, more strongly control trends in treatment effects as compared to aspect. The high ranking of fuel treatment parameters (treatment method and intensity and treatment interval) is encouraging, suggesting that these actions (and changes in them) are likely to have an impact across a range of site and climate conditions. Nonetheless PAWSC and vegetation type also consistently rank high. Collectively this pattern underscores the importance of biophysical setting and its interaction with treatment strategies in determining how a treatment affects forests, water, and fire. Based on this, PAWSC and vegetation type should be considered in fuel treatment selection. This is not always actionable from a management perspective, as often specific locations in the wildland urban interface necessitate treatment to mitigate high severity fire risk—but in modeling or planning possible treatments with a degree of flexibility, the cost-benefit of where to treat should consider PAWSC and vegetation type with weight similar to the type of fuel treatment itself. This is particularly true of treatments aimed at a broader range of forest and water-related goals—key among them are drought mitigation efforts like reduction in forest mortality or increasing water yield, while still aiming to reduce fire severity.

Climate is a less dominant control on fuel treatment effects as compared to the treatment method and intensity, treatment interval, vegetation type, and PAWSC. Though there is a consistent difference in rank order between the climate parameters (climate warming and aridity) and the above four parameters, the margin can be small, as with treatment effects on stand carbon (**Figure 7A**) or conifer canopy fuel gap (**Figure 7F**). Our results indicate that while climate is not a clear primary control on the outcome of a fuel treatment, neither can we ignore it given the often-marginal difference from other, higher ranked, parameters. As focus on fuel treatments used for climate change mitigation increases, the need for inclusion of climate in analyses of fuel treatment effects will also increase. This work serves to contextualize that inclusion of climate as a control on fuel treatments; in more expansive analyses, or those simulating long-term projections, climate (both climate warming and aridity) is a reasonable or even necessary control to include and vary, with the opposite being true in narrower, or shorter term analyses. The role of climate here is also likely underestimated as we simulate climate warming only with a 2°C increase in temperature and our aridity scenarios do not account for the expected increased variability of precipitation (Hayhoe et al., 2018).

Our results are consistent with other research that has considered factors like treatment method, storage capacity, vegetation type, and climate as variables that can influence treatment responses (Finney et al., 2007; Hurteau et al., 2014). Tree-scale interactions between neighboring vegetation, specifically lateral transfers of water and shading, are not typically considered. In this study, the root sharing coefficient reflects variation in tree scale interactions. While the root sharing coefficient is not the dominant factor influencing fuel treatment effects, it is consistently comparable to the climate parameters, and has a particularly large influence on conifer canopy fuel gap. Our research underscores the importance of tree-scale lateral root access in facilitating emergent differences in vegetation heights. While more work is needed to fully understand tree-scale water transfers due to lateral root access, and how this varies with species and canopy structure, the role of tree-scale lateral transfers shown here is noteworthy. Finally, we note that aspect demonstrates a consistently weaker influence on all fuel treatment effects. Inevitably there will be specific cases in which aspect has a more noteworthy influence on treatment effects, but it nonetheless would be the first parameter to exclude when narrowing the scope of analysis.

Model Limitations and Future Work

Though our research makes meaningful strides to better characterize fuel treatments and fuel treatment effects, both through the incorporation of tree-scale lateral transfers, as well as other recent advances to RHESSys, our modeling approach (like any) remains an imperfect approximation of reality. Some limitations include the use of indicators of fire severity rather than natively including fires within the model, and the absences of lateral subsurface water inputs (see Methods). These are not limitations of RHESSys but rather are constraints due to modeling a single "patch family" rather than a hillslope. Focusing on a single patch allowed us to fully explore a complex parameter space. Practical computing would limit this exploration for a full watershed implementation, but future work will investigate watershed scale behaviors for parameter scenarios selected from this study. In this study we did not account for heterogeneity in vegetation size classes nor species differences.

The relationships between scenarios and treatment effects in this research are based on assumptions and limitations specific to our mid-elevation Southern Sierra Nevada site. Despite this, little of the model or scenario parameterization is truly exclusive to our site. Parameter sets were selected specifically to be regionally representative. The results found here are then useful across regions where vegetation, climate, and PAWSC are comparable—Southern Sierra Nevada mid-elevation regions. Beyond the broader application of the results of this work, the methodology developed here, both the modeling methods (RHESSys and multiscale routing) and the general architecture of the scenarios, has merit for use elsewhere. Interest in fuel treatments for fire severity reduction, improved drought resilience, increased water yield, and myriad other purposes is not unique to the Southern Sierras. The methods demonstrated here can be replicated in other regions to build improved understanding of global effects of fuel treatments, which continues to be a key yet challenging goal (Evaristo and McDonnell, 2019; Kirchner et al., 2020). The methods shown in this work also present an opportunity for synthesis with empirical data on fuel treatment effects, and can serve as a foundational step, to preface either more focused modeling work, or to inform the planning of field work. Replication of this work is already planned across a series of sites in the Western United Sates, but with climate-driven increases to fire activity projected for many regions of the world (Moritz et al., 2012), additional locations merit further investigation of fuel treatment effects.

CONCLUSIONS

Interactions between biophysical setting, climate, and fuel treatments are complex and have non-linear effects on forests, water, and fire. As fuel treatments receive more interest, and more often with goals beyond fire severity reduction, it becomes increasingly important to understand and ultimately quantify the range and distribution of likely effects that a treatment may have. This presents a challenging task for modelers and field scientists alike given the intersecting scientific domains and complex interconnected processes. Our research works to address this problem and provide a blueprint for how to robustly identify both the range of expected treatment effects and which factors have the greatest influence on those treatment effects. Across our range of scenarios, we highlight cases where treatment effects deviate from expectations, such as instances of increasing carbon sequestration or decreasing water yields. Even when treatment effects conform to expected direction of change (e.g., increasing water yields), results show substantial variation in the magnitude of effects even within the same watershed. For our mid-elevation Southern Sierra site, fuel treatment parameters (i.e., treatment method and intensity, and treatment interval) along with biophysical parameters (i.e., vegetation type and PAWSC), are important controls on fuel treatment effects. Climate and root sharing coefficient are of lesser, albeit variable importance across fuel treatment effects, while aspect stands out with particularly little influence on fuel treatment effects for this site. Arising from these analyses, we underscore the difficulty in estimating fuel treatment effects over narrow ranges of biophysical and fuel treatment parameters, and the need for greater variation across the parameter space, particularly as treatments are used with multiple goals in mind concerning forests, water, and fire. This approach allows for more focused analyses to further interrogate, at finer spatial and temporal scales, how fuel treatments affect our natural environment.

DATA AVAILABILITY STATEMENT

Datasets generated from this study can be found on HydroShare: Burke, W. (2020). Big Creek Patch Scale RHESSys Simulations, HydroShare, http://www.hydroshare.org/resource/2f41fc04cb8645d0938097af5c57f98e. Code used to generate those datasets and perform analysis can be found on Github: https://github.com/wburke24/BigCreekPatchScale. Specific version/commit of the model used – RHESSys 7.1.1 (3/2/20, commit: 01e391f, full SHA: 01e391f56f0f63e6cf3ff3ac4b21122ed6bfce7b) can be found on Github: https://github.com/RHESSys/RHESSys/tree/01e391f56f0f63e6cf3ff3ac4b21122ed6bfce7b.

AUTHOR CONTRIBUTIONS

WB and CT conceived of initial research and lead research design which was contributed to by MK and MM. WB conducted the modeling and data analysis, lead figure design, and manuscript writing. All authors contributed to figure design and manuscript writing.

FUNDING

This research was supported by funding from National Science Foundation [Hazard SEES program (Grant number: 094878394)]: Land Management Strategies for Confronting Risks and Consequences of Wildfire (EAR-1520847).

ACKNOWLEDGMENTS

The authors thank Janet Choate for contributions to figures, and both the Tague lab and SERI-Fire team for their feedback and contributions.

REFERENCES

Agee, J. K., and Skinner, C. N. (2005). Basic principles of forest fuel reduction treatments. *For. Ecol. Manage.* 211, 83–96. doi: 10.1016/j.foreco.2005.01.034

Allen, C. D., Macalady, A. K., Chenchouni, H., Bachelet, D., McDowell, N., Vennetier, M., et al. (2010). A global overview of drought and heat-induced tree mortality reveals emerging climate change risks for forests. *For. Ecol. Manage.* 259, 660–684. doi: 10.1016/j.foreco.2009.09.001

Anderson, S. E., Bart, R. R., Kennedy, M. C., MacDonald, A. J., Moritz, M. A., Plantinga, A. J., et al. (2018). The dangers of disaster-driven responses to climate change. *Nat. Clim. Chang.* 8, 651–653. doi: 10.1038/s41558-018-0208-8

Asner, G. P., Brodrick, P. G., Anderson, C. B., Vaughn, N., Knapp, D. E., and Martin, R. E. (2016). Progressive forest canopy water loss during the 2012–2015 California drought. *Proc. Natl. Acad. Sci. U. S. A.* 113, E249–E255. doi: 10.1073/pnas.1523397113

Bales, R. C., Hopmans, J. W., O'Geen, A. T., Meadows, M., Hartsough, P. C., Kirchner, P., et al. (2011). Soil moisture response to snowmelt and rainfall in a Sierra Nevada mixed-conifer forest. *Vadose Zone J.* 10, 786–799. doi: 10.2136/vzj2011.0001

Barros, A. M., Ager, A. A., Day, M. A., and Palaiologou, P. (2019). Improving long-term fuel treatment effectiveness in the National Forest System through quantitative prioritization. *Forest Ecol. Manag.* 433, 514–527. doi: 10.1016/J.FORECO.2018.10.041

Bart, R. R., Kennedy, M. C., Tague, C. L., and McKenzie, D. (2020). Integrating fire effects on vegetation carbon cycling within an ecohydrologic model. *Ecol. Modell.* 416:108880. doi: 10.1016/j.ecolmodel.2019.108880

Bart, R. R., Tague, C. L., and Moritz, M. A. (2016). Effect of tree-to-shrub type conversion in lower montane forests of the sierra nevada (USA) on streamflow. *PLoS ONE* 11:e0161805. doi: 10.1371/journal.pone.0161805

Boisramé, G. F., Thompson, S. E., Tague, C., and Stephens, S. L. (2019). Restoring a natural fire regime alters the water balance of a sierra nevada catchment. *Water Resour. Res.* 55, 5751–5769. doi: 10.1029/2018WR024098

Brown, A. E., Zhang, L., McMahon, T. A., Western, A. W., and Vertessy, R. A. (2005). A review of paired catchment studies for determining changes in water yield resulting from alterations in vegetation. *J. Hydrol.* 310, 28–61. doi: 10.1016/j.jhydrol.2004.12.010

Burke, W., and Tague, N. (2019). "Multiscale routing-integrating the tree-scale effects of disturbance into a watershed ecohydrologic model," in *AGU Fall Meeting* (San Francisco, CA). Available online at: https://agu.confex.com/agu/fm19/meetingapp.cgi/Paper/510712

Cabon, A., Mouillot, F., Lempereur, M., Ourcival, J.-M., Simioni, G., and Limousin, J.-M. (2018). Thinning increases tree growth by delaying drought-induced growth cessation in a mediterranean evergreen oak coppice. *For. Ecol. Manage.* 409, 333–342. doi: 10.1016/j.foreco.2017.11.030

Calkin, D., and Gebert, K. (2006). Modeling fuel treatment costs on forest service lands in the western United States. *Western J. Appl. For.* 21, 217–221. doi: 10.1093/wjaf/21.4.217

Clark, J. S., Iverson, L., Woodall, C. W., Allen, C. D., Bell, D. M., Bragg, D. C., et al. (2016). The impacts of increasing drought on forest dynamics, structure, and biodiversity in the United States. *Glob. Change Biol.* 22, 2329–2352. doi: 10.1111/gcb.13160

Dickinson, R. E., Shaikh, M., Bryant, R., and Graumlich, L. (1998). Interactive canopies for a climate model. *J. Clim.* 11, 2823–2836. doi: 10.1175/1520-0442(1998)011<2823:ICFACM>2.0.CO;2

Ellison, D., Futter, M. N., and Bishop, K. (2012). On the forest cover–water yield debate: from demand- to supply-side thinking. *Glob. Chang. Biol.* 18, 806–820. doi: 10.1111/j.1365-2486.2011.02589.x

Evans, A. M., Everett, R. G., Stephens, S. L., and Youlz, J. A. (2011). Comprehensive fuels treatment practices guide for mixed conifer forests: california, central and southern rockies, and the Southwest. *JFSP Synth. Rep.* 12:113. Available online at: https://digitalcommons.unl.edu/jfspsynthesis/12/

Evaristo, J., and McDonnell, J. J. (2019). Global analysis of streamflow response to forest management. *Nature* 570, 455–461. doi: 10.1038/s41586-019-1306-0

Farquhar, G. D., von Caemmerer, S., von, and Berry, J. A. (1980). A biochemical model of photosynthetic CO_2 assimilation in leaves of C 3 species. *Planta* 149, 78–90. doi: 10.1007/BF00386231

Fatichi, S., Vivoni, E. R., Ogden, F. L., Ivanov, V. Y., Mirus, B., Gochis, D., et al. (2016). An overview of current applications, challenges, and future trends in distributed process-based models in hydrology. *J. Hydrol.* 537, 45–60. doi: 10.1016/j.jhydrol.2016.03.026

Fernandes, P. M. (2015). Empirical support for the use of prescribed burning as a fuel treatment. *Curr. For. Rep.* 1, 118–127. doi: 10.1007/s40725-015-0010-z

Filoso, S., Bezerra, M. O., Weiss, K. C. B., and Palmer, M. A. (2017). Impacts of forest restoration on water yield: a systematic review. *PLoS ONE* 12:e0183210. doi: 10.1371/journal.pone.0183210

Finney, M. A., Seli, R. C., McHugh, C. W., Ager, A. A., Bahro, B., and Agee, J. K. (2007). Simulation of long-term landscape-level fuel treatment effects on large wildfires. *Int. J. Wildl. Fire* 16, 712–727. doi: 10.1071/WF06064

Garcia, E. S., Tague, C. L., and Choate, J. S. (2016). Uncertainty in carbon allocation strategy and ecophysiological parameterization influences on carbon and streamflow estimates for two western US forested watersheds. *Ecol. Modell.* 342, 19–33. doi: 10.1016/j.ecolmodel.2016.09.021

Gould, D. (2019a). *Revised Draft Land Management Plan for the Sequoia National Forest USDA*. Available online at: https://www.fs.usda.gov/nfs/11558/www/nepa/3403_FSPLT3_4658766.pdf (accessed July 29, 2020).

Gould, D. (2019b). *Revised Draft Land Management Plan for the Sierra National Forest. USDA*. Available online at: https://www.fs.usda.gov/nfs/11558/www/nepa/3403_FSPLT3_4658767.pdf (accessed July 29, 2020).

Grant, G. E., Tague, C. L., and Allen, C. D. (2013). Watering the forest for the trees: an emerging priority for managing water in forest landscapes. *Front. Ecol. Environ.* 11, 314–321. doi: 10.1890/120209

Hayhoe, K., Wuebbles, D. J., Easterling, D. R., Fahey, D. W., Doherty, S., Kossin, J., et al. (2018). "2018: our changing climate," in *Impacts, Risks, and Adaptation in the United States: Fourth National Climate Assessment, Volume II*, eds D. R. Reidmiller, C. W. Avery, D. R. Easterling, K. E. Kunkel, K. L. M. Lewis, T. K. Maycock, and B. C. Stewart (Washington, DC: U.S. Global Change Research Program), 72–144. doi: 10.7930/NCA4.2018.CH2

Hessburg, P. F., Spies, T. A., Perry, D. A., Skinner, C. N., Taylor, A. H., Brown, P. M., et al. (2016). Tamm review: management of mixed-severity fire regime forests in Oregon, Washington, and Northern California. *For. Ecol. Manage.* 366, 221–250. doi: 10.1016/j.foreco.2016.01.034

Hewlett, J. D., and Hibbert, A. R. (1967). Factors affecting the response of small watersheds to precipitation in humid areas. *For. Hydrol.* 1, 275–290.

Hurteau, M. D., Robards, T. A., Stevens, D., Saah, D., North, M., and Koch, G. W. (2014). Modeling climate and fuel reduction impacts on mixed-conifer forest carbon stocks in the Sierra Nevada, California. *For. Ecol. Manage.* 315, 30–42. doi: 10.1016/j.foreco.2013.12.012

Kennedy, M. C., McKenzie, D., Tague, C., and Dugger, A. L. (2017). Balancing uncertainty and complexity to incorporate fire spread in an eco-hydrological model. *Int. J. Wildl. Fire* 26, 706–718. doi: 10.1071/WF16169

Kirchner, J. W., Berghuijs, W. R., Allen, S. T., Hrachowitz, M., Hut, R., and Rizzo, D. M. (2020). Streamflow response to forest management. *Nature* 578, E12–E15. doi: 10.1038/s41586-020-1940-6

Klos, P. Z., Goulden, M. L., Riebe, C. S., Tague, C. L., O'Geen, A. T., Flinchum, B. A., et al. (2018). Subsurface plant-accessible water in mountain ecosystems with a mediterranean climate. *Wiley Interdiscip. Rev.* 5:e1277. doi: 10.1002/wat2.1277

Liang, S., Hurteau, M. D., and Westerling, A. L. (2018). Large-scale restoration increases carbon stability under projected climate and wildfire regimes. *Front. Ecol. Environ.* 16, 207–212. doi: 10.1002/fee.1791

Liaw, A., and Wiener, M. (2002). Classification and regression by randomForest. *R News* 2, 18–22.

McDowell, N. G., Adams, H. D., Bailey, J. D., and Kolb, T. E. (2007). The role of stand density on growth efficiency, leaf area index, and resin flow in southwestern ponderosa pine forests. *Can. J. For. Res.* 37, 343–355. doi: 10.1139/X06-233

Monteith, J. L. (1965). Evaporation and environment. *Symp. Soc. Exp. Biol.* 19, 205–234.

Moritz, M. A., Batllori, E., Bradstock, R. A., Gill, A. M., Handmer, J., Hessburg, P. F., et al. (2014). Learning to coexist with wildfire. *Nature* 515, 58–66. doi: 10.1038/nature13946

Moritz, M. A., Parisien, M.-A., Batllori, E., Krawchuk, M. A., Dorn, J. V., Ganz, D. J., et al. (2012). Climate change and disruptions to global fire activity. *Ecosphere* 3:art49. doi: 10.1890/ES11-00345.1

North, M., Brough, A., Long, J., Collins, B., Bowden, P., Yasuda, D., et al. (2015). Constraints on mechanized treatment significantly limit mechanical fuels reduction extent in the Sierra Nevada. *J. For.* 113, 40–48. doi: 10.5849/jof.14-058

North, M., Hurteau, M., and Innes, J. (2009). Fire suppression and fuels treatment effects on mixed-conifer carbon stocks and emissions. *Ecol. Appl.* 19, 1385–1396. doi: 10.1890/08-1173.1

Omi, P. N., and Martinson, E. J. (2002). Effects of fuels treatment on wildfire severity. *Fort Collins: Colorado State University: Joint Fire Science Program Governing Board, Western Forest Fire Research Center.* Available online at: https://www.ntc.blm.gov/krc/uploads/399/Effects%20of%20Fuels%20Treatment%20on%20Wildfire%20Severity.pdf (accessed April 4, 2020).

Paluszynska, A., Biecek, P., and Jiang, Y. (2019). *randomForestExplainer: Explaining and Visualizing Random Forests in Terms of Variable Importance*. Available online at: https://CRAN.R-project.org/package=randomForestExplainer (accessed May 17, 2020).

Running, S. W., Nemani, R. R., and Hungerford, R. D. (1987). Extrapolation of synoptic meteorological data in mountainous terrain and its use for simulating forest evapotranspiration and photosynthesis. *Can. J. For. Res.* 17, 472–483. doi: 10.1139/x87-081

Ryan, M. G. (1991). Effects of climate change on plant respiration. *Ecol. Appl.* 1, 157–167. doi: 10.2307/1941808

Safeeq, M., and Hunsaker, C. T. (2016). Characterizing runoff and water yield for headwater catchments in the southern sierra nevada. *J. Am. Water Resour. Assoc.* 52, 1327–1346. doi: 10.1111/1752-1688.12457

Safford, H. D., Stevens, J. T., Merriam, K., Meyer, M. D., and Latimer, A. M. (2012). Fuel treatment effectiveness in California yellow pine and mixed conifer forests. *For. Ecol. Manage.* 274, 17–28. doi: 10.1016/j.foreco.2012.02.013

Saksa, P. C., Conklin, M. H., Battles, J. J., Tague, C. L., and Bales, R. C. (2017). Forest thinning impacts on the water balance of S ierra N evada mixed-conifer headwater basins. *Water Resour. Res.* 53, 5364–5381. doi: 10.1002/2016WR019240

Schenk, H. J., and Jackson, R. B. (2002). Rooting depths, lateral root spreads and below-ground/above-ground allometries of plants in water-limited ecosystems. *J. Ecol.* 90, 480–494. doi: 10.1046/j.1365-2745.2002.00682.x

Sohn, J. A., Saha, S., and Bauhus, J. (2016). Potential of forest thinning to mitigate drought stress: a meta-analysis. *For. Ecol. Manage.* 380, 261–273. doi: 10.1016/j.foreco.2016.07.046

Son, K., Tague, C., and Hunsaker, C. (2016). Effects of model spatial resolution on ecohydrologic predictions and their sensitivity to inter-annual climate variability. *Water* 8:321. doi: 10.3390/w8080321

Spittlehouse, D. L., and Stewart, R. B. (2003). Adaptation to climate change in forest management. *Adapt. Clim. Change* 4:12. Available online at: https://jem-online.org/index.php/jem/article/download/254/173.pdf

Stephens, S. L., McIver, J. D., Boerner, R. E., Fettig, C. J., Fontaine, J. B., Hartsough, B. R., et al. (2012). The effects of forest fuel-reduction treatments in the United States. *Bioscience* 62, 549–560. doi: 10.1525/bio.2012.62.6.6

Tague, C., Seaby, L., and Hope, A. (2009). Modeling the eco-hydrologic response of a mediterranean type ecosystem to the combined impacts of projected climate change and altered fire frequencies. *Clim. Change* 93, 137–155. doi: 10.1007/s10584-008-9497-7

Tague, C. L., and Band, L. E. (2004). RHESSys: regional hydro-ecologic simulation system—an object-oriented approach to spatially distributed modeling of carbon, water, and nutrient cycling. *Earth Interact.* 8, 1–42. doi: 10.1175/1087-3562(2004)8<1:RRHSSO>2.0.CO;2

Tague, C. L., Moritz, M., and Hanan, E. (2019). The changing water cycle: the eco-hydrologic impacts of forest density reduction in mediterranean (seasonally dry) regions. *Wiley Interdiscip. Rev.* 6:e1350. doi: 10.1002/wat2.1350

Tague, C. L., and Moritz, M. A. (2019). Plant accessible water storage capacity and tree-scale root interactions determine how forest density reductions alter forest water use and productivity. *Front. For. Glob. Change* 2:36. doi: 10.3389/ffgc.2019.00036

Thompson, M. P., Bowden, P., Brough, A., Scott, J. H., Gilbertson-Day, J., Taylor, A., et al. (2016). Application of wildfire risk assessment results to wildfire response planning in the southern Sierra Nevada, California, USA. *Forests* 7:64. doi: 10.3390/f7030064

Tsamir, M., Gottlieb, S., Preisler, Y., Rotenberg, E., Tatarinov, F., Yakir, D., et al. (2019). Stand density effects on carbon and water fluxes in a semi-arid forest, from leaf to stand-scale. *For. Ecol. Manage.* 453:117573. doi: 10.1016/j.foreco.2019.117573

Wibbenmeyer, M., Anderson, S., and Plantinga, A. J. (2016). *Risk Salience, Public Pressure, and Agency Action: Wildfire and the Management of Public Lands*. Mimeo. Available online at: https://www.fs.usda.gov/Internet/FSE_DOCUMENTS/fseprd640156.pdf (accessed October 25, 2018).

Conflict of Interest: The authors declare that the research was conducted in the absence of any commercial or financial relationships that could be construed as a potential conflict of interest.

Advantages of publishing in Frontiers

OPEN ACCESS
Articles are free to read for greatest visibility and readership

FAST PUBLICATION
Around 90 days from submission to decision

HIGH QUALITY PEER-REVIEW
Rigorous, collaborative, and constructive peer-review

TRANSPARENT PEER-REVIEW
Editors and reviewers acknowledged by name on published articles

Frontiers
Avenue du Tribunal-Fédéral 34
1005 Lausanne | Switzerland

Visit us: www.frontiersin.org
Contact us: frontiersin.org/about/contact

REPRODUCIBILITY OF RESEARCH
Support open data and methods to enhance research reproducibility

DIGITAL PUBLISHING
Articles designed for optimal readership across devices

FOLLOW US
@frontiersin

IMPACT METRICS
Advanced article metrics track visibility across digital media

EXTENSIVE PROMOTION
Marketing and promotion of impactful research

LOOP RESEARCH NETWORK
Our network increases your article's readership